IMPROVE

Interagency Monitoring of Protected Visual Environments

Spatial and Seasonal Patterns and Temporal Variability of Haze and its Constituents in the United States

Report IV

November 2006

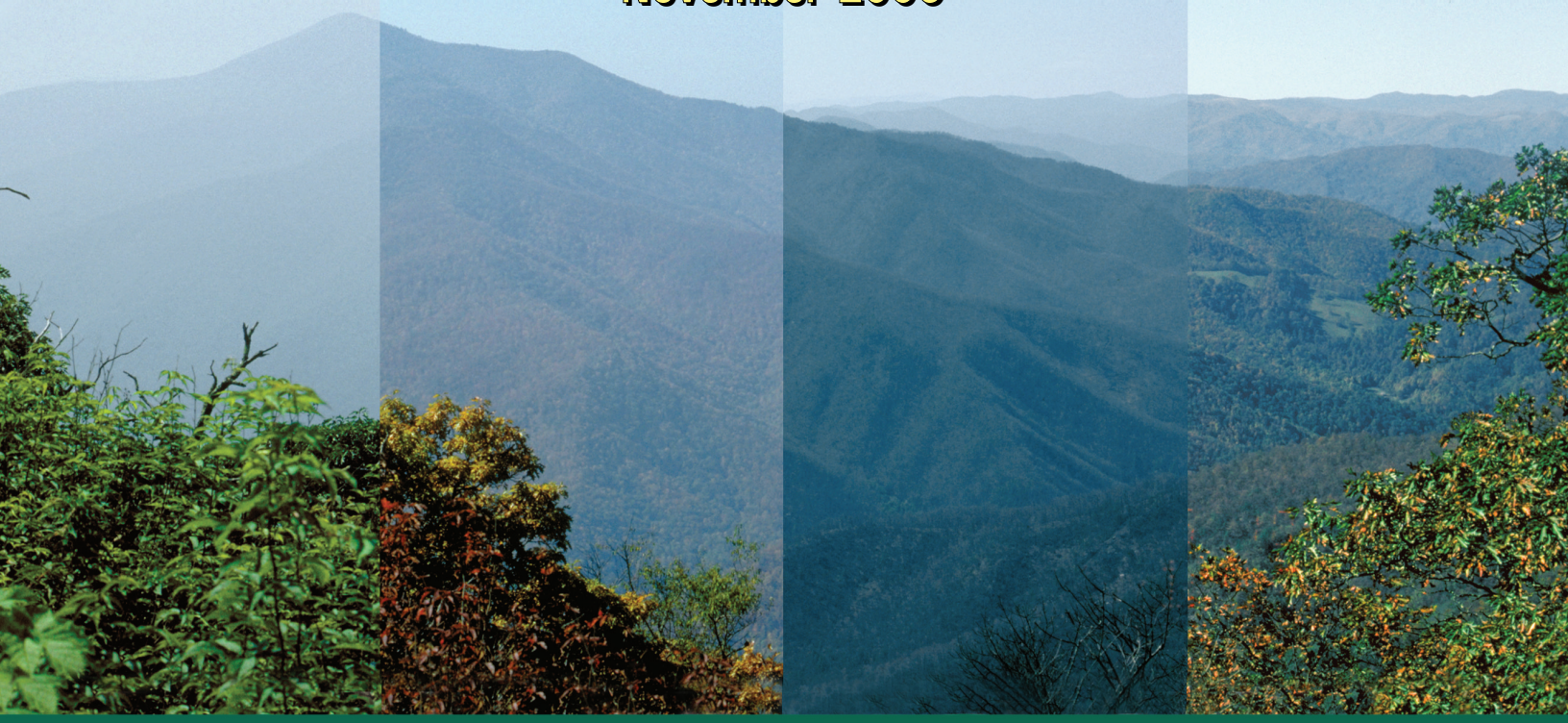

ISSN: 0737-5352-74

CIRA
Cooperative Institute for Research in the Atmosphere

Colorado State University

Spatial and Seasonal Patterns and Temporal Variability of Haze and its Constituents in the United States
Report IV

Principal Author:
Linsey J. DeBell[1]
[1]Cooperative Institute for Research in the Atmosphere
Colorado State University
Fort Collins, CO 80523-1375

Contributors:
Kristi A. Gebhart[2]
Jenny L. Hand[1]
William C. Malm[2]
Marc L. Pitchford[3]
Bret A. Schichtel[2]
Warren H. White[4]

[2]National Park Service
CSU/CIRA
Fort Collins, CO 80523-1375
[3]National Oceanic and Atmospheric Administration
Desert Research Institute
Las Vegas, NV 89119-7363
[4]Crocker Nuclear Laboratory
University of California
Davis, CA 95616-8569

TABLE OF CONTENTS

Appendices A–E available on cd or at
http://vista.cira.colostate.edu/improve/Publications/improve_reports.htm

Appendix A: Annual Average Reconstructed Fine Mass and Aerosol Extinction Budgets for Each Site

Appendix B: Seasonal and Annual Regional Reconstructed Fine Mass and Reconstructed Extinction Budgets

Appendix C: Monthly and Annual Reconstructed Fine Mass and Reconstructed Extinction and their Associated Budgets from the IMPROVE Network for 2000 through 2004

Appendix D: Articles Reporting the Results from IMPROVE Special Monitoring Studies Conducted since 2000

Appendix E: An Assessment of Measurement Errors in the IMPROVE and STN Networks from In-Network and Cross-Network Collocated Data and the Estimated Comparability of Data Collected from the Two Networks

LIST OF FIGURES

LIST OF TABLES

OVERVIEW AND SUMMARY

This report is the fourth in a series of periodic reports that describe the data collected by the Interagency Monitoring of Protected Visual Environments (IMPROVE) monitoring network. The IMPROVE program is a cooperative measurement effort between the U.S. Environmental Protection Agency (EPA), federal land management agencies, and state air agencies designed to

1. establish current visibility and aerosol conditions in mandatory Class I areas (CIAs);
2. identify chemical species and emission sources responsible for existing man-made visibility impairment;
3. document long-term trends for assessing progress towards the national visibility goal;
4. and, with the enactment of the Regional Haze Rule, provide regional haze monitoring representing all visibility-protected federal CIAs where practical.

When the IMPROVE monitoring program was initiated, it was resource and funding limited so that it was not practical to place monitoring stations at all 156 mandatory Class I areas where visibility is an important attribute. Therefore, the first IMPROVE report reflected data that were collected at only 36 sites for the time period March 1988 through February 1991. Over subsequent years the IMPROVE network evolved and a second IMPROVE report was published that covered data gathered between March 1992 and February 1995 at 43 sites. The network is now composed of 110 IMPROVE sites representative of 155 of the 156 visibility-protected federal Class I areas (national parks and wilderness areas). There are an additional ~50 IMPROVE protocol sites operated identically to the 110 IMPROVE sites but which are individually sponsored by federal, state, and tribal organizations (see Figure S.1).

This report provides a broad examination of the IMPROVE data as well as results from special field studies and data analyses conducted since the 2000 IMPROVE report. The IMPROVE data analysis includes the examination of the spatial and seasonal aerosol concentrations and composition for 159 sites from 2000 through 2004 and long-term trends for 38–49 sites, depending upon the parameter examined, using data from 1988 and 2004. A unique aspect of this report compared to previous IMPROVE reports is the inclusion of 84 sites from the EPA's Speciated Trend Network (STN) in the spatial and seasonal pattern analyses. The STN network collects speciated aerosol data similar to the IMPROVE network, but the sites are located primarily in urban/suburban settings. Incorporation of data from these sites into the assessment permits the extension of the spatial and season aerosol patterns from the surrounding remote areas into urban areas, providing insights into the fraction of the particulate matter (PM) that is contributed by regional and local sources.

IMPROVE quality assurance (QA) procedures are continually reviewed and enhanced. During the recent network expansion (2000 to 2002), collocated monitors were installed at a number of IMPROVE sites to provide data needed to assess measurement precision. This report summarizes the current QA procedures and the results of precision estimates from collocated monitors.

S.1 OPTICAL AND AEROSOL DATA

The IMPROVE aerosol samplers (versions I and II) consist of four independent modules. Each module incorporates a separate inlet, filter pack, and pump assembly. It is convenient to consider a particular module, its associated filter, and the parameters measured from the filter as a channel of measurement (e.g., module A). Modules A, B, and C are equipped with a 2.5 μm cyclone, while module D is fitted with a PM_{10} inlet. The D module collects PM_{10} aerosol on Teflon filters. The A, B, and C modules collect $PM_{2.5}$ aerosol on Teflon, nylon, and quartz fiber filters, respectively. The different filter media facilitate the collection of particular aerosol species or a specific form of chemical analysis. Gravimetric analysis is routinely performed on the A and D module filters. Elemental analysis and aerosol absorption measurements are routinely performed on the A module filter. Ion analysis is routinely performed on the B module filter, and carbon analysis is routinely performed on the quartz fiber filter. The samplers are currently operated on a one-day-in-three schedule for a 24-hour sampling duration consistent with the EPA's aerosol monitoring networks. There are aerosol samplers at the 110 IMPROVE sites and the ~50 IMPROVE protocol sites. Current and past IMPROVE and protocol aerosol sampling sites are listed by region in Table S.1, and those in the contiguous 48 states are shown in Figure S.1.

Table S.1. IMPROVE monitoring sites listed according to region. The monitoring site codes are in parentheses.

Alaska	Northeast
• Ambler (AMBL1)*	• Acadia NP (ACAD1)
• Denali NP (DENA1)	• Addison Pinnacle (ADPI1)
• Petersburg (PETE1)	• Bridgton (BRMA1)
• Simeonof (SIME1)	• Cape Cod (CACO1)
• Trapper Creek (TRCR1)	• Casco Bay (CABA1)
• Tuxedni (TUXE1)	• Connecticut Hill (COHI1)*
Appalachia	• Great Gulf WA (GRGU1)
• Arendtsville (AREN1)	• Lye Brook WA (LYBR1)
• Cohutta (COHU1)	• Martha's Vineyard (MAVI1)
• Dolly Sods WA (DOSO1)	• Mohawk Mt. (MOMO1)
• Frostburg (FRRE1)	• Moosehorn NWR (MOOS1)
• Great Smoky Mountains NP (GRSM1)	• Old Town (OLTO1)
• James River Face WA (JARI1)	• Presque Isle (PRIS1)
• Jefferson NF (JEFF1)*	• Proctor Maple R. F. (PMRF1)
• Linville Gorge (LIGO1)	• Quabbin Summit (QURE1)
• Shenandoah NP (SHEN1)	Northern Great Plains
• Shining Rock WA (SHRO1)	• Badlands NP (BADL1)
• Sipsy WA (SIPS1)	• Cloud Peak (CLPE1)
Boundary Waters	• Fort Peck (FOPE1)
• Boundary Waters Canoe Area (BOWA1)	• Lostwood (LOST1)
• Isle Royale NP (ISLE1)	• Medicine Lake (MELA1)
• Isle Royale NP (ISRO1)*	• Northern Cheyenne (NOCH1)
• Seney (SENE1)	• Theodore Roosevelt (THRO1)
• Voyageurs NP #1 (VOYA1)*	• Thunder Basin (THBA1)
• Voyageurs NP #2 (VOYA2)	• UL Bend (ULBE1)
California Coast	• Wind Cave (WICA1)
• Pinnacles NM (PINN1)	Northern Rockies
• Point Reyes National Seashore (PORE1)	• Bridger WA (BRID1)
• San Rafael (RAFA1)	• Cabinet Mountains (CABI1)

Central Great Plains
- Blue Mounds (BLMO1)
- Bondville (BOND1)
- Cedar Bluff (CEBL1)
- Crescent Lake (CRES1)
- El Dorado Springs (ELDO1)
- Great River Bluffs (GRRI1)
- Lake Sugema (LASU1)*
- Lake Sugema (LASU2)
- Nebraska NF (NEBR1)
- Omaha (OMAH1)
- Sac and Fox (SAFO1)
- Tallgrass (TALL1)
- Viking Lake (VILA1)

Central Rockies
- Brooklyn Lake (BRLA1)*
- Great Sand Dunes NM (GRSA1)
- Mount Zirkel WA (MOZI1)
- Rocky Mountain NP (ROMO1)
- Rocky Mountain NP HQ (RMHQ1)*
- Storm Peak (STPE1)*
- Wheeler Peak (WHPE1)
- White River NF (WHRI1)

Colorado Plateau
- Arches NP (ARCH1)*
- Bandelier NM (BAND1)
- Bryce Canyon NP (BRCA1)
- Canyonlands NP (CANY1)
- Capitol Reef NP (CAPI1)
- Hance Camp at Grand Canyon NP (GRCA2)
- Hopi Point #1 (GRCA1)*
- Indian Gardens (INGA1)
- Meadview (MEAD1)
- Mesa Verde NP (MEVE1)
- San Pedro Parks (SAPE1)
- Weminuche WA (WEMI1)
- Zion (ZION1)*
- Zion Canyon (ZICA1)

Columbia River Gorge
- Columbia Gorge #1 (COGO1)
- Columbia River Gorge (CORI1)

Death Valley
- Death Valley NP (DEVA1)

East Coast
- Brigantine NWR (BRIG1)
- Swanquarter (SWAN1)

Great Basin
- Great Basin NP (GRBA1)
- Jarbidge WA (JARB1)

Hawaii
- Haleakala NP (HALE1)
- Hawaii Volcanoes NP (HAVO1)
- Mauna Loa Observatory #1 (MALO1)
- Flathead (FLAT1)
- Gates of the Mountains (GAMO1)
- Glacier NP (GLAC1)
- Monture (MONT1)
- North Absaroka (NOAB1)
- Salmon NF (SALM1)*
- Sula Peak (SULA1)
- Yellowstone NP 1 (YELL1)
- Yellowstone NP 2 (YELL2)

Northwest
- Lynden (LYND1)*
- Mount Rainier NP (MORA1)
- North Cascades (NOCA1)
- Olympic (OLYM1)
- Pasayten (PASA1)
- Snoqualmie Pass (SNPA1)
- Spokane Res. (SPOK1)*
- White Pass (WHPA1)

Not Assigned
- Walker River Paiute Tribe (WARI1)*

Ohio River Valley
- Cadiz (CADI1)
- Livonia (LIVO1)
- M.K. Goddard (MKGO1)
- Mammoth Cave NP (MACA1)
- Mingo (MING1)
- Quaker City (QUCI1)

Oregon and Northern California
- Bliss SP (TRPA) (BLIS1)
- Crater Lake NP (CRLA1)
- Kalmiopsis (KALM1)
- Lassen Volcanic NP (LAVO1)
- Lava Beds NM (LABE1)
- Mount Hood (MOHO1)

Phoenix
- Phoenix (PHOE1)

Puget Sound
- Puget Sound (PUSO1)
- Redwood NP (REDW1)
- Three Sisters WA (THSI1)
- Trinity (TRIN1)

Sierra Nevadas
- Dome Lands WA (DOLA1)*
- Dome Lands WA (DOME1)
- Hoover (HOOV1)
- Kaiser (KAIS1)
- Sequoia NP (SEQU1)
- South Lake Tahoe (SOLA1)*
- Yosemite NP (YOSE1)

Southeast
- Breton (BRET1)
- Cape Romain NWR (ROMA1)
- Chassahowitzka NWR (CHAS1)
- Everglades NP (EVER1)

- Mauna Loa Observatory #2 (MALO2)
- Mauna Loa Observatory #3 (MALO3)*
- Mauna Loa Observatory #4 (MALO4)*

Hells Canyon
- Craters of the Moon NM (CRMO1)
- Hells Canyon (HECA1)
- Sawtooth NF (SAWT1)
- Scoville (SCOV1)*
- Starkey (STAR1)

Lone Peak
- Lone Peak WA (LOPE1)*

Mid South
- Caney Creek (CACR1)
- Cherokee Nation (CHER1)
- Ellis (ELLI1)
- Hercules-Glades (HEGL1)
- Sikes (SIKE1)
- Upper Buffalo WA (UPBU1)
- Wichita Mountains (WIMO1)

Mogollon Plateau
- Bosque del Apache (BOAP1)
- Gila WA (GICL1)
- Hillside (HILL1)*
- Ike's Backbone (IKBA1)
- Mount Baldy (BALD1)
- Petrified Forest NP (PEFO1)
- San Andres (SAAN1)*
- Sierra Ancha (SIAN1)
- Sycamore Canyon (SYCA1)
- Tonto NM (TONT1)
- White Mountain (WHIT1)
- Okefenokee NWR (OKEF1)
- St. Marks (SAMA1)

Southern Arizona
- Chiricahua NM (CHIR1)
- Douglas (DOUG1)
- Organ Pipe (ORPI1)
- Queen Valley (QUVA1)
- Saguaro NM (SAGU1)
- Saguaro West (SAWE1)

Southern California
- Agua Tibia (AGTI1)
- Joshua Tree NP (JOSH1)
- Joshua Tree NP (JOTR1)*
- San Gabriel (SAGA1)
- San Gorgonio (SAGO5)
- San Gorgonio WA (SAGO1)

Urban QA Sites
- Atlanta (ATLA1)
- Baltimore (BALT1)
- Birmingham (BIRM1)
- Chicago (CHIC1)
- Detroit (DETR1)
- Fresno (FRES1)
- Houston (HOUS1)
- New York City (NEYO1)
- Pittsburgh (PITT1)
- Rubidoux (RUBI1)*

Virgin Islands
- Virgin Islands NP (VIIS1)

Washington D.C.
- Washington D.C. (WASH1)

West Texas
- Big Bend NP (BIBE1)
- Guadalupe Mountains NP (GUMO1)
- Salt Creek (SACR1)

NF = National Forest
NM = National Monument
NP = National Park
NWR = National Wildlife Refuge
WA = Wilderness Area
*Discontinued sites

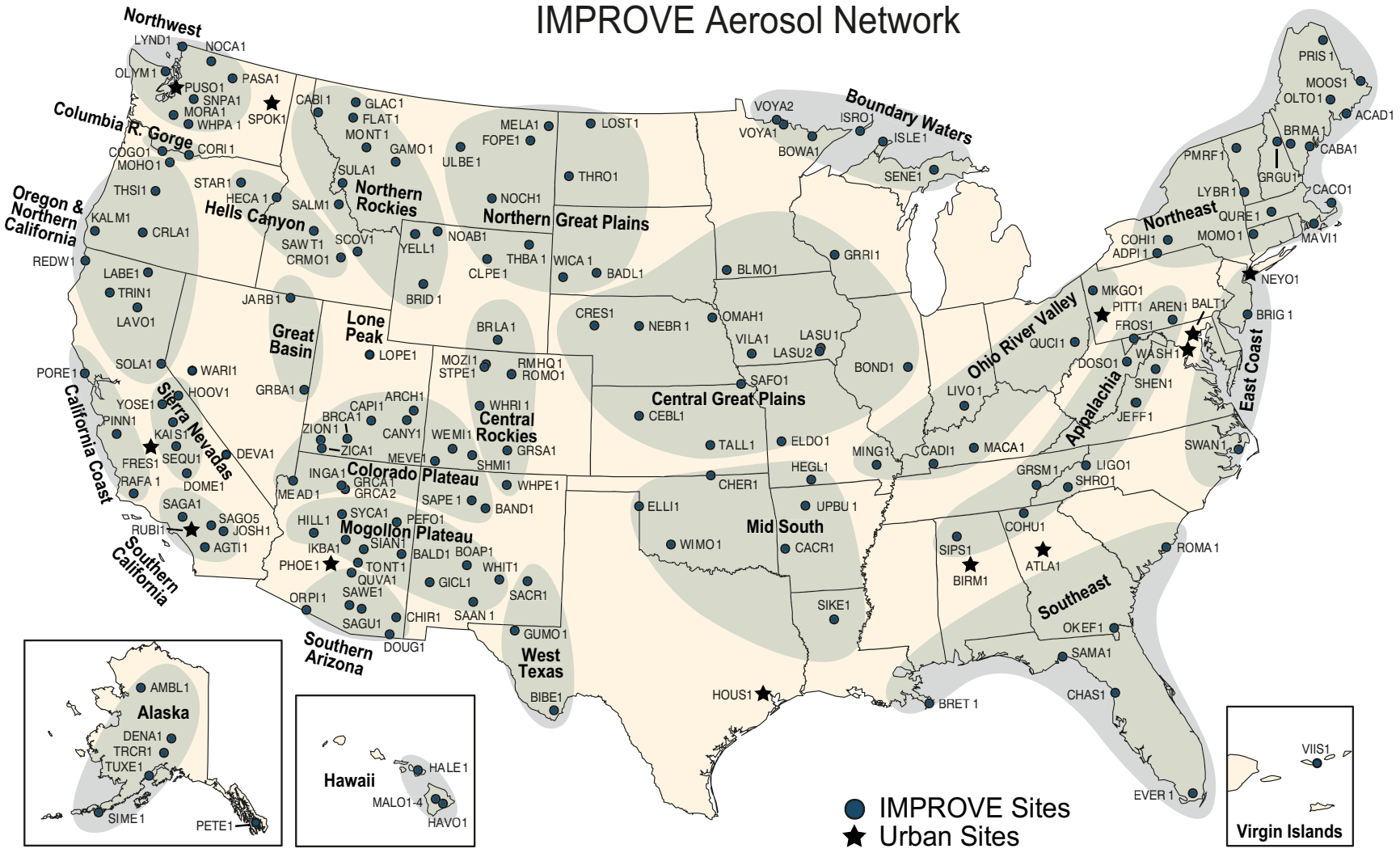

Figure S.1. The locations current and discontinued IMPROVE and IMPROVE protocol monitoring sites as of December 2004. The IMPROVE regions used for grouping the sites in some analyses in this report are indicated by green shading and bold text. Urban sites included in the IMPROVE network for quality assurance purposes are identified by stars.

S.2 SPATIAL TRENDS IN AEROSOL CONCENTRATION AND EXTINCTION

The spatial trends in $PM_{2.5}$ and b_{ext} and their constituents were examined using 2000–2004 data from the integrated IMPROVE and STN data set. PM_{10} is not measured in the STN network, so only coarse mass from the IMPROVE network was examined, and b_{ext} could only be estimated for IMPROVE sites. Appendix E assesses the comparability of data from collocated IMPROVE and STN sites to determine the appropriateness of combining the data from these two networks. It was found that on average the annual STN $PM_{2.5}$, sulfate, nitrate and organics concentrations between the STN and IMPROVE were within 2% of the IMPROVE concentrations. However, the STN fine soil and light-absorbing carbon (LAC) were respectively 30% and 10% lower than that measured by IMPROVE.

The major aerosol species are calculated by scaling measured elemental and ionic concentrations to assumed forms of particulate matter, e.g., ammonium sulfate. The particulate light extinction is calculated from these aerosol species concentrations by multiplying the concentration of a given species by its light-extinction efficiency and summing over all species. Sulfates and nitrates are hygroscopic, so their light-extinction efficiencies increase with relative humidity and are adjusted using a nonlinear relative humidity factor based on monthly averaged relative humidity at each site.

Haziness is characterized by an index with deciview (dv) units, which are related to the logarithm of the sum of the particulate b_{ext} and Rayleigh scattering. A change of 1 dv is usually perceived as a small change in haziness, regardless of the initial haze level. The spatial deciview and reconstructed b_{ext} maps are presented in Figures S.2 and S.3. Because higher b_{ext} leads to higher dv, the geographic trends in visibility (dv) are similar to the trends in reconstructed extinction. In addition, the deciview and reconstructed b_{ext} varies throughout the United States in a way analogous to fine aerosol concentrations.

The greatest particulate b_{ext} occurred in the eastern United States and in southern California, while the smallest values occurred in the nonurban West (e.g., the Great Basin and the Colorado Plateau) and in Alaska. The difference between eastern and western light extinction is even more pronounced than the difference in aerosol concentrations, because relative humidity, and therefore the light-scattering efficiency of sulfate and nitrate, is higher in the East than in the West. The smallest dv values, or best visibility, are in Alaska and a broad region including the Great Basin, most of the Colorado Plateau, and portions of the central Rockies, which have visibility impairment of less than 10 dv. Moving in any direction from this region generally results in increasing dv values. West of the Sierra Nevada and including southern California, one finds dv values greater than 14, with a maximum value of 18.9 dv at Sequoia National Park. The northwest United States and the entire eastern half of the United States have in excess of 14 dv of impaired visibility. The regions east of the Mississippi and south of the Great Lakes have impairment in excess of 20 dv. The highest annual dv was about 24, occurring in the general region of the Ohio River and Tennessee valleys.

Fine aerosols are the most effective in scattering light and are the major contributor to light extinction. Ammonium sulfate is among the most important contributors to b_{ext}. In the eastern United States, sulfate accounted for 45–60% of the reconstructed fine mass in rural locations. The contribution was smaller in the western United States and urban locations,

varying from 15% to 40% of the reconstructed fine mass. The highest ammonium sulfate concentrations were found in the Ohio River valley, where there are significant SO_2 emissions, and the Appalachian Mountains at 6–8 $\mu g/m^3$. Ammonium sulfate concentrations were less than 1 $\mu g/m^3$ in most of the western United States. The urban STN sites had similar ammonium sulfate concentrations to nearby rural sites and rarely exceed 2 times the nearby rural concentrations.

The spatial patterns in extinction and mass concentration attributed to ammonium sulfate were very similar but with steeper gradients observed in extinction (Figures S.4 and S.5). For example, the central eastern United States concentrations are about a factor of 8 larger than those in the interior western United States, but the b_{ext} values are about a factor of 12 larger.

Peak rural organic mass by carbon (OMC) concentrations and OMC b_{ext} (Figure S.6) occurred in the Northwest, in the mountains of California, and in the southeastern United States. A large band through the interior West, from the Mexico border into the upper Midwest, had low rural OMC values. The urban STN sites had high OMC concentrations and light scattering in the interior West, Northeast, and Midwest relative to nearby rural sites (Figure S.7). All of the western states with both urban and rural sites had urban concentrations at least 2 times higher than nearby rural concentrations. In the eastern United States, the urban excess was generally smaller, with the largest excess occurring in the southeastern United States and along the Atlantic seaboard. In the northwestern United States, OMC accounted for more than 50% of the reconstructed fine mass and b_{ext}.

Rural LAC concentrations were low, typically less than 0.5 $\mu g/m^3$. Urban LAC concentrations were higher than neighboring rural sites, with average concentrations about 1 $\mu g/m^3$ or greater at urban centers throughout the United States. These concentrations represent less than 8% of the reconstructed fine mass at all locations. The contribution of LAC to b_{ext} was also small, typically less than 10%.

Rural and urban ammonium nitrate concentrations and nitrate b_{ext} were high in California and the central Great Plains and Great Lakes regions of the Midwest where both NOx and ammonia emissions are high (Figures S.8 and S.9). The highest rural nitrate light scattering was in the Midwest at 20–27 Mm^{-1}. The highest urban extinction coefficients, between 60 and 90 Mm^{-1}, were in metropolitan Los Angeles and the San Joaquin Valley, California. In past IMPROVE reports and spatial analyses, the IMPROVE network did not contain Midwest monitoring sites, and the Midwest nitrate "bulge" was missing from these analyses. All urban sites had excess ammonium nitrate compared to neighboring rural sites. The largest excess occurred in California, the mountainous West, and the Great Lakes regions where it was 2–12 $\mu g/m^3$ or 12–74 Mm^{-1}.

The spatial patterns in fine soil concentrations and light scattering were quite distinct from those for ammonium sulfate, ammonium nitrate, and OMC—it is the only fine aerosol parameter to show peak values in the arid Southwest, where in rural areas it contributes to 20–45% of the reconstructed fine mass and up to 10% of the particulate b_{ext} (Figures S.10 and S.11). For most of the United States, urban soil mass concentrations were in the same concentration range as neighboring rural sites. The exceptions include Alaska, Alabama, Nebraska, and Ohio, where the urban concentrations were over 2 times those at the rural sites in the state. In urban

areas the soil concentrations accounted for less than 20% of the reconstructed fine mass, except for Puerto Rico.

The coarse mass is typically dominated by contributions from soil. However, as shown by comparing Figures S.10 and S.12, there are large differences in the spatial patterns in fine soil and coarse mass concentrations and light scattering. The coarse mass spatial patterns have a large "bulge" in the agriculturally intensive Midwest that is not seen in the fine soil. In addition, coastal sites have high coarse mass values relative to fine soil. At the rural sites, the coarse mass has its highest contributions to light scattering in the Southwest where it contributed to 20% or more of the particulate b_{ext}.

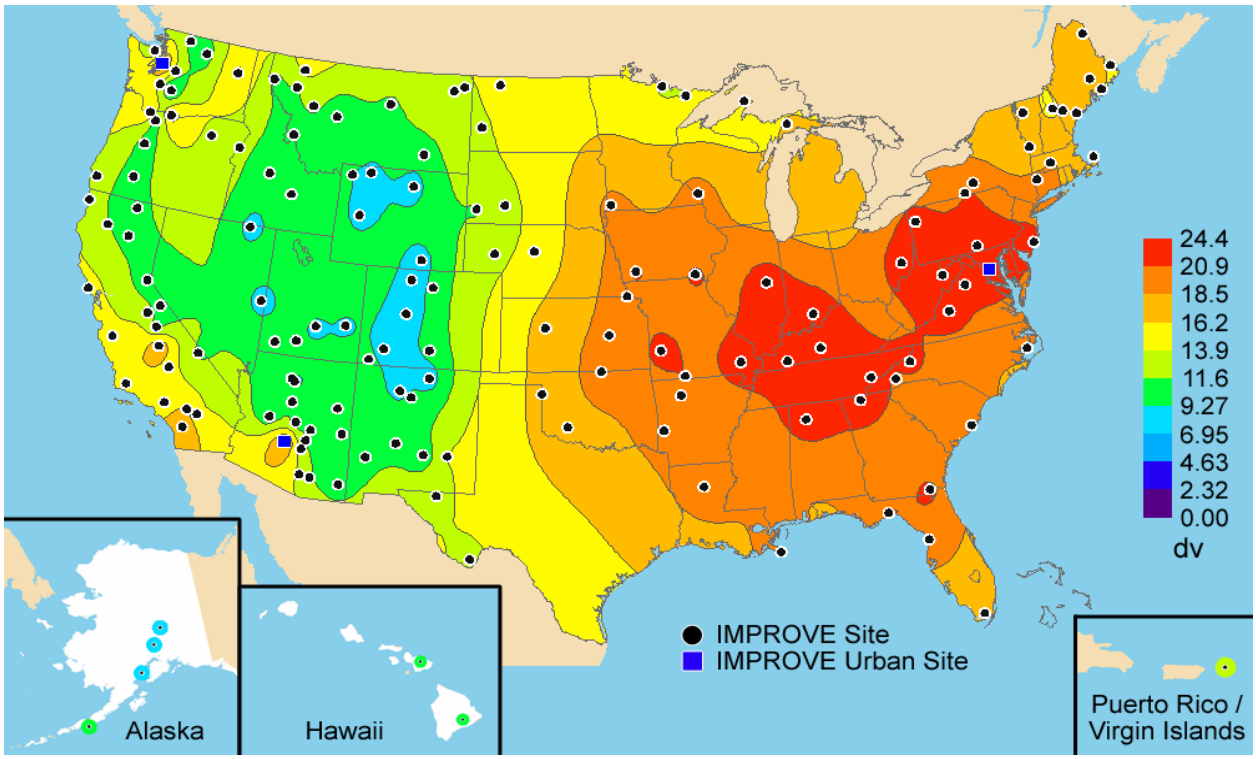

Figure S.2. Five-year average (2000–2004) deciview (DV) using only IMPROVE data.

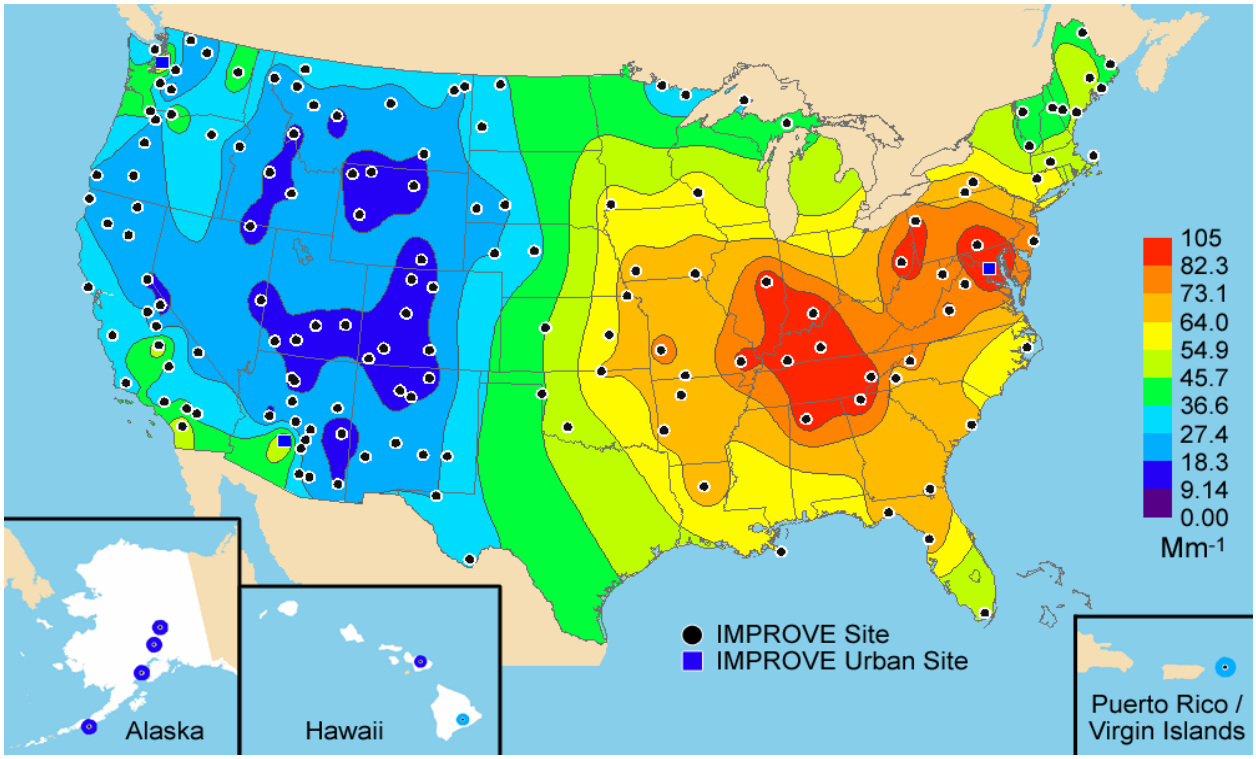

Figure S.3. Five-year average (2000–2004) reconstructed particulate light extinction using only IMPROVE data.

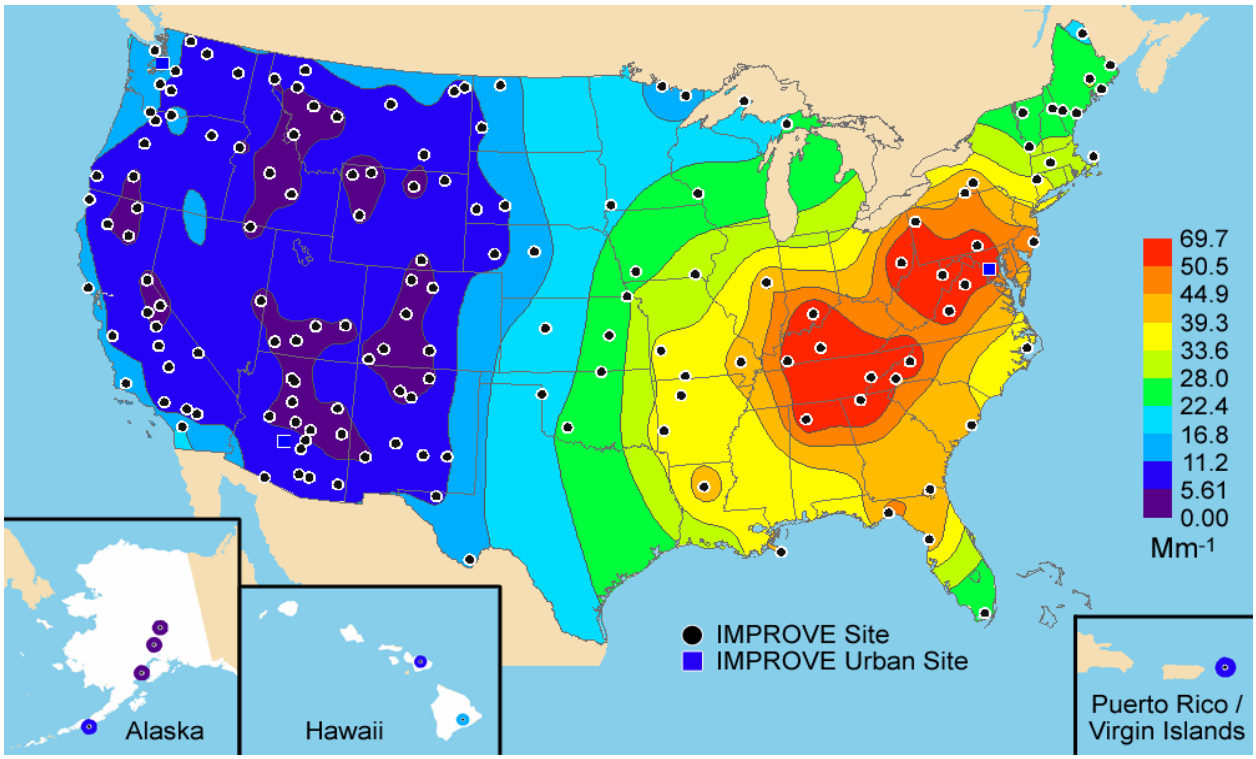

Figure S.4. Five-year average (2000–2004) sulfate light scattering using only IMPROVE data.

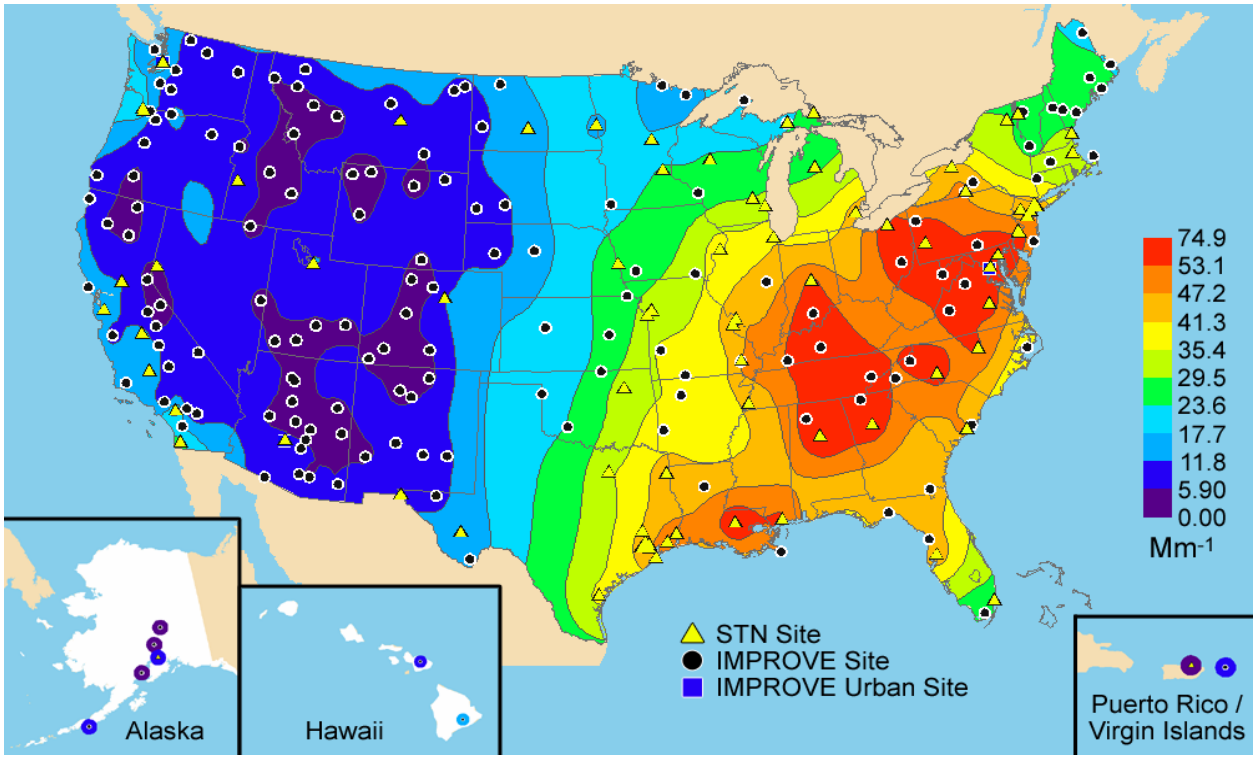

Figure S.5. Five-year average (2000–2004) sulfate light scattering using IMPROVE and STN data.

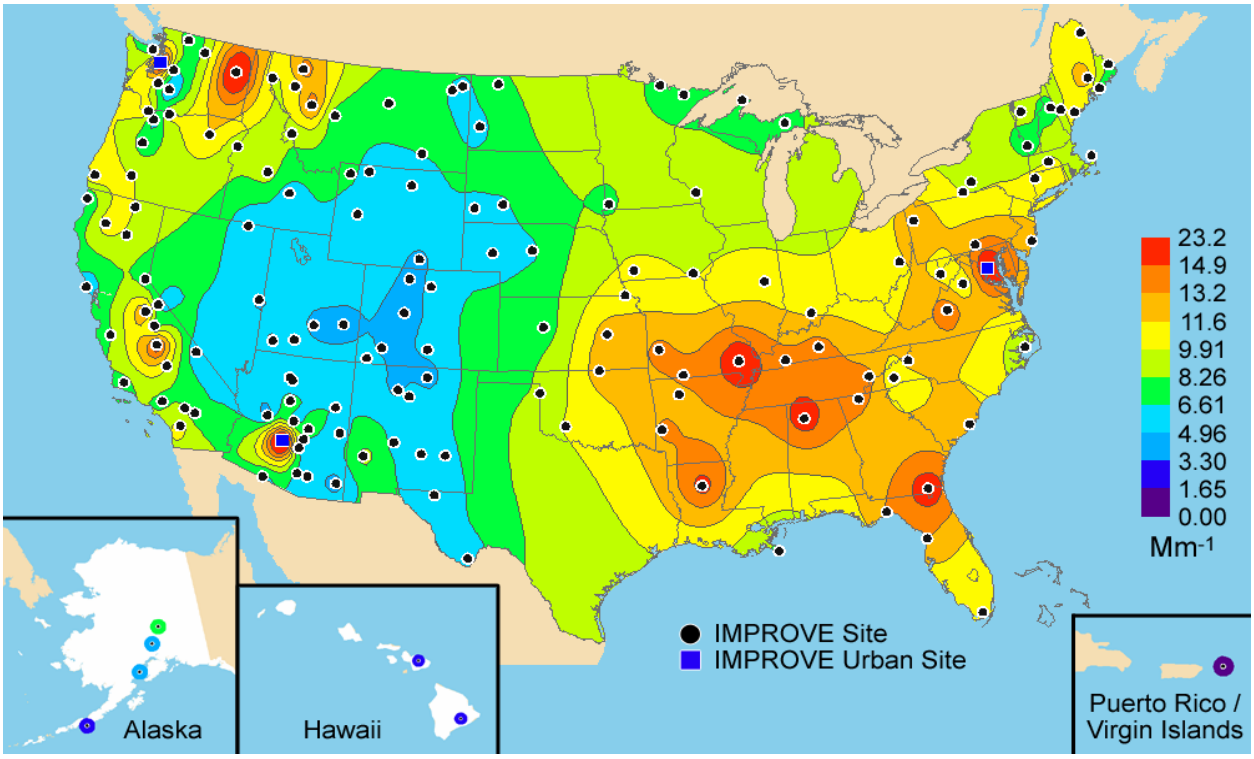

Figure S.6. Five-year average (2000–2004) organic carbon light scattering using only IMPROVE data.

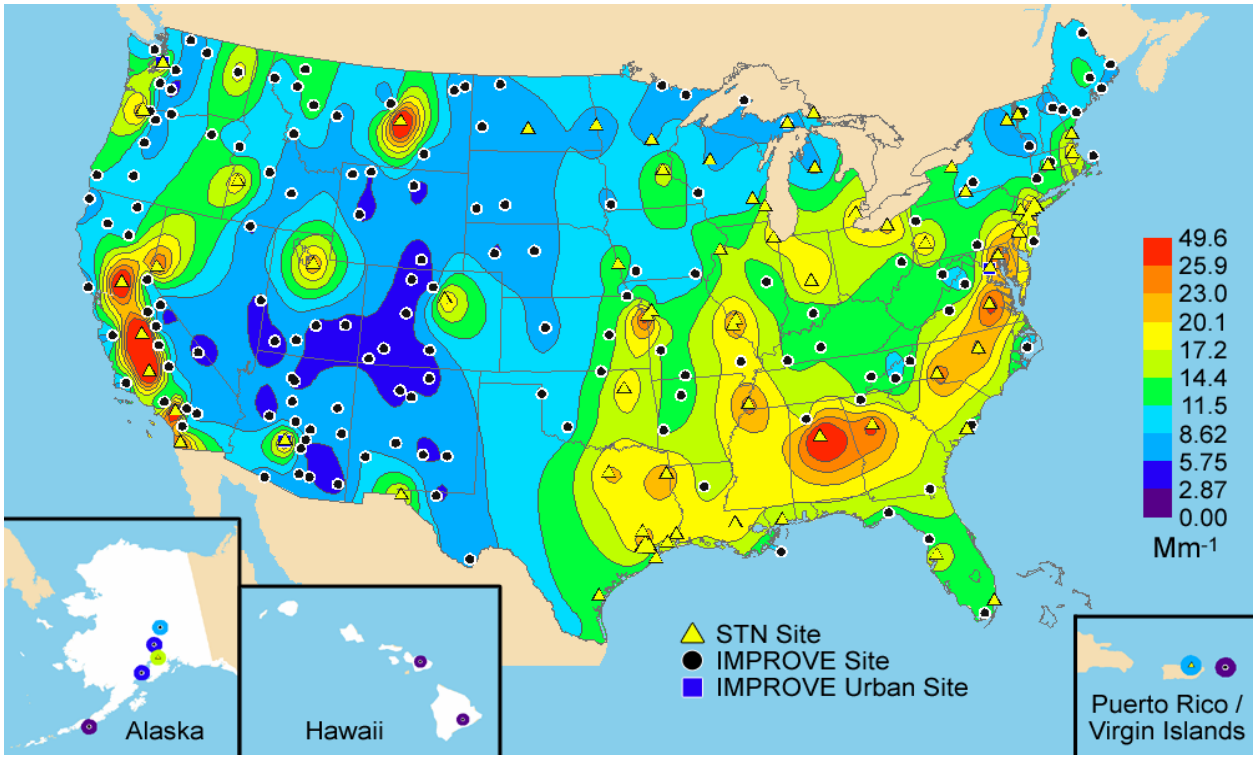

Figure S.7. Five-year average (2000–2004) organic carbon light scattering using IMPROVE and STN data.

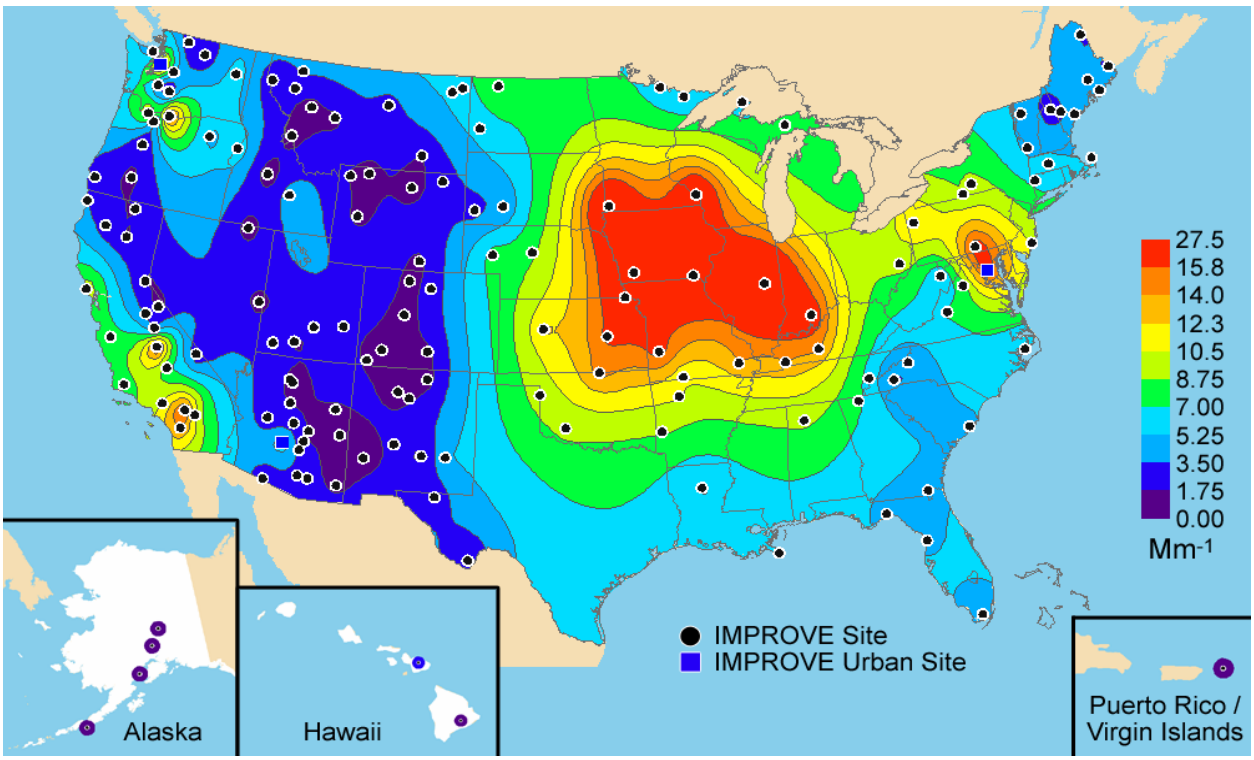

Figure S.8. Five-year average (2000–2004) ammonium nitrate light scattering using only IMPROVE data.

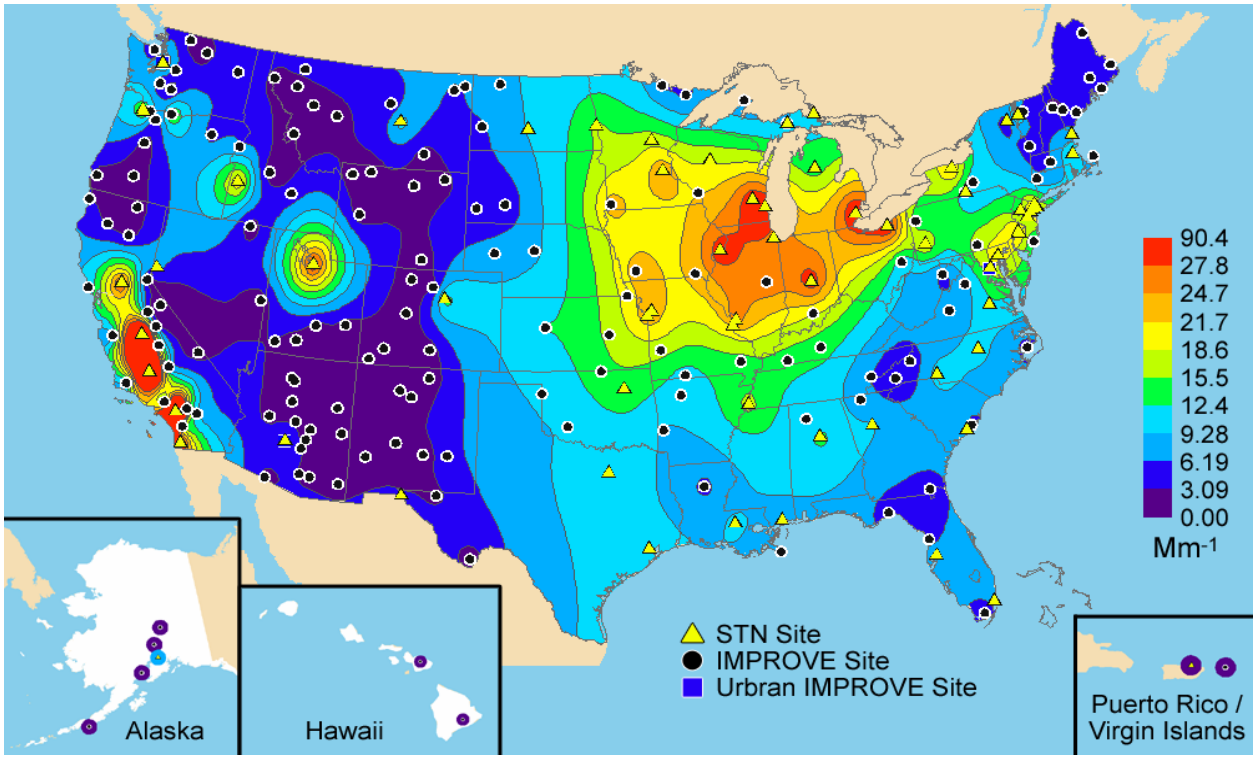

Figure S.9. Five-year average (2000–2004) ammonium nitrate light scattering using IMPROVE and STN data.

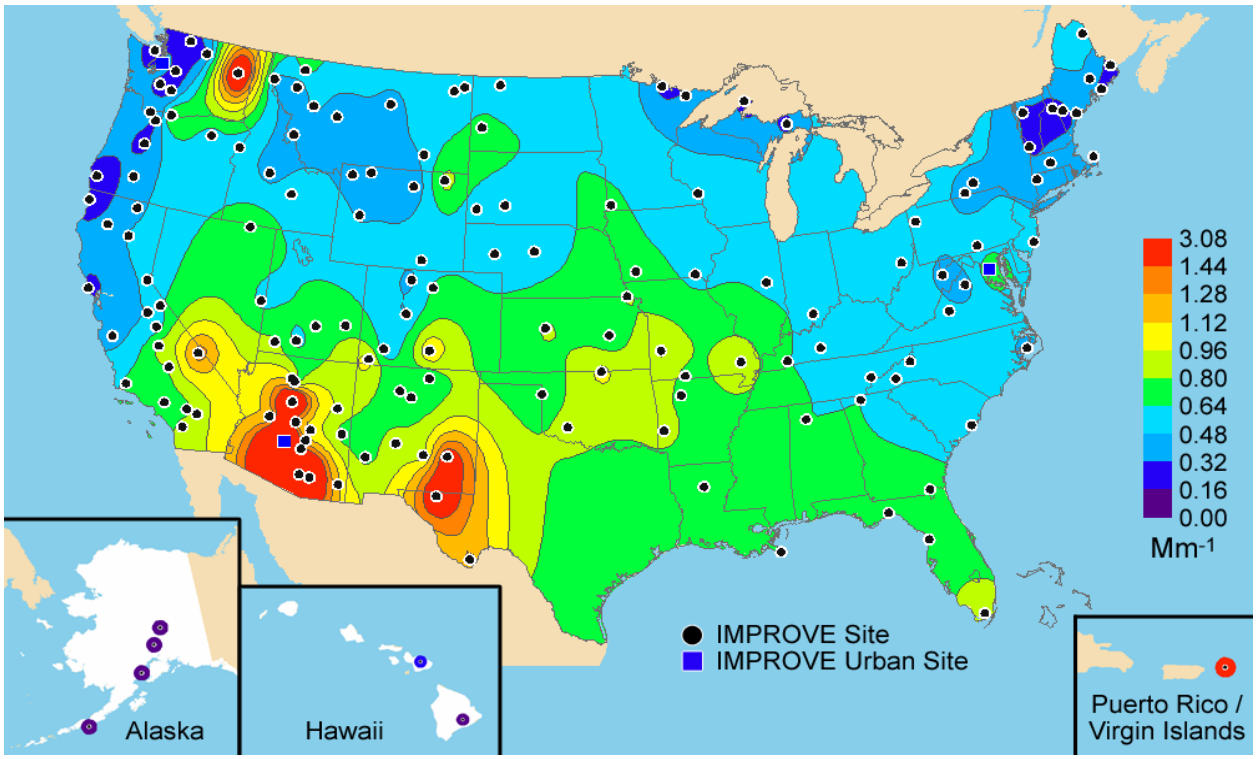

Figure S.10. Five-year average (2000–2004) fine soil light scattering using only IMPROVE data.

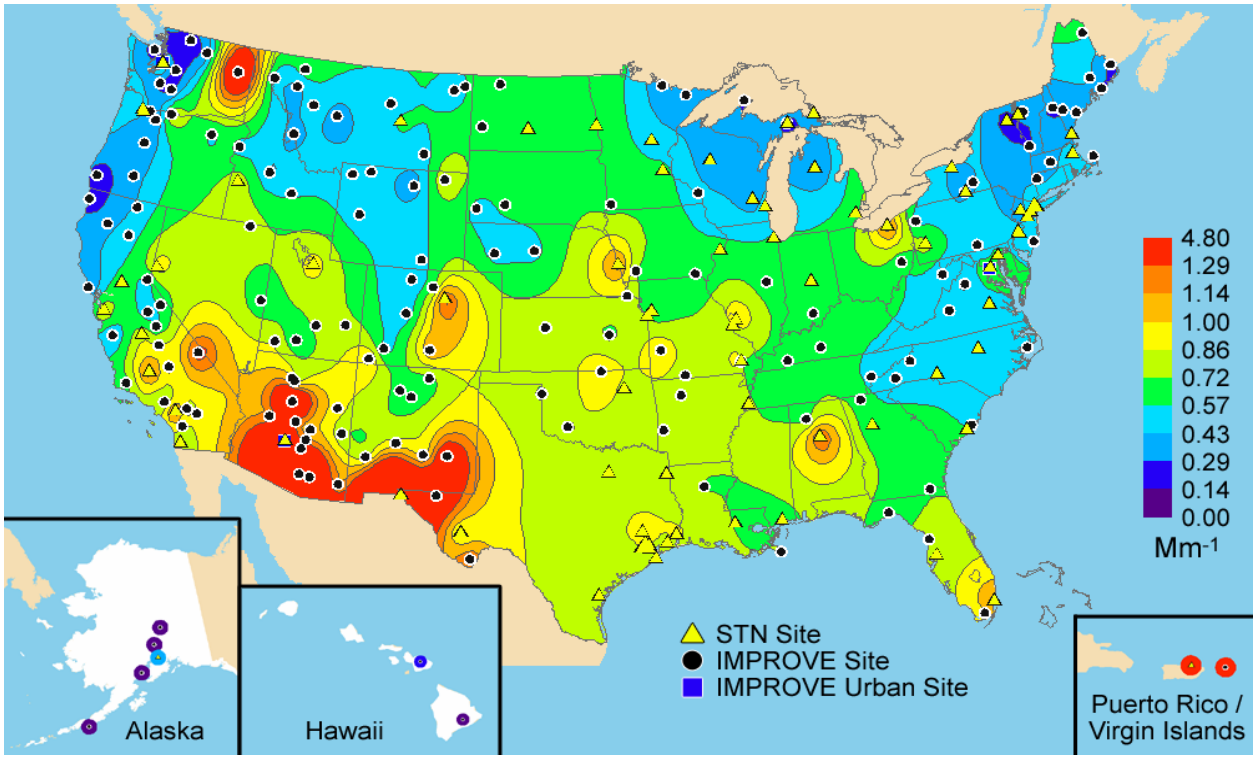

Figure S.11. Five-year average (2000–2004) fine soil light scattering using IMPROVE and STN data. Note comparisons of collocated data indicate the STN fine soil concentrations and light scattering were typically 30% smaller than from the IMPROVE monitors.

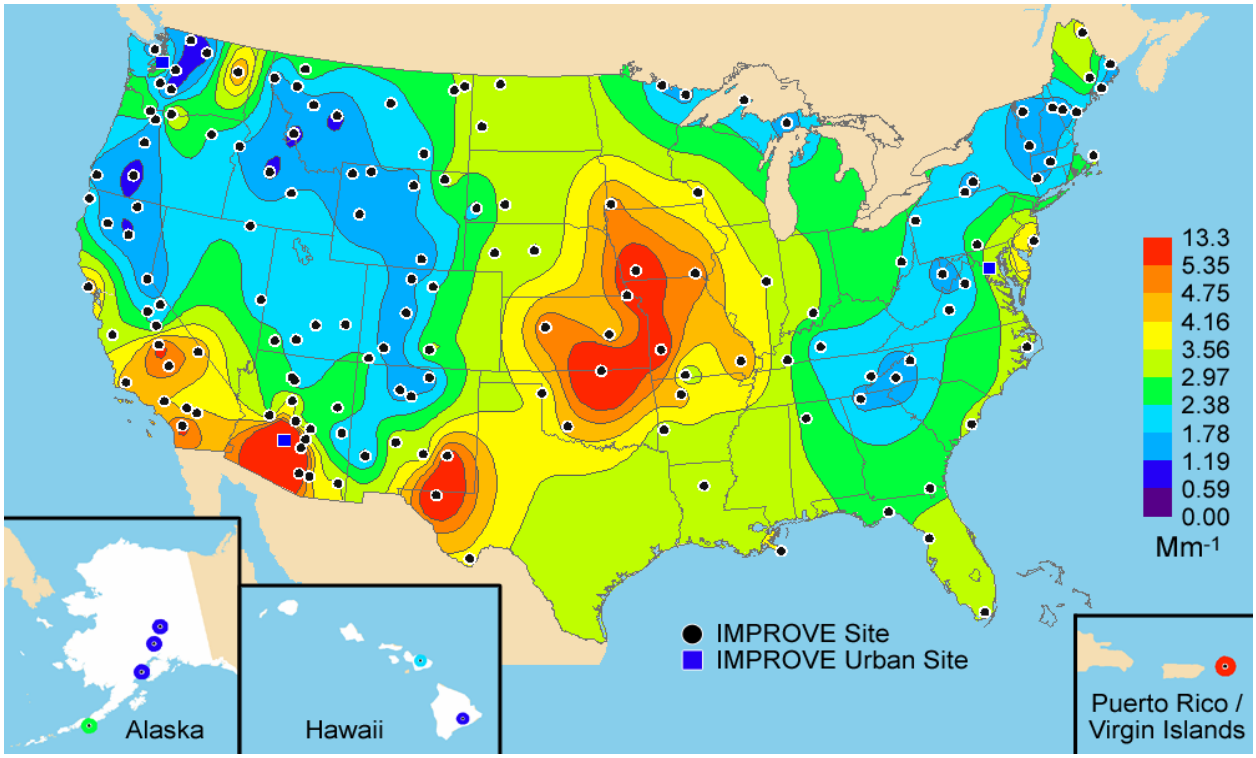

Figure S.12. Five-year average (2000–2004) coarse mass light scattering using only IMPROVE data.

S.3 SPATIAL VARIABILITY OF AVERAGE MONTHLY PATTERNS IN FINE AEROSOL SPECIES CONCENTRATIONS AND AEROSOL EXTINCTION COEFFICIENTS

The seasonal composition of the IMPROVE and STN particulate contributions to b_{ext} for various regions is summarized in Figures S.13, S.14, and S.15. Note that the STN network does not include light scattering by coarse mass. As shown in Figure S.13, in the rural eastern United States, b_{ext} peaks during the summer months, driven by the ammonium sulfate light scattering. The exception is in the central Great Plains and Boundary Waters regions where there are summer and winter peaks. The winter peaks are due to increased ammonium nitrate scattering when ammonium sulfate values are low. At the urban sites, b_{ext} has a summer and a winter peak in most regions. The summer peak is due to increased light scattering by ammonium sulfate and organics, while the winter peak is due to increased ammonium nitrate light scattering. Fine soil, coarse mass, and light absorption are small contributors to b_{ext} during all months in the eastern United States. However, at the Virgin Islands site, fine soil and coarse mass contribute about half of the b_{ext} and peak May–September.

In the rural southwestern United States (Figure S.14), the b_{ext} generally peaks in spring and summer months, when light scattering by ammonium sulfate, organics, and soil are highest. Ammonium nitrate is a small contributor to b_{ext}, except in California where the highest ammonium nitrate light scattering occurs in the colder months from November to March. In the southwestern urban regions, b_{ext} generally peaks between November and February. This b_{ext} peak is caused by increased light scattering by ammonium nitrate as well as organics. Summer peaks in organics also occurred at Denver, Colorado, and in western Nevada. Los Angeles is unique in that b_{ext} peaks during the summer months due to increased light scattering by ammonium sulfate.

In the rural northwestern United States (Figure S.15), the seasonality of b_{ext} is varied. In Alaska and the northern Rockies and northern California/Oregon regions, there are pronounced summer peaks due primarily to increased light scattering from organics compared to winter months. The Northwest region also has a summer peak in b_{ext} due to similar increases in light scattering from organics and ammonium sulfate. The Columbia River Gorge and Hells Canyon regions have winter b_{ext} peaks due to increased ammonium nitrate light scattering. The Hells Canyon region also has a summer b_{ext} peak when light scattering by organics is largest. The b_{ext} in all of the northwestern urban regions peaks in the cold months. Similar to the eastern and southwestern United States, the cold month peaks in b_{ext} were partially due to increased light scattering by ammonium nitrate, as well as increased light scattering by organics at a number of the urban regions. The northwestern urban ammonium sulfate light scattering is unique in that it does not peak in the summer months, and in Boise, Idaho, and Missoula, Montana, ammonium sulfate light scattering actually peaks in the cold months.

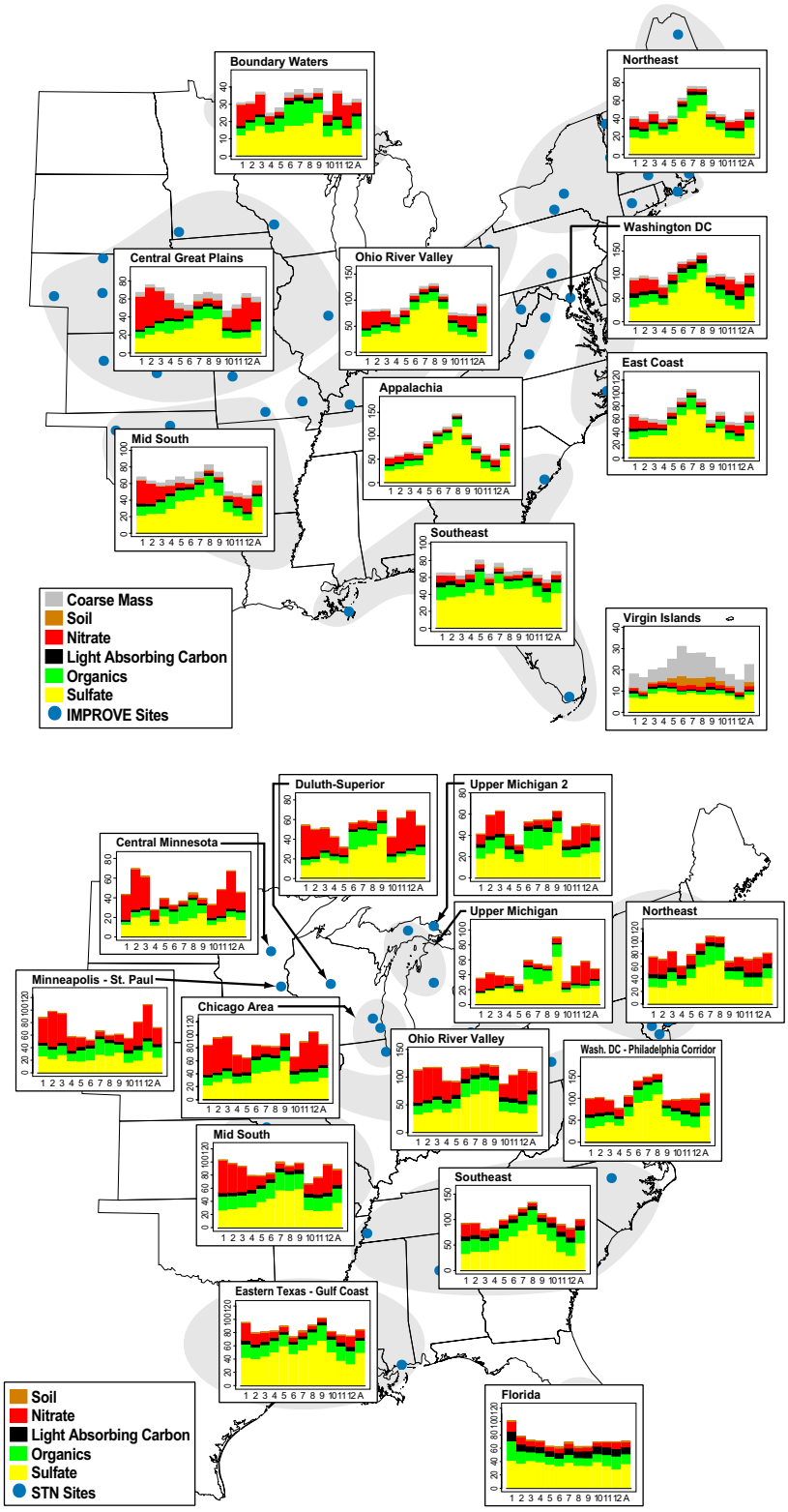

Figure S.13. Monthly particulate contributions to reconstructed b_{ext} (Mm^{-1}) for regions in the eastern United States using IMPROVE data (top) and STN data (bottom). Note, STN does not measure coarse mass.

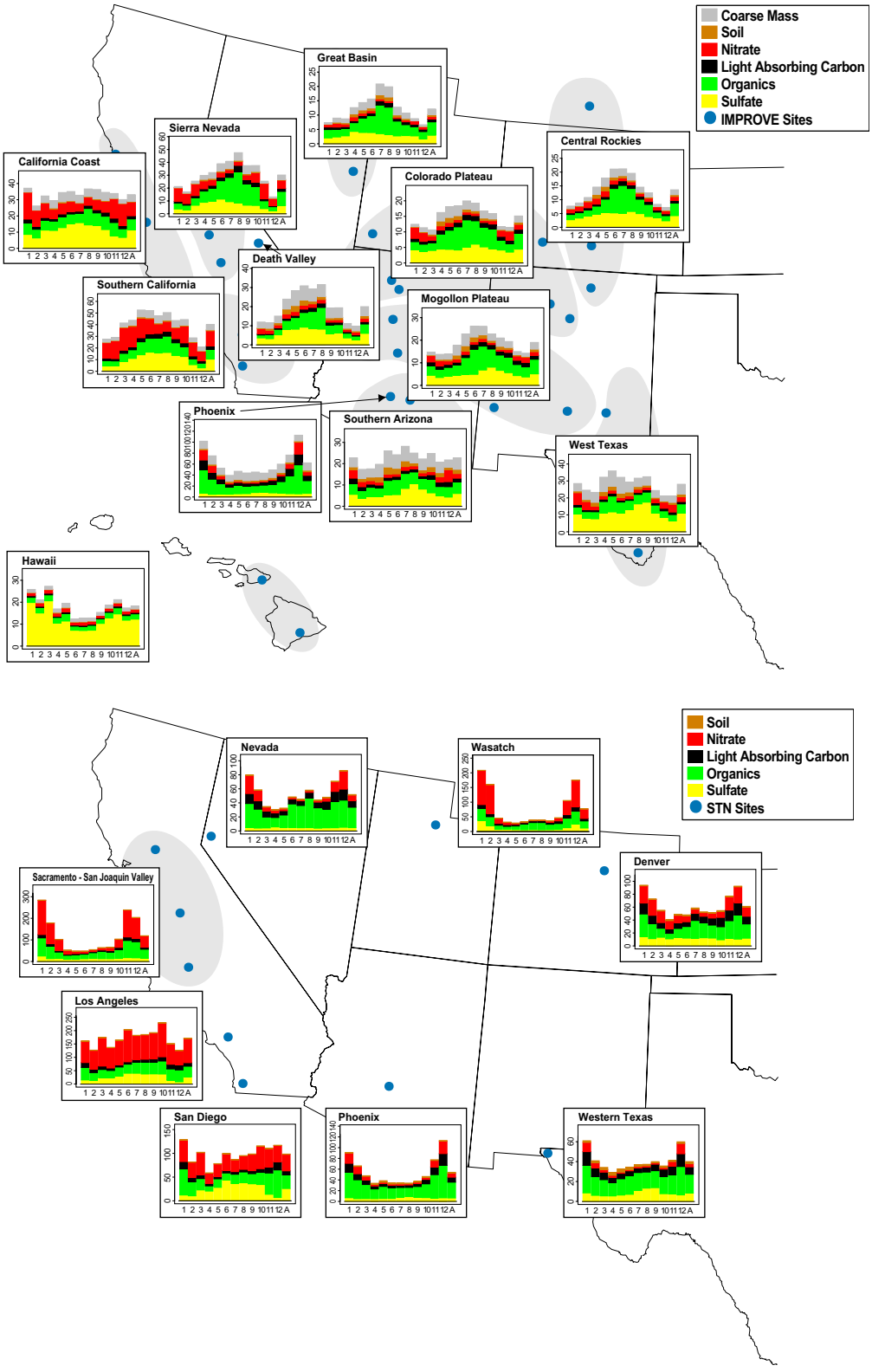

Figure S.14. Monthly particulate contributions to reconstructed b_{ext} (Mm^{-1}) for regions in the southwestern United States using IMPROVE data (top) and STN data (bottom). Note, STN does not measure coarse mass.

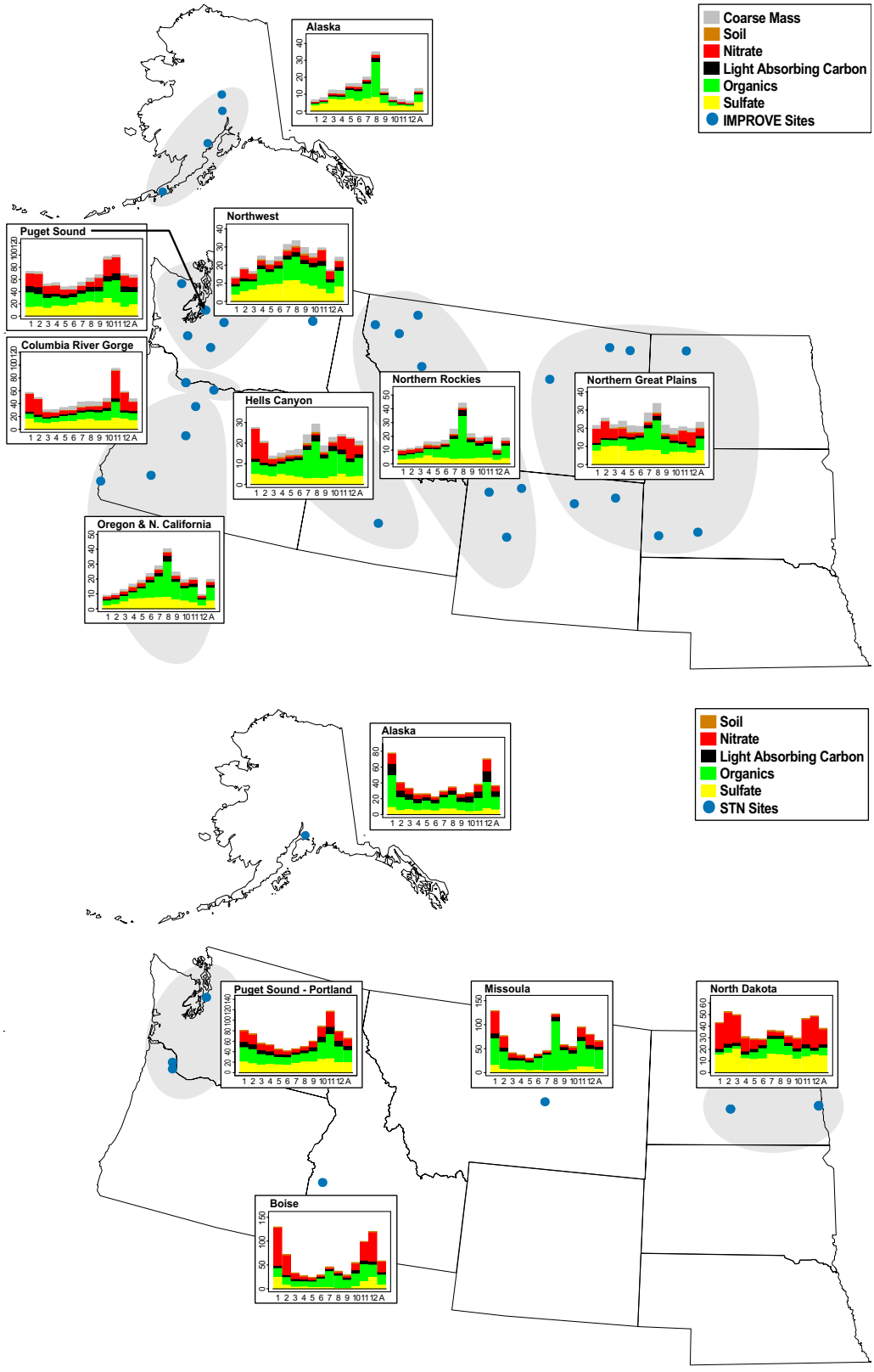

Figure S.15. Monthly particulate contributions to reconstructed b_{ext} (Mm^{-1}) for regions in the northwestern United States using IMPROVE data (top) and STN data (bottom). Note, STN does not measure coarse mass.

S.4 TEMPORAL TRENDS IN FINE AEROSOL SPECIES CONCENTRATIONS AND AEROSOL EXTINCTION

The results of several studies investigating monotonic trends in fine aerosol species concentrations are summarized in this report. Discussions are included on the following topics: the uncertainty in sulfate concentration trends [White et al., 2005], the 10-year spatial and temporal trends in sulfate concentrations and SO_2 emissions [Malm et al., 2002], 10-year trends in visibility [NPS, 2006], >7-year trends in organic and elemental carbon (OC and EC) [Schichtel et al., 2004], and the Visibility Information Exchange Web System (VIEWS) annual summary trends tools.

The effects of sampling and analytical error on time trends derived from routine monitoring were examined in White et al. [2005]. The analysis was based on actual concentration differences observed among three long sulfate series recorded by collocated and independent measurements at Shenandoah National Park. Five-year sulfate trends at this location were shown to include a 1-sigma uncertainty of about 1%/year from measurement error alone. This is significantly more than would be estimated under naive statistical assumptions from the demonstrated precision of the measurements. The excess uncertainty arises from subtle trends in the errors themselves.

Legislative and regulatory mandates have resulted in reduced sulfur dioxide (SO_2) emissions in both the eastern and western United States, with anticipation that concurrent levels of ambient SO_2, SO_4^{2-}, and rainwater acidity would decrease. Spatial and temporal trends in ambient SO_4^{2-} concentrations from 1988 to 1999, SO_2 emissions from 1990 to 1999, and the relationship between these two variables were examined in Malm et al. [2002]. The SO_4^{2-} concentration data came from combining data from IMPROVE and the Clean Air Status and Trends Network (CASTNet). In the East, the largest SO_4^{2-}decreases in the 80th percentile concentrations occurred north of the Ohio River valley, while most monitoring sites south of Kentucky and Virginia showed increasing and decreasing trends that were not statistically significant. Big Bend National Park, Texas, Cranberry, North Carolina, and Lassen Volcanic National Park, California, are the only areas that show a statistically significant increase in SO_4^{2-} mass concentrations. The 1990–1999 annual 80th percentile SO_4^{2-} time series were compared to the annual SO_2 emissions over four broad United States regions. Each region had a unique time series pattern, with the SO_4^{2-} concentrations and SO_2 emissions closely tracking each other over the 10-year period. Both the SO_4^{2-} and SO_2 emissions decreased in the Northeast (28%) and the West (15%), while there was little change in the Southeast and a 15% increase over Texas, New Mexico, and Colorado.

Trends in the haze index, measured in deciviews, were examined for the 10-year period 1995–2004 by the National Park Service (http://www2.nature.nps.gov/air/Pubs/pdf/gpra/Gpra2005_Report_03202006_Final.pdf). Trends in the annual average 20% best and worst days were examined using the Theil regression method for the IMPROVE sites with at least 6 complete years out of the 10-year period. Visibility was stable (insignificant trends) or improving at all IMPROVE sites at the 0.05 significance level. Acadia, Moosehorn, Lye Brook, Dolly Sods, and Shenandoah showed statistically significant improving visibility trends for the clearest days at eastern national park monitoring sites. Great Smoky Mountains, Okefenokee, Mammoth Cave, and Washington, D.C., also had improving

trends on the haziest visibility days. Statistically significant improving trends for the clearest visibility days were observed at 17 sites in the western United States including Alaska. Mount Rainier also had an improving trend on the haziest visibility days. No site included in the analysis had a significant worsening trend on either the clearest or haziest visibility days.

Theil regression was used to examine trends in winter and summer elemental and organic carbon at the 54 sites with 7 or more years of data in Schichtel et al. [2004]. Winter EC concentrations decreased significantly at most monitoring sites in the Pacific coastal states and throughout the eastern United States, with median EC concentrations decreasing from 50% to 75% over a 10-year time period. Winter OC concentrations from Washington State to northern California showed similar significant decreases, but Acadia, Maine, was the only monitoring site in the eastern United States with a significant downward trend. Unlike EC, wintertime OC increased at a number of monitoring sites in the southeastern United States, though not significantly. Most sites in the Intermountain West did not show significant winter trends in either EC or OC.

VIEWS is a web-based system that presents data and tools to summarize and display data to aid those who are implementing the Regional Haze Rule enacted in 1999 by the EPA to reduce regional haze and improve visibility in national parks and wilderness areas. As part of this effort, a long-term temporal trends tool was developed that allows a user to quickly create and browse trends of aerosol concentrations and their contribution to light extinction over any monitoring site's sampling period. Various temporal aggregation and smoothing options are available, including the Regional Haze Rule metrics for tracking trends in haze. In addition, a Theil regression analysis can be conducted on each temporal trend.

S.5 IMPROVE DATA QUALITY ASSURANCE

The IMPROVE program's quality assurance system, data validation procedures, and results from a collection of nitrate data quality studies are described in Chapter 5. The first section provides an overview of the IMPROVE network's quality assurance system and the data validation procedures conducted by CIRA (the Cooperative Institute for Research in the Atmosphere). Section 5.2 summarizes the results from a historical data validation review of IMPROVE data collected from 1988 through 2003. Section 5.3 summarizes the results from several studies designed to investigate potential data quality issues related to IMPROVE's nitrate measurements.

S.6 SPECIAL STUDIES ASSOCIATED WITH THE IMPROVE PROGRAM

The results of four special studies conducted in association with the IMPROVE program since the 2000 IMPROVE report are summarized. The Big Bend Regional Aerosol and Visibility Observational (BRAVO) study is summarized in section 6.1. Big Bend National Park is located in southwestern Texas along the Mexican-Texas border. During the 1990s, the haze at Big Bend and other sites in west Texas and southern New Mexico increased, further obscuring Big Bend's and nearby regions' scenic beauty. In response to the increased haze, the BRAVO study was conducted. This was an intensive monitoring study sampling aerosol physical, chemical, and optical properties, as well atmospheric dispersion using synthetic tracers from July through October 1999. The monitoring was followed by a multiyear assessment of the causes of

haze in Big Bend National Park, Texas, with the primary purpose to identify the source regions and source types responsible for the haze at Big Bend.

The Yosemite Aerosol Characterization Study (YACS) is summarized in section 6.2. YACS was an intensive field measurement campaign conducted by a number of U.S. research groups from 15 July to 4 September 2002 at Yosemite National Park, California. The objectives of the study were to determine appropriate values for converting analyzed aerosol carbon mass to ambient aerosol organic carbon mass; develop an improved understanding of the visibility-impairment-related characteristics of a smoke/organic carbon-dominated aerosol, including the role of relative humidity in modifying visibility impairment; and examine the sources contributing to high aerosol organic carbon mass concentrations.

The findings from the review of the IMPROVE equation for estimating ambient light extinction coefficients are summarized in section 6.3. Compliance under the Regional Haze Rule is based on IMPROVE protocols for reconstructing aerosol $PM_{2.5}$ mass concentrations and light extinction coefficients (b_{ext}) from speciated mass concentrations. Hand and Malm (http://vista.cira.colostate.edu/improve/Publications/GrayLit/016_IMPROVEeqReview/IMPROVEeqReview.htm) recently reviewed the assumptions and some associated uncertainties inherent in the IMPROVE formulation for reconstructing light extinction. Refinements were suggested when data exist to support modifications to the assumptions used to derive the IMPROVE equation. However, refinements of several of the assumptions are not possible at this time because existing data do not warrant them or because further measurements are required. The suggested refinements of the IMPROVE equation include

- changing the R_{oc} factor used to compute particulate organic matter from 1.4 to 1.8;
- modifying the f(RH) scattering enhancement curve to reflect some water associated with particles below a relative humidity of 40%;
- including sea salt in reconstructed mass and extinction equations;
- modifying values of dry mass scattering efficiencies to reflect current data and functional relationships between mass scattering efficiency and mass concentration;
- site-specific Rayleigh scattering based on elevation and the annual average temperature of a monitoring site;
- the addition of a NO_2 light absorption term used at sites with available data.

The results of a coarse mass speciation study are included in section 6.4. To more fully investigate the composition of coarse particles, a program of coarse particle sampling and speciation analysis at nine of the IMPROVE sites was initiated 19 March 2003 and operated through the year 2004. The study was motivated by a few short-term special studies at national parks and showed that coarse mass (2.5–10 μm) is not limited to only crustal minerals but can also consist of a substantial amount (≈ 40–50%) of carbonaceous material and inorganic salts such as calcium nitrate and sodium nitrate. Crustal minerals (soil) were the single largest contributor to coarse mass (CM) at all but one monitoring location. The average fractional contributions ranged from a high of 76% at Grand Canyon National Park to a low of 34% at Mount Rainier National Park. The second largest contributor to CM was organic mass, which on an average annual fractional basis was highest at Mount Rainier at 59%. At Great Smoky

Mountains National Park, organic mass contributed 40% on average, while at four sites organic mass concentrations contributed between 20% and 30% of the CM. Nitrates were on average the third largest contributor to CM concentrations. The highest fractional contributions of nitrates to CM were at Brigantine National Wildlife Refuge, Great Smoky Mountains National Park, and San Gorgonio wilderness area at 10–12%. Sulfates contributed less than about 5% at all sites.

REFERENCES

Malm, W. C., B. A. Schichtel, R. B. Ames, and K. A.Gebhart (2002), A 10-year spatial and temporal trend of sulfate across the United States, *J. Geophys. Res.*, *107*.

National Park Service (2006), 2005 Annual performance & progress report: Air quality in national parks, available at http://www2.nature.nps.gov/air/Pubs/pdf/gpra/Gpra2005_Report_03202006_Final.pdf.

Schichtel, B. A., W. C. Malm, and W. H. White (2004), Organic and elemental carbon long-term trends and spatial patterns in rural United States, presented at the Regional and Global Perspectives on Haze: Causes, Consequences and Controversies-Visibility Specialty Conference, Air & Waste Management Association, Asheville, NC, October 25-29.

White, W. H., L. L. Ashbaugh, N. P. Hyslop, and C. E. Mcdade (2005), Estimating measurement uncertainty in an ambient sulfate trend, *Atmos. Environ., 39*, 6857-6867.

CHAPTER 1: IMPROVE NETWORK – PURPOSE, DESIGN, AND HISTORY

INTRODUCTION: REPORT OBJECTIVES

This report is the fourth in a series of periodic reports that describe the data collected by the Interagency Monitoring of Protected Visual Environments (IMPROVE) monitoring network. The objectives of this report were to

1. describe the spatial and seasonal variation of aerosol species contributing to visibility impairment from January 2000 through December 2004 for the combined data set from the IMPROVE network and the Environmental Protection Agency's (EPA) Speciation Trends Network (STN);
2. provide a first estimate of the apportionment of visibility impairment to these chemical species;
3. document long-term trends (7–16 years) of various aerosol species and visibility;
4. review a number of special studies that were designed to examine the robustness of algorithms used to make extinction estimates from aerosol mass concentrations;
5. and evaluate and qualify certain uncertainties in the IMPROVE measurements and examine the intercomparability of the data from IMPROVE and the STN.

1.1 OBJECTIVES OF VISIBILITY MONITORING UNDER THE IMPROVE PROGRAM

The Regional Haze Rule [U.S. EPA, 1999] requires monitoring representative of each of the 156 visibility-protected federal Class I areas (CIAs), as shown in Figure 1.1. The monitoring is conducted in order to track progress toward the goal of returning visibility in our national parks and wilderness areas (CIAs) to natural visibility conditions. Required monitoring under the Regional Haze Rule began in 2000. The deciview index, calculated from speciated ambient particle concentrations, was selected to track haze levels. This entails sampling and analysis of the major aerosol components using methods patterned after those utilized since 1987 by the IMPROVE network [Joseph et al., 1987; Sisler, 1996] and consistent with the aerosol monitoring portion of the 1999 Visibility Monitoring Guidance document issued by the EPA [U.S. EPA, 1999].

The IMPROVE program is a cooperative measurement effort designed to

1. establish current visibility and aerosol conditions in mandatory CIAs;
2. identify chemical species and emission sources responsible for existing man-made visibility impairment;
3. document long-term trends for assessing progress towards the national visibility goal;
4. and, with the enactment of the Regional Haze Rule, provide regional haze monitoring representing all visibility-protected federal CIAs where practical.

The program is managed by the IMPROVE steering committee that consists of representatives from the U.S. EPA; the four federal land managers (FLMs)—the National Park Service, U.S. Forest Service, Fish and Wildlife Service, and Bureau of Land Management; the National Oceanic and Atmospheric Administration; four organizations representing state air quality organizations—the State and Territorial Air Pollution Program Administrators/Association of Local Air Pollution Control Officials (STAPA/ALAPCO), Western Regional Air Partnership (WRAP), Northeast States for Coordinated Air Use Management (NESCAUM), and Mid-Atlantic Regional Air Management Association (MARAMA); and an associate member, the State of Arizona Department of Environmental Quality.

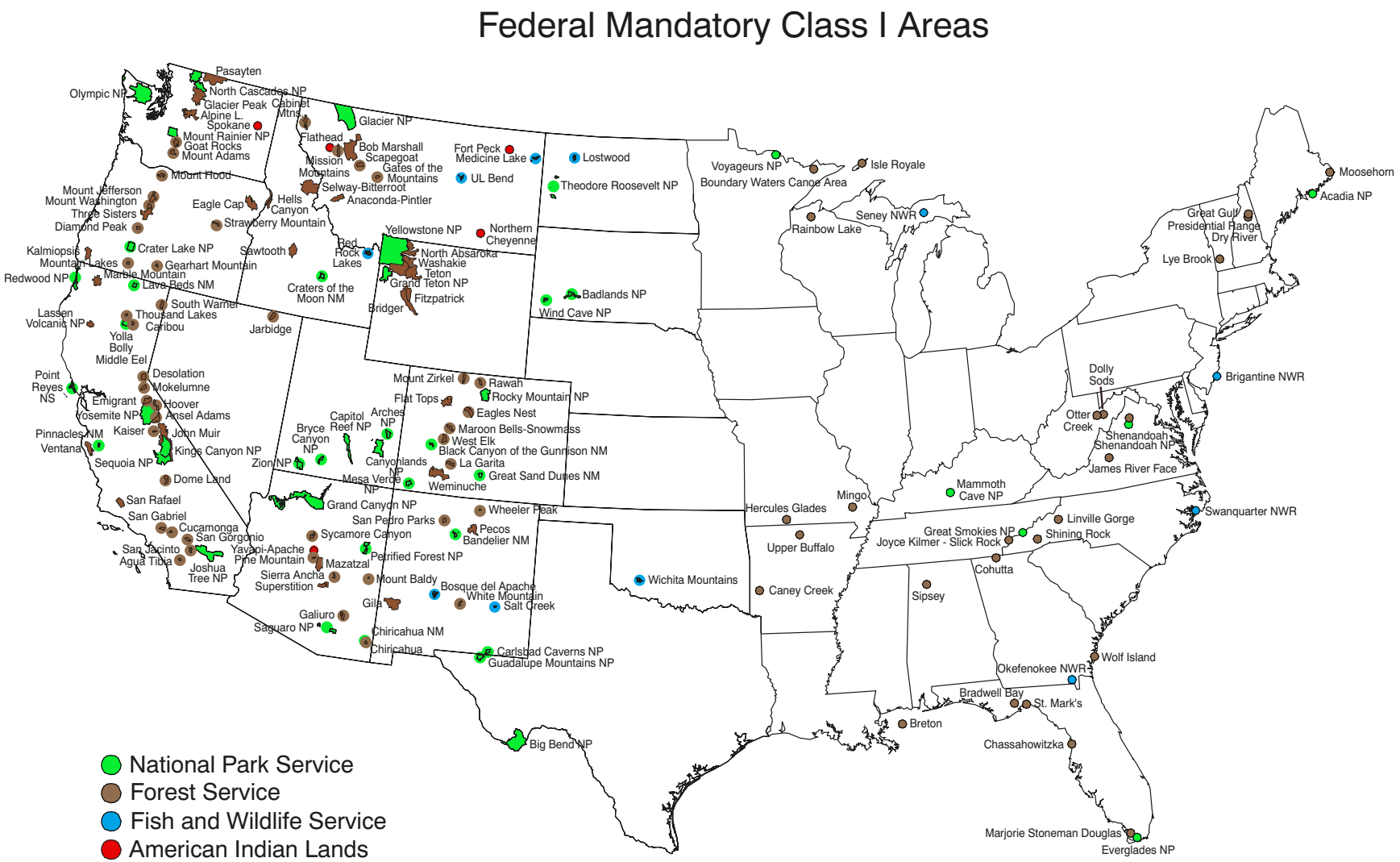

Figure 1.1. All Class I areas of the contiguous United States are identified on the map. The color coding identifies the managing agency of each Class I area.

1.2 OVERVIEW OF THE IMPROVE MONITORING NETWORK

1.2.1 Current and Historical Sampler Siting

The IMPROVE network initially consisted of 30 monitoring sites in CIAs, 20 of which began operation in 1987, with the others starting in the early 1990s (Table 1.1). An additional approximately 40 sites, most in remote areas, that used the same instrumentation and monitoring and analysis protocols (called IMPROVE protocol sites) began operation prior to 2000 and were operated individually by federal or state organizations. Adjustments to the number of monitoring sites in the network or the suite of measurements collected at an individual site have happened on several occasions, due in some cases to scientific considerations and in others to resource and funding limitations. Many of the sites also included optical monitoring with a nephelometer, a transmissometer, and/or color photography to document scenic appearance. The optical monitoring sites are detailed below in section 1.2.3.

Beginning in 1998, the EPA began providing supplemental support to IMPROVE to expand the network in order to provide the representative speciated particle monitoring required under the Regional Haze Rule for each of the 156 mandatory federal CIAs (Figure 1.1, Table 1.2) where it is practical to do so. The expansion was not as straightforward as installing a new monitoring site within the boundaries of each of the 156 CIAs that did not already have an IMPROVE site. For one thing, many CIAs are designated national wilderness areas, for which the Wilderness Act restricts the siting of man-made items, including environmental monitoring equipment [The Wilderness Act, 1964]. Additionally, even for CIAs where monitoring is allowed (e.g., national parks), practical requirements such as power, security, and access occasionally make it difficult to find a suitable monitoring site within the CIA boundary.

Since regional haze impacts are by definition those that are distributed over a broad geographic region, a representative monitoring site does not necessarily need to be located in the CIA being represented. The practical significance of this concept is that it is possible for a site to 1) be located outside of the CIA boundaries and 2) represent more than one CIA when they are located within the same regional haze region. A clustering process, designed to limit the number of sites necessary for tracking progress under the Regional Haze Rule, identified 110 CIA clusters that require monitoring [Malm et al., 2000]. Locations for the necessary monitoring sites were chosen through a selection process detailed in Malm et al. [2000] that included reviewing the locations of existing IMPROVE sites, horizontal distance from the CIA, site elevation, and local pollution sources. The selection process was completed by the end of 1999 and installations began shortly after. At the time of this report, the network has been expanded to 167 sites, including a representative site for each of these 110 clusters and additionally to fill in the spatial gaps where CIAs are sparse or absent. These monitoring sites provide data that aid in understanding spatial patterns and are often installed to assist the sponsoring agency, such as a state, tribe, or the EPA, in meeting planning or quality assurance responsibilities.

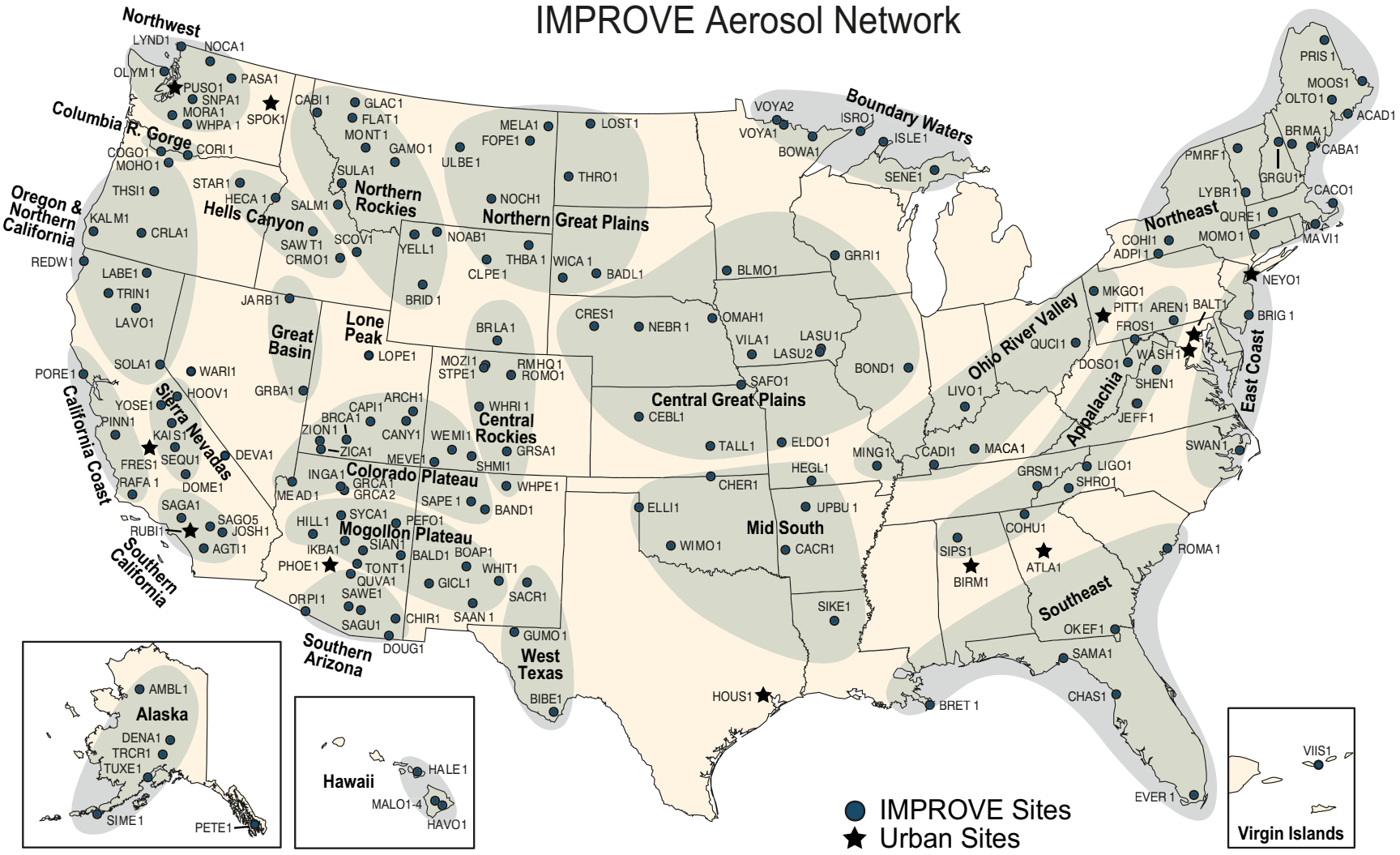

Figure 1.2. The locations of IMPROVE and IMPROVE protocol sites are shown for all discontinued and current sites as of December 2004. The IMPROVE regions used for grouping the sites in some analyses in this report are indicated by green shading and bold text. Urban sites included in the IMPROVE network for quality assurance purposes are identified by stars.

Table 1.1. Discontinued and current IMPROVE particulate monitoring sites. The site groupings are displayed in Figure 1.2.

IMPROVE Site Group	Site Name	Site Code	State	Latitude	Longitude	Elevation (m)	Dates of Operation
Alaska	Ambler	AMBL1	AK	67.099	-157.863	78	07/2004-08/2005
	Denali NP	DENA1	AK	63.723	-148.968	658	03/1988-present
	Petersburg	PETE1	AK	56.611	-132.812	0	07/2004-present
	Simeonof	SIME1	AK	55.325	-160.506	57	09/2001-present
	Trapper Creek	TRCR1	AK	62.315	-150.316	155	09/2001-present
	Tuxedni	TUXE1	AK	59.992	-152.666	15	12/2001-present
Appalachia	Arendtsville	AREN1	PA	39.923	-77.308	267	04/2001-present
	Cohutta	COHU1	GA	34.785	-84.626	735	05/2000-present
	Dolly Sods WA	DOSO1	WV	39.105	-79.426	1182	09/1991-present
	Frostburg	FRRE1	MD	39.706	-79.012	767	04/2004-present
	Great Smoky Mountains NP	GRSM1	TN	35.633	-83.942	811	03/1988-present
	James River Face Wilderness	JARI1	VA	37.627	-79.513	290	06/2000-present
	Jefferson NF	JEFF1	VA	37.617	-79.483	219	09/1994-05/2000
	Linville Gorge	LIGO1	NC	35.972	-81.933	969	03/2000-present
	Shenandoah NP	SHEN1	VA	38.523	-78.435	1079	03/1988-present
	Shining Rock WA	SHRO1	NC	35.394	-82.774	1617	07/1994-present
	Sipsy Wilderness	SIPS1	AL	34.343	-87.339	286	03/1992-present
Boundary Waters	Boundary Waters Canoe Area	BOWA1	MN	47.947	-91.496	527	08/1991-present
	Isle Royale NP	ISLE1	MI	47.46	-88.149	182	11/1999-present
	Isle Royale NP	ISRO1	MI	47.917	-89.15	213	06/1988-07/1991
	Seney	SENE1	MI	46.289	-85.95	215	11/1999-present
	Voyageurs NP #1	VOYA1	MN	48.413	-92.83	426	03/1988-09/1996
	Voyageurs NP #2	VOYA2	MN	48.413	-92.829	429	11/1999-present
California Coast	Pinnacles NM	PINN1	CA	36.483	-121.157	302	03/1988-present
	Point Reyes National Seashore	PORE1	CA	38.122	-122.909	97	03/1988-present
	San Rafael	RAFA1	CA	34.734	-120.007	957	02/2000-present
Central Great Plains	Blue Mounds	BLMO1	MN	43.716	-96.191	473	07/2002-present
	Bondville	BOND1	IL	40.052	-88.373	263	03/2001-present
	Cedar Bluff	CEBL1	KS	38.77	-99.763	666	06/2002-present
	Crescent Lake	CRES1	NE	41.763	-102.434	1207	07/2002-present
	El Dorado Springs	ELDO1	MO	37.701	-94.035	298	06/2002-present
	Great River Bluffs	GRRI1	MN	43.937	-91.405	370	07/2002-present
	Lake Sugema	LASU1	IA	40.688	-91.988	210	06/2002-11/2004
	Lake Sugema	LASU2	IA	40.693	-92.006	229	12/2004-present

IMPROVE Site Group	Site Name	Site Code	State	Latitude	Longitude	Elevation (m)	Dates of Operation
	Nebraska NF	NEBR1	NE	41.889	-100.339	883	07/2002-present
	Omaha	OMAH1	NE	42.149	-96.432	430	08/2003-present
	Sac and Fox	SAFO1	KS	39.979	-95.568	293	06/2002-present
	Tallgrass	TALL1	KS	38.434	-96.56	390	09/2002-present
	Viking Lake	VILA1	IA	40.969	-95.045	371	06/2002-present
Central Rockies	Brooklyn Lake	BRLA1	WY	41.366	-106.242	3196	09/1993-12/2003
	Great Sand Dunes NM	GRSA1	CO	37.725	-105.519	2498	05/1988-present
	Mount Zirkel WA	MOZI1	CO	40.538	-106.677	3243	07/1994-present
	Rocky Mountain NP HQ	RMHQ1	CO	40.362	-105.564	2408	03/1988-02/1991
	Rocky Mountain NP	ROMO1	CO	40.278	-105.546	2760	09/1990-present
	Storm Peak	STPE1	CO	40.445	-106.74	3220	12/1993-07/1994
	Wheeler Peak	WHPE1	NM	36.585	-105.452	3366	08/2000-present
	White River NF	WHRI1	CO	39.154	-106.821	3414	07/1993-present
Colorado Plateau	Arches NP	ARCH1	UT	38.783	-109.583	1722	03/1988-05/1992
	Bandelier NM	BAND1	NM	35.78	-106.266	1988	03/1988-present
	Bryce Canyon NP	BRCA1	UT	37.618	-112.174	2481	03/1988-present
	Canyonlands NP	CANY1	UT	38.459	-109.821	1798	03/1988-present
	Capitol Reef NP	CAPI1	UT	38.302	-111.293	1897	03/2000-present
	Hopi Point #1	GRCA1	AZ	36.066	-112.154	2164	03/1988-08/1998
	Hance Camp at Grand Canyon NP	GRCA2	AZ	35.973	-111.984	2267	09/1997-present
	Indian Gardens	INGA1	AZ	36.078	-112.129	1166	10/1989-present
	Meadview	MEAD1	AZ	36.019	-114.068	902	09/1991-09/1992 02/2003-present
	Mesa Verde NP	MEVE1	CO	37.198	-108.491	2172	03/1988-present
	San Pedro Parks	SAPE1	NM	36.014	-106.845	2935	08/2000-present
	Weminuche WA	WEMI1	CO	37.659	-107.8	2750	03/1988-present
	Zion Canyon	ZICA1	UT	37.198	-113.151	1215	12/2002-present
	Zion	ZION1	UT	37.459	-113.224	1545	03/2000-08/2004
Columbia River Gorge	Columbia Gorge #1	COGO1	WA	45.569	-122.21	230	09/1996-present
	Columbia River Gorge	CORI1	WA	45.664	-121.001	179	06/1993-present
Death Valley	Death Valley NP	DEVA1	CA	36.509	-116.848	130	10/1993-present
East Coast	Brigantine NWR	BRIG1	NJ	39.465	-74.449	5	09/1991-present
	Swanquarter	SWAN1	NC	35.451	-76.207	-4	06/2000-present

IMPROVE Site Group	Site Name	Site Code	State	Latitude	Longitude	Elevation (m)	Dates of Operation
Great Basin	Great Basin NP	GRBA1	NV	39.005	-114.216	2066	05/1992-present
	Jarbidge WA	JARB1	NV	41.893	-115.426	1869	03/1988-present
Hawaii	Haleakala NP	HALE1	HI	20.809	-156.282	1153	02/1991-present
	Hawaii Volcanoes NP	HAVO1	HI	19.431	-155.258	1259	03/1988-present
	Mauna Loa Observatory #1	MALO1	HI	19.536	-155.577	3439	03/1995-present
	Mauna Loa Observatory #2	MALO2	HI	19.536	-155.577	3439	03/1995-present
	Mauna Loa Observatory #3	MALO3	HI	19.539	-155.578	3400	04/1996-05/1996
	Mauna Loa Observatory #4	MALO4	HI	19.539	-155.578	3400	04/1996-05/1996
Hells Canyon	Craters of the Moon NM	CRMO1	ID	43.461	-113.555	1818	05/1992-present
	Hells Canyon	HECA1	OR	44.97	-116.844	655	08/2000-present
	Sawtooth NF	SAWT1	ID	44.17	-114.927	1990	01/1994-present
	Scoville	SCOV1	ID	43.65	-113.033	1500	05/1992-05/1997
	Starkey	STAR1	OR	45.225	-118.513	1259	03/2000-present
Lone Peak	Lone Peak WA	LOPE1	UT	40.445	-111.708	1768	12/1993-08/2001
Mid South	Caney Creek	CACR1	AR	34.454	-94.143	683	06/2000-present
	Cherokee Nation	CHER1	OK	36.956	-97.031	342	09/2002-present
	Ellis	ELLI1	OK	36.085	-99.935	697	06/2002-present
	Hercules-Glades	HEGL1	MO	36.614	-92.922	404	03/2001-present
	Sikes	SIKE1	LA	32.057	-92.435	45	03/2001-present
	Upper Buffalo WA	UPBU1	AR	35.826	-93.203	723	12/1991-present
	Wichita Mountains	WIMO1	OK	34.732	-98.713	509	03/2001-present
Mogollon Plateau	Mount Baldy	BALD1	AZ	34.058	-109.441	2509	02/2000-present
	Bosque del Apache	BOAP1	NM	33.87	-106.852	1390	04/2000-present
	Gila WA	GICL1	NM	33.22	-108.235	1776	04/1994-present
	Hillside	HILL1	AZ	34.429	-112.963	1511	04/2001-06/2005
	Ike's Backbone	IKBA1	AZ	34.34	-111.683	1298	04/2000-present
	Petrified Forest NP	PEFO1	AZ	35.078	-109.769	1766	03/1988-present
	San Andres	SAAN1	NM	32.687	-106.484	1326	10/1997-08/2000
	Sierra Ancha	SIAN1	AZ	34.091	-110.942	1600	02/2000-present
	Sycamore Canyon	SYCA1	AZ	35.141	-111.969	2046	09/1991-present
	Tonto NM	TONT1	AZ	33.655	-111.107	775	04/1988-present
	White Mountain	WHIT1	NM	33.469	-105.535	2064	01/2002-present
Northeast	Acadia NP	ACAD1	ME	44.377	-68.261	157	03/1988-present
	Addison Pinnacle	ADPI1	NY	42.091	-77.21	512	04/2001-present
	Bridgton	BRMA1	ME	44.107	-70.729	234	03/2001-present
	Casco Bay	CABA1	ME	43.833	-70.064	27	03/2001-present

IMPROVE Site Group	Site Name	Site Code	State	Latitude	Longitude	Elevation (m)	Dates of Operation
	Cape Cod	CACO1	MA	41.976	-70.024	49	04/2001-present
	Connecticut Hill	COHI1	NY	42.401	-76.653	519	04/2001-07/2006
	Great Gulf WA	GRGU1	NH	44.308	-71.218	454	06/1995-present
	Lye Brook WA	LYBR1	VT	43.148	-73.127	1015	09/1991-present
	Martha's Vineyard	MAVI1	MA	41.331	-70.785	3	01/2003-present
	Mohawk Mt.	MOMO1	CT	41.821	-73.297	522	09/2001-present
	Moosehorn NWR	MOOS1	ME	45.126	-67.266	78	12/1994-present
	Old Town	OLTO1	ME	44.933	-68.646	51	07/2001-present
	Proctor Maple Research Facility	PMRF1	VT	44.528	-72.869	401	12/1993-present
	Presque Isle	PRIS1	ME	46.696	-68.033	166	03/2001-present
	Quabbin Summit	QURE1	MA	42.298	-72.335	318	03/2001-present
Northern Great Plains	Badlands NP	BADL1	SD	43.743	-101.941	736	03/1988-present
	Cloud Peak	CLPE1	WY	44.334	-106.957	2471	06/2002-present
	Fort Peck	FOPE1	MT	48.308	-105.102	638	06/2002-present
	Lostwood	LOST1	ND	48.642	-102.402	696	12/1999-present
	Medicine Lake	MELA1	MT	48.487	-104.476	606	12/1999-present
	Northern Cheyenne	NOCH1	MT	45.65	-106.557	1283	06/2002-present
	Thunder Basin	THBA1	WY	44.663	-105.287	1195	06/2002-present
	Theodore Roosevelt	THRO1	ND	46.895	-103.378	853	12/1999-present
	UL Bend	ULBE1	MT	47.582	-108.72	891	01/2000-present
	Wind Cave	WICA1	SD	43.558	-103.484	1296	12/1999-present
Northern Rockies	Bridger WA	BRID1	WY	42.975	-109.758	2627	03/1988-present
	Cabinet Mountains	CABI1	MT	47.955	-115.671	1441	07/2000-present
	Flathead	FLAT1	MT	47.773	-114.269	1580	06/2002-present
	Gates of the Mountains	GAMO1	MT	46.826	-111.711	2387	07/2000-present
	Glacier NP	GLAC1	MT	48.511	-113.997	975	03/1988-present
	Monture	MONT1	MT	47.122	-113.154	1282	03/2000-present
	North Absaroka	NOAB1	WY	44.745	-109.382	2483	01/2000-present
	Salmon NF	SALM1	ID	45.159	-114.026	2788	12/1993-08/2000
	Sula Peak	SULA1	MT	45.86	-114	1896	08/1994-present
	Yellowstone NP 1	YELL1	WY	44.565	-110.4	2442	03/1988-07/1996
	Yellowstone NP 2	YELL2	WY	44.565	-110.4	2425	07/1996-present
Northwest	Lynden	LYND1	WA	48.953	-122.559	28	10/1996-08/1997
	Mount Rainier NP	MORA1	WA	46.758	-122.124	439	03/1988-present
	North Cascades	NOCA1	WA	48.732	-121.065	569	03/2000-present
	Olympic	OLYM1	WA	48.007	-122.973	600	07/2001-present

IMPROVE Site Group	Site Name	Site Code	State	Latitude	Longitude	Elevation (m)	Dates of Operation
	Pasayten	PASA1	WA	48.388	-119.927	1627	11/2000-present
	Snoqualmie Pass	SNPA1	WA	47.422	-121.426	1049	07/1993-present
	Spokane Res.	SPOK1	WA	47.904	-117.861	552	07/2001-06/2005
	White Pass	WHPA1	WA	46.624	-121.388	1827	02/2000-present
Not Assigned	Walker River Paiute Tribe	WARI1	NV	38.952	-118.815	1250	06/2003-11/2005
Ohio River Valley	Cadiz	CADI1	KY	36.784	-87.85	192	03/2001-present
	Livonia	LIVO1	IN	38.535	-86.26	282	03/2001-present
	Mammoth Cave NP	MACA1	KY	37.132	-86.148	235	09/1991-present
	Mingo	MING1	MO	36.972	-90.143	111	05/2000-present
	M.K. Goddard	MKGO1	PA	41.427	-80.145	380	04/2001-present
	Quaker City	QUCI1	OH	39.943	-81.338	366	05/2001-present
Oregon and Northern California	Bliss SP (TRPA)	BLIS1	CA	38.976	-120.103	2131	11/1990-present
	Crater Lake NP	CRLA1	OR	42.896	-122.136	1996	03/1988-present
	Kalmiopsis	KALM1	OR	42.552	-124.059	80	03/2000-present
	Lava Beds NM	LABE1	CA	41.712	-121.507	1460	03/2000-present
	Lassen Volcanic NP	LAVO1	CA	40.54	-121.577	1733	03/1988-present
	Mount Hood	MOHO1	OR	45.289	-121.784	1531	03/2000-present
	Redwood NP	REDW1	CA	41.561	-124.084	244	03/1988-present
	Three Sisters WA	THSI1	OR	44.291	-122.043	885	07/1993-present
	Trinity	TRIN1	CA	40.786	-122.805	1014	07/2000-present
Phoenix	Phoenix	PHOE1	AZ	33.504	-112.096	342	04/2001-present
Puget Sound	Puget Sound	PUSO1	WA	47.57	-122.312	98	03/1996-present
Sierra Nevada	Dome Lands WA	DOLA1	CA	35.699	-118.202	914	08/1994-10/1998
	Dome Lands WA	DOME1	CA	35.728	-118.138	927	02/2000-present
	Hoover	HOOV1	CA	38.088	-119.177	2561	07/2001-present
	Kaiser	KAIS1	CA	37.221	-119.155	2598	01/2000-present
	Sequoia NP	SEQU1	CA	36.489	-118.829	519	03/1992-present
	South Lake Tahoe	SOLA1	CA	38.933	-119.967	1900	03/1989-06/1997
	Yosemite NP	YOSE1	CA	37.713	-119.706	1603	03/1988-present
Southeast	Breton	BRET1	LA	29.119	-89.207	11	06/2000-present
	Chassahowitzka NWR	CHAS1	FL	28.748	-82.555	4	04/1993-present
	Everglades NP	EVER1	FL	25.391	-80.681	1	09/1988-present
	Okefenokee NWR	OKEF1	GA	30.741	-82.128	48	09/1991-present
	Cape Romain NWR	ROMA1	SC	32.941	-79.657	5	09/1994-present
	St. Marks	SAMA1	FL	30.093	-84.161	8	06/2000-present
Southern Arizona	Chiricahua NM	CHIR1	AZ	32.009	-109.389	1555	03/1988-present

IMPROVE Site Group	Site Name	Site Code	State	Latitude	Longitude	Elevation (m)	Dates of Operation
	Douglas	DOUG1	AZ	31.349	-109.54	1230	06/2004-present
	Organ Pipe	ORPI1	AZ	31.951	-112.802	504	01/2003-present
	Queen Valley	QUVA1	AZ	33.294	-111.286	661	04/2001-present
	Saguaro NM	SAGU1	AZ	32.175	-110.737	941	06/1988-present
	Saguaro West	SAWE1	AZ	32.249	-111.218	714	04/2001-present
Southern California	Agua Tibia	AGTI1	CA	33.464	-116.971	508	11/2000-present
	Joshua Tree NP	JOSH1	CA	34.069	-116.389	1235	02/2000-present
	Joshua Tree NP	JOTR1	CA	34.069	-116.389	1228	09/1991-07/1992
	San Gabriel	SAGA1	CA	34.297	-118.028	1791	12/2000-present
	San Gorgonio WA	SAGO1	CA	34.194	-116.913	1726	03/1988-present
Urban QA Sites	Atlanta	ATLA1	GA	33.688	-84.29	243	04/2004-present
	Baltimore	BALT1	MD	39.255	-76.709	78	06/2004-present
	Birmingham	BIRM1	AL	33.553	-86.815	176	04/2004-present
	Chicago	CHIC1	IL	41.751	-87.713	195	11/2003-09/2005
	Detroit	DETR1	MI	42.229	-83.209	180	11/2003-present
	Fresno	FRES1	CA	36.782	-119.773	100	09/2004-present
	Houston	HOUS1	TX	29.67	-95.129	7	05/2004-09/2005
	New York City	NEYO1	NY	40.816	-73.902	45	08/2004-present
	Pittsburgh	PITT1	PA	40.465	-79.961	268	04/2004-present
	Rubidoux	RUBI1	CA	34	-117.416	248	09/2004-09/2005
Virgin Islands	Virgin Islands NP	VIIS1	VI	18.336	-64.796	51	10/1990-present
Washington D.C.	Washington D.C.	WASH1	DC	38.876	-77.034	15	03/1988-present
West Texas	Big Bend NP	BIBE1	TX	29.303	-103.178	1067	03/1988-present
	Guadalupe Mountains NP	GUMO1	TX	31.833	-104.809	1672	03/1988-present
	Salt Creek	SACR1	NM	33.46	-104.404	1072	04/2000-present

NF = National Forest
NM = National Monument
NP = National Park
NWR = National Wildlife Refuge
WA = Wilderness Area

Table 1.2. Class I areas and the representative monitoring site.

Class I Area Name	Site Name	Site Code
Acadia	Acadia NP	ACAD1
Agua Tibia	Agua Tibia	AGTI1
Alpine Lakes	Snoqualmie Pass	SNPA1
Anaconda-Pintler	Sula Peak	SULA1
Ansel Adams	Kaiser	KAIS1
Arches	Canyonlands NP	CANY1
Badlands	Badlands NP	BADL1
Bandelier	Bandelier NM	BAND1
Big Bend	Big Bend NP	BIBE1
Black Canyon of the Gunnison	Weminuche WA	WEMI1
Bob Marshall	Monture	MONT1
Bosque del Apache	Bosque del Apache	BOAP1

Class I Area Name	Site Name	Site Code
Boundary Waters Canoe Area	Boundary Waters Canoe Area	BOWA1
Breton	Breton	BRET1
Bridger	Bridger WA	BRID1
Brigantine	Brigantine NWR	BRIG1
Bryce Canyon	Bryce Canyon NP	BRCA1
Cabinet Mountains	Cabinet Mountains	CABI1
Caney Creek	Caney Creek	CACR1
Canyonlands	Canyonlands NP	CANY1
Cape Romain	Cape Romain NWR	ROMA1
Capitol Reef	Capitol Reef NP	CAPI1
Caribou	Lassen Volcanic NP	LAVO1
Carlsbad Caverns	Guadalupe Mountains NP	GUMO1
Chassahowitzka	Chassahowitzka NWR	CHAS1
Chiricahua NM	Chiricahua NM	CHIR1
Chiricahua W	Chiricahua NM	CHIR1
Cohutta	Cohutta	COHU1
Crater Lake	Crater Lake NP	CRLA1
Craters of the Moon	Craters of the Moon NM	CRMO1
Cucamonga	San Gabriel	SAGA1
Denali	Denali NP	DENA1
Desolation	Bliss SP (TRPA)	BLIS1
Diamond Peak	Crater Lake NP	CRLA1
Dolly Sods	Dolly Sods WA	DOSO1
Dome Land	Dome Lands WA	DOME1
Eagle Cap	Starkey	STAR1
Eagles Nest	White River NF	WHRI1
Emigrant	Yosemite NP	YOSE1
Everglades	Everglades NP	EVER1
Fitzpatrick	Bridger WA	BRID1
Flat Tops	White River NF	WHRI1
Galiuro	Chiricahua NM	CHIR1
Gates of the Mountains	Gates of the Mountains	GAMO1
Gearhart Mountain	Crater Lake NP	CRLA1
Gila	Gila WA	GICL1
Glacier	Glacier NP	GLAC1
Glacier Peak	North Cascades	NOCA1
Goat Rocks	White Pass	WHPA1
Grand Canyon	Hance Camp at Grand Canyon NP	GRCA2
Grand Teton	Yellowstone NP 2	YELL2
Great Gulf	Great Gulf WA	GRGU1
Great Sand Dunes	Great Sand Dunes NM	GRSA1
Great Smoky Mountains	Great Smoky Mountains NP	GRSM1
Guadalupe Mountains	Guadalupe Mountains NP	GUMO1
Haleakala	Haleakala NP	HALE1
Hawaii Volcanoes	Hawaii Volcanoes NP	HAVO1
Hells Canyon	Hells Canyon	HECA1
Hercules-Glade	Hercules-Glades	HEGL1
Hoover	Hoover	HOOV1
Isle Royale	Isle Royale NP	ISLE1
James River Face	James River Face WA	JARI1
Jarbidge	Jarbidge WA	JARB1
John Muir	Kaiser	KAIS1

Class I Area Name	Site Name	Site Code
Joshua Tree	Joshua Tree NP	JOSH1
Joyce Kilmer-Slickrock	Great Smoky Mountains NP	GRSM1
Kaiser	Kaiser	KAIS1
Kalmiopsis	Kalmiopsis	KALM1
Kings Canyon	Sequoia NP	SEQU1
La Garita	Weminuche WA	WEMI1
Lassen Volcanic	Lassen Volcanic NP	LAVO1
Lava Beds	Lava Beds NM	LABE1
Linville Gorge	Linville Gorge	LIGO1
Lostwood	Lostwood	LOST1
Lye Brook	Lye Brook WA	LYBR1
Mammoth Cave	Mammoth Cave NP	MACA1
Marble Mountain	Trinity	TRIN1
Maroon Bells-Snowmass	White River NF	WHRI1
Mazatzal	Ike's Backbone	IKBA1
Medicine Lake	Medicine Lake	MELA1
Mesa Verde	Mesa Verde NP	MEVE1
Mingo	Mingo	MING1
Mission Mountains	Monture	MONT1
Mokelumne	Bliss SP (TRPA)	BLIS1
Moosehorn	Moosehorn NWR	MOOS1
Mount Adams	White Pass	WHPA1
Mount Baldy	Mount Baldy	BALD1
Mount Hood	Mount Hood	MOHO1
Mount Jefferson	Three Sisters WA	THSI1
Mount Rainier	Mount Rainier NP	MORA1
Mount Washington	Three Sisters WA	THSI1
Mount Zirkel	Mount Zirkel WA	MOZI1
Mountain Lakes	Crater Lake NP	CRLA1
North Absaroka	North Absaroka	NOAB1
North Cascades	North Cascades	NOCA1
Okefenokee	Okefenokee NWR	OKEF1
Olympic	Olympic	OLYM1
Otter Creek	Dolly Sods WA	DOSO1
Pasayten	Pasayten	PASA1
Pecos	Wheeler Peak	WHPE1
Petrified Forest	Petrified Forest NP	PEFO1
Pine Mountain	Ike's Backbone	IKBA1
Pinnacles	Pinnacles NM	PINN1
Point Reyes	Point Reyes National Seashore	PORE1
Presidential Range-Dry River	Great Gulf WA	GRGU1
Rawah	Mount Zirkel WA	MOZI1
Red Rock Lakes	Yellowstone NP 2	YELL2
Redwood	Redwood NP	REDW1
Rocky Mountain	Rocky Mountain NP	ROMO1
Roosevelt Campobello	Moosehorn NWR	MOOS1
Saguaro	Saguaro NM	SAGU1
Saint Marks	St. Marks	SAMA1
Salt Creek	Salt Creek	SACR1
San Gabriel	San Gabriel	SAGA1
San Gorgonio	San Gorgonio WA	SAGO1
San Jacinto	San Gorgonio WA	SAGO1

Class I Area Name	Site Name	Site Code
San Pedro Parks	San Pedro Parks	SAPE1
San Rafael	San Rafael	RAFA1
Sawtooth	Sawtooth NF	SAWT1
Scapegoat	Monture	MONT1
Selway-Bitterroot	Sula Peak	SULA1
Seney	Seney	SENE1
Sequoia	Sequoia NP	SEQU1
Shenandoah	Shenandoah NP	SHEN1
Shining Rock	Shining Rock WA	SHRO1
Sierra Ancha	Sierra Ancha	SIAN1
Simeonof	Simeonof	SIME1
Sipsey	Sipsy WA	SIPS1
South Warner	Lava Beds NM	LABE1
Strawberry Mountain	Starkey	STAR1
Superstition	Tonto NM	TONT1
Swanquarter	Swanquarter	SWAN1
Sycamore Canyon	Sycamore Canyon	SYCA1
Teton	Yellowstone NP 2	YELL2
Theodore Roosevelt	Theodore Roosevelt	THRO1
Thousand Lakes	Lassen Volcanic NP	LAVO1
Three Sisters	Three Sisters WA	THSI1
Tuxedni	Tuxedni	TUXE1
UL Bend	UL Bend	ULBE1
Upper Buffalo	Upper Buffalo WA	UPBU1
Ventana	Pinnacles NM	PINN1
Virgin Islands	Virgin Islands NP	VIIS1
Voyageurs	Voyageurs NP #2	VOYA2
Washakie	North Absaroka	NOAB1
Weminuche	Weminuche WA	WEMI1
West Elk	White River NF	WHRI1
Wheeler Peak	Wheeler Peak	WHPE1
White Mountain	White Mountain	WHIT1
Wichita Mountains	Wichita Mountains	WIMO1
Wind Cave	Wind Cave	WICA1
Wolf Island	Okefenokee NWR	OKEF1
Yellowstone	Yellowstone NP 2	YELL2
Yolla Bolly-Middle Eel	Trinity	TRIN1
Yosemite	Yosemite NP	YOSE1
Zion	Zion	ZION1

NF = National Forest
NM = National Monument
NP = National Park
NWR = National Wildlife Refuge
WA = Wilderness Area

1.2.2 Aerosol Sampling and Analysis

The current IMPROVE protocol for particle sampling requires that the sampler operate at ambient temperatures. To accomplish this, samplers are generally housed in a ventilated shelter that provides shielding from direct sunlight. Shelter design across the network is varied to meet differing practical and aesthetic concerns for specific sites.

A few protocol changes with respect to the particle monitoring in the network were implemented as part of the expansion to make the IMPROVE network more consistent with the EPA's fine mass and fine speciation particulate monitoring networks and to add additional quality control measures. The primary changes included changing the twice-weekly, 24-hour duration sampling schedule to an every-third-day schedule that corresponds to the schedule of the national particulate networks operated by state and local governments and the addition of replicate sampling and analysis for $PM_{2.5}$ mass and composition to evaluate measurement uncertainty. A new version of the IMPROVE particle sampler was designed and produced at the University of California, Davis, to allow for these protocol changes. The version I sampler is described in previous IMPROVE-related publications [Malm et al., 1989; Malm et al., 1994; Malm et al., 2000], and the version II IMPROVE sampler is described below. Installation of the version II samplers at all 110 IMPROVE sites, new and existing, began in November 1999 and continued through the spring of 2000. All sites installed since 2000 have the version II sampler.

The IMPROVE samplers (versions I and II) consist of four independent modules (see Figure 1.3). Each module incorporates a separate inlet, filter pack, and pump assembly. It is convenient to consider a particular module, its associated filter, and the parameters measured from the filter as a channel of measurement (e.g., module A). Modules A, B, and C are equipped with a 2.5 μm cyclone, while module D is fitted with a PM_{10} inlet. For module B, the sampled air is drawn through a carbonate denuder tube in the inlet to remove gaseous nitric acid.

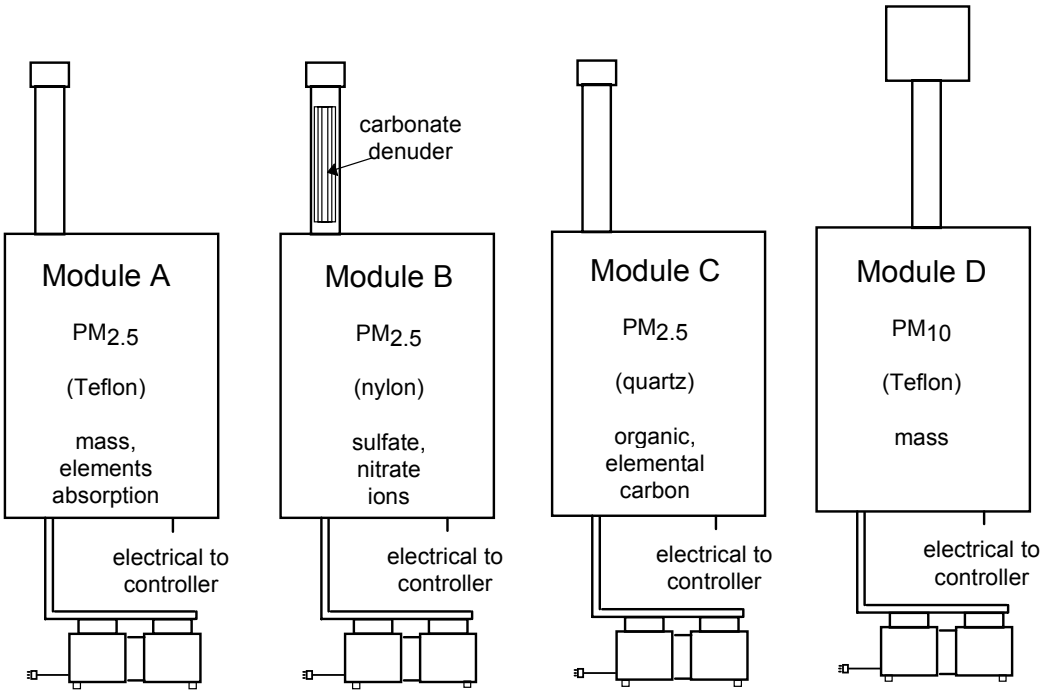

Figure 1.3. Schematic view of the IMPROVE sampler showing the four modules with separate inlets and pumps. The substrates with analyses performed for each module are also shown.

For the version II sampler, the objective was to build a sampler that would be comparable to the version I sampler from a sample collection perspective but use then state-of-the-art microprocessor technology to increase the control and provide feedback on operating status. The version II sampler was designed to be identical to the version I sampler in the design of the four

sampling modules (shown in Figure 1.3), including using the same sample collection substrates (filter materials) and the same materials and dimensions for each module, from the sample inlet to the face of the filter, and with the same flow rates. Preliminary tests of the samplers confirmed the qualitative comparability of the aerosol samples collected via the version I and II samplers [Malm et al., 2000; Eldred et al., 2001].

One of the improvements in the version II sampler is a microprocessor-based controller that can be programmed to sample any period of time on any schedule, which replaced the 7-day timer/controller. The microprocessor includes a memory card reader/writer that is used to record flow rate, sample temperature, and other performance-related information reported every 15 minutes throughout the sample period. For the original version I sampler, the flows were manually checked at the beginning and end of each sample period, and the seasonal mean site temperature and pressure were used for flow calculations. Beyond the improved tracking and calculation of flow and sample air volume, the microprocessor also permits programming changes to be distributed to the controller on chips that are installed during annual maintenance visits. This allows for programming changes to be implemented consistently and without requiring programming in the field.

To accommodate the new sampling schedule, the version II sampler has a four-filter manifold for each module, in place of the version I sampler two-filter manifolds. The manifold with the solenoids sits directly above the filter cassettes and is raised or lowered as a unit to unload and load the filters. The four filter cassettes are held in a cartridge (shown in Figure 1.4) that is designed to only allow one orientation in the sampler. Fully prepared date- and site-labeled filter cartridges, along with memory cards, are sent from the analysis laboratory to the field and are returned in special mailing containers to prevent confusion concerning the order of sampling among the filters. If filter change service is performed on a sample day, the operator moves the cassette containing that day's filter to the open position in the newly loaded cartridge. The few minutes that it takes to perform this sample change is recorded by the microprocessor on the memory card so that the correct air volume is used to calculate concentrations.

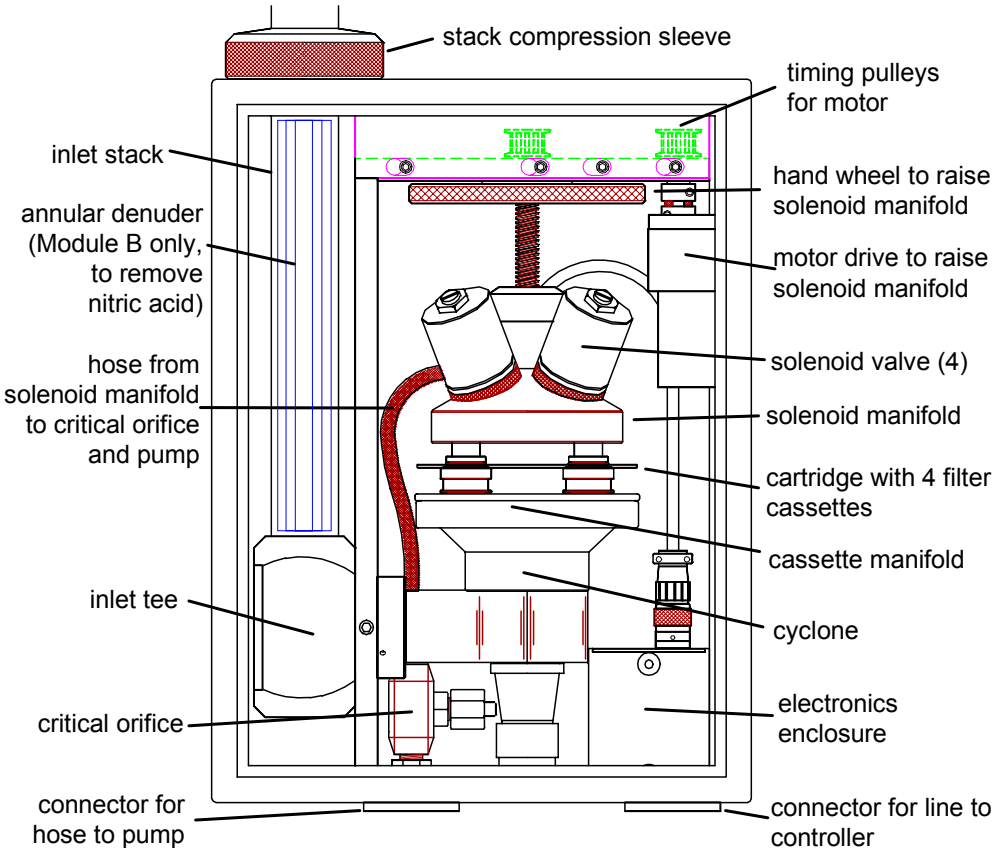

Figure 1.4. Schematic of a new version of the IMPROVE sampler $PM_{2.5}$ module.

Additionally, the version II IMPROVE sampler makes it simple to add a fifth module at the monitoring sites to accommodate replicate sampling and analysis for mass and composition. This quality assurance module will be operated for each sample period and will collect a replicate sample for one of the four modules (A, B, C, or D) so that, over time, relative precision information can be developed for each parameter. Starting in 2003, collocated modules were installed at 24 sites across the network, providing ~4% replication for each of the four modules (Table 1.3).

Table 1.3. Sites with a fifth collocated module.

Site Name	Site	A	B	C	D	Start Date	End Date
Mesa Verde NP	MEVE1	X				8/13/2003	
Olympic NP	OLYM1	X				11/8/2003	
Proctor Maple Research Facility	PMRF1	X				9/3/2003	
Sac and Fox	SAFO1	X				11/20/2003	
St. Marks	SAMA1	X				11/18/2004	
Trapper Creek	TRCR1	X				6/22/2004	
Big Bend NP	BIBE1		X			8/30/2003	
Blue Mounds	BLMO1		X			9/16/2004	
Frostburg	FRRE1		X			4/15/2004	
Gates of the Mountains	GAMO1		X			9/23/2003	
Lassen Volcanic NP	LAVO1		X			4/18/2003	
Mammoth Cave NP	MACA1		X			5/12/2003	

Site Name	Site	A	B	C	D	Start Date	End Date
Everglades NP	EVER1			X		7/11/2003	
Hercules-Glades	HEGL1			X		8/24/2004	
Hoover	HOOV1			X		8/13/2003	
Medicine Lake	MELA1			X		9/25/2003	
Saguaro West	SAWE1			X		3/25/2004	
Seney	SENE1			X		8/10/2003	
Houston	HOUS1				X	4/30/2004	9/1/2005
Jarbidge WA	JARB1				X	6/30/2004	
Joshua Tree NP	JOSH1				X	8/7/2003	
Quabbin Summit	QURE1				X	9/4/2003	
Swanquarter	SWAN1				X	11/9/2004	
Wind Cave	WICA1				X	9/17/2004	

NP = National Park
WA = Wilderness Area

In both the version I and II samplers, the four modules independently collect aerosol samples onto a variety of filter types (Figure 1.3). The D module collects PM_{10} aerosol on Teflon filters. The A, B, and C modules collect $PM_{2.5}$ aerosol on Teflon, nylon, and quartz fiber filters, respectively. The different filter media facilitate the collection of particular aerosol species or a specific form of chemical analysis. Gravimetric analysis is routinely performed on the A and D module filters. Elemental analysis and aerosol absorption measurements are routinely performed on the A module filter. Ion analysis is routinely performed on the B module filter, and carbon analysis is routinely performed on the quartz fiber filter.

The gravimetric analysis performed on both the $PM_{2.5}$ A and PM_{10} D module Teflon filters allows for the estimation of the coarse aerosol fraction through differencing. Teflon filters are prone to losses of semivolatile NH_4NO_3 and thus provide only a lower estimate of the actual ambient aerosol concentrations [Hand and Malm, 2006]. Unfortunately, nylon filters that effectively capture the NH_4NO_3 are not ideal for gravimetric analysis because they are heavier than Teflon filters, and thus the calculation of aerosol mass through pre- and post-weighing is more error prone since aerosol mass represents a smaller fraction of the total mass. The quartz filters are not suitable for gravimetric analysis because they are more friable and subject to the same NH_4NO_3 losses as Teflon. A further complication on the interpretation of the gravimetric measurements is the variable size cut on the $PM_{2.5}$ modules. The size cut of the cyclone used to collect and separate $PM_{2.5}$ aerosols is controlled by the flow rate of the sampler. Variations in the flow rate can have impacts on the size range of aerosols being collected and termed “fine”. This issue can be important when interpreting fine mass versus coarse mass, as well as affect the chemical composition of the fractions since different aerosol types tend to be dominant in each size fraction.

The forms of elemental analysis conducted past and present in the IMPROVE network are proton elastic scattering analysis (PESA), proton induced X-ray emission (PIXE), and X-ray fluorescence (XRF). Since the network’s inception, PESA has been and continues to be used for quantifying elemental hydrogen. PIXE has been used for quantifying nearly all elements with atomic weights ≥11 (Na) and ≤82 (Pb). Beginning in 1992, analysis of the heavier elements, those with atomic weights from 26 (Fe) to 82 (Pb), was changed from PIXE to XRF with a Mo anode source. PIXE was discontinued in late 2001 and analysis of the lighter elements with atomic weights from 11 (Na) to 25 (Mn) was changed from PIXE to XRF using a Cu anode

source. Also, in late 2001, the analysis of Fe was changed from Mo anode XRF to Cu anode XRF. In both cases the change from PIXE to XRF provided lower minimum detection limits (mdl) for most elements of interest, as well as better sample preservation for reanalysis. The exceptions were Na, Mg, Al, and to a lesser extent Si, where the change to Cu XRF resulted in significantly increased mdl and uncertainty. The details on the transitions from PIXE to XRF are provided in section 1.3 below.

The material collected from the B module nylon filters is extracted ultrasonically in an aqueous solution that is subsequently analyzed by ion chromatography for the anions sulfate, nitrate, nitrite, and chloride. Nylon filters have been shown to be more effective at capturing and retaining NO_3 from semivolatile NH_4NO_3 than Teflon filters [Yu et al., 2005]. Field blanks for the B module are collected to correct for positive artifacts of all the reported anions. A field blank nylon filter is placed in an unused port in the filter cassette, so it is exposed to all aspects of the filter handling process, except it does not have sample air drawn through it [McDade et al., 2004]. Approximately 70 field blanks are collected each month, constituting around 4% of the total filters collected [McDade et al., 2004]. Each site receives a nylon filter field blank every two to three months, on average [McDade et al., 2004]. A single artifact correction is applied for each species for every site in the network for the time period being processed. Currently, the data are processed in monthly batches; prior to June 2002, seasonal quarters were used. The artifact correction is calculated as the median of the filter blank values and is subtracted from all reported concentrations. Analysis of artifacts on the nylon filter suggests that sulfate ion artifacts are typically less than 10% of the ambient concentration, and nitrate artifacts range between 10% and 20% for the filters used prior to 2004 [McDade et al., 2004]. The filters introduced in 2004 were significantly cleaner, with typical median blank values of 0.00 (below the mdl) for sulfate and nitrate and 0.01 $\mu g/m^3$ for chloride, which is approximately 100 times smaller than the chloride blank values observed prior to 2004.

Module C utilizes quartz fiber filters that are analyzed by thermal optical reflectance (TOR) for particulate organic and elemental carbon (OC and EC, respectively) [Chow et al., 1993]. Quartz filter field blanks are also collected at approximately the same frequency as for nylon filters, and they are analyzed for the components of OC and EC. These field blanks are examined routinely to identify potential problems, but they are not used for artifact corrections in the IMPROVE database. In the IMPROVE program, secondary filters (after-filters) are used to correct for positive artifacts resulting from the adsorption of organic gases onto the filter. The after-filters are placed directly behind the primary quartz filter and are collected at six sites, Chiricahua, AZ; Grand Canyon, AZ; Yosemite, CA; Okefenokee, GA; Shenandoah, VA; and Mount Rainier, WA, to determine the artifact corrections for OC and EC. The Chiricahua and Okefenokee sites were added in 2001. The number of sites is limited by financial and logistical constraints and was selected to cover a variety of regions and aerosol conditions. The quartz after-filters are collected during every sampling period at the six after-filter sites. Typical artifacts for OC can correspond to half of the reported ambient concentration [McDade et al., 2004]. Negative artifacts due to the volatilization of particulate organics are not accounted for because they are thought to be small [Turpin et al., 2000], although some studies suggest they could be important [Hand and Malm, 2006].

1.2.3 Optical Sampling and Analysis

Optical monitoring is conducted at a subset of the IMPROVE sites (Tables 1.4 and 1.5). Routine optical monitoring includes light extinction as measured by transmissometers and aerosol scattering as measured by nephelometers.

Transmissometers are calibrated to measure the irradiance, at a wavelength of 550 nm, of a light source after the light has traveled over a finite atmospheric path. The transmittance of the path is calculated by dividing the measured irradiance at the end of the path by the calibrated initial intensity of the light source. Bouger's law is applied to calculate the extinction. Because of the relatively clean atmospheres found in the western United States, path lengths of a few kilometers are required to achieve the necessary sensitivity to resolve extinctions near the Rayleigh limit.

The transmissometers used in IMPROVE are the Optec, Inc., LPV-2 instruments, which have been in use since 1986. Their use in remote locations such as national parks is discussed by Molenar et al. [1989], while their use in urban settings is presented by Dietrich et al. [1989]. Data processing algorithms that incorporate corrections for interferences are thoroughly discussed by Molenar and Malm [1992].

Molenar et al. [1989] discuss the inherent uncertainties associated with the measurement. The accuracy of the transmission measurement, as determined by field and laboratory calibrations, is better than 1%. However, the accuracy of the derived extinction is dependent on the accuracy of the transmission measurement in field conditions. The transmission calculation is determined from an absolute (as opposed to relative) measurement of irradiance of a light source of known intensity that is located some known distance from the receiver. The measurement is made through optics that are exposed to the ambient atmosphere but are assumed to be free of dust or other films that tend to build up on the optical surfaces. The uncertainties associated with these parameters contribute to the overall uncertainty of the measurement. For a typical 5-km path length, the estimated uncertainty is about 4 Mm^{-1}.

Table 1.4. Transmissometer receiver and transmitter locations.

Location	Site Name	Receiver Lon (deg)	Lat (deg)	Elevation (m)	Bearing (deg)	Transmitter Lon (deg)	Lat (deg)	Elevation (m)	Mean Elevation	Elevation Angle (deg)	Distance	Start Date	End Date	Sponsor
ACAD1	Acadia NP	-68.26	44.37	134	134	-68.23	44.35	466	300	5	4	9/1/1987	8/31/1993	NPS
BADL1	Badlands NP	-101.9	43.79	806	239	-101.95	43.77	805	805	-0.01	4.151	12/1/1987		NPS
BAND1	Bandelier NM	-106.26	35.78	2011	315	-106.3	35.81	2143	2077	1.65	4.058	9/1/1988		NPS
BRID1	Bridger WA	-109.79	42.93	2390	11	-109.77	42.97	2568	2479	2.01	5.083	9/1/1988		USFS
CANY1	Canyonlands NP	-109.82	38.46	1806	73	-109.75	38.48	1774	1790	-0.29	6.426	12/1/1986		NPS
CHIR2	Chiricahua NM	-109.39	32.01	1567	97	-112.54	32.01	1682	1625	2.07	3.18	12/1/1998		NPS
CHIR1	Chiricahua NM	-109.39	32.01	1567	84	-109.32	32.01	2235	1901	6.26	6.123	12/1/1988	2/28/1999	NPS
GLAC1	Glacier NP	-113.94	48.56	968	232	-113.99	48.53	975	972	0.08	5.276	12/1/1988		NPS
GRBA1	Great Basin NP	-114.21	38.99	2130	315	-114.24	39.02	2365	2248	3.44	3.913	9/1/1992		NPS
GRCA1	Grand Canyon NP	-111.99	36	2256	81	-111.93	36.01	2170	2213	-0.85		12/1/1986		NPS
	Grandview (on the rim)													
GRCW1	Grand Canyon NP	-112.12	36.07	2145	205	-112.09	36.11	755	1450	-15.78	5.11	12/1/1989		NPS
	Yavapai (in canyon)													
GUMO1	Guadalupe Mountains NP	-104.81	31.83	1616	249	-104.86	31.82	1317	1467	-3.53	4.858	12/1/1988		NPS
PEFO1	Petrified Forest NP	-109.77	35.08	1772	173	-109.75	34.94	1690	1731	-0.3	15.44	8/1/1987	8/31/1987	NPS
PEFO2	Petrified Forest NP	-109.8	34.9	1690	48	-109.75	34.95	1700	1695	0.1	5.938	6/1/1987		NPS
PINN1	Pinnacles NM	-121.15	36.47	448	317	-121.18	36.5	428	438	-0.25	4.799	3/1/1988	8/31/1993	NPS
ROMO1	Rocky Mountain NP	-105.58	40.36	2535	305	-105.63	40.39	2932	2734	4.31	5.274	12/1/1987	8/31/1997	NPS
ROMO2	Rocky Mountain NP	-105.58	40.37	2502	302	-105.63	40.39	2932	2717	5.01	4.921	9/1/1998		NPS

Location	Site Name	Receiver Lon (deg)	Lat (deg)	Elevation (m)	Bearing (deg)	Transmitter Lon (deg)	Lat (deg)	Elevation (m)	Mean Elevation	Elevation Angle (deg)	Distance	Start Date	End Date	Sponsor
SAGO1	San Gorgonio WA	-116.91	34.19	1710	211	-116.94	34.16	1731	1721	0.29	4.099	3/1/1988		USFS
SHEN2	Shenandoah NP	-78.43	38.51	1073	310	-78.44	38.52	1061	1717	-0.49	1.412	6/1/1991		NPS
TONT1	Tonto NM	-111.03	33.62	733	115	-111.11	33.65	786	760	0.42	7.203	3/1/1989	8/31/1991	USFS
YELL1	Yellowstone NP	-110.69	44.97	1836	125	-110.65	44.95	1951	1894	1.54	4.285	6/1/1989	8/31/1993	NPS
YOSE2	Yosemite NP	-119.7	37.71	1608	236	-119.75	37.69	1475	1542	-1.71	4.468	12/1/1994		NPS
YOSE1	Yosemite NP	-119.7	37.71	1608	242	-119.73	37.7	1370	1489	-5.04	2.711	9/1/1988	11/30/1994	NPS

NM = National Monument
NP = National Park
WA = Wilderness Area

Integrating nephelometers measure the scattering of light over a defined band of visible wavelengths from an enclosed volume of air. Historically, integrating nephelometers used in most major field studies have underestimated scattering because of

1. modification of the ambient aerosol by heating when a large fraction of the sampled aerosol is hygroscopic;
2. inlet, sampling train, and optical chamber designs that limit the size of particles that make it into the sampling chamber;
3. optical geometry that causes a truncation of the true scattering volume;
4. and electronics that display large nonlinear drifts in zero and span values.

The Optec NGN-2 ambient integrating nephelometer was developed to minimize these limitations. The instrument, which measures light scattering at an effective wavelength of 550 nm, is described in some detail by Molenar et al. [1989]. It is an "open air" design that has minimal heating characteristics, and because it is open it allows a larger distribution of particle sizes to pass through the instrument. However, the cutpoint of the instrument has not been characterized. It is also designed with solid-state electronics that are very stable over wide temperature and humidity shifts. It still has an inherent limitation of an abbreviated acceptance angle in that it only samples light scattered between 5° and 175°. Calibration of the instrument and data validation and processing algorithms are also discussed in detail in Molenar and Malm [1992]. Unlike transmissometers, where an uncertainty in transmittance leads to an additive error in extinction, uncertainties in nephelometer calibration lead to a multiplicative error in measured scattering. Typical uncertainties for the Optec instrument are on the order of 5–10% [Molenar and Malm, 1992].

During high humidity and precipitation events, the nephelometer can report erroneously high scattering values. This is due to water condensing on the walls of the nephelometer and spray from rain drops impacting the screen on the nephelometer inlet. This water collects in the light trap and reflects light directly into the scattered-light detector, causing extremely high readings. In order to minimize this problem, the door of the nephelometer closes during heavy precipitation events, and a wick was added to the light trap to facilitate the removal of any collected water.

Table 1.5. IMPROVE nephelometer network site locations.

Site	Code	State	Latitude	Longitude	Elevation	Dates of Operation
Upper Buffalo WA	UPBU1	AR	35.83	-93.20	722	12/1991-present
Muleshoe Ranch	MUSR1	AZ	32.35	-110.23	1402	07/1997-present
Rucard Canyon	RUCA1	AZ	31.78	-109.30	1637	02/1997-05/2001
Indian Gardens	INGA1	AZ	36.08	-112.13	1166	10/1989-present
Sycamore Canyon	SYCA1	AZ	35.14	-111.97	2046	09/1991-07/1992
Hance Camp at Grand Canyon NP	GRCA2	AZ	35.97	-111.98	2267	09/1997-present
Sierra Ancha	SIAN1	AZ	34.09	-110.94	1600	02/2000-present
McFadden Peak	MCFD1	AZ	34.00	-111.00	2175	10/1997-02/2000
Phoenix	PHON1	AZ				12/1996-present
Estrella Mountain Regional Park	ESTR1	AZ	33.39	-112.38	290	
Petrified Forest NP	PEFO3	AZ	34.91	-109.80	1690	

Site	Code	State	Latitude	Longitude	Elevation	Dates of Operation
Tucson Central	TUCN1	AZ			762	04/1997-present
Tucson Mountain #1	TUMO1	AZ	32.28	-111.17	754	12/1996-present
Ike's Backbone	IKBA1	AZ	34.34	-111.68	1297	04/2000-present
Humble Mountain	HUMB1	AZ	33.98	-111.78	1586	03/1997-present
Mazatzal	MAZA1	AZ	33.91	-111.43	2164	03/1997-08/2000
Tucson	CRAY1	AZ	32.20	-110.88	1707	
Greer Arizona	GRER1	AZ	34.07	-109.43	2513	
Tucson Mountain #2	TUMO2	AZ				
Lake Tahoe Blvd.	LTBV1	CA	38.95	-118.04	1902	
Bliss SP (Tahoe Regional Planning Agency)	BLIS1	CA	38.98	-120.10	2130	11/1990-present
Mount Zirkel WA	MOZI1	CO	40.54	-106.68	3243	07/1994-present
Okefenokee NWR	OKEF1	GA	30.74	-82.13	48	09/1991-present
Cedar Bluff	CEBL1	KS	38.77	-99.76	665	
Mammoth Cave NP	MACA1	KY	37.13	-86.15	235	09/1991-present
Acadia NP	ACAD1	ME	44.38	-68.26	157	03/1988-present
Seney NWR	SENY1	MI	46.29	-84.05	216	
Boundary Waters Canoe Area	BOWA1	MN	47.95	-91.50	526	08/1991-present
Shining Rock WA	SHRO1	NC	35.39	-82.77	1617	07/1994-present
Great Gulf WA	GRGU1	NH	44.31	-71.22	453	06/1995-present
Brigantine NWR	BRIG1	NJ	39.47	-74.45	5	09/1991-present
Gila WA	GICL1	NM	33.22	-108.24	1775	04/1994-present
Jarbidge WA	JARB1	NV	41.89	-115.43	1869	03/1988-present
Quaker City	QUAK1	OH	39.94	-80.66	372	01/1900-present
Wichita Mountains	WIMO1	OK	34.73	-98.71	509	03/2001-present
Three Sisters WA	THSI1	OR	44.29	-122.04	885	07/1993-present
Cape Romain NWR	ROMA1	SC	32.94	-79.66	4	09/1994-present
Great Smoky Mountains NP	GRSM1	TN	35.63	-83.94	810	03/1988-present
Big Bend NP	BIBE1	TX	29.30	-103.18	1066	03/1988-present
Lone Peak WA	LOPE1	UT	40.44	-111.71	1768	12/1993-present
James River Face WA	JARI1	VA	37.63	-79.51	289	06/2000-present
Shenandoah NP	SHEN1	VA	38.52	-78.43	1079	03/1988-present
Virgin Islands NP	VIIS1	VI	18.34	-64.80	51	10/1990-present
Lye Brook WA	LYBR1	VT	43.15	-73.13	1015	09/1991-present
Snoqualmie Pass	SNPA1	WA	47.42	-121.43	1049	07/1993-present
Columbia River Gorge	CORI1	WA	45.66	-121.00	178	06/1993-present
Mount Rainier NP	MORA1	WA	46.76	-122.12	439	03/1988-present
Columbia River Gorge #2	COGO2	WA	45.57	-122.21	243	
Mayville	MAYV1	WI	43.44	-87.47	306	
Dolly Sods WA	DOSO1	WV	39.11	-79.43	1182	09/1991-present
Green River Visibility Study	GRVS1	WY	41.84	-109.61	1950	06/1996-10/2000

NP = National Park
NWR = National Wildlife Refuge
SP = State Park
WA = Wilderness Area

1.3 PROTOCOL AND EQUIPMENT CHANGES

While consistency through time is critical to a monitoring program interested in trends, changes in protocol are inevitable. Significant changes in sampling, analysis, and data processing have occurred in the history of the IMPROVE network. Most of the changes were

implemented to improve the quality or usefulness of the IMPROVE data set or to increase the overall effectiveness of the network within available resources. Some of the key changes, including the reasoning behind the decision and the ramifications for the IMPROVE data set, are described below and listed in Table 1.6.

1.3.1 Analytical Changes

1.3.1.1. Transition from PIXE to XRF

Elemental analysis was transitioned from proton induced X-ray emission (PIXE) to X-ray fluorescence (XRF) in two stages. The initial transition was elected to lower the mdl of parameters important to aerosol source apportionment. The first transition from PIXE to XRF using a Mo anode occurred in mid 1992 and applied to the analysis of elements with atomic weights from Fe to Pb. The second transition from PIXE to XRF using a Cu anode occurred in late 2001 and applied to the analysis of the lighter elements with atomic weights from Na to Mn. Also, in late 2001, the analysis of Fe was changed from Mo anode XRF to Cu anode XRF. These transitions had both positive and negative impacts on the data quality of the elemental measurements.

One of the positives was the improved detection limits for most elements of interest. Another positive development was the decreased filter degradation with the XRF system as compared to PIXE and PESA. The proton beam used for PIXE and PESA weakens the bonds in the Teflon filters. Over long exposures and high doses, the samples become brittle and will fall apart from small disturbances such as applying vacuum or vibration. Dependent on the filter loadings, a sample can be destroyed with as little as 100 seconds of proton exposure at 50 nano amps, which is a typical exposure condition for rural IMPROVE samples. This filter destruction places a limitation on the PIXE and PESA quality control system because it prevents the repeated reanalysis of the same samples. The option of reanalyzing the same batch of filters numerous times, either as part of a precision study or over time as a check on calibration drift, is a significant addition to the quality control measures of the IMPROVE program.

A negative impact of the move to XRF as compared to PIXE was poorer quantification of the lightest elements Na, Mg, and Al. This is because the number of X-rays detected for Na, Mg, Al, and to a lesser extent Si using the Cu XRF system is much lower than with PIXE. The physical configuration and operating procedures for the XRF systems have continued to evolve to address quality issues as they are identified.

1.3.1.2. Alternate Nylon Filter Extraction Procedure

The filter extraction process for ion analysis was changed from the basic anion eluent to deionized water. This was first done for three sites in 1997 to allow for NH_4^+ analysis (Table 1.6). Starting in 2001, deionized water was used for all sites for the same purpose. The transition dates and the affected sites are detailed in Table 1.6. Recent studies have shown that both extraction solutions are equally effective at extracting particulate nitrate from nylon filters when sonication is used [Yu et al., 2005].

1.3.2 Sampling Equipment Changes

1.3.2.1. Transition from Version I to Version II IMPROVE Sampler

As described in section 1.2, the IMPROVE sampler was modified to accommodate the transition from the twice-weekly, 24-hour duration sampling schedule to an every-third-day schedule, the addition of replicate sampling, and analysis for $PM_{2.5}$ mass and composition to evaluate precision. The new schedule corresponds to the schedule of the EPA's national particulate network operated by state and local governments. The updated sampler is comparable from a sample collection perspective but uses microprocessor technology to increase control and provide feedback on operating status. The changes were implemented into the network through the installation of version II samplers during late1999 through early 2001.

1.3.2.2. Denuder Coating Modified

The module B denuder coating was altered in 1996 to include glycerin to maintain the efficiency of the denuder for capturing SO_2 and HNO_3 gases for the entire year in which each denuder is deployed. The glycerin was expected to keep the denuder wet and thereby more reactive. Recent studies have shown that qualitatively comparable nitrate concentrations are collected with both the original and current denuder coatings [Ashbaugh et al., 2004; Yu et al., 2005]. The IMPROVE sampler B module inlet/denuder sampling train has been exposed to known concentrations of nitric acid in the laboratory, and nitric acid removal efficiencies have been shown to lie consistently between 98% and 99%.

1.3.2.3. Changes in Nylon Filter Size

Larger nylon filters (47 mm) were initially used to ensure that the pressure drop at the filter, which can impact sampler flow rate and thereby the cutpoint for the sample, was not too high. Improved filter quality allowed the move to smaller 25 mm filters in 1994 that were consistent in size with the other modules and, due to the smaller size, had smaller artifact corrections due to manufacturing contamination, all without negative impacts on pressure drop. In 1996, procuring nylon filters of sufficient quality at the 25 mm size became difficult. With the development of the version II sampler (deployment in 2000–2001), it was decided to increase the nylon filter size to 37 mm so that the sampler would experience less pressure drop. Tests involving collocated samples with 25 and 37 mm diameter filters showed qualitatively comparable nitrate concentrations [McDade et al., 2004].

1.3.2.4. Changes in Nylon Filter Manufacturer

Prior to 1996, IMPROVE purchased nylon filters from Pall/Gelman. However, since Pall/Gelman ceased manufacturing those filters in 1996, IMPROVE transitioned to MSI/Osmonics. Unfortunately, the MSI/Osmonincs filters exhibited increased and inconsistent contamination levels of all major ions (especially chloride) as compared to the Pall/Gelman filters. Pall/Gelman resumed manufacturing nylon filters, and after testing at Crocker Nuclear Laboratory (CNL) confirmed that the pressure drops and artifact-corrected ambient concentrations were statistically equivalent to the MSI/Osmonics filters, IMPROVE transitioned back to Pall/Gelman filters in January of 2004. The new Pall/Gelman filters have significantly

lower monthly median artifact values for all major ions as compared to both the MSI/Osmonics filters and the original Pall/Gelman filters.

1.3.3 Data Processing Changes

1.3.3.1. Change in the Reporting of Gravimetric Measurements

Beginning in 2002, it was decided that gravimetric measurements below measurement detection limit, even those less than 0, would be retained in the data set so as not to bias statistical analyses. With the resubmission of data for the period 2000–2004 in October 2005, below mdl gravimetric measurements were added back into the IMPROVE database for that period. This change made the decision-making process for the reporting of the gravimetric data set consistent with the speciation analyses.

1.3.3.2. Change in Batch Size Used in Data Processing Routines at CNL

In 2002 it was decided to change the batch size used in the data processing routines—blank corrections, data validation, and reporting—from seasonal quarters to months. The transition from seasonal quarters to months allowed for the release of a calendar year of data as soon as the December data were fully validated. The downsides of this protocol change include less robust blank correction and uncertainty statistics, noncompatibility with the existing filter storage system, and data management system inefficiencies in the XRF lab.

1.3.3.3. Change in Flow Rate Validation Flag Definitions

In 2005, flow rate validation flags were redefined to be more objective and quantitative in nature and make more complete use of the 15-minute flow rate data [McDade, 2005]. The new flags were adopted for future use and also applied to the 2000–2004 data so that they were determined quantitatively and consistently across the entire Regional Haze Rule 5-year base period. The data prior to 2000 do not use the new flow validation flags. The version I sampler did not collect 15-minute flow rate data, and thus the necessary data are not available to formulate the new flags for data prior to 2000.

1.3.3.4. Change in Flow Rate Calculations

Flow rates were recalculated for the 2000–2004 period to correct an error in the calculation that existed prior to January 2004 [McDade, 2005]. The flow calibration coefficients were incorrectly referenced to the temperature at the time of annual calibration rather than a standard temperature. The range of bias resulting from the calculation error extended from about a 5% high to about a 4% low, with over 80% of the instances falling within a bias of ±2%. A single calibration temperature was applied at each site for the entire period between calibrations, typically about a year. Thus the bias did not appear as random fluctuations but rather as offsets in annual blocks of data. The pre-2000 temperature data are not of sufficient quality to warrant applying the small calibration temperature correction.

1.3.3.5. Spectral Corrections to S and Al Data from the XRF Cu Anode System

In both PIXE and XRF analysis, sulfur is subject to a small positive interference from lead, and aluminum is subject to a small positive interference from bromine. The corrections are

S (corrected) = S - 0.74*Pb
Al (corrected) = Al - 0.62*Br

These corrections were initially not applied to the XRF data from December 2001 through 2004; the corrections were applied to the 2000–2004 redelivery and will be applied to future XRF data.

1.3.3.6. Change in the Reporting of Organic Pyrolyzed Carbon (OP) Concentrations

In the TOR carbon analysis, the sample is first heated in a non-oxidizing He atmosphere to volatilize the OC. During this phase of the analysis, some of the OC on the filter pyrolyzes to EC in the absence of O_2. The organic pyrolyzed carbon (OP) fraction corrects the OC and EC fractions for this pyrolyzed carbon. However, oxidizing minerals [Fung, 1990; Sciare et al., 2003], catalysts [Lin and Friedlander, 1988a,b] in the sampled aerosol, or oxygen leaks in the TOR analyzer can oxidize [Chow et al., 2005] EC, which can be released during the non-oxidizing phase of the TOR analysis. In these cases, the OP fraction can be negative. Previously, negative OP values were reported as 0. With the resubmission of the carbon analysis data for 2000–2004, the negative OP values were reported unmodified.

Approximately one in ten OP values was affected by this change [Chow et al., 2005]. This change in reporting procedure will also be applied to future data deliveries. While the OP correction could be applied to data prior to 2000, it was decided that this one small correction did not warrant the effort involved in reprocessing 12 years of data.

Table 1.6. Major network-wide changes in sampling, analysis and data reporting.

Change Date	Change Description
9/15/1990	Ion analysis contractor switched from Research Triangle Institute (RTI) to Global Geochemistry Company (GGC). Ion samples extracted using anion eluent.
6/1/1992	Analysis of elements with atomic weights from Fe to Pb was changed from PIXE to XRF by Mo anode, decreasing their minimum detection limits (mdl). The cyclotron time for the PIXE analysis was reduced increasing the mdl for elements below FE.
3/1/1994	Optical absorption measurement changed from Laser Integrating Plate Method (LIPM) to Hybrid Integrating Plate/Sphere Analysis (HIPS).
6/1994	Changed nylon filter size from 47mm diameter to 25mm.
4/1995-present	Began removing Module A filter masks, effectively changing the sample area from 2.2 sq. cm to 3.5 sq. cm. Transition still in progress as of the date of this writing.
5/23/1995	Ion analysis switched to Research Triangle Institute (RTI). Ion samples extracted using anion eluent.
1996	Added glycerin to Module B denuder. The new model denuders were installed during annual maintenance visits.
10/1996	Changed nylon filter manufactures from Gelman to MSI.
6/1/1997	Ion samples extracted using DI water at GRSM1, SHEN1, DOSO1. All other sites extracted with anion eluent.
1/28/1999	Ion samples extracted using DI water at all sites.
12/1999 - 4/2001	Transitioned the new and existing 110 IMPROVE sites to version II IMPROVE samplers.
4/2000 -1/2001	Changed nylon filter size from 25 mm to 37 mm.

Change Date	Change Description
10/11/2000	Ion samples extracted using anion eluent at all sites except GRSM1, SHEN1, and DOSO1 where extraction is with DI water.
4/5/2001	Ion samples extracted using DI water at all sites.
12/1/2001	Analysis of elements with atomic weights from Na to Mn was changed from PIXE to XRF by Cu anode.
2002	Started reporting below-mdl gravimetric measurements.
6/1/2002	Changed from quarterly to monthly medians to estimate artifact corrections from field blanks & secondary filters.
10/1/2002	Standardized XRF run times at 1000 seconds.
3/2003	Installation of collocated extra modules began.
11/2003	Installation of collocated modules with Speciated Trends Network began.
1/2004	Changed module B filter supplier from Osmonics to Pall-Gelman.
9/2004	Changed from monthly to quarterly medians to estimate artifact corrections from field blanks & secondary filters.
10/2005	Redelivery of 2000–2004 data to back-correct data for several data processing changes including new definitions of the flow rate validation flags, a correction to the flow rate calculation, a correction to the XRF results, and a change in the way negative OP fractions were reported.

1.4 THE COMPARISON OF CONCENTRATIONS FROM COLLOCATED IMPROVE AND STN MONITORING SITES

Chapters 2 and 3 examine the annual spatial patterns and the seasonal patterns of the major fine aerosol constituents from 159 IMPROVE sites from 2000 through 2004. The IMPROVE network collects samples in primarily remote rural areas, thus providing little information on the aerosol composition and concentrations in and near population centers. To fill in these gaps, data from the EPA's Speciated Trend Network (STN) from 84 sites were incorporated into the spatial and seasonal pattern analyses. The STN collects speciated aerosol data similar to the IMPROVE network, but the sites are located primarily in urban/suburban settings. Incorporation of the STN data extends the spatial aerosol patterns from the surrounding remote areas into urban areas, providing insights into the fraction of the particulate matter (PM) that is contributed by regional and local sources.

IMPROVE and the STN both collect 24-hour $PM_{2.5}$ samples on similar filter media on a 1-in-3-day sampling schedule for quantifying $PM_{2.5}$ mass and its chemical constituents. Both networks use similar gravimetric analysis for quantifying $PM_{2.5}$ mass, ion chromatography for NO_3^- and $SO_4^=$, and XRF for elements including S, Al, Fe, Ca, Si, and Ti. However, IMPROVE uses thermal optical reflectance (TOR) to measure carbon, and the STN uses thermal optical transmittance (TOT). These two techniques are known to produce similar total carbon concentrations but different splits between OC and light-absorbing carbon (LAC) concentrations. The TOR analysis generally has higher LAC concentrations than the TOT technique. IMPROVE and the STN also use different samplers and different standard operating procedures for sample collection and analysis and maintain independent quality assurance programs.

The two networks have collocated IMPROVE and STN samplers in several urban and rural locations. These collocated data were compared to identify potential biases between the annual IMPROVE and STN concentrations that could impact the interpretation of results from the combined data sets. This was done using data from six collocated sites in 2002 and five collocated sites in 2003. For each site and year, annual averages of the major particulate

composite components were calculated, resulting in 11 pairs of annual average values for each particulate component. The calculation of the composite components and their aggregation are described in Chapter 2. A summary of the results for $PM_{2.5}$ and the major particulate composite components are presented in Table 1.7. Appendix E provides a detailed analysis of the differences between a subset of the IMPROVE and STN measured species. Note that the STN does not generally blank correct the OC concentration to account for positive artifacts, but IMPROVE does. The EPA has developed OC adjustments for the STN concentrations to correct for the positive artifacts. The STN OC concentrations used in this analysis were adjusted for the carbon artifact. Appendix E contains a comparison of the unadjusted STN and IMPROVE carbon concentrations.

As shown in Table 1.7, the errors between the annual average values were 16% or smaller for all parameters except fine soil, which was 35%. The bias was 1.3% or smaller for $PM_{2.5}$, ammonium sulfate, ammonium nitrate, and organics. However, the bias for LAC was -10.4%, indicating the IMPROVE annual average LAC is 10% greater than for the STN. For the fine soil, the IMPROVE annual average concentrations were 30% greater than for the STN.

The spatial and seasonal analyses in Chapters 2 and 3 used 5-year average values. Therefore, the random error between the IMPROVE and STN data will likely be smaller than reported in Table 1.7. This, combined with the fact that $PM_{2.5}$, ammonium sulfate, ammonium nitrate, and organics have small biases, indicates that the IMPROVE and STN data are sufficiently similar to combine the data. These results indicate that the STN LAC concentrations will be systematically smaller than IMPROVE's by about 10%. This bias needs to be considered when comparing the IMPROVE and STN concentrations. The 30% bias in the fine soil is sufficiently large that the combined fine soil patterns should be treated as suspect.

Table 1.7. Comparison of annual average concentrations between collocated IMPROVE and STN monitoring sites.

	$PM_{2.5}$	Ammonium Sulfate	Ammonium Nitrate	Organics	Light Absorbing Carbon	Fine Soil
Average IMPROVE ($\mu g/m^3$)	9.1	3.3	1.1	4.0	0.6	1.4
Average STN ($\mu g/m^3$)	9.2	3.2	1.0	4.1	0.5	0.9
[1]Error (%)	8.3	5.5	13.2	16.0	15.9	35.5
[2]Bias (%)	1.3	-0.6	-0.5	-0.8	-10.4	-30.8

[1] $Error = median\left(\left|\frac{\overline{X_i} - \overline{Y_i}}{\overline{Y_i}}\right|\right)$ where $\overline{X_i}$ and $\overline{Y_i}$ are the annual average STN and IMPROVE concentrations, respectively.

[2] $Bias = \frac{1}{N}\sum_{i}^{N}\frac{\overline{X_i} - \overline{Y_i}}{\overline{Y_i}}$ where N is the number of annual average concentrations.

REFERENCES

Ashbaugh, L. L., C. E. McDade, W. H. White, P. Wakabayashi, J. L. Collett Jr., and X-Y Yu (2004), Efficiency of IMPROVE network denuders for removing nitric acid, presented at Regional and Global Perspectives on Haze: Causes, Consequences and Controversies-Visibility Specialty Conference, Air & Waste Management Association, Asheville NC, October 25-29.

Chow, J. C., J. G Watson, L. C. Pritchett, W. R. Pierson, C A. Frazier, and R G. Purcell (1993), The DRI thermal/optical reflectance carbon analysis system: description, evaluation, and applications in U.S. air quality studies, *Atmos. Environ*., ***27(A)***(8), 1185-1201.

Chow, J. C., J. G.Watson, L.-W. A. Chen, M.-C. O. Chang, and G. Paredes-Miranda (2005), Comparison of the DRI/OGC and model 2001 thermal/optical carbon analyzers, http://vista.cira.colostate.edu/improve/Publications/GrayLit/013_CarbonAnalyzer/IMPROVECarbonAnalyzerAssessment.pdf.

Dietrich, D.L., J. D. Molenar, and J. F. Faust (1989), Transmissometer extinction measurements in an urban environment, In *Visibility and Fine Particles*, C.V. Mathai, Ed., AWMA, Pittsburgh, pages 374-383.

Eldred, R. A., L. L. Ashbaugh, M. L. Pitchford, and W. C. Malm (2001), Spatial trends from the expanded IMPROVE network, presented at Regional Haze and Global Radiation Balance--Aerosol Measurements & Models: Closure, Reconciliation & Evaluation, A&WMA, Bend OR, October.

Fung, K. K. (1990), Particulate carbon speciation by MnO_2 oxidation, *Aerosol Sci. Technol. 12*(1), 122-127.

Hand, J. L., and W. C. Malm (2006), Review of the IMPROVE equation for estimating ambient light extinction coefficients, http://vista.cira.colostate.edu/improve/Publications/GrayLit/016_IMPROVEeqReview/IMPROVEeqReview.htm.

Joseph, D. B., J. Metsa, W. C. Malm, and M. L. Pitchford (1987), Plans for IMPROVE: a federal program to monitor visibility in class I areas, In: *Visibility Protection: Research and Policy Aspects*, P.S. Bhardwaja (Ed.), APCA, Pittsburgh PA.

Lin, C., and S. K. Friedlander (1988a), Soot oxidation in fibrous filters. 1. Deposit structure and reaction mechanisms, *Langmuir, 4*(4), 891-898.

Lin, C., and S. K. Friedlander (1988b), Soot oxidation in fibrous filters. 2. Effects of temperature, oxygen partial pressure, and sodium additives; *Langmuir, 4*(4), 898-903.

Malm, W. C., K. A. Gebhart, D. A. Latimer, T. A. Cahill, R. A. Eldred, R. Pielke, R. Stocker, and J. Watson (1989), National Park Service Report on the Winter Haze Intensive Tracer Experiment, Final Report, 1989.

Malm, W. C., J. F. Sisler, D. Huffman, R. A. Eldred, and T. A. Cahill (1994), Spatial and seasonal trends in particle concentration and optical extinction in the United States, *J. Geo. Res*., *99*(D1), 1347-1370.

Malm, W. C., J. F. Sisler, M. L. Pitchford, M. Scruggs, R. Ames, S. Copeland, K. A. Gebhart, and D. E. Day (2000), IMPROVE (Interagency Monitoring of Protected Visual Environments): Spatial and seasonal patterns and temporal variability of haze and its constituents in the United States: Report III, CIRA Report ISSN: 0737-5352-47, Colo. State Univ., Fort Collins.

McDade, C. E., R. A. Eldred, and L. L. Ashbaugh (2004), Artifact corrections in IMPROVE, internal report.

McDade, C. E. (2005), Data redelivery summary, http://vista.cira.colostate.edu/improve/Publications/GrayLit/018_IMPROVEDataResubmission/DataRedeliverySummary2005.pdf.

Molenar, J. F, D. L. Dietrich, and R. M. Tree (1989), Application of a long-range transmissometer to measure the ambient atmospheric extinction coefficient in remote pristine environments, In *Visibility and Fine Particles*, C.V. Mathai, Ed., AWMA, Pittsburgh, 374-383.

Molenar, J. F., and W. C. Malm (1992), Ambient optical monitoring techniques, presented at the Conference on Visibility and Fine Particles, Vienna, Austria, September.

Sciare, J., H. Cachier, K. Oikonomou, P. Ausset, R. Sarda-Esteve, and N. Mihalopoulos (2003), Characterization of carbonaceous aerosols during the MINOS campaign in Crete, July-August 2001: A multi-analytical approach, *Atmos. Chem. Phys., 3*, 1743-1757.

Sisler, J. F. (1996), Spatial and seasonal patterns and long term variability of the composition of the haze in the United States: An analysis of data from the IMPROVE network, Cooperative Institute for Research in the Atmosphere, Colorado State University, ISSN 0737-5352-32.

The Wilderness Act, Public Law 88-577 (1964), 16 USC section 1131.

Turpin, B. J., P. Saxena, and E. Andrews (2000), Measuring and simulating particulate organics in the atmosphere: problems and prospects, *Atmos. Environ., 34*, 2983-3013.

U.S. EPA (1999), Regional Haze Regulations; Final Rule, 40 CFR 51, Federal Register, 64, 35714-35774.

Yu, X-Y., T. Lee, B. Ayres, S. M. Kreidenweis, J. L. Collett, Jr., and W. C. Malm (2005) Particulate nitrate measurement using nylon filters, *J. Air Waste Manage. Assoc., 55*, 1100-1110.

CHAPTER 2: SPATIAL DISTRIBUTIONS OF RECONSTRUCTED MASS AND MASS BUDGETS AND RECONSTRUCTED LIGHT EXTINCTION AND LIGHT-EXTINCTION BUDGETS

INTRODUCTION

The fine aerosol species at most IMPROVE sites can be classified into five major types: sulfates, nitrates, organics, light-absorbing carbon, and soil. However, at coastal locations such as the Virgin Islands and Brigantine, sea salt can be an important contributor to fine mass concentrations. The standard methods for apportionment of measured mass to the various aerosol species and the assumptions involved in those calculations are reviewed in section 2.1.

Atmospheric light extinction is a fundamental metric used to characterize air pollution impacts on visibility. It is the fractional loss of intensity in a light beam per unit of distance due to scattering and absorption by the gases and particles in the air. Light extinction (b_{ext}) can be expressed as the sum of light scattering by particles (b_{sp}), scattering by gases (b_{sg}), absorption by particles (b_{ap}), and absorption by gases (b_{ag}). The model used to reconstruct the light extinction coefficient from aerosol measurements and other visibility metrics for the sites are presented and examined below in section 2.2.

Spatial trends in reconstructed fine mass and the mass attributed to each of the major aerosol types are examined for the IMPROVE network and the IMPROVE and STN networks in section 2.4. The spatial trends in particulate extinction and the percent extinction attributed to each of the major aerosol types are examined in section 2.5 for the IMPROVE network and the IMPROVE and STN networks.

2.1 ESTIMATION OF AEROSOL SPECIES MASS

Table 2.1 presents the standard equations used in the IMPROVE program and those used in this report for estimating the aerosol species concentrations. The methodology behind those formulas and the limitations of the reconstructed fine mass (RCFM) aerosol model are discussed below.

The molecular form of sulfate depends on its degree of neutralization, for which routine measurements of the ammonium ion are required. The IMPROVE network does not measure the NH_4^+ ion, and there are inherent sampling issues with respect to ammonium measurements [Hand and Malm, 2006]. The molar ratio of ammonium to sulfate ranges from 2 for fully neutralized ammonium sulfate to 0 for sulfuric acid. Many authors have shown that aerosol sulfate acidity can vary temporally and spatially. Acidic aerosols have been measured at many locations throughout the United States [Gebhart et al., 1994; Liu et al., 1996; Day et al., 1997; Lowenthal et al., 2000; Lefer and Talbot, 2001; Quinn et al., 2002; Chu, 2004; Hogrefe et al., 2004; Schwab et al., 2004; Tanner et al., 2004; Zhang et al., 2005]. Special studies at IMPROVE sites have also demonstrated variability. At Great Smoky Mountains National Park during the summer of 1995 (Southeastern Aerosol and Visibility Study, SEAVS), ammonium-to-sulfate molar ratios of 1.1 were observed [Hand et al., 2000]. During the Big Bend Regional Aerosol

and Visibility Observational (BRAVO) study at Big Bend National Park, Lee et al. [2004] found ammonium-to-sulfate molar ratios of 1.54 on average. On average, fully neutralized ammonium sulfate was measured at Yosemite National Park during the summer of 2002 [Malm et al., 2005]. Seasonal and spatial variations in aerosol acidity complicate the selection of a single form of ammoniated sulfate, and regular measurements of the NH_4^+ ion at IMPROVE sites do not exist. Because the ammonium ion is not routinely measured in the IMPROVE program, sulfates will be assumed to be in the form of ammonium sulfate for the purpose of examining general spatial and temporal trends in sulfate aerosol mass concentrations.

Nitrate aerosols are assumed to be in the form of ammonium nitrate, but special studies have shown that at some locations fine nitrates are the fine tail of the coarse particle nitrate size distribution, such as sodium or calcium nitrate that has resulted from the reaction of nitric acid vapor with sea salt or soil dust [Malm et al., 2003; Lee et al., 2004; Hand and Malm, 2006]. The form of nitrate is difficult to predict since it depends on a number of factors including temperature, relative humidity, the presence of other aerosol species, and the cutpoint of the impactor [Hand and Malm, 2006]. Furthermore, Hand and Malm [2006], in a special study involving speciated and size-resolved aerosol samples from several IMPROVE sites, found that when fine mode total nitrate concentrations were roughly greater than 0.5 $\mu g/m^3$, ammonium nitrate contributed over 70% of the observed total nitrate in the fine mode. Given that the measurements necessary to accurately determine the form of ammonium nitrate are unavailable and the indication that higher levels of nitrate in the fine mode are probably associated with NH_4NO_3, assuming that nitrate is in the form of ammonium nitrate is reasonable for reconstructing fine mass.

An average ambient particulate organic compound is assumed to have a constant fraction of carbon by weight. Historically in the IMPROVE program, organic carbon mass concentration (OMC) from module C was assumed to be [OMC] = 1.4[OC], where OC is organic carbon as determined by thermal optical reflectance (TOR). The value of 1.4 was based on an experiment conducted by Grosjean and Friedlander [1975] in urban Pasadena, California, in 1973. They found that the carbon content of these samples averaged 73%. White and Roberts [1977] suggested an OC to OMC conversion factor (OMC/OC) of 1.4 based on this data, and this value was incorporated into the IMPROVE reconstructed fine mass equation. More recently, the ratio of OMC to OC used by IMPROVE has been changed to a value of 1.8, based on the suggestion of Hand and Malm [2006] and the studies summarized therein indicating that a correction factor of 1.4 is probably unreasonably low for the IMPROVE network and that 1.8 is a reasonable consensus value based on the available data.

Soil taxonomy charts show variability across the United States with soil type, with the southwestern United States differing from the eastern United States and many finer differentiations beyond that. Soil composition can also vary due to long-range intercontinental and transcontinental transport. Several studies have shown that contributions of Asian dust to U.S. fine soil aerosol concentrations can be significant episodically, affecting aerosol concentrations and mineralogy across the United States in the spring [VanCuren and Cahill, 2002; Jaffe et al., 2003; VanCuren, 2003; DeBell et al., 2004]. In the late spring to midsummer, transport of North African dust to the United States occurs regularly, affecting aerosol concentrations in the Virgin Islands, the eastern United States [Perry et al., 1997; Prospero, 1999], and even as far west as Big Bend National Park [Hand et al., 2002]. Due to the spatial

and temporal variability in dust sources, it is very difficult to characterize an appropriate aerosol soil composition for each measurement site. Soil mass concentrations are therefore estimated by a general method that sums the oxides of elements that are typically associated with soil (Al_2O_3, SiO_2, CaO, K_2O, FeO, Fe_2O_3, TiO_2), with a correction for other compounds such as MgO, Na_2O, H_2O, and carbonates [Malm et al., 1994]. The soil K is estimated from the Fe and Fe/K ratios because of the nonsoil K contributions from other sources, including smoke. Elemental concentrations are multiplied by factors that represent the mass concentrations of the oxide forms, with several corrections made to account for the previously mentioned compounds.

Coarse mass concentrations (CM) are estimated by differencing the PM_{10} mass measurement and the $PM_{2.5}$ measurement. Deviations from the nominal flow rate due to filter clogging from high aerosol loading and other operational problems can cause the cutpoint of the $PM_{2.5}$ A module to vary and affect which modes of the size distribution are being classified as fine and coarse.

Because Teflon filters are prone to losses of semivolatile NH_4NO_3 and thus provide only a lower estimate of the actual ambient aerosol concentrations, comparisons of reconstructed fine mass using the IMPROVE equation and gravimetric fine mass can be highly affected. Other factors such as retained water on the Teflon filter can also impact reconstructed fine mass to gravimetric fine mass comparisons.

Table 2.1. IMPROVE equations.

Aerosol Type	Traditional IMPROVE Equation	Revised Equation	Assumptions
Ammonium Sulfate	4.125*[S]	Same	All elemental S is from sulfate. All sulfate is in the form of ammonium sulfate.
Ammonium Nitrate	1.29*[NO_3]	Same	Denuder efficiency is close to 100% for HNO_3. All nitrate is in the form of ammonium nitrate.
Organic Mass by Carbon (OMC)	1.4*[OC]	1.8*[OC]	Average organic molecule is 55% (70% for the 1.4 correction factor) carbon.
Light-Absorbing Carbon (LAC)	[LAC]	Same	
STN Light-absorbing Carbon (LAC_STN)	NA	[LAC_STN]	
Adjusted STN Organic Carbon (OC_STN)	NA	[OC_STN]-[blank correction]	Organic carbon from STN NIOSH adjusted for method specific blank correction.
Total Carbon	NA	[OC]+[LAC] or [OC_STN]+[LAC_STN]	No organic carbon correction.

Aerosol Type	Traditional IMPROVE Equation	Revised Equation	Assumptions
Soil	2.2*[Al]+2.49*[Si]+1.63*[Ca]+ 2.42*[Fe]+1.94*[Ti]	same	Soil potassium=0.6*[Fe] FeO and Fe_2O_3 are equally abundant. A factor of 1.16 is used for MgO, Na_2O,H_2O, CO_3.
Reconstructed Fine Mass	[Ammonium Sulfate]+ [Ammonium Nitrate]+[LAC]+[OMC]+ [Soil]	same	Represents dry ambient fine aerosol mass. Comparability of OC and OC_STN.
Coarse Mass	[PM_{10}]-[$PM_{2.5}$]	Same	A $PM_{2.5}$ cut point on the fine mass sample. A PM_{10} cut point on the coarse mass sample.

2.2 RECONSTRUCTING LIGHT EXTINCTION FROM AEROSOL MEASUREMENTS

The light-extinction coefficient, b_{ext} (expressed as inverse megameters, Mm^{-1}), is the sum

$$b_{ext} = b_{scat} + b_{abs} = b_{sg} + b_{sp} + b_{ag} + b_{ap} \quad (2.1)$$

where b_{scat} is the sum of scattering by gases and scattering by particles, and b_{abs} is the sum of absorption by gases and particles. Light extinction due to the gaseous components of the atmosphere are relatively well understood and well estimated for any atmospheric condition. Absorption of visible light by gases in the atmosphere is primarily by NO_2 and can be directly and accurately estimated from NO_2 concentrations by multiplying by the absorption efficiency. Scattering by gases, b_{sg}, is described by the Rayleigh scattering theory [van de Hulst, 1981]. Rayleigh scattering depends on the density of the atmosphere; the highest values are at sea level (about 12 Mm^{-1}) and they diminish with elevation (8 Mm^{-1} at about 12,000′) and vary somewhat at any elevation due to atmospheric temperature and pressure variations. Rayleigh scattering can be accurately determined for any elevation and meteorological condition.

Particle light extinction is more complex than that caused by gaseous components. Light-absorbing carbon (e.g., diesel exhaust soot and smoke) and some crustal minerals are the only commonly occurring airborne particle components that absorb light. All particles scatter light, and, generally, particle light scattering is the largest of the four light extinction components. If the index of refraction as a function of particle size is well characterized, Mie theory can be used to accurately calculate the light scattering and absorption by those particles. However, it is rare that these particle properties are known, so assumptions are used in place of missing information to develop a simplified calculation scheme that provides an estimate of the particle light extinction from the available data set.

2.2.1 Extinction Model

The traditional IMPROVE algorithm for estimating light extinction from IMPROVE particle monitoring data assumes that absorption by gases (b_{ag}) is 0, that Rayleigh scattering (b_{sg}) is 10 Mm^{-1} for each monitoring site regardless of site elevation and meteorological condition, and that particle scattering and absorption (b_{sp} and b_{ap}) can be estimated by multiplying the concentrations of each of six major components by typical component-specific light extinction efficiencies. The component extinction efficiency values are constants, except for the sulfate and nitrate extinction efficiency terms that include a water growth factor that is a function of relative humidity (displayed as f(RH)), multiplied by a constant dry extinction efficiency. Expressed as an equation, the algorithm used in this report for estimating light extinction from IMPROVE data takes the following form where the particle component concentrations are indicated in the brackets. The formulas for the composite components are given in section 2.1.

$$\begin{aligned} b_{ext} \approx\ & 3 \times f(RH) \times [Ammonium\ Sulfate] \\ & + 3 \times f(RH) \times [Ammonium\ Nitrate] \\ & + 4 \times [Organic\ Mass] \\ & + 10 \times [Elemental\ Carbon] \\ & + 1 \times [Fine\ Soil] \\ & + 0.6 \times [Coarse\ Mass] \\ & + 10 \end{aligned} \qquad (2.2)$$

The units for light extinction and Rayleigh scattering are inverse megameters (Mm^{-1}); component concentrations shown in brackets are in microgram per meter cubed ($\mu g/m^3$); dry efficiency terms are in units of meters squared per gram (m^2/g); and the water growth terms, f(RH), are unitless.

Among the implicit assumptions for this formulation of the algorithm are that

- the six particle component terms plus a constant Rayleigh scattering term are sufficient for a good estimate of light extinction;

- constant dry extinction efficiency terms rounded to one significant digit for each of the six particle components (e.g., for both sulfate and nitrate the value is 3) works adequately for all locations and times; and

- light extinction contributed by the individual particle components can be adequately estimated as separate terms, as they would be if they were in completely separate particles (externally mixed), though they often are known to be internally mixed in particles.

A relatively simple algorithm for estimating light extinction using only the available monitoring data requires assumptions such as these.

The issue of estimating aerosol optical properties from bulk aerosol measurements that do not allow for determining the mixing state of the aerosol has been addressed. Ouimette and

Flagan [1982] have shown that, from basic theoretical considerations, if an aerosol is mixed externally, or if in an internally mixed aerosol the index of refraction is not a function of composition or size, and the aerosol density is independent of volume, then

$$b_{ext} = \sum_i \alpha_i m_i \tag{2.3}$$

where α_i is the specific scattering or absorption efficiency and m_i is the mass of the individual species.

Furthermore, Malm and Kreidenweis [1997] demonstrated from a theoretical perspective that specific scattering of mixtures of organics and sulfates were insensitive to the choice of internal or external mixtures. Sloane [1983, 1984, 1986], Sloane and Wolff [1985], and more recently, Lowenthal et al. [1995], Malm et al. [1997], and Malm [1998] have shown that differences in estimated specific scattering between external and internal model assumptions are usually less than about 10%. In the absence of a detailed microphysical and chemical structure of ambient aerosols, the above studies demonstrate that a reasonable estimate of aerosol extinction can be achieved by assuming each species is externally mixed.

Implicit to the extinction model is an assumed linear relationship between aerosol mass and extinction. It is well known that sulfates and other hygroscopic species form solution droplets that increase in size as a function of relative humidity (RH). Therefore, if scattering is measured at various relative humidities, the relationship between measured scattering and hygroscopic species mass can be quite nonlinear. The approach of Gebhart and Malm [1989] and Malm et al. [1989] for estimating the effect of RH on aerosol scattering is the basis for the method employed in the IMPROVE extinction model. In their approach, the hygroscopic species are multiplied by a relative humidity scattering enhancement factor, f(RH), that is calculated on a sampling-period-by-sampling-period basis using Mie theory and an assumed size distribution and laboratory-measured aerosol growth curve. However, because the growth factor and light-scattering efficiency for ambient aerosols have previously been observed to be rather smooth [Waggoner et al., 1981; Sloane 1983, 1984, 1986; Wexler and Seinfeld, 1991; Day et al., 2000; Malm et al., 2000a], the laboratory growth curves, as measured by Tang [1996], were smoothed between the deliquescence and crystallization points to obtain a “best estimate" for the sulfate and nitrate species growth (Figure 2.1).

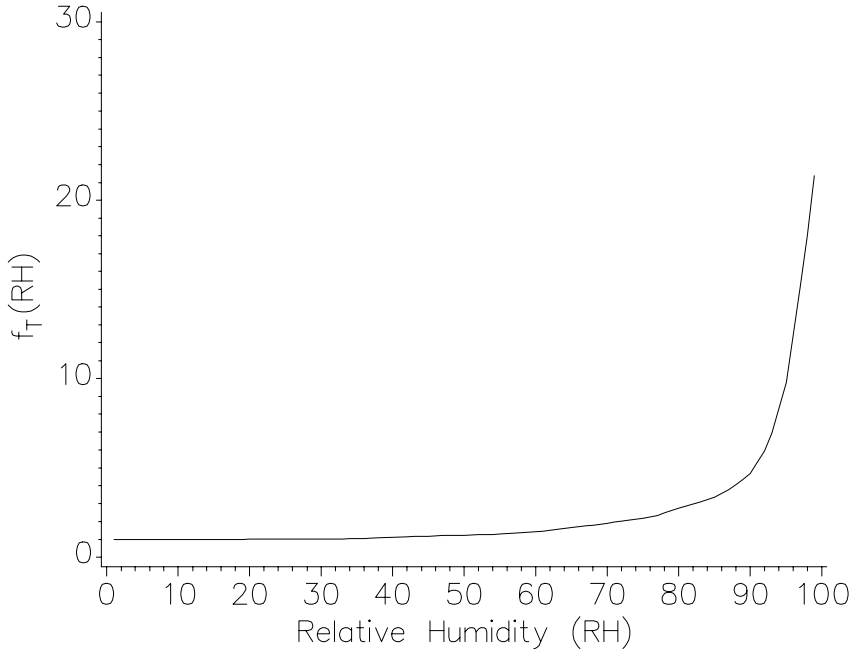

Figure 2.1. RH factors (f_T (RH)) derived from Tang's ammonium sulfate growth curves smoothed between the crystallization and deliquescence points.

For the data used in this report, the f(RH) values for each sample are calculated using the algorithm outlined in the Regional Haze Rule Guidelines for Tracking Progress [U.S. EPA, 2003]. Under this algorithm, f_{SO4}(RH) values for each sampling period are calculated by assuming a typical site-specific RH value, a lognormal sulfate mass size distribution with a geometric mass mean diameter of 0.3 μm and a geometric standard deviation, σ_g, of 2.0, and growth curves that are smoothed between the crystallization and deliquescence points. The f_{NO3}(RH) associated with nitrates is assumed to be the same as for sulfates, while f_{org}(RH) for organics is set equal to 1.0.

Month-specific climatological mean RH values were chosen to eliminate the confounding effects of interannual variations in relative humidity while maintaining typical regional and seasonal humidity patterns. The EPA produced a lookup table with recommended monthly f(RH) values for each Class I area based on analysis of a 10-year record (1988–1997) of hourly relative humidity data from 292 National Weather Service stations across the 50 states and the District of Columbia, as well as from 29 IMPROVE and IMPROVE protocol monitoring sites, 48 Clean Air Status and Trends Network (CASTNet) sites, and 13 additional sites administered by the National Park Service. The daily ammonium sulfate and ammonium nitrate extinction coefficients for each site are calculated using this lookup table.

In a recent review, estimates of particle scattering by the IMPROVE algorithm (i.e., excluding the light-absorbing carbon and Rayleigh terms) were compared to directly measured particle scattering data at the 21 monitoring sites that have hourly averaged nephelometer and relative humidity data [IMPROVE technical subcommittee for algorithm review, 2006]. The results indicated that the algorithm performed reasonably well over a broad range of particle light scattering values and monitoring locations. However, the algorithm does tend to underestimate

the highest extinction values and overestimate the lowest extinction values. A revised algorithm that reduces these biases has recently been approved by the IMPROVE steering committee as an alternative method for calculating reconstructed extinction. The new algorithm with revised terms in bold has the following form:

$$
\begin{aligned}
b_{ext} \approx\ & \\
& 2.2 \times f_s(RH) \times [\text{Small Sulfate}] + 4.8 \times f_L(RH) \times [\text{Large Sulfate}] \\
& + 2.4 \times f_s(RH) \times [\text{Small Nitrate}] + 5.1 \times f_L(RH) \times [\text{Large Nitrate}] \\
& + 2.8 \times [\text{Small Organic Mass}] + 6.1 \times [\text{Large Organic Mass}] \\
& + 10 \times [\text{Elemental Carbon}] \\
& + 1 \times [\text{Fine Soil}] \\
& + 1.7 \times f_{ss}(RH) \times [\text{Sea Salt}] \\
& + 0.6 \times [\text{Coarse Mass}] \\
& + \text{Rayleigh Scattering (Site Specific)} \\
& + 0.33 \times [NO_2 \text{ (ppb)}]
\end{aligned}
\qquad (2.4)
$$

The apportionment of the total concentration of sulfate compounds into the concentrations of the small and large size fractions is accomplished using the following equations:

$$[\text{Large Sulfate}] = \frac{[\text{Total Sulfate}]}{20\ \mu g/m^3} \times [\text{Total Sulfate}], \text{ for } [\text{Total Sulfate}] < 20\ \mu g/m^3$$

$$[\text{Large Sulfate}] = [\text{Total Sulfate}], \text{ for } [\text{Total Sulfate}] \geq 20\ \mu g/m^3$$

$$[\text{Small Sulfate}] = [\text{Total Sulfate}] - [\text{Large Sulfate}]$$

The same equations are used to apportion total nitrate and total organic mass concentrations into the small and large size fractions. The algorithm used for calculating the new terms and the technical justification of the changes are detailed here: http://vista.cira.colostate.edu/improve/Publications/GrayLit/019_RevisedIMPROVEeq/RevisedIMPROVEAlgorithm3.doc.

Comparisons of the revised and original IMPROVE extinction algorithms indicated that the composition associated with the average best and worst haze days was fairly insensitive to algorithm selection [IMPROVE technical subcommittee for algorithm review, 2006]. Therefore only results utilizing the original algorithm, modified to include the new organic mass to organic carbon ratio, are shown here. Speciated extinction values calculated using the new and original algorithm are available from the IMPROVE website at http://vista.cira.colostate.edu/views/Web/Data/DataWizard.aspx. Interested readers can explore both data sets by either downloading the data for themselves or utilizing the data exploration tools provided by the VIEWS website at http://vista.cira.colostate.edu/views/Web/General/AnnualSummary.aspx.

Visibility, expressed as the reconstructed deciview (dv), is calculated from the reconstructed total extinction values. The dv is a visibility metric based on the light extinction coefficient that expresses incremental changes in perceived visibility [Pitchford and Malm, 1994]. Because the dv expresses a relationship between changes in light extinction and perceived visibility, it can be useful in describing visibility trends. A 1-dv change is about a 10% change in extinction coefficient, which is a small but perceptible scenic change under many circumstances. The dv is defined by the following equation:

$$dv = 10\,\mathbf{ln}(b_{ext}/10) \tag{2.5}$$

The dv scale is near 0 for pristine atmosphere (dv = 0 for Rayleigh condition at about 1.8 km elevation) and increases as visibility is degraded.

2.3 COMPLETENESS CRITERIA

For the following analyses, data from a particular site are only included if they meet certain completeness criteria. The completeness criteria used in Chapters 2 and 3 of the report are designed to ensure that as many sites as possible are included in the analyses without jeopardizing the robustness or representativeness of the results. These criteria are not the same criteria as applied under Regional Haze Rule guidelines, which have different objectives than this report. The goal of these analyses was to look at general trends in the central tendency of the aerosol parameters, rather than analyzing the individual days that make up the worst and best haze days.

Since results are supposed to be representative of the 5-year period 2000–2004, it was decided that the equivalent of two-fifths of the potential samples, or ~2 years' worth, needed to be valid for the site to be considered complete. Furthermore, similar criteria are applied to each of the four seasons, ensuring that the annual averages are not overly biased by exclusion of samples from a particular season. A site was required to have its first valid sample on or before 1 February 2003 to be included in the following analyses, figures, and tables. Additionally, it was required that each seasonal bin have at least 50 valid samples. Seasonal distribution of the valid samples beyond the minimum per bin was not examined. These criteria are applied at the parameter level, not the record level, e.g., completeness is assessed for organic carbon independently of sulfate or any other parameter of interest. These requirements are a slight departure from similar analyses reported in prior IMPROVE reports where filtering only took into account the start date of the site in question.

In keeping with the parameter-level application of completeness criteria, the sorting and aggregation of data by time and space are also conducted at the parameter level. This process and its implications are detailed in Malm et al. [2000b] and will be described here briefly. As an example, the calculation of the average RCFM for Acadia for the 2000–2004 period will be used to illustrate this topic. Two approaches can be taken in calculating this "average", the sum of the averages or the average of the sums:

1) $Avg(RCFM)=Avg(NO_3)+ Avg(SO_4)+ Avg(OMC)+ Avg(LAC)+ Avg(SOIL)$

2) $Avg(RCFM)= Avg(NO_3+SO_4+OMC+LAC+SOIL)$

The second approach, the average of the sums, requires that each sample day be complete, with valid measurements for all five major parameters for inclusion in the 5-year average. The problems with using the stricter completeness criteria dictated by approach 2 include unacceptably small sample sizes in some data aggregates and the exclusion of some records where very high or low aerosol concentrations have resulted in invalid values for a subset of the parameters. The analyses in this report make use of the first equation since it includes all valid samples for a parameter regardless of the sampling completeness for an individual date, and in that sense the data aggregates more accurately represent the average atmospheric conditions.

2.4 SPATIAL TRENDS IN AEROSOL CONCENTRATIONS IN THE UNITED STATES

Estimated spatial trends of annual average species concentrations across the United States were presented by Malm et al. [1994] for the 3-year period of March 1988 through February 1991 using data collected at 36 monitoring sites. Of the 36 monitoring sites, only 4 (including Washington, D.C.) were located in the eastern United States, and therefore any east/west or north/south trends east of a line from North Dakota to Texas were speculative at best. The spatial variability of the 2001 annual average aerosol species concentrations were reported in Malm et al. [2004] using data collected at 143 sites, 49 of which were eastern United States monitoring sites, allowing for a significantly better understanding of spatial and short-term temporal (monthly) trends in that region of the country.

Here, the spatial variability of the annual average aerosol species concentrations for the 5-year period January 2000 through December 2004 is explored. The annual average aerosol components are presented in Figures 2.2–2.9 as isopleth maps. Data collected at 157 IMPROVE monitoring sites and 69 STN monitoring sites met the completeness criteria for all five RCFM components; an additional 2 IMPROVE sites and 15 STN sites met completeness criteria for a subset of the RCFM components. All sites that met completeness criteria for a given RCFM component were included in the analysis and are depicted on the maps. The isopleth values between the monitoring sites are not meant to represent the concentrations in these areas; instead, they are meant to help identify large spatial patterns in the monitored data. Spatial patterns in both aerosol concentration and percent contribution to reconstructed fine mass are explored for each aerosol component. Additionally, the change in spatial patterns that results from the addition of urban sites from the STN is also examined. IMPROVE sites are indicated on the maps with circles and STN sites are indicated with triangles.

2.4.1 Fine Particle Ammonium Sulfate Mass

Figure 2.2, panels a and c, show isopleths maps of fine particulate sulfur interpreted as ammonium sulfate and the fractions of reconstructed fine mass that are attributed to ammonium sulfate, expressed as a percentage of RCFM for the IMPROVE network. Panels b and d show the same results for the IMPROVE and STN networks. Sulfates are primarily a product of sulfur dioxide (SO_2) emissions and photochemical reactions in the atmosphere. For example, sulfates tend to be highest in areas of significant SO_2 emissions such as the eastern United States where SO_2 is emitted from coal-fired stationary sources [Malm et al., 1994, 2002]. The highest annual average rural ammonium sulfate mass concentrations were found in the central eastern United

States, where concentrations at most sites were in the 4.5–6.5 μg/m^3 range (Appendix A). The addition of the STN sites stretches the Ohio River valley high concentration region, where concentrations were greater than 5.25 μg/m^3, in all directions. From the high concentration region, ammonium sulfate concentrations decrease to the northeast, southeast, and west. The higher sulfate concentration isopleths were extended farther west by the addition of the east Texas and Gulf Coast STN sites, as compared to the rural spatial trends identified in the analysis of IMPROVE. The east-to-west gradient is particularly striking, with concentrations in the central eastern United States a factor of 8 higher than the western sites. Both the rural noncontiguous United States sites in Hawaii and the Virgin Islands and the urban site in Puerto Rico had concentrations between 1 and 2.25 μg/m^3. The rural and urban sites in Alaska had ammonium sulfate concentrations in the 0.5–1 μg/m^3 range.

In general, the east-to-west gradient is so much stronger than the urban-to-rural gradients that the latter are difficult to identify in the isopleth maps. Urban ammonium sulfate concentrations generally did not exceed 2 times nearby rural concentrations. The exceptions to this were the urban sites, STN and IMPROVE, in the northwestern states of Oregon, Washington, Colorado, Utah, and Idaho, which had ammonium sulfate concentrations at least 2 times higher than nearby rural concentrations. Given the mountainous locations of many of the IMPROVE sites in these states, the impact of elevation on the urban-rural contrast must be considered. The rural sites in Colorado and Idaho were all between 600 and 2000 m above Denver and the Wasatch Front STN sites, correspondingly. There were significant elevation gradients (>1000 m) between the urban and rural sites in Oregon, Washington, and Utah as well, but there were also rural sites at similar elevations to the urban sites (within 50 m) that still showed urban concentrations of at least 2 times rural concentrations. Elevation gradients likely contribute to at least a portion of the sites in these states exhibiting high urban-rural contrast in ammonium sulfate. Because of the relatively low contrast between urban and nearby rural sites, the general spatial trends observed in rural concentrations were not greatly modified by the addition of urban sites to the analysis. However, there were noticeable changes such as the extension of the high concentration region in the central eastern United States. Of the five RCFM components, spatial trends in ammonium sulfate were the least affected by the addition of urban sites to the analysis.

Referring to Figures 2.2c and 2.2d and Appendix A, which lists the annual average concentrations for 2000–2004, there were 25 sites in the eastern United States and Hawaii where ammonium sulfates make up over 50% of RCFM. The fractional contribution of ammonium sulfate to RCFM generally decreases to the west and to the east along the Atlantic coast. Much of the northwestern United States had less than a 20% ammonium sulfate contribution to RCFM. Fractional contributions increase again along the Pacific coast, particularly at the coastal sites in California—Agua Tibia, Point Reyes National Seashore, Redwoods National Park, and San Rafael—where the percent contributions were all 30% or greater, which makes them more similar to sites east of the Continental Divide than the other western sites. The general patterns observed here in the 2000–2004 period for the combined IMPROVE and STN data set are consistent with those observed by Malm et al. [2004] for the 2001 IMPROVE data and are not significantly altered by the addition of the 82 urban STN sites.

2.4.2 Fine Particle Carbon Mass

Organic aerosols have their origin in both primary emissions and from secondary aerosol formation. For instance, primary organic carbon emissions have been linked to meat cooking, road dust, mobile sources, fire-related activity, and industrial activities in the Los Angeles Basin [Rogge et al., 1996] and, more generally, to fire-related activity in all parts of the United States [Hawthorne et al.,1992; Schmidt et al., 2002], while secondary organic aerosols are formed from gaseous precursors that have both biogenic [Hatakeyama et al., 1989; Izumi and Fukuyama, 1990; Kavouras et al., 1998a, 1998b; Jang and Kamens, 1999] and anthropogenic [Izumi and Fukuyama, 1990; Odum et al., 1996, 1997; Holes et al., 1997; Jang and Kamens, 2001] origins. Light-absorbing carbon particles are produced from the combustion of carbon-based fuels, with the major sources including diesel engines, biomass burning, and coal combustion [Bond and Bergstrom, 2005].

The side-by-side analysis of urban and rural carbon measurements is complicated by different measurement techniques for IMPROVE and the STN and by the differences in the average carbon multiplier for urban and rural areas. The separation point between OC and light-absorbing carbon (LAC) is procedurally defined, and thus the reported OC and LAC fractions from the IMPROVE and STN networks are not expected to be equal. Another major distinction between the IMPROVE and STN carbon measurements is the lack of blank correction for the reported STN measurements. However, the STN OC measurements reported here are blank corrected as described in Appendix E. Given that the OC and LAC are not expected to be equal, it was surprising that collocated IMPROVE and STN data showed the blank-corrected OC measurements from the STN to be quite comparable with less than a 1% difference between annual averages in the organic carbon concentrations. However, the STN LAC average concentrations were ~10% lower than from the collocated IMPROVE samplers. Furthermore, urban and rural aerosols have been shown to be best modeled with different carbon multipliers, with lower values recommended for urban aerosols [Turpin and Lim, 2001]. Therefore spatial trends in LAC and OC between STN and IMPROVE sites should be considered to have greater uncertainty than spatial trends observed in ammonium sulfate and nitrate. Since total carbon (TC) measurements are expected to be equivalent and are also free of the complication of an assumed organic carbon multiplier, spatial trends in TC are examined even though TC is not a component of the RCFM model.

The rural IMPROVE TC mass concentrations for the contiguous United States ranged from 0.6 to 3.0 $\mu g/m^3$, with ~80% of the sites having concentrations less than 2 $\mu g/m^3$ (Figure 2.3a). The noncontiguous U.S. sites—Alaskan, Virgin Island, and Hawaiian—all had TC concentrations less than 0.5 $\mu g/m^3$. The highest rural TC concentrations, greater than 2.5 $\mu g/m^3$, were found at the same sites, with peak OMC concentrations in the southeastern United States and the Sierra Nevada region (Appendix A). Intermediate TC concentrations of 1.5–2.25 $\mu g/m^3$ are found throughout much of the eastern and northwestern (including northern California) United States and in the Sierra Nevada and southern California regions. The TC concentrations at the STN urban sites ranged from 0.9 $\mu g/m^3$ in upstate New York to 7.8 $\mu g/m^3$ in the San Joaquin Valley of California, with ~60% of the sites having concentrations between 2 and 4 $\mu g/m^3$ (Figure 2.3b). All of the western states with urban and rural sites available for comparison (Alaska, California, Oregon, Washington, Montana, Idaho, Nevada, Utah, Arizona, Texas, Kansas, and Nebraska) had urban TC concentrations at least 2 times higher than nearby rural

concentrations. In the East, this high degree of contrast between urban and rural concentrations was only present in Alabama, North Carolina, Ohio, and New Hampshire.

Organic mass by carbon concentrations and fractional contributions to RCFM are shown in Figure 2.4a–d. OMC concentrations were above 1 $\mu g/m^3$ at nearly all IMPROVE sites. Of the eight sites with organic mass concentrations below 1 $\mu g/m^3$, five are sites located outside of the contiguous United States (Simeonof and Tuxedni, Alaska; Hawaii Volcanoes National Park and Haleakala, Hawaii; and the Virgin Islands) and two are among the highest elevation sites in this analysis (Wheeler Peak, New Mexico, and White River, Colorado); the eighth site, White Pass, Washington, is the highest elevation site in the Northwest region. Peak rural values of 4–5 $\mu g/m^3$ occurred at the Spokane reservation in the Northwest, Sequoia National Park in the Sierra Nevada region, Mingo in the mid-South region, and at several sites in the southeastern United States. A large band through the interior West from the Mexico border into the upper Midwest had rural OMC concentrations less than 2 $\mu g/m^3$ at most sites. Most of the rural eastern and northwestern United States, along with northern and southern California and the Sierra Nevada mountains, had OMC concentrations in the 2–4 $\mu g/m^3$ range.

Using the same adjustment factor for calculating urban and rural OMC concentrations, the OMC concentrations at the three urban IMPROVE sites were between 4.5 and 6 $\mu g/m^3$. Phoenix and Puget Sound concentrations were 2–5 times higher than the nearby rural sites, indicating large local sources. Compared to the analysis of ammonium sulfate, the addition of the urban STN sites more extensively altered the spatial trends in peak OMC mass concentrations. Localized high concentration areas outside of the southeastern United States and California were identified with the inclusion of the urban sites. The STN urban sites had OMC concentrations ranging from 1.3 $\mu g/m^3$ in upstate New York to 12.4 $\mu g/m^3$ in the San Joaquin Valley of California with ~60% of the sites having concentrations between 2 and 6 $\mu g/m^3$. All of the western states with urban and rural sites available for comparison (Alaska, California, Oregon, Washington, Montana, Idaho, Nevada, Utah, Arizona, Texas, Kansas, and Nebraska) had urban concentrations at least 2 times higher than nearby rural concentrations. In the East, this high degree of contrast between urban and rural concentrations was only present in Alabama, Kansas, North Carolina, and New Hampshire; the other eastern states where a comparison was possible had urban concentrations that did not exceed 2 times nearby rural concentrations.

There was greater dissimilarity between the spatial trends in the fractional contribution of OMC to RCFM and the trends in OMC concentrations than was the case for ammonium sulfate. The highest OMC contributions to RCFM all occurred in Alaska and the northwestern United States where they were nearly all above 40% and exceeded 60% at approximately half of these sites. In rural southern California, the Colorado and Mogollon plateaus, the northern Great Plains, the Rockies, the Boundary Waters, New England, and the southeastern United States, percent contributions of OMC were typically in the 30–50% range. Organics only contributed in the range of 20–30% to RCFM in the remainder of the rural contiguous United States, principally from the Central Great Plains through the Ohio River valley and northern Appalachia range into upstate New York, with additional pockets in the arid Southwest and along the coasts. Puerto Rico and Hawaii also had OMC contributions in the 20–30% range. The Virgin Islands was the only location to have organics contribute less than 20% to RCFM. The most obvious effects of adding the urban STN sites to the analysis are the extension of the high contributions regions in

the Northwest, south to central California, and east to eastern Montana and adding hot spots to the high contribution region in the southeastern United States.

Rural light-absorbing carbon mass concentrations, with a few exceptions, were below 0.5 $\mu g/m^3$; the four exceptions, Old Town, Maine; M.K. Goddard, Pennsylvania; Mingo, Missouri; and James River Face Wilderness, Virginia, all had concentrations very near to 0.5 $\mu g/m^3$ (Figure 2.5a). The highest average LAC concentrations, those greater than 0.4 $\mu g/m^3$, occurred in the eastern United States and California, with over half of these sites concentrated in the Ohio River valley and Appalachian region. The high LAC concentration region in the East roughly corresponds to the high ammonium sulfate region. Similar to OMC, there is a large low concentration band through the interior West, where LAC concentrations were generally less than 0.2 $\mu g/m^3$. Much of the rural eastern and northwestern United States, along with the Sierra Nevada and southern California regions, had LAC concentrations in the 0.2–0.4 $\mu g/m^3$ range. Urban LAC concentrations ranged from 0.2 in upstate New York to 2.3 $\mu g/m^3$ in Puerto Rico, with ~70% of the sites having concentrations between 0.3 and 1 $\mu g/m^3$. Light-absorbing carbon contributes less than 10% to RCFM at all rural sites, with the highest fractional contributions occurring at Glacier National Park, Montana; Old Town, Maine; and Snoqualmie Pass and Mount Rainier National Park, Washington (Figure 2.5b). Urban LAC contributions were less than 10%, with the exceptions of Alaska, southeastern Florida, and Puerto Rico where contributions were 10%, 15%, and 26%, respectively.

2.4.3 Fine Particle Ammonium Nitrate Mass

The annually averaged nitrate concentrations and the nitrate fractions of RCFM are shown in Figure 2.6a–d. The fine particulate nitrate mass concentrations were interpreted as ammonium nitrate. Since nitrate concentrations are dependent on a number of factors, including nitrogen oxide and ammonia emissions, photochemical reactions, temperature, humidity, and the presence of other aerosol species, many factors contribute to where high aerosol nitrate concentrations are formed. Rural ammonium nitrate concentrations were highest at the central and southern California sites and in the Midwest, where both nitrogen oxide and ammonia emissions are high [U.S. EPA, 2000]. Urban IMPROVE and STN sites indicate additional high concentration areas in the Sacramento Valley of California, Idaho, Utah, Colorado, Texas, New York, and Pennsylvania. The highest concentrations occur at the urban sites in southern California, peaking at 14 $\mu g/m^3$ in Los Angeles. The Central Great Plains region is the largest area of high ammonium nitrate concentrations, with rural concentrations typically between 2 and 3 $\mu g/m^3$ and the urban concentrations between 3 and 4 $\mu g/m^3$. From the high concentration region in the Midwest, rural ammonium nitrate concentrations generally decrease to the east, south, and west until higher concentrations are again encountered along the Pacific coast. The extreme Northeast and the interior West have concentrations that are typically less than 0.5 $\mu g/m^3$.

Similar to TC, the western states of Alaska, California, Oregon, Washington, Montana, Idaho, Nevada, Utah, and Arizona all had urban concentrations at least 2 times higher than nearby rural concentrations. In the East, urban ammonium nitrate concentrations less commonly exceeded 2 times nearby rural concentrations. The exceptions in the East, where a high degree of urban-rural contrast existed, were North Carolina, Ohio, Tennessee, Massachusetts, New Hampshire, and Vermont. Additionally, the states that had the largest absolute differences

between the highest urban concentrations and surrounding rural sites, 2–4 μg/m^3, were Colorado, Utah, Idaho, New York, Michigan, and Ohio. Central and southern California had urban excess ammonium nitrate concentrations in the 2–12 μg/m^3 range, but northern California and Oregon were in the 0.75–1.25 μg/m^3 range. The comparison of the northern Minnesota rural sites to urban sites results in urban excess values of ~2 μg/m^3, but the southern Minnesota rural sites were within 0.5 μg/m^3 of the highest urban concentrations.

The spatial trends in the fractional contribution of nitrates to RCFM reflect the spatial trends in nitrate concentration. The highest percent contributions of 25–45% occur in the Midwest, central and southern California, and urban Idaho and Utah. The areas surrounding the highest contribution regions—parts of the Midwest, northern California, the Northeast, the Northwest, and southern Arizona—all have contributions in the 10–20% range. Nitrate contributions were generally less than 10% in New England, the Southeast, the interior West, and much of the northwestern United States.

2.4.4 Fine Particle Soil Mass

Figure 2.7a–d shows the annual average spatial distribution for the 2000–2004 period of fine soil mass concentrations and the soil fractions of RCFM. The highest rural fine soil concentrations were found in the arid Southwest at Sycamore Canyon and the west and east units of Saguaro National Park, Arizona, at 2.61, 3.08, and 2.18 μg/m^3, respectively. The Virgin Islands, the Queen Valley in southern Arizona, and the west Texas sites of Guadalupe Mountain and Salt Creek all had concentrations in the 1.5–2 μg/m^3 range. Rural soil mass concentrations in the range of 1–1.5 μg/m^3 were found in southern Colorado; the Death Valley National Monument, California; El Dorado Springs, Missouri; in the Cherokee Nation, Oklahoma; and throughout most of Arizona. For most of the rural United States, soil mass concentrations were between 0.5 and 1 μg/m^3, with the Great Lakes area, the northern Rockies, Alaska, Hawaii, and the northwestern and northeastern United States generally having soil concentrations less than 0.5 μg/m^3. The spatial patterns in fine soil were quite distinct from those for ammonium sulfate, ammonium nitrate, and organic mass by carbon—it is the only fine aerosol parameter to show peak concentrations in the arid Southwest.

The peak soil concentration of 4.8 μg/m^3 occurs at an urban STN site in El Paso, Texas. The annual average soil concentration at this site in El Paso is 2–3 times the other STN El Paso site and the IMPROVE sites in western Texas. The next highest urban site, the IMPROVE Phoenix, Arizona, site, had at 2.93 μg/m^3 a comparable concentration to the peak rural concentrations in Arizona. The STN Puerto Rico site and the IMPROVE Spokane site also have soil concentrations greater than 2 μg/m^3. The Spokane reservation site had annual soil concentrations that were between 2 and 10 times the other urban and rural sites in Washington and northwestern Montana. Urban soil mass concentrations in the range of 1–2 μg/m^3 were found in Arizona and west Texas, as well as in Alabama, California, Colorado, Florida, Missouri, Nebraska, and Ohio. For most of the United States, urban soil mass concentrations were in the same concentration range as at nearby rural sites. The exceptions include Alaska, Alabama, Nebraska, and Ohio where the urban concentrations were over 2 times those at the rural sites in the state. Soil concentrations in Denver were twice those at the northern Colorado sites and the Weminuche Wilderness and similar to the Great Sand Dunes and Mesa Verde national parks.

The additions of the STN Missoula site and the southwestern Pennsylvania site extend the 0.5–1 $\mu g/m^3$ isopleth west and north, respectively.

As was the case with ammonium nitrate, the spatial trends in fractional contribution of soil to RCFM reflect the spatial trends in soil concentration. The highest fractional contribution from soil occurs in the Virgin Islands at 51%. The Virgin Islands and Barbados have both been shown to have significant dust aerosol inputs from the African deserts [Perry et al., 1997; Prospero, 1999]. From there the highest fractional contributions were associated with the highest soil concentrations; Sycamore Canyon and the west and east units of Saguaro National Park had soil contributions in the range of 35–45%. Soil contributions ranged from 30% to 35% at Chiricahua National Monument, Queen Valley, and Hillside, Arizona; Great Sand Dunes National Monument, Colorado; Death Valley National Park, California; and Guadalupe Mountains National Park, Texas. Most of the remaining rural southwestern sites, including the IMPROVE Phoenix site, had soil contributions in the 20–30% range. Puerto Rico was the only STN site to have soil contributions greater than 20% (Appendix A). Outside of the southwestern United States, the rural interior West and the Everglades National Park, Florida, had soil contributions in the 10–20% range. Florida also has regular inputs of dust aerosol from Africa [Perry et al., 1997; Prospero, 1999]. STN sites in western Texas; Phoenix, Arizona; Denver, Colorado; southeast Florida; and central North Dakota also had contributions of 10–20%. In the rural East, Alaska, Hawaii, and along the Pacific coast, soil and, at most urban sites, soil contributions to RCFM were less than 10%.

2.4.5 Reconstructed Fine Mass

The highest rural RCFM concentrations, those greater than 11.5 $\mu g/m^3$, were concentrated in the Ohio River valley and Appalachian region (Figure 2.8a). On a mass basis, these sites were all dominated by ammonium sulfate, with the exception of Mingo, Missouri, where OMC and ammonium sulfate contributed almost an equal fraction to RCFM. But the high RCFM concentrations in this region were not simply due to high ammonium sulfate concentrations; the high RCFM region represents the convergence of the high ammonium sulfate region with the high LAC region and the high OMC region to the south and west and the high ammonium nitrate region to the north and west. All of the sites besides Mingo fell into the top ten sites with the highest ammonium sulfate concentrations; Mingo was in the top ten for OMC and LAC. Additionally, two-thirds of these sites fell into the top ten for an additional two parameters, a combination of either ammonium nitrate, OMC, or LAC.

From this high concentration region, RCFM concentrations decrease in all directions but remain above 6 $\mu g/m^3$ in the eastern United States, with the exception of several sites to the north in the Boundary Waters region and in northern New England. To the west, concentrations decrease until the central interior West, where low concentrations of all the RCFM components contribute to low RCFM concentrations between 2 and 4 $\mu g/m^3$. The higher RCFM concentrations, 4–6 $\mu g/m^3$ in Arizona, New Mexico, and Death Valley to the south of the low concentration region, were driven by a combination of higher soil concentrations and higher ammonium sulfate concentrations. In contrast, the higher concentrations of again 4–6 $\mu g/m^3$, northwest (northern California, Oregon, Washington, and Montana) of the low concentration area, were driven primarily by higher OMC concentrations and, to a lesser extent, higher ammonium sulfate and ammonium nitrate concentrations. The higher RCFM concentrations in

central and southern California, 4–10 μg/m^3, were due to various combinations of higher OMC, ammonium nitrate, ammonium sulfate, and soil concentrations.

Urban RCFM concentrations ranged from 5 to 31 μg/m^3, with the peak concentrations in Los Angeles and the San Joaquin Valley, California, and Birmingham, Alabama (Figure 2.8b, Appendix A). Close to half of the IMPROVE rural sites had RCFM concentrations less than the minimum urban concentration, and the maximum rural concentration was similar in value to the median urban concentration, 12.9 and 12.7 μg/m^3, respectively. Most of the western states with urban and rural sites available for comparison (Alaska, California, Oregon, Washington, Montana, Idaho, Nevada, Utah, Arizona, Texas) had urban RCFM concentrations at least 2 times higher than nearby rural concentrations. This high degree of contrast was not present in the East where urban RCFM concentrations never exceeded 2 times nearby rural concentrations.

2.4.6 Coarse Mass

The spatial trends in rural coarse mass (CM) (Figure 2.9) were very different than for RCFM (Figure 2.8a). Whereas the highest RCFM concentrations were in the central eastern United States, the highest CM concentrations, 8–15 μg/m^3, were concentrated farther west in the middle of the United States and in the arid Southwest and southern California. These regions were identified in emissions estimates as having high PM_{10} emissions [U.S. EPA, 2000]. Coarse mass concentrations were also very high, 13.4 μg/m^3, in the Virgin Islands. From the central Great Plains, CM concentrations trended toward increasingly lower concentrations in the range of 2–6 μg/m^3 to the north, east, and west until reaching the coasts. The sites along the Pacific, Gulf, and Atlantic coasts typically had moderate to high CM concentrations in the 4–8 μg/m^3 range. The CM concentrations were generally very low, 1–2 μg/m^3, in the following northwestern regions—the northern Rockies, Oregon and northern California, the Northwest, and Alaska. Similarly, low concentrations also occurred at Hawaii Volcanoes National Park, Hawaii; Shining Rock Wilderness, North Carolina; Lye Brook Wilderness, Vermont; and Seney, Michigan. The midwestern sites added since the 2000 IMPROVE report [Malm et al., 2000b] greatly aid in identifying the spatial trends in CM—the high CM region in the central Great Plains was not identifiable with the pre-2000 network configuration.

The spatial patterns in CM differ from those of fine soil in that the elevated-CM regions in the middle of the United States and along the coasts were not reflected in the fine soil measurements. The disparity in spatial patterns for fine soil and CM may reflect regional patterns in the fractional contribution of soil to CM. The results of a special study of speciated CM samples at nine IMPROVE sites throughout the United States that investigated the relative contributions of the major aerosol types included in the RCFM model to coarse mass concentrations [Malm et al., 2006] generally support this hypothesis. The study was initiated between 19 March 2003 and 23 December 2003 at Mount Rainier, Washington; Bridger, Wyoming; Sequoia and San Gorgonio, California; Grand Canyon, Arizona; Bondville, Illinois; Upper Buffalo, Arkansas; Great Smoky Mountains, Tennessee; and Brigantine, New Jersey, with each site operating for one year. Crustal minerals were the single largest contributor to CM at all but one monitoring location. Annual average fractional soil contributions to CM ranged from 79% at the Grand Canyon to 32% at Mount Rainier. Bondville and Upper Buffalo, which were both to the west of the high-CM region, had annual average CM soil contributions of 57% and

63%, respectively. Brigantine, along the east coast of the United States, had fine soil contributions of 44%.

a) Ammonium sulfate concentrations for the IMPROVE network

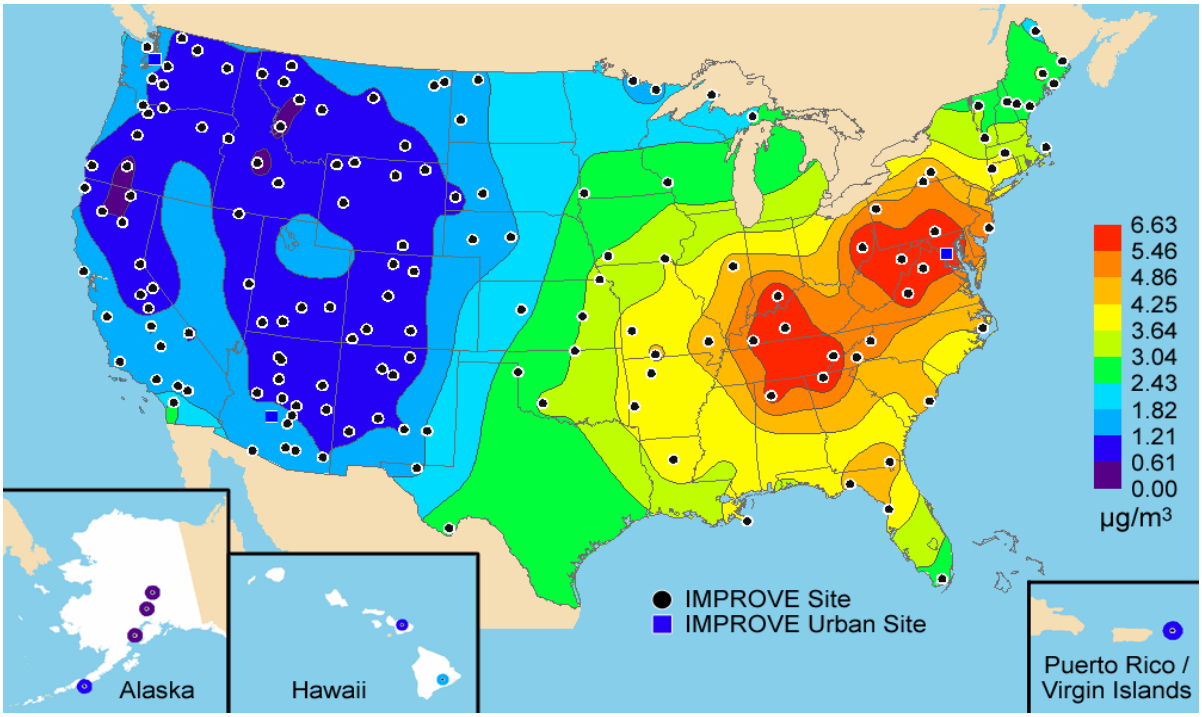

b) Ammonium sulfate concentrations for the IMPROVE and STN networks

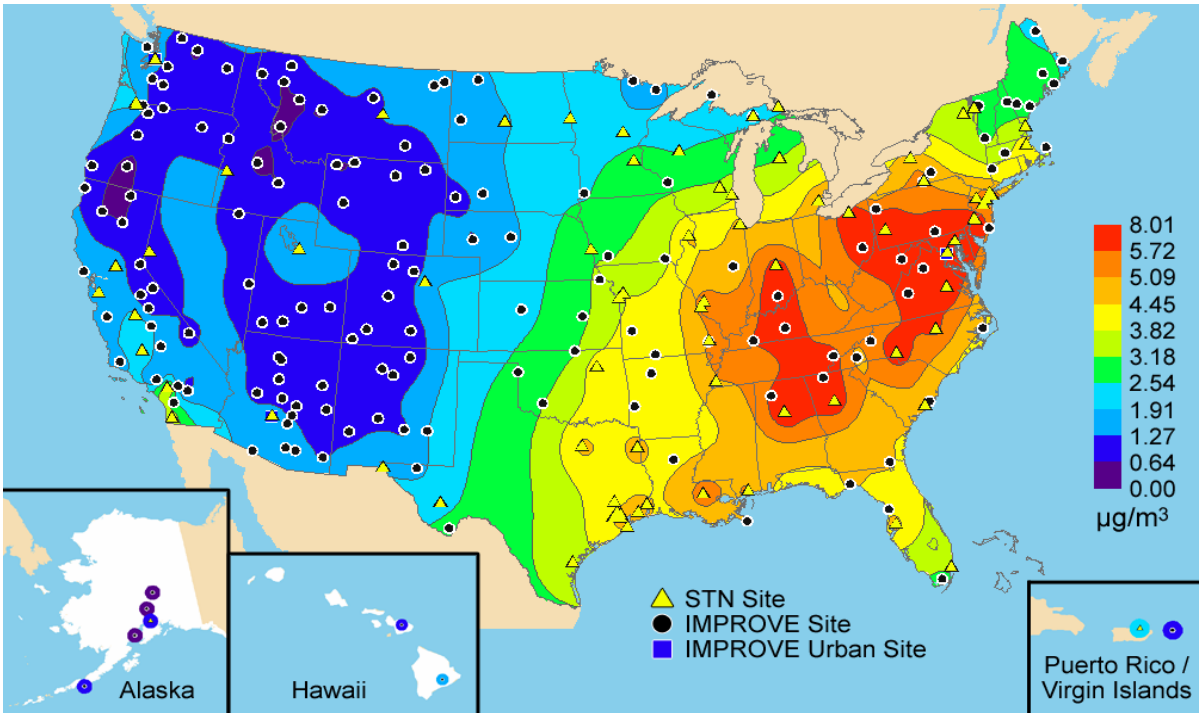

c) Ammonium sulfate fractional contribution to reconstructed fine mass for the IMPROVE network

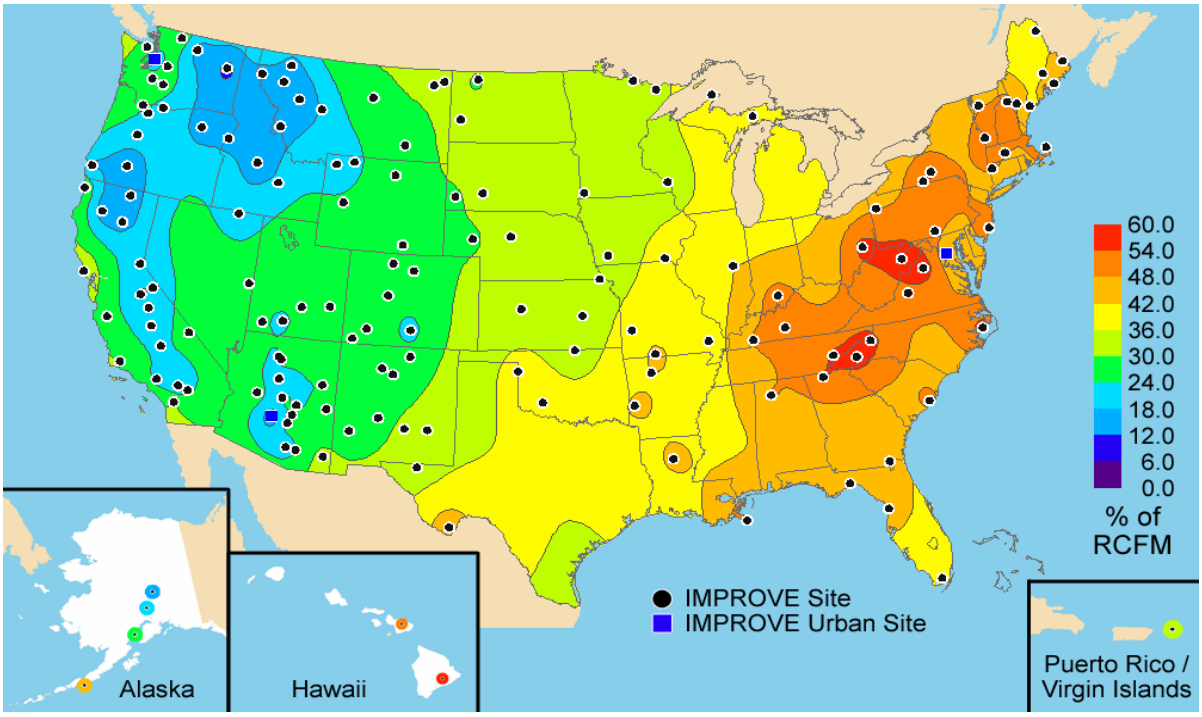

d) Ammonium sulfate fractional contribution to reconstructed fine mass for the IMPROVE and STN networks

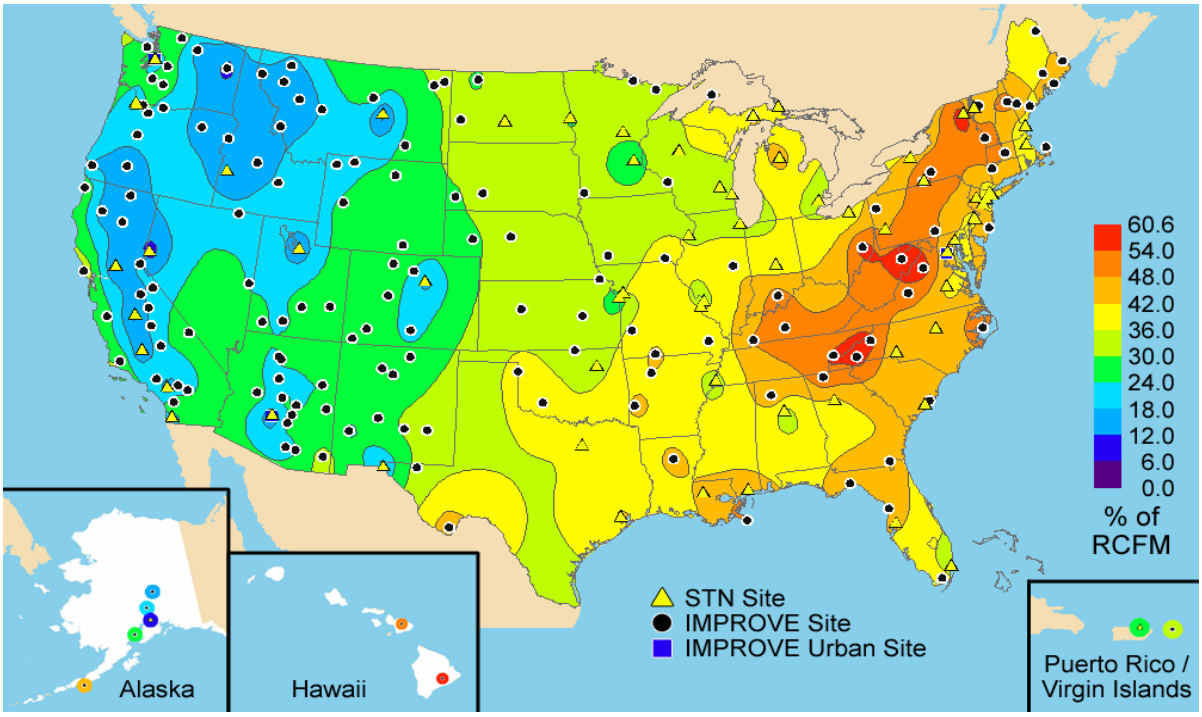

Figure 2.2. Isopleth maps of annual ammonium sulfate concentrations in panels a and b and percent contributions to reconstructed fine mass in panels c and d. Panels a–d include all sites from the IMPROVE network that met the prescribed completeness criteria including the urban sites from 2000–2004. Panels b and d also include all sites from the STN network that met the prescribed completeness criteria.

a) Total carbon concentrations for the IMPROVE network

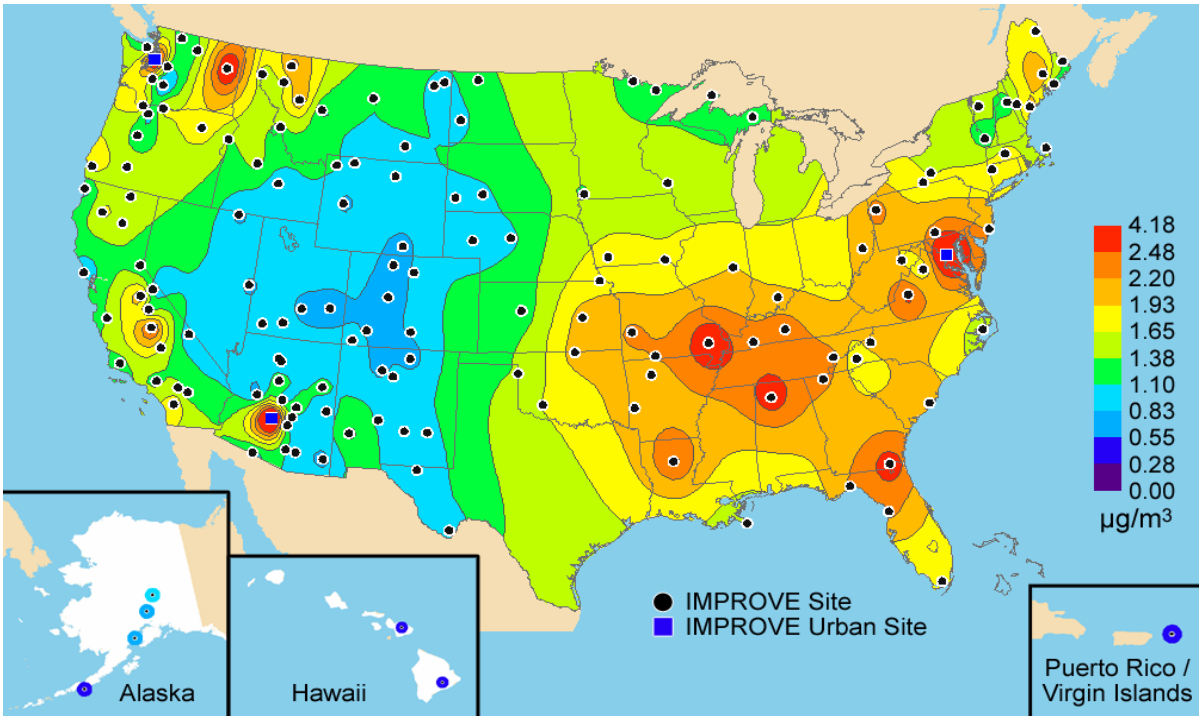

b) Total carbon concentrations for the IMPROVE and STN networks

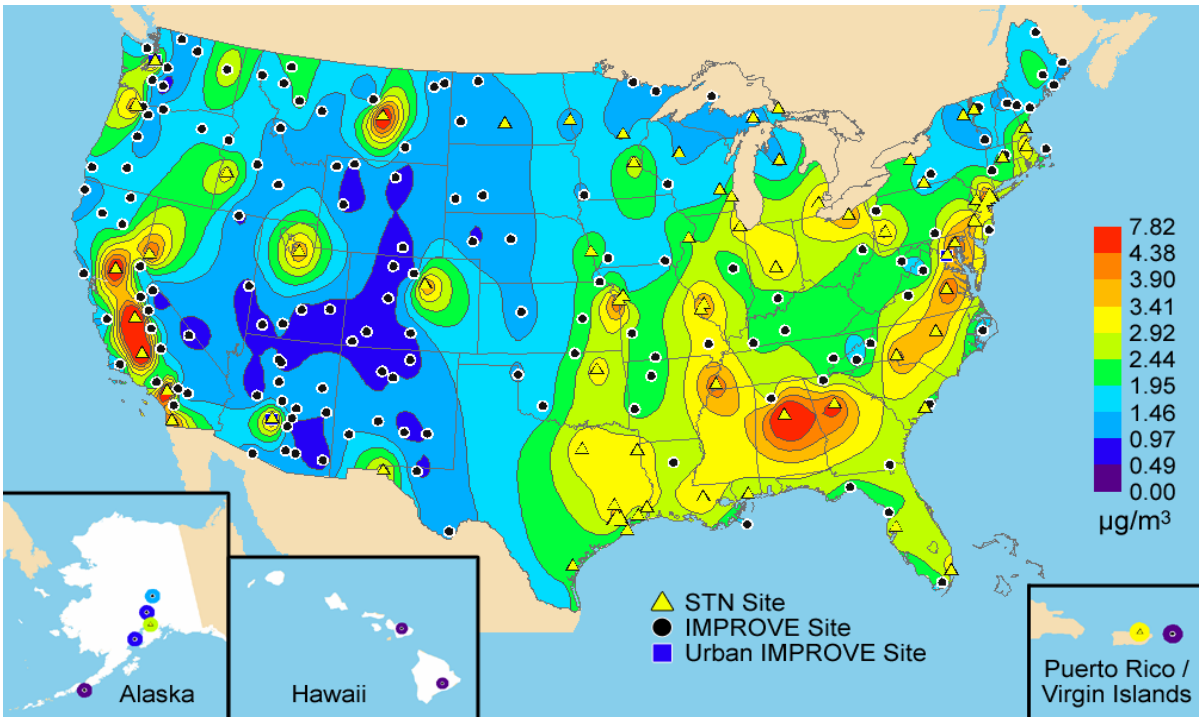

Figure 2.3. Isopleth maps of annual total carbon concentrations. Panels a and b include all sites from the IMPROVE network that met the prescribed completeness criteria including the urban sites for 2000–2004. Panel b also includes all sites from the STN network that met the prescribed completeness criteria.

a) Organic mass by carbon concentrations for the IMPROVE network

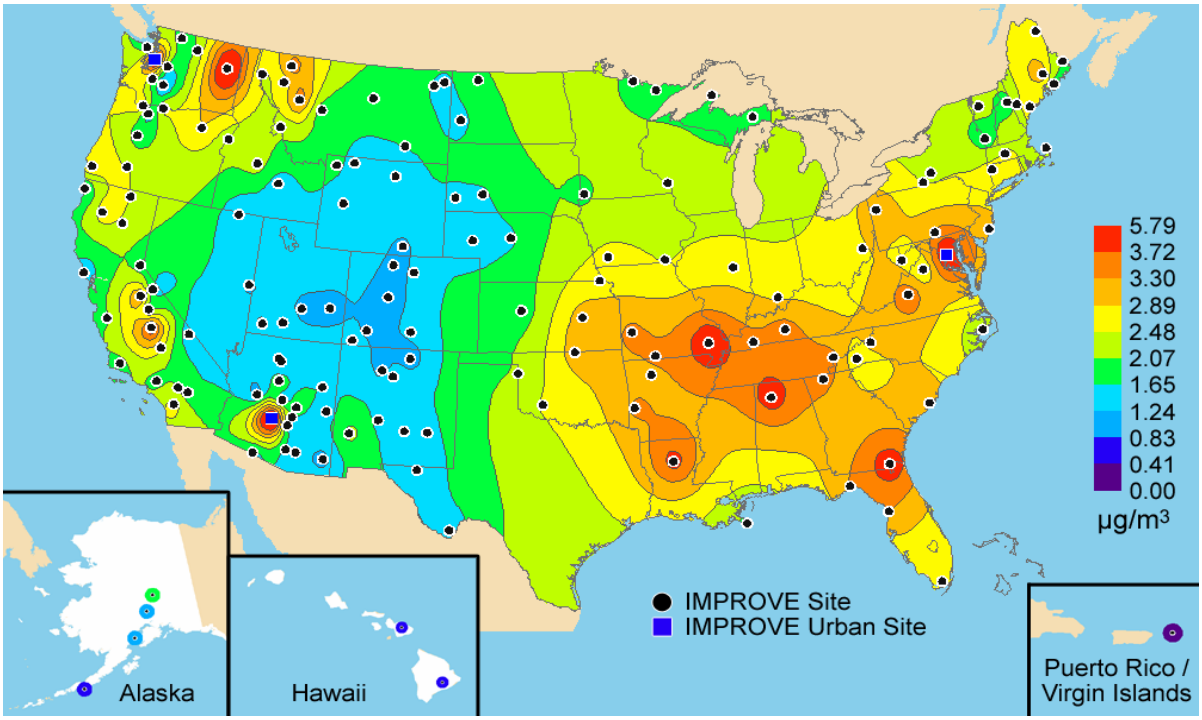

b) Organic mass by carbon concentrations for the IMPROVE and STN networks

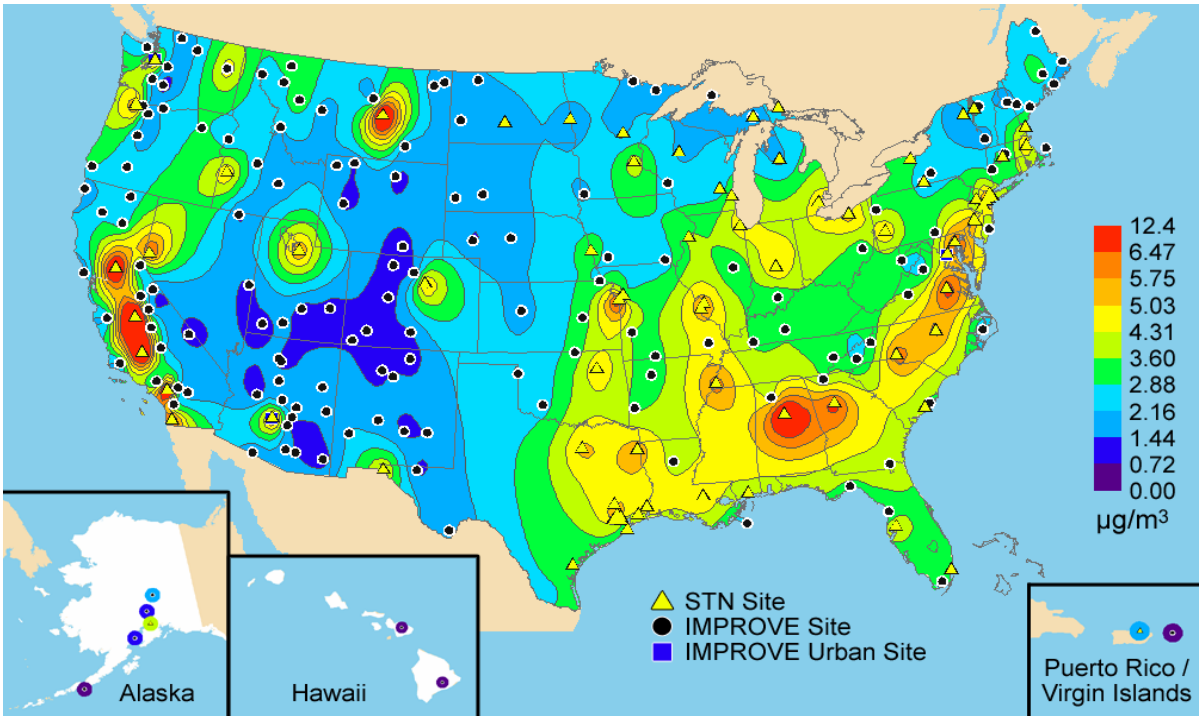

c) Organic mass by carbon fractional contribution to reconstructed fine mass for the IMPROVE network

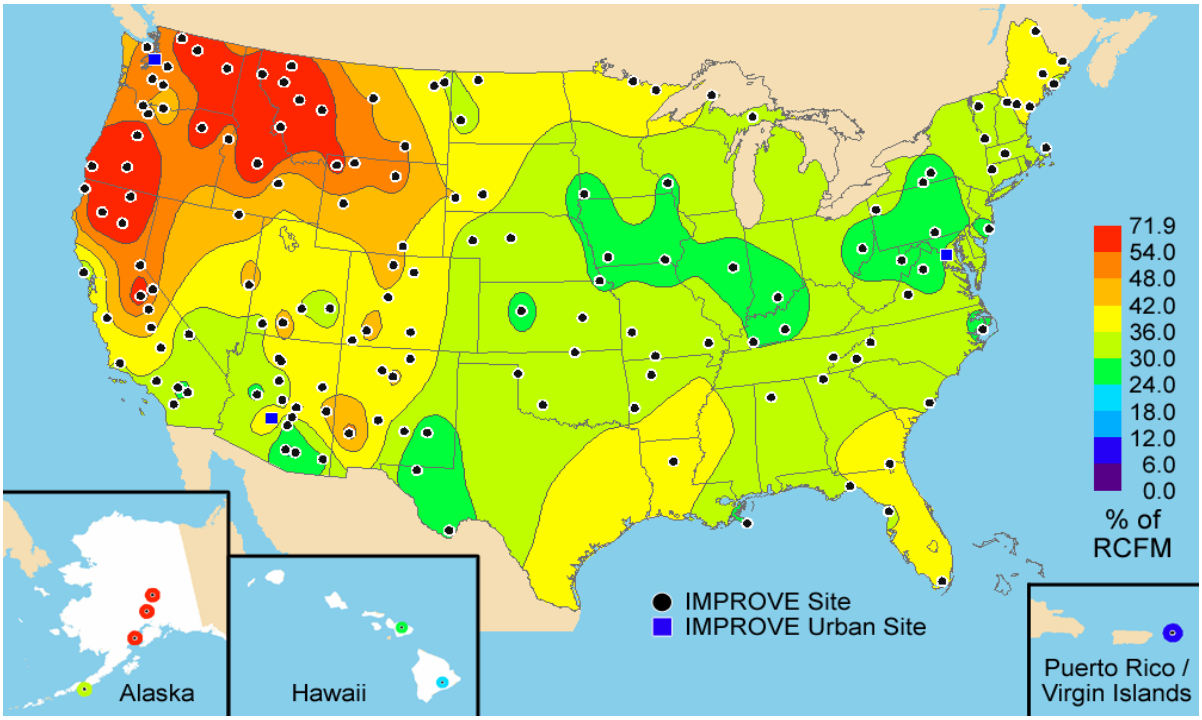

d) Organic mass by carbon fractional contribution to reconstructed fine mass for the IMPROVE and STN networks

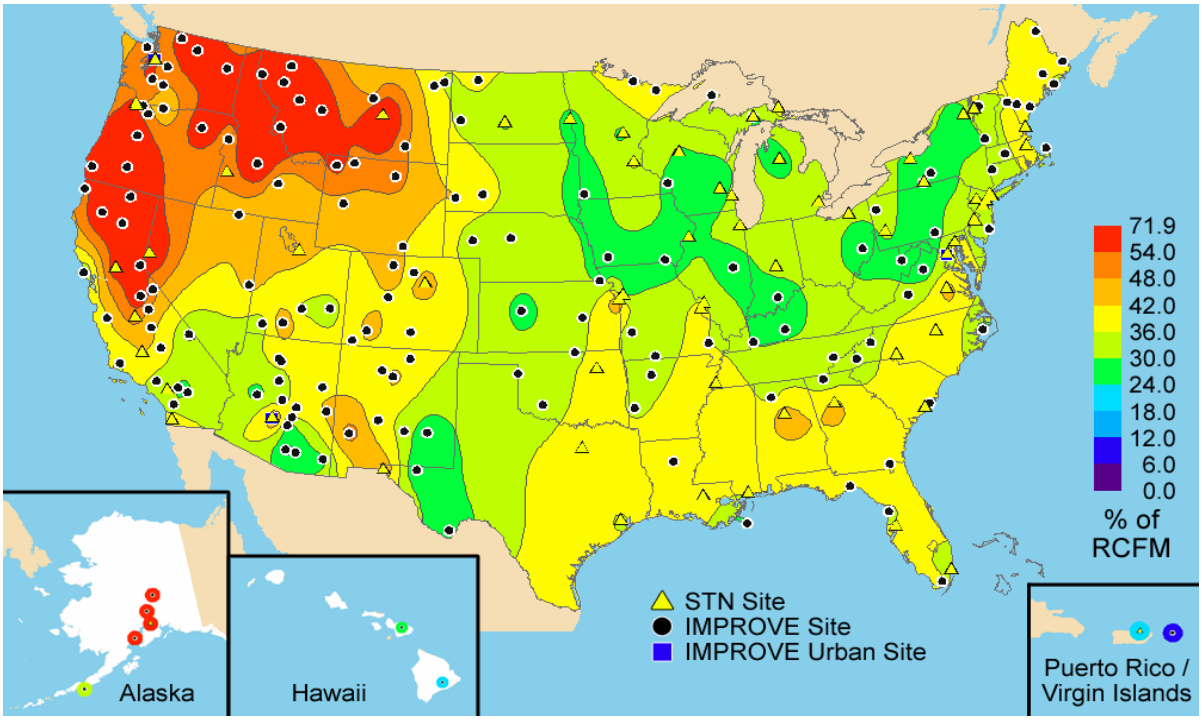

Figure 2.4. Isopleth maps of annual organic carbon concentrations in panels a and b and percent contributions to reconstructed fine mass in panels c and d. Panels a–d include all sites from the IMPROVE network that met the prescribed completeness criteria including the urban sites for 2000–2004. Panels b and d also include all sites from the STN network that met the prescribed completeness criteria.

a) Light-absorbing carbon concentrations for the IMPROVE network

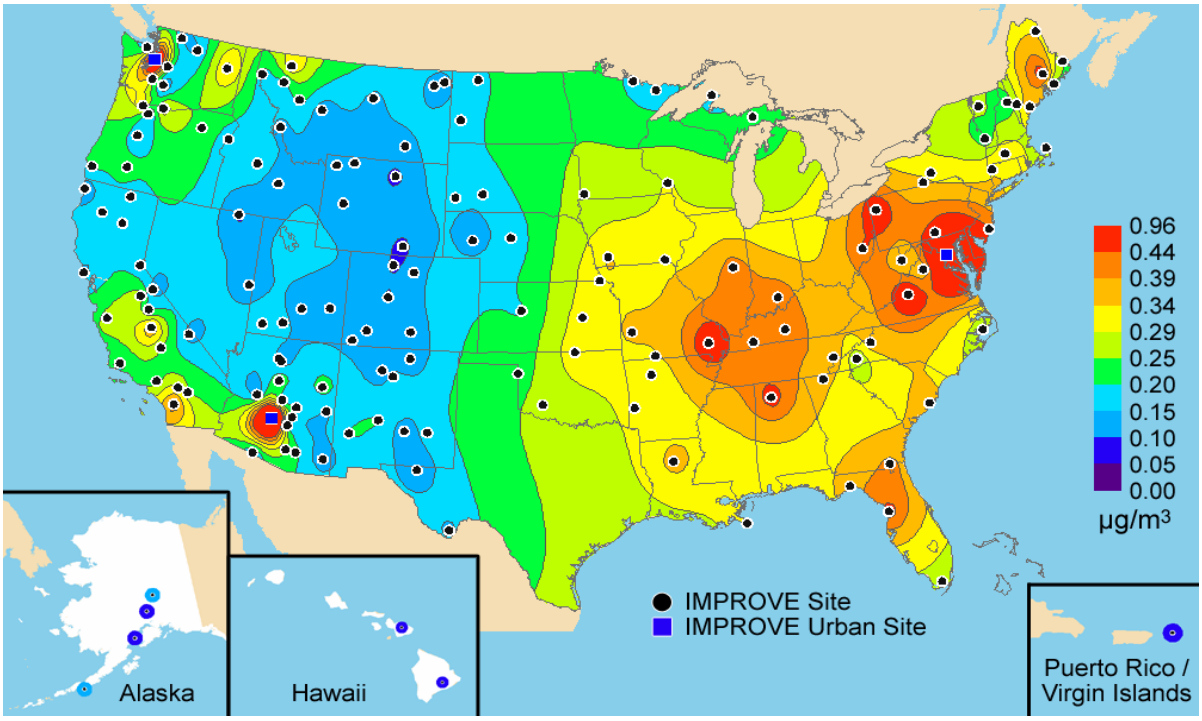

b) Light-absorbing carbon concentrations for the IMPROVE and STN networks

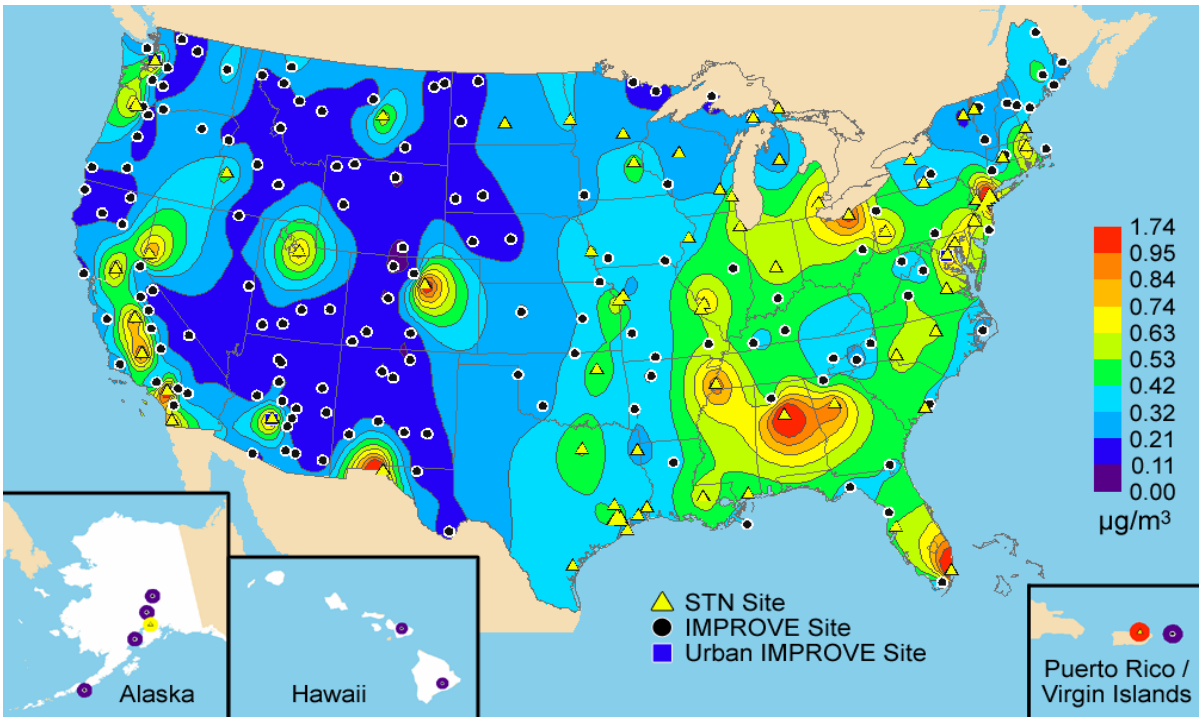

c) Light-absorbing carbon fractional contribution to reconstructed fine mass for the IMPROVE network

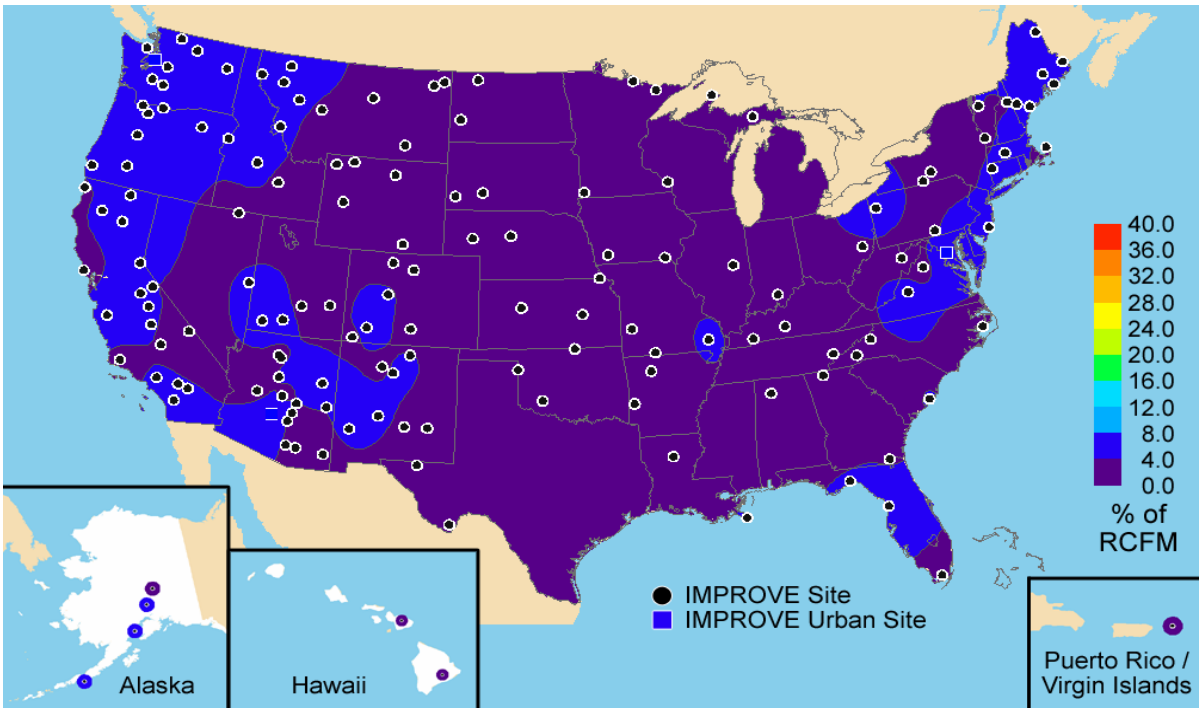

d) Light-absorbing carbon fractional contribution to reconstructed fine mass for the IMPROVE and STN networks

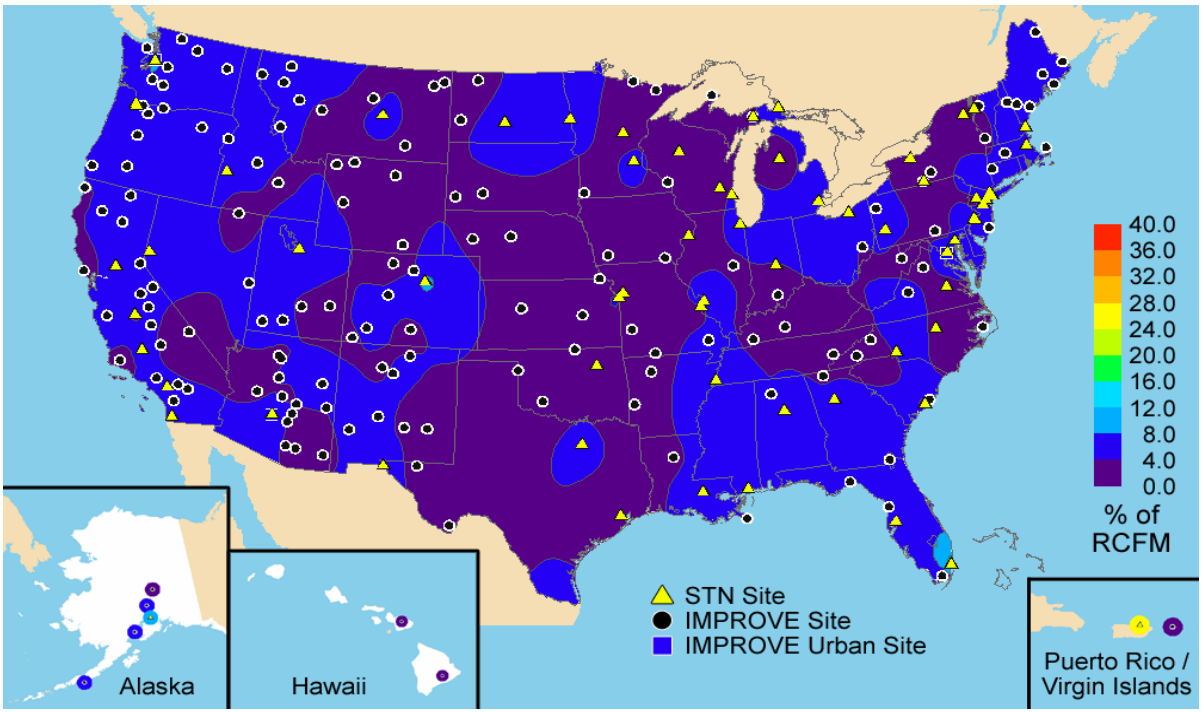

Figure 2.5. Isopleth maps of annual light-absorbing carbon concentrations in panels a and b and percent contributions to reconstructed fine mass in panels c and d. Panels a–d include all sites from the IMPROVE network that met the prescribed completeness criteria including the urban sites for 2000–2004. Panels b and d also include all sites from the STN network that met the prescribed completeness criteria.

a) Ammonium nitrate concentrations for the IMPROVE network

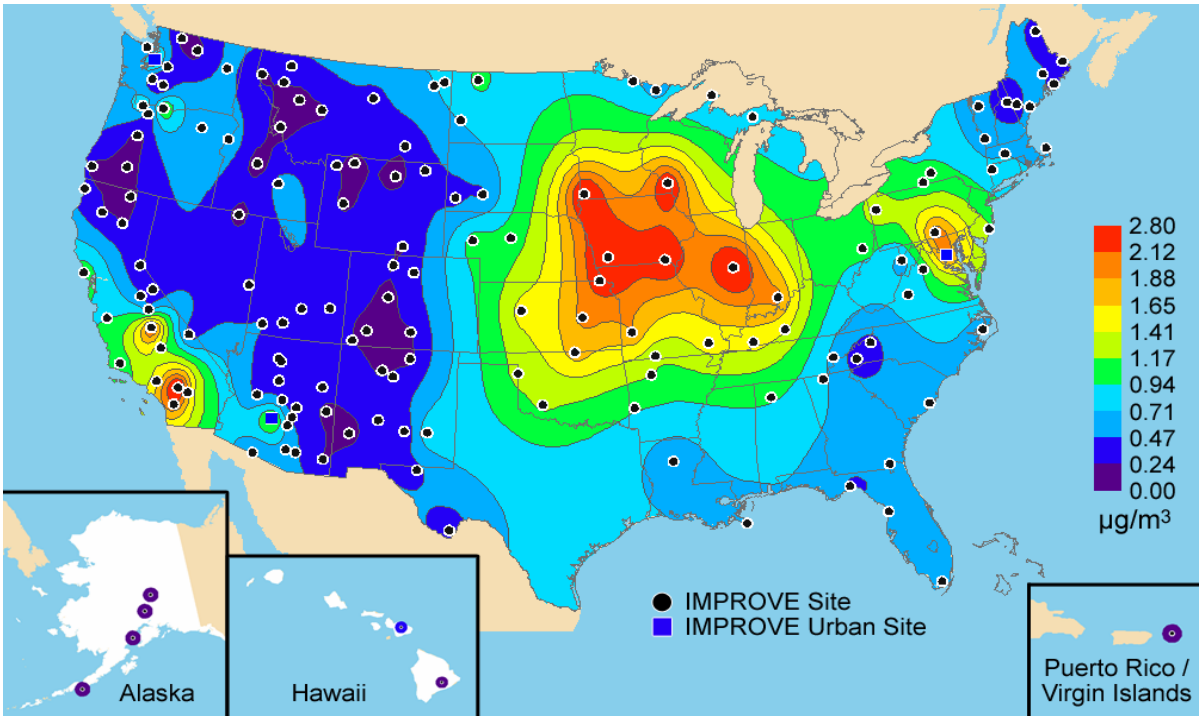

b) Ammonium nitrate concentrations for the IMPROVE and STN networks

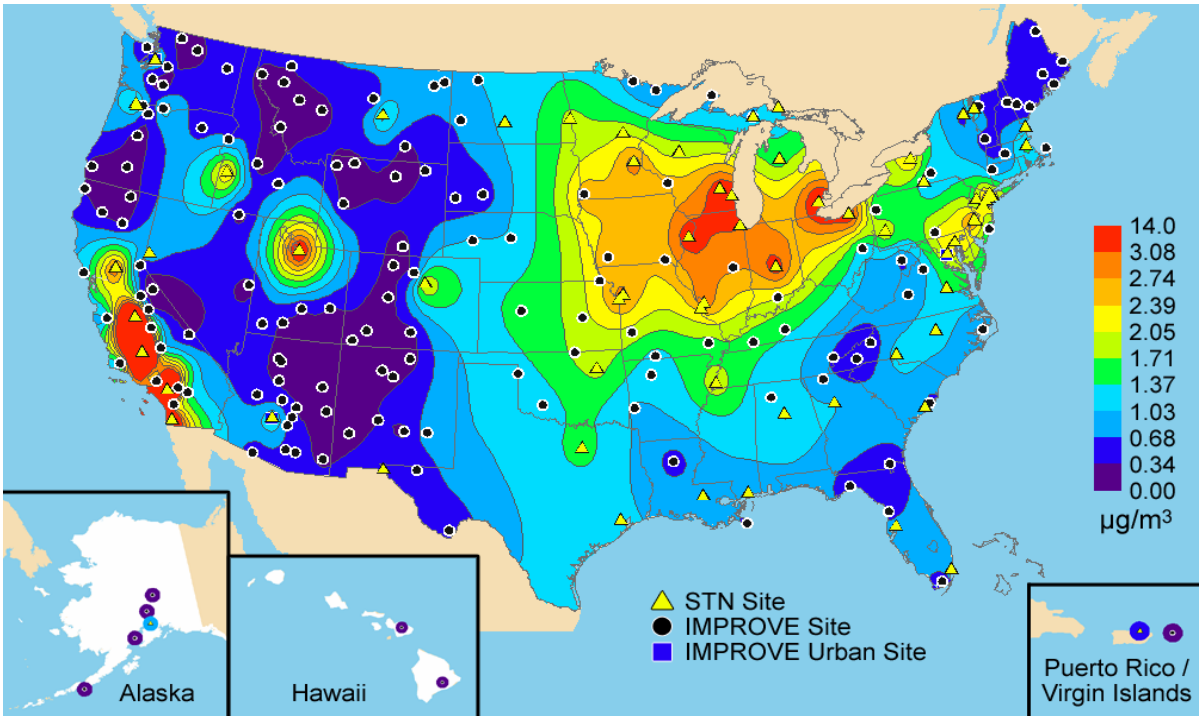

c) Ammonium nitrate fractional contribution to reconstructed fine mass for the IMPROVE network

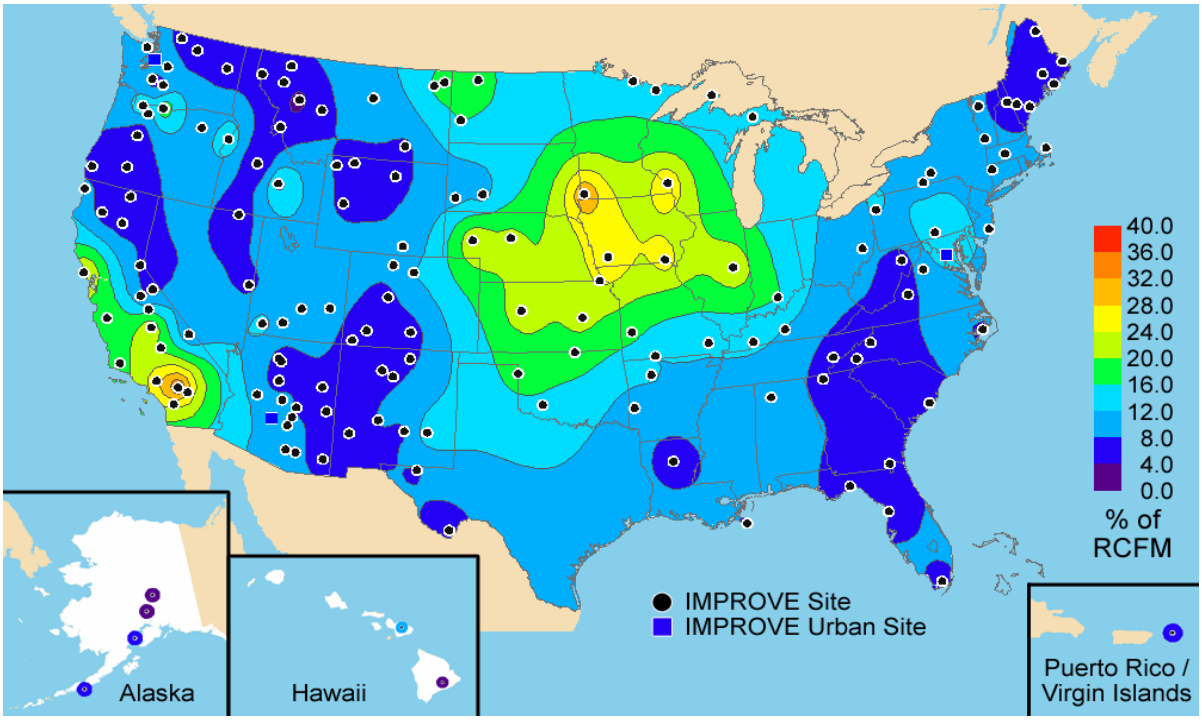

d) Ammonium nitrate fractional contribution to reconstructed fine mass for the IMPROVE and STN networks

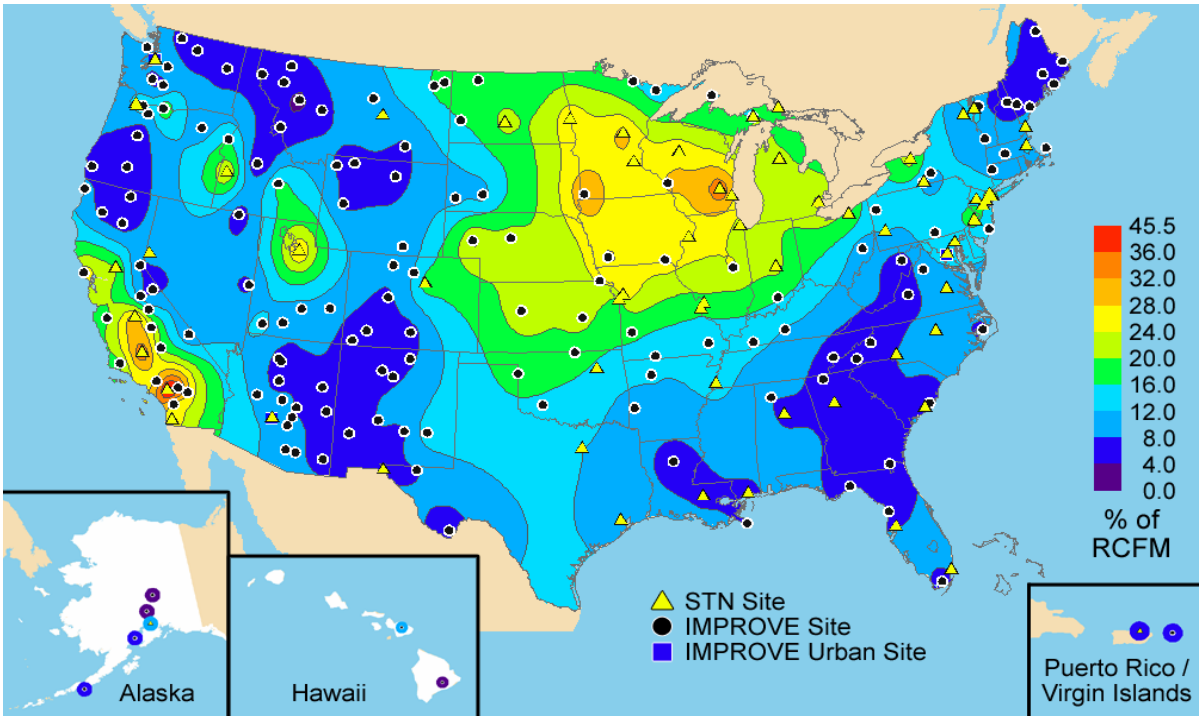

Figure 2.6. Isopleth maps of annual ammonium nitrate concentrations in panels a and b and percent contributions to reconstructed fine mass in panels c and d. Panels a–d include all sites from the IMPROVE network that met the prescribed completeness criteria including the urban sites for 2000–2004. Panels b and d also include all sites from the STN network that met the prescribed completeness criteria.

a) Fine soil concentrations for the IMPROVE network

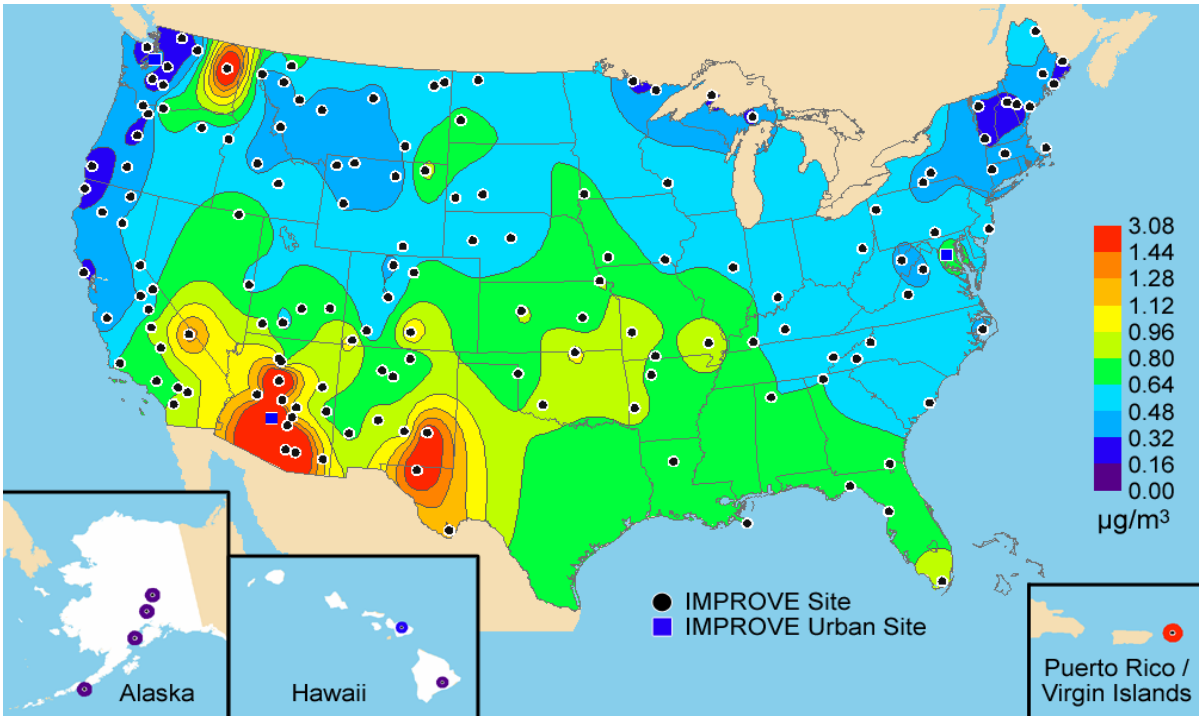

b) Fine soil concentrations for the IMPROVE and STN networks

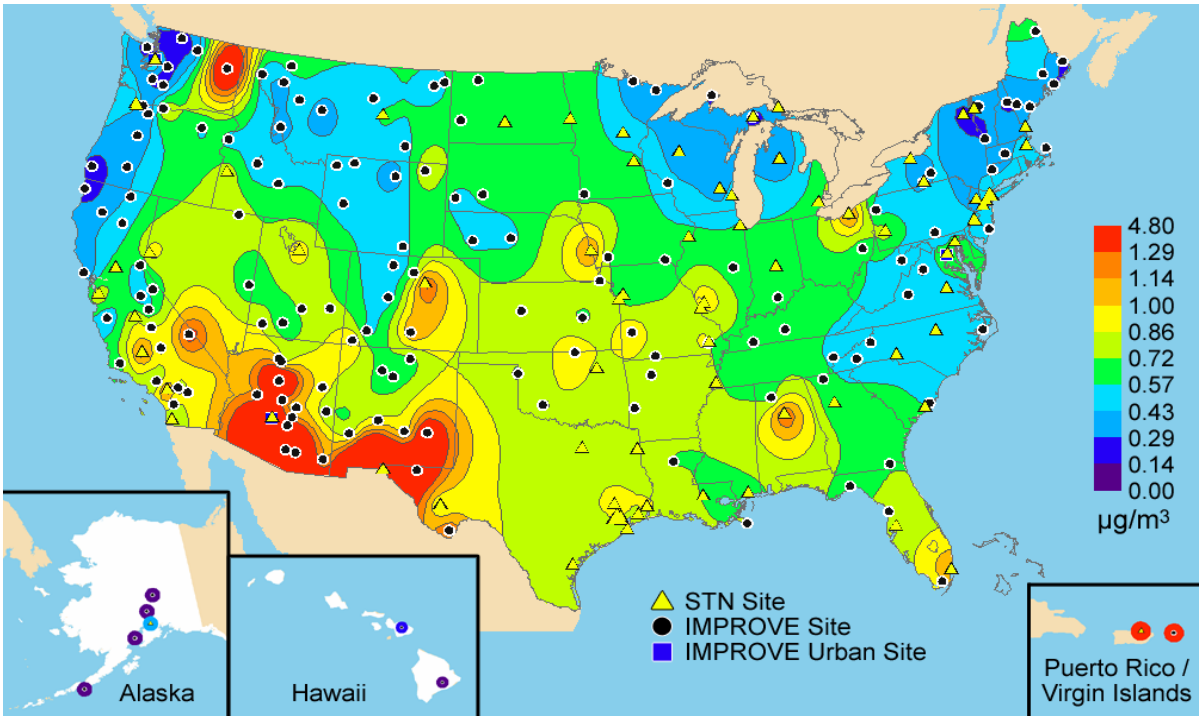

c) Fine soil fractional contribution to reconstructed fine mass for the IMPROVE network

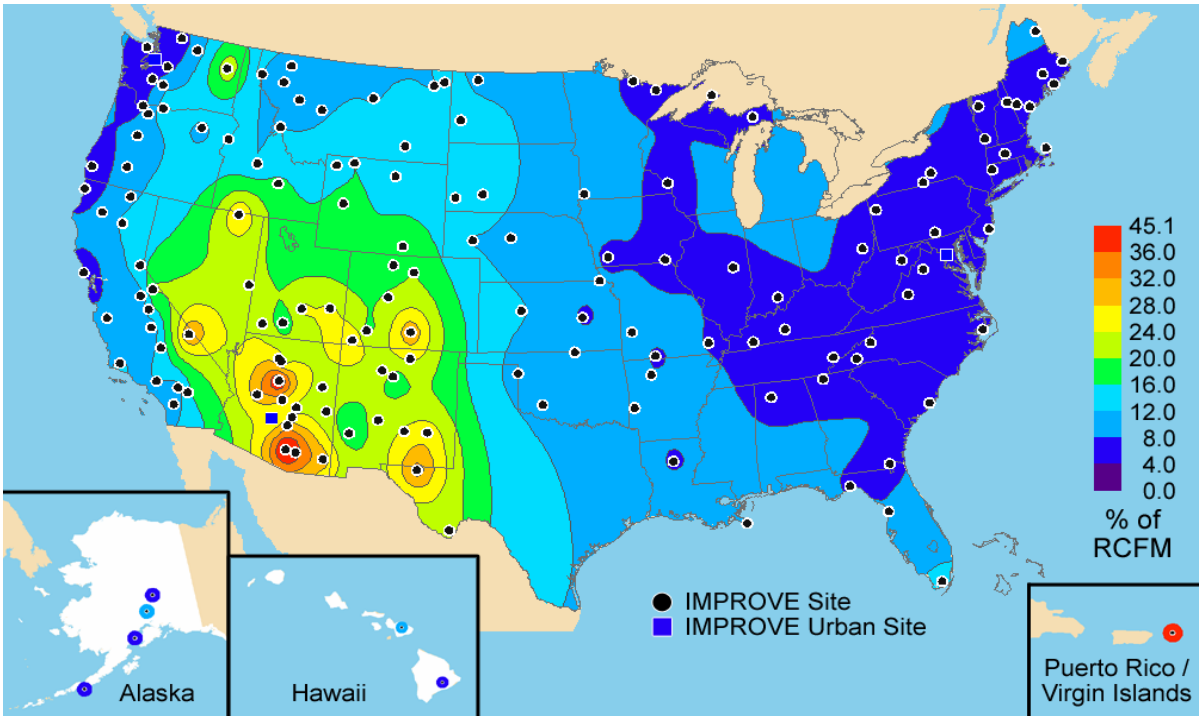

d) Fine soil fractional contribution to reconstructed fine mass for the IMPROVE and STN networks

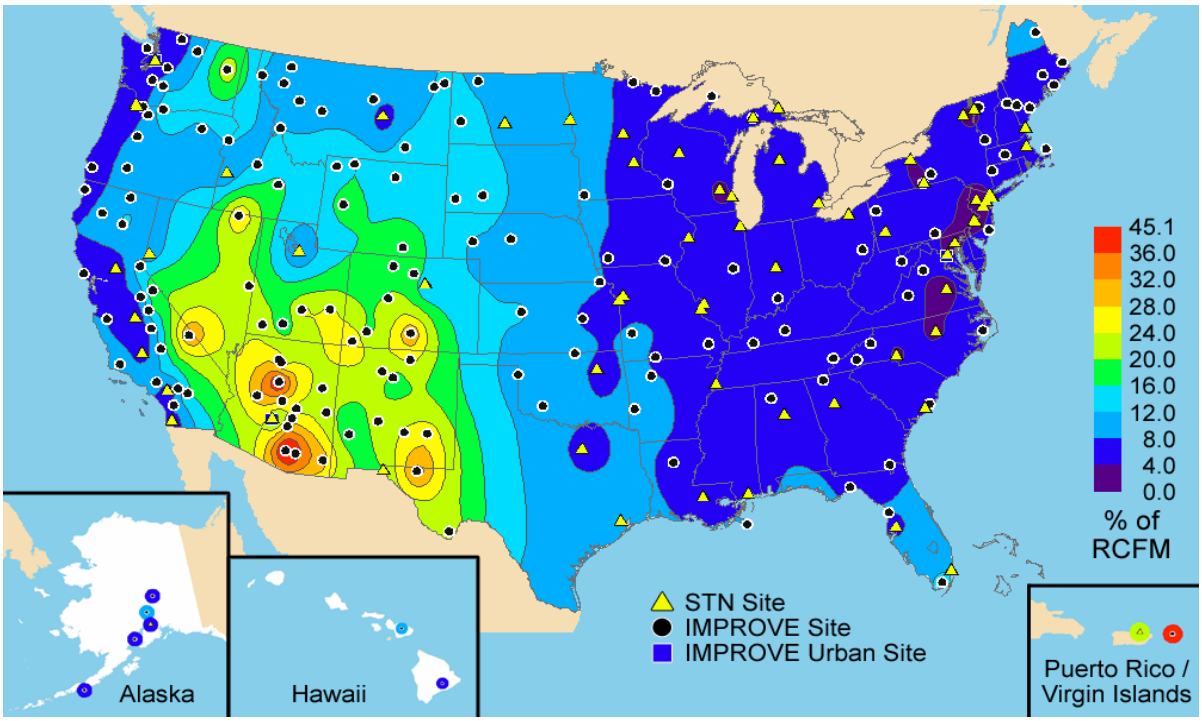

Figure 2.7. Isopleth maps of annual soil concentrations in panels a and b and percent contributions to reconstructed fine mass in panels c and d. Panels a–d include all sites from the IMPROVE network that met the prescribed completeness criteria including the urban sites for 2000–2004. Panels b and d also include all sites from the STN network that met the prescribed completeness criteria.

a) Reconstructed fine mass for the IMPROVE network

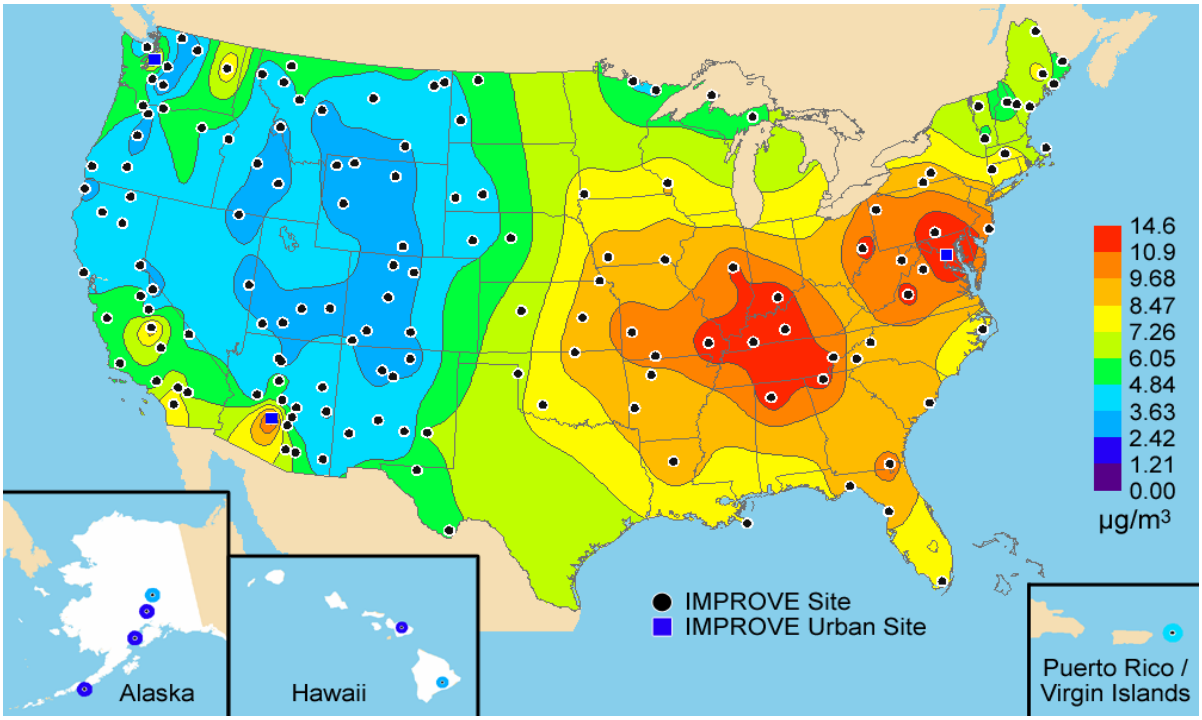

b) Reconstructed fine mass for the IMPROVE and STN networks

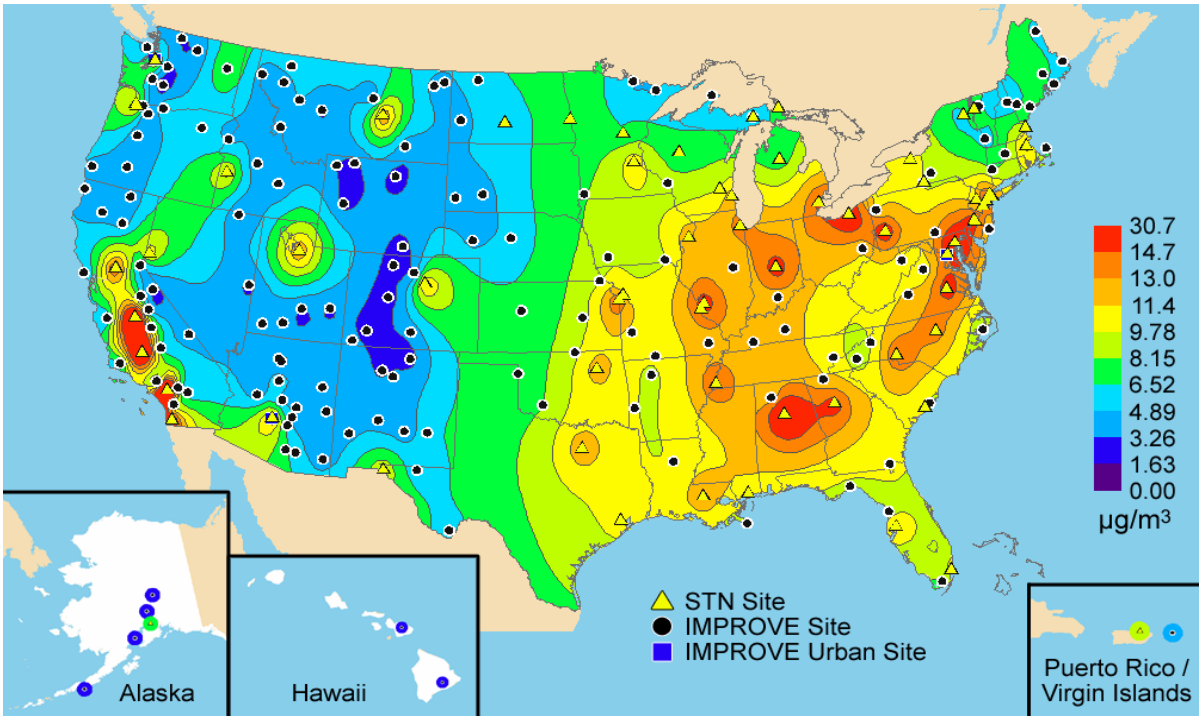

Figure 2.8. Isopleth maps of annual reconstructed fine mass concentrations. Panels a and b include all sites from the IMPROVE network that met the prescribed completeness criteria including the urban sites for 2000–2004. Panel b also includes all sites from the STN network that met the prescribed completeness criteria.

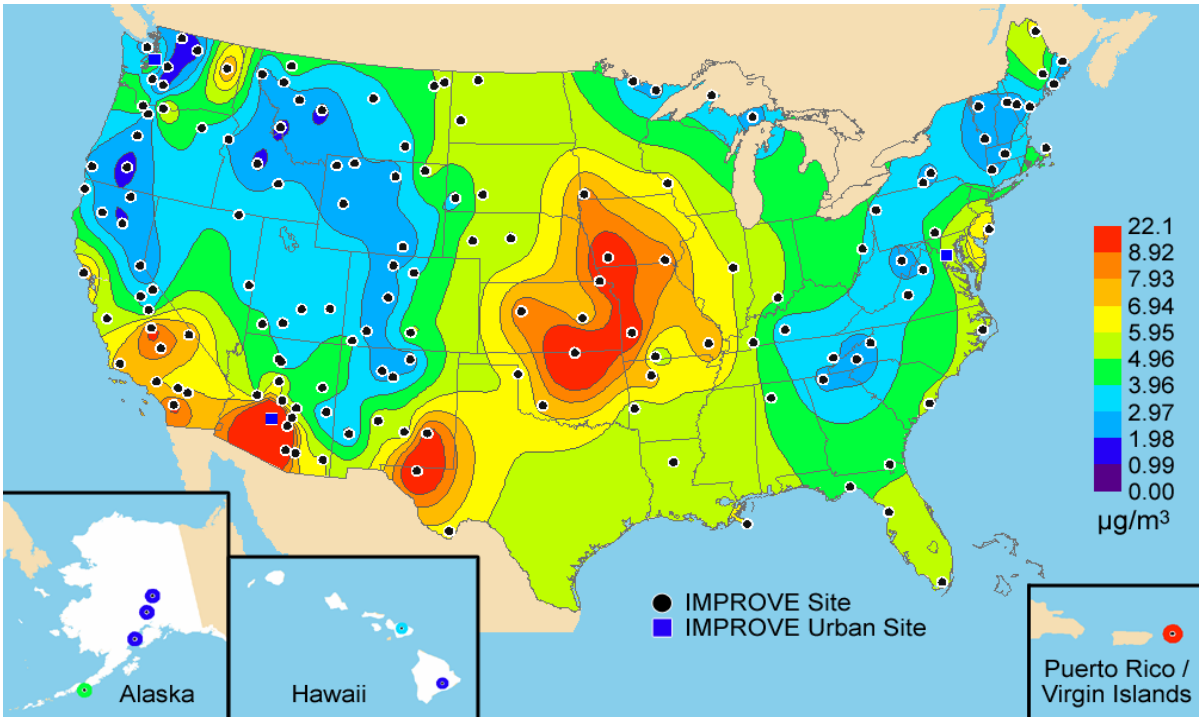

Figure 2.9. Isopleth map of annual coarse mass concentrations; includes all sites from the IMPROVE network that met the prescribed completeness criteria including the urban sites for 2000–2004.

2.5 SPATIAL TRENDS IN PARTICULATE EXTINCTION IN THE UNITED STATES

Spatial patterns in the reconstructed particulate extinction were similar to those observed for aerosol concentrations since reconstructed particle extinction is calculated from aerosol concentrations. However, because specific scattering of sulfates and nitrates were larger than other fine aerosols because of associated water, light-absorbing carbon has relatively high specific extinction, and coarse particle scattering contributes to total particulate extinction, the extinction budgets are somewhat different from fine aerosol budgets. Total particulate extinction was not calculated for the STN, and therefore fractional contributions to total particulate extinction were also not calculated for the STN because CM is not measured by this network.

2.5.1 Fine Particle Ammonium Sulfate Extinction

Figure 2.10 shows the ammonium sulfate light extinction coefficient averaged over the 5-year period 2000–2004 and the fractional contribution of ammonium sulfate to total particulate extinction expressed as a percentage for the same period. The spatial patterns in extinction and mass concentration attributed to ammonium sulfate were very similar but with steeper gradients observed in extinction. The east-to-west gradient in ammonium sulfate extinction is even stronger than that for concentrations, with extinction coefficients in the central eastern United States over a factor of 12 higher than the low extinction values found at the interior West sites rather than the factor of 8 observed in mass concentrations.

Both the peak ammonium sulfate mass concentration and extinction coefficient occurred at the STN southwestern Pennsylvania site. Similar to ammonium sulfate concentrations, the highest annual average rural and urban ammonium sulfate extinction coefficients, between 60 and 75 Mm^{-1}, were found in the central eastern United States. Extinction coefficients decrease in all directions from the high coefficient region, with extinction coefficients less than 5 Mm^{-1} through much of the interior West (Appendix A). The exception in the interior West is the urban Wasatch Front site, where the extinction coefficient was 12 Mm^{-1}. Along the Pacific coast, rural extinction coefficients were typically in the 5–10 Mm^{-1} range, with a few rural sites in the 10–20 Mm^{-1} range. Urban sites along the Pacific Coast were in the 15–25 Mm^{-1} range.

In the East, ammonium sulfate contributes at least 50% to reconstructed particulate extinction at most IMPROVE sites, with contributions of 70–80% in the Appalachian region (Figure 2.10b) and Hawaii. Ammonium sulfate contributions to particulate extinction were between 10% and 20% at four rural sites in the West including Yosemite National Park, California; Sawtooth National Forest, Idaho; Monture, Montana; and Sycamore Canyon, Arizona, as well as Phoenix, Arizona, an urban site, and Spokane, Washington, a heavily influenced rural site. Typical contributions in the interior West were 20–30%. Sites along the Pacific coast and in the middle of the United States had intermediate ammonium sulfate contributions of 30–50%.

2.5.2 Fine Particle Carbon Extinction

Figure 2.11 shows isopleths of the light extinction attributed to organic carbon and the fractional contribution of organics to particulate extinction. Because no humidity dependence for organics was considered, the spatial trends in organic carbon extinction coefficients were the same as for mass concentrations. The largest region of high rural organic carbon extinction coefficients (12–18 Mm^{-1}) was the southeastern United States; coefficients in this range were also present in the Sierra Nevada region of California and in the northern Rockies of Montana (Appendix A). The urban sites in the southeastern United States and California have OMC extinction coefficients that were even higher than the surrounding rural areas, with extinction coefficients greater than 18 Mm^{-1} at most urban sites and a peak value of 50 Mm^{-1} in the San Joaquin Valley of California. Additional localized high concentration areas in the Northwest, the interior West, and the midwestern United States were identified with the inclusion of the urban sites. The lowest extinction coefficients (1.5–4 Mm^{-1}) were at the sites with the lowest OMC concentrations, which were Simeonof and Tuxedni, Alaska; Hawaii Volcanoes National Park and Haleakala, Hawaii; the Virgin Islands; Wheeler Peak, New Mexico; White River, Colorado; and White Pass, Washington.

With the exception of two sites in Arizona, Sycamore Canyon and Saguaro National Monument East, the contribution of OMC to reconstructed particulate extinction at IMPROVE sites is less than its contribution to RCFM. The greatest contributions of organic carbon to particulate extinction occur in the northwestern United States, with peak contributions of 50–60% of extinction at Trinity, Lassen Volcanic National Park, and Crater Lake National Park in the Oregon/northern California region; at Sula Peak and Monture in the northern Rockies of Montana; at Denali National Park in Alaska; and at Sawtooth National Forest in the Hells Canyon region of Idaho. Most sites in the interior mountainous West, including the northern Sierra Nevada, have extinction contributions in the 30–50% range. The remaining areas west of

the eastern border of Colorado were typically in the 20–30% isopleth, whereas most sites east of that line were in the 10–20% isopleth. The only site where organics contributed less than 10% to particulate extinction was the Virgin Islands.

The light extinction attributed to aerosol absorption by light-absorbing carbon and the fractional contribution of LAC to particulate extinction are shown in Figure 2.12. Again, because there is no humidity dependence for estimating the extinction attributed to LAC, the spatial trends in LAC extinction and concentration were the same. Peak rural LAC concentrations and extinction coefficients were found at Old Town, Maine; M.K. Goddard, Pennsylvania; Mingo, Missouri; and James River Face Wilderness, Virginia. The highest LAC extinction coefficients and concentrations were found at the STN sites in southeastern Florida, El Paso, Texas, New Jersey, and Puerto Rico. Unlike OMC, the percent contributions of LAC to particulate b_{ext} were, with the exception of Simeonof, Alaska, greater than their contributions to RCFM. The peak LAC extinction coefficients were primarily in the eastern United States, whereas the peak contributions to particulate b_{ext} were found in the West.

2.5.3 Fine Particle Ammonium Nitrate Extinction

Similar to ammonium sulfate, the hygroscopicity of ammonium nitrate is also accounted for in the ammonium nitrate extinction coefficients; thus the spatial trends in ammonium nitrate extinction coefficients were generally the same but not identical to those in ammonium nitrate concentrations. The isopleths of ammonium nitrate extinction coefficients and the fractional contribution of ammonium nitrate to particulate b_{ext} expressed as a percentage are shown in Figure 2.13. Rural ammonium nitrate extinction coefficients were highest at the central and southern California sites and in the Midwest, where ammonium nitrate concentrations were highest, and lowest in the interior West, where again the concentrations were lowest (Appendix A). Whereas the rural extinction coefficients were highest, 20–27 Mm-1, in the Midwest, the highest urban extinction coefficients, between 60 and 90 Mm^{-1}, were in metropolitan Los Angeles and the San Joaquin Valley, California. Outside of the Midwest and California, the Wasatch Front in Utah was the only site to have ammonium nitrate extinction coefficients greater than 30 Mm^{-1}. Also, similar to ammonium sulfate, there is a stronger gradient between the lowest to the highest coefficients observed at the rural sites, with a factor of 20 range in coefficients as compared to a factor of 13 observed in concentrations.

Ammonium nitrate consistently makes larger contributions, in the range of 1–7 percentage points, to particulate b_{ext} than to RCFM at the IMPROVE sites. The peak ammonium nitrate contribution to reconstructed particulate extinction of 40% is found in the San Gorgonio Wilderness, California. Contributions of greater than 30% were also found at Point Reyes National Seashore, Joshua Tree National Park, and San Gabriel, California; Lake Sugema and Viking Lake, Iowa; Great River Bluffs and Blue Mounds, Minnesota; and Columbia River Gorge, Washington.

2.5.4 Fine Particle Soil Extinction

Figure 2.14 shows the annual average spatial distribution for the 2000–2004 period of fine soil mass extinction coefficients and the soil fractions of total particulate extinction. The spatial trends in fine soil extinction are identical to the spatial trends in fine soil mass

concentrations—fine soil is assumed to be nonhygroscopic and its mass scattering efficiency is estimated to be 1 m^2/g. To reiterate from section 2.4, the highest rural fine soil concentrations, and therefore extinction coefficients, not surprisingly were found in the arid Southwest at Sycamore Canyon and the west and east units of Saguaro National Park, Arizona, at 2.61, 3.08, and 2.18 Mm^{-1}, respectively (Appendix A). The Virgin Islands, the Queen Valley in southern Arizona, and the west Texas sites of Guadalupe Mountains and Salt Creek all had coefficients in the 1.5–2 Mm^{-1} range. Rural fine soil extinction coefficients in the range of 1–1.5 Mm^{-1} were found in southern Colorado; the Death Valley National Monument, California; El Dorado Springs, Missouri; in the Cherokee Nation, Oklahoma; and throughout most of Arizona. For most of the rural United States, soil extinction coefficients were between 0.5 and 1 Mm^{-1}, with the Great Lakes area, the northern Rockies, Alaska, Hawaii, and the northwestern and northeastern United States generally having soil concentrations less than 0.5 Mm^{-1}. The peak soil extinction of 4.8 Mm^{-1} occurs at the urban STN site in El Paso, Texas. The STN Puerto Rico site and the IMPROVE Phoenix and Spokane sites have soil coefficients greater than 2 Mm^{-1}. Urban soil extinction coefficients in the range of 1–2 Mm^{-1} are found in Arizona and west Texas, as well as in Alabama, California, Colorado, Florida, Missouri, Nebraska, and Ohio.

Whereas fractional fine soil contributions to RCFM were as high as 50%, contributions to particulate b_{ext} were all under 12%. In all cases, the contribution of fine soil to reconstructed particulate extinction is significantly less than its contribution to fine mass. In the most extreme example, fine soil contributed 51% to RCFM but only 9% to particulate b_{ext} at the Virgin Islands site. The largest contributions of fine soil to particulate b_{ext}, between 5% and 12%, were in the arid southwestern United States and the Virgin Islands.

2.5.5 Coarse Mass Particle Extinction

Figure 2.15 shows the CM extinction coefficients and the CM fractions of reconstructed extinction expressed as a percentage of particulate b_{ext}. Coarse mass is assumed to be composed of soil and to be nonhygroscopic and therefore to have an estimated mass scattering efficiency of 0.6 m^2/g. The spatial trends in CM were the same as for CM concentrations and were quite distinct from the spatial trends in RCFM (see section 2.4). The highest CM concentrations, and therefore CM extinction coefficients, 5–9 Mm^{-1}, were concentrated farther west in the middle of the United States and in the arid Southwest and southern California (Appendix A). Coarse mass extinction coefficients were also very high, 8.02 Mm^{-1}, in the Virgin Islands. From the central Great Plains, CM coefficients trended toward increasingly lower coefficients in the range of 1–4 Mm^{-1} to the north, east, and west until reaching the coasts. The sites along the Pacific, Gulf, and Atlantic coasts typically had moderate to high CM coefficients in the 3–4 Mm^{-1} range. The CM coefficients were generally very low, 0.5–1.5 Mm^{-1}, in the following northwestern regions—the northern Rockies, Oregon and northern California, the Northwest, and Alaska. Similarly, low coefficients also occurred at Hawaii Volcanoes National Park, Hawaii; Shining Rock Wilderness, North Carolina; Lye Brook Wilderness, Vermont; and Seney, Michigan. The most significant contribution from CM to particulate b_{ext}, 35.7%, occured at the Virgin Islands. Contributions of 20–30% were found in Death Valley, California, western Texas, and southern Arizona. Moving from this region, west to the California coast and north to increasingly higher latitudes and moving farther inland, CM contributes between 10% and 20% to reconstructed particulate extinction. Throughout most of the Northwest and all of the eastern United States, CM contributions were less than 10%.

2.5.6 Total Reconstructed Particulate Extinction (b_{ext})

Total reconstructed particulate extinction was not calculated for the STN because CM is not measured by this network. The highest rural particulate b_{ext} coefficients, those greater than 90 Mm^{-1}, were concentrated in the central eastern United States (Figure 2.16) and the lowest, those less than 15 Mm^{-1}, were concentrated in the interior West and Alaska (Appendix A). The high particulate b_{ext} region represents the intersect of the regions of high mass concentrations of ammonium sulfate, ammonium nitrate, OMC, and LAC in a region of comparatively high average relative humidity. The spatial trends in b_{ext} were very similar to those in RCFM; however, the east-to-west gradient between the lowest values in the interior West and the highest values in the East is stronger for the extinction coefficients (over a factor of 9 change) than for mass concentrations (over a factor of 7).

2.5.7 Visibility Expressed in Deciviews

Another way of displaying visibility estimates from aerosol data is by using the deciview (dv) scale. The dv scale was designed to linearly relate to humanly perceived differences in visibility, which is not the case for light extinction. Particle-free or Rayleigh conditions have a dv value of 0, and a change of 1 dv is a small but often noticeable change in perceived visibility.

Figure 2.17 shows isopleths of dv averaged over the 2000–2004 period. While the spatial patterns in visibility impairment were the same as for reconstructed particulate extinction, taking the log of aerosol extinction to calculate the dv has the effect of reducing the strength of the observed east-to-west gradient in dv as compared to Mm^{-1}. The broad region that includes the Great Basin, most of the Colorado Plateau, and portions of the Rocky Mountains and Hells Canyon had visibility impairment of less than 10 dv (Appendix A). Moving in any direction from this region generally results in a gradient of increasing dv. The Alaska sites also had visibility impairment of 10 dv or less. Hawaii and the Virgin Islands were in the 10–12 dv range. Visibility impairments of 10–15 dv were found throughout much of the remainder of the West and in the Boundary Waters area. The Columbia River Gorge in Washington, San Gorgonio, Agua Tibia, and Sequoia National Park in California, and the western urban sites all had the highest visibility impairments for the West of 10–20 dv. With the exception of the Boundary Waters area, the eastern United States had visibility impairments of greater than 15 dv. The highest annual dv value was reported at Mammoth Cave National Park and Washington, D.C., with an impairment of 24 dv.

a) Ammonium sulfate extinction for the IMPROVE network

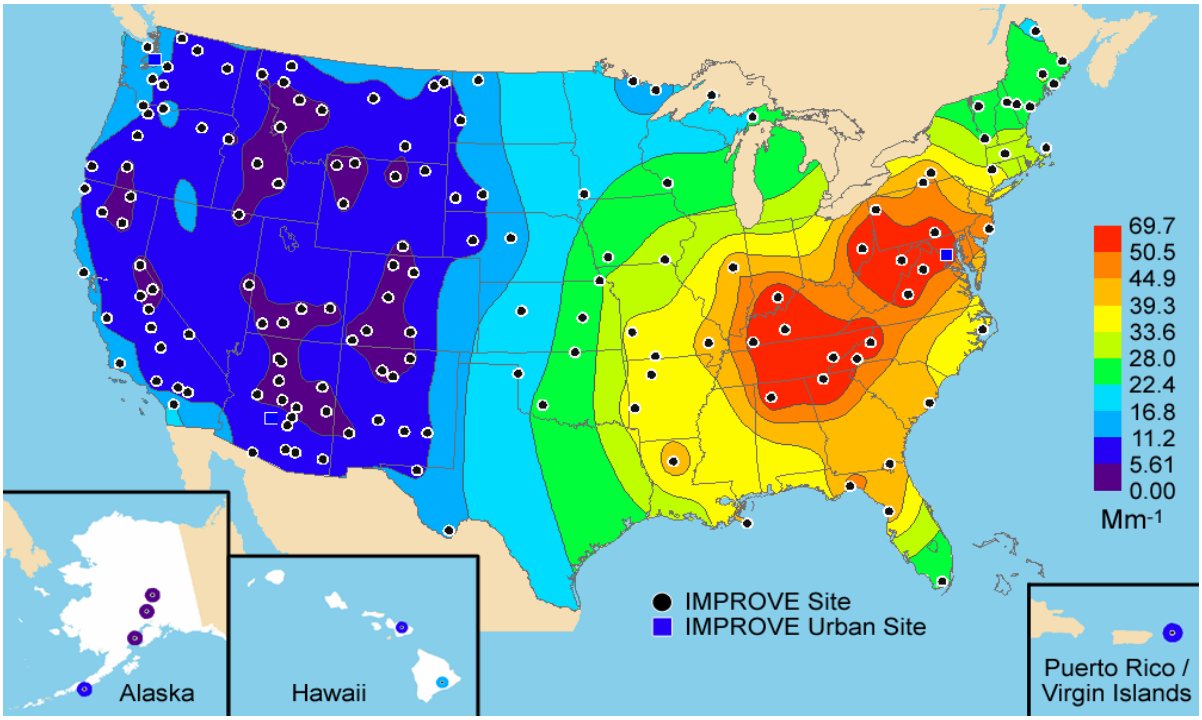

b) Ammonium sulfate extinction for the IMPROVE and STN networks

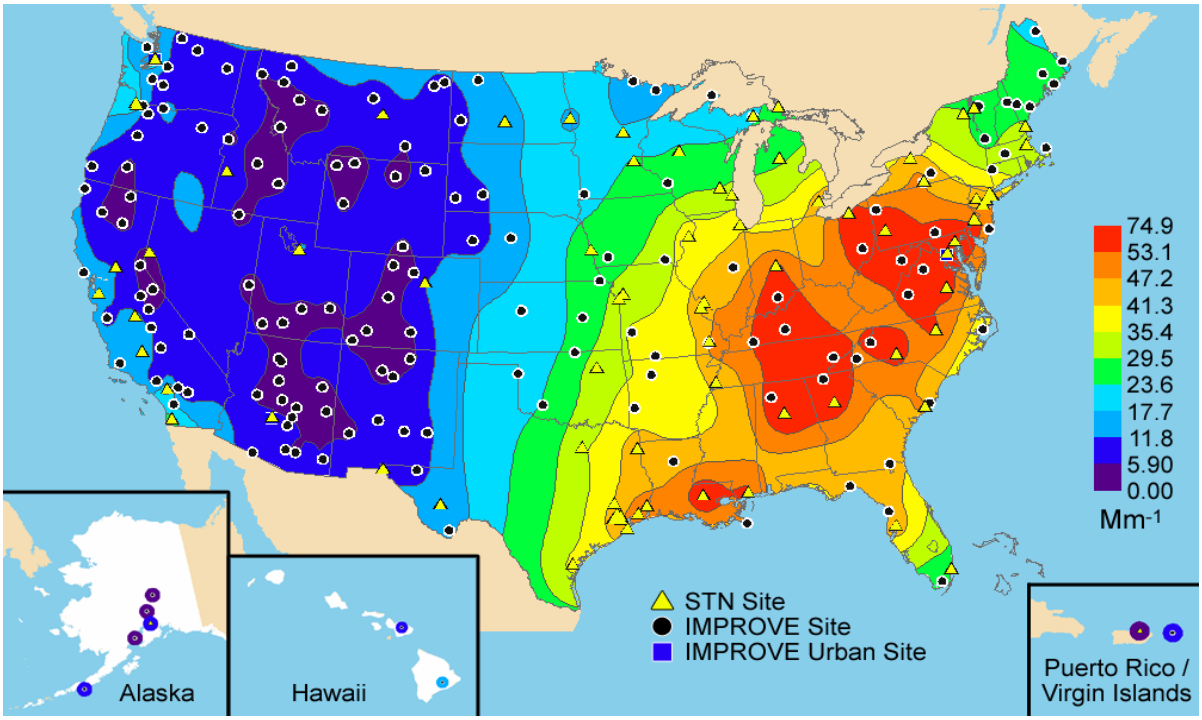

c) Ammonium sulfate fractional contribution to reconstructed particulate extinction for the IMPROVE network

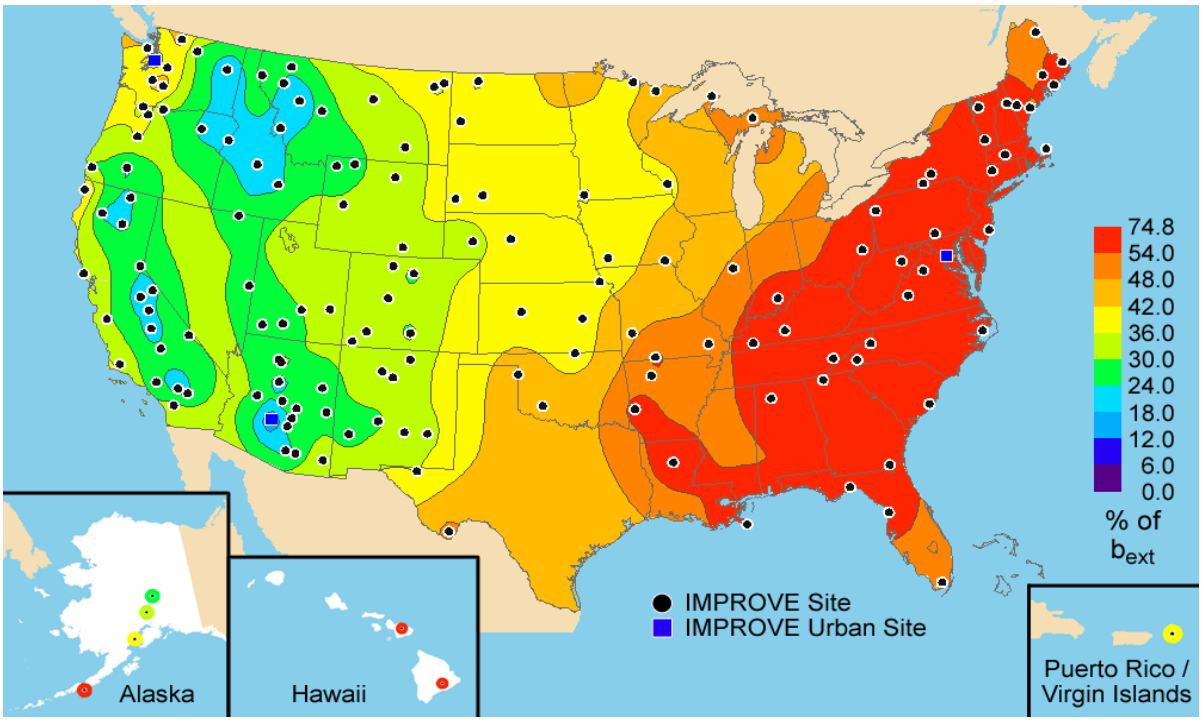

Figure 2.10. Isopleth maps of annual ammonium sulfate extinction coefficients in panels a and b and percent contribution to reconstructed particulate extinction in panel c. Panels a, b, and c include all sites from the IMPROVE network that met the prescribed completeness criteria including the urban sites for 2000–2004. Panel b also includes all sites from the STN network that met prescribed completeness criteria.

a) Organic carbon extinction for the IMPROVE network

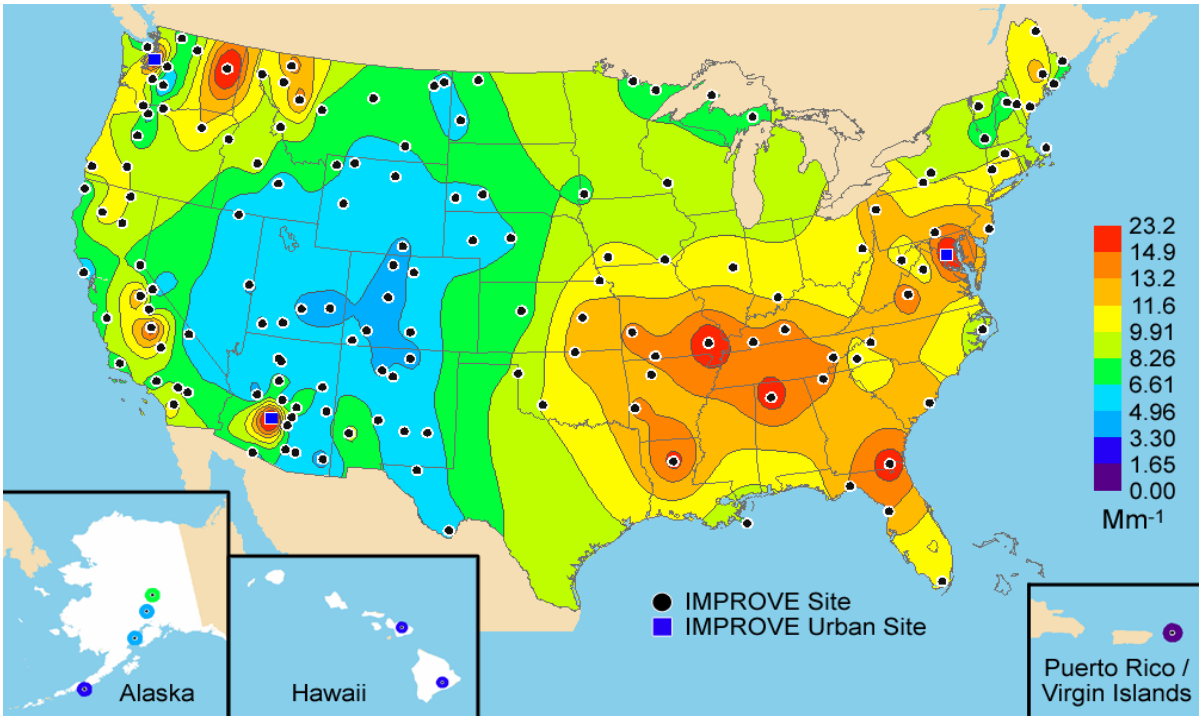

b) Organic carbon extinction for the IMPROVE and STN networks

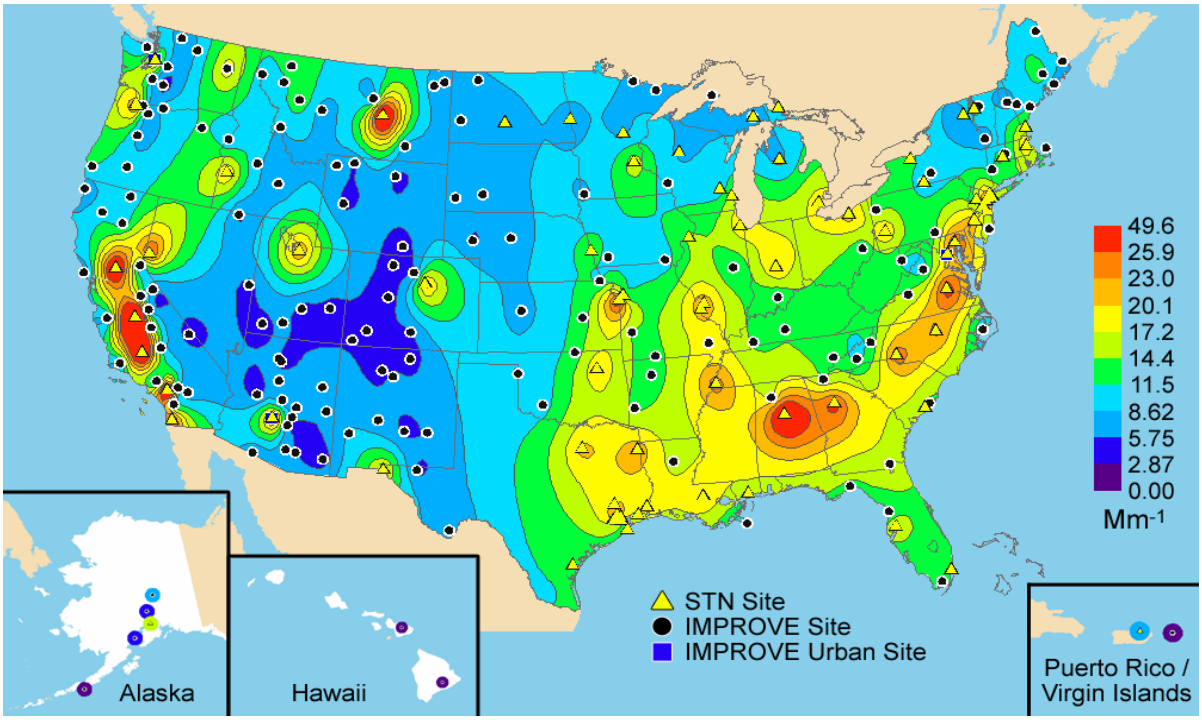

c) Organic carbon fractional contribution to reconstructed particulate extinction for the IMPROVE network

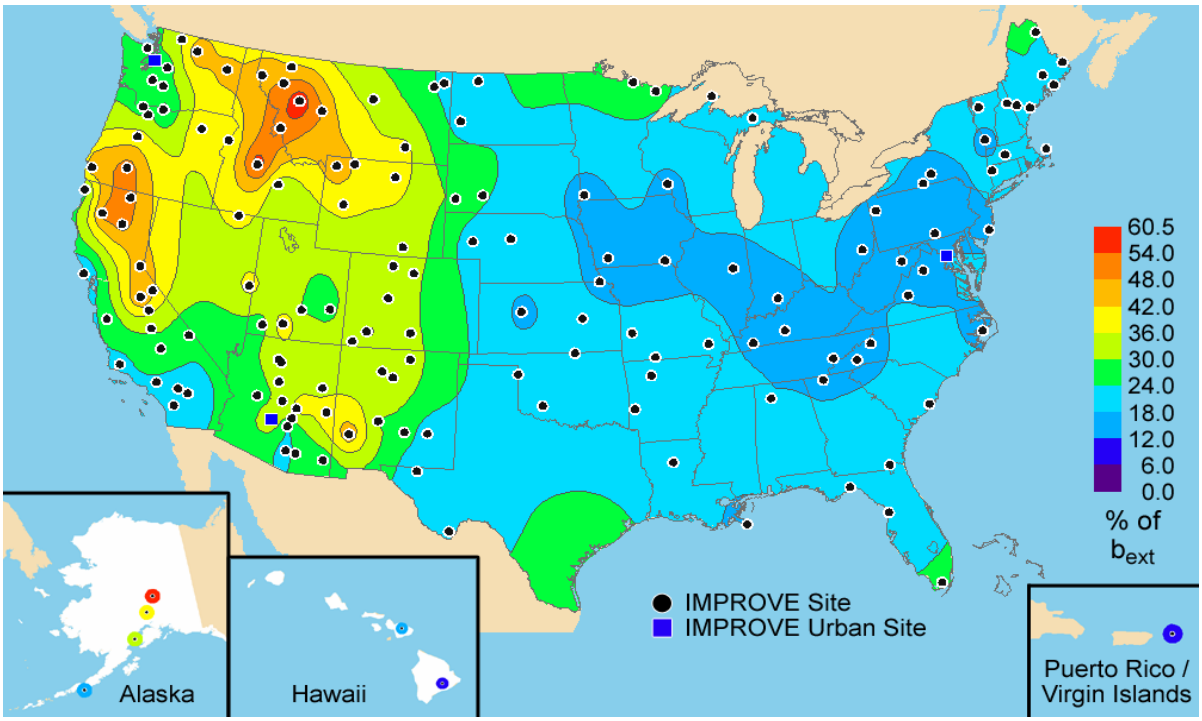

Figure 2.11. Isopleth maps of annual organic mass by carbon extinction coefficients in panels a and b and percent contribution to reconstructed particulate extinction in panel c. Panels a, b, and c include all sites from the IMPROVE network that met the prescribed completeness criteria including the urban sites for 2000–2004. Panel b also includes all sites from the STN network that met prescribed completeness criteria.

a) Light-absorbing carbon extinction for the IMPROVE network

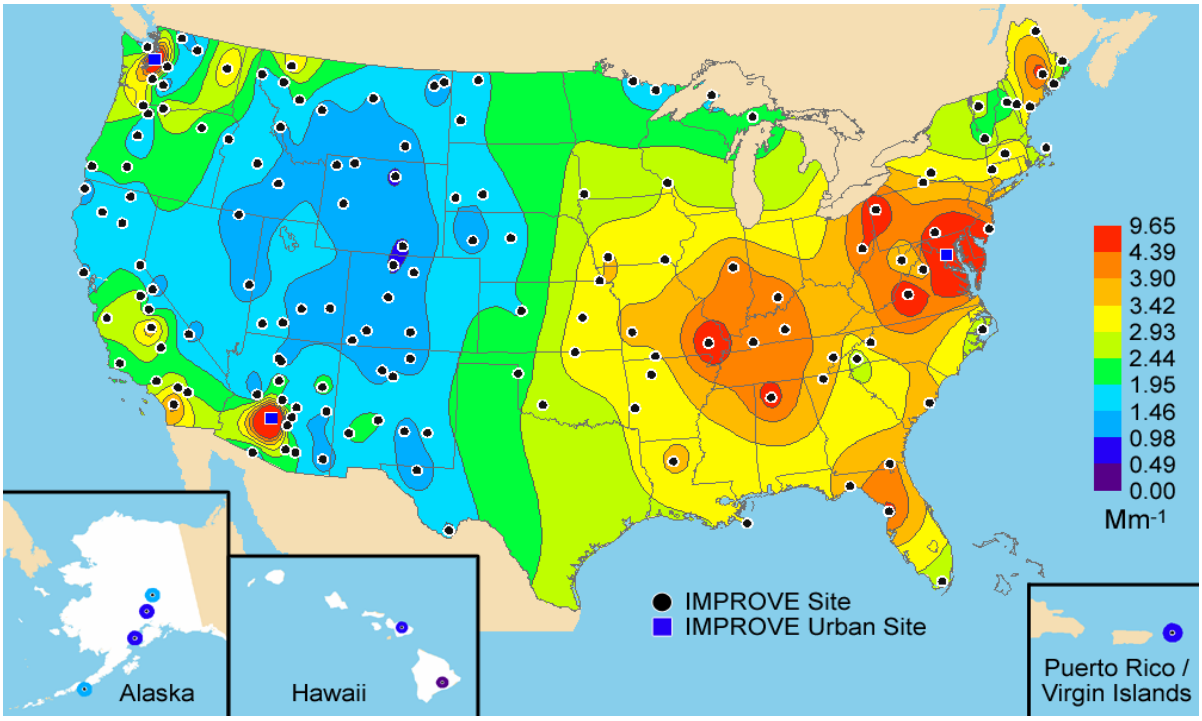

b) Light-absorbing carbon extinction for the IMPROVE and STN networks

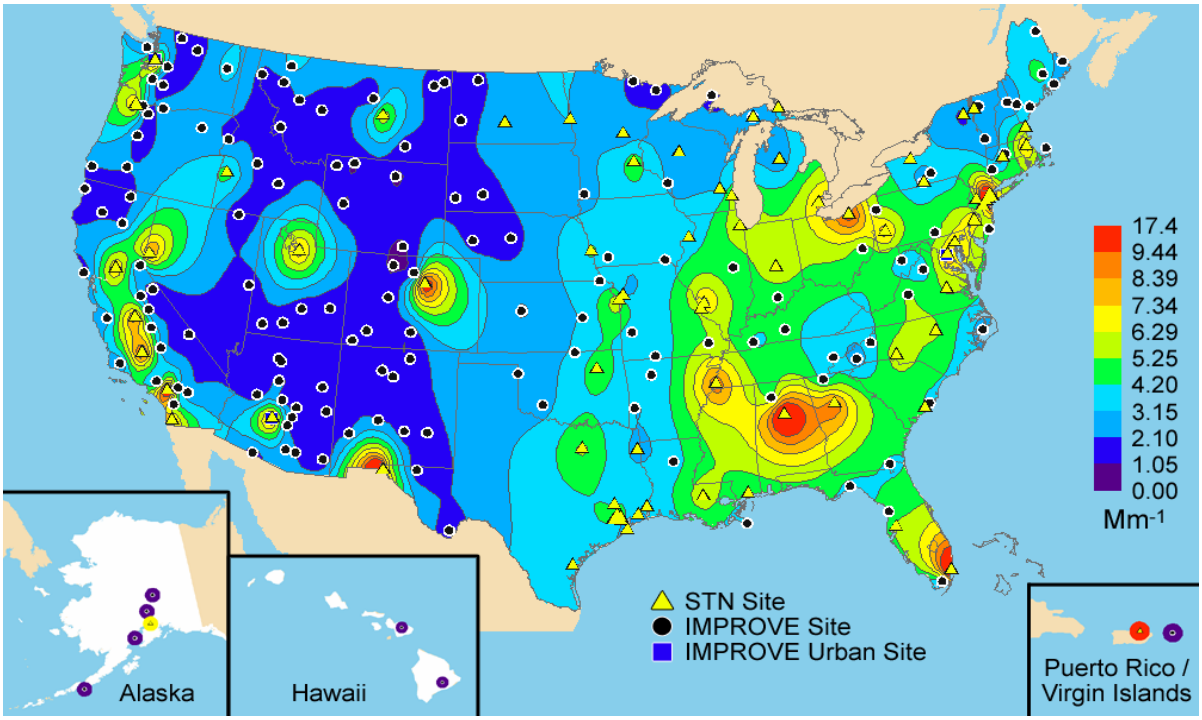

c) Light-absorbing carbon fractional contribution to reconstructed particulate extinction for the IMPROVE network

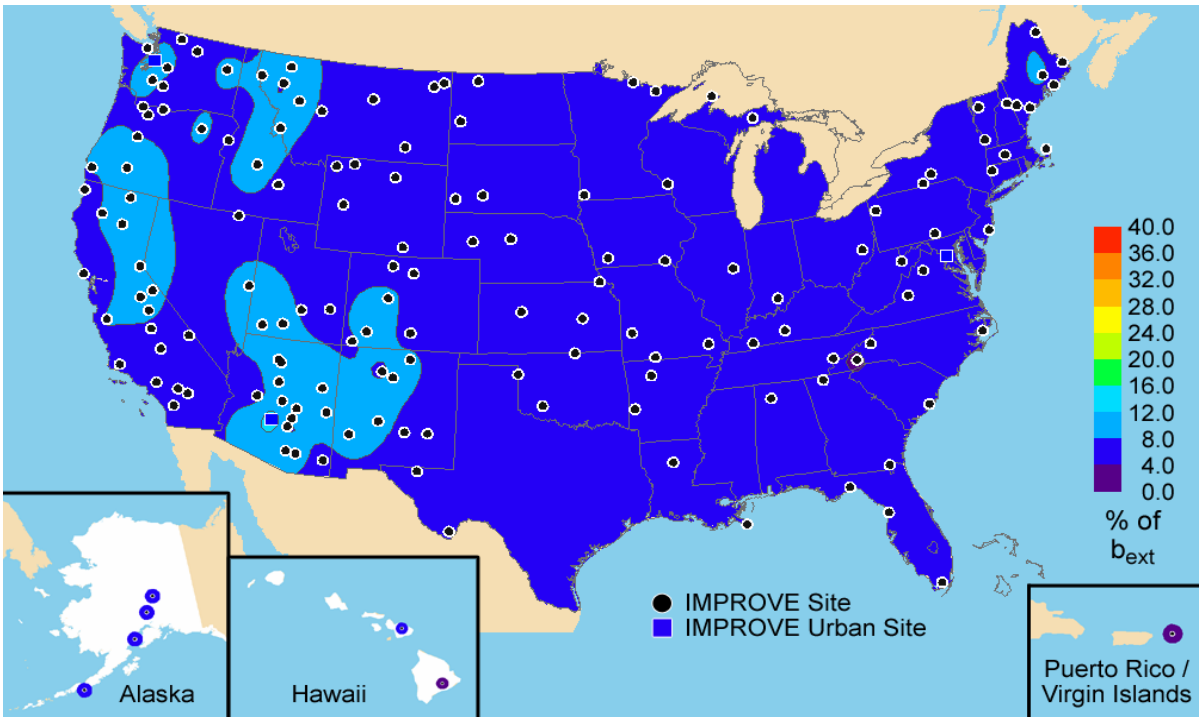

Figure 2.12. Isopleth maps of annual light-absorbing carbon extinction coefficients in panels a and b and percent contribution to reconstructed particulate extinction in panel c. Panels a, b, and c include all sites from the IMPROVE network that met the prescribed completeness criteria including the urban sites for 2000–2004. Panel b also includes all sites from the STN network that met prescribed completeness criteria.

a) Ammonium nitrate extinction for the IMPROVE network

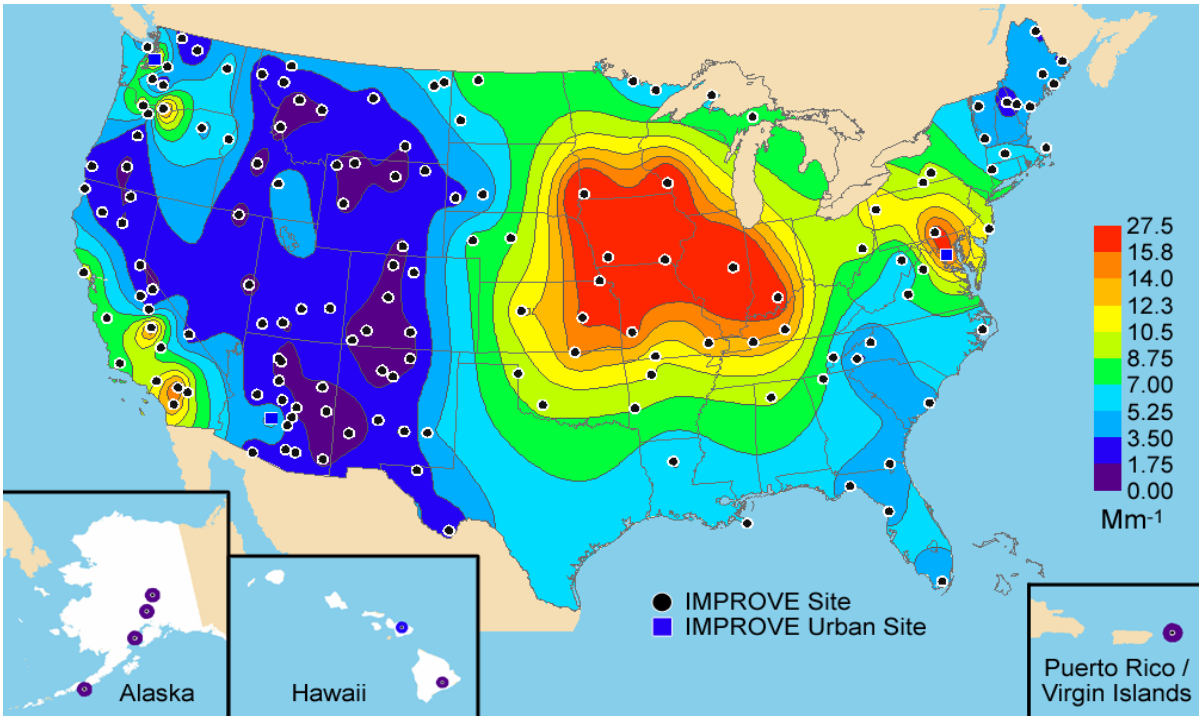

b) Ammonium nitrate extinction for the IMPROVE and STN networks

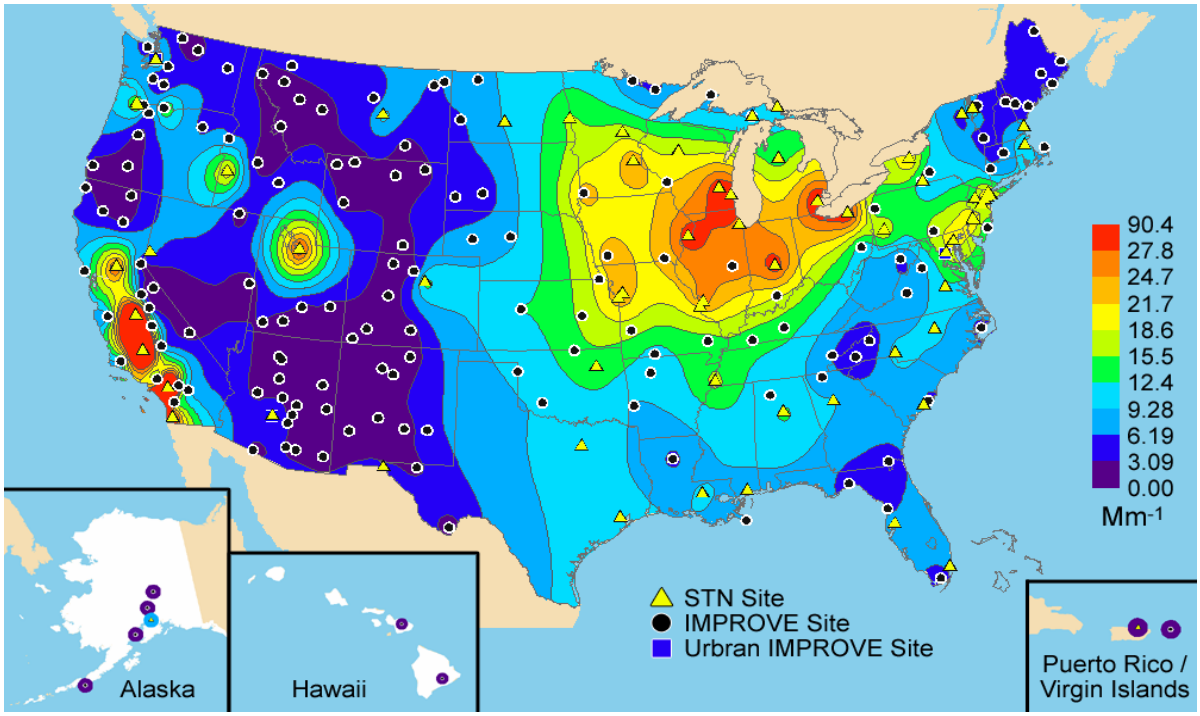

c) Ammonium nitrate fractional contribution to reconstructed particulate extinction for the IMPROVE network

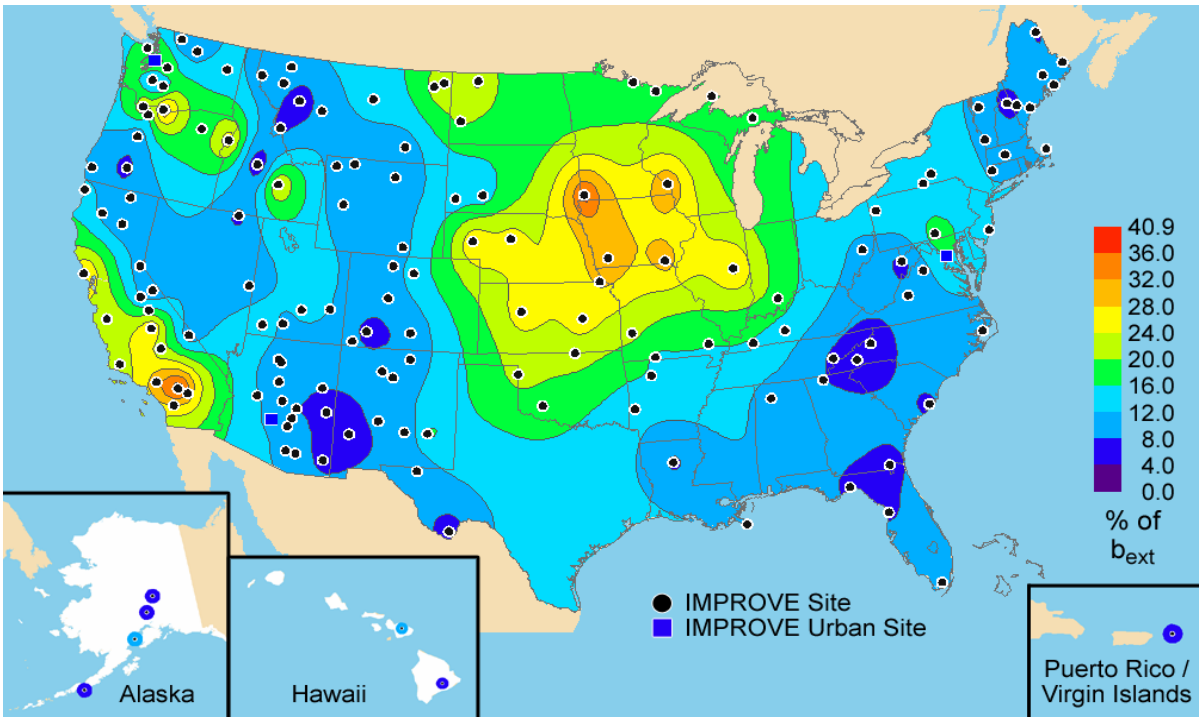

Figure 2.13. Isopleth maps of annual ammonium nitrate extinction coefficients in panels a and b and percent contribution to reconstructed particulate extinction in panel c. Panels a, b, and c include all sites from the IMPROVE network that met the prescribed completeness criteria including the urban sites for 2000–2004. Panel b also includes all sites from the STN network that met prescribed completeness criteria.

a) Fine soil extinction for the IMPROVE network

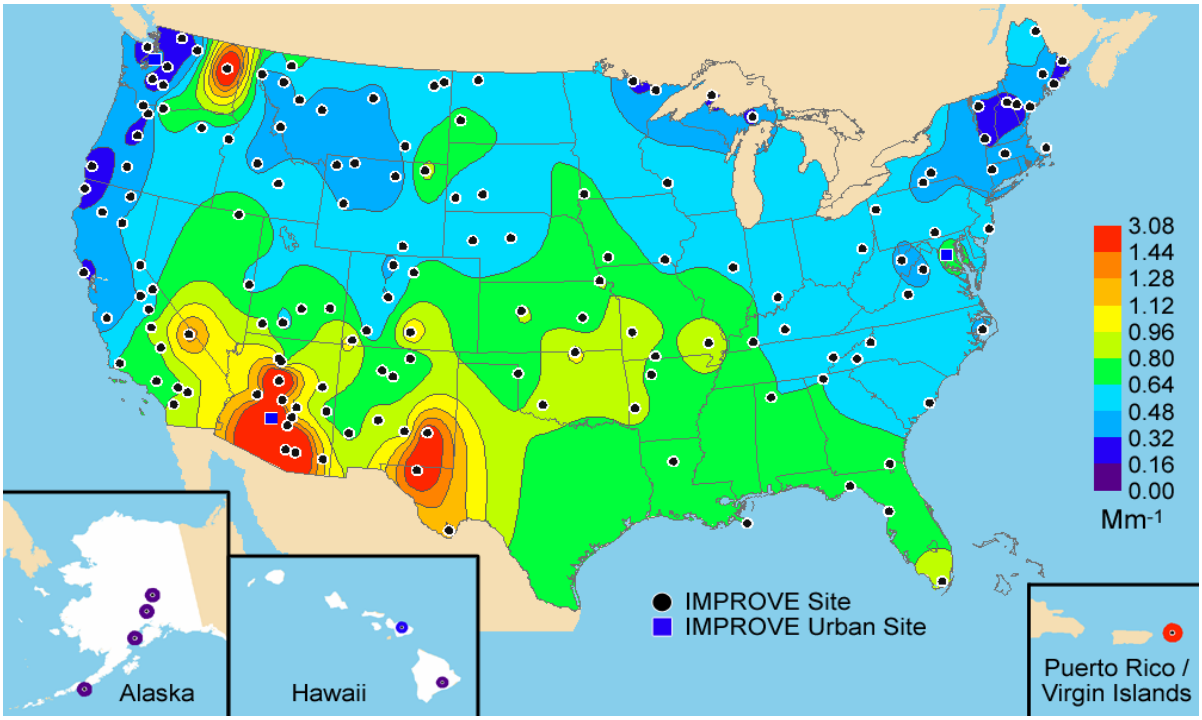

b) Fine soil extinction for the IMPROVE and STN networks

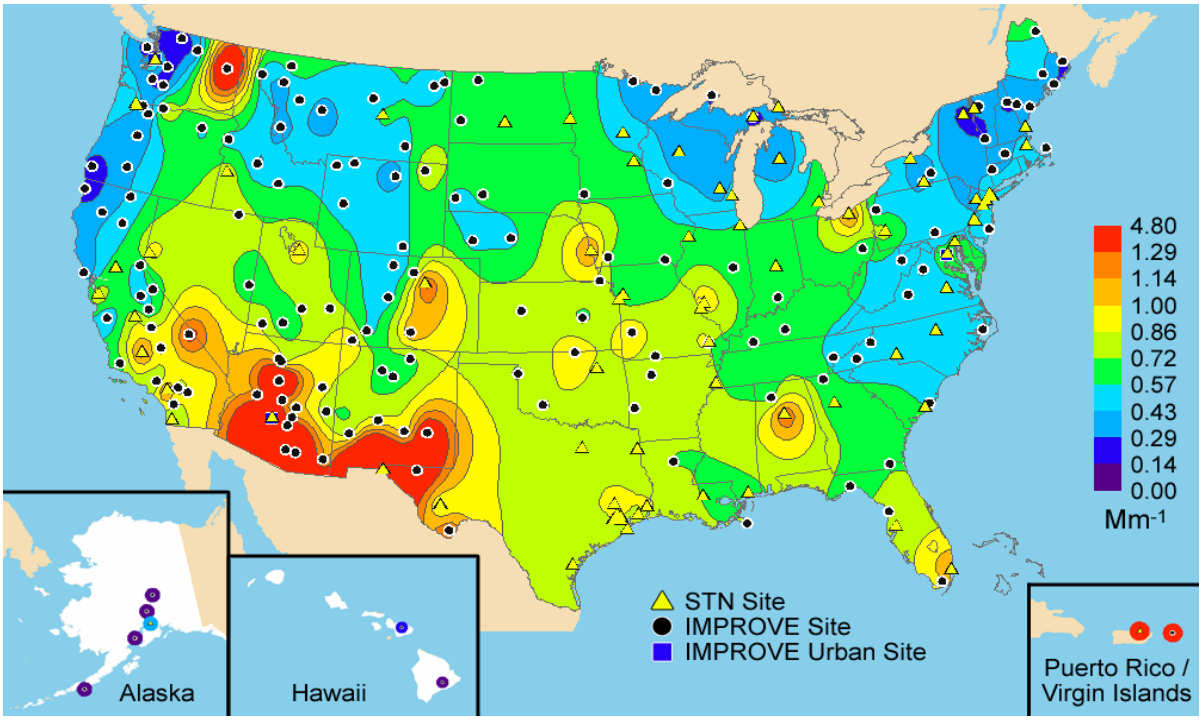

c) Fine soil fractional contribution to reconstructed particulate extinction for the IMPROVE network

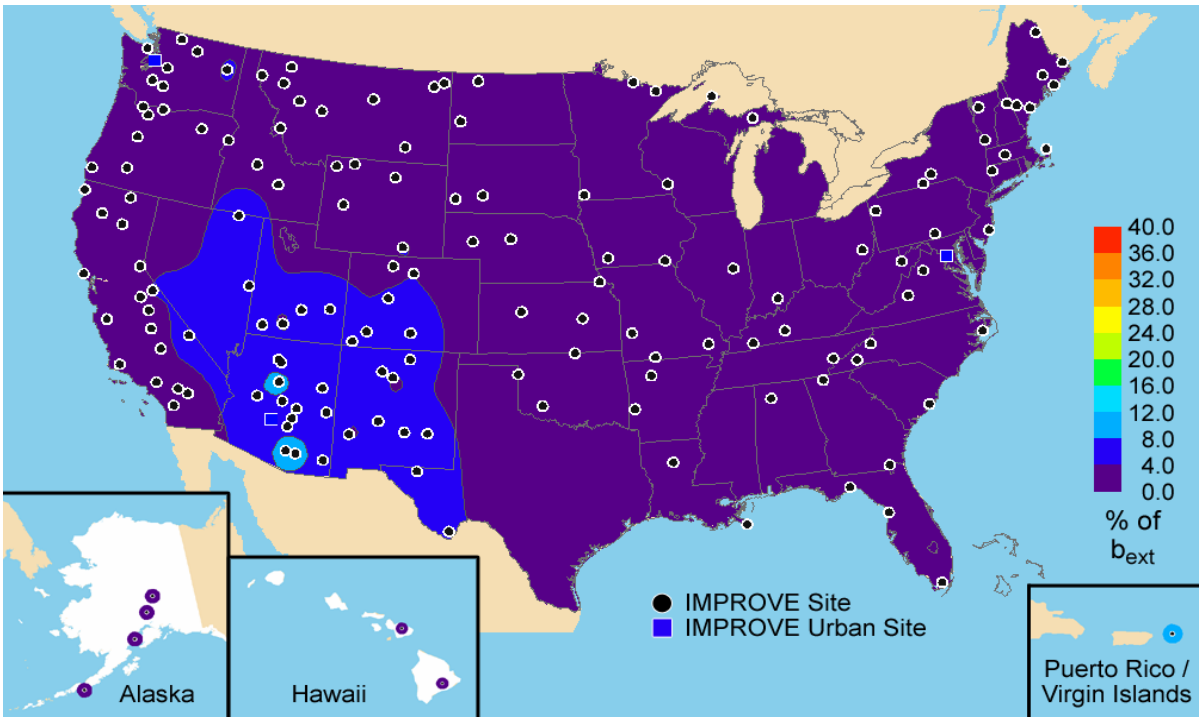

Figure 2.14. Isopleth maps of annual fine soil extinction coefficients in panels a and b and percent contribution to reconstructed particulate extinction in panel c. Panels a, b, and c include all sites from the IMPROVE network that met the prescribed completeness criteria including the urban sites for 2000–2004. Panel b also includes all sites from the STN network that met prescribed completeness criteria.

a) Coarse mass extinction for the IMPROVE network

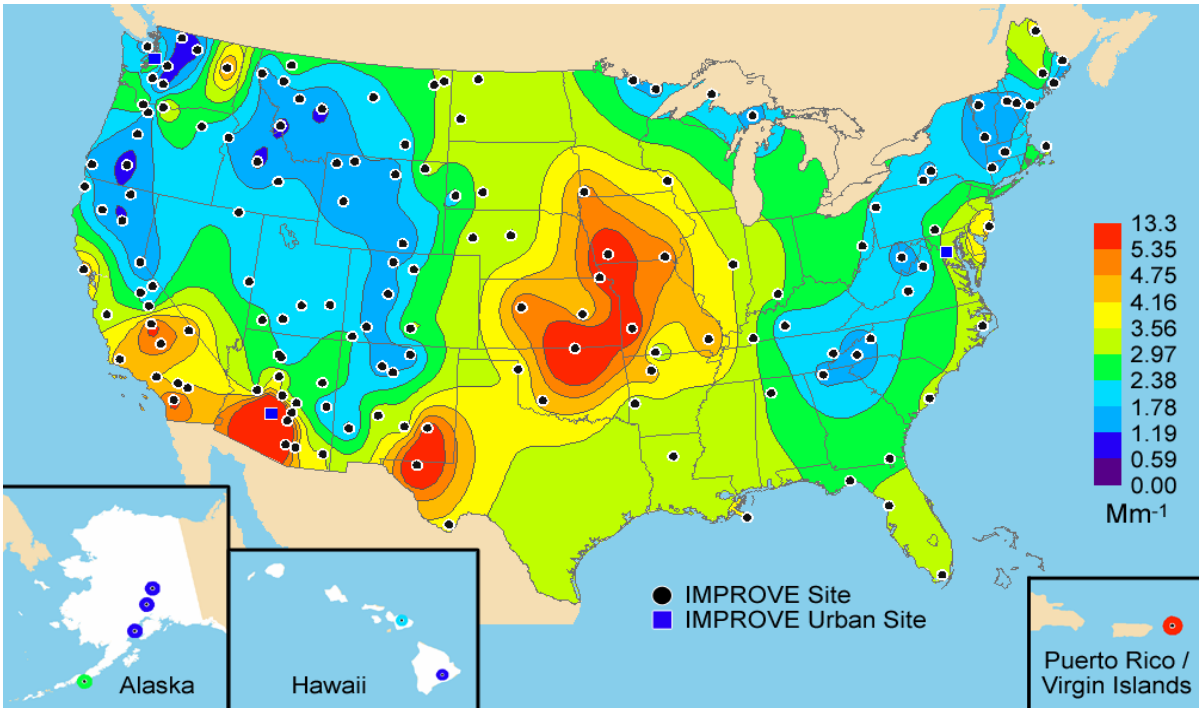

b) Coarse mass contribution to reconstructed particulate extinction for the IMPROVE network

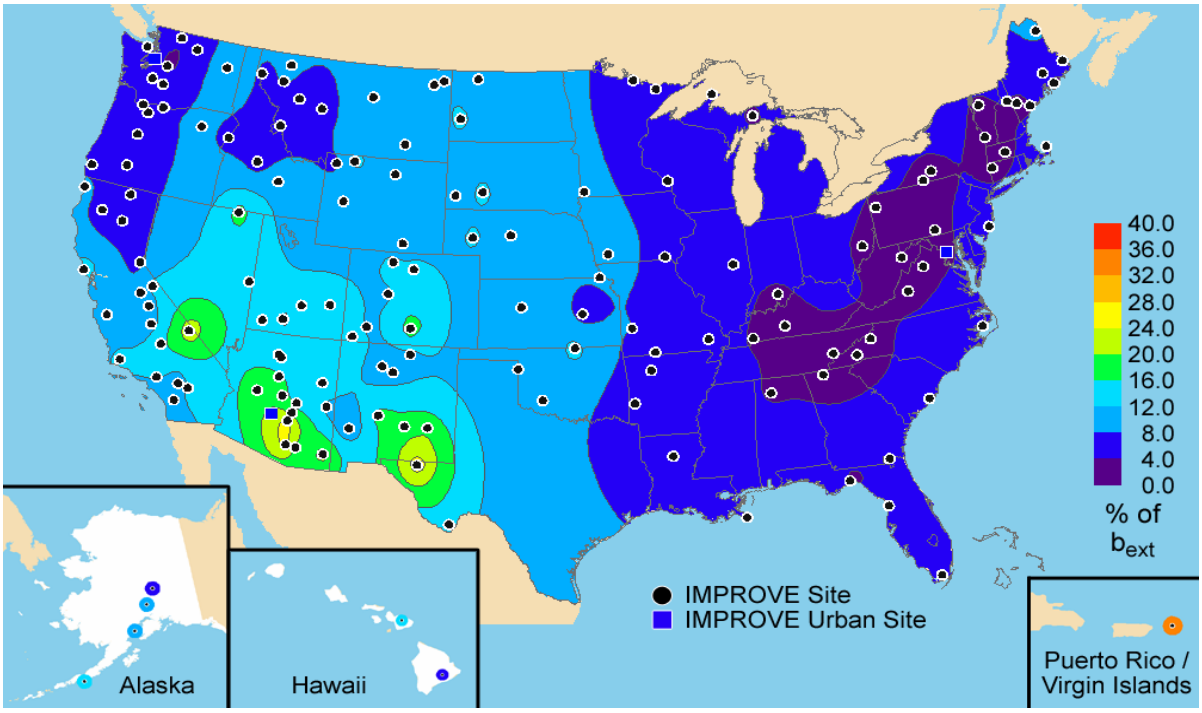

Figure 2.15. Isopleth maps of annual coarse mass extinction coefficients in panel a and percent contribution to reconstructed particulate extinction in panel b. Panels a and b include all sites from the IMPROVE network that met the prescribed completeness criteria including the urban sites for 2000–2004.

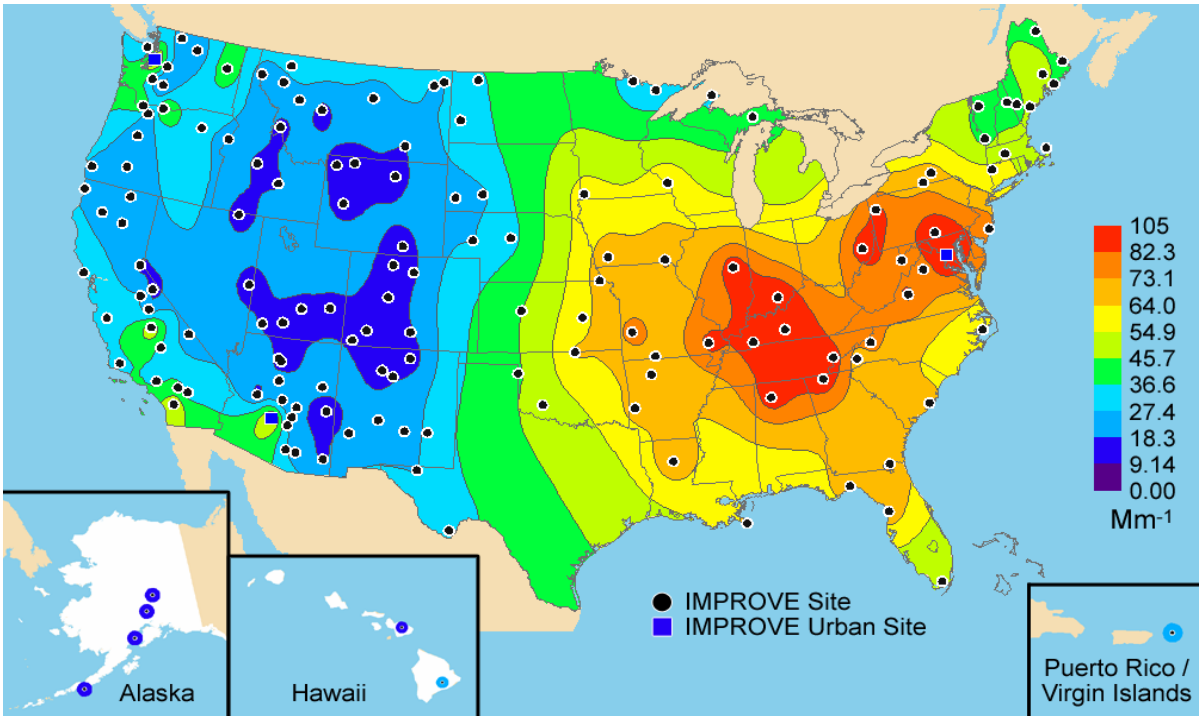

Figure 2.16. Isopleth map of annual total reconstructed particulate extinction in panel a. Includes all sites from the IMPROVE network that met the prescribed completeness criteria including the urban sites for 2000–2004. Rayleigh scattering was not included.

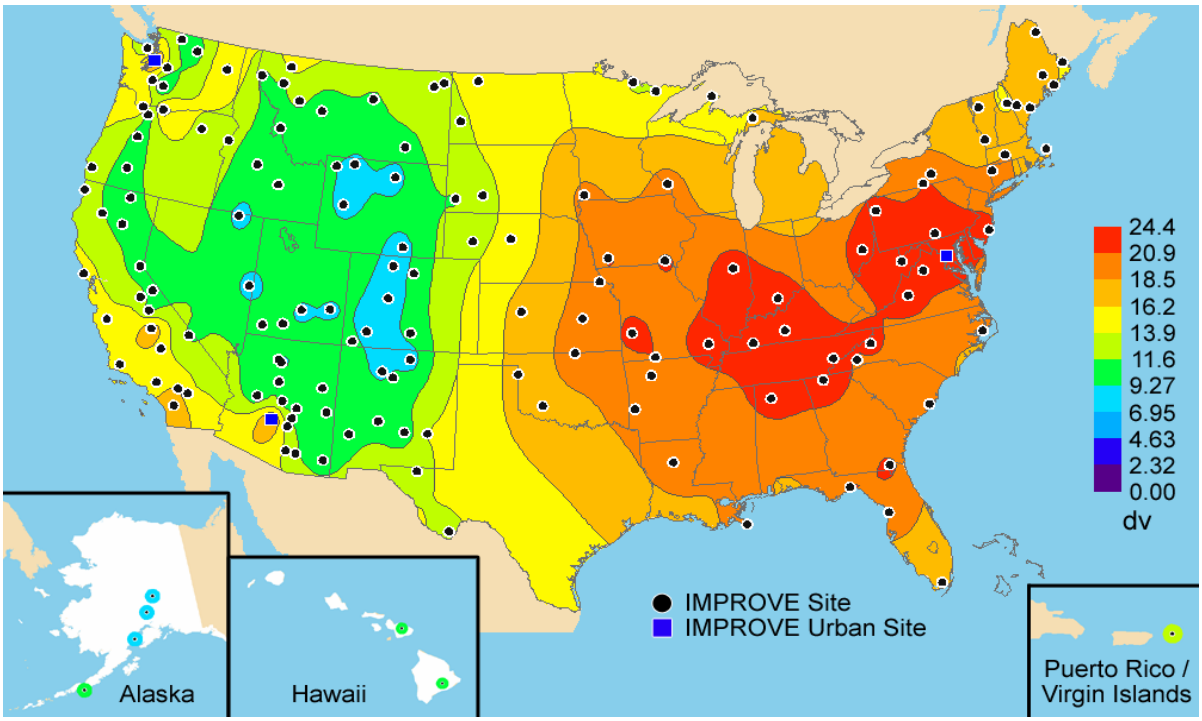

Figure 2.17. Isopleth map of annual visibility in deciviews in panel a. Includes all sites from the IMPROVE network that met the prescribed completeness criteria including the urban sites for 2000–2004.

REFERENCES

Bond, T. C., and R. W. Bergstrom (2005), Light absorption by carbonaceous particles: An investigative review, *Aerosol Science and Technology, 39*, 1-41.

Chu, S.-H. (2004), $PM_{2.5}$ episodes as observed in the speciation trends network, *Atmos. Environ., 38,* 5237-5246.

Day, D. E., W. C. Malm, and S. M. Kreidenweis (1997), Seasonal variations in aerosol composition and acidity at Shenandoah and Great Smoky Mountains National Park, *J. Air & Waste Manage. Assoc., 47*, 411-418.

Day, D. E., W. C. Malm, and S. M. Kreidenweis (2000), Aerosol light scattering measurements as a function of relative humidity, *J. Air & Waste Manage. Assoc.*, 5169-5176.

DeBell, L. J., M. Vozzella, R. W. Talbot, and J. E. Dibb (2004), Asian dust storm events of 2001 and associated pollutants observed in New England by the Atmospheric Investigation, Regional Modeling, Analysis and Prediction (AIRMAP) monitoring network, *J. Geophys. Res., 109*, D01304, doi:10.1029/2003JD003733.

Gebhart, K. A., and W. C. Malm (1989), An investigation of the size distributions of particulate sulfate concentrations measured during WHITEX, In *Transactions of the AWMA/EPA Int'l Specialty Conference on Visibility and Fine Particles*, edited by C.V. Mathai, Air and Waste Management Association, 157-169.

Gebhart, K. A., W. C. Malm, and D. E. Day (1994), Examination of the effects of sulfate acidity and relative humidity on light scattering at Shenandoah National Park, *Atmos. Environ., 28*(5), 841-849.

Grosjean, D., and S. K. Friedlander (1975), Gas-particle distribution factors for organics and other pollutants in the Los Angeles atmosphere, *J. Air Pollution Control Assoc., 25*, 1038-1044.

Hand, J. L., R. B. Ames, S. M. Kreidenweis, D. E. Day, and W. C. Malm (2000), Estimates of particle hygroscopicity during the Southeastern Aerosol and Visibility Study, *J. Air & Waste Manage. Assoc., 50*, 677-685.

Hand, J. L., S. M. Kreidenweis, D. E. Sherman, J. L. Collett, Jr., S. V. Hering, D. E. Day, and W. C. Malm (2002), Aerosol size distributions and visibility estimates during the Big Bend Regional Aerosol Visibility and Observational Study (BRAVO), *Atmos. Environ., 36*, 5043-5055.

Hand, J. L., and W. C. Malm (2006), Review of the IMPROVE equation for estimating ambient light extinction coefficients, http://vista.cira.colostate.edu/improve/Publications/GrayLit/016_IMPROVEeqReview/IMPROVEeqReview.htm

Hatakeyama, S., K. Izumi, T. Fukuyama, and H. Akimoto (1989), Reactions of ozone with alpha-pinene and beta-pinene in air: Yields of gaseous and particulate products, *J. Geophys. Res., 94*, 13,013-13,024.

Hawthorne, S. B., D. J. Miller, J. J. Langenfeld, and M. S. Krieger (1992), PM_{10} to high volume collection and quantification of semi- and nonvolatile phenols, methoxylated phenols, alkanes, and polycyclic aromatic hydrocarbons from winter urban air and their relationship to wood smoke, *Environ. Sci. Technol., 26*, 2251-2283.

Hogrefe O., J. J. Schwab, F. Drewnick, G. G. Lala, S. Peters, K. J. Demerjian, K. Rhoads, H. D. Felton, O. V. Rattigan, L. Husain, and V. A. Dutkiewicz (2004), Semicontinuous $PM_{2.5}$ sulfate and nitrate measurements at an urban and rural location in New York: PMTACS-NY summer 2001 and 2002 campaigns, *J. Air & Waste Manage. Assoc., 54*, 1040-1060.

Holes, A., A. Esebi, D. Grosgean, and D. Allen (1997), FTIR analysis of aerosol formed in the presence of the photo oxidation of 1,2,4–trimethylbenene, *Aerosol Sci. Technol., 26*, 516–526.

IMPROVE technical subcommittee for algorithm review (2006), Revised IMPROVE Algorithm for Estimating Light Extinction from Particle Speciation Data, http://vista.cira.colostate.edu/improve/Publications/GrayLit/019_RevisedIMPROVEeq/RevisedIMPROVEAlgorithm3.doc.

Izumi, K., and T. Fukuyama (1990), Photochemical aerosol formation from aromatic hydrocarbons in the presence of NOx, *Atmos. Environ., Part A, 241*, 1433-1441.

Jaffe, D., J. Snow, and O. Cooper (2003), The April 2001 Asian dust events: transport and substantial impact on surface particulate matter concentrations across the United States, *EOS transactions, November 18*.

Jang, M., and R. M. Kamens (1999), Newly characterized products and composition of secondary aerosols from the reaction of alpha-pinene with ozone, *Atmos. Environ., 33*, 459-474.

Jang, M., and R. M. Kamens (2001), Atmospheric secondary aerosol formation by heterogeneous reactions of aldehydes in the presence of a sulfuric acid aerosol catalyst, *Environ. Sci. Technol., 35*, 4758-4766.

Kavouras, I. G., N. Mihalopoulos, and E. G. Stephanou (1998a), Formation of atmospheric particles from organic acids produced by forests, *Nature, 395*, 683-686.

Kavouras, I. G., N. Mihalopoulos, and E. G. Stephanou (1998b), Secondary aerosol formation vs. primary organic aerosol emission: In situ evidence for chemical coupling between monoterpene acid photochemical products and new particle formation over forests, *Environ. Sci. Technol., 33*, 1028-1037.

Lee, T., S. M. Kreidenweis, and J. L. Collett, Jr. (2004), Aerosol ion characteristics during the Big Bend Regional Aerosol and Visibility Observational Study, *J. Air & Waste Manage. Assoc., 54*, 585-592.

Lefer, B. L., and R. W. Talbot (2001), Summertime measurements of aerosol nitrate and ammonium at a northeastern U.S. site, *J. Geophys. Res., 106*(D17), 20365-20378.

Liu L.-J. S., R. Burton, W. E. Wilson, and P. Koutrakis (1996), Comparison of aerosol acidity in urban and semi-rural environments, *Atmos. Environ., 30*(8), 1237-1245.

Lowenthal, D.H., C. F. Rogers, P. Saxena, J. G. Watson, and J. C. Chow (1995), Sensitivity of estimated light extinction coefficients to model assumptions and measurement errors, *Atmos. Environ., 29*, 751-766.

Lowenthal, D. H., J. G. Watson, and P. Saxena (2000), Contributions to light extinction during project MOHAVE, *Atmos. Environ., 34*, 2351-2359.

Malm, W. C., H. Iyer, J. Watson, and D. A. Latimer (1989), Survey of a variety of receptor modeling techniques, In *Transactions of the AWMA/EPA Int'l Specialty Conference on Visibility and Fine Particles*, edited by C.V. Mathai, Air and Waste Management Association.

Malm, W. C., J. F. Sisler, D. Huffman, R. A. Eldred, and T. A. Cahill (1994), Spatial and seasonal trends in particle concentration and optical extinction in the United States, *J. Geo. Res., 99*(D1), 1347-1370.

Malm, W. C., and S. M. Kreidenweis (1997), The effects of models of aerosol hygroscopicity on the apportionment of extinction, *Atmos. Environ., 31*, 1965-1976.

Malm, W. C., D. E. Day, and S. M. Kreidenweis (1997), Comparison of measured and reconstructed scattering during an intensive field study at Great Smoky Mountains National Park, paper #97-WA70.02, presented at the Air and Waste Management 90th Annual Meeting, Pittsburgh, PA.

Malm, W. C. (1998), Examining the relationship between aerosol concentration and partial scattering efficiencies near the Grand Canyon, Presented at the 91st Annual Meeting of the Air and Waste Management Association, Pittsburgh, PA.

Malm, W. C., D. E. Day, and S. M. Kreidenweis (2000a), Light scattering characteristics of aerosols at ambient and as a function of relative humidity: part II---a comparison of measured scattering and aerosol concentrations using statistical models. *J. Air and Waste Management Association, 50*, 174-182.

Malm, W. C., J. F. Sisler, M. L. Pitchford, M. Scruggs, R. Ames, S. Copeland, K. A. Gebhart, and D. E. Day (2000b), Spatial and seasonal patterns and temporal variability of haze and its constituents in the United States: Report III, Cooperative Institute for Research in the Atmosphere, Colorado State University, ISSN 0737-5352-47.

Malm, W. C., B. A. Schichtel, R. B. Ames, and K. A Gebhart (2002), A 10-year spatial and temporal temporal trend of sulfate across the United States, *J. Geo. Res., 107*(D22), 4627, doi:10.1029/2002JD002107.

Malm W. C., D. E. Day, S. M. Kreidenweis, J. L. Collett, Jr., T. Lee (2003), Humidity dependent optical properties of fine particles during the Big Bend Regional Aerosol and Visibility Observational study (BRAVO), *J. Geophys. Res. 108*(D9), 4279, doi:10.1029/2002JD002998.

Malm W. C, B. A. Schichtel, M. L. Pichford, L. L. Ashbaugh, and R. A. Eldred (2004), Spatial and monthly trends in fine particle concentration in the United States, *J. Geophys. Res. 109*, D03306, doi:10.1029/2003JD003739.

Malm W. C., D. E. Day, C. Carrico, S. M. Kreidenweis, J. L. Collett, Jr., G. McMeeking, T. Lee, and J. Carrillo (2005), Inter-comparison and closure calculations using measurements of aerosol species and optical properties during the Yosemite Aerosol Characterization Study, *J. Geophys. Res., 110*, D14.

Malm, W. C., M. L. Pitchford, C. McDade, and L. L. Ashbaugh (2006), Coarse particle speciation at selected locations in the rural continental United States, *Atmos. Environ,* accepted.

Odum, J. R., T. Hoffmann, F. Bowman, D. Collins, R. C. Flagan, and J. H. Seinfeld (1996), Gas/particle partitioning and secondary organic aerosol yields, *Environ. Sci. Technol., 30*, 2580-2585.

Odum, J. R., P. W. Jungkamp, R. J. Griffin, H. J. L. Forstner, R. C. Flagan, and J. H. Seinfeld (1997), Aromatics, reformulated gasoline, and atmospheric organic aerosol formation, *Environ. Sci. Technol., 31*, 1890-1897.

Ouimette, J. R., and R. C. Flagan (1982), The extinction coefficient of multicoponent aerosols, *Atmos. Environ., 16*, 2405.

Perry, K. D., T. A. Cahill, R. A. Eldred, and D. D. Dutcher (1997), Long-range transport of North African dust to the eastern United States, *J. Geophys. Res., 102*(D10), 11225-11238.

Pitchford, M. L., and W. C. Malm (1994), Development and applications of a standard visual index, *Atmos. Environ., 28*(5), 1049-1054.

Prospero, J. M. (1999), Long-term measurements of the transport of African mineral dust to the southeastern United States: Implications for regional air quality, *J. Geophys. Res., 104*(D13), 15,917-15,927.

Rogge, W. F., L. M. Hildemann, M. A. Mazurek, G. R. Cass, and B. R. T. Simoneit (1996), Mathematical modeling of atmospheric fine particle associated primary organic compound concentrations, *J. Geophys. Res., 101*, 19,379-19,394.

Quinn, P. K., T. L. Miller, T. S. Bates, J. A. Ogren, E. Andrews, and G. E. Shaw (2002), A 3-year record of simultaneously measured aerosol chemical and optical properties at Barrow, Alaska, *J. Geophys. Res., 107*(D11), 4130, 10:1029/2001JD001248.

Schmidt, K. M., J. P. Menakis, C. C. Hardy, W. J. Hann, and D. L. Bunnell (2002), Development of course-scale spatial data for wildland fire and fuel management, Gen. Tech. Rep. RMRS-87, USDA For. Serv. Rocky Mt. Res. Stn., Fort Collins, Colo.

Schwab, J. J., H. D. Felton, and K. L. Demerjian (2004), Aerosol chemical composition in New York state from integrated filter samples: Urban/rural and seasonal contrasts, *J. Geophys. Res., 109*(D16S05), doi:10.1029/2003JD004078.

Sloane C. S. (1983), Optical properties of aerosols-comparison of measurements with model calculations, *Atmos. Environ., 17*, 409-416.

Sloane C. S. (1984), Optical properties of aerosols of mixed composition, *Atmos. Environ., 18*, 871-878.

Sloane C. S., and G. T. Wolff (1985), Change in aerosol optical properties with change in chemical composition, *Atmos. Environ., 19*, 669-680.

Sloane C.S. (1986), Effects of composition on aerosol light scattering efficiencies, *Atmos. Environ., 20*, 1025.

Tang, I. N. (1996), Chemical and size effects of hygroscopic aerosols on light scattering coefficients, *J. Geophys. Res., 101*(D14), 19245-19250.

Tanner, R. L., W. J. Parkhurst, M. L. Valente, and W. D. Phillips (2004), Regional composition of PM2.5 aerosols measured at urban, rural, and "background" sites in the Tennessee valley, *Atmos. Environ., 38*, 3143-3153.

Turpin, B. J., and H. J. Lin (2001), Species contributions to PM2.5 mass concentrations: Revisiting common assumptions for estimating organic mass, *Aerosol Science and Technology, 35*, 602-610.

U.S. EPA (2000), National Air Pollutant Emissions Trends, 1900-1998, Office of Air Quality Planning and Standards, EPA-454/R-00-002.

U.S. EPA (2003), Guidance for Tracking Progress Under the Regional Haze Rule, Contract No. 68-D-02-0261, Work Order No. 1-06.

VanCuren, R. A., and T. A. Cahill (2002), Asian aerosols in North America: Frequency and concentration of fine dust, *J. Geophys. Res., 107*(D24), 4804, doi:10.1029/2002JD002204.

VanCuren, R. A. (2003), Asian aerosols in North America: Extracting the chemical composition and mass concentration of the Asian continental aerosol plume from long-term aerosol records in the western United States, *J. Geophys. Res., 108*(D20), 4623, doi:10.1029/2003JD003459.

van de Hulst, H. C. (1981), Light Scattering by Small Particles, Dover Publications, New York.

Waggoner, A. P., R. E. Weiss, N. C. Ahlquist, D. S. Covert, S. Will, and R. J. Charlson (1981), Optical characteristics of atmospheric aerosols, *Atmos. Environ., 15*, 1891-1909.

Wexler, A., and J. Seinfeld (1991),Second-generation inorganic aerosol model, *Atmos. Environ., 25A*, 2731.

White, W. H., and P. T. Roberts (1977), On the nature and origins of visibility-reducing aerosols in the Los Angels Air Basin, *Atmos. Environ., 11*, 803-812.

Zhang, Q., M. R. Canagaratna, J. T. Jayne, D. R. Worsnop, and J.-L. Jimenez (2005), Time- and size-resolved chemical composition of submicron particles in Pittsburgh: Implications for aerosol sources and processes, *J. Geophys. Res., 110*, D07S09, doi:10.1029/2004JD004649.

CHAPTER 3: SPATIAL VARIABILITY OF AVERAGE MONTHLY PATTERNS IN FINE AEROSOL SPECIES CONCENTRATIONS AND PARTICULATE EXTINCTION COEFFICIENTS

INTRODUCTION

In this section, the spatial variability in the seasonal patterns in aerosol composition and concentration are explored for the IMPROVE and STN networks. Additionally, the spatial variability in the seasonal patterns in particulate extinction coefficients is discussed and contrasted to those in aerosol concentrations for the IMPROVE network. Aerosol composition is influenced by both the nature of pollutant emissions and atmospheric characteristics that determine dispersion, transformation, and deposition. It seems likely that these influential factors would be similar during the same times of the year for relatively compact groupings of monitoring sites. Thus it may be reasonable to examine temporal and spatial patterns in annual and monthly averages on a regional basis. Regional groupings of sites in the IMPROVE network have been developed based on examination of seasonal patterns in aerosol composition and concentration in context of the sites' geographical locations and the expected spatial extent of regional fine aerosols [Sisler et al., 1993; Sisler et al., 1996; Malm et al., 2000; Malm et al., 2004]. The rural sites included in this analysis have been grouped into 26 previously defined regions; the three urban IMPROVE sites are analyzed individually. Variations in seasonal composition among sites within the regional groupings were not explicitly examined in this assessment but can be significant, especially for regions with significant terrain features and large emissions gradients and for sites at substantially different elevations. For example, Shining Rock and James River Face wilderness areas are both in the Appalachian region, but at James River Face the January sulfate concentration is about a factor of 1.8 greater than at Shining Rock, and the January organics are about a factor of 3 greater (see Appendix C). Only the 160 sites meeting the completeness criteria outlined in section 3.3 are included.

For the purposes of comparison, STN sites meeting the completeness criteria described in section 3.3 were grouped into regions based upon qualitative analysis of the aerosol data from 2000 through 2004. Stacked bar charts of monthly averaged data for the 69 sites with complete data for the five reconstructed fine mass (RCFM) components were examined for comparability in monthly patterns of aerosol composition and concentrations. Sites in the same geographic area that also had similar patterns in each of the five RCFM components, expressed both as concentrations and as fractional contribution to RCFM, were grouped into regions. The 69 sites were grouped into 27 regions, 14 of which contain only a single site. Quantitative comparability between sites in terms of monthly values or seasonal patterns was not explored.

Monthly and annual average aerosol species concentrations for the IMPROVE rural regions and urban sites are presented graphically in Figures 3.1, 3.3, and 3.5 as stacked bar charts of ammonium sulfate, organic and light-absorbing carbon, ammonium nitrate, and soil concentrations by month with the last bar representing the annual average. The graphics have been scaled to the maximum monthly concentrations. The STN regions are similarly summarized in Figures 3.2, 3.4, and 3.6. The fractional contributions to fine mass are shown in Figures 3.7, 3.9, and 3.11 for IMPROVE and in Figures 3.8, 3.10, and 3.12 for the STN. In these cases the y

axis is the percent contribution to RCFM. Similar graphs of particulate extinction for IMPROVE and the STN are in Figures 3.13–3.21, where the y axis is either extinction in Mm^{-1} or percent contribution to reconstructed particulate extinction. Similar charts for the IMPROVE sites (data not regionally averaged) are in Appendix C. The regional seasonal and annual average reconstructed fine mass and extinction budgets are presented in tabular form in Appendix B.

3.1 SPATIAL VARIABILITY OF AVERAGE MONTHLY PATTERNS IN FINE AEROSOL SPECIES CONCENTRATIONS

In this section, the spatial variability in the seasonal patterns of each of the major aerosol types is explored. In particular, regional differences and urban-rural differences in the timing of maximum and minimum concentrations and fractional contributions are examined. Additionally, the spatial variability in the degree of seasonality as measured by the contrast between the maximum and minimum concentrations is also explored.

3.1.1 Fine Particle Ammonium Sulfate Mass

In general, ammonium sulfate concentrations tend to be higher during the summer and early fall months (June–September). The regional monthly maximum occurred during these months in ~70% of the IMPROVE and STN regions. The regions with maximum concentrations in the remainder of the year were primarily urban. The following urban regions had winter maxima: Boise, Minneapolis-St. Paul, Denver, Missoula, and the Wasatch Front. Spring maxima occurred in the urban regions of North Dakota, Florida, northwestern Nevada, central Minnesota, urban as well as rural Alaska and the rural regions of Hells Canyon, the northern Great Plains, the northern Rockies, and the Virgin Islands. The monthly minimums were less varied and occurred during winter in over 85% of the regions. The exceptions were almost exclusively urban, with Boise, urban Alaska, Denver, Minneapolis-St. Paul, Upper Michigan 2, and North Dakota all having fall minimums and Missoula having a spring minimum. The only rural region to not have a winter minimum was Hawaii, where the minimum occurred in summer.

Not surprisingly, because SO_2 emissions are highest there, the highest monthly ammonium sulfate concentrations occurred in the central eastern United States, where maximum rural and urban concentrations were comparable. Including both STN and IMPROVE regions, the maximum monthly concentration of ~11.4 $\mu g/m^3$ occurred in August in the IMPROVE Appalachian and Washington, D.C., regions and the STN Washington, D.C.-Philadelphia corridor region. The lowest monthly concentrations, 0.2–0.3 $\mu g/m^3$, occurred in the western rural regions of Oregon and northern California, the Great Basin, Alaska, the Sierra Nevada, and the Northwest. In general, in the eastern contiguous United States the regional maximum monthly concentrations ranged from 3 to 11.4 $\mu g/m^3$, and the minimums were 1.4–3.9 $\mu g/m^3$. In the western contiguous United States, including the low sulfate concentration regions of the northern Great Plains and Boundary Waters, the maximum monthly concentrations ranged from 4.1 to 6.6 $\mu g/m^3$ (0.8–2.8 $\mu g/m^3$, excluding the urban Wasatch Front in Utah and Los Angeles and San Diego in California) and the minimums ranged from 0.2 to 1.6 $\mu g/m^3$.

Ten of the 57 regions did not exhibit a distinct seasonal cycle in ammonium sulfate concentrations. These exceptions were Minneapolis-St. Paul, Boundary Waters, the northern

Great Plains, North Dakota, the Sacramento and San Joaquin valleys, and the Virgin Islands, which qualitatively appeared to have minimal seasonality and had ratios of the highest to lowest monthly ammonium sulfate concentrations of less than 2. The ratios of the maximum to the minimum monthly concentration ranged from 1.4 in Denver to 7.2 in the Sierra Nevada, with a median value of 2.5. The highest ratios, above 4.5, were all found in California in the Sierra Nevada, southern California, Los Angeles, San Diego, Oregon, northern California, and Death Valley regions. A higher degree of seasonality was present in a greater proportion, ~2/3 as compared to ~1/3, of the rural regions as compared to the urban regions. An above-median ratio was considered indicative of a higher relative degree of seasonality as compared to other regions.

There was greater variability in the timing of the maximum and minimum monthly ammonium sulfate percent contributions to RCFM as compared to the variability in the timing of maximum and minimum ammonium sulfate concentrations. The maximum occurred during summer in ~60% of the regions, and the minimum occurred in winter in ~75% of the regions. Many of the rural and urban regions in the southwestern, north-central, and southeastern United States exhibited minimal seasonality in the percent contribution of ammonium sulfate to RCFM. The highest percent contributions, 50–70%, occurred exclusively in the IMPROVE network. The regions with these high ammonium sulfate contributions included both regions with high (in the top quartile) ammonium sulfate concentrations–Washington, D.C., the mid-South, Southeast, Northeast, Ohio River valley, East Coast, and Appalachia—and those with low to moderate concentrations (in the bottom 25–50th quartiles)—Alaska, Hawaii, and the Virgin Islands.

3.1.2 Fine Particle Organic Carbon Mass

There was greater regional variability in the seasonality of organic mass by carbon concentration (OMC) as compared to ammonium sulfate. A double peak structure with both a summer and winter peak in OMC was observed in the seasonal cycle of OMC in some regions (see the STN Nevada region for an example). In general, the OMC mass concentrations are at a minimum in winter or spring, with ~80% of the regions having their minimum during these seasons. Approximately 70% of rural regions had winter minima. Hawaii and the Virgin Islands were the only rural regions to exhibit summertime minima. All of the western urban regions had spring minima, with the exception of Phoenix where the minimum occurred in summer. The eastern urban regions were more varied, with spring minima observed in ~40% of the regions, winter minima in ~30% of the regions, and either June or fall minima observed in several regions.

Maximum OMC concentrations tended to occur in summer; ~60% of the regions had maxima during this period, but maxima occur in all seasons, depending on region. While summer and fall monthly maxima occur in both urban and rural areas, spring maxima occur exclusively in rural regions, and winter maxima occur exclusively in urban regions and in the heavily polluted Columbia River Gorge region. Most western urban regions had OMC maxima between November and January; the exceptions were Los Angeles with an October maximum and Missoula and western Nevada with August maxima. In contrast, eastern urban areas typically had maxima between July and September. The exceptions to the eastern norm were Florida with a January maximum, Duluth-Superior with a June maximum, and the Southeast with a November maximum. The rural regions typically had maxima occurring between May and August; the regions with maxima outside of this timespan included the central Great Plains

with an April maximum, the mid-South and the Virgin Islands with September maxima, and the Columbia River Gorge with a November maximum.

The highest monthly average OMC concentration of 28.39 $\mu g/m^3$ was in Missoula, Montana, during August. High concentrations were also found during the winter in the urban Sacramento and San Joaquin valleys, STN Phoenix, and San Diego at 23.74, 17.85, and 17.25 $\mu g/m^3$, respectively. The lowest minimum monthly concentrations of OMC were in the rural regions of Alaska, the Virgin Islands, Death Valley, the central Rockies, and Hawaii at 0.17, 0.26, 0.39, 0.46, and 0.48 $\mu g/m^3$, respectively. Overall, the maximum monthly concentrations ranged from 0.6 to 7.7 $\mu g/m^3$ in rural regions and from 5.3 to 28.4 $\mu g/m^3$ in urban regions, and the minimums ranged from 0.2 to 2.6 $\mu g/m^3$ in the rural areas and 3.0 to 9.5 $\mu g/m^3$ in urban areas.

A number of urban regions, including the Southeast, mid-South and Ohio River valley, Puerto Rico, and eastern Texas-Gulf coast regions, exhibited minimal seasonality with maximum to minimum OMC concentration ratios of less than 1.5. The maximum to minimum ratios ranged from 1.3 in the urban Southeast to 30 in rural Alaska, with a median value of 2.3. The highest ratios, those greater than 5, occurred in the following rural western regions: the central and northern Rockies, northern Great Plains, Death Valley, Oregon and North California, the Sierra Nevada, and Alaska. Similar to the patterns observed in ammonium sulfate concentrations, a higher degree of seasonality was present in a greater proportion, about two-thirds as compared to about one-third, of the rural regions as compared to the urban regions.

Approximately half of the regions scattered around the United States, including Alaska and Hawaii, exhibited minimal seasonality in the percent contribution of OMC to RCFM. Again, a lack of seasonality was much more common in urban regions than rural regions, with approximately two-thirds of the urban regions showing fairly constant contributions of OMC to RCFM throughout the year. The percent contributions of OMC tended to be at a minimum in winter and spring and at a maximum in summer, with a high degree of variability depending on region. The maximum monthly percent contribution ranged from 24% to 89% and the minimum ranged from 5% to 64%.

3.1.3 Fine Particle Light-Absorbing Carbon Mass

Similar to the OMC concentrations, maxima and minima in the monthly light-absorbing carbon concentrations were regionally variable. Western urban regions had spring or summer light-absorbing carbon (LAC) minima. The eastern urban regions were variable in the timing of the monthly minimum concentrations, with minima occurring in every season. However, spring minima were marginally dominant, occurring in ~40% of the eastern urban regions. The monthly minima also occurred in every season in the rural regions; springtime was again marginally dominant, with ~40 of the rural regions having their minima in this season. Peak LAC concentrations occurred more or less equally in summer, fall, and winter, with timing depending upon region; rural west Texas was the only region to have had a springtime maximum. Summer maxima were typical of rural regions, fall maxima were typical of eastern urban regions, and winter maxima were typical of western urban regions. Approximately one-third of the regions had minimum monthly OMC and LAC concentrations in the same month, and about half of the regions had maximums in the same month. The regions with temporally

matched OMC and LAC minima were equally split between urban and rural, whereas about two-thirds of the regions with matched maxima were rural.

The maximum monthly LAC concentrations ranged from 0.06 to 2.66 $\mu g/m^3$ and the minimums ranged from 0.03 to 1.93 $\mu g/m^3$. The highest maximum monthly concentrations occurred at the urban sites Denver, Los Angeles, Phoenix (IMPROVE and STN), and Puerto Rico at 1.90, 1.94, 1.95 and 2.19, and 2.66 $\mu g/m^3$, respectively. The lowest minimum monthly concentrations occurred in rural Alaska, Virgin Islands, Hawaii, and Death Valley at 0.03, 0.04, 0.04, and 0.05 $\mu g/m^3$, respectively

The ratio of the maximum to minimum monthly LAC concentrations ranged from 1.3 in the urban Northeast to 6.8 in rural Alaska. The highest ratios, those greater than 4, occurred in Oregon and northern California, the Sierra Nevada, Death Valley, urban and rural Alaska, Phoenix, and the northern Rockies. The lowest ratios, those less than 1.4, occurred in the urban Northeast, urban and rural mid-South, North Dakota, Upper Michigan 2, and Puerto Rico. Approximately 35% of the regions exhibited minimal seasonality in LAC; all were in the central or eastern United States.

The timing of the minima and maxima in percent contribution of LAC to RCFM varied depending on region, with contributions dipping in spring or summer and peaking in fall or winter in most regions. The maximum monthly percent contributions ranged from 3% to 26% and the minimums ranged from 0.6% to 15%. Approximately a quarter of the regions exhibited minimal seasonality in the percent contribution of LAC; most were in the central and eastern United States.

3.1.4 Fine Particle Ammonium Nitrate Mass

While ammonium sulfate and rural organic carbon concentrations tend to peak during the summer months, ammonium nitrates are typically highest during the winter season, because the cooler winter season temperatures favor particulate nitrate over gaseous nitric acid equilibrium. The monthly maximums occurred in November–March in most regions with the following exceptions: maximums in late spring in the Great Basin, southern California, Hawaii, and Puerto Rico; in summer in Death Valley, the Virgin Islands, Oregon and northern California, and rural Alaska; and in October in Los Angeles, San Diego, and the IMPROVE Puget Sound site. If the assumption of ammonium nitrate is valid for these regions, then the warm season nitrate maxima are interesting, particularly in hot regions such as the tropics, Death Valley, and southern California. The minimums in monthly ammonium nitrate occurred between June and September in all regions with the following exceptions: the minima occurred in spring in San Diego; in late fall in Death Valley and the Northwest; and in summer in southern California, Los Angeles, Oregon and northern California, rural Alaska, the Great Basin, and the Virgin Islands.

The highest monthly average concentrations occur in the urban regions of Los Angeles, Sacramento, and the Wasatch Front at 19.9, 16.9, and 12.6 $\mu g/m^3$, respectively. The highest rural monthly averages occurred in the central Great Plains, Ohio River valley, and the mid-South at 3.1, 3.2, and 5.0 $\mu g/m^3$, respectively, and were approximately 4 to 6 times smaller than those in Los Angeles. The lowest monthly maximums, 0.2–0.3 $\mu g/m^3$, occurred in rural Alaska, Hawaii, Oregon and northern California, the Great Basin, and the northern Rockies. These

regions also had some of the lowest monthly minimum ammonium nitrate concentrations at less than 0.15 $\mu g/m^3$.

The only regions that exhibited minimal seasonality in ammonium nitrate concentrations were Hawaii and Puerto Rico. The highest ratios between the maximum and minimum concentrations within a region occurred in the Boundary Waters, Hells Canyon, Boise, Missoula, central Minnesota, and Wasatch Front regions, where the ratios were between 11 and 33. The lowest ratios, less than 2, occurred in Puerto Rico, Hawaii, the Northwest, and the Great Basin. In contrast to the patterns observed in ammonium sulfate and OMC concentrations, a higher degree of seasonality was present in a greater proportion of the urban regions as compared to the rural regions. About two-thirds of urban sites had above-median ratios as compared to about one-third of rural regions with above-median ratios.

In most regions, on a fractional basis nitrates make their greatest contribution to RCFM from November to March, with most of the maximum contributions occurring during the winter months. The exceptions were Los Angeles and Hawaii, where the maximum ammonium nitrate contributions occurred during summer. The minimum nitrate contributions occurred in June–September, except in Hawaii, San Diego, and Los Angeles, which all had wintertime minima. The maximum monthly percent contributions ranged from 5% to 51% and the minimums ranged from 2% to 30%. The largest percent contributions, 40–50%, occurred in regions of California, the Midwest, and urban Idaho and Utah. The only regions with minimal seasonality were Puget Sound and Portland, Florida, and Puerto Rico.

3.1.5 Fine Particle Soil Concentrations

Several regions displayed minimal seasonality in fine soil concentrations; all were urban and included Puget Sound and Portland, Los Angeles, Denver, IMPROVE Phoenix, and STN Northeast. However, they were the anomaly, with most regions having clear seasonality, with minimum monthly soil concentrations in fall and winter and maximum concentrations in spring or summer. San Diego, where soil concentrations were at a minimum in June and at a maximum in November, was an exception to this general pattern. The Northwest and the Sacramento and San Joaquin valleys regions also had fall maxima. There was a west-to-east gradient in the timing of the soil maxima, with spring maxima more common in the West (including Hawaii and Alaska) and summer maxima more common in the East (including the Virgin Islands and Puerto Rico).

The highest maximum monthly soil concentrations, 3–4.5, $\mu g/m^3$, were found in the arid Southwest regions of Death Valley, southern Arizona, STN Phoenix, and urban west Texas and in the eastern noncontiguous United States regions of Puerto Rico and the Virgin Islands. The lowest maximum monthly soil concentrations, less than 0.5 $\mu g/m^3$, occurred in the rural noncontiguous United States regions of Alaska and Hawaii and in the Boundary Waters and upper Michigan regions. The northwestern United States had the lowest minimum monthly soil concentrations, less than 0.1 $\mu g/m^3$, in the regions of rural Alaska, the Northwest, Oregon and northern California, and the northern Rockies. Not surprisingly, the regions with the highest minima, 1–2.5 $\mu g/m^3$, were found in the arid southwestern regions of southern Arizona, IMPROVE/STN Phoenix, and urban west Texas.

The ratio of maximum to minimum soil concentrations was greatest in the Virgin Islands where it was 20. The ratios were also quite high, 10–15, in the northwestern United States regions of the Northwest, Oregon and northern California, the Great Basin, and the northern Rockies. The lowest ratios, less than 2, occurred in the urban regions of Puget Sound and Portland, IMPROVE Phoenix, Los Angeles, Denver, northwest Nevada, the Northeast, and Washington, D.C. Similar to the patterns observed in ammonium sulfate and OMC concentrations, a higher degree of seasonality was present in a greater proportion of the rural regions as compared to the urban regions. The breakdown was similar, with about two-thirds of rural sites having an above-median ratio as compared to about one-third of urban regions meeting the same criteria.

In most regions, on a fractional basis soil makes the greatest contribution to RCFM during spring and summer, with approximately half of the regions having maximum soil contributions in April. Minimum soil contributions occurred primarily from November through February; the only exceptions were San Diego, Los Angeles, Alaska, and Death Valley, where the minimums occurred during summer. Maximum fractional contributions ranged from 4% in upper Michigan to 70% in the Virgin Islands. Minimum contributions ranged from 1% in the Sacramento and San Joaquin valleys to 27% in southern Arizona.

The broad-scale regional and temporal trends in the soil concentrations are indicative of large-scale transport mechanisms rather than local wind-blown mechanisms. A number of researchers have documented the impact of Saharan dust during the spring–summer months in the Virgin Islands and in the southeastern United States [Perry et al., 1997; Prospero et al., 2002]. The elevated spring–summer soil and the increasing southeast gradient over the eastern United States are consistent with this region being impacted by North African dust. It is also known that the western United States is periodically impacted by large dust plumes originating in Asia [Husar et al., 2001; VanCuren and Cahill, 2002] during the spring season. The widespread elevated springtime dust from northern Nevada to Texas is an indication of long-range-transport dust, particularly in the mountainous regions where local origins of dust are expected to be low.

In addition to potential Asian dust influences, the western United States is affected by local dust sources. The western United States and Mexico have three large dust source regions [Prospero et al., 2002], one located west and southwest of Salt Lake City, Utah, a second defined by the Salton Trough of southernmost California and northern Mexico, and the third in Mexico just south of the United States-Mexico border in the southern Mimbres Basin. The dust activity from these source regions begins in April–May and peaks in June–July, with dust extending from west Texas to the Mogollon Rim and to the Great Basin. The Owens Valley in California and eastern Washington are also important dust sources. The timing and locality of the highest fine soil aerosol concentrations are similar to those of these North American dust sources.

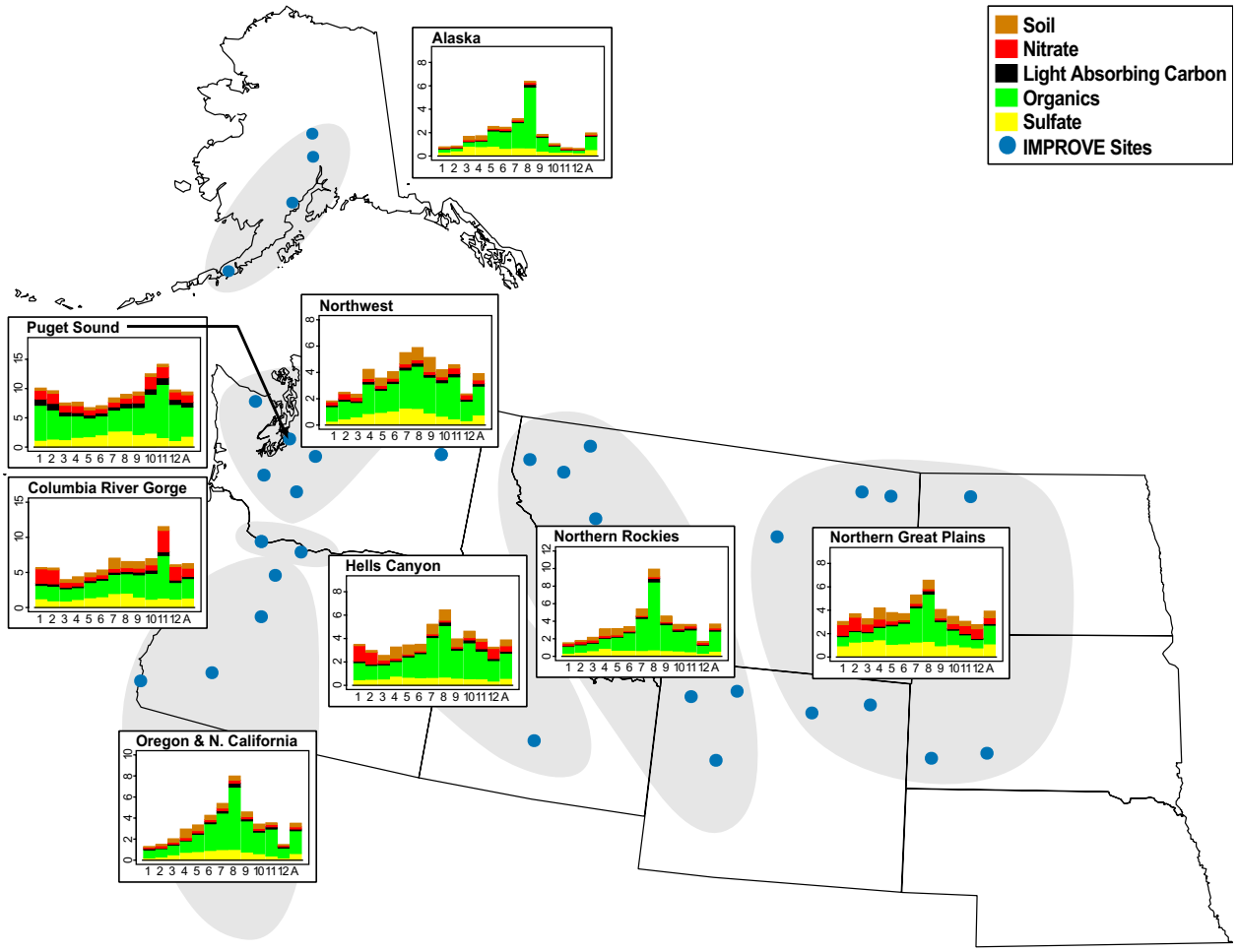

Figure 3.1. Map of stacked bar charts of monthly mean concentrations (µg/m^3) of fine aerosol species in the northwestern U.S. regions of the IMPROVE network.

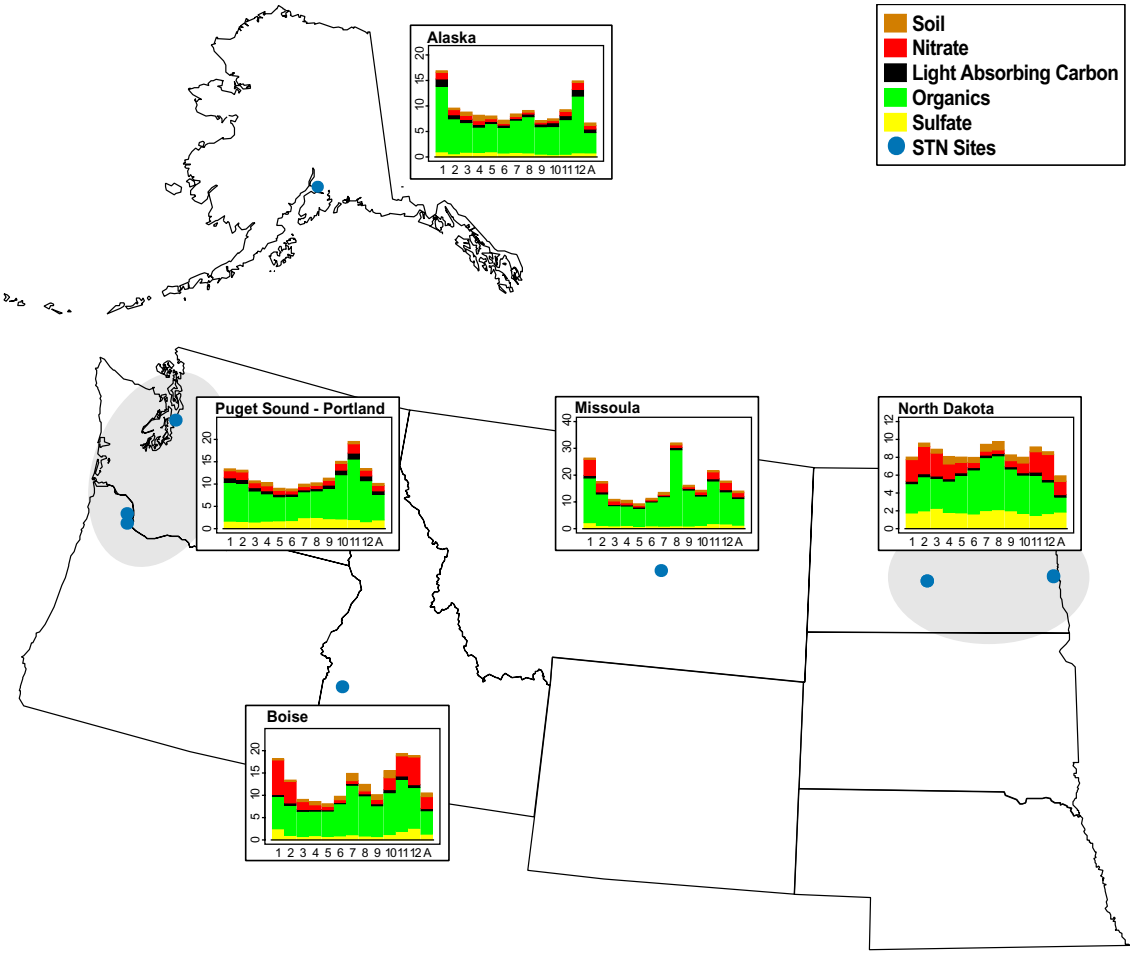

Figure 3.2. Map of stacked bar charts of monthly mean concentrations (µg/m^3) of fine aerosol species in the northwestern U.S. regions of the STN network.

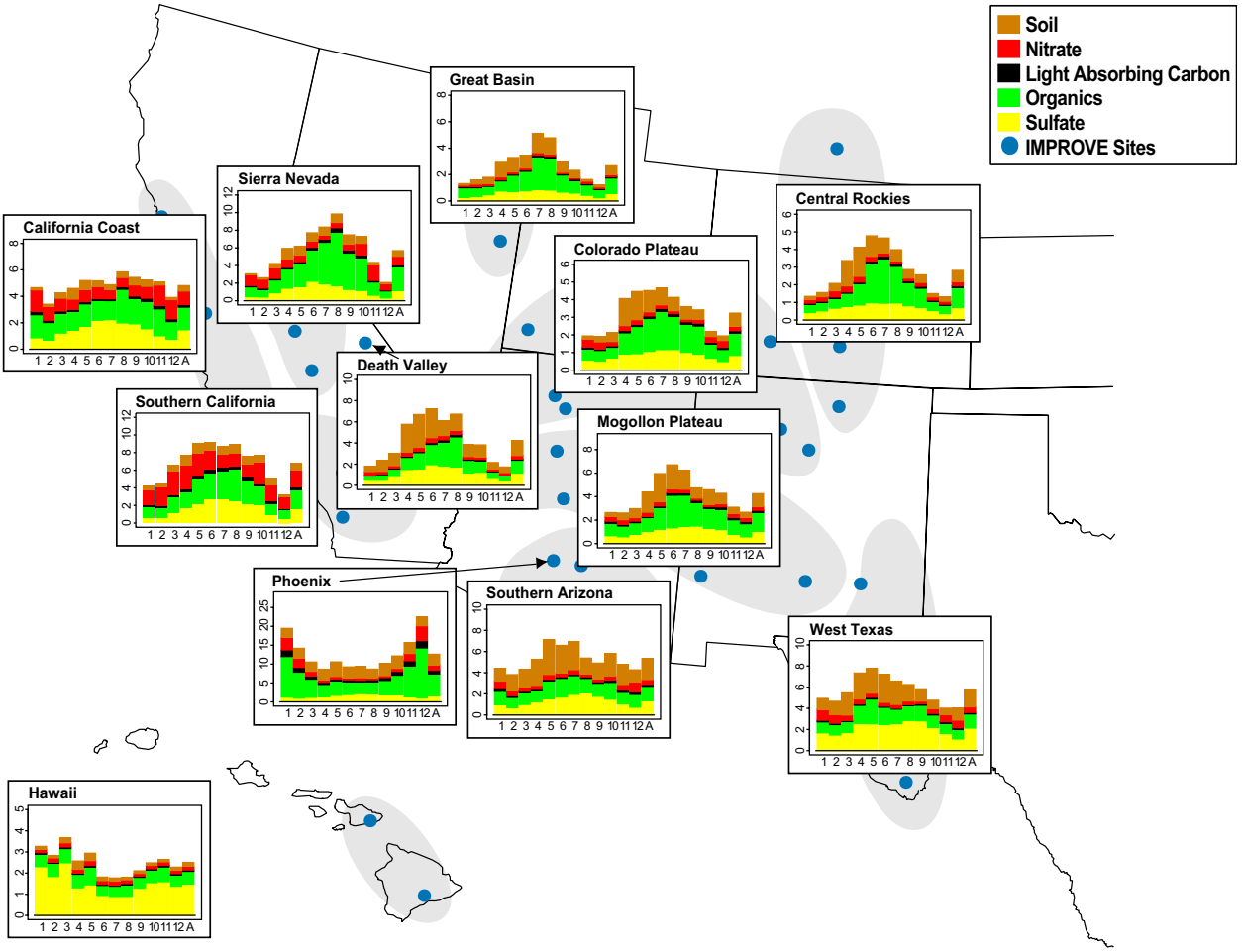

Figure 3.3. Map of stacked bar charts of monthly mean concentrations (µg/m^3) of fine aerosol species in the southwestern U.S. regions of the IMPROVE network.

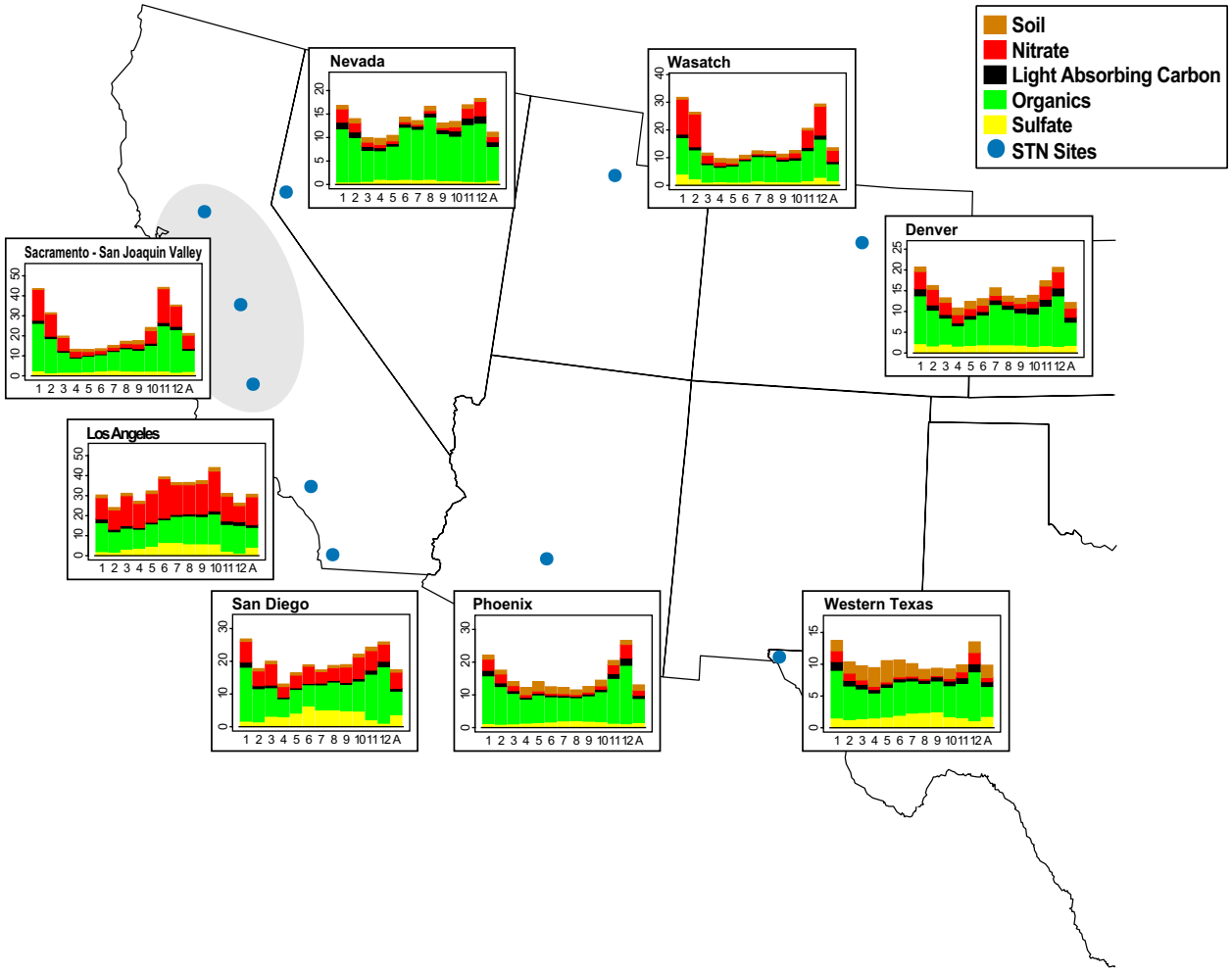

Figure 3.4. Map of stacked bar charts of monthly mean concentrations (µg/m^3) of fine aerosol species in the southwestern U.S. regions of the STN network.

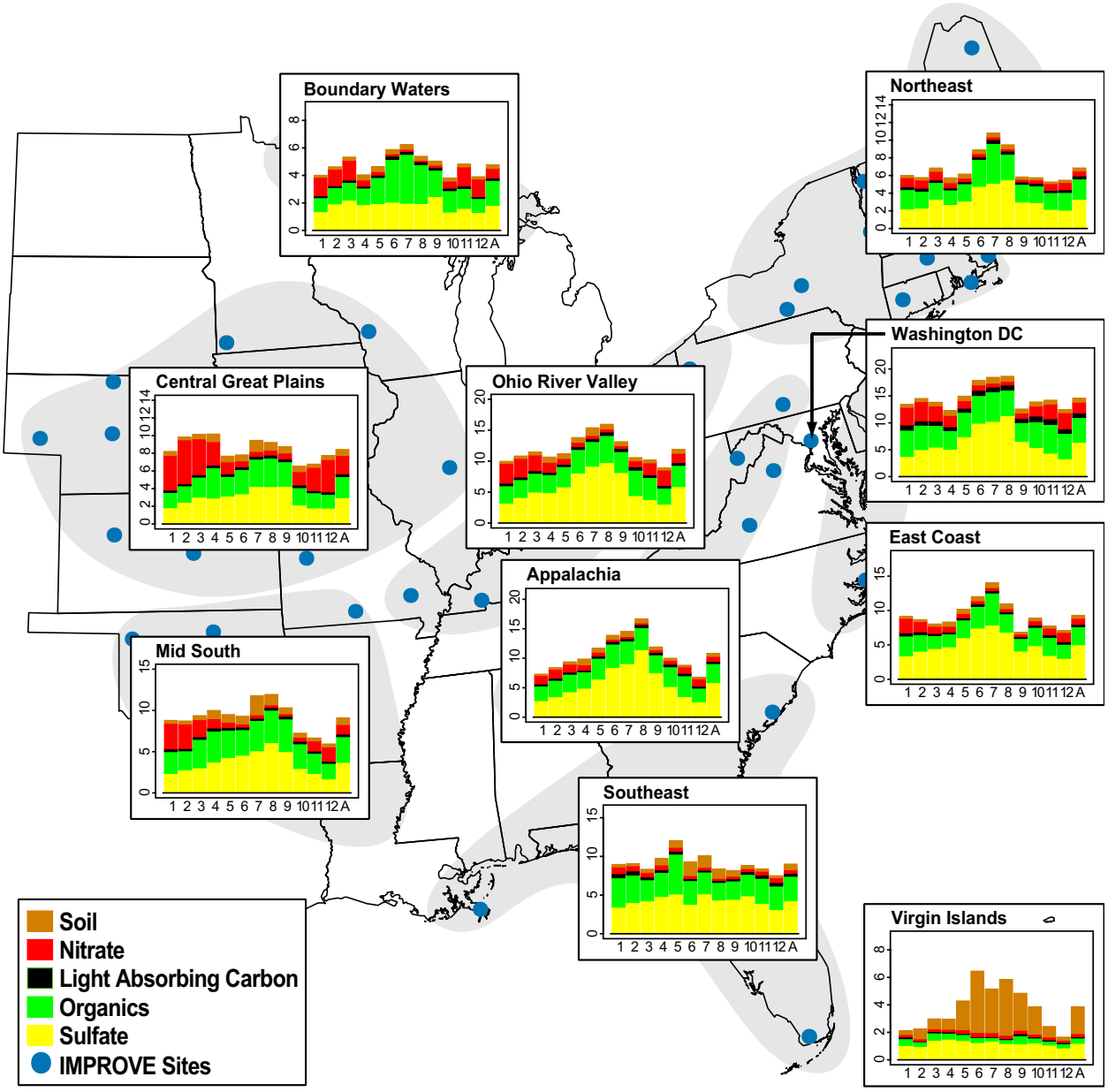

Figure 3.5. Map of stacked bar charts of monthly mean concentrations (µg/m^3) of fine aerosol species in the eastern U.S. regions of the IMPROVE network.

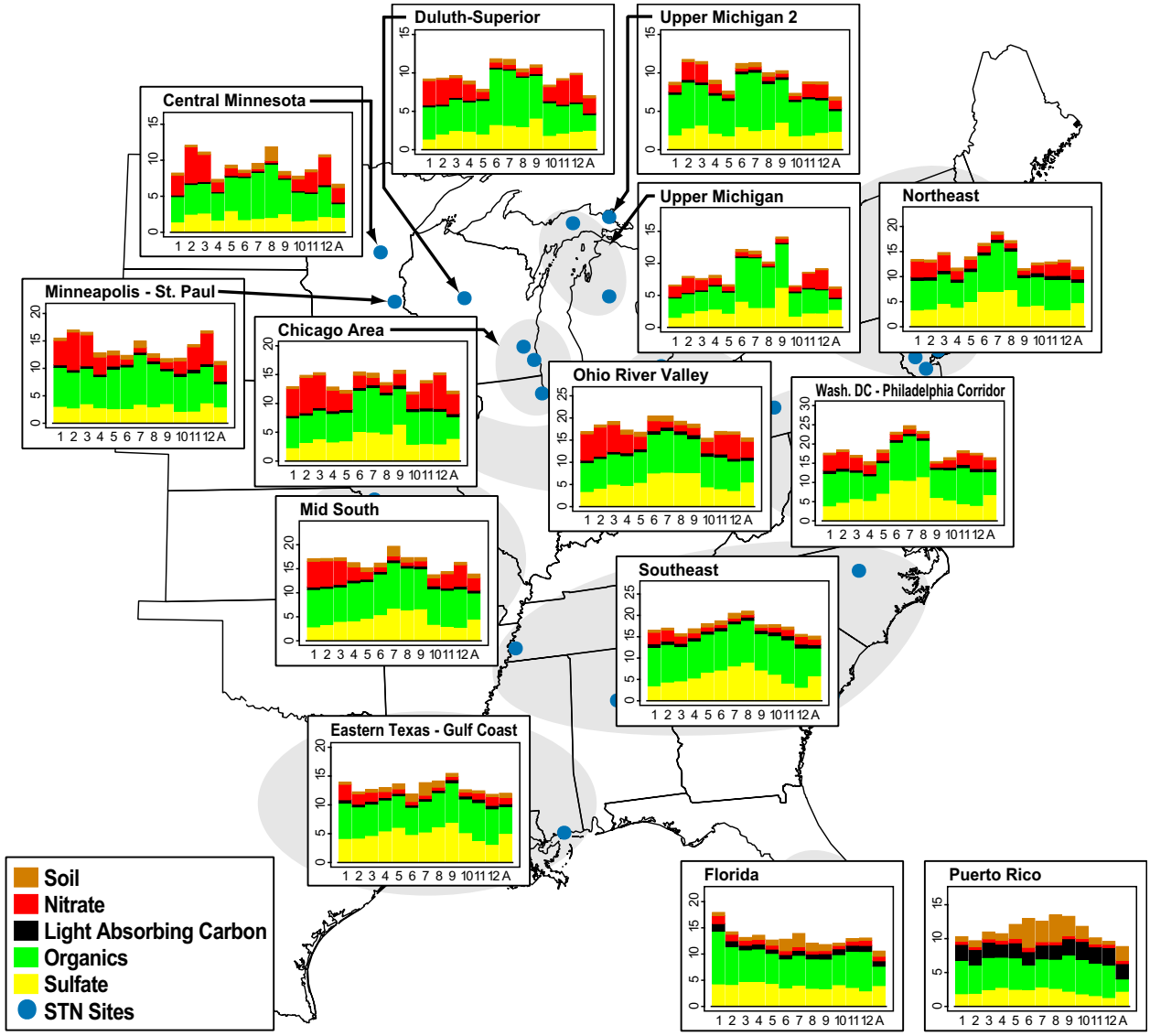

Figure 3.6. Map of stacked bar charts of monthly mean concentrations (µg/m^3) of fine aerosol species in the eastern U.S. regions of the STN network.

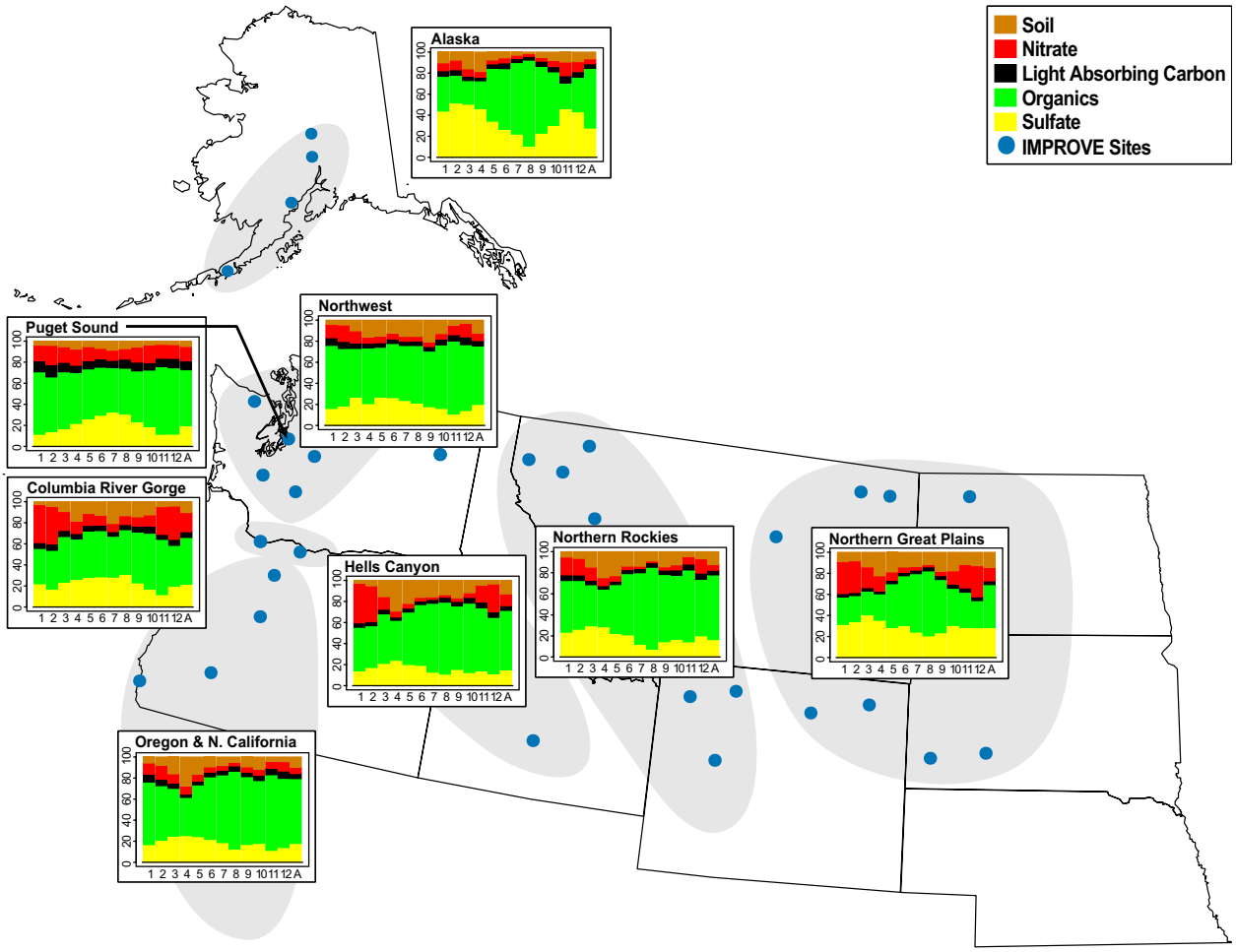

Figure 3.7. Map of stacked bar charts of monthly percent contribution to reconstructed fine mass (%) of fine aerosol species in the northwestern U.S. regions of the IMPROVE network.

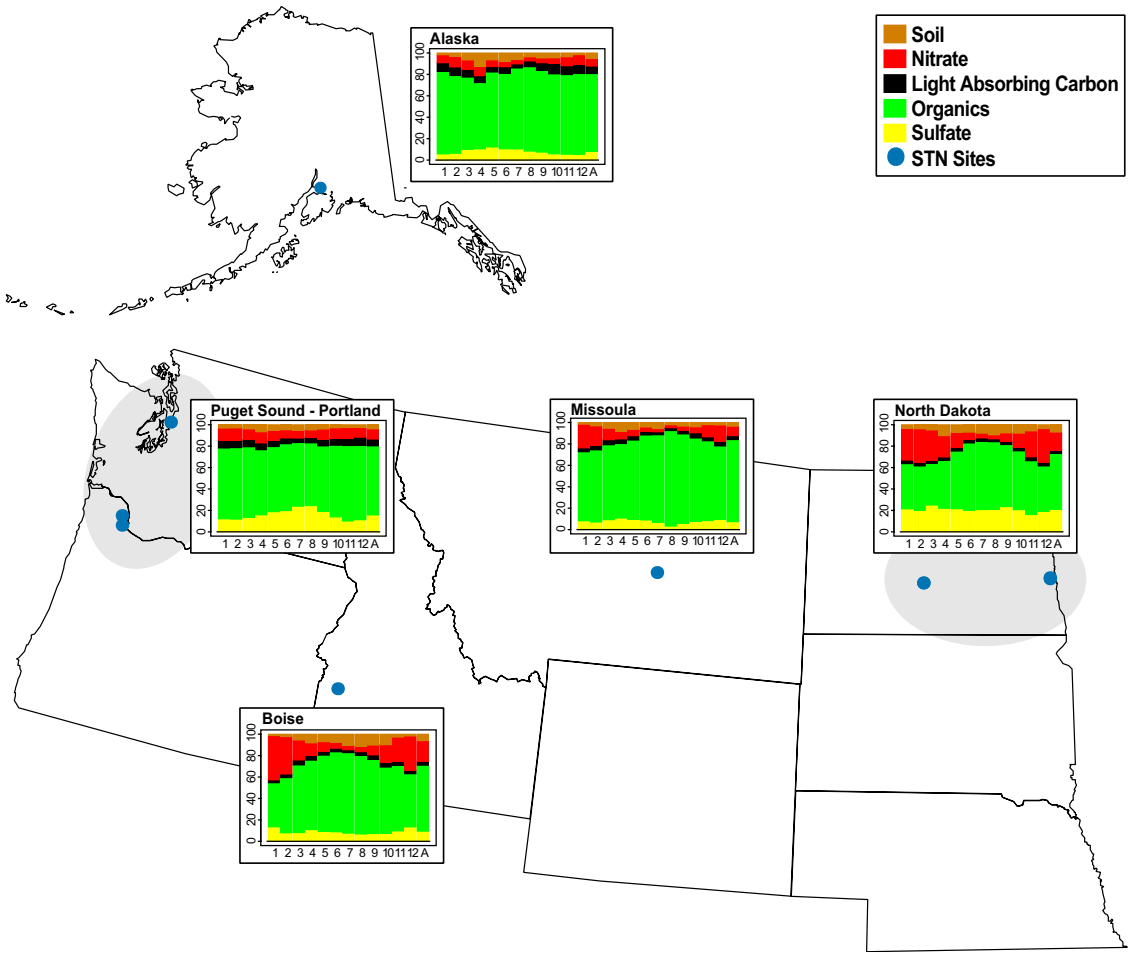

Figure 3.8. Map of stacked bar charts of monthly percent contribution to reconstructed fine mass (%) of fine aerosol species in the northwestern U.S. regions of the STN network.

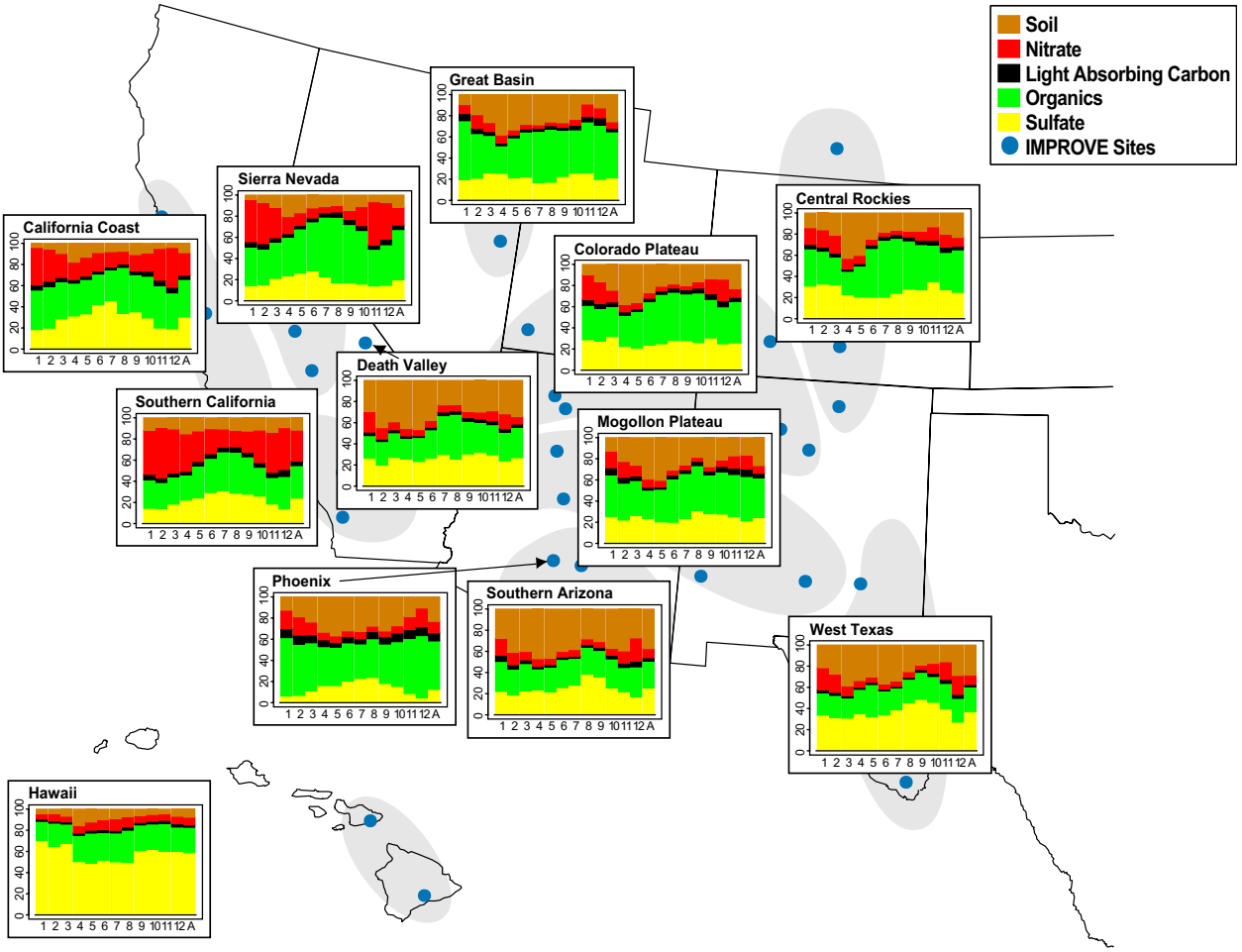

Figure 3.9. Map of stacked bar charts of monthly percent contribution to reconstructed fine mass (%) of fine aerosol species in the southwestern U.S. regions of the IMPROVE network.

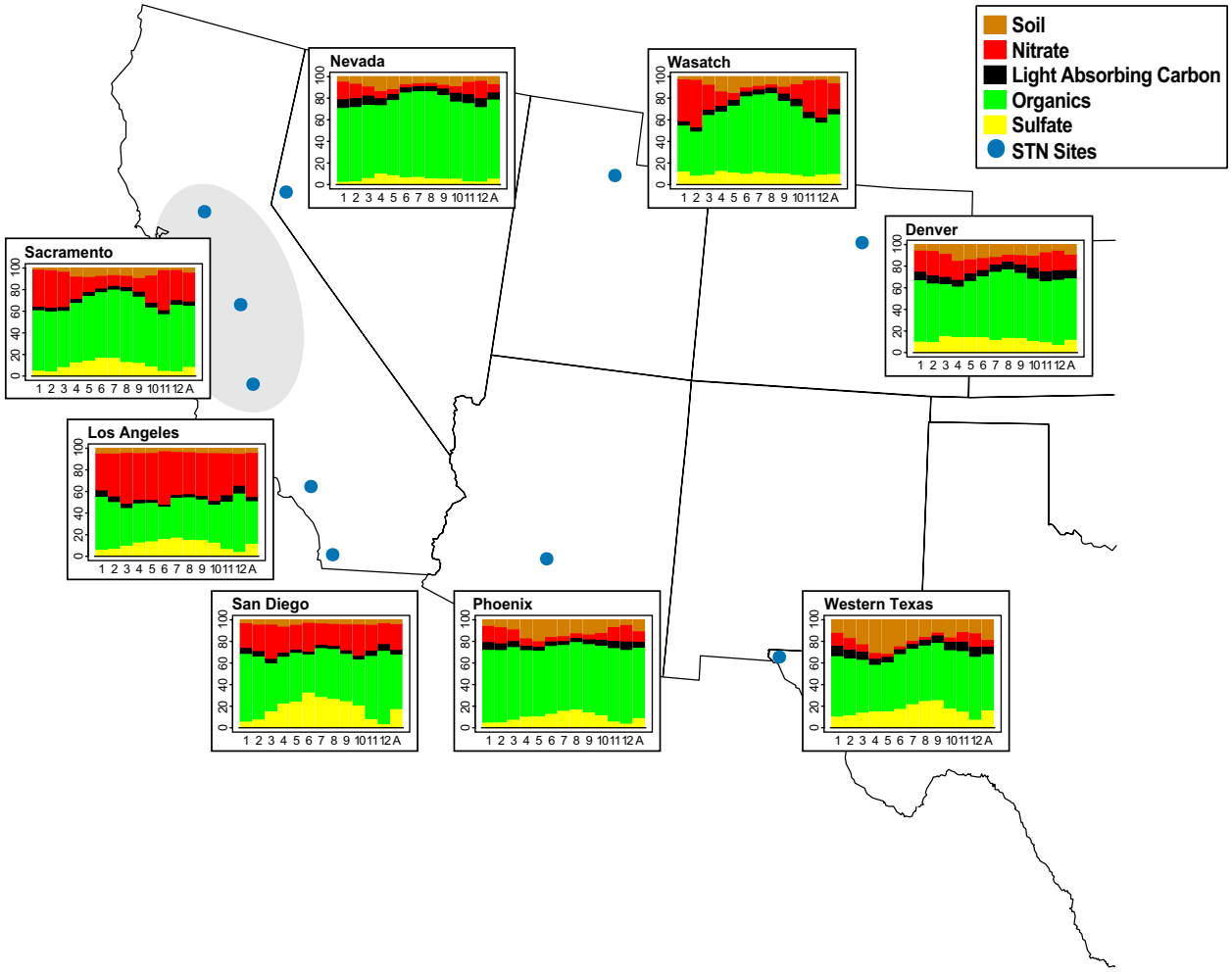

Figure 3.10. Map of stacked bar charts of monthly percent contribution to reconstructed fine mass (%) of fine aerosol species in the southwestern U.S. regions of the STN network.

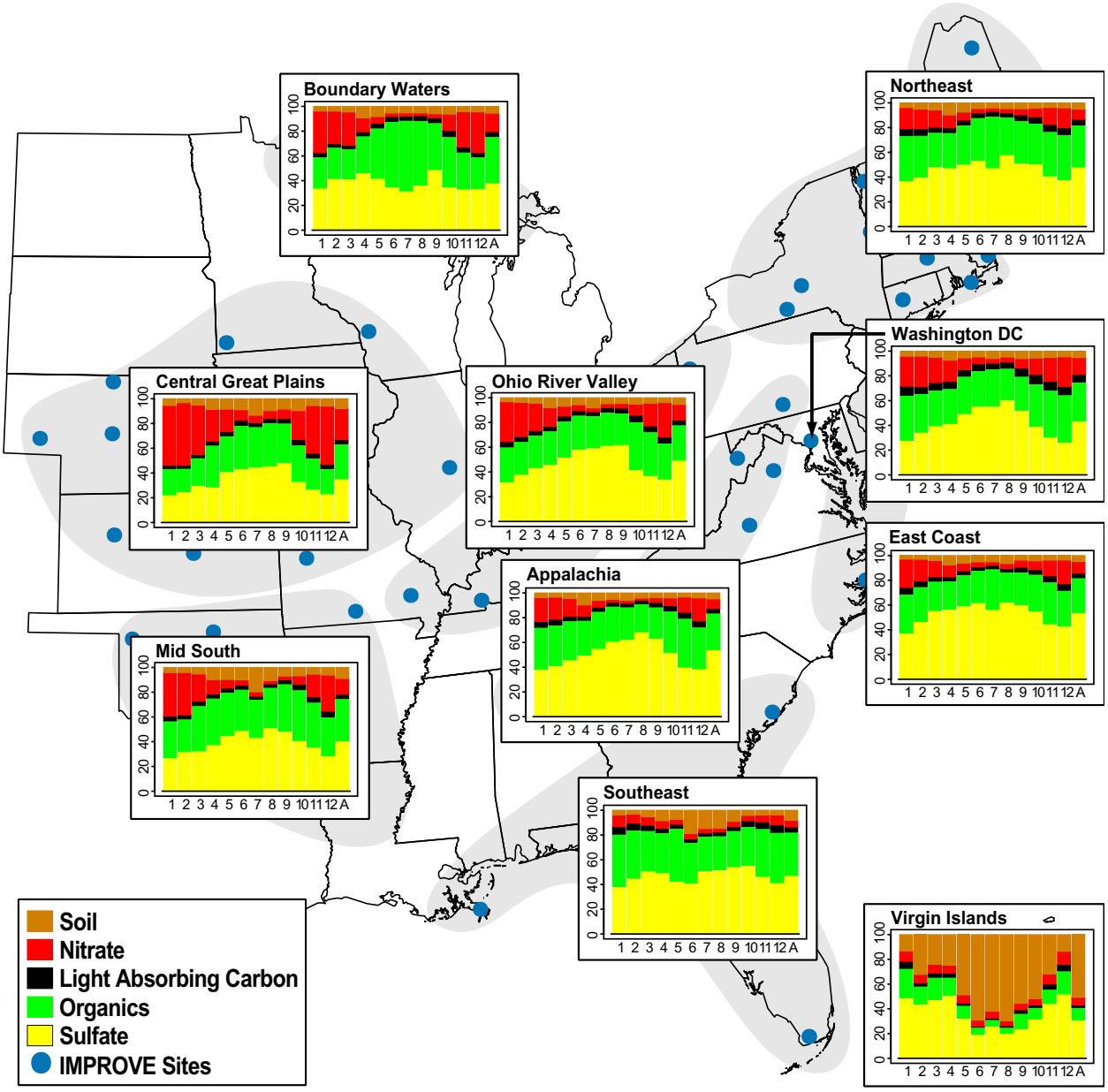

Figure 3.11. Map of stacked bar charts of monthly percent contribution to reconstructed fine mass (%) of fine aerosol species in the eastern U.S. regions of the IMPROVE network.

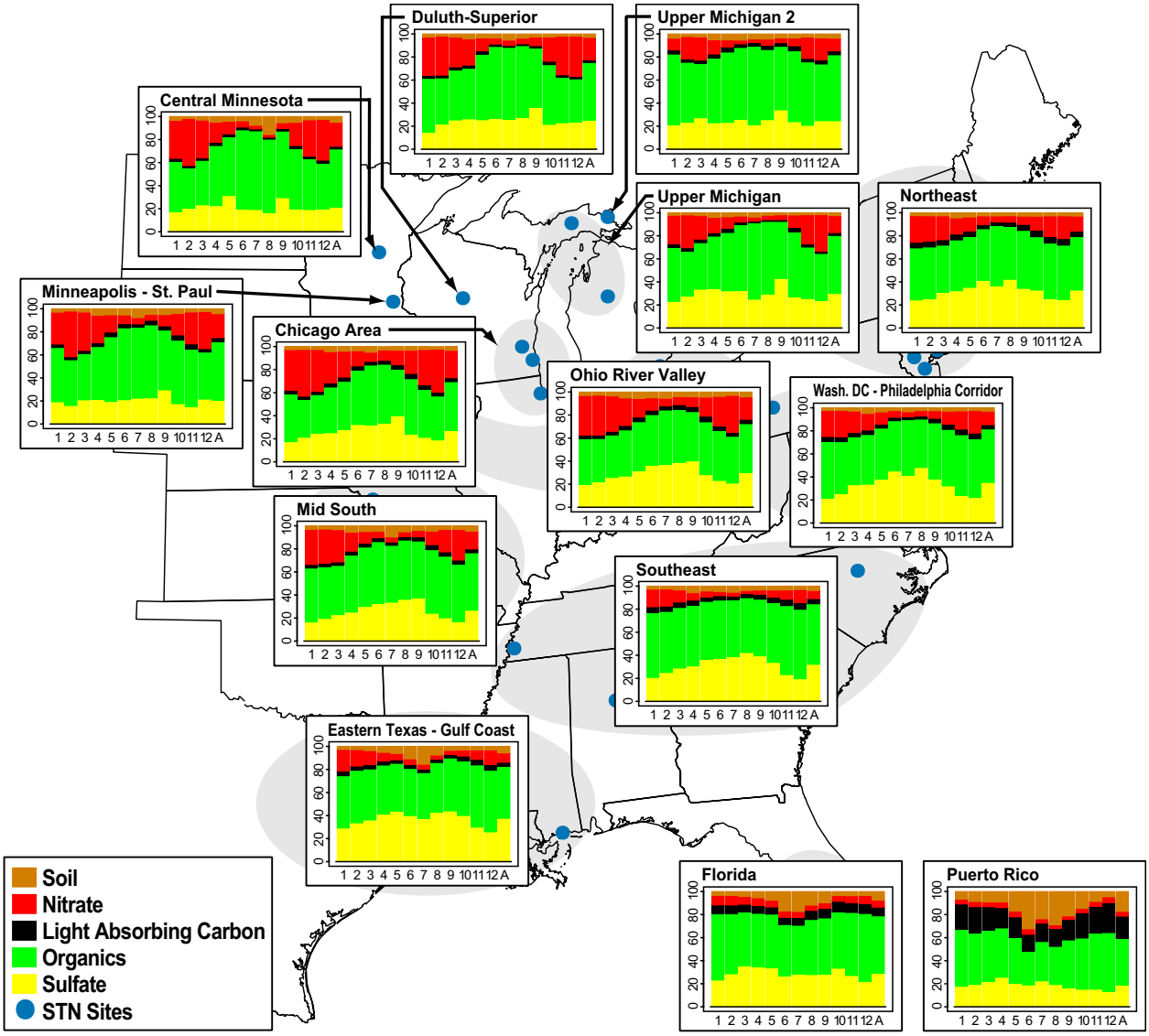

Figure 3.12. Map of stacked bar charts of monthly percent contribution to reconstructed fine mass (%) of fine aerosol species in the eastern U.S. regions of the STN network.

3.2 SPATIAL VARIABILITY OF AVERAGE MONTHLY PATTERNS IN PARTICULATE EXTINCTION COEFFICIENTS

In this section, the spatial variability in the seasonal patterns in particulate extinction and how they differ from aerosol mass concentration are explored for the IMPROVE network. Spatial and temporal patterns in the reconstructed particulate extinction are similar to those observed for aerosols since reconstructed particulate extinction is calculated from aerosol concentrations. However, because specific scattering of sulfates and nitrates is larger than other fine aerosols because of associated water, light-absorbing carbon has relatively high specific extinction, and coarse particle scattering contributes to total particulate extinction, the extinction budgets are somewhat different from fine aerosol budgets. Additionally, the temporal and spatial trends in relative humidity further modify the patterns observed in aerosol concentrations. Coarse mass (CM) is not measured by the STN so the seasonal patterns in the particulate extinction components are explored without an analysis of the total particulate extinction budget.

3.2.1 Fine Particle Ammonium Sulfate Extinction

In general, the seasonal patterns in ammonium sulfate extinction were similar to those in ammonium sulfate mass concentrations, the main difference being enhanced fractional contributions in extinction. Additionally, the seasonality, as indicated by the ratio of the maximum to the minimum monthly average, was increased in extinction in about one-third of the rural regions as compared to mass concentrations. The seasonality in relative humidity can act to either enhance or suppress the seasonality in ammonium sulfate concentrations. The rural regions where extinction had a slightly higher degree of seasonality (an increase of less than 1 in the max/min ratio) were primarily in the eastern United States. The only rural regions to show a large (greater than 1) change in the max/min ratio were all in the West and had larger max/min ratios in ammonium sulfate concentrations compared to extinction coefficients. The opposite was true in the urban regions where seasonality was increased in extinction for approximately 65% of both eastern and western regions. The only two regions to have a large change in the max/min ratio were the Wasatch Front in Utah and Boise, Idaho, both of which had greater seasonality in extinction coefficients.

For nearly all IMPROVE regions, both the maximum and minimum monthly contributions of ammonium sulfate to reconstructed particulate extinction were greater than the maximum and minimum contributions to reconstructed fine mass. The exceptions were Phoenix and the Virgin Islands, where the maximum contributions to concentrations were greater, and the Great Basin and Mogollon Plateau, where the minimum contributions were greater.

In most regions the maximum and minimum monthly values in ammonium sulfate mass concentrations and extinction coefficients occurred within a month of each other. The timing of maximum and minimum contributions to reconstructed particulate extinction and mass was also similar for most IMPROVE regions; comparison was possible for the STN regions. In several regions, the timing of the maxima or minima differed by more than 2 months when comparing mass concentration and extinction coefficients, with no real impact on the overall seasonal pattern. However, a few regions had markedly different seasonal patterns in ammonium sulfate extinction as compared to mass concentrations. Rural Alaska had a spring peak in ammonium sulfate mass concentrations but a summertime peak in extinction because of the lower springtime

f(RH) values. Columbia River Gorge, Puget Sound, and Portland went from a summertime peak in concentrations to a fall peak in extinction due to the comparably higher f(RH) values that are at a minimum in summer in this region. In the Great Basin region, where f(RH) is also at a minimum in summer, the ammonium sulfate maximum shifted from summer in the mass concentration to spring in extinction. In the Virgin Islands, there is both a winter and spring peak in the fractional contribution of ammonium sulfate to reconstructed fine mass and reconstructed particulate extinction. The maximum percent contribution of ammonium sulfate to RCFM occurred during the winter peak, whereas it occurred during the spring peak for reconstructed particulate extinction.

The rural maximum monthly ammonium sulfate extinction coefficient ranged from 4.3 Mm^{-1} in the Great Basin to 121.2 Mm^{-1} in Appalachia, and rural monthly minimums ranged from 1.7 Mm^{-1} in the Great Basin to 31.1 Mm^{-1} in the Southeast. The urban regional monthly maximum ranged from 5.8 in northwest Nevada to 110.0 in the Washington, D.C.-Philadelphia corridor; the minimum ranged from 3.0 in Boise Idaho to 33.2 in the Ohio River valley. Maximum monthly ammonium sulfate contributions to reconstructed particulate extinction ranged from 20% in Phoenix to 82% in Appalachia, and the minimum contributions ranged from 5% in Phoenix to 55% in Hawaii.

3.2.2 Fine Particle Organic Carbon Extinction

The seasonal patterns in OMC extinction were the same as for OMC concentration because no humidity dependence for organics was considered. However, the seasonal patterns in percent contribution of OMC to extinction were influenced by the seasonality of the humidity-impacted terms of reconstructed particulate extinction. In contrast to ammonium sulfate, the contributions of OMC to reconstructed particulate extinction were generally reduced as compared to its contributions to reconstructed fine mass in the IMPROVE regions; comparison was possible for the STN regions. The only exception was southern Arizona where very low relative humidity suppressed the growth of sulfate and nitrate, which resulted in both the maximum and minimum monthly OMC contributions to extinction being higher by one to two percentage points than for the maximum and minimum contributions to mass. There were several regions where the timing of the minimum or maximum contribution differed by more than 2 months when comparing seasonal patterns in reconstructed particulate extinction to those in reconstructed mass. However, only Hells Canyon exhibited a noticeable change in the overall seasonal pattern, with a shift from a springtime to a winter minimum in percent OMC contribution.

The rural maximum monthly OMC extinction coefficients ranged from 2.4 Mm^{-1} in the Virgin Islands to 31.0 Mm^{-1} in the northern Rockies, and monthly minimums ranged from 0.7 Mm^{-1} in Alaska to 10.4 Mm^{-1} in the rural Ohio River valley. The urban maximum ranged from 13.1 Mm^{-1} in North Dakota to 102.5 Mm^{-1} in Missoula, and the minimum ranged from 0.9 Mm^{-1} in upper Michigan to 27.1 Mm^{-1} in Los Angeles. Maximum monthly contributions to reconstructed particulate extinction ranged from 11% in the Virgin Islands to 70% in the northern Rockies, and the minimum contributions ranged from 4% in the Virgin Islands to 27% in Phoenix.

3.3 Fine Particle Light-Absorbing Carbon Extinction

Similar to OMC, the seasonal patterns in LAC extinction were the same as for LAC mass concentration because no humidity dependence for LAC was considered. In all IMPROVE regions where comparison was possible, the maximum and minimum percent contributions of LAC were greater in reconstructed particulate extinction than in reconstructed mass. While there were several regions where the timing of the minimum or maximum contribution differed by more than 2 months when comparing seasonal patterns in contributions to reconstructed particulate extinction to those in reconstructed mass, none had a noticeable impact in the overall seasonal pattern in LAC contributions.

The rural maximum monthly LAC extinction coefficients ranged from 0.8 Mm^{-1} in Hawaii to 5.7 Mm^{-1} in the Ohio River valley, and monthly minimums ranged from 0.3 Mm^{-1} in Alaska to 3.8 Mm^{-1} in the Ohio River valley. The urban maximum ranged from 2.6 Mm^{-1} in Duluth-Superior to 21.9 Mm^{-1} in Phoenix, and the minimum ranged from 1.5 Mm^{-1} in upper Michigan to 8.6 Mm^{-1} in Los Angeles. Maximum monthly contributions to reconstructed particulate extinction ranged from 4% in Hawaii to 17% in Phoenix, and the minimum contributions ranged from 1% in the Virgin Islands to 10% in Phoenix.

3.3.1 Fine Particle Ammonium Nitrate Extinction

Like ammonium sulfate, the seasonal patterns in ammonium nitrate extinction were typically similar to those in ammonium nitrate mass concentrations, with the main difference being enhanced fractional contributions in extinction. For ammonium nitrate, the seasonality as indicated by the ratio of the maximum to the minimum monthly average was increased in extinction as compared to concentrations in approximately two-thirds of the rural regions and half of the urban regions. Many of the urban and rural western regions had significantly larger max/min ratios (greater than 1 increase in ratio) in extinction as compared to concentration; this was not true in the East. The only large changes in ratio, where the seasonality was higher for concentration, occurred in the eastern urban regions of central Minnesota and Minneapolis-St. Paul.

For nearly all IMPROVE regions, both the maximum and minimum monthly contributions of ammonium nitrate to reconstructed particulate extinction were greater than the maximum and minimum contributions to reconstructed fine mass. The exceptions were the Virgin Islands where the maximum contribution and Phoenix where the minimum contribution to reconstructed mass were greater.

In most regions, the maximum and minimum monthly values in ammonium nitrate mass concentrations and extinction coefficients occurred within a month of each other, as did the maximum and minimum contributions to reconstructed particulate extinction and mass. In several regions, the timing of the maxima or minima differed by more than 2 months when comparing mass concentration and extinction coefficients with no real impact on the overall seasonal pattern. However, in Death Valley the seasonal pattern in extinction coefficients with a winter peak and late fall minimum was quite different from the pattern in mass concentrations of a summer peak and late fall minimum.

The rural maximum monthly ammonium nitrate extinction coefficients ranged from 1.4 Mm^{-1} in the Great Basin to 43.2 Mm^{-1} in the Columbia River Gorge, and monthly minimums ranged from 0.5 Mm^{-1} in the Great Basin to 8.2 Mm^{-1} in southern California. The urban maximums ranged from 1.7 Mm^{-1} in urban west Texas to 16.9 Mm^{-1} in the Sacramento and San Joaquin valleys, and the minimums ranged from 0.1 Mm^{-1} in west Texas to 8.0 Mm^{-1} in Los Angeles. Maximum monthly contributions to reconstructed particulate extinction ranged from 9% in the Virgin Islands to 56% in the central Great Plains, and the minimum contributions ranged from 2% in Appalachia to 17% in southern California.

3.3.2 Fine Particle Soil Extinction

Soil, like OMC and LAC, is assumed to have no humidity dependence, and therefore the seasonal patterns in extinction coefficients are the same as those for mass concentrations. In all IMPROVE regions, the maximum and minimum percent contributions of soil were greater in reconstructed fine mass than in reconstructed particulate extinction. While there were several regions where the timing of the minimum or maximum contribution differed by more than 2 months when comparing seasonal patterns in reconstructed particulate extinction to those in reconstructed mass, none had a noticeable impact in the overall seasonal pattern in soil contributions.

The rural maximum monthly soil extinction coefficients ranged from 0.3 Mm^{-1} in Alaska to 4.5 Mm^{-1} in the Virgin Islands, and monthly minimums ranged from 0.1 Mm^{-1} in Alaska to 1.2 Mm^{-1} in southern Arizona. Urban maximums ranged from 0.5 Mm^{-1} in upper Michigan to 3.9 Mm^{-1} in Phoenix; minimums ranged from 0.1 Mm^{-1} in upper Michigan to 2.4 Mm^{-1} in Phoenix. Maximum monthly contributions to reconstructed particulate extinction ranged from 1% on the East Coast to 14% in the Virgin Islands, and the minimum contributions ranged from 0.3% in the Columbia River Gorge to 5% in southern Arizona.

3.3.3 Coarse Particle Mass Extinction

Since no humidity dependence for CM is assumed in the extinction model, the seasonal patterns in extinction coefficients and mass concentrations are comparable. While the seasonal patterns in CM concentrations are not discussed in this report since the prior discussion was focused on the reconstructed fine mass model, seasonal coarse mass values can be found in Appendix B. In general, the seasonal patterns in CM are very similar to those in soil, with the maximum and minimum extinction coefficients in CM and soil occurring within a month of each other in over half and over three-quarters of the regions, respectively. Thus, peak CM extinction coefficients are typically in spring or summer, and minimum values are typically in fall or winter.

However, several regions that had a spring maximum in soil extinction coefficients had a summer maximum in CM; these included Boundary Waters, Hells Canyon, the Northeast, the northern Great Plains, and southern California. One region, the East Coast, had the reverse situation of a springtime maximum in CM and a summertime maximum in soil. Additionally, several regions that had fall time minima in soil extinction had winter minima in CM; these were Hawaii, the East Coast, and the mid-South. The central Rockies had the reverse situation of a winter minimum in soil and a fall maximum in CM. Exceptions to the spring-summer maximum

in CM extinction coefficients included several regions that had spring or summertime maximums in soil but had fall maxima in CM; these were Alaska, the California coast, the Sierra Nevada, Oregon and northern California, the Ohio River valley, Phoenix, and Washington, D.C. Washington, D.C., was also an exception to the fall-winter minimum in CM extinction coefficients with its minimum monthly extinction value occurring in June.

The ratios of maximum to minimum CM extinction coefficients were lower than the ratios in soil extinction in most regions, particularly in regions with a high degree of seasonality in soil concentrations. The maximum to minimum ratio in CM extinction coefficients ranged from 1.5 to 12, with a median value of 3, whereas soil ratios ranged from 1.5 to 20, with a median value of 5. Different seasonal patterns in CM and soil might indicate different sources for the two aerosol types.

The maximum monthly CM extinction coefficients ranged from 1.7 Mm^{-1} in Alaska to 15.3 Mm^{-1} in Phoenix, and monthly minimums ranged from 0.3 Mm^{-1} in Hells Canyon to 10.5 Mm^{-1} in Phoenix. Maximum monthly contributions to reconstructed particulate extinction ranged from 4% in Appalachia to 45% in the Virgin Islands, and the minimum contributions ranged from 1% in Death Valley to 14% in Hells Canyon.

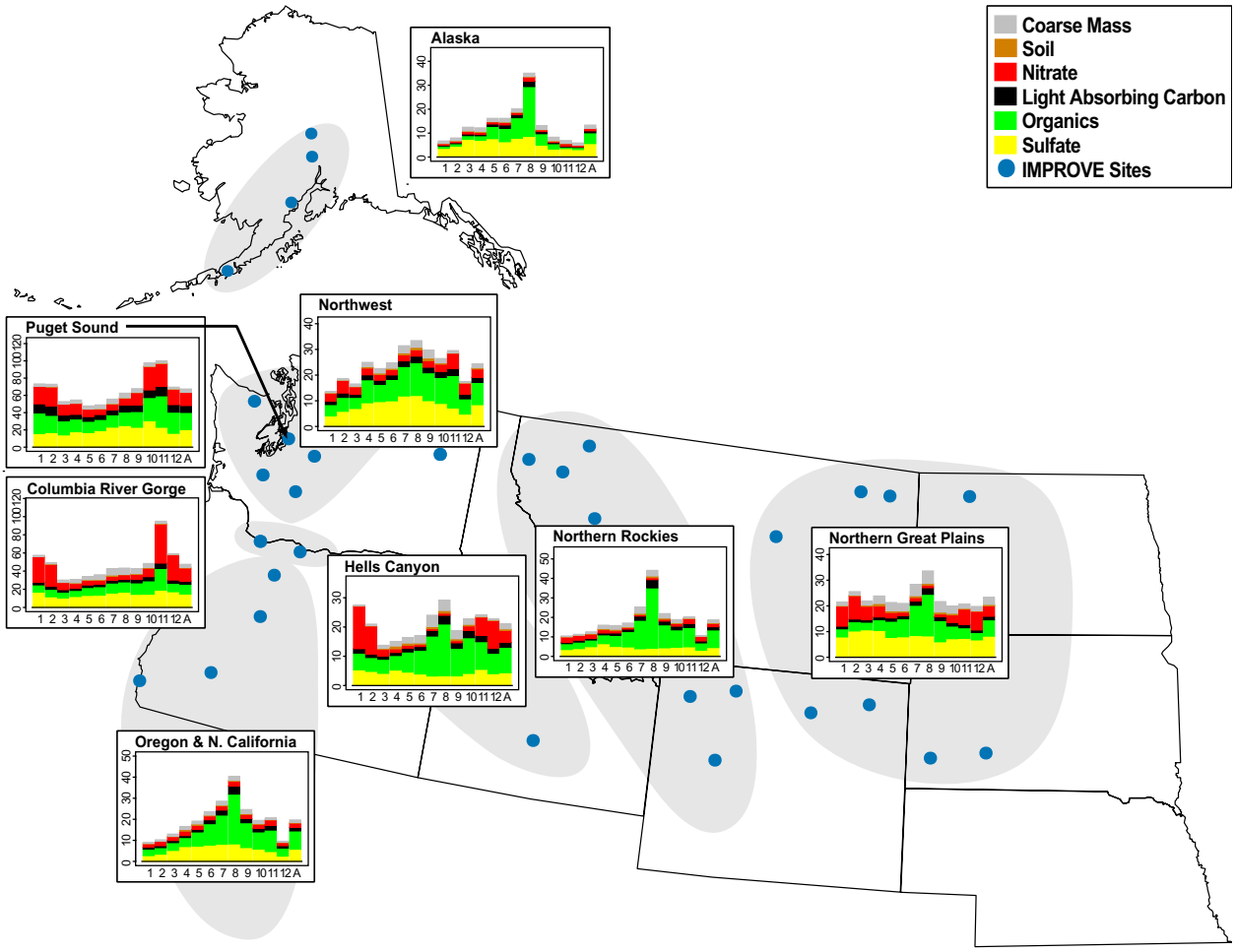

Figure 3.13. Map showing stacked bar charts of monthly distributions of particulate extinction coefficients for the northwestern U.S. regions of the IMPROVE network. Starting from the base of the chart, ammonium sulfate, organics, light-absorbing carbon, ammonium nitrate, soil, and coarse mass are the order of presentation.

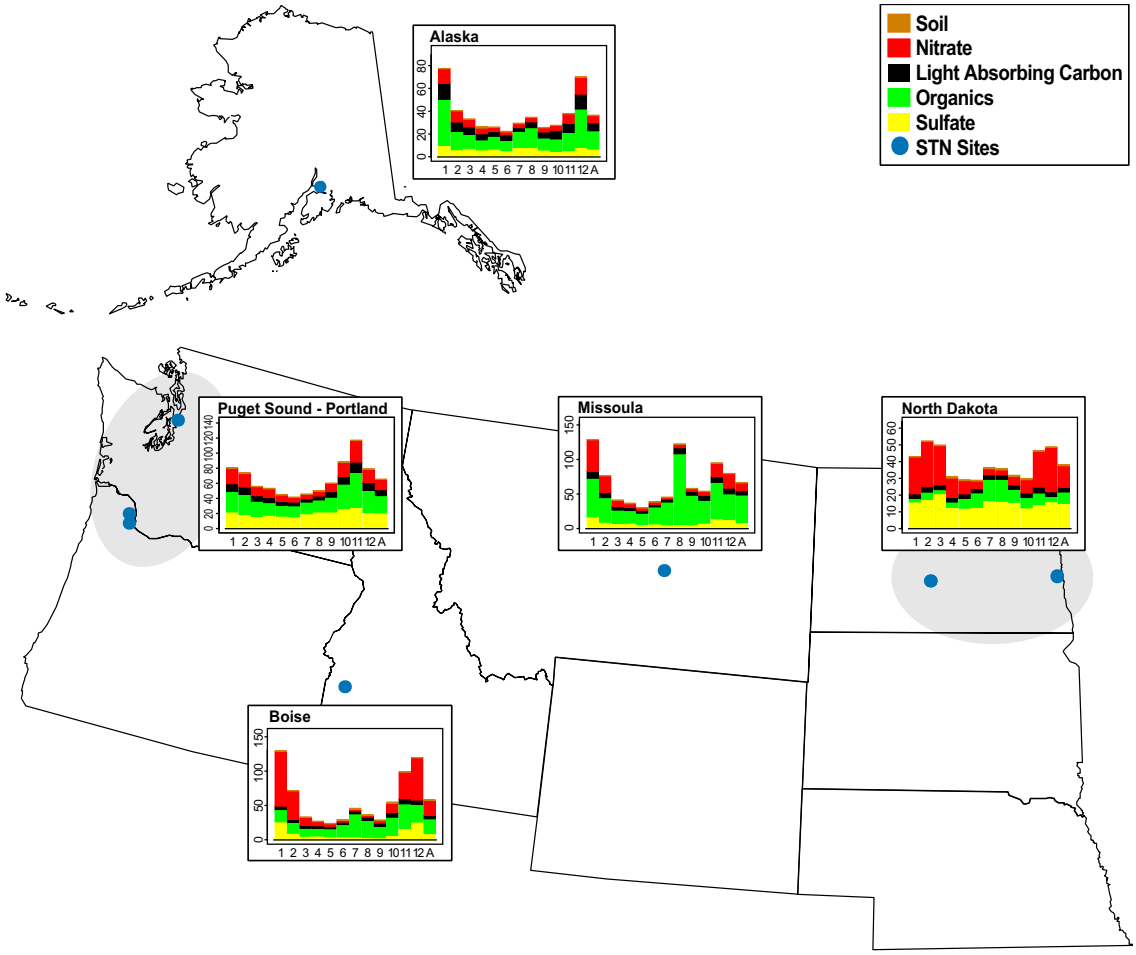

Figure 3.14. Map showing stacked bar charts of monthly distributions of fine particulate extinction coefficients (Mm^{-1}) for the northwestern U.S. regions of the STN network. Starting from the base of the chart, ammonium sulfate, organics, light-absorbing carbon, ammonium nitrate, and soil are the order of presentation. Coarse mass measurements were not available for STN and so are not included.

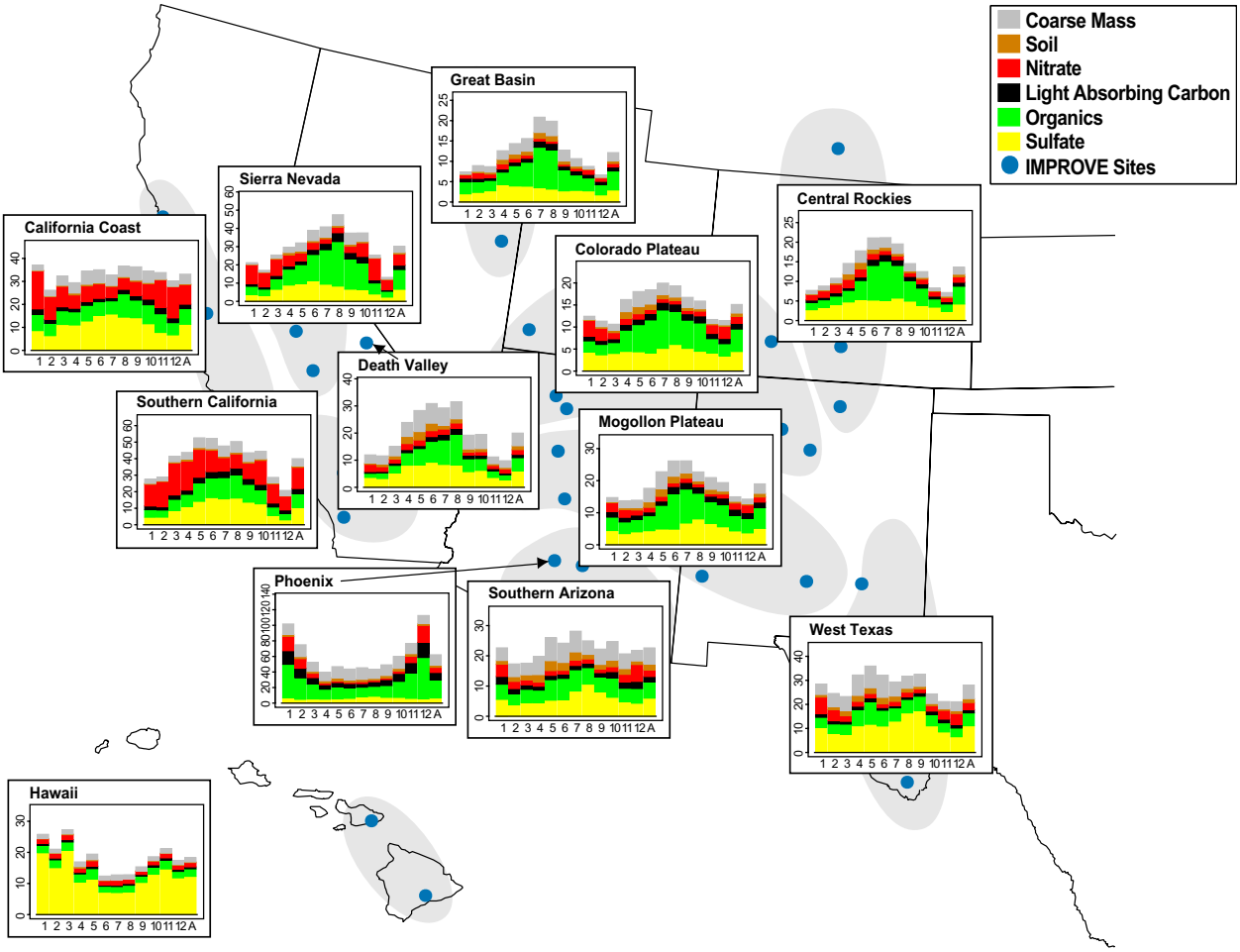

Figure 3.15. Map showing stacked bar charts of monthly distributions of particulate extinction coefficients (Mm^{-1}) for the southwestern U.S. regions of the IMPROVE network. Starting from the base of the chart, ammonium sulfate, organics, light-absorbing carbon, ammonium nitrate, soil, and coarse mass are the order of presentation.

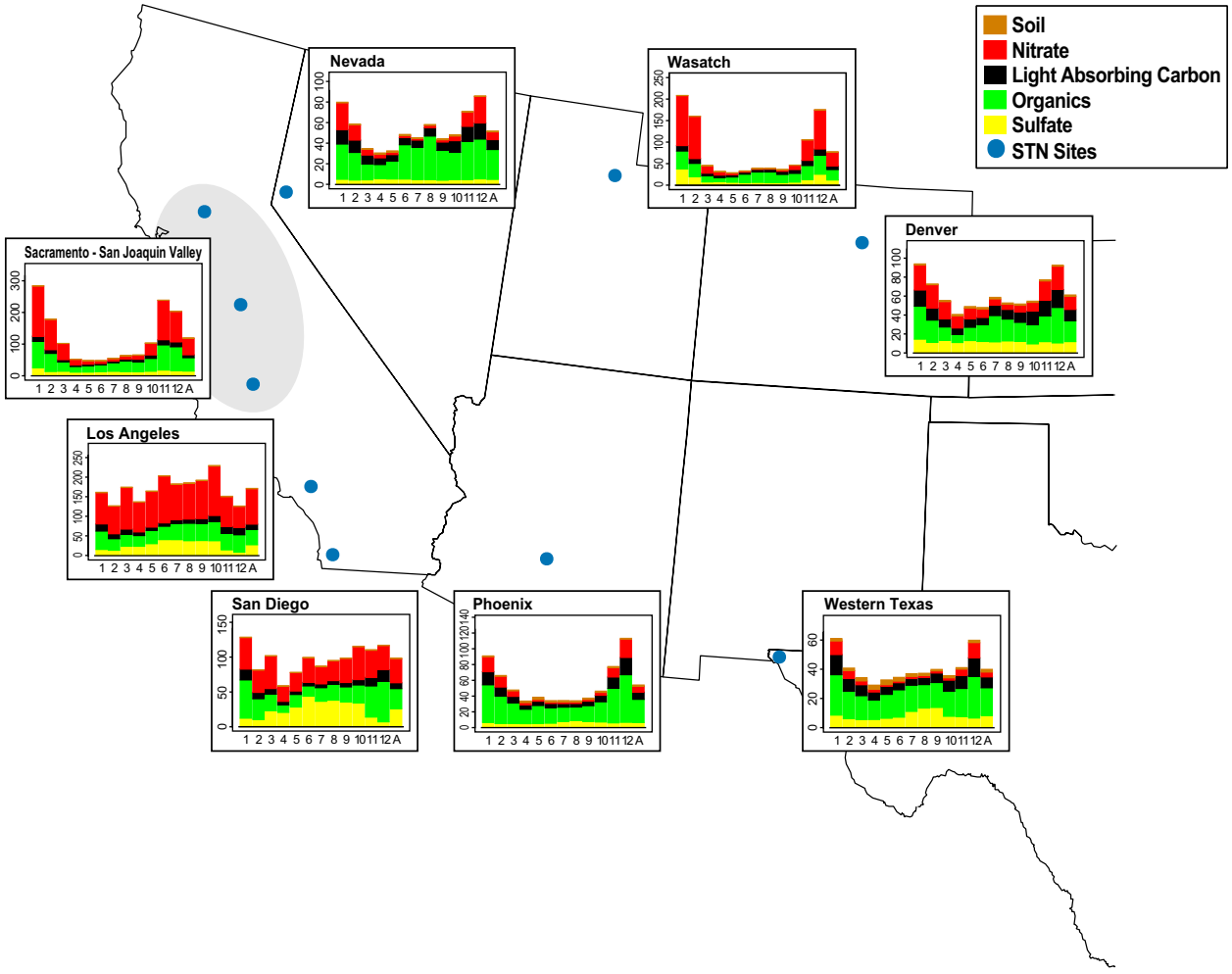

Figure 3.16. Map showing stacked bar charts of monthly distributions of fine particulate extinction coefficients (Mm^{-1}) for the southwestern U.S. regions of the STN network. Starting from the base of the chart, ammonium sulfate, organics, light-absorbing carbon, ammonium nitrate, and soil are the order of presentation. Coarse mass measurements were not available for STN and so are not included.

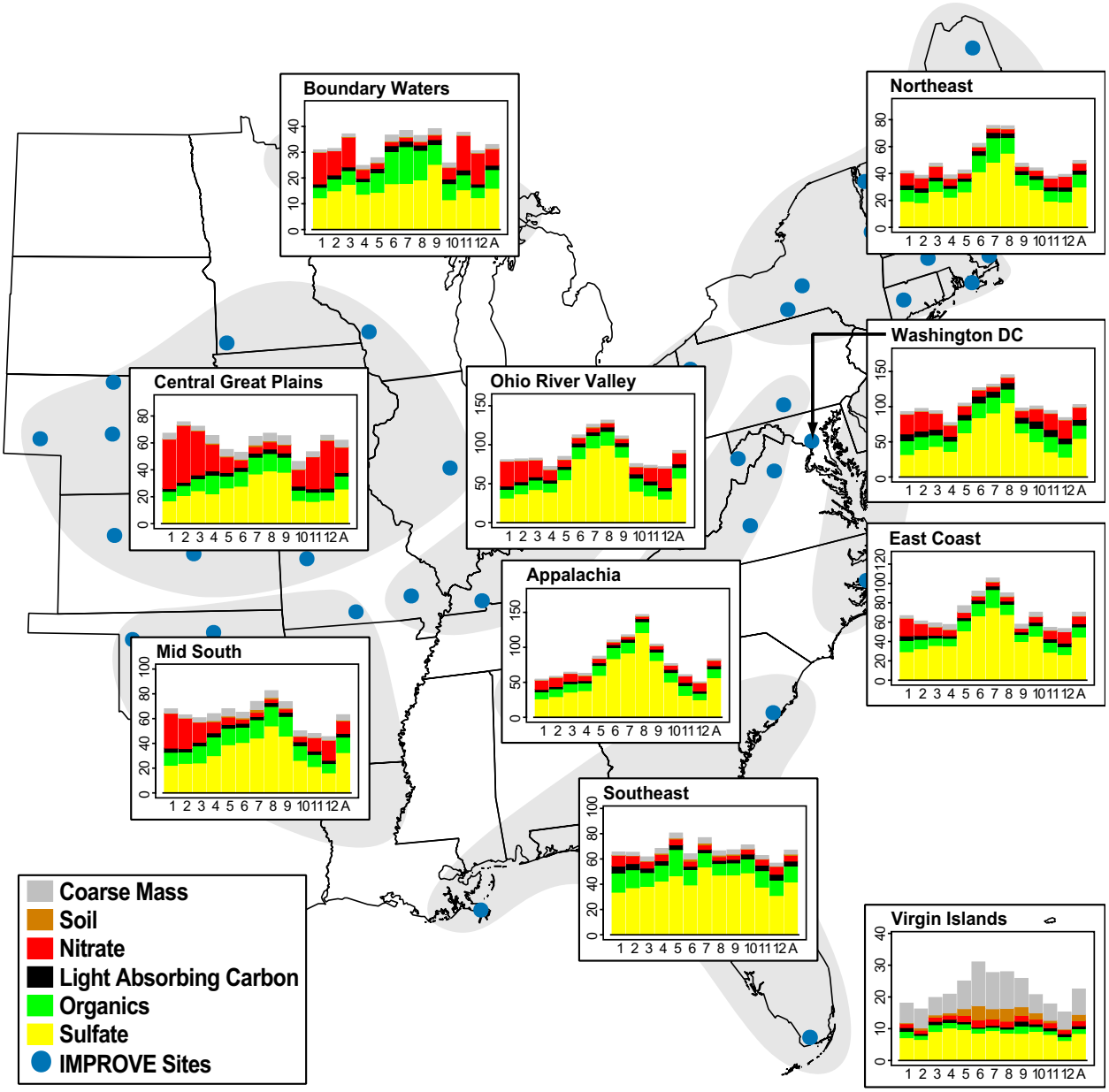

Figure 3.17. Map showing stacked bar charts of monthly distributions of particulate extinction coefficients (Mm^{-1}) for the eastern U.S. regions of the IMPROVE network. Starting from the base of the chart, ammonium sulfate, organics, light-absorbing carbon, ammonium nitrate, soil, and coarse mass are the order of presentation.

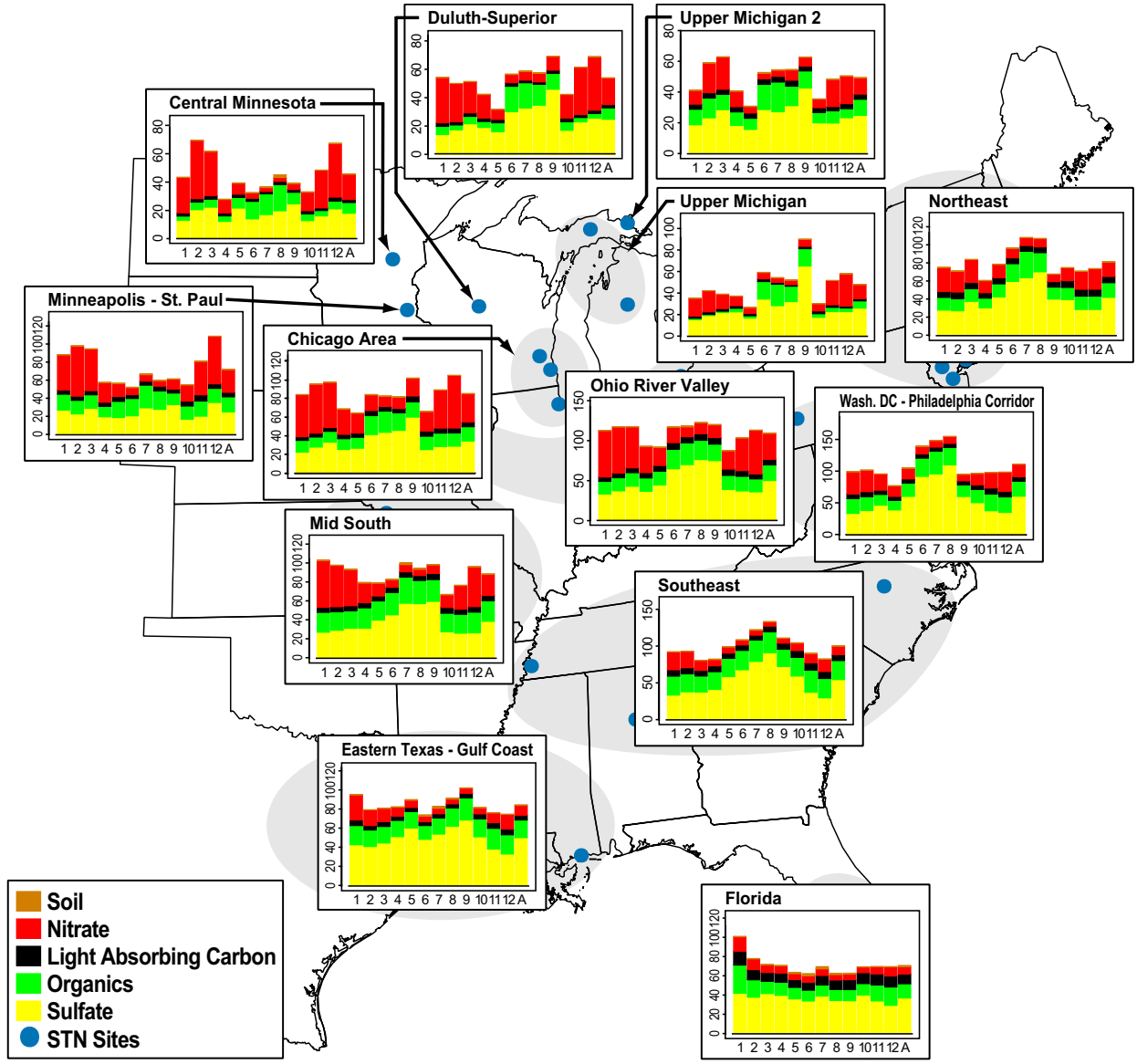

Figure 3.18. Map showing stacked bar charts of monthly distributions of fine particulate extinction coefficients (Mm^{-1}) for the eastern U.S. regions of the STN network. Starting from the base of the chart, ammonium sulfate, organics, light-absorbing carbon, ammonium nitrate, and soil are the order of presentation. Coarse mass measurements were not available for STN and so are not included.

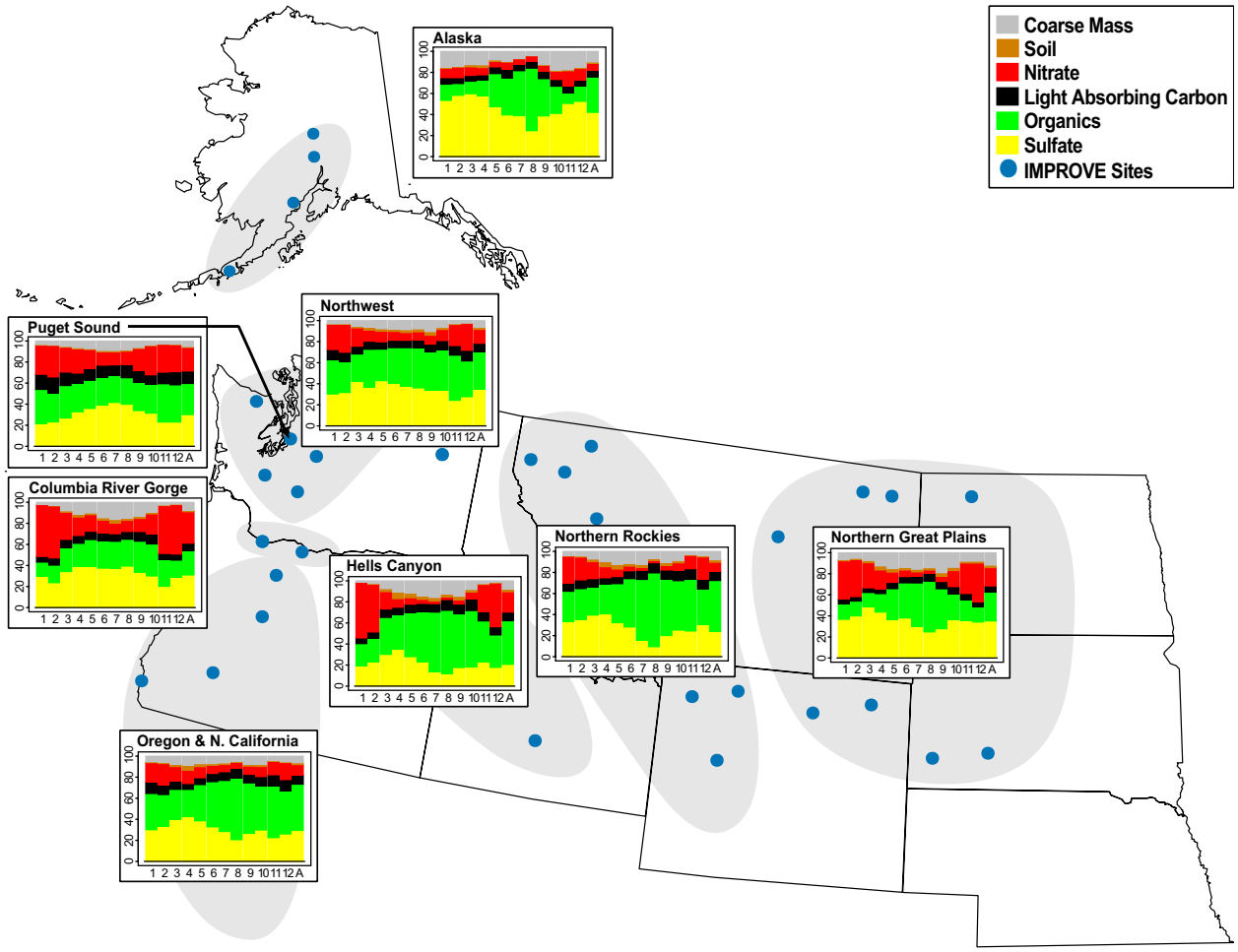

Figure 3.19. Map showing stacked bar charts of monthly percent contribution to reconstructed particulate extinction (%) for particulate extinction coefficients for the northwest U.S. regions of the IMPROVE network. Starting from the base of the chart, ammonium sulfate, organics, light-absorbing carbon, ammonium nitrate, soil, and coarse mass are the order of presentation.

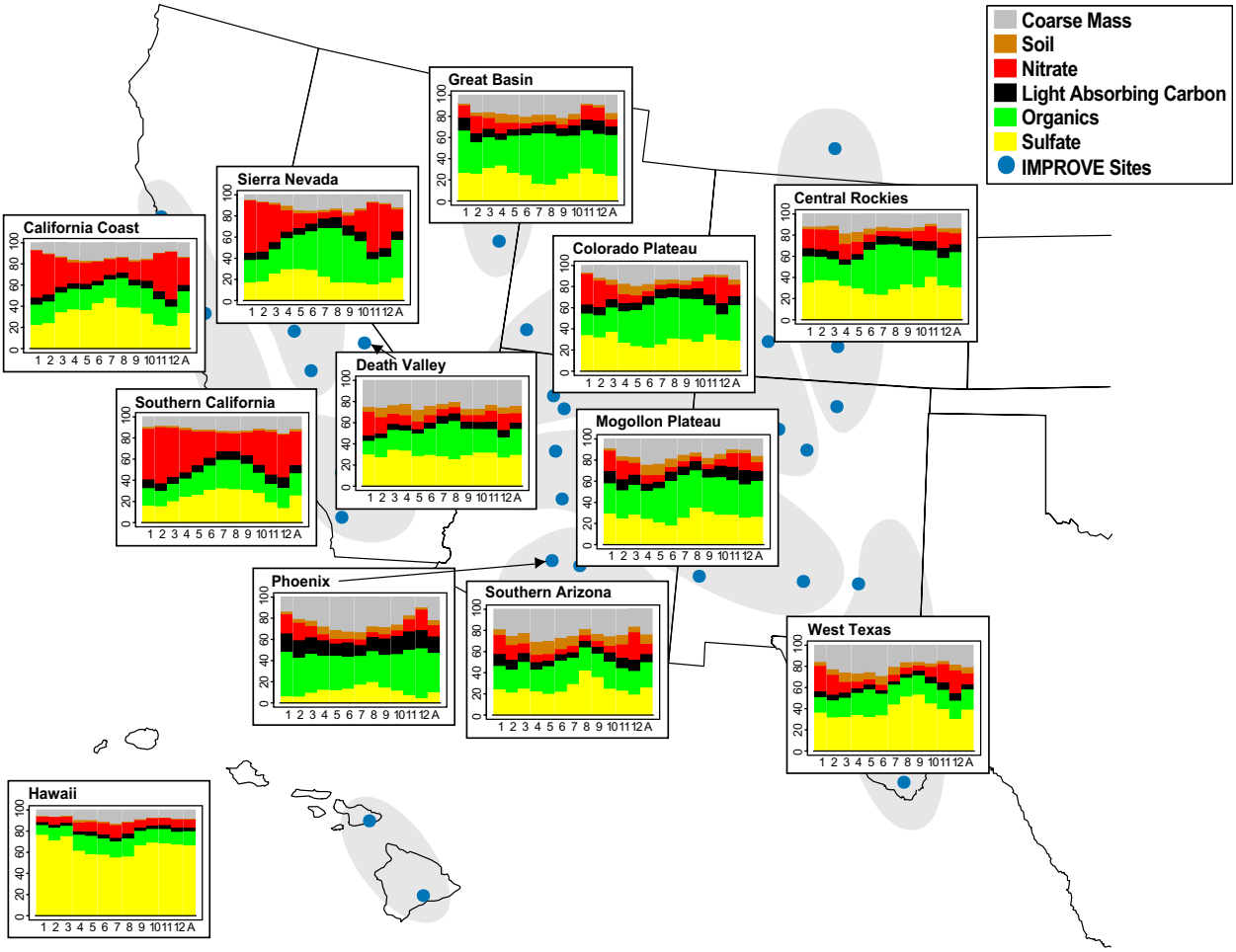

Figure 3.20. Map showing stacked bar charts of monthly percent contribution to reconstructed particulate extinction (%) for particulate extinction coefficients for the southwest U.S. regions of the IMPROVE network. Starting from the base of the chart, ammonium sulfate, organics, light-absorbing carbon, ammonium nitrate, soil, and coarse mass are the order of presentation.

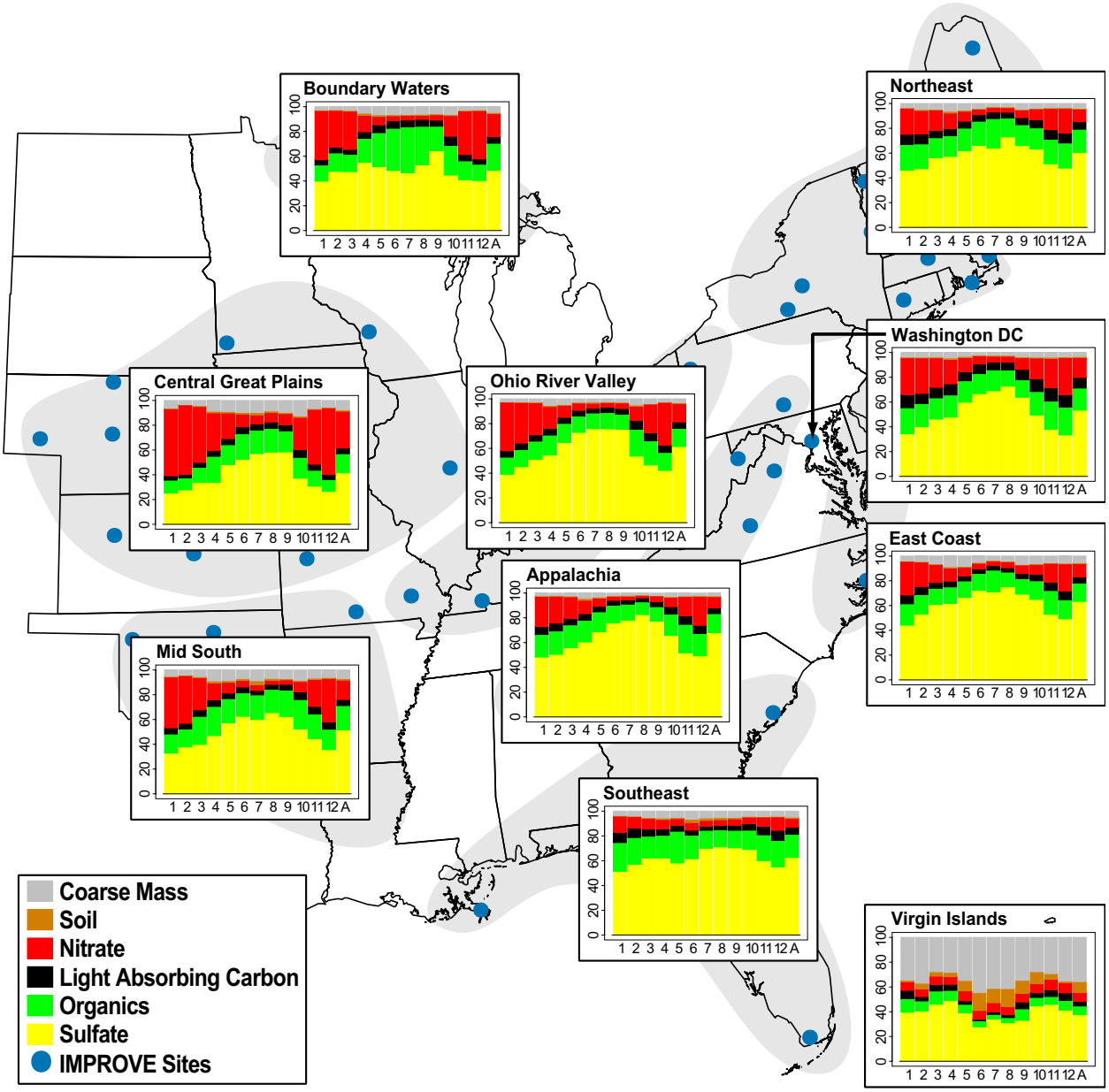

Figure 3.21. Map showing stacked bar charts of monthly percent contribution to reconstructed particulate extinction (%) for particulate extinction coefficients for the eastern U.S. regions of the IMPROVE network. Starting from the base of the chart, ammonium sulfate, organics, light-absorbing carbon, ammonium nitrate, soil, and coarse mass are the order of presentation.

REFERENCES

Husar, R. B., et al. (2001), Asian dust events of April 1998, *J.Geophys. Res.*, *106*, 18,317-18,330.

Malm, W. C., J. F. Sisler, M. L. Pitchford, M. Scruggs, R. Ames, S. Copeland, K. A. Gebhart, and D. E. Day (2000), Spatial and seasonal patterns and temporal variability of haze and its constituents in the United States: Report III, Cooperative Institute for Research in the Atmosphere, Colorado State University, ISSN 0737-5352-47.

Malm W. C, B. A. Schichtel, M. L. Pichford, L. L. Ashbaugh, and R. A. Eldred (2004), Spatial and monthly trends in fine particle concentration in the United States, *J. Geophys. Res., 109*, D03306, doi:10.1029/2003JD003739.

Perry, K. D., T. A. Cahill, R. A. Eldred, and D. D. Dutcher (1997), Long-range transport of North African dust to the eastern United States, *J. Geophys. Res.*, *102*(D10), 11225-11238.

Prospero, J. M., P. Ginoux, O. Torres, S. E Nicholson, and T. E. Gill (2002), Environmental characterization of global sources of atmospheric soil dust identified with the Nimbus 7 Total Ozone Mapping Spectrometer (TOMS) absorbing aerosol product, *Rev. Geophys., 40*(1), 1002, doi:10.1029/2000RG000095.

Sisler, J. F., D. Huffman, D. A. Latimer, W. C. Malm, and M. L. Pitchford (1993), Spatial and temporal patterns and the chemical composition of the haze in the United States: An analysis of data from the IMPROVE network 1988-1991, Cooperative Institute for Research in the Atmosphere, Colorado State University, ISSN 0737-5352-26.

Sisler, J. F., W. C. Malm, and K. A. Gebhart (1996), Spatial and seasonal patterns and long term variability of the composition of the haze in the United States: An analysis of data from the IMPROVE network, Cooperative Institute for Research in the Atmosphere, Colorado State University, ISSN 0737-5352-32.

VanCuren, R. A., and T. A. Cahill (2002), Asian aerosols in North America: Frequency and concentration of fine dust, *J. Geophys. Res., 107*(D24), 4804, doi:10.1029/2002JD002204.

CHAPTER 4: TEMPORAL TRENDS IN FINE AEROSOL SPECIES CONCENTRATIONS AND AEROSOL EXTINCTION

INTRODUCTION

The results of several studies investigating monotonic trends in fine aerosol species concentrations will be summarized here, with the originals available in Appendix D. Topics explored since the last IMPROVE report in 2000 include the 10-year spatial and temporal trends in sulfate concentrations and SO_2 emissions [Malm et al., 2002], the uncertainty in sulfate concentration trends [White et al., 2005], 10-year trends in visibility [NPS, 2006], >7-year trends in organic and elemental carbon [Schichtel et al., 2004], and the Visibility Information Exchange Web System (VIEWS) annual summary trends tools. The IMPROVE program often uses Theil regression statistics for calculating trends; the original reference is not widely available so there is a discussion of Theil regression and associated statistics available from the IMPROVE website. A detailed discussion and algorithm for performing Theil regression in SAS, by Hess et al. [2002], is available at http://vista.cira.colostate.edu/improve/Publications/GrayLit/026_TheilReg/TheilRegressionl.pdf.

4.1 Estimating Measurement Uncertainty in an Ambient Sulfate Trend

The Regional Haze Rule seeks restoration of natural visibility conditions through steady improvements over the next six decades. Documenting change on this timescale entails particle measurements that will support accurate comparisons between different eras, even as monitoring methods evolve [White, 1997; Weatherhead et al., 1998]. Such absolute measurement stability is a requirement not encountered in the shorter, more intensive field campaigns typically mounted to support source apportionment and model validation studies.

It is sometimes asserted that measurement errors should have little impact on trend estimates. Random errors are as likely to cancel as to reinforce each other in successive observations, and the estimated imprecision of an average accordingly declines with the square root of the number of observations going into it. Fixed biases are even less of a concern; zero offsets cancel when observations from different periods are subtracted, and scaling factors cancel when ratios are taken.

The problem with such theoretical analyses is that actual measurement series generally include nonideal errors. Figure 4.1 shows an example of such nonideality, a year-long trend in observed differences between collocated measurements of $SO_4^=$ at Big Bend National Park. The errors that generate these differences are clearly neither independent in successive observations nor constant across all observations. The collocated precision of the measurements is an excellent 2.5%, but there is a difference of about 5%/year between the time trends of the two measurement series.

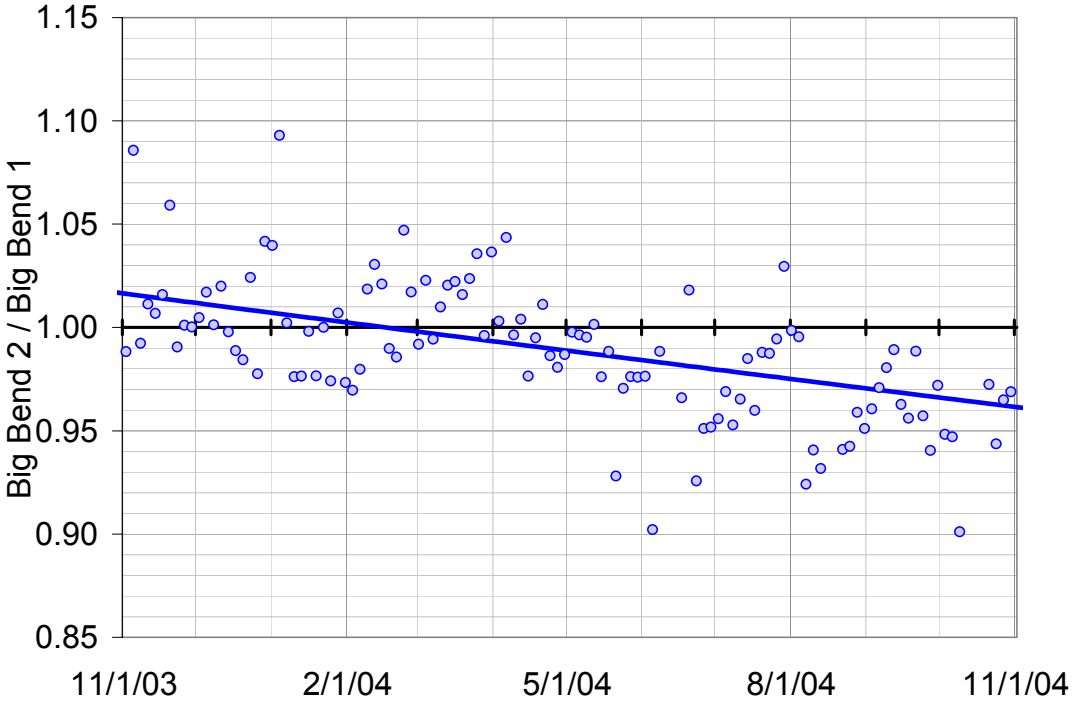

Figure 4.1. Ratio of 24-hour sulfate concentrations measured by collocated and routine IMPROVE B modules at Big Bend NP.

A case study of the trend uncertainty produced by actual patterns of measurement error was undertaken by White et al. [2005] with data from Shenandoah National Park. IMPROVE and the Clean Air Status and Trends Network (CASTNet) have conducted collocated particle monitoring at this site since 1988. The analysis was based on the three independent series recorded for 24-hour sulfur (IMPROVE proton induced X-ray emission/X-ray fluorescence—PIXE/XRF), 24-hour sulfate (IMPROVE ion chromatography—IC), and 168-hour sulfate (CASTNet IC). These redundant determinations allowed the uncertainties of measurement to be isolated from those of meteorological variability and incomplete sampling.

Table 4.1 presents a selection of the results. Five-year sulfate trends can be estimated from both the sulfur and sulfate series, and these trends are expected to agree in the absence of measurement error. Equivalently, any trends observed in the series of ratios can be attributed to the effects of errors. It can be seen that spurious trends of as much as 3% per year were recorded over 5-year periods. The overall uncertainty of 5-year sulfate trends was estimated to be at least 1% per year from measurement error alone, significantly more than would be expected under naive statistical assumptions from the demonstrated precision of the measurements. The excess uncertainty arises from subtle trends in the errors themselves.

Table 4.1. Five-year trends in measurement differences at Shenandoah NP.

	SO_4/3S	
Period	**Decrease/yr**	**+/-**
6/88 – 5/93	0.3%	0.6%
6/89 – 5/94	-0.5%	0.7%
6/90 – 5/95	0.1%	0.7%

	SO_4/3S	
Period	**Decrease/yr**	**+/-**
6/91 – 5/96	2.3%	0.8%
6/92 – 5/97	2.8%	0.7%
6/93 – 5/98	2.6%	0.7%
6/94 – 5/99	2.0%	0.6%
6/95 – 5/00	0.8%	0.5%
6/96 – 5/01	-0.6%	0.6%
6/97 – 5/02	-1.5%	0.7%
6/98 – 5/03	-3.5%	0.8%
$rms/\sqrt{2}$	**1.3%**	0.5%

4.2 A 10-YEAR SPATIAL AND TEMPORAL TREND OF SULFATE ACROSS THE UNITED STATES

4.2.1 Introduction

Emissions of sulfur dioxide (SO_2) into the atmosphere result in the formation of fine (<2.5 mm) particulate sulfate via a number of physiochemical mechanisms. Fine sulfates significantly impair visibility, deposit to susceptible aquatic and terrestrial ecosystems, and have the potential to be harmful to human health. A number of legislative and regulatory mandates have reduced SO_2 emissions both in the eastern and the western United States in an attempt to ameliorate these potentially deleterious effects. In response to the regulations and other socioeconomic pressures, SO_2 emissions have been declining over much of the United States [U.S. EPA, 2001].

This chapter builds upon previous work by examining the spatial and temporal trends of $SO_4^=$ over the United States. The CASTNet $SO_4^=$ data and the IMPROVE monitoring program data were combined to investigate changes in the spatial trends of the 90th percentile $SO_4^=$ concentrations across the United States between two time periods (1990–1994 and 1995–1999) and the yearly temporal trends of the 20th and 80th percentile. Also, the trends in SO_2 emissions and $SO_4^=$ concentrations were compared for regions in both the western and eastern United States. The spatial trends in the 90th percentile will not be discussed here but can be found in the full article in Appendix D.

The IMPROVE and CASTNet monitoring sites used in this analysis are presented in Figure 1 in Malm et al. [2002]. The CASTNet, or CASTNet Deposition Network (CDN), was established as a result of the 1990 Amendments to the Clean Air Act, with the goal to determine the effect of emissions reductions mandated by the act on air quality and deposition. Important differences between the samplers deployed by the CASTNet and IMPROVE networks are summarized in Table 4.2 and should be kept in mind when comparing their respective data. The trends in SO_2 emissions were examined using annual SO_2 emission rates from the EPA's National Emission Trends (NET) database [U.S. EPA, 2000]. The data were obtained by downloading 15 years (1985–1999) of county-level emission data from the EPA's AIRData website.

Table 4.2. Important differences between samplers deployed in the CASTNet and IMPROVE networks.

Protocol	CASTNet	IMPROVE
Sampler type	Filter pack	Modular
Sampling frequency	Weekly	Twice weekly (Wednesday and Saturday), 24-hour
Collection substrate	Teflon	Teflon (for elemental S), nylon (Nylasorb) for NO_3^- ions
Inlet size cut	Non-size-selective	$PM_{2.5}$ cyclone
Inlet denuder	None	Na_2CO_3 (for nylon collection substrate, intended to remove HNO_3)
Inlet height	10 m agl	~ 3 m above ground level (agl)

4.2.2 Yearly Temporal Trends of the 20th and 80th Percentile $SO_4^=$ Concentrations

In this section, the temporal trends in the yearly 20th and 80th percentile sulfate mass concentrations are examined. Characterization of trends can be a highly subjective exercise in that slopes and their significance can vary depending on the technique employed. Using an ordinary least squares (OLS) regression approach is questionable with such small data sets, as the results can be highly influenced by outliers. In another approach developed by Theil [1950], outlier data points do not as significantly influence the results. Slopes of trend lines are calculated for each site by first finding the slope between all possible pairs of data points. The median value in the case of an odd number of pairs is selected as the estimated slope, or in the case of an even number of pairs, the average of the two slopes that straddle the median is used as the estimate. The significance of the Theil trend is found by calculating the probability that a random re-ordering of the same observations would yield a trend as consistent as the one observed. The slope estimates ($\mu g/m^3/yr$) are the trend lines for the periods under consideration. For the IMPROVE data set, slope estimates are only shown for those sites that have at least 75 data points (two 24-hour samples per week ≈72% data recovery) for 7 years out of approximately 12 years of data. For the CASTNet data set, trends were calculated for sites with 40 data points (weekly samples ≈77% data recovery) for at least 7 out of 11 years of data.

Trends in yearly 80th percentile sulfate concentration at all, except two, monitoring sites west of the Rocky Mountains show some decrease in sulfate concentration (Figure 4.2). The exceptions are Lassen Volcanic National Park, California, where the sulfate concentration shows a statistically significant increase of about 24%, and Hopi Point in the Grand Canyon National Park, which had an insignificant increase of 1%. There are two sites, Indian Gardens in the Grand Canyon National Park, Arizona (4000 feet below rim), and Pinnacles National Monument, California, that exhibit about a 40% reduction that is statistically significant. Six additional sites also show statistically significant decreases.

In the East, the largest decreases occurred north of the Ohio River valley, while all monitoring sites south of Kentucky and Virginia showed increasing and decreasing trends that are not statistically significant. The maximum percent decrease occurred at Dolly Sods Wilderness Area, West Virginia, at a rate of 73% for the 11-year period, while many sites showed statistically significant decreases in excess of 50%.

East of the Rocky Mountains, Big Bend, Texas, and Cranberry, North Carolina, are the only areas that show statistically significant increases in $SO_4^=$ mass concentrations of 32% and 15%, respectively, while Guadalupe Mountains, Great Sand Dunes, Badlands and Mammoth Cave National Parks, Upper Buffalo Wilderness Area, and Chassahowitzka National Wildlife Refuge showed increasing trends that were not statistically significant.

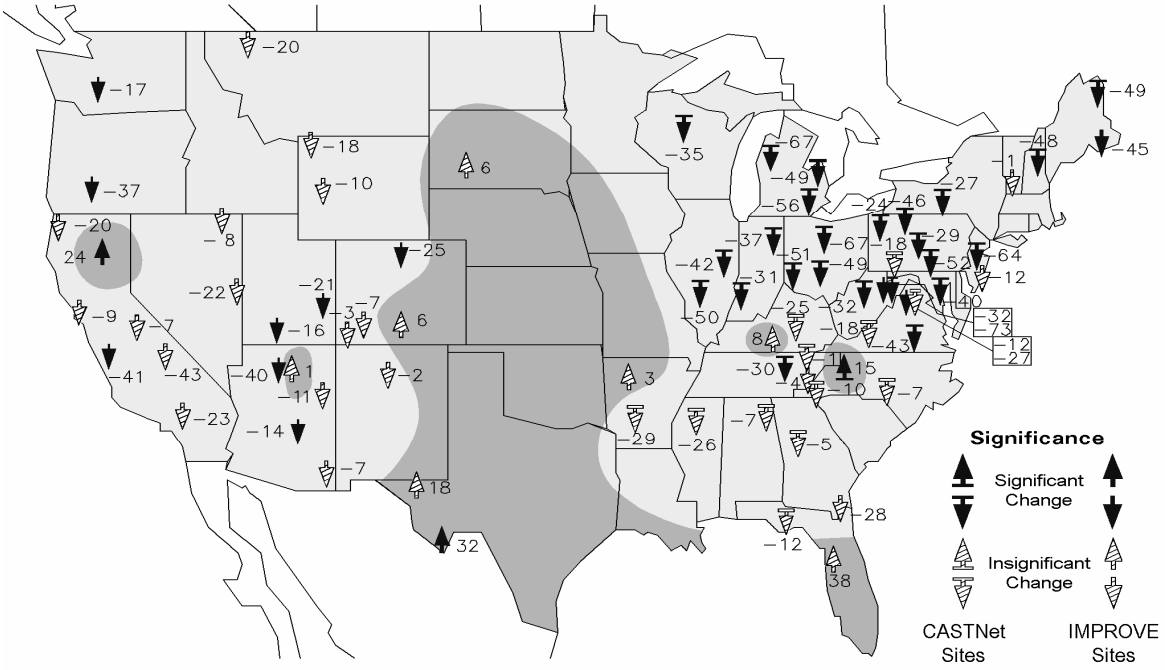

Figure 4.2. Summary of the results of Theil regressions for the 80th percentile SO_4^{2-} (3*S for IMPROVE program) concentrations from 1989 to 1999. Solid up or down arrows show which sites have trends with a significance level of at least 10%. Arrows with enclosed hatch lines show whether the trend was up or down but not statistically significant. Arrows with a bar across the tail represent CASTNet sites, while arrows without the bar show IMPROVE monitoring sites. The numbers are the percent changes from the overall median of the 80th percentile.

The spatial patterns of the 20th percentile $SO_4^=$ concentrations are similar to the 80th percentile map shown in that most of the western United States shows a downward trend in 20th percentile sulfate concentrations (Figure 4.3). In the East, all but eight sites north of the northern border of Tennessee and North Carolina have statistically significant downward trends, while those sites south of this border show statistically insignificant increasing and decreasing trends.

It is of interest to point out that for the 80th percentile trends, the largest decreases were observed in the central eastern United States with somewhat smaller but still significant trends in the Northeast, while for the 20th percentile sulfate concentrations the spatial relationship of trends between the central and northeastern United States is reversed.

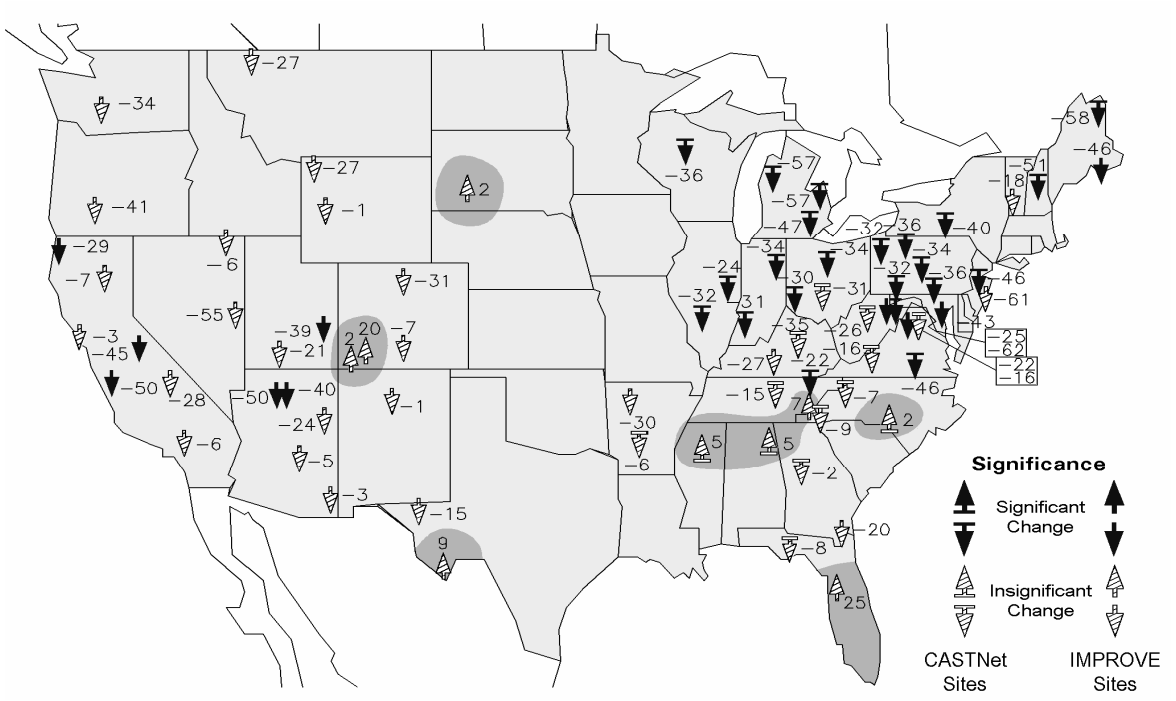

Figure 4.3. Summary of the results of Theil regressions for the 20th percentile SO_4^{2-} (3*S for IMPROVE program) concentrations from 1989 to 1999. Solid up or down arrows show which sites have a trend with a significance level of at least 10%. Arrows with enclosed hatch lines show whether the trend was up or down but not statistically significant. Arrows with a bar across the tail represent CASTNet sites, while arrows without the bar show IMPROVE monitoring sites. The numbers are the percent changes from the overall median of the 20th percentile.

4.2.3 Yearly Temporal Trends of NET SO_2 Emissions

The trends in the NET SO_2 emission fields were examined for each state by first aggregating the county-level emissions over each state for each year from 1990 to 1999. The slope of the 10-year trend for each state was estimated using the Theil regression. In the northern half of the eastern United States from Missouri to Maine, most states had statistically significant decreasing trends from 10% to 60% and ~30% over the entire region (Figure 4.4). States along the Ohio River valley, which have the highest SO_2 emissions in the country, had statistically significant decreases as high as 35% in Ohio and 44% in Indiana. Over most of the southeastern states from Arkansas to Florida, the SO_2 emissions have increased with significant increases in Arkansas (87%), Louisiana (48%), and North Carolina (37%). Tennessee and Georgia, with some of the highest SO_2 emission rates in the region, had significant decreases of 35% and 42%, respectively.

In the central part of the United States extending from Texas to North Dakota, the SO_2 emissions have also been increasing. Statistically significant increases were found in Texas (14%), New Mexico (10%), Colorado (11%), Wyoming (31%), North Dakota (35%), and Minnesota (9%). Decreases were found for Oklahoma (26%) and South Dakota (4%); however, these were not significant. Throughout most of the western United States, the SO_2 emissions have decreased from 8% in Idaho to 37% in California. Statistically significant decreases of 30% were also found in Oregon and Montana.

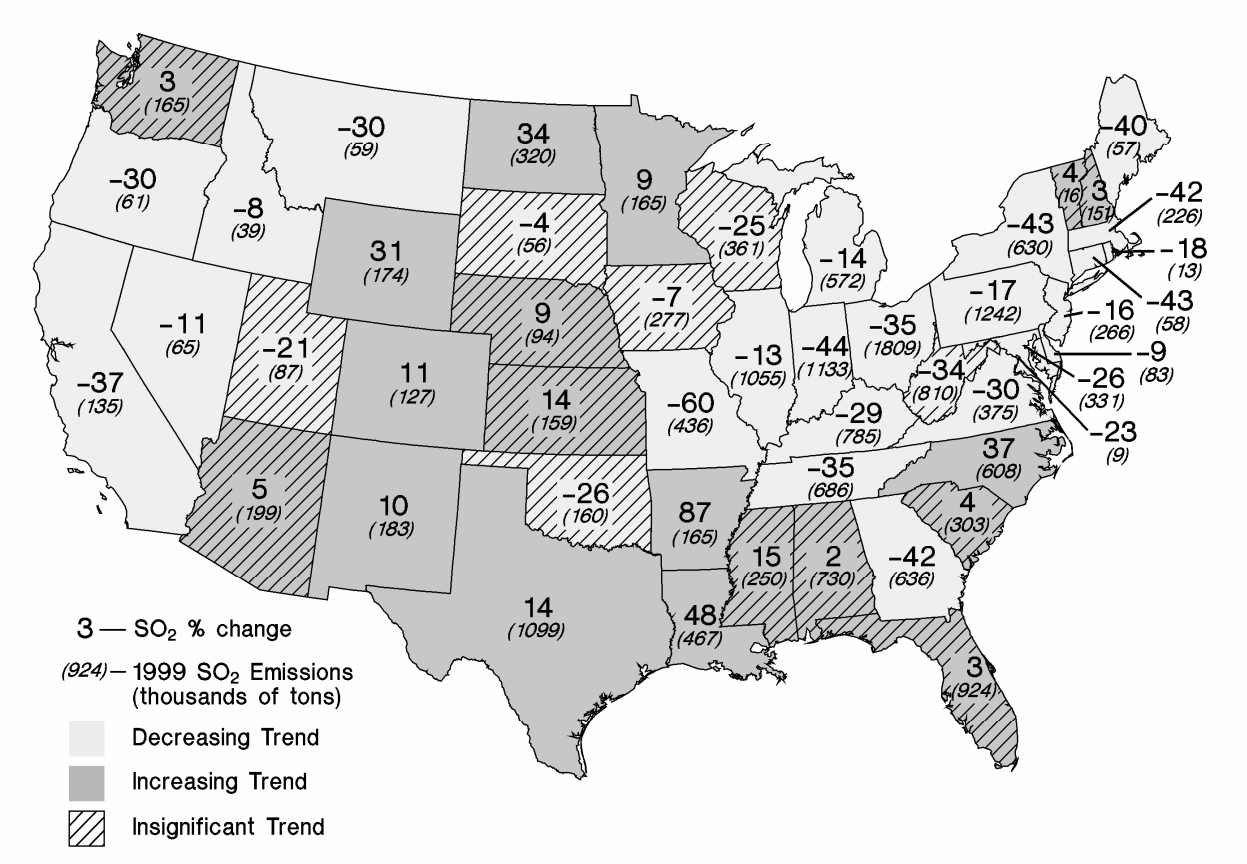

Figure 4.4. The percent change in the NET SO_2 emissions for each state in the conterminous United States from 1990 through 1999. The light gray states have decreasing trends, while the dark gray states have increasing trends. States without hatch marks have trends that are significant with two-sided P values below 0.1. The percent changes were calculated by dividing the change in emissions over the 10-year period by the 1990 emissions estimated from the trend line. The 1999 SO_2 emission rates for each state are in parentheses.

4.2.4 Regional Comparisons of SO_2 Emissions and $SO_4^=$ Concentrations

The 1990 to 1999 annual SO_2 emission and 80th percentile $SO_4^=$ concentration time series were qualitatively compared over broad northeastern, southeastern, south-middle, and western United States regions. Each region had a unique time series pattern, with the $SO_4^=$ concentrations and SO_2 emissions closely tracking each other over the 10-year time period (Figure 4.5). In the western United States from Arizona to Washington, both SO_2 emissions and concentrations steadily declined about 15% throughout the 1990s. In the south-middle United States, they steadily increased about 15%. In the northeastern United States, the SO_2 emissions and $SO_4^=$ concentrations declined ~7% from 1990 to 1994, then decreased nearly 20% between 1994 and 1995, and leveled off afterward. In the southeastern United States, the $SO_4^=$ concentrations and SO_2 emissions did not change appreciatively over the time period, but each had a decreasing trend in the early 1990s followed by an increasing trend since 1995–1996.

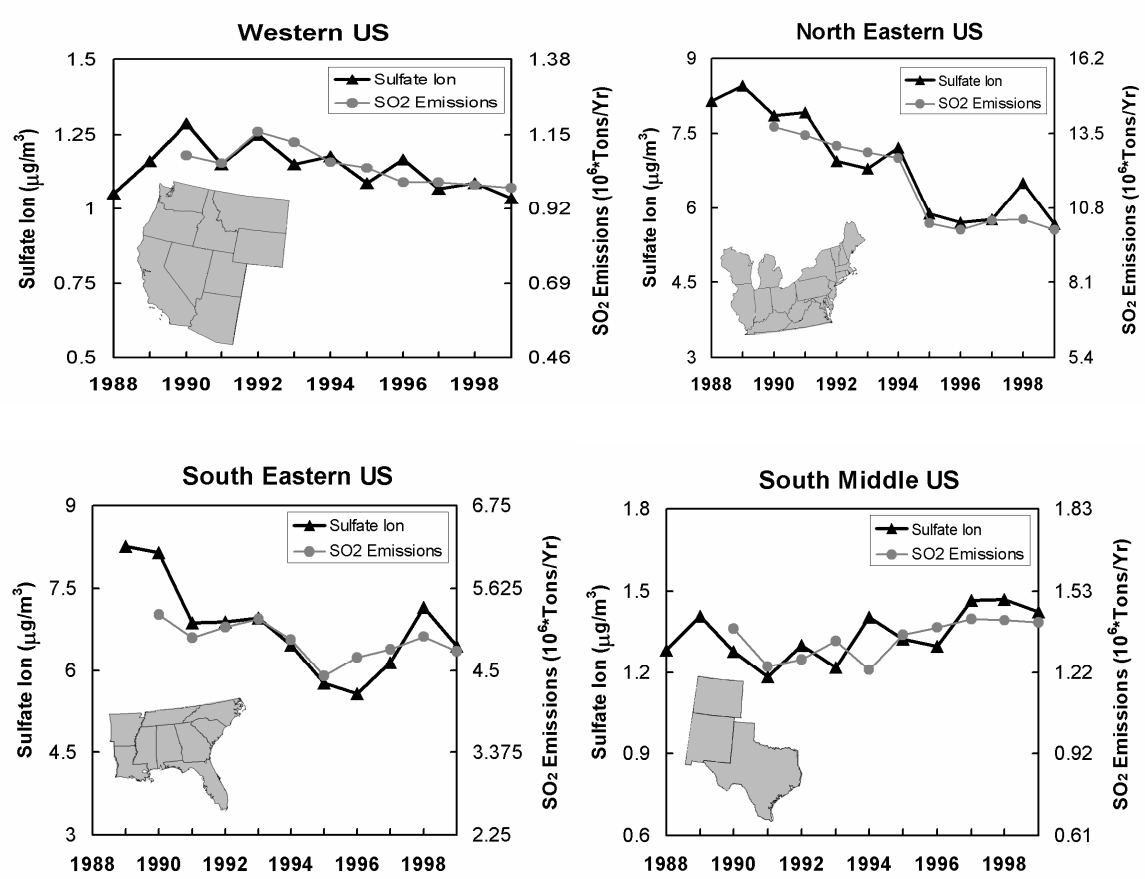

Figure 4.5. Comparison of the 80th percentile SO_4^{2-} concentrations (3*S for IMPROVE program) and NET SO_2 emissions aggregated over northeastern, southeastern, south-middle, and western United States regions. In each plot the SO_4^{2-} and SO_2 emission scales have a factor of 3 change between the low and high values.

4.3 Trends in the Haze Index

Trends in the haze index were examined for the 10-year period 1995–2004 by the National Park Service [NPS, 2006]. The haze index is measured in deciviews, a visibility metric based on the light extinction coefficient that expresses incremental changes in perceived visibility (Chapter 2). The haze index values were calculated as prescribed under the Regional Haze Rule (RHR) guidance for tracking progress [U.S. EPA, 2003]. The RHR guidance outlines missing variable treatment and completeness criteria for constructing annual average deciview values for the 20% best and 20% worst visibility days. Trends in the annual average 20% best and worst days were examined using the Theil regression method (see section 4.2 for a description of the regression method) for the IMPROVE sites with at least 6 complete years out of the 10-year period. Visibility was stable (insignificant trends) or improving at all IMPROVE sites at the 0.05 significance level. Acadia, Moosehorn, Lye Brook, Dolly Sods, and Shenandoah showed statistically significant improving visibility trends for the clearest days at eastern national park monitoring sites (Figure 4.6). Great Smoky Mountains, Okefenokee, Mammoth Cave, and Washington, D.C., also had improving trends on the haziest visibility days (Figure 4.7). Statistically significant improving trends for the clearest visibility days were observed at 17 sites in the western United States including Alaska. Mount Rainer also had an improving trend

on the haziest visibility days. No site included in the analysis had a significant worsening trend on either the clearest or haziest visibility days.

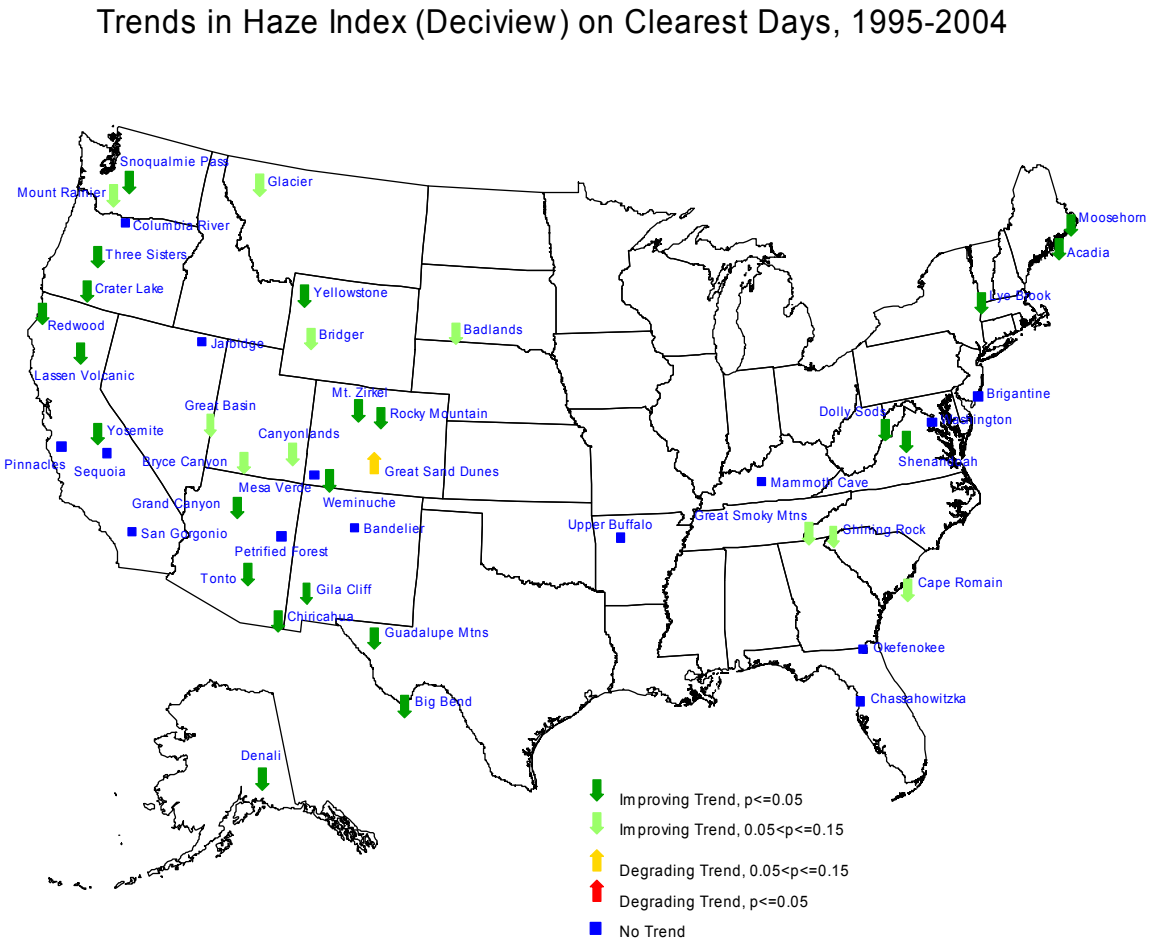

Figure 4.6. Theil trends in the haze index of the annual average 20% best visibility days.

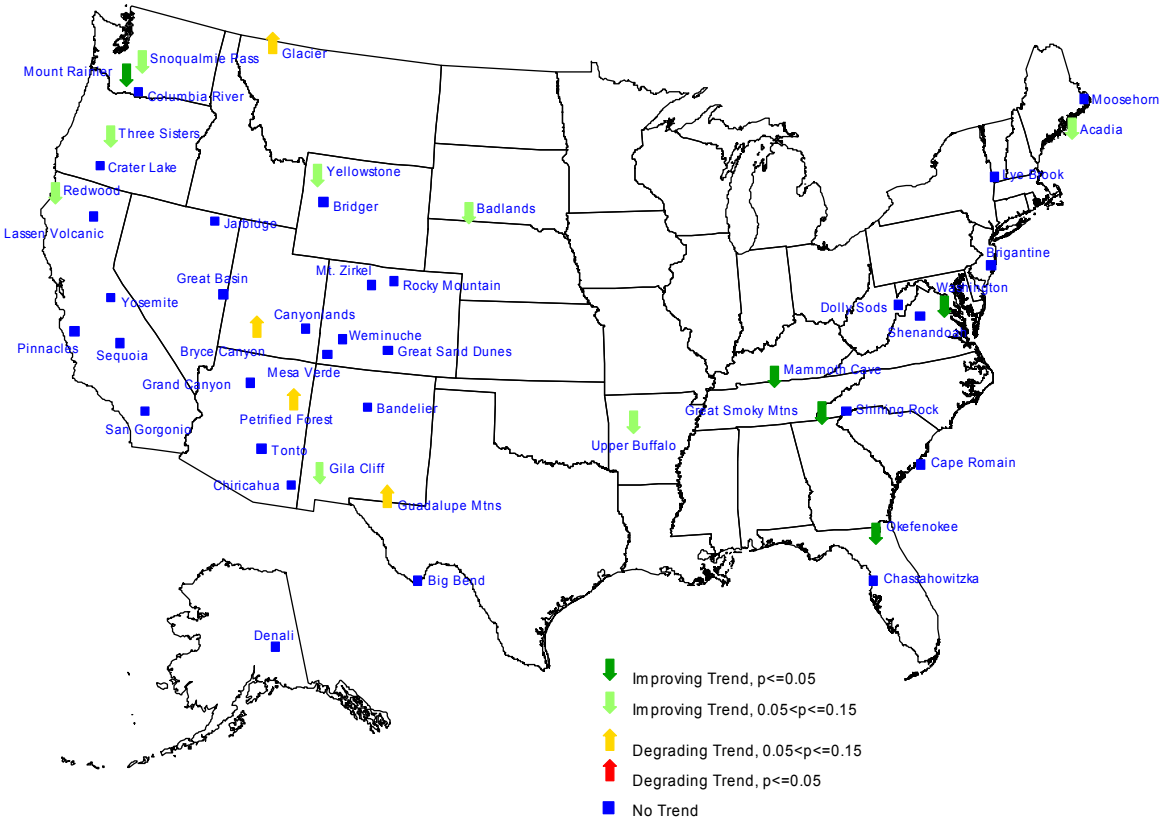

Figure 4.7. Theil trends in the haze index of the annual average 20% worst visibility days.

4.4 Organic and Elemental Carbon Long-Term Trends and Spatial Patterns in the Rural United States

4.4.1 Introduction

Carbonaceous aerosols are a complex mixture of organic carbon compounds and soot composed predominately of elemental carbon. These compounds are a major component of the fine aerosol mass [Malm et al., 2004], and their mass fraction is increasing as sulfate aerosols decrease [Malm et al., 2002]. Scattering and absorption by organic and elemental carbon are key factors in atmospheric transparency and the balance of solar radiation [White and Macias, 1989; Malm et al., 1994; Hegg et al., 1997; Hansen et al., 2000], which is important to the regional haze regulations and climate change. Carbonaceous emissions from wood burning and fossil fuel combustion may also have possible health effects [Lewis et al., 1988; U.S. EPA, 2000].

Carbonaceous aerosols arise from a wide array of sources, including diesel combustion and cooking in urban areas and smoke from fires and biogenic emissions from plants in rural areas. Planned changes in wildfire management are likely to increase the carbon contributions of smoke [Fox et al., 1999]. Combined with new diesel engine standards [Lloyd and Cackette, 2001] and other vehicle technology trends, the concentrations and chemical character of the

carbonaceous materials will change over time. In addition, other changes in the chemical environment can alter the rates of formation of secondary organic aerosols, further changing carbonaceous materials' concentrations and chemical character.

The long-term trends in carbonaceous material are a response to past changes in emissions and reactive environment. Understanding these responses and their causes will aid in future actions to reduce carbonaceous aerosol concentrations. Seasons are examined because source emissions and relevant atmospheric processes often vary with season, which could lead to seasonal variations in the trends of carbonaceous material.

4.4.2 EC and OC Long-Term Trends

Theil regression was used to examine trends in winter and summer elemental and organic carbon at the 54 sites with 7 or more years of data. Winter elemental carbon (EC) concentrations decreased significantly at most monitoring sites in the Pacific coastal states and throughout the eastern United States, with median EC concentrations decreasing from 50% to 75% over a 10-year time period (Figure 4.8). Winter organic carbon (OC) concentrations (Figure 4.9) from Washington State to northern California showed similar significant decreases, but Acadia, Maine, was the only monitoring site in the eastern United States with a significant downward trend. Unlike EC, wintertime OC increased at a number of monitoring sites in the southeastern United States, though not significantly. Most sites in the intermountain West did not show significant winter trends in either EC or OC.

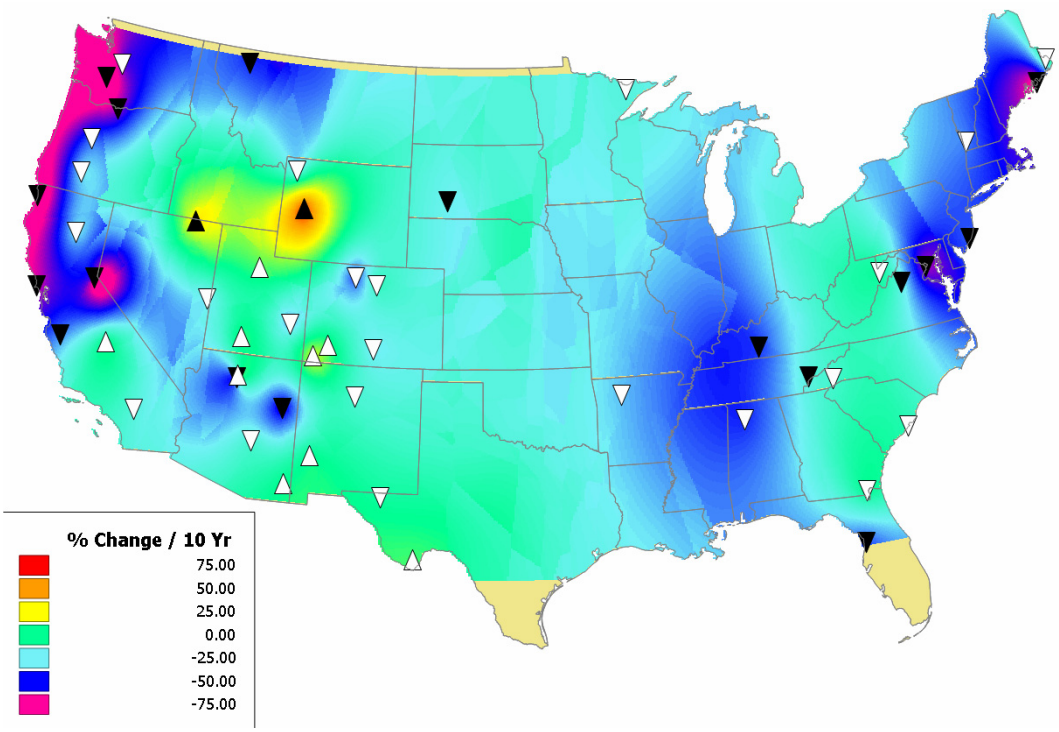

Figure 4.8. The wintertime elemental carbon trend using IMPROVE data from monitoring sites with a minimum of 7 years of data. The triangles indicate a increasing (up) or decreasing (down) trend, and black arrows have a significant trend at the 0.05 level. The isopleths are the slope of the trend line as the % change from the median EC concentration per 10 years.

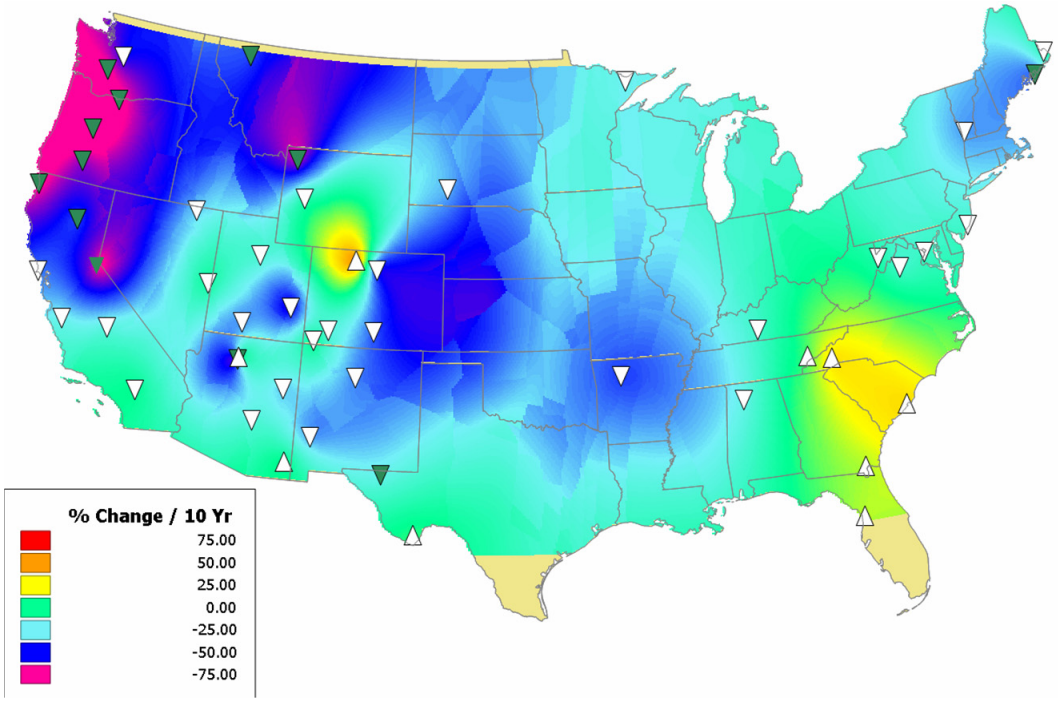

Figure 4.9. The wintertime organic carbon trend using IMPROVE data from monitoring sites with a minimum of 7 years of data.

EC and OC displayed significant summer concentration trends at only a few sites (Figures 4.10 and 4.11). However, there were some coherent spatial patterns in the trends that were observed. Summertime EC and OC both decreased at most sites from Washington State to northern California and in Maine. A number of monitoring sites from Montana to New Mexico had increases of over 30% in the median summer OC and EC concentrations over a 10-year period, though the trends were not statistically significant. In the middle and late 1990s this region experienced increased wild fire, which likely drove the large increases in the observed carbon.

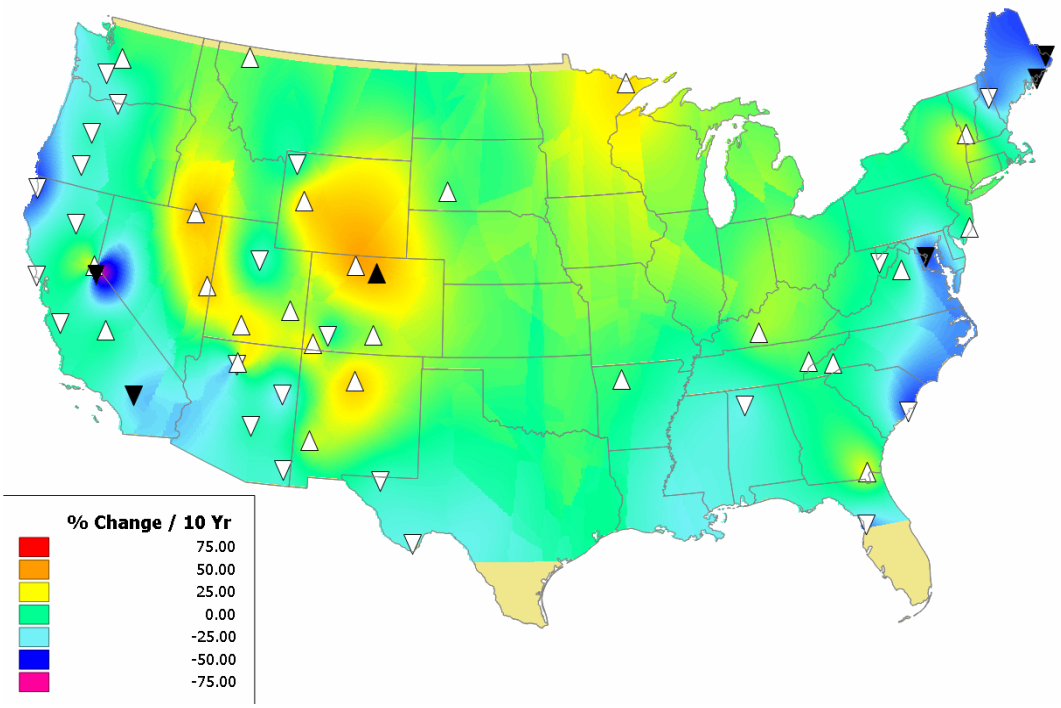

Figure 4.10. The summertime elemental carbon trend using IMPROVE data from monitoring sites with a minimum of 7 years of data.

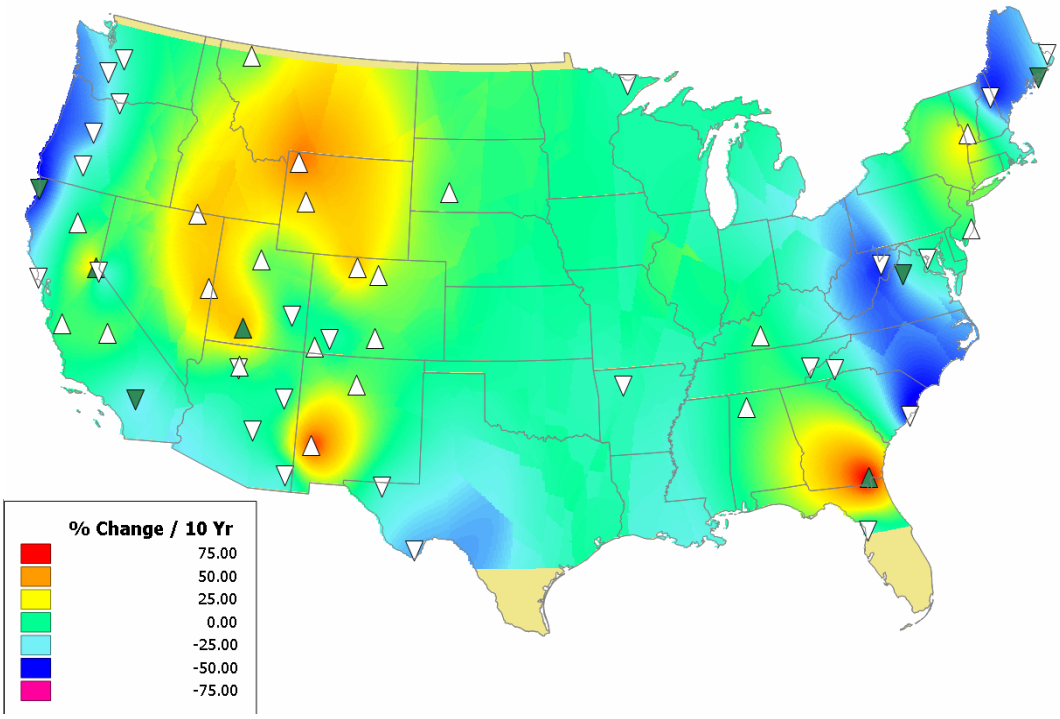

Figure 4.11. The summertime organic carbon trend using IMPROVE data from monitoring sites with a minimum of 7 years of data.

OC and EC can be emitted from separate sources, e.g., secondary biogenic organic carbon, or at different ratios from the same source, e.g., fire and automobile traffic. The differing trends in OC and EC in the Northeast imply a change in the mix of sources contributing to carbonaceous aerosols there. Alternatively, these trends could be the result of changes or drifts in the sampling and analysis of the carbonaceous material. The samples have been analyzed using the same set of thermal optical reflectance (TOR) instruments over the past 15 years, and subtle changes may have occurred as the instruments have aged. In addition, the positive OC and EC artifact corrections have changed over time. For example, the EC artifact correction has been decreasing since the early 1990s.

4.5 VIEWS Annual Summary Trends Tools

VIEWS is an online exchange of air quality data, research, and ideas designed to understand the effects of air pollution on visibility and to support the Regional Haze Rule enacted by the U.S. EPA to reduce regional haze and improve visibility in national parks and wilderness areas. The Annual Summary section of the VIEWS web site provides access to data products described in the VIEWS scope of work. It also provides browsing capabilities of the IMPROVE aerosol database using graphical interfaces.

On the trends page of the annual summary section, the user can click on a map icon to view trend data for a selected parameter at that site (currently, http://vista.cira.colostate.edu/views/web/AnnualSummaryDev/Trends.aspx). Annual data aggregations can be selected by calculated aerosol extinction percentile group and averaging period (either annual averages or 5-year rolling averages). The timeline plot has two modes, "Single" and "Multi". In "Single" mode, the timeline will display the most recent selection. In "Multi" mode, each additional selection adds another timeline to the display. Up to four timelines can be superimposed in "Multi" mode.

The annual data aggregations for the 20% best and 20% worst visibility days represent the finalized calculation procedures as specified in guidance documents for the RHR. Daily IMPROVE data, including daily data substitutions where applicable, are available in the Annual Summary and by selecting the IMPROVE regional haze (IRHR) program in other VIEWS tools.

REFERENCES

Fox, D. G., W. C. Malm, B. Mitchell, and R. W. Fisher (1999), Where there's fire, there's smoke: Fine particulate and regional haze, *Environmental Manager* (EM), November.

Hansen, J., M. Sato, R. Ruedy, A. Lacis, and V. Oinas (2000), *Proc. Natl. Acad. Sci.*, *97*, 9875-9880.

Hegg, D. A., J. Livingston, P. V. Hobbs, T. Novakov, and P. Russell (1997), *J. Geophys. Res., 102*, 25,293-25,303.

Hess, A., P. Patterson, and H. Iyer (2002), A SAS Macro for Theil Regression, Colorado State University, Fort Collins, ISSN 0737-5352-57.

Lewis, C. W., R. E. Baumgardner, R. K. Stevens, L. D. Claxton, and J. Lewtas (1988), *Env. Sci. Tech., 22*, 968-971.

Lloyd, A. C., and T. A. Cackette (2001), *JAWMA, 51*, 809-847.

Malm, W. C., J. F. Sisler, D. Huffman, R. A. Eldred, and T. A. Cahill (1994), *J. Geophys. Res., 99*, 1347-1370.

Malm, W. C., B. A. Schichtel, R. B. Ames, and K. A. Gebhart (2002), A 10-year spatial and temporal trend of sulfate across the United States, *J. Geophys. Res., 107*(D22), 4627, doi:10.1029/2002JD002107.

Malm, W. C., B.A. Schichtel, M. L. Pitchford, L. L. Ashbaugh, and R. A. Eldred (2004), *J. Geophys. Res.,* **,***109*, doi:10.1029/2003JD003739.

NPS (2006), 2005 Annual performance & progress report: Air quality in national parks, available at http://www2.nature.nps.gov/air/Pubs/pdf/gpra/Gpra2005_Report_03202006_Final.pdf.

Schichtel, B. A., W. C. Malm, and W. H. White (2004), Organic and elemental carbon long-term trends and spatial patterns in rural United States, presented at the Regional and Global Perspectives on Haze: Causes, Consequences and Controversies-Visibility Specialty Conference, Air & Waste Management Association, Asheville, NC, October 25-29.

Theil, H. (1950), A rank-invariant method of linear and polynomial regression analysis, *Proc. Kon. Ned. Akad. V. Wetensch. A,, 53*, 386 – 392, 521–525, 1397–1412.

U.S. EPA (2000), Health assessment document for diesel exhaust, EPA/600/8-90-157.

U.S. EPA, (2001), National air quality and emissions trends report, 1999, EPA 454/R-01-004, Natl. Tech. Inf. Serv., Dept. of Commerce, Springfield, VA.

U.S. EPA (2003), Guidance for tracking progress under the regional haze rule, EPA-454/B-03-004.

Weatherhead, E. C., G. C. Reinsel, G. C. Tiao, X.-L. Meng, D. Choi, W.-K. Cheang, T. Keller, J. DeLuisi, D. J. Wuebbles, J. B. Kerr, A. J. Miller, S. J. Oltmans, and J. E. Frederick (1998), Factors affecting the detection of trends: Statistical considerations and applications to environmental data, *Journal of Geophysical Research, 103,* 17149-17161.

White, W. H., and E. S. Macias (1989), *Aerosol Science and Technology, 10*, 111-117.

White, W. H. (1997), Deteriorating air or improving measurements? -- On interpreting concatenate time series, *Journal of Geophysical Research, 102*, 6813-6821.

White, W. H., L. L. Ashbaugh, N. P. Hyslop, and C. E. McDade (2005), Estimating measurement uncertainty in an ambient sulfate trend, *Atmospheric Environment, 39,* 6857–6867.

CHAPTER 5: IMPROVE DATA QUALITY ASSURANCE

This chapter provides a summary of the IMPROVE program's quality assurance system, data validation procedures, and results from a collection of nitrate data quality studies. The first section provides an overview of the IMPROVE network's quality assurance system and the data validation procedures conducted by CIRA. Section 5.2 summarizes the results from a historical data validation review of IMPROVE data collected from 1988 through 2003. Section 5.3 summarizes the results from several studies designed to investigate potential data quality issues related to IMPROVE's nitrate measurements.

5.1 OVERVIEW OF THE IMPROVE NETWORK'S QUALITY ASSURANCE SYSTEM AND DATA VALIDATION PROCEDURES CONDUCTED BY CIRA

The IMPROVE program is a cooperative measurement effort designed to identify chemical species and emission sources responsible for existing man-made visibility impairment and to document long-term trends for assessing progress towards the national visibility goal. With the enactment of the Regional Haze Rule (RHR), an additional goal has become to establish current visibility and aerosol conditions in mandatory visibility-protected federal areas (VPFAs). In order to meet these objectives, the program has the responsibility for ensuring that a data set of suitable quality for scientific inquiry and for regulatory use is gathered, analyzed, and made available to the stakeholders. To meet this responsibility, IMPROVE maintains a continually evolving quality assurance (QA) program to ensure that the data quality objectives of the RHR are met or exceeded and additionally to ensure that the data quality objectives meet the needs of the stakeholders.

The data validation system is a key component of the QA program. The role of the validation system is to verify that the measurement quality objectives (MQOs) of the program are met for every data point and that appropriate actions, such as flagging the data, are taken when the MQOs cannot be met. The task of data validation is shared among several organizations, including the Crocker Nuclear Laboratory (CNL) at the University of California, Davis, the Cooperative Institute for Research in the Atmosphere (CIRA) at Colorado State University, the Desert Research Institute (DRI) at the University of Nevada, and the Research Triangle Institute (RTI) in North Carolina.

The validation system is linked to the data management and quality control (QC) systems. The data management system controls the flow of data from the sampler to the final database, the validation system ensures that proper decisions are made along the way, and the QC system informs the decision-making process. Efforts to better integrate these systems are underway. One component of this process is the development of new validation tools and tests to augment the current data validation process. The new validation application utilizes web-based interfaces, interactive data selection from the CIRA IMPROVE database, on-the-fly calculation of diagnostic statistics and/or composite parameters, and on-line charting capabilities.

The full data validation system spans a wide scope of tests from simple checks on sample identity to complex checks on temporal comparability. The new tools incorporate all of the data validation tests historically performed on the concentration values. They also include tests that were too cumbersome and resource intensive to implement in the past. New tests will be added

as needed to address issues that are identified as part of our on-going QC program and as additional supporting data sets are incorporated into the database. Both the QA and the data validation systems are described in the following sections.

5.1.1 Sampling and Analysis

The standard IMPROVE sampler has four independent sampling modules: A, B, and C collect $PM_{2.5}$ particles (0–2.5 μm), and D collects PM_{10} particles (0–10 μm). Module A utilizes a Teflon filter that is analyzed for gravimetric mass and elemental concentrations by X-ray fluorescence (XRF), proton elastic scattering analysis (PESA), and, prior to December 2001, by proton induced X-ray emission (PIXE). Beginning in 1992, analysis of the heavier elements, those with atomic weights from Fe to Pb, was changed from PIXE to XRF with a Mo anode source. PIXE was discontinued in December 2001, and analysis of the lighter elements with atomic weights from Na to Mn was changed from PIXE to XRF with a Cu anode source. Additionally, the Fe measurements from the Cu XRF system were reported to the final database instead of those from the Mo system. Module B utilizes a nylon filter and is analyzed primarily for anions by ion chromatography (IC). Module C utilizes a quartz filter and is analyzed for organic and elemental carbon by thermal optical reflectance (TOR) carbon analysis. Module D utilizes a Teflon filter and is analyzed for gravimetric mass. The reader is referred to section 5.1.6 for an overview on data acquisition, quality control, and data management and to the appropriate standard operating procedures (SOPs) for a detailed description of activities related to sampling and analysis.

The IMPROVE system has been designed to include internal measurement redundancy, a valuable asset for data validation. Examples include Fe from both XRF systems, $SO_4^=$ and S from modules B and A, respectively, and various modeled relationships that allow for the intercomparison of results from the independent modules (see section 5.1.3 and section 5.1.7 for more detail).

5.1.2 Overview of the IMPROVE QA System

This overview is an introduction to those components of the QA system required to understand the data validation procedures. For a complete review of the IMPROVE QA system, the reader is referred to the IMPROVE Quality Management Plan (QMP) and the IMPROVE Quality Assurance Project Plan (QAPP) and associated SOPs. The quality control and data management systems are described in section 5.1.6. Some changes in the sampling and/or analytical systems described in section 5.1.6 are not yet contained in the QA documentation but have been adopted by IMPROVE and will be reflected in revised documents expected in 2006. All documents are available from the IMPROVE website (http://vista.cira.colostate.edu/improve).

5.1.2.1. Roles and Responsibilities

The QA process for the IMPROVE program is carried out by multiple organizations at various stages in the life history of the data. These organizations include the laboratories contracted to collect, analyze, and validate the data: CNL, DRI, and RTI. CIRA is contracted to perform additional data validation and distribution and analysis of the data. The National Park

Service is responsible for providing technical oversight to all aspects of the program in response to the IMPROVE steering committee. In addition to the internal QA performed by the organizations listed above, the EPA oversees all management system reviews (MSRs) or technical system audits (TSAs) on any of the agencies involved.

5.1.2.2. Data Quality Objectives

The primary goal for IMPROVE under the new RHR guidelines for tracking progress is to be able to make a valid comparison between consecutive 5-year averages of the 20% worst and 20% best visibility days. The IMPROVE program is in the process of reviewing and refining their data quality objective (DQO) to ensure that it is consistent with these new guidelines. As part of that review process, all the MQOs are also being reviewed and may be revised as necessary. The MQOs include measurement specific objectives in precision, accuracy, minimum quantifiable limit (mql) or minimum detection limit (mdl), data completeness, data representativeness, and data comparability. Secondary objectives of analyzing the data set, including trace elements, for source apportionment and other related subjects will also be taken into account when reviewing the MQOs.

5.1.2.2.1. Precision, Accuracy, and MQL/MDL

For current specific MQOs regarding precision, accuracy, and mql/mdl, the reader is referred to the IMPROVE QAPP. The MQO review process will include a thorough assessment of the current capabilities of the IMPROVE sampling program. The recent addition since 2003 of 24 collocated sampler modules to assess the precision of IMPROVE measurements will aid the review process, as well as add greatly to the program's QA/QC capabilities. The collocated data will also be used to assess uncertainty estimates.

5.1.2.2.2. Completeness

Under the RHR guidelines for tracking progress, stringent data completeness requirements have been established. The new tracking progress guidelines have placed additional significance on collecting a complete set of high quality samples from every IMPROVE site. A sampling day is only considered complete if valid measurements are obtained from the key analyses: $PM_{2.5}$ gravimetry, PM_{10} gravimetry, ion analysis, elemental analysis, and carbon analysis. For a year of data from a site to be included for tracking progress, 75% of the possible samples for the calendar year must be complete, 50% of the possible samples for each calendar quarter must be complete, and no more than 10 consecutive sampling periods may be missing [U.S. EPA, 2003].

5.1.2.2.3. Representativeness

Site selection criteria have been developed to ensure that all sites are as representative as possible of the regional air shed that they are intended to monitor. If at any point a site is found to be unrepresentative, then it another site determined to be representative may be selected.

5.1.2.2.4. Comparability

The particle measurements must remain consistent through the years to fulfill the needs of the RHR. Maintaining comparability through both space and time is crucial to trend analysis and data analysis and interpretation. No one procedure, policy, or test can maintain comparability. Rather it is an issue that must be constantly addressed and weighed when considering any and all changes introduced at all levels, from sampling through data processing. Some specific measures that have been adopted to address this issue are collocating samplers at the new and old locations for several months prior to officially moving a site, testing new sampling equipment or components at a field station in Davis prior to use in the network, checking each filter lot for consistency and quality, and determining the comparability between new and old analysis equipment prior to using new analytical equipment.

5.1.2.3. Documentation

Appropriate documentation is critical for maintaining 1) internal communication, 2) consistency in procedures over time, and 3) the confidence of our stakeholders. Critical documents to the QA system include the QMP, QAPP, SOPs, and the annual QA report. The QA documents are available from the IMPROVE website at http://vista.cira.colostate.edu/improve/Publications/publications.htm.

5.1.3 Data Validation

The data validation checks have been designed to assess the following: that uncertainty, accuracy, and mql objectives are being met; that there is internal consistency between the redundant measurements; and that spatial and temporal comparability is being maintained.

The IMPROVE program defines four levels of data validation:

Table 5.1. Data validation levels as defined by IMPROVE.

Level 0 Data obtained directly from the instruments with no editing or corrections	**Level 1** Data undergo initial reviews for completeness, accuracy and internal consistency (Performed by QA and operational personnel at CNL) • Sample Identification • Operator Observations • Sampler Flags • Laboratory Checks (per SOPS) • Range Checking • Flow Rate Audits • Exposure Duration Checks • Elapsed Time before Retrieval Checks • Holding Times Checks • Mass Balance Checks • Field Operations Database Review • Lab Operations Database Review • Flow Rate Analysis • Flagged Samples Review • QC Samples and Analytical Accuracy and Precision Review

Level 2 Data undergo additional reviews for confirming compliance with MQOs prior to public release (Performed by QA personnel at CNL and CIRA) • Internal Consistency Analysis • Outlier Analysis • Data Completeness • Collocated Bias and Precision • Mass Reconstruction Analysis	**Level 3** Data undergo additional review through the activities of the end users (Performed by QA personnel at CIRA and data users) • Time Series Analysis • Spatial Analysis • Optical Reconstruction Analysis • Modeling • Other

CNL performs level 1 and 2 validation on every monthly batch of data, both during the analysis process and after all four modules have been analyzed. RTI and DRI also conduct various level 1 checks on all data they submit to CNL. Any inconsistencies or other problems identified in this review are corrected prior to sending the data to CIRA. CIRA performs additional level 2+ validations on the data batch, but in the context of larger subsets of the data, on approximately a quarterly basis. The data validation procedures that are performed by CNL are described in section 5.1.7.

Starting with the data collected during 2000, CIRA began a formal validation process to complement the work done by CNL. This process was expanded with the 2004 data and is now conducted for every data delivery during the 30-day preliminary data review period. The focus remains on identifying the more subtle data quality problems that affect large batches of data. The decisions of CNL, DRI, and RTI regarding the validity of individual data points are accepted and not examined outside of the context of data integrity checks.

5.1.3.1. Data Integrity Tests Performed at CIRA

The data validation process at CIRA is designed to ensure that the data set being delivered meets some basic expectations in terms of integrity and reasonableness. The CIRA data management system is designed to automatically ingest data files delivered by CNL, assuming that the file is in the standard format and that all metadata is properly accounted for in CIRA's IMPROVE database. A series of data integrity tests have been designed to make sure that 1) the file is compatible with the system as it is currently defined, 2) all metadata contained in the file have been previously defined in CIRA's system, and 3) every record in the file meets rules defined to ensure completeness and appropriateness of the data. Failures at any level of this process can indicate that the data file contains errors and requires redelivery, or that the CIRA database or ingest process need updates beyond what are contained in the data file being ingested. Specifically the integrity tests check for

- new file formats,
- sites, parameters, or validation flags without metadata records in the CIRA database,
- duplicate records,
- the presence of CNL internal communication flags,
- the improper use or mapping of validation flags,
- the presence of records with data values, uncertainty, and measurement detection limits inconsistently reported as being valid or invalid,

- successful transformation to a fully normalized schema without data loss or errors, and
- data delivery completeness.

5.1.3.2. Spatial and Temporal Comparability Checks Performed at CIRA

The concept of reasonableness of the delivered data is primarily judged against the past—how a specific site compares to other sites and additional internal consistency tests. Maintaining comparability across the network in both space and time is crucial. Time series analyses of the composite variables included in the RHR calculations are conducted to monitor for changes that may be related to the data collection and processing, rather than a true representation of ambient conditions. Spatial analysis is limited in scope and incorporated into other data validation checks.

It is the task of the laboratories responsible for sampling and analysis to develop procedures and policies for catching and preventing recurrent data quality problems. Therefore, the validation process is intentionally an exploratory process at this stage, since it is presumed that the contractors have already applied rigorous tests to ensure that the data are of sufficient quality to be considered valid. Data exploration is a critical element of the validation process for discovering unanticipated data quality problems.

These checks are performed approximately quarterly by CIRA with the participation of key individuals from CNL and the National Park Service. The process is for the most part subjective, and therefore the conclusions about behaviors that are indicative of data quality problems are analyst dependent. The goal of CIRA's validation efforts is to discover potential problems with a monitoring site's data or with the analysis method, proving that there is an actual problem that requires additional research by the laboratories and in some cases lab or field studies. The results from the CIRA data validation process are posted on the IMPROVE webpage at http://vista.cira.colostate.edu/improve/Data/QA_QC/qa_qc_Branch.htm.

The major components of the exploratory validation process are described below. The test descriptions are categorized by aerosol type.

5.1.3.2.1. Mass

The IMPROVE reconstructed fine mass (RCFM) model provides a way to evaluate mass closure between the speciated mass concentrations from the A, B, and C modules and the gravimetric mass measurements from the A module. The algorithm for RCFM in the current version of the validation software has the following form:

[RCFM] $\mu g/m^3$ = ammonium sulfate + ammonium nitrate + fine soil + organic mass + light absorbing carbon

where
Ammonium Nitrate = 1.29*[NO_3^-]
Ammonium Sulfate = 4.125*[S]
Fine Soil = 2.2*[Al]+2.49*[Si]+1.63*[Ca]+2.42*[Fe]+1.94*[Ti]

Organic Mass by Carbon = 1.9*([OC1]+[OC2]+[OC3]+[OC4]+[OP])
Light Absorbing Carbon = [EC1]+[EC2]+[EC3]-[OP]

Key assumptions on which this model is based include the following:

1) All aerosol sulfur is in the form of $(NH_4)_2SO_4$.
2) All aerosol nitrate is in the form of NH_4NO_3.
3) All Al, Ca, Si, Fe, and Ti are of crustal source;
4) All crustal material is made up of the same basic oxides.
5) The average organic molecule is ~50% carbon by mass.
6) The A, B, and C modules all have cut points of 2.5 μm.

Significant deviations in the agreement between reconstructed and measured mass can occur for a number of reasons:

a) Ambient conditions violate the key assumptions underlying the reconstruction model, for example, the presence of aerosol types not represented in the RCFM model.
b) Sampling conditions violate the key assumptions underlying the reconstruction model, for example, different collection efficiencies for volatile aerosol types on the three different filter types.
c) Sampling problems exist on any or all of the independent modules.
d) Inaccurate analytical detection or quantification of any of the measured values in the reconstruction model or of gravimetric fine mass.
e) Unaccounted for negative and positive artifacts.

Large deviations between reconstructed and measured mass can be indicative of data quality problems. Conversely, they can also indicate the inappropriateness of the reconstruction model for that sample. Specific examples of situations that can lead to poor agreement between reconstructed and measured mass include the following:

a) Ammonium nitrate volatilization from the Teflon filter on the A module, which is not accounted for in the reconstruction model, can lead to reconstructed mass being greater than measured mass. Nitrate is well quantified on nylon filters. This discrepancy highlights a limitation of our gravimetric mass measurements. In regions where ammonium nitrate is a significant contributor to aerosol fine mass concentrations, RCFM likely provides a better estimate of the true atmospheric conditions.
b) Sea salt is not accounted for by the reconstruction model. This can lead to reconstructed mass being less than measured mass at coastal sites. The model could be modified to achieve better mass closure between the modules, especially at coastal sites.
c) Incomplete aerosol collection, for example, due to a clogged inlet, on the B or C module can lead to reconstructed mass being less than measured mass. Incomplete collection on the A module will lead to the reverse situation. This is a data quality problem that results in invalid data for the affected modules.
d) Variations in cut points on the A, B, or C module when coarse mass nitrate or organics are present in the aerosol can lead to poor comparison between reconstructed mass and measured mass. Depending on the severity, this is a data quality problem that can result in invalid data for the affected modules.

Time series of RCFM, gravimetric fine mass, and the ratio of the two are examined for deviations from 1) the general behavior at that site and 2) the general behavior observed at other sites. Figure 5.1 is an example of the time series used to validate mass closure between measured and reconstructed fine mass.

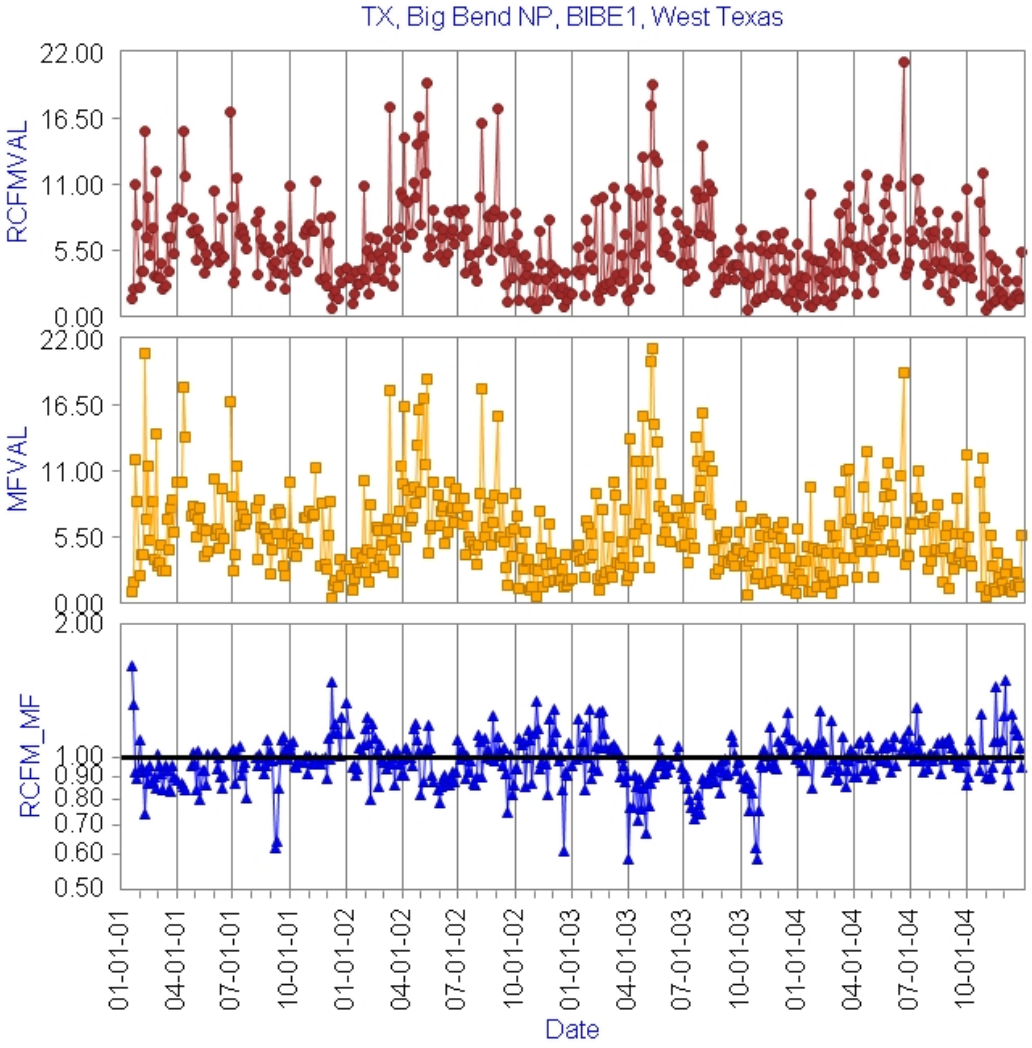

Figure 5.1. An example of the data validation charts from the fall 2004 report. Reconstructed fine mass concentrations, measured fine mass, and the reconstructed fine mass to measured fine mass concentration ratios are shown for the 2001–2004 time period at BIBE1. Definitions of all terms used in the axis titles can be found in the glossary in section 5.1.5 of this document.

5.1.3.2.2. Sulfate

In our data validation process it is assumed that all aerosol sulfur is in the form of sulfate, and thus 3*[S] should equal $[SO_4^{=}]$ within measurement uncertainty. The most basic check on these measurements is time series plots of $[SO_4^{=}]$, [S], and $[SO_4^{=}]$/[S]. Time series of $[SO_4^{=}]$, [S], and $[SO_4^{=}]$/[S] are examined for deviations from 1) the general behavior at that site, 2) the general behavior observed at other sites, and 3) obvious deviations of $[SO_4^{=}]$/[S] from 3. Figure 5.2 is an example of the time series used to validate agreement between the independent $[SO_4^{=}]$

and [S] measurements. Additionally, a more quantitative approach utilizing the Z score (equation 1) and some basic assumptions about the measurements is possible, given that two estimates of the same parameter are available. The Z test and the T test both follow the same general formula and can be used to test if two numbers are equal within their uncertainty. The T test differs from the Z test in that it allows for the populations to have unknown variances. If the underlying populations from which the two numbers are drawn are normal, then the test scores will follow a standard normal in the case of known variability and a t distribution with properly calculated degrees of freedom in the case of estimated variability. The formulas for calculating the Z score and T score are

$$\text{Z score} = ([SO_4^{=}]-3*[S])/\sqrt{(\sigma_{SO4}^2+(3*\sigma_S)^2)} \quad (1)$$

where σ represents a known measurement uncertainty;

$$\text{T score} = ([SO_4^{=}]-3*[S])/\sqrt{(\bar{\sigma}_{SO4}^2+(3*\bar{\sigma}_S)^2)} \quad (2)$$

where $\bar{\sigma}$ represents a statistically estimated measurement uncertainty.

In our case we are comparing two independent measurements, $[SO_4^{=}]$ and 3*[S], with the assumption that their difference should be 0 within measurement uncertainty. We are treating each measurement as an estimate of the true atmospheric sulfate value and the uncertainty that is uniquely reported for each sample as an estimate of the true variance for that measurement reported in terms of the standard deviation. Since our measurement uncertainties are based on a theoretical understanding, we are treating the samples as having known variability, and therefore are loosely referring to them as Z scores. The Z scores indicate how many standard deviations of the difference apart $[SO_4^{=}]$ are from 3*[S]. This interpretation of the Z score is independent of any assumptions about distributions of the underlying populations or the test scores. Z scores can be positive or negative. A positive Z score indicates that the $[SO_4^{=}]$ value is greater than 3*[S]; a negative Z score indicates the reverse.

If the measurement errors are symmetrical, then the Z scores will also be symmetrical. Furthermore, if the measurement errors are distributed normally, then the Z scores will follow a standard normal distribution. If neither is the case, then the Z scores will still represent a standardized score that measures the distance, in standard deviations of the difference, between the paired samples. However, no assumptions about the distribution of the Z scores can be made independently of assumptions about the sample populations.

In this case, the population of interest is not our time series of $[SO_4^{=}]$ and [S], which follow an approximately lognormal distribution, but the theoretical population of all potential $[SO_4^{=}]$ and [S] samples that could have been collected at the same point in time and space as our sample date of interest. On a theoretical level, assuming all S is in the form of sulfate and a well-mixed air mass, we would expect these potential measurements to both pull from a single population. Additionally, we would expect our measurements to only have unbiased random errors associated with sampling and analysis. So under ideal sampling and analytical conditions, we would expect the calculated Z scores to minimally follow a symmetrical distribution and possibly a standard normal distribution.

Additionally, according to Chebychev's rule [Rice, 1995], in any distribution the proportion of scores between the mean and k standard deviations is at least $1–1/k^2$ scores. So even if our test scores do not follow a normal distribution, if all of our parameters are reasonably accurate, we can minimally expect that at least 89% of the scores would reside symmetrically between the mean, 0, and ±3. If the test scores do follow a normal distribution, then 99% of the scores would reside between ±3. For the purposes of this procedure, sample pairs with calculated Z scores outside of the range [-3, 3], which is comparable to pairs that are not equivalent within 3σ uncertainty, are defined as "outlier" pairs.

In the validation process, the data set is explored using calculated Z scores for all samples with reported [S], σ_S, $[SO_4^=]$, and σ_{SO4} to see if certain assumptions are met. It is assumed that, given accurate measurements and well-estimated measurement uncertainty, the following should be true:

- At most, 10% of the sample pairs should be outliers.
- The Z scores should be symmetrically distributed above and below 0.
- This symmetry should persist through time, space, and all quantifiable (concentration>10*mdl) aerosol concentrations.

Figures 5.3–5.4 are examples of the time series of the calculated Z scores used to validate agreement between the independent $[SO_4^=]$ and [S] measurements. Most of the actual analysis is done on statistical summaries of the Z scores, such as the monthly percentages of Z scores <-3 and Z scores >3, depicted in Figure 5.4, rather than the individual Z scores calculated for every data point depicted in Figure 5.3.

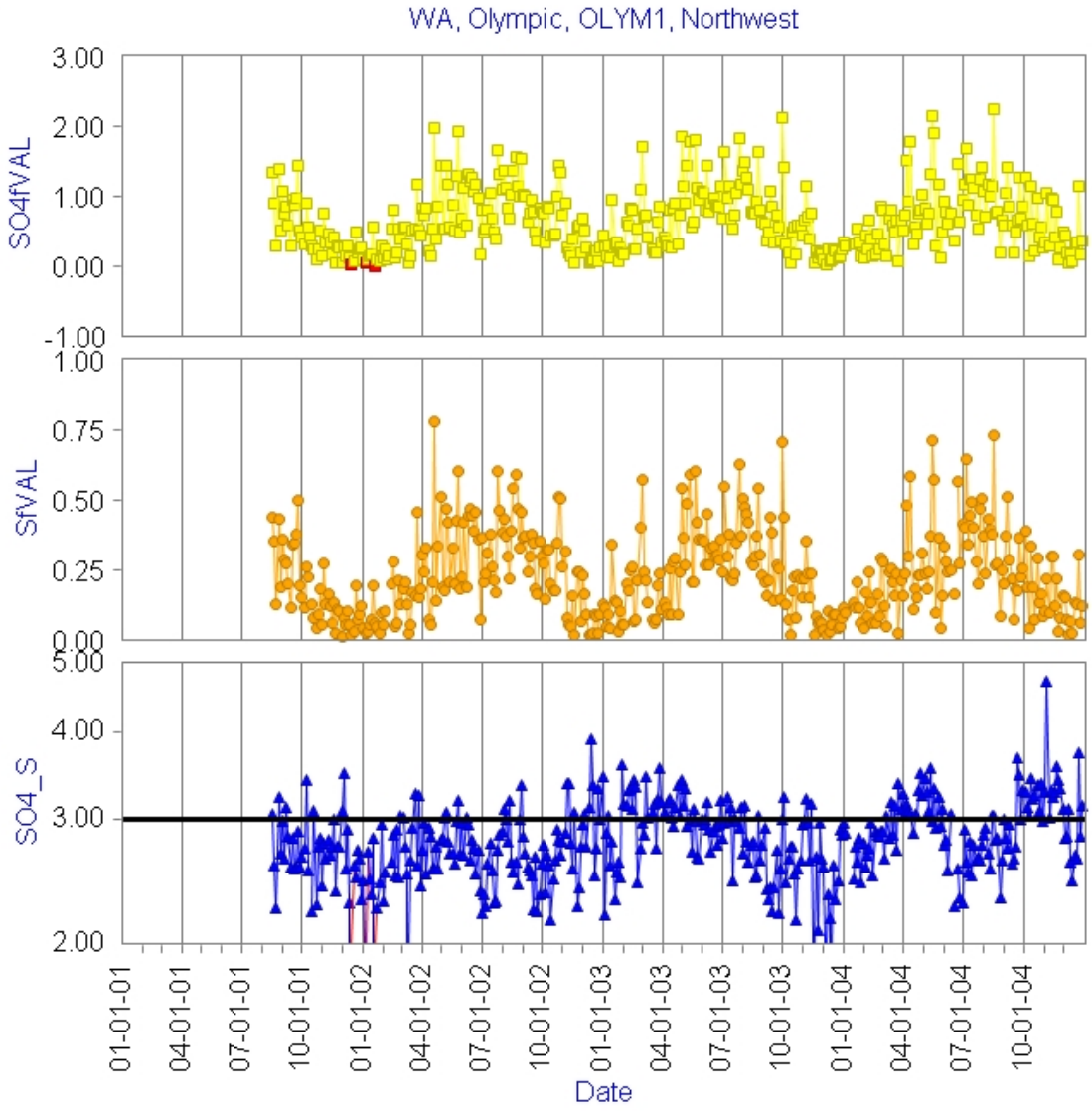

Figure 5.2. An example of the data validation charts from the fall 2004 report. Sulfate concentrations, sulfur concentrations, and the sulfate to sulfur concentration ratios are shown for the 2001–2004 time period at OLYM1. Definitions of all terms used in the axis titles can be found in the glossary in section 5.1.5 of this document.

*Data points shown in red indicate values below mdl.

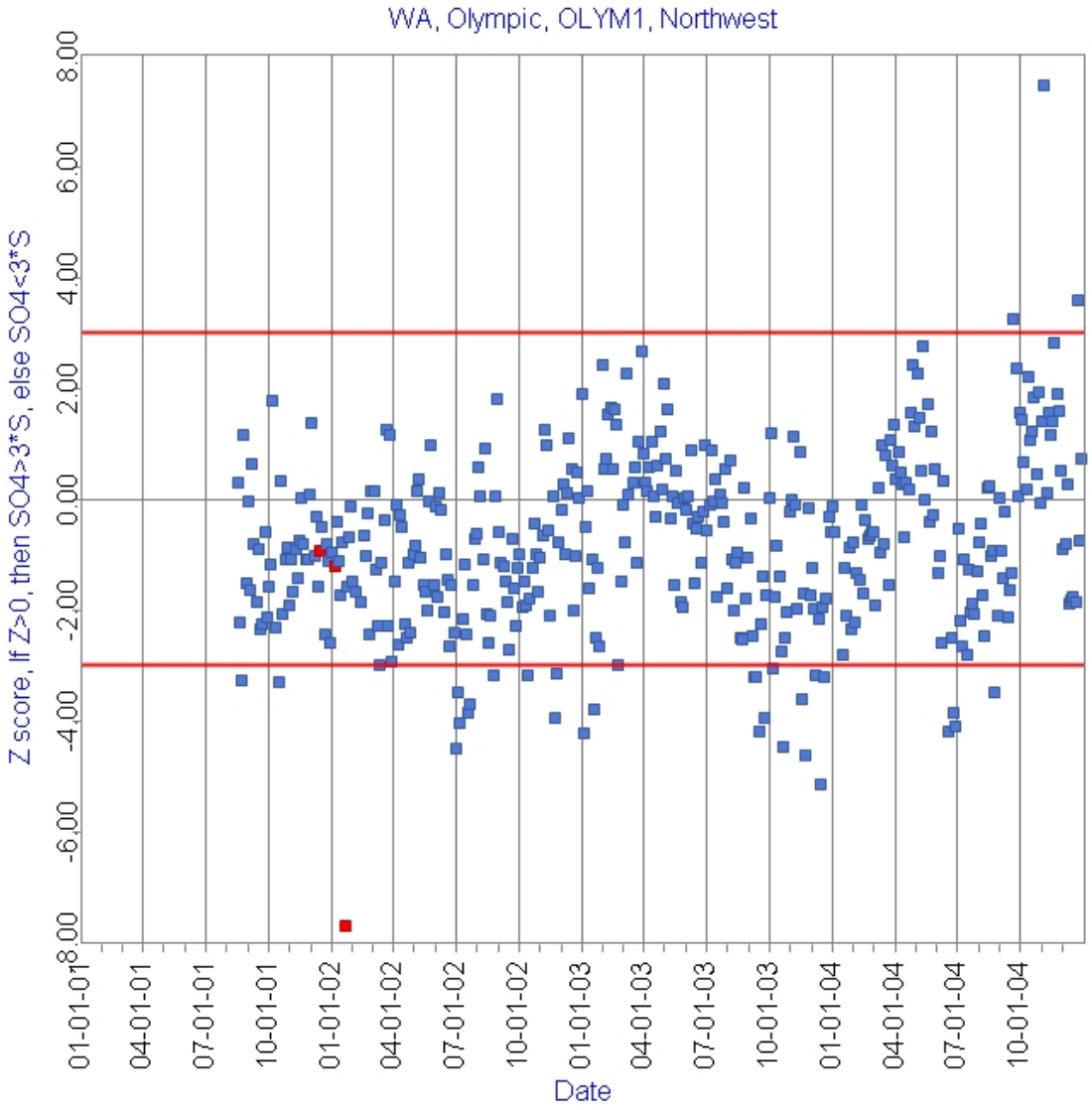

Figure 5.3. An example of the data validation charts from the fall 2004 report. Z scores calculated from the sulfate and sulfur concentrations and reported uncertainties are shown for the 2001–2004 time period at OLYM1. Definitions of all terms used in the axis titles can be found in the glossary in section 5.1.5 of this document.

*Data points shown in red indicate values below mdl.

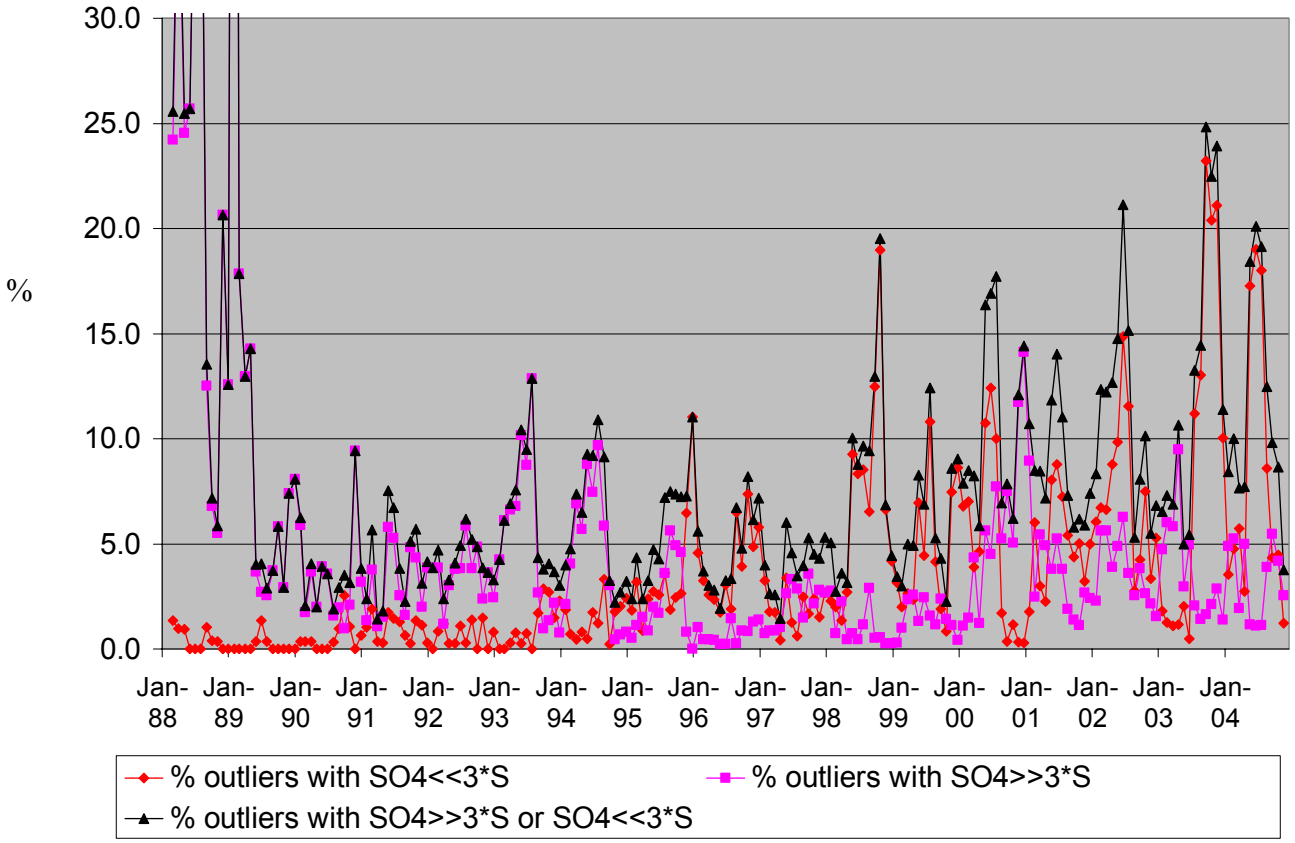

Figure 5.4. The percentage of valid sample pairs with significant disagreement between $SO_4^=$ and 3*S are calculated for each month. This provides a way of tracking 1) the overall magnitude of the number of sample pairs with poor agreement relative to the number of samples collected, as well as 2) the direction of bias at the network level.

5.1.3.2.3. Soil Elements

With the exception of the collocated QC modules, there are no redundant measurements of the soil elements, so all validation efforts at this level focus on 1) internal consistency between the elements for a given sample and 2) consistency through time and, to a lesser extent, space, for the elements individually and in relation to each other. Internal consistency between the soil elements is examined using soil enrichment factors (elemental ratio in aerosol/elemental ratio in average crustal rock), which roughly show if the soil elements in the aerosol sample are found in the same ratio as they would be in average crustal rock. Iron is the most stable element from the XRF systems, so it was selected as the reference element in calculating the enrichment factors. Individual samples are not examined for departures from the expected value of 1 for the enrichment factor; rather, the relative number of these samples and the typical value of the enrichment factor are monitored. Three-panel time series charts are produced for each site for Al, Ca, Si, and Ti as the elements of interest in the first, Fe in the second, and the enrichment factor $((X/Fe_{aerosol})/(X/Fe_{average\ crustal\ rock}))$ for the element of interest in the third panel. The charts are examined primarily for changes in behavior in any of the three metrics over time that could indicate data quality problems.

Additionally, the IMPROVE SOIL parameter is examined in relation to the A module cut point and RCFM. Time series of the three parameters are examined for trends in SOIL that appear related to changes in cut point rather than emissions patterns. Figures 5.5–5.9 are examples of the time series plots used to validate the SOIL parameter.

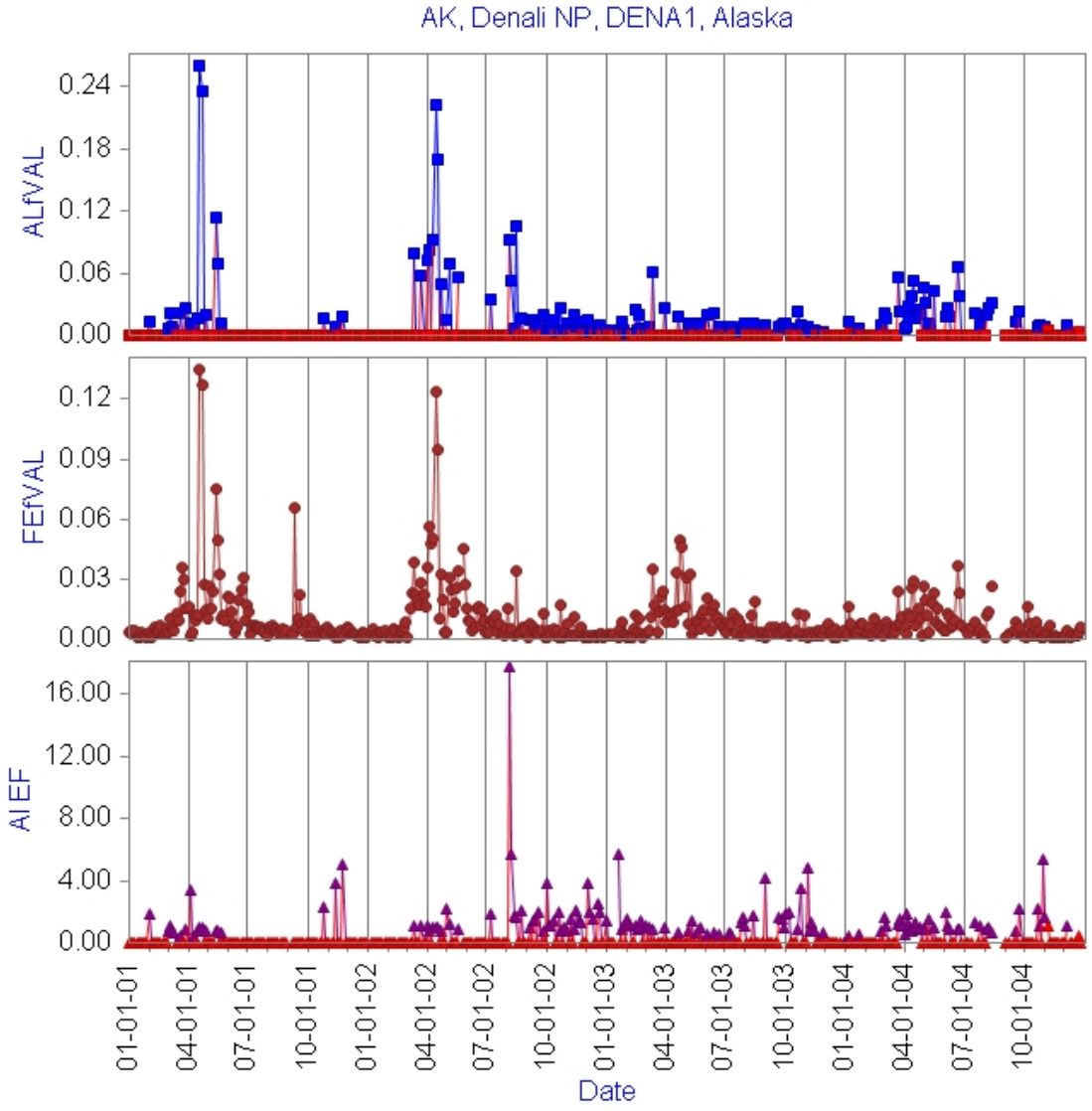

Figure 5.5. An example of the data validation charts from the fall 2004 report. Aluminum concentrations, iron concentrations, and the aluminum to iron enrichment factors are shown for the 2001–2004 time period at DENA1. Definitions of all terms used in the axis titles can be found in the glossary in section 5.1.5 of this document.

*Data points shown in red indicate values below mdl.

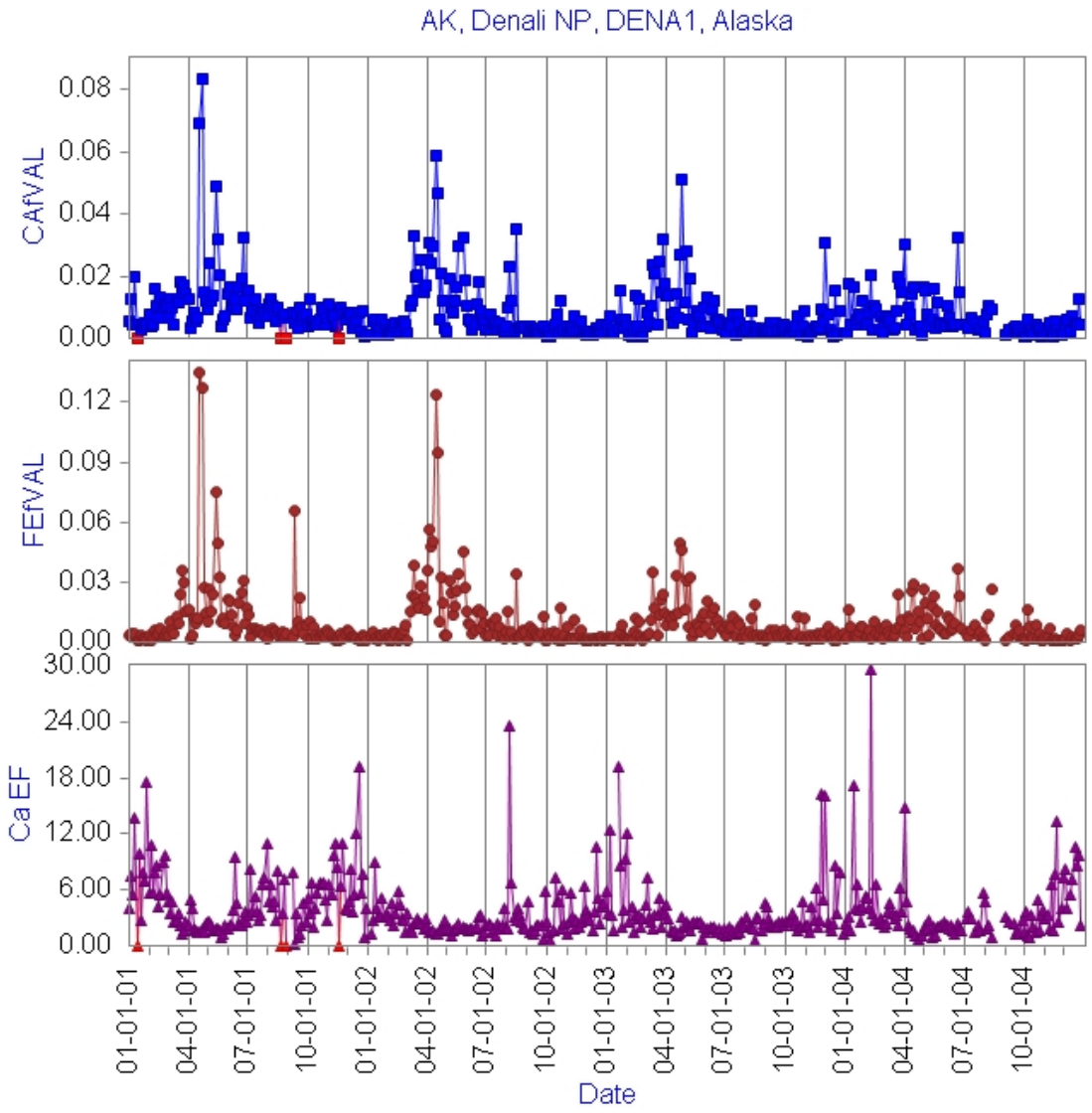

Figure 5.6. An example of the data validation charts from the fall 2004 report. Calcium concentrations, iron concentrations, and the calcium to iron enrichment factors are shown for the 2001–2004 time period at DENA1. Definitions of all terms used in the axis titles can be found in the glossary in section 5.1.5 of this document.

*Data points shown in red indicate values below mdl.

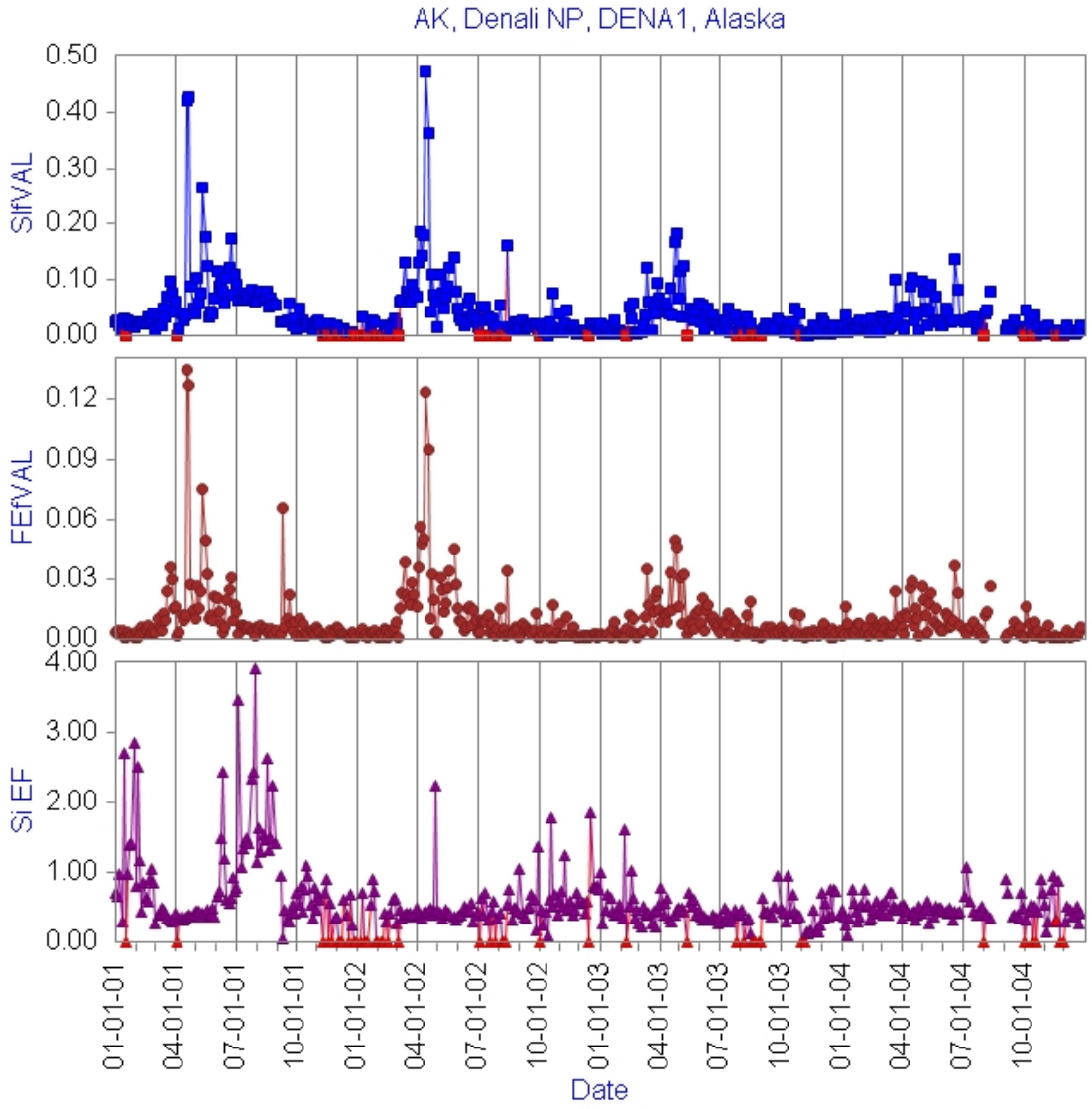

Figure 5.7. An example of the data validation charts from the fall 2004 report. Silicon concentrations, iron concentrations, and the silicon to iron enrichment factors are shown for the 2001–2004 time period at DENA1. Definitions of all terms used in the axis titles can be found in the glossary in section 5.1.5 of this document.

*Data points shown in red indicate values below mdl.

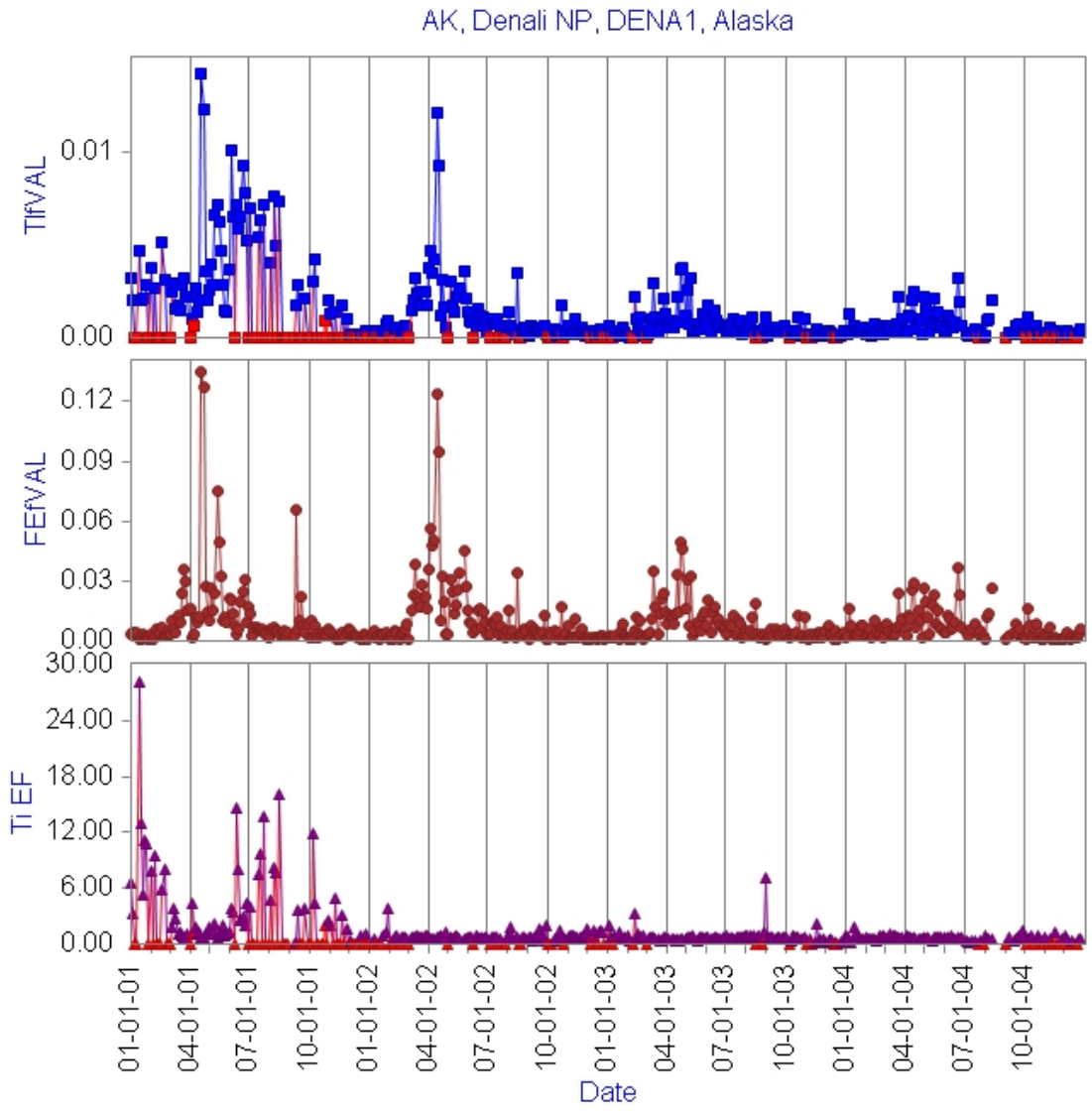

Figure 5.8. An example of the data validation charts from the fall 2004 report. Titanium concentrations, iron concentrations, and the titanium to iron enrichment factors are shown for the 2001–2004 time period at DENA1. Definitions of all terms used in the axis titles can be found in the glossary in section 5.1.5 of this document.

*Data points shown in red indicate values below mdl.

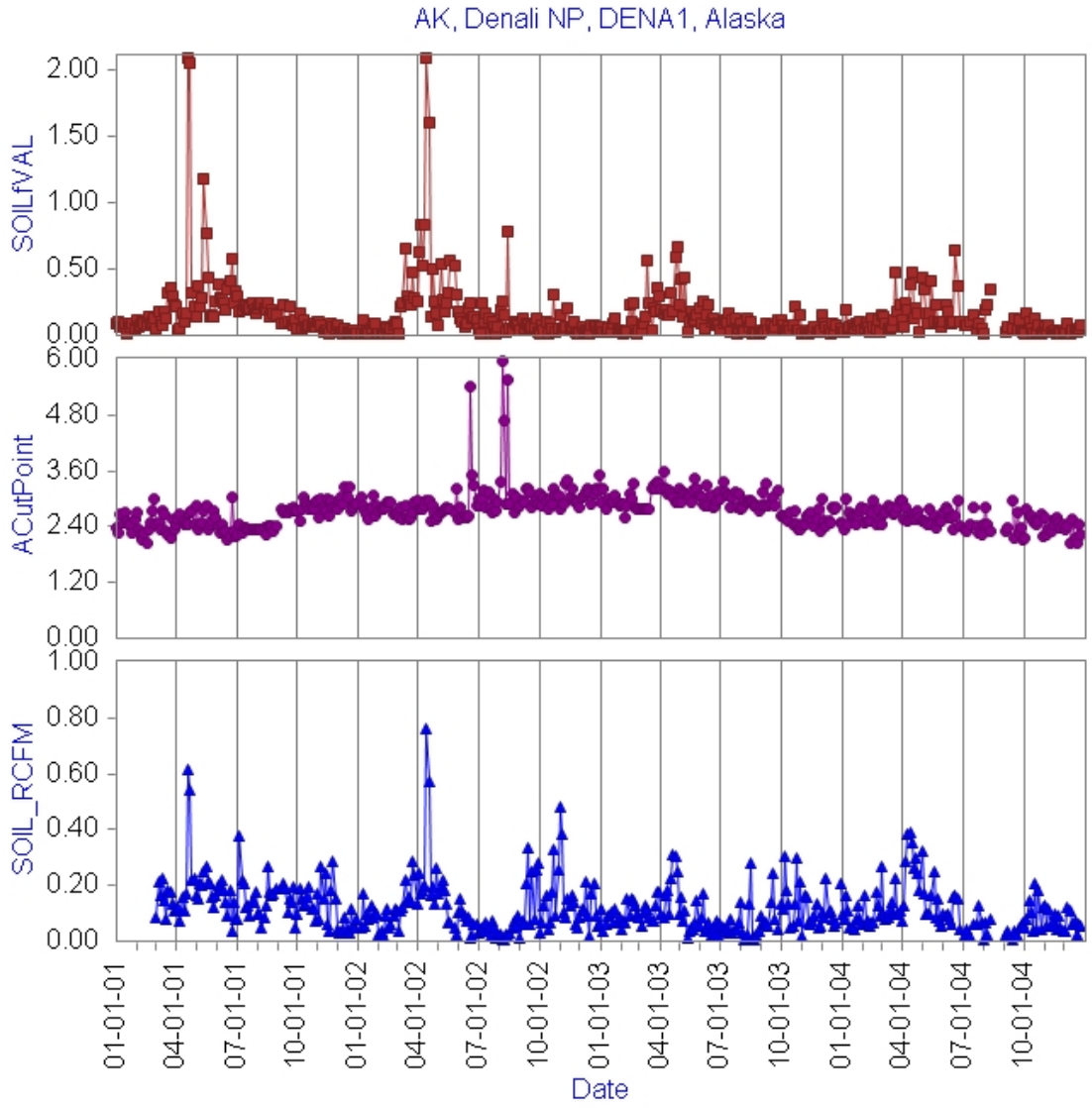

Figure 5.9. An example of the data validation charts from the fall 2004 report. Soil concentrations, the A module cut point and the soil to reconstructed mass concentration ratios are shown for the 2001–2004 time period at DENA1. Definitions of all terms used in the axis titles can be found in the glossary in section 5.1.5 of this document.

5.1.3.2.4. Carbon

In validating the carbon fractions organic carbon (OC) and elemental carbon (EC), the focus at this level is on analyzing time series of the data for abnormalities from 1) the general behavior at that site and 2) the general behavior observed at other sites. Spatial and seasonal variability in OC, EC, and the OC/EC ratio are expected given the varied sources and production pathways for carbonaceous aerosol. Figure 5.10 is an example of the time series of OC, EC, and OC/EC used for validating the carbon data.

The PESA hydrogen measurement can be used as an additional external validation of the OC measurement. Organic mass from hydrogen (OMH) concentrations, an estimate of organic

mass, are calculated from the hydrogen and sulfur concentrations by assuming that all sulfur is in the form of ammonium sulfate, no hydrogen is associated with nitrates or water, and the remaining hydrogen measured by PESA is from organic compounds. It is assumed that the volatile ammonium nitrate and water are quickly lost from the filter as soon as vacuum is applied to conduct the PESA analysis. Although OMH is merely an approximation of organic carbon mass concentration (OMC), the two parameters should correlate well when the sampled aerosol is consistent with the assumption of sulfur being in the form of ammonium sulfate and all other measured hydrogen being associated with the carbon aerosol. Time series of OMC, OMH, and OMH/OMC are analyzed for abnormalities from the general behavior at that site and the general behavior observed at neighboring sites. Figure 5.11 is an example of the time series of OMC, OMH, and OMH/OMC used for validating the organic carbon data.

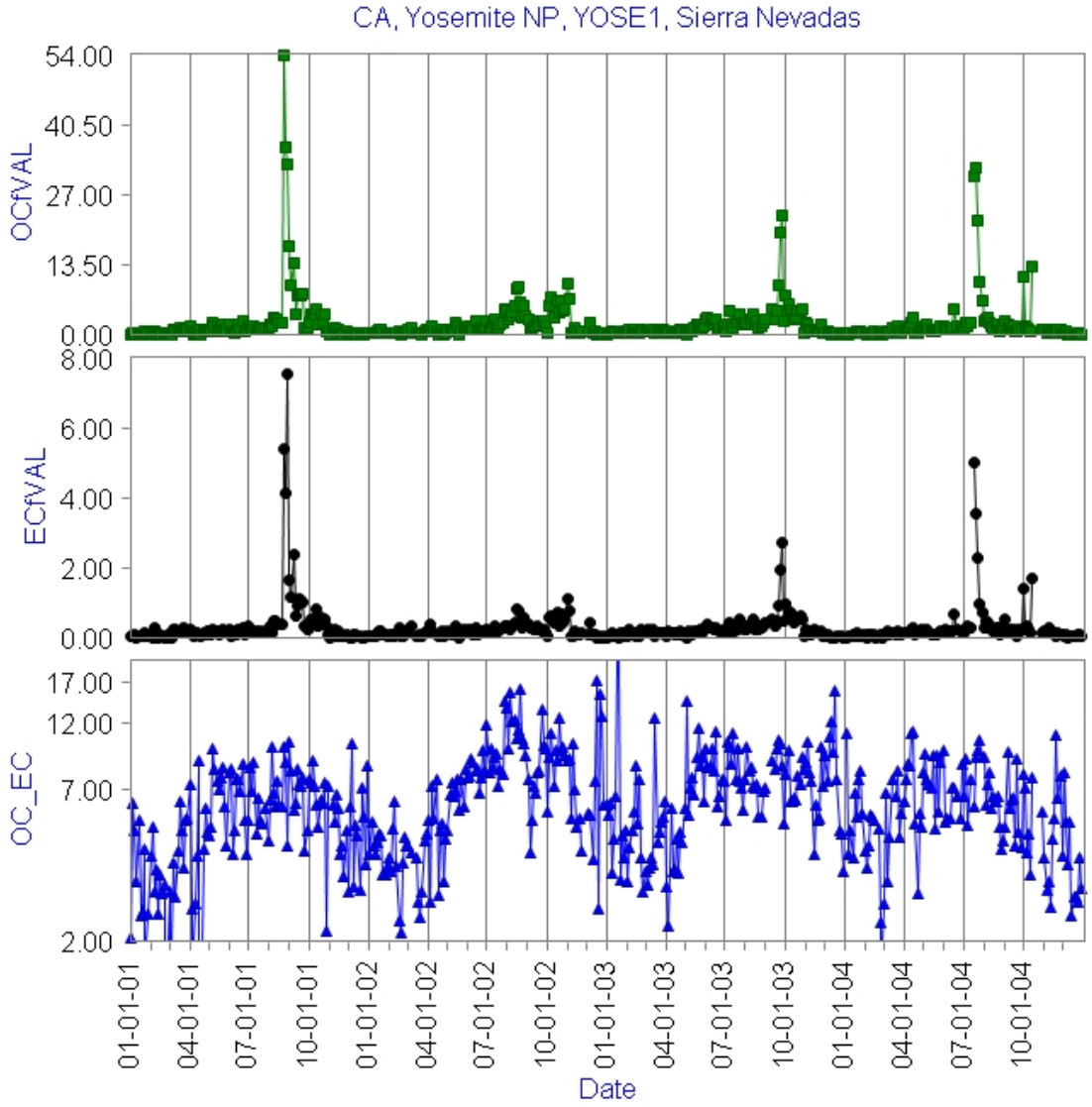

Figure 5.10. An example of the data validation charts from the fall 2004 report. Organic carbon concentrations, elemental carbon concentrations, and the organic carbon to elemental carbon concentration ratios are shown for the 2001–2004 time period at YOSE1. Definitions of all terms used in the axis titles can be found in the glossary in section 5.1.5 of this document.

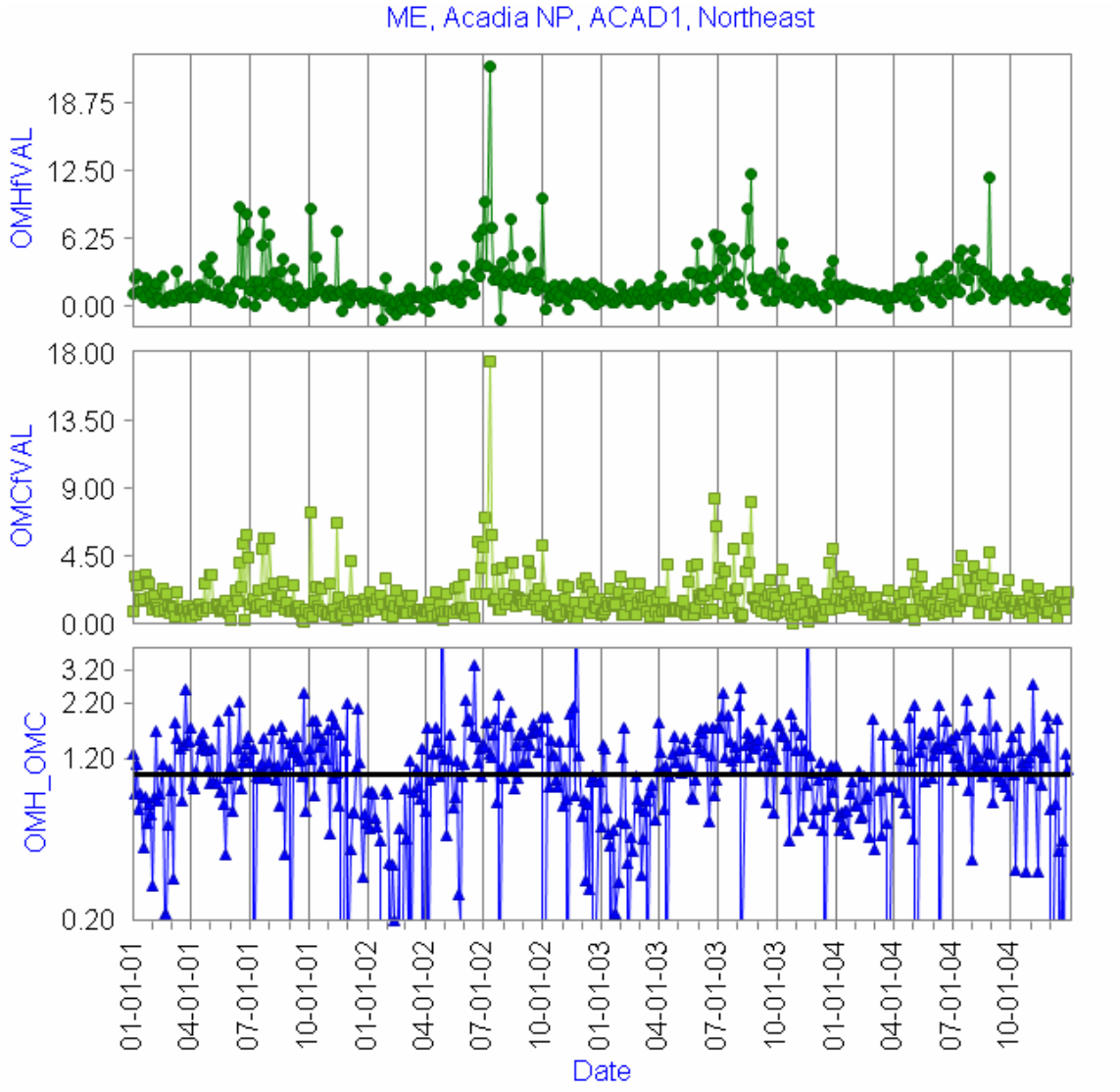

Figure 5.11. An example of the data validation charts from the fall 2004 report. OMC concentrations, OMH concentrations, and the OMH to OMC concentration ratios are shown for the 2001–2004 time period at ACAD1. Definitions of all terms used in the axis titles can be found in the glossary in section 5.1.5 of this document.

5.1.3.2.5. Nitrate

With the exception of the collocated QC modules, there are no redundant measurements of NO_3^-, so the validation efforts at this level are focused on analyzing time series of the data for abnormalities from 1) the general behavior at that site and 2) the general behavior observed at other sites. NO_3^- is examined in relation to RCFM, allowing for analysis of changes in behavior in both the absolute and relative NO_3^- concentrations. Figure 5.12 is an example of the time series used to validate NO_3^-.

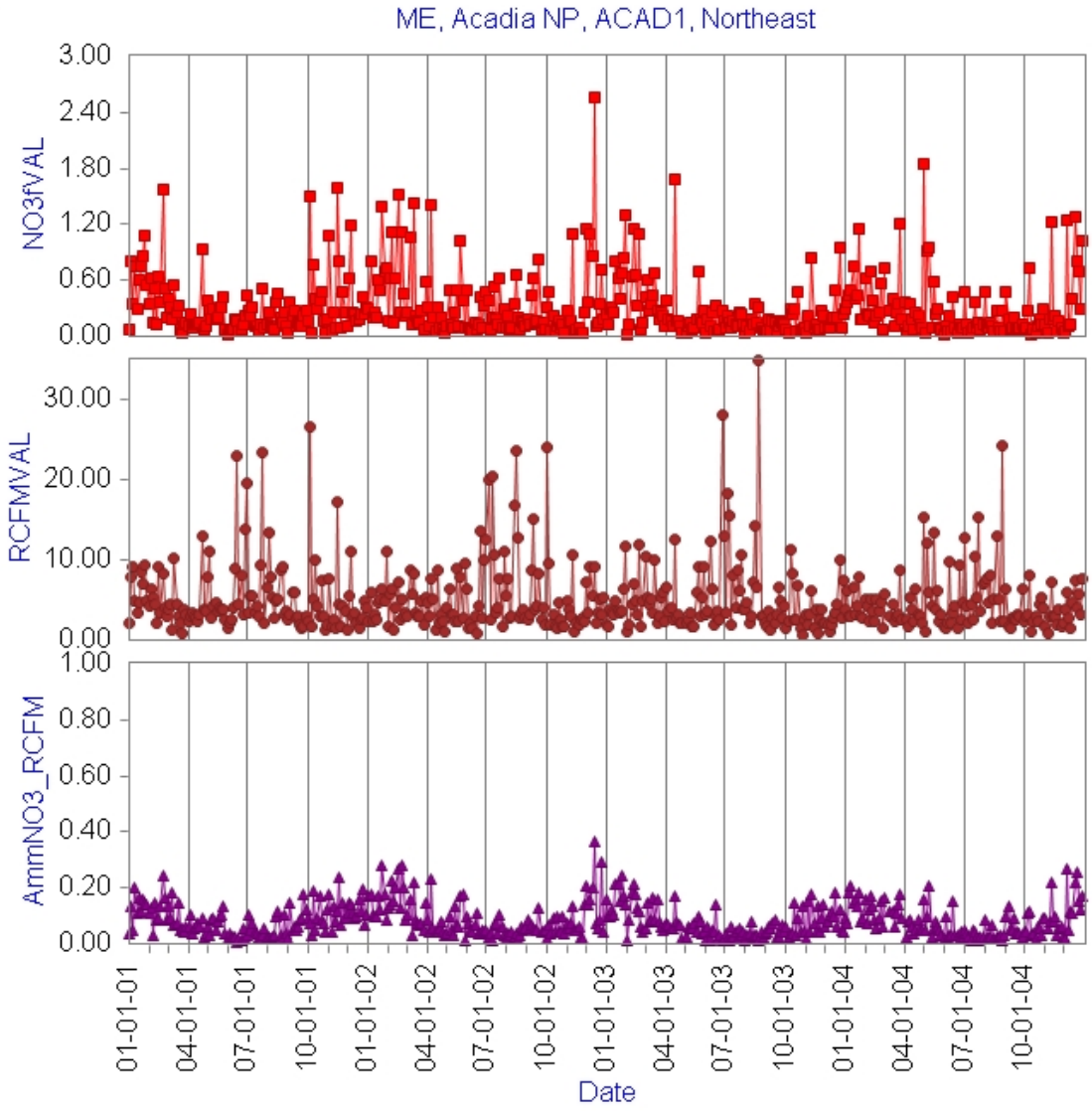

Figure 5.12. An example of the data validation charts from the fall 2004 report. Nitrate concentrations, reconstructed fine mass concentrations, and the ammonium nitrate to reconstructed fine mass concentration ratios are shown for the 2001–2004 time period at ACAD1. Definitions of all terms used in the axis titles can be found in the glossary in section 5.1.5 of this document.

5.1.3.2.6. Cut Point

In the IMPROVE sampler, the aerosol cut point of each module is controlled by controlling the flow rate of that module. Significant sustained deviations from nominal flow rate have occurred at over 75% of the IMPROVE sites for the duration of months to years. Starting with the introduction of the version II sampler in 2000, CNL established a policy whereby these data are flagged as low/high flow rate (LF), really high flow rate (RF), or clogging filter (CG), depending upon the degree of discrepancy between the actual and nominal flow rate (see section 5.1.7 for details). The version I sampler did not provide the necessary flow data to support a flow-rate-based flagging system. The current flagging system employed at CNL accounts for samples with nonnominal flow rates; however, it treats each sample on an individual basis and is

not designed for addressing long-term problems. During the CIRA validation process, sustained periods of time where any one of the three fine aerosol modules (A, B, or C) had a cut point outside of the range (1.5 µm, 3.5µm) are documented. The purpose of CIRA's additional validation process is to document when caution in interpreting the results of cut-point-sensitive analyses involving sites for a particular time period is suggested. Figure 5.13 is an example of the time series figures used by CIRA for validating cut point.

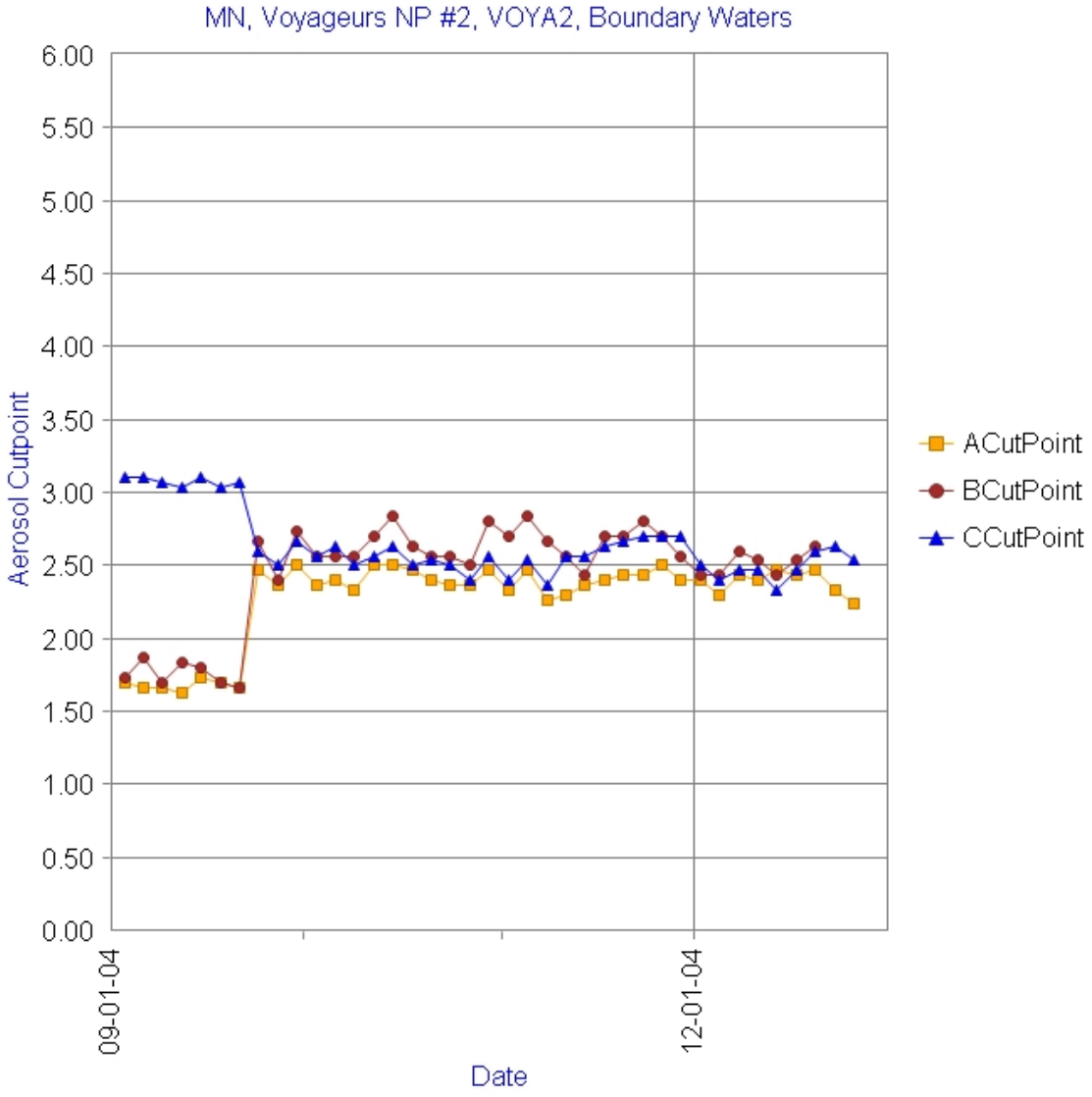

Figure 5.13. An example of the data validation charts from the fall 2004 report. Equation 3 in section 5.1.7 is used to calculate the A, B, and C module cut points from the reported flow rates. The cut points for the A, B, and C modules are shown for the fall–December 2004 data delivery batch at VOYA2. Definitions of all terms used in the axis titles can be found in the glossary in section 5.1.5 of this document.

5.1.4 Examples of Data Quality Issues Discovered by CIRA in the 2004 Data

The primary outcome of the data validation procedures performed by CNL, DRI, and RTI is the qualified data set delivered to CIRA. The QA personnel from these institutions assess the

validity of the data on a data point by data point basis and apply validation flags to communicate the status of the individual data points to the user. The evolving flagging system is designed to communicate whether a data value is valid, questionable, or invalid, and, if the data are not valid, why. The types of problems identified and corrected through this process include misidentified filters, damaged samples, nonroutine sampling conditions, and nonroutine analysis conditions.

Occasionally, the results of the data validation process point to inconclusive or questionable results and the need for reanalysis of either individual or batches of samples. In these cases, the involved samples are, where possible, reanalyzed, and the data validation process starts over with the new results. Problems that are not resolved through reanalysis will result in data being identified and flagged as invalid.

The data validation process at CIRA historically was part of data analysis studies and identified more subtle data quality problems that were difficult to detect with a single batch of data. The outcomes of these past checks have included small special studies, some still in progress, to understand data inconsistencies for identified issues as well as changes in data collection and data management practices and procedures. Examples of the special studies generated by these data validation efforts include

- collocated sample collection with 25 mm and 37 mm nylon filters to determine if changes in face velocity affect the data,
- testing of module B denuder coatings, and
- testing of alternate nylon filter extraction protocols.

Starting with the data collected during 2000, CIRA began a formal validation process that was expanded with the 2004 data and is now conducted for every data delivery during the 30-day preliminary data review period. The focus remains on identifying the more subtle data quality problems that affect large batches of data. The decisions of CNL, DRI, and RTI regarding the validity of individual data points are accepted and not examined outside of the context of data integrity checks. An example to illustrate the distinction is the quantitative validation checks on the comparability of $SO_4^=$ and S. The initial tests conducted at CNL are designed to identify temporally sequential sample pairs with significant disagreement that may indicate that the filters were swapped during the weighing process, whereas the tests at CIRA are designed to assess if the number of sample pairs in a batch of data that have significant disagreement between $SO_4^=$ and S is 1) statistically significant or 2) a change from past behavior for that site.

Data quality problems identified during the first year of routine secondary data validation at CIRA have included identifying sampling problems, data processing errors, and data reporting errors. An additional goal of the process is the quantitative tracking of certain data quality metrics in order to assess trends and transitions in the overall quality of the IMPROVE data set. The special studies resulting more recently from CIRA's validation efforts include

- testing of clogged inlets,
- fully characterizing the cyclone and the effect of changing flow rate on cut point, and
- fully characterizing the XRF systems.

Data reporting errors have included the unintentional inclusion of internal validation flags in the data deliveries, the incorrect use or mapping of validation flags, and the incorrect file format. All of the identified data reporting problems were resolved through data resubmissions, usually within the 30-day review period.

Some of the data processing errors were more complicated and have resulted in broader solutions. One such error identified in the fall 2004 data was erroneously calculated flow rates in the cases where the nominal flow readings were used to calculate the flow rate. The error was identified during the visual inspection of the cut points for each site as an anomalous drop in cut point in all three modules in a handful of data records (Figure 14). The anomaly was reported to CNL, and their review found an error in how the flows were calculated. The error was introduced to the CNL data management system when the code for calculating the flow rates was rewritten to accommodate an updated operating system. The flow rate calculation program was corrected and the fall 2004 data were redelivered.

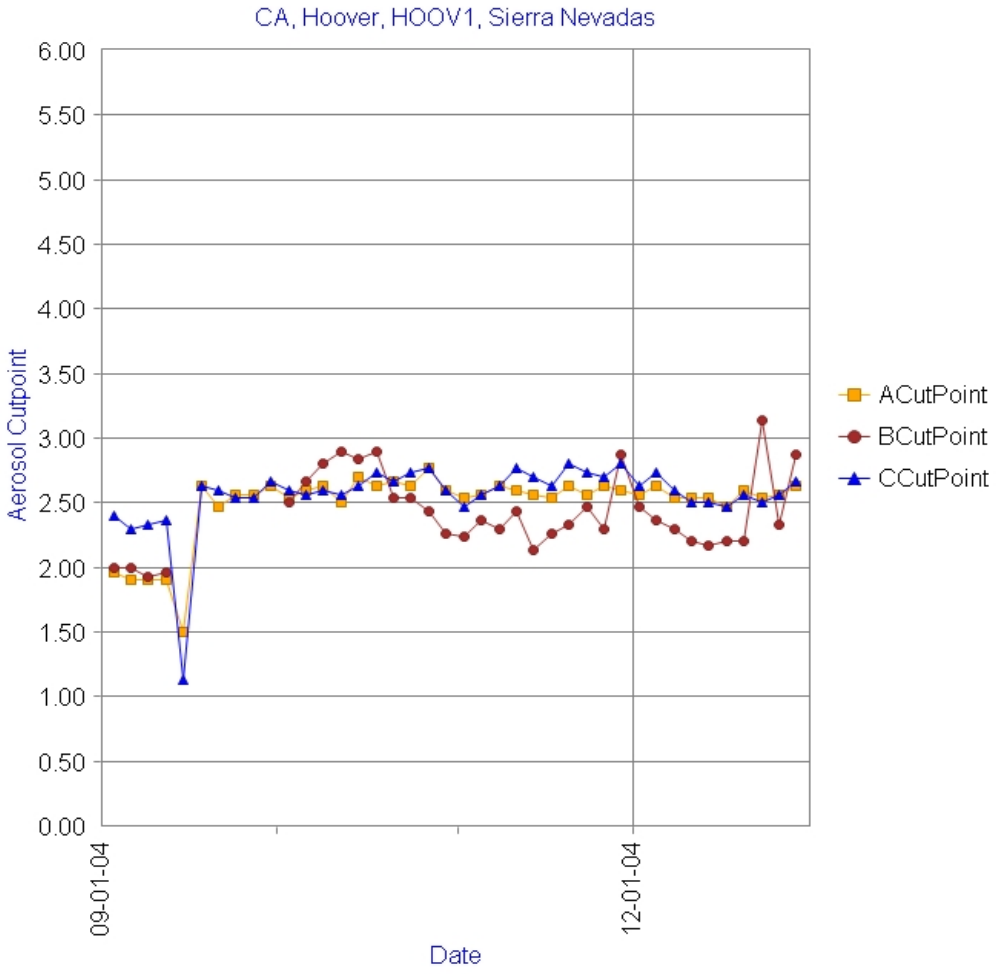

Figure 5.14. An example of the flow rate problem discovered in the data validation charts from the fall 2004 report. Equation 3 in section 5.1.7 is used to calculate the A, B, and C module cut points from the reported flow rates. The cut points for the A, B, and C modules are shown for the fall–December 2004 data delivery batch at HOOV1. Definitions of all terms used in the axis titles can be found in the glossary in section 5.1.5 of this document.

The routine data integrity checks also led to the discovery of undocumented changes to the delivery files. Further communication with the QA personnel at CNL confirmed that the CNL data management system lacks write protections and change tracking. In response to these findings, CNL has accelerated their efforts to thoroughly update and redesign their data management system.

Unlike the data reporting and data processing errors that were primarily found through automated data integrity tests, the sampling problems were identified through CIRA's exploratory data validation process. The most significant discovery in 2004 was an inlet clogging problem associated with a particular inlet design that was difficult to clean. The clogging resulted in incomplete sample collection for the affected modules at Chassahowitzka National Wildlife Refuge (CHAS1), Mingo (MING1), and Swanquarter (SWAN1) for several years. This problem was identifiable at CHAS1 and SWAN1 through on-going degradation in the internal consistency tests (Figure 5.15, a and b) and at MING1 through a decreasing trend in the OC and EC that was not present at neighboring sites (not displayed). The combination of two factors related to the CNL data validation system allowed this sampling problem to remain undetected for 1–2 years at three sites. The first factor was that their validation system did not allow the evaluation of data in context of past behavior, and the second was the assumption that poor comparability between associated samples is due to uncontrollable random errors unless a known problem can be identified.

Once the problem was identified, CNL took several key steps to address the underlying problem. All sites that showed any internal consistency problems and that had the same inlet design as at the identified three sites had new inlets of a more easily maintained design installed. These sites had new inlets mailed to them and the site operators were instructed as to how to install the new inlets. During the 2005 and 2006 field seasons, the remaining sites with the problematic inlets will have had new inlets installed during their annual maintenance visit. As part of this effort, the field technicians were retrained on the importance of cleaning the inlets as part of the annual site maintenance. The clogged inlets from CHAS1, SWAN1, and MING1, along with those removed from unaffected or less-affected sites, were used to study the impacts of inlet clogging on sample collection. The results of these studies indicated that the inlet needed to be almost completely clogged before it had a noticeable impact on sample collection. The analysis of $S/SO_4^{=}$, OMH/OMC, and LRNC/LAC ratios was also added to the CNL data validation process.

a)

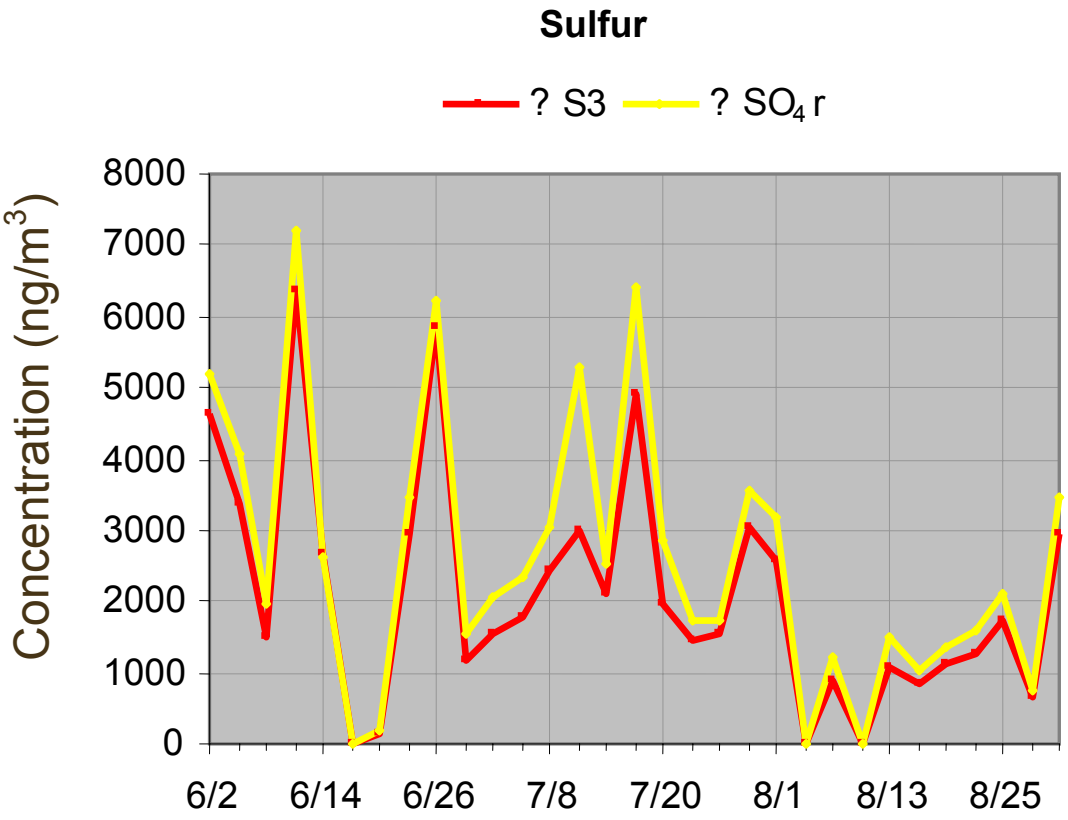
Sulfur
? S3
? SO4 r
Concentration (ng/m3)
8000
7000
6000
5000
4000
3000
2000
1000
0
6/2
6/14
6/26
7/8
7/20
8/1
8/13
8/25

b)

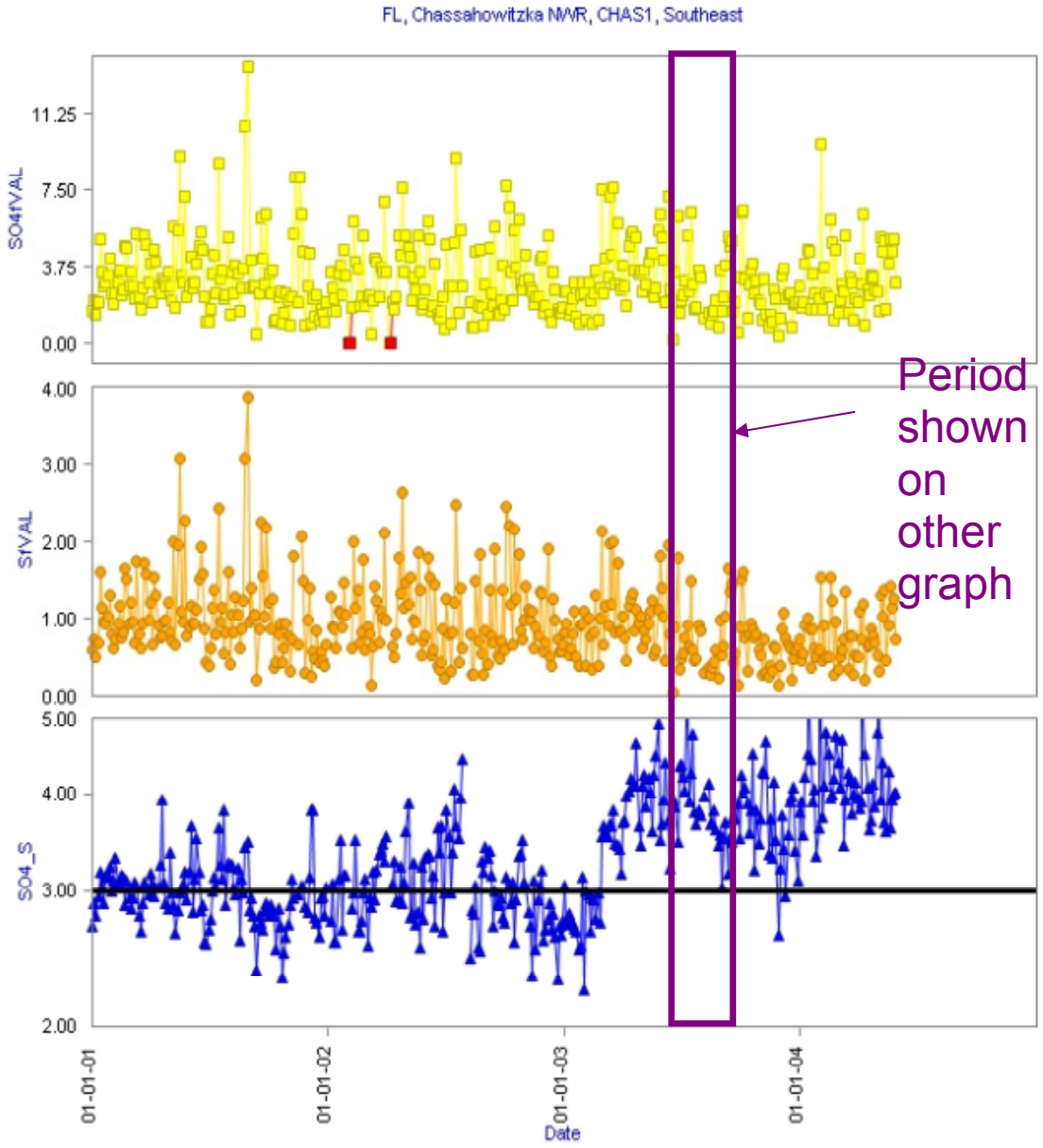

Figure 5.15. An example of the data validation charts from CNL (a) and from CIRA's summer 2004 report (b). Panel a shows sulfate and three times sulfur concentrations for summer 2004 at CHAS1. Panel b shows sulfate concentrations, sulfur concentrations, and the sulfate to sulfur concentration ratios for 2001–2004 at CHAS1. While the incomplete sampling on the A module is obvious in panel b, the sulfate to sulfur discrepancies in panel a do not look similarly alarming. The sampling problem, which is obvious starting in early 2003, was not caught until the 2004 data were examined at CIRA and was not fully acted upon until the summer of 2004. Definitions of all terms used in the axis titles can be found in the glossary in section 5.1.5 of this document.

5.1.5 Glossary of Terms

Quality control (QC) tests: technical activities designed to control errors

Quality assurance (QA) program: a program that includes all of the planning, implementation, documentation, assessment, reporting, and quality improvement activities of the organization that together ensure that a process, item, or service is the type and quality needed and expected by the customer [U.S. EPA, 2000].

Raw IMPROVE Measurements
Measured Fine Mass ($PM_{2.5}$) = **MFVAL** = [$PM_{2.5}$]
Sulfate concentration: **SO4fVal** = [$SO_4^{=}$]
Sulfur concentration: **SfVal** = [S]
SO4UNC = Reported [$SO_4^{=}$] uncertainty
SUNC = Reported [S] uncertainty
Aluminum: **AlfVal** = [Al]
Calcium: **CafVal** = [Ca]
Iron: **FefVal** = [Fe]
Silicon: **SifVal** = [Si]
Titanium: **TifVal** = [Ti]
A_Flow = Reported average flow rate of the A module
B_Flow = Reported average flow rate of the B module
C_Flow = Reported average flow rate of the C module

Parameters Calculated Using IMPROVE Algorithms
Ammonium Nitrate: **AmmNO3** = [AmmNO3] µg/m3 = 1.29*[NO_3^-]
Ammonium Sulfate: AmmSO4 = [AmmSO4] µg/m3 = 4.125*[S]
Organic Carbon: **OCfVal** = [OC] µg/m3 = [OC1]+[OC2]+[OC3]+[OC4]+[OP]
Organic Mass by Carbon: OMC = [OMC] µg/m3 = 1.9*([OC1]+[OC2]+[OC3]+[OC4]+[OP])
Organic Mass by Hydrogen: OMH = 11*([H]-0.25*[S])
Light Absorbing Carbon: **ECfVal**: [EC] µg/m3 = [EC1]+[EC2]+[EC3]-[OP]
Fine Soil: **SOIL** = [SOIL] µg/m3 = 2.2*[Al]+2.49*[Si]+1.63*[Ca]+2.42*[Fe]+1.94*[Ti]
Reconstructed Fine Mass: **RCFMVAL** = [RCFM] µg/m3 = =
AmmSO4+AmmNO3+OMC+EC+SOIL
A Module Cut Point: **ACutPoint** = 2.5-0.334*(A_Flow-22.75)
B Module Cut Point : **BCutPoint** = 2.5-0.334*(B_Flow-22.75)
C Module Cut Point : **CCutPoint** = 2.5-0.334*(C_Flow-22.75)

Other Parameters Utilized in the Validation Tests
Organic Carbon to Light Absorbing Carbon Ratio: **OC_EC** = [OC]/[EC]
Reconstructed Fine Mass to Measured Fine Mass Ratio: **RCFM_MF** = [RCFM]/[$PM_{2.5}$]
Ammonium Nitrate to Reconstructed Fine Mass Ratio: **AmmNO3_RCFM** =
[AmmNO3]/[RCFM]
SOIL to Reconstructed Fine Mass Ratio: **SOIL_RCFM** = [SOIL]/[RCFM]
Sulfate to Sulfur Ratio: **SO4_S** = [$SO_4^{=}$]/[S]
Aluminum Enrichment Factor: **Al EF** = [Al]/[Fe] $_{aerosol}$ / [Al]/[Fe] $_{average\ crustal\ rock}$
Calcium Enrichment Factor: **Ca EF** = [Ca]/[Fe] $_{aerosol}$ / [Ca]/[Fe] $_{average\ crustal\ rock}$

Silicon Enrichment Factor: **Si EF** = $[Si]/[Fe]_{aerosol} / [Si]/[Fe]_{average\ crustal\ rock}$
Titanium Enrichment Factor: **Ti EF** = $[Ti]/[Fe]_{aerosol} / [Ti]/[Fe]_{average\ crustal\ rock}$
Z Score = $([SO_4^{=}] -3*[S])/\sqrt{(SO_4^{=}UNC^2+(3*SUNC)^2)}$

All parameter codes used in the axis titles of the charts are displayed in bold.

5.1.6 Data Acquisition, Quality Control, and Data Management

To reiterate from section 5.1.1, the standard IMPROVE sampler has four independent sampling modules: A, B, and C collect $PM_{2.5}$ particles (0–2.5 μm), and D collects PM_{10} particles (0–10 μm). Module A utilizes a Teflon filter that is analyzed for gravimetric mass and elemental concentrations by X-ray fluorescence (XRF), proton elastic scattering analysis (PESA), and, prior to December 2001, by proton induced X-ray emission (PIXE). Module B utilizes a nylon filter and is analyzed primarily for anions by ion chromatography (IC). Module C utilizes a quartz filter and is analyzed for OC and EC by thermal optical reflectance (TOR) carbon analysis. Module D utilizes a Teflon filter and is analyzed for gravimetric mass.

5.1.6.1. A.1 Sample Handling

Samples are processed on a monthly basis. Separate files are kept for field logs, results from each analysis procedure (weights, laser absorption, XRF, IC, and carbon), comments, flow rates, and sampler calibrations. Each module and filter cassette is color-coded and designated by a letter. Custom software tracks each sample by site, sample date, and start time. Each sample's intended sampling date and location is assigned by the computer. Additionally, the computer also assigns when field blanks or after-filters should be included in the shipment. Samples can be pre-weighed or post-weighed on any one of four balances; they are all calibrated and cross-checked twice daily to ensure consistency. Laboratory blanks are weighed on each balance twice each day, then are loaded into cassettes, stored on a shelf for 6 weeks, and weighed again.

When sample shipments are received for processing, the log sheets are checked and the flow, elapsed time, and temperature are downloaded from a flash memory card that stores the electronic data from the sampler. The sample boxes are then sorted alphabetically for all subsequent processing. At this point, the computer knows the sample box has been received (by site and sample date) and prompts the sample-handling technician through all the sample handling steps. The nylon and quartz filters are removed from cassettes and placed into Petri dishes for shipping to the appropriate analysis contractor. Filter labels are transferred to the Petri dishes from the cassette holder as the filters are unloaded. The computer records their position in the queue of samples.

The Teflon filters are post-weighed, and the net weight is immediately calculated to confirm that the difference is positive. The PM_{10} net weights are also compared to the $PM_{2.5}$ net weights to ensure that the PM_{10} mass is greater than the $PM_{2.5}$ mass. Whenever a discrepancy is found, the weighing technician must call a supervisor before continuing. After being post-weighed, the $PM_{2.5}$ and PM_{10} Teflon filters are mounted into slides and the slides are filed into slide trays. The $PM_{2.5}$ slide trays are delivered to the XRF lab for analysis. The gravimetric analysis of both the A and D module Teflon filters allows for the estimation of the coarse aerosol fraction by subtracting the $PM_{2.5}$ mass from the PM_{10} mass.

After all the used samples are processed, the empty box is sent to the pre-weigh station to be prepared for the next round of samples. The software prompts the technician to weigh the correct filters for the box and prints filter labels and log sheets to go with them. Sample boxes are checked and rechecked several times before being shipped to sites.

5.1.6.2. A.2 Sample Analysis

The $PM_{2.5}$ Teflon filters are analyzed for elemental content by CNL. The forms of elemental analysis conducted past and present in the IMPROVE network are PESA, PIXE, and XRF. PESA has been and continues to be used for quantifying elemental hydrogen. PIXE was initially used for quantifying all other elements reported—nearly all elements with atomic number ≥11 (which is Na) and ≤82 (which is Pb). Beginning in 1992, analysis of the heavier elements, those with atomic weights from Fe to Pb, was changed from PIXE to XRF with a Mo anode source. PIXE was discontinued in late 2001, and analysis of the lighter elements with atomic numbers from Na to Mn was changed from PIXE to XRF with a Cu anode source. Additionally, the Fe measurements from the Cu XRF system were reported to the final database instead of those from the Mo system. In both cases, the change from PIXE to XRF provided lower minimum detection limits (mdl) for particular elements of interest, as well as better sample preservation for reanalysis.

Under current procedures, XRF runs are carried out in 1-month sample batches (e.g., all samples collected in March). Once each month on the Mo system, and once each week on the Cu system, a set of standard foils is run. The Cu system is more subject to change due to the helium atmosphere it runs in and is therefore checked more frequently. The standard foils serve two purposes: 1) to obtain the relationship between X-ray energy and the multi-channel analyzer bin number that the X-rays are counted in and 2) to check the overall calculation against the standard amount. For elements with atomic weights ≥Si, the values reported for each foil must agree with the known amount within 5%, or the analysis is aborted until the reason is found.

Several of the standards are more heavily loaded than routine sample filters and must be run at a lower X-ray tube current. After establishing that the standards are measured correctly, a designated set of previously analyzed samples is run at the normal operating current. These samples have been analyzed multiple times as a check of the system against drift. They contain a range of values typical of those in the network and serve a similar function to a multipoint calibration. The reanalysis samples are checked against the prior known values by a separate regression for each element. The Cu system is checked using a set of low atomic number elements that includes S, Ca, Ti, Fe, and others, and the Mo system is checked using a set of higher atomic number elements appropriate to that system. If any of the regression slopes differ by more than 5%, the run is stopped and the reason is found and corrected. Problems with the replicate analysis are rarely seen once the standards are checked and approved. The regression analysis is more appropriate for the reanalysis samples than a point-by-point test, because statistical counting uncertainties can affect any individual point.

The nylon filters are analyzed by RTI using IC for the major anions Cl^-, NO_3^- and $SO_4^=$, with the primary parameter of interest being the NO_3^-. Multipoint calibrations and QA/QC standards are run daily prior to any samples. Analysis of samples does not proceed unless the observed values for $SO_4^=$ differ by less than 10% from the known values.

The IMPROVE quartz filters are analyzed by DRI for OC and EC using TOR. IMPROVE has used the same TOR protocol since 1988 for measuring OC and EC fractions of total carbonaceous aerosol. Fractionation of the aerosol is controlled and defined by changes in the analysis temperature and atmosphere and changes in filter reflectance. The OC fractions are evolved first in an inert, ultrahigh-purity helium environment; O_2 is then introduced to the sampling chamber to evolve the EC fractions. Evolved carbon for each fraction is quantified using a flame ionization detector (FID) gas chromatograph (GC). The GC is calibrated daily using National Institute of Standards and Technology (NIST) traceable CH_4 and CO_2 calibration gases. In addition, semiannually the calibration slopes derived from the two gases and the potassium hydrogen phthalate (KHP) and sucrose-spiked filter punches are averaged together to yield a single calibration slope for a given analyzer. This slope represents the response of the entire carbon analyzer to generic carbon compounds and includes the efficiencies of the oxidation and methenator zones and the sensitivity of the FID. Note that the current calibration procedure is based only on the total carbon; currently, no routine procedure exists to check the accuracy of the OC/EC split.

Comparability between aerosol carbon measurements, particularly the fractions, is highly dependent on measurement protocol. Recent analysis of the DRI/Oregon Graduate Center (OGC) analyzers used for IMPROVE carbon analysis since 1987 revealed that certain variables were not controlled as well as previously thought in these instruments [Chow et al., 2005]. The possibility exists that poorly controlled aspects of the instrumentation may have caused changes in the OC/EC ratio over time. A small leak in the instrument allowed the diffusion of ambient air into the sampling chamber; the level of oxygen contamination in the helium atmosphere could have changed over time, affecting the stability of the OC/EC ratio. Furthermore, the OC/EC ratio can also be impacted for individual samples by the presence of oxidizing minerals or catalysts (such as NaCl), further complicating the situation. However, total carbon, OC, and EC seemed to be reproducible within measurement uncertainty for filters back to 1999. The Model 2001 carbon analyzer includes an updated protocol and is slated for implementation starting with samples collected in 2005.

The IMPROVE system has been designed to include internal measurement redundancy, a valuable asset for data validation. Examples include Fe from both XRF systems, $SO_4^=$ and S from modules B and A, respectively, and various modeled relationships that allow for the intercomparison of results from the independent modules (see section 5.1.7 for more detail). When all samples for a month have been analyzed and the data sets are complete, they are combined by custom software into a single data table that is then reviewed site-by-site for internal consistency.

5.1.7 Data Validation Activities at CNL

5.1.7.1. Flow Rate Audits and Analysis Performed by CNL

Flow rate accuracy is a critical aspect of overall system accuracy. The A, B, and C modules of the IMPROVE sampler are intended to sample fine aerosol with a cut point of 2.5 µm. The cut points of the modules are controlled by the flow rate for that module. Based on the design of the sampler, flow rate is inversely related to cut point as shown in Figure 5.16 and modeled in equation 3:

$$d_{50} = 2.5 - 0.334 * (Q - 22.75) \quad (3)$$

where Q = flow rate (L/min) and d_{50} = aerodynamic diameter at which 50% of the particles are collected (µm).

Equation 3 was developed based on flow rates between 18 and 24 L/min. Beyond these flow rates, equation 3 may not be valid.

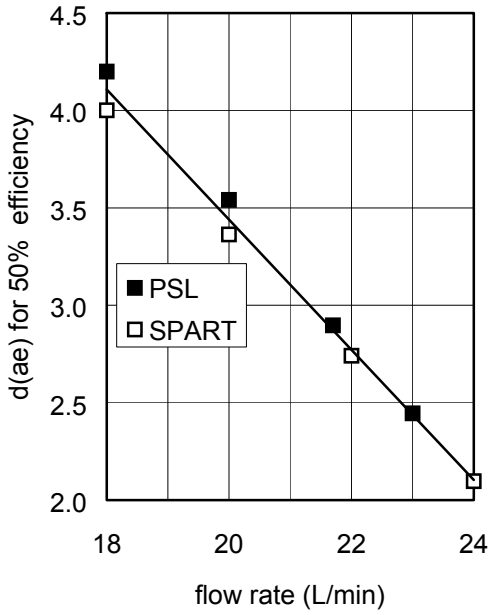

Figure 5.16. The plot shows the 50% cut point as a function of flow rate as determined by two separate collection efficiency tests. The collection efficiency of the IMPROVE cyclone was characterized at the Health Sciences Instrumentation Facility at the University of California at Davis. The efficiency was measured as a function of particle size and flow rate using two separate methods: PSL and SPART. The PSL method uses microspheres of fluorescent polystyrene latex particles (PSL) produced by a Lovelace nebulizer and a vibrating stream generator and analyzed by electron micrographs. The SPART method uses a mixture of PSL particles produced by a Lovelace nebulizer and analyzed by a single particle aerodynamic relaxation time (SPART) analyzer. The aerodynamic diameter for 50% collection, d50, was determined for each flow rate.

Efforts are made to maintain the flow rate at a nominal rate of 22.8 L/min in order to achieve the desired cut point. These efforts include annual calibrations of the sampler, as well as

periodic internal and external flow rate audits to test if the system is within tolerable limits for meeting the MQOs. Corrective action is taken if an audit indicates problems. However, there are a variety of reasons why the average flow rate of a given 24-hour sample may vary from the nominal rate, from clogging due to heavy aerosol loading on the filter to equipment failure. A flagging system is in place to qualify samples with severe deviations from the nominal flow rate and therefore from a cut point of 2.5 μm (Table 5.2). However, only those samples flagged as clogged filter (CL) are considered invalid, thus allowing even those samples that would have estimated cut points outside of the range 1–4 μm (assuming linearity outside of the documented range of equation 3) to be considered qualified valid samples. Currently, all flow-related validation criteria are based only on individual samples; there are no population level checks on how many samples can be flagged as LF or RF.

Table 5.2. Flow rate-related validation flag definitions and application criteria.

Validation Flag	Definition	Concentration Reported?	Criteria
CL	Clogged Filter	No	Flow rate less than 15 L/min for more than 1 hour
CG	Clogging Filter	Yes	Flow rate less than 18 L/min for more than 1 hour [1]
LF	Low/high flow rate	Yes	Average flow rate results in cut point outside 2-3 μm (corresponds to flow rates < 21.3 L/min or > 24.3 L/min).
RF	Really low/high flow rate	Yes	Flow greater than 27 L/min for more than 1 hour [2]

5.1.7.2. Accuracy, Uncertainty, and MQL Checks on QC Samples Performed at CNL

A positive feature of the IMPROVE data set is the calculation and reporting of uncertainty and mdl for every data point. The uncertainty estimate is useful for quantitative comparisons of similar data such as the collocated data and $SO_4^=$ and S. The mdl is useful for evaluating the robustness of the measured values. The uncertainty and mdl calculations are in part based on the results of select QC tests.

All calibration standards for XRF, IC, and TOR are NIST traceable. Calibrations are performed prior to analyzing every batch of samples. Adjustments are made to the systems until they are in agreement with the known standards within a tolerable range for meeting the MQOs for accuracy.

Replicate samples are run as part of every batch to ensure that the system's precision remains within tolerable limits for meeting the MQOs. A further test on the precision of the overall sampling and analytical system is collocated samplers. The observed differences in collocated data are directly comparable to the MQOs. Also, the observed differences in collocated data are compared to the estimated uncertainties reported with each data value to determine if the reported values are accurate.

New data validation tests to ensure MQO conformance will likely be developed as part of the MQO review and revision process.

5.1.7.3. Internal Consistency Checks Performed at CNL

5.1.7.3.1. Iron

Both X-ray systems are equally sensitive for iron, and comparisons of the iron measurements from the two systems are a routine part of CNL's QA system. A scatter plot of iron from the Cu and Mo XRF systems is examined for every data batch. Valid data are expected to have a correlation slope of 1±0.05.

5.1.7.3.2. Mass

Given accurate cut points on both the A and D modules, valid sample sets are expected to have PM_{10} masses that are equivalent to or greater than $PM_{2.5}$ masses. Therefore, every sample in the batch is analyzed to see if PM_{10}-$PM_{2.5} \geq 0$, within measurement uncertainty, both at the time of weighing and after all modules have been analyzed. Cases where PM_{10}-$PM_{2.5} \leq 0$ are evaluated for potential filter swaps.

Additionally, the RCFM from the speciated concentrations and the measured fine (MF) mass are expected to be roughly equivalent for a sample set. Every sample in the batch is analyzed to see if RCFM and MF agree within subjective expectations after all modules have been analyzed. The qualitative analysis is based on the visual inspection of time series figures by the QA manager. Large discrepancies between RCFM and MF can indicate data quality problems in any one or a subset of the measurements involved in the comparison.

5.1.7.3.3. Sulfate

A quality assurance check for the A and B modules consists of comparison of the measured concentrations of sulfur and sulfate. The comparison also provides an external check on the IC and XRF systems. Since both modules should be sampling simultaneously and have the same flow and aerosol size cut point, and assuming all aerosol sulfur is in the form of sulfate, the collected data should be equivalent. Every sample in the batch is analyzed to see if $SO_4^=$ and 3*S agree within subjective expectations after all modules have been analyzed. The qualitative analysis is based on the visual inspection of time series figures by the QA manager. Additionally, a quantitative check on the agreement of the two measurements is used to evaluate temporally consecutive sample pairs for potential filter swaps.

5.1.7.3.4. Carbon

A correlation plot of the concentration of organic mass from hydrogen analysis (OMH) and the concentration of organic mass from carbon analysis (OMC) is examined as an external validation check on the carbon measurements from the C module. OMH concentrations are determined by assuming that all sulfur is in the form of ammonium sulfate, no hydrogen is associated with nitrates or water, and the remaining hydrogen measured by PESA is from organic compounds. It is assumed that the volatile ammonium nitrate and water are quickly lost from the filter as soon as vacuum is applied to conduct the PESA analysis. OMC concentrations are derived through TOR analysis. Although OMH is merely an approximation of OMC, the two parameters should correlate well under certain sampling conditions. The data set is analyzed to

see if OMH is in agreement with OMC within subjective expectations after all modules have been analyzed. The analysis is qualitative and based on the judgment of the QA manager.

5.2 OUTCOMES FROM A HISTORICAL REVIEW OF IMPROVE DATA

5.2.1 Introduction

A historical review of the IMPROVE data collected from 1988 through 2003 was conducted in late 2004 through early 2005. The results of that study are summarized here with the details available at http://vista.cira.colostate.edu/DatawareHouse/IMPROVE/Data/AEROSOL/Data/QA_QC/1988_2003/. It should be noted that changes in the data resulting from redeliveries received after the data were retrieved from the database are not reflected in this study, nor are changes in our understanding of the relationship between flow rate and cut point based upon a study that was conducted after the validation of this data was completed.

5.2.2 Measured Fine Mass versus Reconstructed Fine Mass Review

The closure comparison of gravimetric fine mass to RCFM provides a check on the consistency of results from the three sampling modules and all four major analytical methods. The theory behind these comparisons is given above in the data validation overview section 5.1.3. Large discrepancies from 1 in the RCFM/FM ratio can indicate data quality problems that can be further explored and sometimes explained by either additional relationships among the data records or associated metadata. Eight anomalies, at least in part identified by deviations from typical behavior in the RCFM/FM ratio, were identified. Anomaly 1 affected eight sites and was related to unexplained anomalies in nitrate measurements. Anomalies 2–4 affected four sites and were related to unexplained anomalies in carbon measurements. Anomaly 5 affected three sites and was not found to be related to any particular measurement. Anomalies 6 and 7 affected seven sites and were linked to sampling problems, and the affected data have been invalidated. Anomaly 8 affected one site and appeared to be related to deviations from 2.5 in the cut point of the A module, resulting in additional coarse mass being sampled on this module as compared to the B and C modules. Associated figures and detailed descriptions of the observed anomalies are available from the IMPROVE webpage.

5.2.3 Sulfate Review

Time series and scatter plots of $[SO_4]$ and [S] and their ratio can be useful for qualitatively diagnosing potential problems with either measurement method; the details are discussed above in section 5.1.3.2.2. The combined analyses of time series and scatter charts above indicate that the degree of agreement and the direction of bias in the $[SO_4]$ to [S] relationship for a sample pair are dependent on when the samples were collected and/or analyzed, where the samples were collected, and the sample sulfate concentrations. To quantify these general observations, the spatial, temporal, and concentration distributions of sample pairs where $[SO_4]$ and [S] do not agree within 3σ uncertainty were investigated and are described below. These results were also compared to statistical expectations for a population of samples with accurate measurements and well-quantified measurement uncertainties.

Z scores calculated from [SO_4] and [S] and their uncertainties can be useful for quantitatively diagnosing potential problems with either measurement method; the details are discussed above in section 5.1.3.2.2. When the IMPROVE data set is taken as a whole, the sulfur measurements do not have an unexpected number of pairs that are more than 3σ apart. However, once the temporal, spatial, and concentration dimensions of the population are taken into account, the outlier sample pairs are clustered in certain spatial or temporal subsets of the data. The clusters are typically not symmetrical in terms of bias direction. The bottom line is that the expectation of random distribution of the outliers is violated, and the expectation of at most 10% of the population being in extreme disagreement is also violated for all data set fractions that take the key dimensions of the population into account. Therefore, we would suggest that the poor agreement in many of these sample pairs is not due to random chance but the reflection of real analytical and/or sampling problems specific to certain conditions. More generally, these results indicate that either the SO_4 and/or the S measurements are not accurate under some conditions, and/or one or both of the estimated measurement uncertainties are an underprediction of the true uncertainty under some conditions. However, they also indicate that the measurements are consistently accurate under some conditions and that the estimated uncertainties are accurate or even an overestimate of the actual uncertainty under some conditions.

The network-wide patterns in terms of dominant bias direction are likely due to problems in our analytical process or to sampling media (see Figure 5.4). It appears that local conditions can override the network-wide patterns, suggesting that sampling conditions are a key component to producing comparable [SO_4] and [S] measurements. Sampling conditions could alternately play the role of enhancing the network-level signal at particular sites or dampening it—either reducing or increasing the comparability of those particular [SO_4] and [S] measurements. Additional investigation is required to understand what factors in terms of analytical and sampling equipment and procedure might be negatively or positively impacting the comparability of our measurements. The fact that low Z scores dominate at low concentrations and high Z scores dominate at high concentrations suggests there may be different underlying problems causing sample pairs with [SO_4]<<3*[S] (low Z scores) and those with [SO_4]>>3*[S] (high Z scores). Furthermore, the correlation between sulfate offsets and flow offsets in the collocated data and the correlation between the percentage of valid samples with Z<-3 and blank concentration hint at a connection between flow problems, blank corrections, and the poor agreement between [SO_4] and [S] at low concentrations, even those well over 10*mdl, for at least the recent past. Associated figures, tables, and detailed descriptions of the observed discrepancies are available on the IMPROVE webpage.

5.2.4 Soil

With the exception of the collocated QC modules, there are no redundant measurements of the soil elements, so all validation efforts at this level focus on 1) internal consistency between the elements for a given sample and 2) consistency through time and, to a lesser extent, space, for the elements individually and in relation to each other. Internal consistency between the soil elements is examined using soil enrichment factors (elemental ratio in aerosol/elemental ratio in average crustal rock), which roughly show if the soil elements in the aerosol sample are found in the same ratio as they would be in average crustal rock. Iron is the most stable element from the XRF systems, so it was selected as the reference element in calculating the enrichment factors.

Individual samples are not examined for departures from the expected value of 1 for the enrichment factor; rather, the relative number of these samples and the typical value of the enrichment factor are monitored. Additionally, trends in soil concentration and A module cut point were examined to highlight instances where long-term deviations from nominal flow rate appeared to produce trends in soil concentrations. The details of how the soil elements are examined are discussed above in section 5.1.3.2.3. Associated figures and detailed descriptions of the observed anomalies are available from the IMPROVE webpage. The main observations from the historical analysis of the soil elements were as follows:

- It seems that Al data have been particularly sensitive to analytical and data processing changes.
- The possibility that the PIXE system was contaminated with titanium should be explored.
- Persistent offsets from nominal flow in the A module appear to have resulted in trends in absolute and relative soil concentrations. This could have significant impacts for trends analysis at sites where soil is a dominant fraction of the aerosol.
- The soil elements taken as an ensemble, but not as a composite variable such as SOIL, seem to be more revealing of analytical inconsistencies and problems.

Associated figures and detailed descriptions of the observed anomalies are available from the IMPROVE webpage.

5.2.5 Carbon

In validating the carbon fractions OC and EC, the focus at this level was on analyzing time series of the data for abnormalities from 1) the general behavior at that site and 2) the general behavior observed at other sites. Background information can be found in section 5.1.3.2.4. Spatial and seasonal variability in OC, EC, and the OC/EC ratio are expected given the varied sources and production pathways for carbonaceous aerosol. Furthermore, the anomalies documented in this report may be an accurate reflection of true atmospheric conditions at the site or may be a reflection of data quality problems related to sampling or analytical conditions. In each case below, RCFM/FM ratios were used to try and determine if data quality problems were behind the reported anomaly. The historical review identified 12 anomalies affecting, in total, 29 sites. The anomalies related to trends observed in OC, EC, or the OC/EC ratio, changes in the seasonality of OC, EC, or the OC/EC ratio, and changes in the central tendency of OC, EC, or the OC/EC ratio. Associated figures and detailed descriptions of the observed anomalies are available from the IMPROVE webpage.

5.2.6 Nitrate

With the exception of the collocated QC modules, there are no redundant measurements of NO_3^-, so the validation focused on analyzing time series of the data for abnormalities from 1) the general behavior at that site and 2) the general behavior observed at other sites. NO_3^- was examined in relation to RCFM, allowing for analysis of changes in behavior in both the absolute and relative NO_3^- concentrations. Two anomalies affecting multiple sites were identified in the historical record from 1988 to 2003. The first (also identified and studied prior to this analysis) was low wintertime nitrate concentrations observed at 22 sites from 1996–1997 to 1999–2000 [McDade, 2004]. These low concentrations may have resulted from measurement abnormalities during that

period. However, there is no definitive evidence to support that claim, and thus the data must be considered valid until shown otherwise. The second anomaly was high NO_3 values and ammonium NO_3/RCFM ratios from 2000 to 2003 at 33 sites; again there is no evidence that these values are invalid; however, data quality problems are a potential cause. An additional three anomalies that were isolated in nature were also identified. The first was reduced range in ammonium nitrate concentrations at Badlands National Park (BADL1) after 1999. The second was high NO_3/RCFM at HAVO1 during mid 2003. The third anomaly was ammonium nitrate to RCFM ratios that were unusually low during 2003 at SACR1 due to unusually high RCFM values. Data quality problems relating to nonnominal flow rates on the A module are a potential source of the anomaly. Associated figures and detailed descriptions of the observed anomalies are available from the IMPROVE webpage.

5.2.7 Cut Point

In the IMPROVE sampler, the aerosol cut point of each module is controlled by controlling the flow rate of that module. Significant sustained deviations from nominal flow rate have occurred at the majority of IMPROVE sites for the duration of months to years. The current data validation system treats each sample on an individual basis and is not designed for addressing long-term problems. The associated report documents sustained periods of time where any one of the three fine aerosol modules (A,B, or C) had cut points outside of the range (1.5 m, 3.5 m), based upon the cut-point-to-flow-rate relationship available at the time of this analysis. It should be noted that the data were considered valid under IMPROVE program standards at the time of this study. Furthermore, the results from a subsequent study of the relationship between flow rate and cut point for the IMPROVE sampler indicate that the relationship is much less sensitive than previously thought. Associated figures and detailed descriptions of the observed anomalies are available from the IMPROVE webpage.

5.3 NITRATE SAMPLING METHODS INVESTIGATION

5.3.1 Introduction

The results from a collection of field studies designed to investigate nitrate sampling methods will be summarized here, with the original papers available in Appendix D. This study was motivated by the lower winter nitrate concentrations and variability measured at many (though not all) IMPROVE sites from 1996 through 2000. Coincidently, glycerin was added to the B module denuder starting in 1996. However, with no further change to the denuder, nitrate concentrations returned to pre-1996 levels in 2001. A study consisting of several month-long field sampling campaigns at specially selected IMPROVE sites was conducted to better understand the effects of denuder coating and filter type on IMPROVE ammonium nitrate sampling [Ashbaugh et al., 2004; Yu et al., 2005; Yu et al., 2006].

5.3.2 Methods

5.3.2.1. Field Sites

Field campaigns, each approximately 1 month in duration, were carried out at Bondville, Illinois (February 2003), San Gorgonio Wilderness Area, California (April 2003 and July 2004), Grand Canyon National Park, Arizona (May 2003), Brigantine National Seashore, New Jersey (November 2003), and Great Smoky Mountains National Park, Tennessee (July–August 2004). Bondville was chosen because of its historically high winter nitrate concentrations. The San Gorgonio site, located in the San Bernardino National Forest east of Los Angeles, historically has the highest NH_4NO_3 concentrations among all IMPROVE sites [Malm et al., 1994]. Grand Canyon was selected to represent sites in the southwestern United States, and a spring measurement period was selected as a period when fine particle nitrate concentrations are typically higher in the IMPROVE data record.

The Brigantine site was selected to represent a rural location on the Atlantic seaboard, where nitrate is historically high in autumn and where sea salt may be an important aerosol constituent. The final study at Great Smoky Mountains National Park was designed to evaluate ammonium loss under polluted summertime conditions when the local aerosol is usually strongly acidic.

5.3.2.2. Sampling and Analysis Protocol for Filter Comparisons

During the campaigns, 24-hour samples were collected daily at 8:00 a.m. local standard time. The annular denuder/filter pack systems (URG-3000C) used in the study were manufactured by University Research Glassware Inc. A schematic diagram of the three denuder/ filter pack sampling train configurations is shown in Yu et al. [2005], Figure 1. Three sampling configurations were chosen to allow for comparisons between two extraction methods for nylon filters and between nylon and Teflon filters.

Denuders were cleaned and coated daily. All filters were handled in an ammonia-free glove box, an enclosed Plexiglas box with an ammonia scrubber (Perma Pure Inc.). Denuders were extracted using 10 ml of deionized water immediately in the field, and the aliquots were refrigerated before IC analysis. Filters were stored in clean sample tubes in a freezer inside clean

Ziploc bags with ammonia-removing towels (1% phosphorous acid) until extraction. For the first sampling train configuration, the front nylon filter was extracted using 5 ml of deionized water for 30–45 min in an ultrasonic bath. The backup nylon filter was extracted ultrasonically using a 5 ml 1.8mM Na_2CO_3/1.7mM $NaHCO_3$ solution (anion IC eluent) to recover collected nitric acid volatilized from the first filter. From the second sampling train configuration, the nylon filter was extracted using the Na_2CO_3/$NaHCO_3$ solution to compare with nylon filters extracted using deionized water. From the third configuration, the Teflon filters were extracted using deionized water and sonication. Then, 50 µl ethanol was added to wet the hydrophobic Teflon filter surface before extraction [Wolfson, 1980]. The extracts were analyzed by IC for both anions and cations.

5.3.2.3. Sampling and Analysis Protocol for Denuder Comparisons

At each site, five IMPROVE ion modules were operated, each with a different denuder configuration: 1) a freshly coated denuder, 2) a denuder that had operated for a year at Joshua Tree National Monument (and was exposed to high levels of nitric acid during that time), 3) an anodized aluminum denuder with no coating, 4) a Na_2CO_3-coated denuder without glycerin, and 5) no denuder. For the module with no denuder, the bare aluminum surfaces of the inlet tube and rain shield could remove some nitric acid.

The freshly coated denuder represents an IMPROVE site immediately after annual maintenance. The used denuder was selected to represent a worst-case exposed denuder at the end of its annual cycle. The denuder without glycerin was used in the IMPROVE network prior to summer 1996. Bare aluminum denuders and the bare aluminum surfaces of sampler inlets have been shown to collect nitric acid, so these configurations were included to complete the test. Filters were subsequently analyzed by IC according to IMPROVE standard operating procedures.

5.3.3 Conclusions

5.3.3.1. Particulate Nitrate Measurement Using Nylon Filters

Five field experiments were conducted at selected IMPROVE aerosol monitoring sites to examine issues related to sampling of aerosol ammonium nitrate. Different annular denuder/filter pack configurations were utilized to evaluate measurement precision, the efficiency of NO_3^- extraction from nylon filters by deionized water, and losses of particulate NO_3^- from denuded nylon and Teflon filters.

Deionized water was observed to be as efficient as a basic carbonate/bicarbonate solution in extracting particulate NO_3^- sampled on nylon filters in all five of the campaigns. Laboratory study of the filter extraction procedure indicated that sonication is probably needed to ensure complete recovery of NO_3^- collected on the filter.

$PM_{2.5}$ NO_3^- loss from denuded nylon and Teflon filters was examined in each field campaign as well. NO_3^- losses from denuded nylon filters were extremely small (<1%) at all of the sites, confirming the utility of nylon filters for providing a single-filter sampling solution for measurement of fine particle anion concentrations. As expected, significant NO_3^- losses occurred from the denuded Teflon filters, with average losses of 18% at Bondville, 45% at San Gorgonio

in April, 42% at Grand Canyon, and 52% at Brigantine. Some correlation was observed between the fraction of NO_3^- lost and the daily variation in temperature and RH, as well as the fraction of ambient N(V) in the gas phase.

This work represents an important evaluation of the efficiency of deionized water extraction of particulate NO_3^- collected on nylon filters at a variety of nonurban locations and seasons where NO_3^- composes a significant fraction of fine particle mass. It also adds to the existing body of literature on the magnitude of NO_3^- volatilization from denuded Teflon filters, while confirming the efficiency of nylon filters in preventing NO_3^- loss through recapture of volatilized HNO_3.

5.3.3.2. Loss of Fine Particle Ammonium from Denuded Nylon Filters

Ammonium loss from denuded nylon and Teflon filter media was examined in the same five rural field studies. The degree of ammonium loss from denuded nylon filters varied between campaigns, ranging from an average of 10% in Bondville, Illinois, in February to 28% in San Gorgonio, California, in July. Ammonium losses from denuded Teflon filters were generally somewhat lower than observed for nylon filters, possibly reflecting higher pressure drops across nylon filters. Losses of ammonium tended to increase with increasing diurnal temperature and relative humidity swings, although these relationships were often weak. Ammonium loss also increased with the degree of gas-particle equilibrium perturbation caused by upstream removal of gaseous ammonia, as predicted by previous investigators. For sampling approaches where ammonia is not denuded upstream, losses are probably lower than observed here, although positive artifacts resulting from ammonia collection by acidic particles can be problematic in this approach.

Although NH_4NO_3 volatilization is typically considered the major source of ammonium loss, observations in Great Smoky Mountains National Park indicate that more ammonium is lost than can be explained by this mechanism. It is hypothesized that organic ammonium salts, such as ammonium oxalate, may also contribute to observed losses of ammonium from filter media. Relatively large amounts of oxalate and succinate were observed in Great Smoky Mountains National Park particle extracts where ammonium losses exceeded aerosol nitrate concentrations.

While loss of nitrate was demonstrated to be negligible from denuded nylon filters, loss of ammonium cannot be ignored and should be considered in future sampling system design. One possible remedy is to capture volatilized ammonia with a backup acid-coated filter or denuder, an approach often used in intensive research air sampling efforts. The costs of implementing such a solution for existing large monitoring networks, however, could be substantial.

5.3.3.3. Efficiency of IMPROVE Network Denuders for Removing Nitric Acid

The denuder used in the IMPROVE network operates efficiently to remove nitric acid during the 1-year period it remains in the field. The sodium carbonate coating is not necessary for proper operation in most cases, nor is glycerin required to maintain efficiency. It is possible that a denuder exposed to 2-years' equivalent of IMPROVE sampling would show reduced efficiency for removing nitric acid, but it is not clear that this is the case.

REFERENCES

Ashbaugh, L. L., C. E. McDade, W. H. White, P. Wakabayashi, J. L. Collett Jr., and X-Y Yu (2004), Efficiency of IMPROVE network denuders for removing nitric acid, Regional and Global Perspectives on Haze: Causes, Consequences and Controversies-Visibility Specialty Conference, Air & Waste Management Association, Asheville, NC, October 25-29.

Chow, J. C., J. G. Watson, L.-W. A. Chen, M.-C. O. Chang, and G. Paredes-Miranda (2005), Comparison of the DRI/OGC and Model 2001 thermal/optical carbon analyzers, http://vista.cira.colostate.edu/improve/Publications/GrayLit/013_CarbonAnalyzer/IMPROVECarbonAnalyzerAssessment.pdf.

Malm, W. C., J. F.Sisler, D. Huffman, R.A. Eldred, and T. A. Cahill (1994), Spatial and seasonal trends in particle concentration and optical extinction in the United States. *Journal of Geophysical Research Atmospheres 99* (D1), 1347–1370.

McDade, C. (2004), Summary of IMPROVE Nitrate Measurements, internal report.

Rice, J. A. (1995), Mathematical Statistics and Data Analysis, Duxbury Press, Belmont, CA.

U.S. EPA (2000), EPA quality manual for environmental programs, Office of Environmental Information Quality Staff, Washington, D.C.

U.S. EPA (2003), Guidance for Tracking Progress under the Regional Haze Rule, Office of Air Quality Planning and Standards, Research Triangle Park, NC.

Wolfson, J. M. (1980), Determination of microgram quantities of inorganic sulfate in atmospheric particulates, *Journal of the Air Pollution Control Association 30*(6), 688–690.

Yu, X., T. Lee, B. Ayres, S. M. Kreidenweis, W. C. Malm, and J. L. Collett, Jr. (2005), Particulate nitrate measurement using nylon filters, *J. Air Waste Manage. Assoc.*, *55*, 1100-1110.

Yu, X., T. Lee, B. Ayres, S. M. Kreidenweis, W. C. Malm, and J. L. Collett Jr. (2006), Loss of fine particle ammonium from denuded nylon filters, *Atmospheric Environment, 40*, 4797–4807.

CHAPTER 6: SPECIAL MONITORING STUDIES & DATA ANALYSES ASSOCIATED WITH THE IMPROVE PROGRAM

The results of four special studies conducted in association with the IMPROVE program are summarized here. The Big Bend Regional Aerosol and Visibility Observational (BRAVO) study is summarized in section 6.1 with details available in the full report available at http://vista.cira.colostate.edu/improve/Studies/BRAVO/Studybravo.htm and in associated journal articles. The Yosemite Aerosol Characterization Study (YACS) is summarized in section 6.2, details can be found on the web at http://vista.cira.colostate.edu/improve/Studies/YACS/studyYACS.htm and in associated journal articles. Section 6.3 summarizes the findings from the review of the improve equation for estimating ambient light extinction coefficients, the details are available in the full report at http://vista.cira.colostate.edu/improve/Publications/GrayLit/016_IMPROVEeqReview/IMPROVEeqReview.htm and in associated journal articles. The results of a coarse mass speciation study are included in section 6.4.

6.1 EXECUTIVE SUMMARY: BIG BEND REGIONAL AEROSOL AND VISIBILITY OBSERVATIONAL (BRAVO) STUDY RESULTS: AIR QUALITY DATA AND SOURCE ATTRIBUTION ANALYSES RESULTS FROM THE NATIONAL PARK SERVICE / COOPERATIVE INSTITUTE FOR RESEARCH IN THE ATMOSPHERE

Big Bend National Park is located in southwestern Texas along the Mexican-Texas border (Figure 6.1). During the 1990s, the haze at Big Bend and other sites in west Texas and southern New Mexico increased, further obscuring Big Bend's and nearby regions scenic beauty. In response to the increased haze, the Big Bend Regional Aerosol and Visibility Observational (BRAVO) study was conducted. This was an intensive monitoring study sampling aerosol physical, chemical, and optical properties, as well atmospheric dispersion using synthetic tracers from July through October 1999. The monitoring was followed by a multiyear assessment of the causes of haze in Big Bend National Park, Texas, with the primary purpose to identify the source regions and source types responsible for the haze at Big Bend. Secondary research objectives of the study were to learn more about the chemical, physical, and optical properties of aerosols responsible for haze. BRAVO study participants include the National Park Service (NPS), the U.S. Environmental Protection Agency (EPA), the Texas Commission on Environmental Quality (TCEQ), and the Electric Power Research Institute (EPRI), among others.

In support of BRAVO, the NPS and Cooperative Institute for Research in the Atmosphere (CIRA) at CSU analyzed the measured aerosol data to better understand the chemical, physical, and optical properties of Big Bend's haze, and conducted a number of complementary qualitative and quantitative haze source apportionment analyses. All source apportionment techniques went through extensive validation and evaluation tests and only those techniques which passed these tests were applied to Big Bend's haze. In addition to the analysis of the BRAVO study data, long-term Big Bend air quality and meteorological data were analyzed to determine the representativeness of the BRAVO time period to other seasons and years.

This Executive Summary summarizes the key findings from the analyses and their implications concerning Big Bend's haze with a focus on the apportionment of particulate sulfate and its contribution to Big Bend's haze. The body of this technical report provides detailed descriptions of the methods, evaluation and validation procedures and results from the multiple analyses employed by the NPS/CIRA group and the reconciliation between all source attribution techniques.

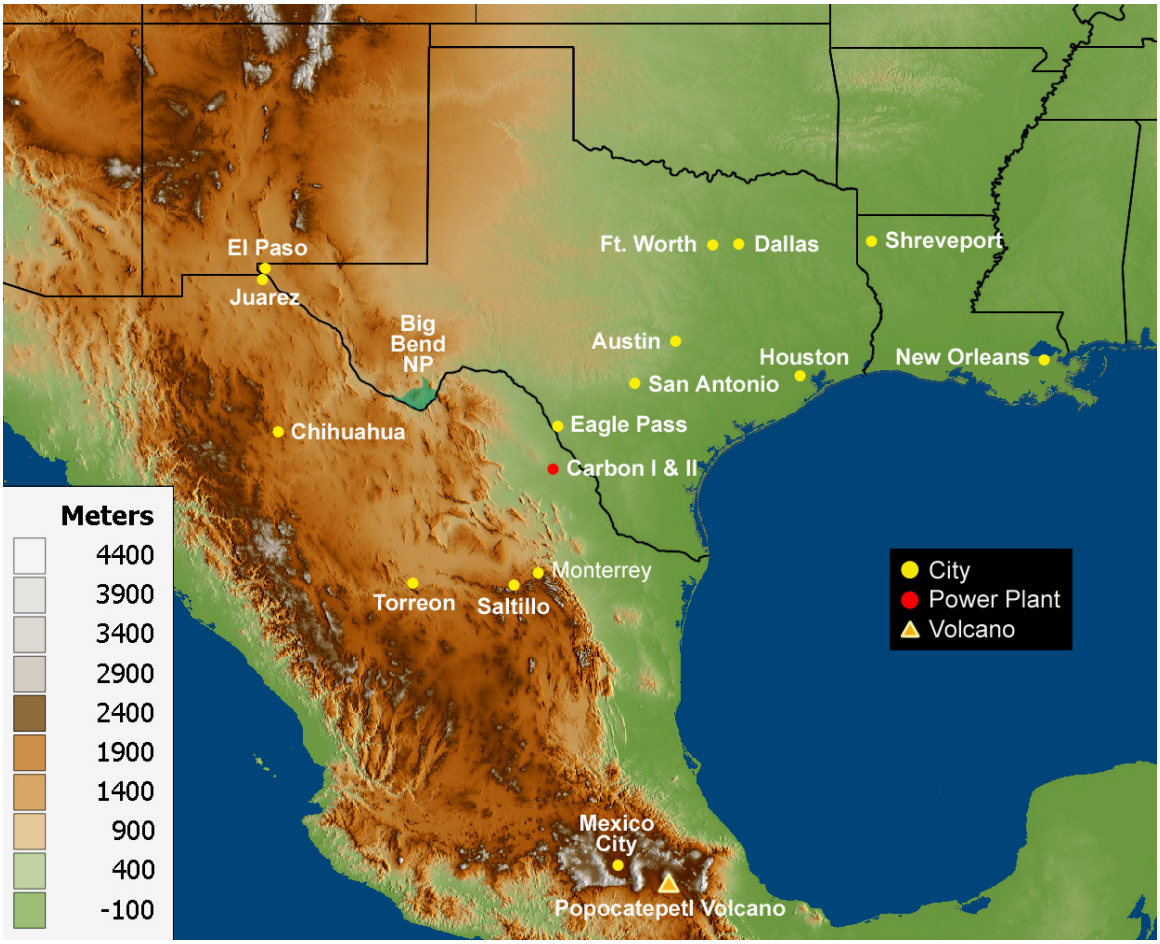

Figure 6.1. A terrain map of Texas and Mexico as well as some major cities and points of interest from the BRAVO study.

6.1.1 Characterization of Big Bend's Haze

Haze is caused by scattering and absorption of light by suspended fine liquid or solid particles in ambient air, known collectively as atmospheric aerosol. The sum of the light scattering and absorption is known as the light extinction and can be thought of as the fraction of light lost per unit of distance. The units of light extinction are inverse distance, e.g., 1/(million meters) or Mm^{-1}. Higher light extinction levels correspond to hazier conditions.

Detailed particle size and chemical composition measurements made at Big Bend during the BRAVO study were used to develop advanced estimates for each day's contributions to light extinction by the major aerosol components. These compare well to direct optical measurements of light scattering and light extinction. Figure 6.2 shows the daily particulate light extinction (sum of light scattering and absorption) contributions by the major aerosol components. As shown, there is a distinct difference in the particulate extinction budget in the first and second half of the BRAVO study. From July 1–August 15, the light extinction is primarily due to ammoniated sulfates (35%), organics (20%), and coarse mass (30%). In the second half of the study, post-August 15, the ammoniated sulfates account for 50% of the particulate extinction

while organics and coarse mass each account for about 20%. On the haziest 1/5th of the days, sulfate compounds accounted for about 55% of the particulate b_{ext} and organics 15%.

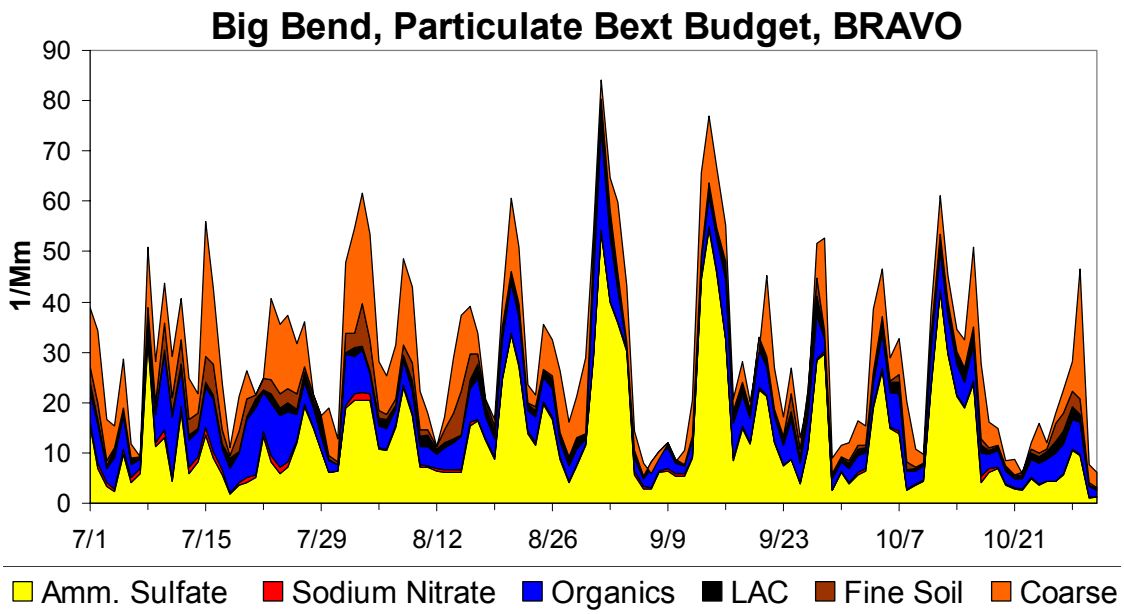

Figure 6.2. Big Bend's particulate light extinction budget during BRAVO.

The BRAVO period can be put into a larger climatological context by examining Big Bend's extinction budget over a long time period. Figure 6.3 shows the five-year (1998 through 2002) light extinction budget from measurements made every three days at Big Bend National Park in the IMPROVE monitoring network. In general, there are two periods of high haze at Big Bend National Park – one in spring when particulate sulfate and carbonaceous compounds contribute in similar amounts to haze and another in late-summer/fall when particulate sulfate compounds are the largest contributors to haze. Similar to the BRAVO period, the particulate sulfate compounds usually contribute more to haze than any other individual aerosol component. Carbonaceous particulate matter – organic compounds and light absorbing carbon (LAC) – generally constitute the second largest individual aerosol component contributing to haze at Big Bend National Park and on some days are the single largest contributor to haze. Information from other studies shows that during late spring episodes, concentrations of carbonaceous compounds are increased due to biomass burning in Mexico and Central America. Dust, represented by a combination of fine soil and coarse mass, contributes as much to haze as particulate sulfate compounds during the months of March and April.

On average, sulfate compounds contribute more to light extinction on the haziest days (53%) than for average days (48%). The contribution of carbonaceous (i.e., organic and light absorbing carbon) compounds to light extinction remained the about the same at 23% on average and the haziest days. The coarse mass is also a major contributor to the particulate light extinction, accounting for about 17% of the particulate light extinction on average and 15% on the haziest days. Since the sulfates accounted for more than half of the particulate extinction on the highest haze days, the lower contribution of organics and the fact that they have a potentially large contribution from smoke and other natural sources lead us to concentrate on understanding the source attribution of sulfate.

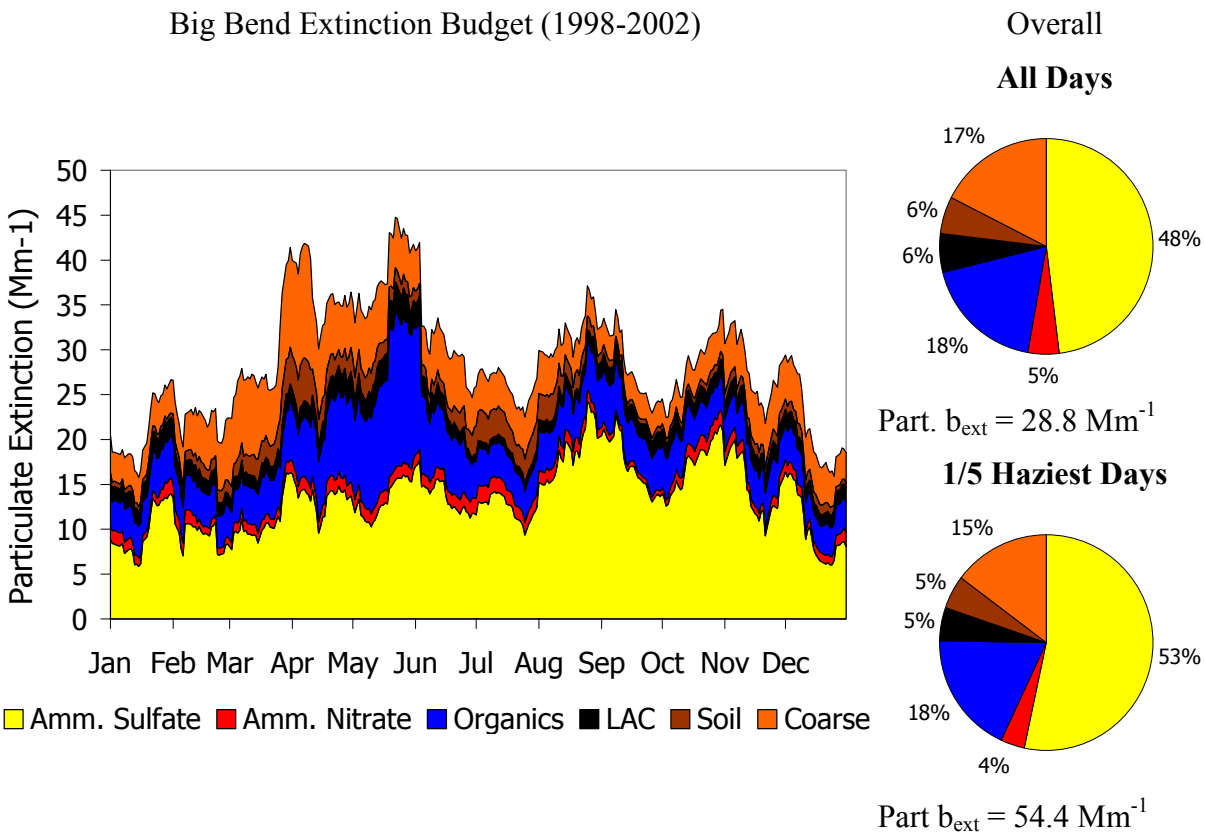

Figure 6.3. Big Bend National Park five-year light extinction budget. All days with that fall on the same day of the year were averaged together, then the data were smoothed using a 15-day moving average.

6.1.2 Apportionment of Big Bend's Sulfate Haze

Ambient particulate sulfate compounds result from direct emissions of sulfate (primary sulfate) or are produced by chemical transformation (oxidation) of SO_2 emissions in the atmosphere (secondary sulfate). Secondary sulfates constitute most of the particulate sulfate compounds measured at ambient monitoring sites, such as Big Bend National Park. The extent of the oxidation of SO_2 to secondary sulfate depends on the oxidative capacity of the atmosphere, which is influenced in large part by nitrogen oxides (NO_x) and volatile organic carbon emissions. Oxidation of SO_2 to sulfate can be slow, often requiring one to two days to convert about half of the SO_2 to particulate sulfate compounds. However, this extent of transformation can occur much more rapidly, from a few hours to several minutes, in the presence of mists, fogs, and clouds. Meanwhile, atmospheric dispersion and deposition processes are reducing the ambient SO_2 and sulfate concentrations during transport from emission sources to distant monitoring locations. Consequently, it is typically challenging to establish causal relationships between measured ambient particulate sulfate concentrations and SO_2 emissions sources.

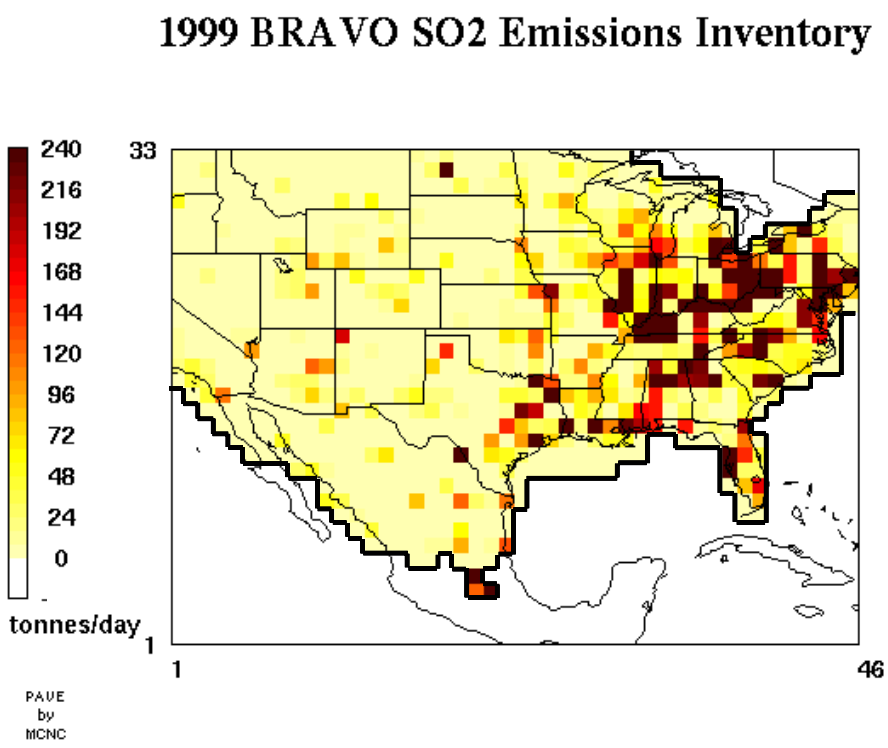

Figure 6.4. (Left) SO_2 emissions based on the 1999 BRAVO emissions inventory used in the REMSAD and CMAQ-MADRID modeling. No emissions were included beyond the black outline shown in the figure. Mexico City and Popocatepetl volcano emissions are located in the three most southern emission grid cells.

Figure 6.4 presents the SO_2 emission inventory used in the BRAVO study. As noted on the map the BRAVO study emission inventory did not include sources in southern Mexico (except for Mexico City and the Popocatepetl volcano), Cuba, or other Caribbean islands. Effects of sources outside of the modeling domain, beyond the frames of Figure 6.4, were accounted for in BRAVO study modeling by use of four-month average boundary conditions obtained from global model simulations. The largest SO_2 emissions are in the eastern United States where about 14 million tonnes/year are emitted. In Texas approximately 1 million tonnes of SO_2 are emitted each year, almost all in eastern Texas, and the western U.S. emissions are about 1.7 million tonnes/year. In Mexico, SO_2 emissions are estimated to be about 2.5 million tonnes/year, with 1.5 million tonnes/year from the Popocatepetl volcano. There are a few high-emitting locations in northern Mexico, including the Carbón I & II coal-fired power plants located about 200 km east-southeast of Big Bend and at urban and industrial areas near Monterrey in northeastern Mexico.

U.S. SO_2 emission inventories have been in development for over 30 years, and in the 1990s continuous emission monitors were placed into the largest SO_2 point sources. Therefore the U.S. SO_2 emission inventory is considered to be of a high quality. However, less information was available about the Mexican SO_2 emissions and significant uncertainties in the inventory remain. For example, a recently produced emission inventory for Mexico differs from the BRAVO emissions inventory for SO_2 emissions, with emissions by as much as a factor of two larger in some regions. In addition, uncertainties in Carbón SO_2 emissions exist and emissions of 154,000 and 245,000 tonnes/year were used.

The Popocatepetl volcano in central Mexico near Mexico City has been active for a number of years including during the BRAVO study period and is the largest single SO_2 emissions source in North America. Limited modeling of the flow of its emissions indicated that it likely had little effect on Big Bend haze during the BRAVO study period. The effects of emissions from southern Mexico, Cuba, and other areas outside of the BRAVO study emissions inventory are also thought to be small at Big Bend.

6.1.2.1. Spatial Patterns of Aerosol Components

Examination of the spatial and temporal patterns in several fine particulate species, including sulfate, measured during BRAVO suggests that there are unique sources for different aerosol types and that transport patterns are seasonal with more transport from Mexico to southern Texas during the summer than during the fall and conversely more transport from the eastern United States during the fall than during the summer. These findings are consistent with the back trajectory analyses. Sulfate concentrations at Big Bend were highest during four episodes, September 1 and 2, 14 and 15, October 12, and August 22. The four episodes were characterized by different trace element concentrations and different spatial patterns in sulfate, indicating differing contributions from different source types for each episode. Sulfate concentrations measured within a few hundred km are generally highly correlated in time, but measurements in southwestern Texas were not highly correlated with measurements in northeast Texas, and different regions of the state also had different seasonal patterns in sulfate concentrations, indicating they are influenced by different sources. Highest sulfate concentrations measured during BRAVO were in northeast Texas during the summer, while highest concentrations at Big Bend were during the fall. Spatial patterns in sulfate concentrations show influence from the Carbón I & II power plants, especially north and west of the plants, though the contribution is not quantifiable by these analyses.

Spatial and temporal patterns in the iron concentrations and the abrupt drop in Al/Ca ratios from summer to fall are evidence of Saharan dust episodes during the summer.

The trace element most associated with sulfur at Big Bend is selenium, which is usually associated with coal combustion. Selenium concentrations were highest in northeast Texas, with evidence of selenium sources within the state, at the Carbón I & II plants, and possibly entering Texas from the east.

6.1.2.2. Airmass Transport to Big Bend during BRAVO Days with High and Low Particulate Sulfate Concentrations

All other things being the same, a source region's potential to contribute to haze at Big Bend increases for time periods when air parcels frequently pass over and spend more time over the source region prior to transport to Big Bend. These airmass transport characteristics can be estimated from trajectories, where a trajectory gives the estimated location of air parcels every hour prior to their being transported to Big Bend. Residence time analysis is used to aggregate the number of air parcels that resided over an area for selected periods of time at Big Bend (e.g., a month) or selected receptor site conditions (e.g., haziest days at Big Bend). This is related to the aggregate of time all trajectories resided over a given area. While the residence time is dependent on airmass transport frequency from a given region to Big Bend and the time it spends

over the region, it has been shown that the difference in the residence time from one region to another is primarily dependent on different transport frequencies.

On days with the 20% highest particulate sulfur concentrations during the BRAVO study, air parcels were most likely to have previously resided over northern Mexico, Texas, and the eastern United States (Figure 6.5a). These tended to be low-level and low-speed air parcels, which are conducive to the accumulation of pollutants from sources. In contrast, on days with the 20% lowest particulate sulfate concentrations, air parcels were most often previously over northern Mexico and the Gulf of Mexico as well as over the western United States and infrequently over eastern Texas or the eastern United States (Figure 6.5b). The transport over Mexico tended to be low level but high speed, which is not conducive to the accumulation of emissions into the air parcels.

The examination of transport pathways during individual particulate sulfate episodes showed that there were three common pathways associated with elevated sulfate at Big Bend, from eastern Texas, the southeastern United States., and northeastern Mexico (Figure 6.6). The largest concentrations occurred when transport over several of these regions occurred. For example, the September 1 episode had transport over all three regions and had the highest concentrations during the BRAVO study. Elevated sulfate was also associated with prior transport over the Midwest (Missouri, Kentucky, and Tennessee), though this was infrequent and airmasses tended to be elevated and had higher speeds relative to the other three regions.

These results show that the transport from eastern Texas and the southeastern United States is associated with elevated sulfate concentrations at Big Bend and is not associated with low sulfate concentrations. These results, combined with the fact that eastern Texas and the Southeast have high sulfur dioxide emissions, support the notion that these areas contribute to the sulfate concentrations and haze at Big Bend. Northeastern Mexico appears to be a common transport pathway during both high and low sulfate days. However, the time airmasses spend over northern Mexico prior to reaching Big Bend is greater on the high sulfate days than the low sulfate days. The increased time allows for potentially greater accumulation of SO_2 emissions and time for transformation to sulfate.

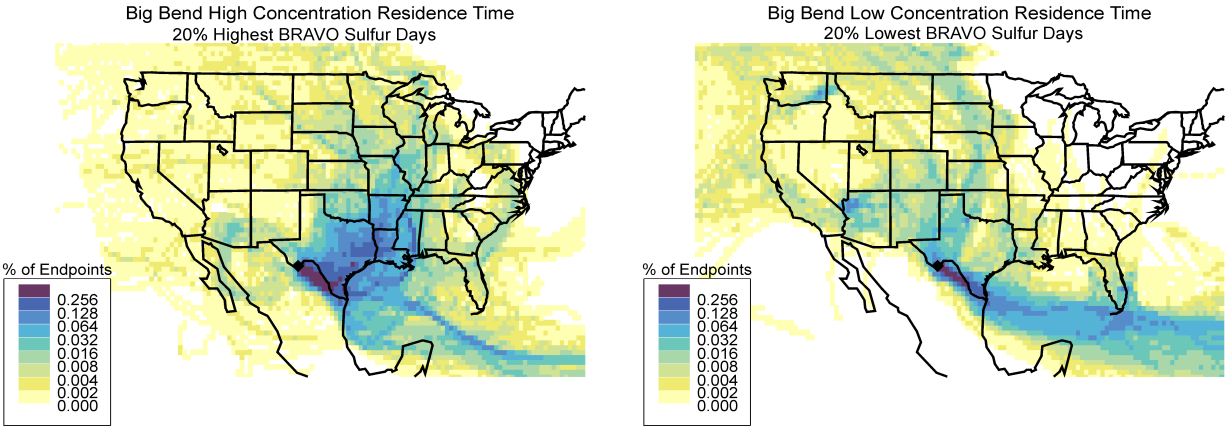

Figure 6.5. Fraction of time that air parcels spent during ten-day trajectories for periods with the a) 20% highest concentrations of particulate sulfate compounds and b) for the periods with the 20% lowest concentrations of particulate sulfate during the BRAVO study period July through October 1999.

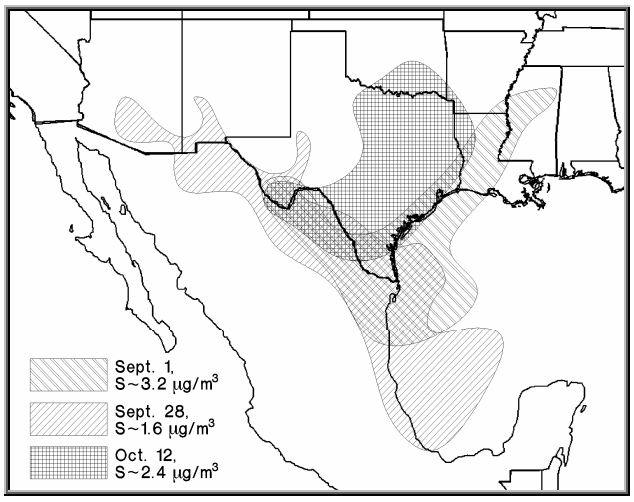

Figure 6.6. Airmass transport patterns to Big Bend, TX, during three sulfate episodes. Each isopleth shows the most likely pathway the airmass traversed prior to impacting Big Bend.

6.1.2.3. Quantitative Source Apportionment of Big Bend's Sulfate Haze

NPS/CIRA employed numerous methods to identify the source types (e.g., power plants) or source regions (e.g., Texas, the eastern United States, the western United States, and Mexico) that contribute to the particulate sulfate compounds that influence Big Bend haze and to estimate the magnitude of their contributions. The techniques fall into three categories, receptor-oriented modeling, source-oriented modeling, and hybrid modeling combining features from both source and receptor modeling.

Airmass-History-Based Receptor Models: Several airmass-history-based receptor analysis methods were used for source attribution. These methods developed statistical relationships between the Big Bend particulate sulfate concentrations and airflow prior to reaching Big Bend. Variations of the trajectory methods included the use of two methods of estimating wind over North America (EDAS from the National Weather Service and MM5 applied specifically for the BRAVO study) and the use of back-trajectories from Big Bend employed in Trajectory Mass Balance (TrMB), and forward transport and dispersion from all potential source regions used in Forward Mass Balance Regression (FMBR).

Extensive testing of TrMB and FMBR applied to both sets of wind information showed adequate overall performance when used to attribute artificial tracer released as part of the BRAVO study. Additional evaluations showed that these airmass history regression models were accurate within their stated precision when applied to synthetic sulfate concentration with known attribution results. Only the combination of airmass history model and meteorological data inputs that passed these evaluations was used for attribution of measured sulfate.

An inherent characteristic of these techniques is the estimation of the average relationship between air transport from an area and that area's contribution to sulfate. Therefore, these techniques were used only for estimating average attributions. These techniques are subjected to increased uncertainties due to collinearity of transport from multiple source regions. For example, transport from the eastern United States typically traversed Texas in route to Big Bend. In addition, other issues can bias the results. For example, it was found that FMBR tended to

enhance attributions to nearby source regions and reduce attribution from more distant source regions.

Regional Air Quality Source-Oriented Models: The REMSAD regional air quality model was used to estimate the effects of transport, dispersion, chemical transformation, and deposition on emissions, and thereby to predict particulate sulfate concentrations throughout the modeling domain, including at Big Bend. The difference in predicted concentrations between air quality model prediction with all emissions (base case) and those with emissions for a specific source or source region set to zero (emissions sensitivity case) is interpreted as the particulate sulfate attributed to the specific source or source region. The CMAQ-MADRID air quality model was also operated by EPRI and Atmospheric and Environmental Research (AER).

Eulerian air quality models are limited by the soundness of emissions and meteorological data, as well as the accuracy of transformation, deposition, dispersion, and other numerical algorithms. Biases and uncertainties identified in any of these processes can adversely affect their source attribution estimates. The Eulerian models were tested against the BRAVO tracer data to evaluate their capability of simulating dispersion in Texas where it was found that they could reproduce the tracer concentrations within the inherent uncertainty of the tracer data. Also, the simulated sulfate and SO_2 concentrations and sulfate apportionments were extensively compared to measured data. It was found that both models tended to underestimate particulate sulfate compound concentrations in the first half of the BRAVO study period when sources in Mexico were determined to have the largest contribution. Both models also tended to overestimate particulate sulfate concentrations when flow was from the eastern United States.

Hybrid Modeling - Synthesis Inversion Analysis of Air Quality Models: Concerns about possible systematic biases that could be the result of Mexico's SO_2 emissions and/or transformation chemistry biases resulted in the development of a hybrid modeling approach. This approach entailed the development of statistical relationships between the daily source attribution results from REMSAD and CMAQ-MADRID and the measured particulate sulfate concentrations in and around Big Bend.

The synthesis inversion technique was unable to resolve distant source regions with small source contributions. To minimize problems caused by this behavior, attribution results for these sources were held close to their originally modeled values. Thus, any sulfate that may have been improperly attributed to small distant sources by the Eulerian models runs was most likely attributed to source regions near Big Bend in the synthesized method. The technique also systematically underestimated the measured sulfate data. It is not known if this underestimation impacts one source region more than another.

It was determined that Synthesized CMAQ-MADRID combined with the attribution of Carbón power plants from Synthesized REMSAD provided the best available estimates of the source attribution for particulate sulfate at Big Bend during the BRAVO study period, henceforth referred to as the BRAVO Estimate.

Figure 6.7 shows the study period-averaged attribution results for nine methods as well as the BRAVO Estimate results. CMAQ-MADRID and Synthesized CMAQ-MADRID attribution did not include the Carbón power plants. TAGIT was a source attribution technique employed

by the Desert Research Institute (DRI) to attribute Carbón power plants' contribution to Big Bend's sulfate.

As shown in Figure 6.7, during the BRAVO study period U.S. sources contributed to about 55% (BRAVO Estimate) of the particulate sulfate at Big Bend, with a range among methods of 44% to 67%. The Mexico sources contributed about 38% of Big Bend's particulate sulfate, with a range among methods of 23% to 55%. The eastern United States was the largest U.S. contributor at ~30%, followed by Texas at ~17%, and the western United States at ~9%, with ranges among the methods of 16% to 42%, 16% to 30%, and 0% to 14%, respectively. The Carbón power plants in Mexico contributed to about 20% of the particulate sulfate at Big Bend, more than any other single SO_2 emissions facility, with a range among the methods of 14% to 26%.

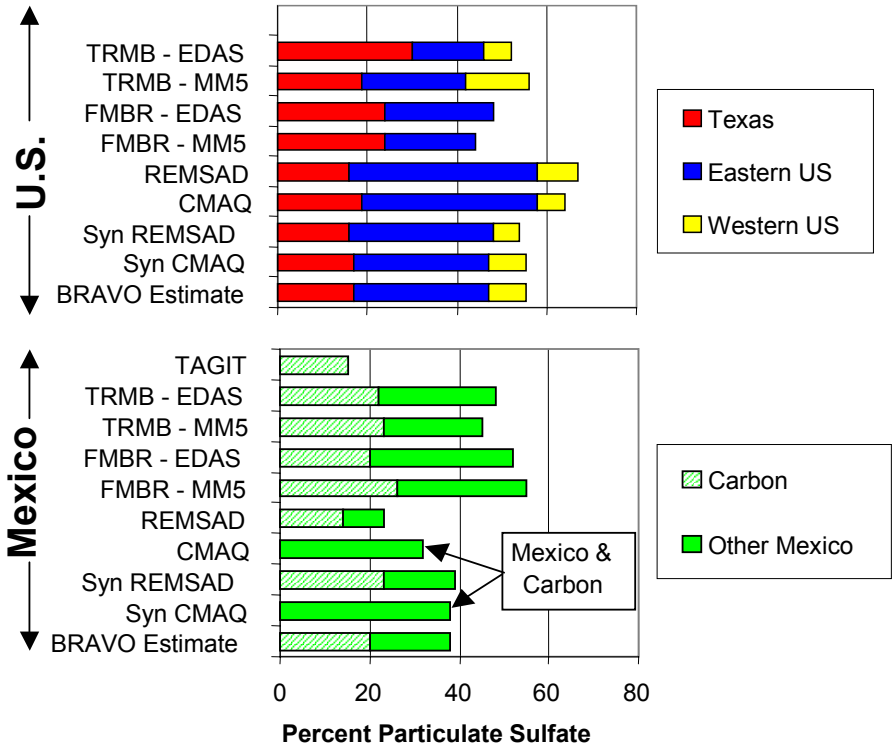

Figure 6.7. Estimates by several data analysis and modeling methods of the study-period averaged percent contributions to particulate sulfate at Big Bend by U.S. and Mexico sources. TAGIT only attributed the Carbón power plants, while CMAQ and Synthesized CMAQ attribution did not distinguish Carbón from Mexico.

Figure 6.8 presents a smoothed daily attribution using the BRAVO Estimate method. The top plot in Figure 6.8 shows attribution in absolute concentrations for direct comparison to the measured particulate sulfate concentrations, while the bottom plot shows the percent fraction of the predicted amount by each source region. As shown, each source region's contribution to Big Bend particulate sulfate had unique characteristics over the BRAVO study period. Sources in Mexico were the largest contributors to sulfate in July and August, contributing from 0.5 to 1.5 $\mu g/m^3$ every day. During the largest peak in late July, sources in Mexico contributed to about 2 $\mu g/m^3$, constituting about 90% of the modeled particulate sulfate. In September and October

contributions by sources in Mexico decreased to roughly less than 1 μg/m^3. Sources in Texas contributed very little to sulfate concentrations in July, with three episodes in the middle months of the study period having peak values from about 0.8 to 1.5 μg/m^3. During two episodes in October, sources in Texas had peak contributions of about 1.2 to 2.8 μg/m^3 of particulate sulfate and constituted to over 60% of the largest peak in October. Sources in the eastern United States contributed to sulfate concentrations mostly in the middle two months of the study period with several peak contributions exceeding 1 μg/m^3. The largest of these contributions is greater than 5 μg/m^3 and constitutes about 80% of the largest peak particulate sulfate measured during the BRAVO study period.

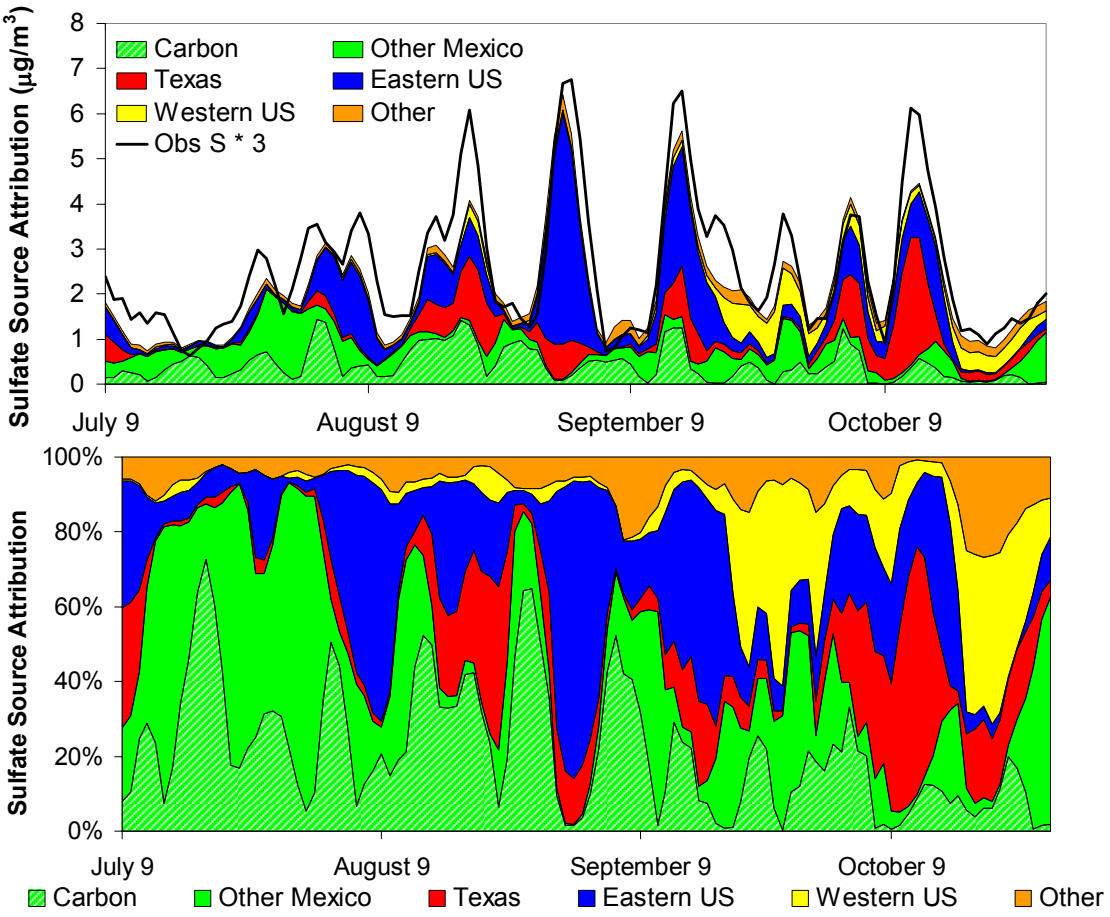

Figure 6.8. Smoothed daily estimates by source regions to particulate sulfate concentration (top plot) and fraction of total predicted particulate sulfate (bottom plot) at Big Bend during the study period.

6.1.2.4. The Contribution of Sulfur Source Regions to Particulate Haze Levels at Big Bend National Park during the BRAVO Study Period

Both the fraction of light extinction associated with particulate sulfate (see Figure 6.2) and the fraction of particulate sulfate attributed to each source region (see Figure 6.8) varied considerably throughout the BRAVO study period. This information was combined to show variation in the absolute and percent fractional contribution by sulfur source regions to Big Bend light extinction (shown in the top and bottom plots of Figure 6.9, respectively). Pie diagrams are shown in Figure 6.10 to illustrate the differences in particulate sulfate contributions by various

source regions to light extinction for the study period's 20% haziest days compared to the study period's 20% least hazy days. The numbers of 20% haziest days during each month of the BRAVO study from July through October are 1, 8, 10, and 4, respectively, while the numbers per month for the 20% least hazy days were 3, 1, 10, and 9, respectively.

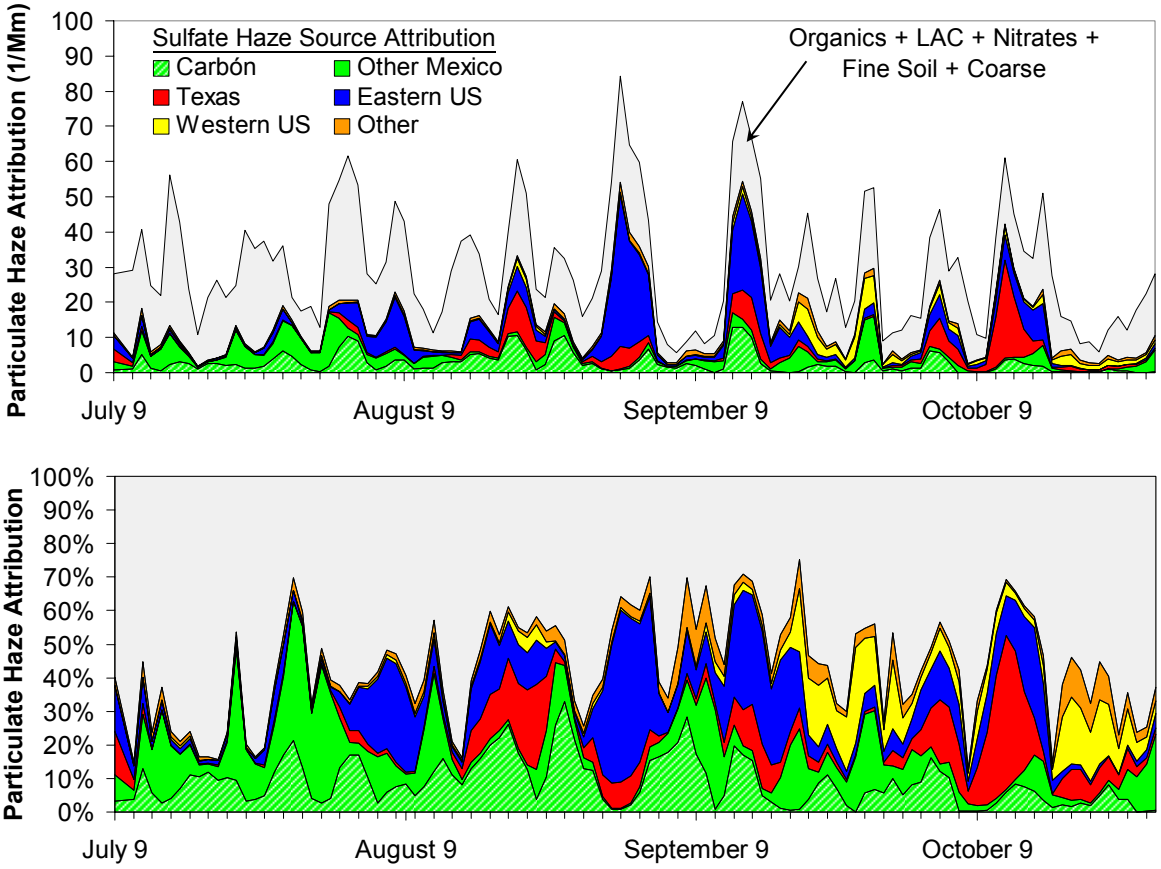

Figure 6.9. Estimated contributions to particulate haze by various particulate sulfate source regions. The top plot shows the absolute haze contributions by the various particulate sulfate sources as well as the total particulate haze level (black line). The bottom plot shows the fractional contribution to haze by the various sources.

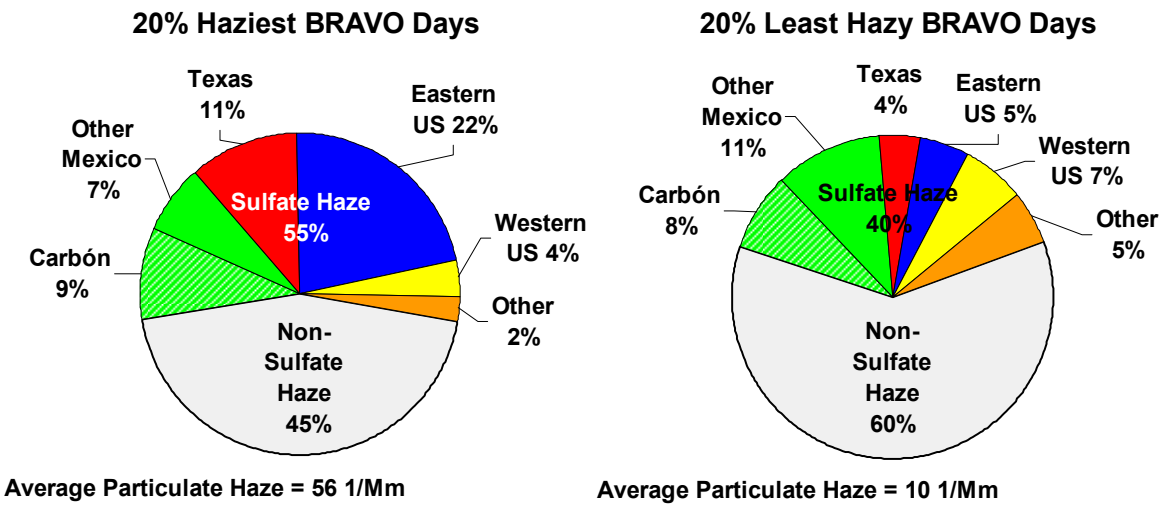

Figure 6.10. Estimated contributions by particulate sulfate source regions to Big Bend particulate haze levels for the 20% haziest days and the 20% least hazy days of the BRAVO study period.

The SO_2 sources in Mexico generally contributed a moderate 5 Mm^{-1} to 15 Mm^{-1} of the light extinction on most days during the study period, but during some of the minor haze episodes in July and August their relative contributions were 40% to 60% of the average particulate light extinction. SO_2 sources in Texas contributed to less than 5 Mm^{-1} on most days during the study period, but during one of the few periods of higher contribution these sources contributed to nearly 30 Mm^{-1}, corresponding to about 50% of the particulate light extinction on the haziest day in October. SO_2 sources in the eastern United States also contributed to less than 5 Mm^{-1} on most days during the study period, but during the two haziest episodes of the study period these sources contributed to about 50 Mm^{-1} and about 30 Mm^{-1}, respectively, corresponding to about 50% and 30% of the light extinction.

The sulfate contribution to particulate light extinction is higher on the haziest days compared to the least hazy days (55% compared to 40%). This increase in the sulfate contribution on the haziest days compared to the least hazy days is driven by increased relative contributions from the eastern United States and Texas. The relative contribution of sulfate on the haziest days from Texas increased by about a factor of 3 (4% to 11%), and from the eastern United States it increased by about a factor of 4 (5% to 22%) compared to the least hazy days. In contrast, the relative contributions for the Carbón I & II power plants remained about the same at 8% to 9%, and the contribution of other sources in Mexico decreased from 11% on the least hazy days to 7% on the haziest days. The relative contribution of sulfate sources in the western United States to Big Bend's sulfate haze also decreased from 7% on the least hazy days to 4% on the haziest days. These results are consistent with the observation that the Texas and eastern U.S. sources had their largest sulfate contributions during the highest sulfate episodes.

The nonsulfate haze is primarily due to dust (fine soil and coarse particles) and carbonaceous (organic and carbon) compounds. Compared to the least hazy days, the haziest days have a higher relative contribution to light extinction by dust (25% compared to 19%) and a lower relative contribution by carbonaceous particles (19% compared to 39%).

6.1.3 Application of the Source Attribution Results to Other Months and Years

In order to assess the applicability of haze attribution results for the BRAVO study to other years or other times of year, it is necessary to compare the four-month study period with the same months in other years and with other months of the year. Emissions and meteorology are the two most important factors that influence haze levels. Between 1999 and the present, the annual emissions responsible for particulate sulfate concentrations in North America have not appreciably changed (U.S. emissions have decreased about 15%, but less is known about emission trends in Mexico). Seasonal variations in SO_2 emissions and in the SO_2 to particulate sulfate oxidation rate make extrapolations of the BRAVO study results to other months of the year prone to additional uncertainty. One of the most influential meteorological processes affecting the haze at Big Bend is the airflow patterns that determine which potential source regions are upwind of Big Bend. In spite of the uncertainties inherent in such a simple approach, comparisons of the meteorological flow patterns from the residence time analysis were used alone in an attempt to assess the applicability of BRAVO study results to other years and times of year.

Residence time plots convey information about both the frequency of transport over potential source regions and its duration over the regions. However, it was shown that the residence time transport patterns are primarily driven by the variations in transport frequency over regions as opposed to duration variations. Consequently, a change that doubles the residence time over a source region for a specific month can be thought of as doubling the probability of influence of that source region during that month. In this example the monthly averaged contribution would likely double because the numbers of impacting periods would about double, but the amount of the peak impact is not expected to change much.

During the BRAVO study period, airflow to Big Bend was mostly similar to the airflow conditions during the five-year period. However, in September 1999 there was typically less flow over the eastern United States than for the five-year average, implying that the BRAVO results may underestimate the average haze contributions by that region's sources. In addition, during October 1999 there was typically more flow over Texas and less flow over Mexico, implying that the average October BRAVO haze contributions may be overestimated for Texas and underestimated for Mexico compared to the five-year average. While the estimated average contributions by these source regions may change, the peak contributions are likely not affected by the atypical frequency of flow.

Comparing the airflow patterns for the BRAVO study period to that of the other months of the year (Figure 6.11), it is evident that SO_2 sources in Mexico are likely to contribute less from November through March. This is because airflow across Mexico is less in general and is over lower emission density regions of Mexico to the west of Big Bend. SO_2 sources in Mexico are likely to be contributing to the particulate sulfate portion of the Big Bend haze during the months of April through June comparable to their contributions for the BRAVO study months of July and August. Sources in Texas are likely to contribute little to the particulate sulfate portion of the Big Bend haze for the months from November through June since the airflow is not frequently over the high emissions regions of east Texas, similar to July 1999. Eastern U.S. sources are unlikely to contribute to Big Bend haze during the months from November through March since airflow to Big Bend is rarely over that region during those months. During the

months from April to June, the eastern U.S. sources may contribute a modest amount to sulfate haze, comparable to that estimated for July and early August.

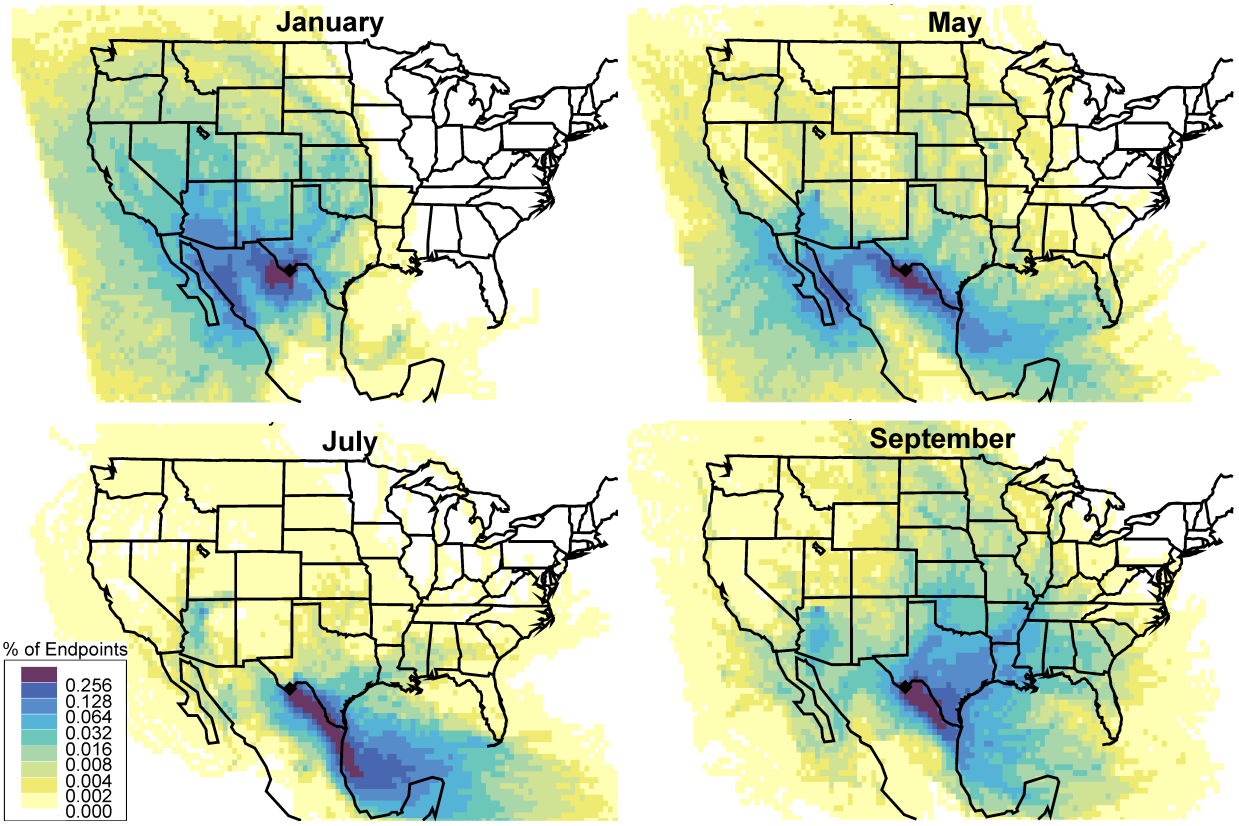

Figure 6.11. Examples of geographic distribution of the fraction of time that air parcels spend during the five days prior to arriving at Big Bend National Park for the months of January, May, July, and September based upon a five-year analysis period (1998 to 2002).

6.1.4 Implications

There is no single answer to the question of what sources are responsible for the haze at Big Bend National Park; sources in both the United States and Mexico are responsible. Mexican SO_2 emissions contribute to the sulfate haze most frequently, but to generate the haziest events that occur in the late summer and fall, contributions from Texas and the eastern United States must occur. The greatest individual contributor to haze is the Carbón I & II power plant in northern Mexico. Substantial changes of that facility's emissions would likely result in small but noticeable changes in haze levels on many days, but it would not make much difference to the worst haze episodes during late summer and early fall. To substantially affect all of the haze episodes during the late summer and fall where U.S. contributions are large at Big Bend will require SO_2 emission changes in both Texas and the eastern United States. Because of the high frequency of air transported to Big Bend from the southeast along a corridor on both sides of the Rio Grande River, emission changes there have a potential to affect haze levels at Big Bend, especially during June through September when transport from this region is most frequent.

The clearest days at Big Bend also had low sulfate concentrations. The visual scene on a clear day is more sensitive to small changes in haze than a hazy or moderately hazy day. These

days were primarily associated with contributions from the Carbón I & II power plants and other sources in northeast Mexico. Reduction in emissions from Carbón would likely result in creating more clear days. On the other hand, growth along this border region will likely further reduce the number of clear days.

6.2 EXECUTIVE SUMMARY: THE YOSEMITE AEROSOL CHARACTERIZATION STUDY

The Yosemite Aerosol Characterization Study (YACS) was an intensive field measurement campaign conducted by a number of U.S. research groups from 15 July to 4 September 2002 at Yosemite National Park (NP), California. This summary describes the major findings of the study in the context of outstanding issues related to the Regional Haze Rule and to visibility and air quality concerns specific to Yosemite NP.

Aerosol composition measurements have been conducted in Yosemite NP since 1988 as part of the Interagency Monitoring of Protected Environments (IMPROVE) network. The long-term data record (1988–2004) clearly shows a seasonal trend in organic aerosol mass concentrations, with peaks in the summer and early fall (Figure 6.12). The long-term Yosemite data show that organic carbon contributes between 40 and 60% of the monthly average fine aerosol mass. These fractions are much higher than most IMPROVE sites in the eastern United States. Not only the total fine particulate mass concentration, but also the fraction attributable to organic species, increases during summer and fall. Furthermore, the variability in organic aerosol mass concentrations becomes much larger in those seasons.

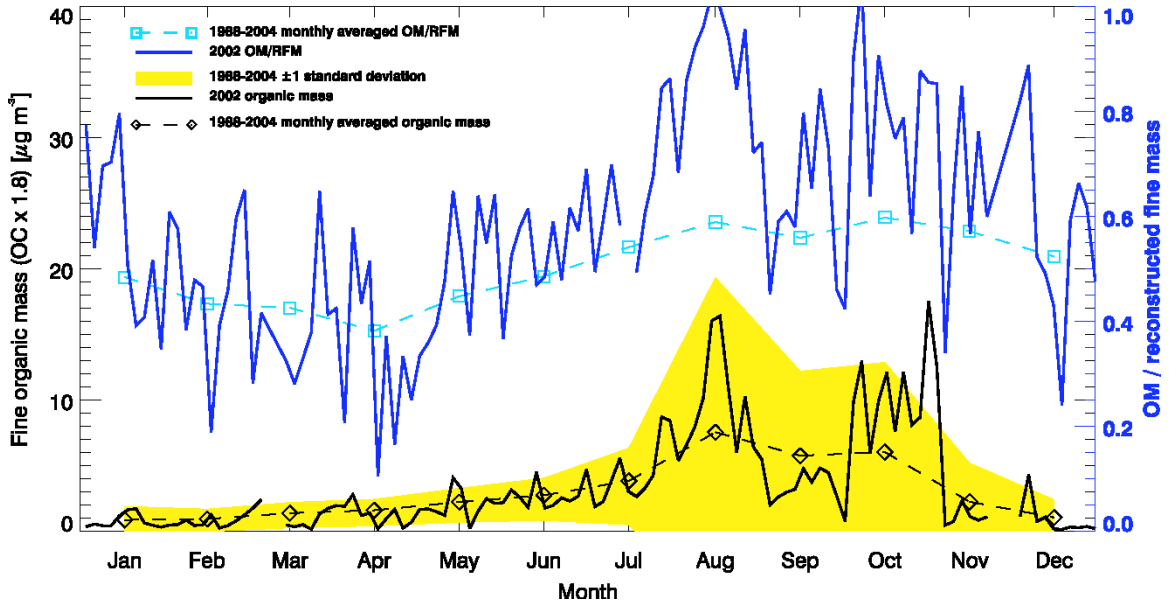

Figure 6.12. Annual variation of organic carbon mass concentrations in the fine mode of the aerosol ($PM_{2.5}$), from data obtained from the IMPROVE database (http://vista.cira.colostate.edu/views/). A measure of interannual variability is indicated by the yellow shaded area, which envelops one standard deviation in the data. Blue lines indicate the fraction of fine particulate mass concentration apportioned to organic carbon over the long-term average and for 2002.

These observations suggest an important role for organic carbon in air quality and visibility degradation in Yosemite NP. However, at the time this study was planned, several key properties of aerosol organic carbon were unknown, all of which affect estimates of visibility impairment.

- First, organic carbon in atmospheric aerosols exists in molecular forms that incorporate hydrogen, oxygen, nitrogen, and possibly other elements. However, the standard IMPROVE analytical technique measures only carbon concentrations, and thus a multiplication factor that accounts for additional weight contributed by other elements is needed to determine the total organic aerosol mass concentration in the atmosphere. Although a factor of 1.4 is used for this conversion in the Regional Haze Rule, recent studies suggested this factor may not be appropriate for many of the rural and remote locations represented in IMPROVE. The study design included measurements that could be used to constrain total mass and thus to deduce appropriate conversion factors for summertime Yosemite aerosols.
- Second, it was unknown whether the organic carbon fraction of the total aerosol could absorb water in response to increases in ambient relative humidity; standard IMPROVE and Regional Haze Rule visibility calculations assume it cannot. The absorption of water can dramatically increase total atmospheric aerosol mass concentrations and also tends to enhance extinction per unit mass. Both effects can significantly increase estimates of visibility impairment and thus need to be accurately modeled. To address these questions, the study design included measurements to quantify the increase in extinction, as a function of relative humidity, due to water uptake by aerosol organic carbon.
- Finally, the standard IMPROVE measurements can provide little insight into the sources of aerosol organic particulate matter, although the increased variability and occurrence of higher organic aerosol mass concentrations during years having severe wildfire seasons suggest that wildfire emissions are important. However, tourism in Yosemite NP follows a similar seasonal trend. Elucidation of the respective contributions of wildfire emissions and transportation sources to particulate organic matter concentrations in Yosemite NP was a third key objective of the Yosemite Aerosol Characterization Study. Sampling occurred at the elevated Turtleback Dome site, the location of the long-term IMPROVE monitors, and at a ground-level site in Yosemite Valley.

6.2.1 Study Objectives

- Determine appropriate values for converting analyzed aerosol carbon mass to ambient aerosol organic carbon mass.
- Develop an improved understanding of the visibility-impairment-related characteristics of a smoke/organic carbon-dominated aerosol, including the role of relative humidity in modifying visibility impairment.
- Examine the sources contributing to high aerosol organic carbon mass concentrations.

6.2.2 Study Findings

- **Accurate modeling of the effects of aerosols on summertime visibility in Yosemite NP requires revision of several commonly applied assumptions.**
  - The total mass of organic compounds present in fine particulate matter at Turtleback Dome was better represented by multiplying elemental carbon concentrations by 1.8, rather than by 1.4 (Figure 6.13). The commonly applied 1.4 factor underestimated the total mass concentration of fine-mode organic aerosol by more than 25%. This higher

multiplier suggests that a significant fraction of the aerosol organic matter comprised highly oxygenated organic species.

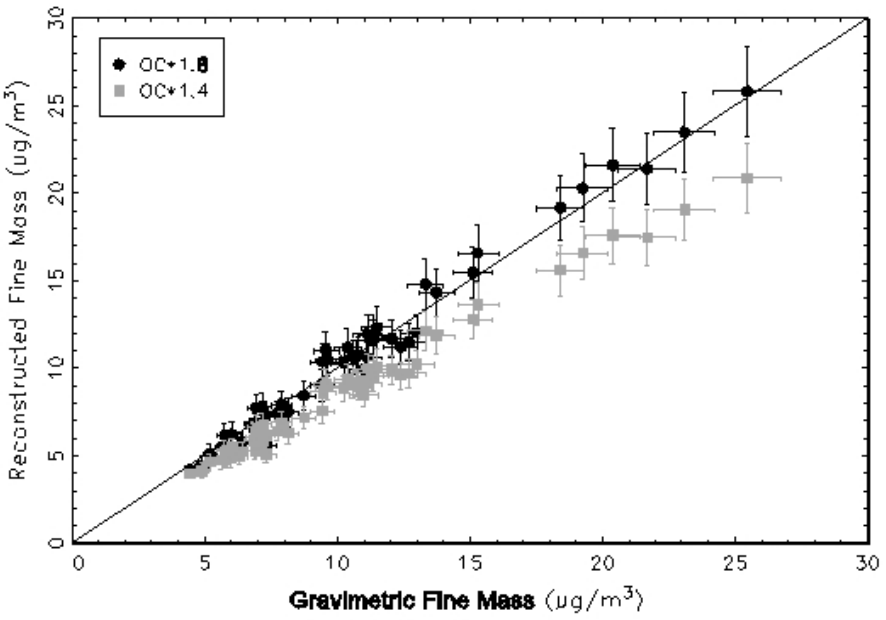

Figure 6.13. Fine mass concentrations reconstructed from individual species concentration measurements, plotted against fine mass concentrations determined by gravimetry (weighing of filters). Reconstructions are shown for two assumptions regarding the elemental-to-molecular mass conversion for organic carbon.

- The average dry mass scattering efficiency of the $PM_{2.5}$ aerosol was determined to be close to 4 m^2 g^{-1}, the same value used in the IMPROVE protocols to estimate dry light scattering coefficients of organic carbon particulate matter. However, during periods of high fine mass concentrations dominated by organic carbon and influenced by fire emissions, the dry mass scattering efficiencies ranged as high as 6 m^2 g^{-1}. The standard IMPROVE formula thus underestimates the contribution of organic carbon to total light scattering by as much as 50% during these periods.
- Light absorption was better modeled if it was assumed that elemental carbon was mixed with other constituents in individual particles, rather than assuming it was present as a separate mode. Single-particle analyses by electron microscopy also suggested that aerosol constituents were mostly found together in individual particles. IMPROVE formulas base the optical properties of elemental carbon on the assumption that it is not mixed with other aerosol species.
- At 85% relative humidity, aerosol light scattering coefficients are enhanced by a factor of 1.1 to 1.3 due to the presence of condensed water in the aerosol phase. This is much lower than the factors expected for aerosols dominated by sulfate compounds.
- Nitrate in the fine particle mode was associated most often with reacted sea salt and was only occasionally present as ammonium nitrate, which is the assumed molecular form in IMPROVE conversion equations. The reacted sea salt is present primarily in the coarse mode, although some of this mass is captured and detected on the $PM_{2.5}$ filter samples. Nitrate associated with coarse sea salt particles has a lower impact on visibility per unit

mass than is assumed for fine mode ammonium nitrate in the IMPROVE equations. However, this is partially compensated for by lower estimates of nitrate species mass concentrations, because the molecular mass of sodium nitrate is slightly larger than that for ammonium nitrate.

- **Organic carbon was the dominant component of fine particulate matter in Yosemite NP during summer 2002, and $PM_{2.5}$ mass concentrations were higher than long-term average concentrations.**
  - Figure 6.14 shows the study-averaged fine ($PM_{2.5}$) aerosol composition as observed at Turtleback Dome and at the Yosemite Valley site, along with an estimate of the coarse mass concentration (PM_{10}-$PM_{2.5}$). Organic carbon represented, on average, more than 70% of the fine mass concentration at both sites.
  - The average $PM_{2.5}$ mass concentration in Yosemite Valley during the study was 16 ± 5 µg m^{-3}, and at Turtleback Dome it was 10 ± 4 µg m^{-3}. This compares with July–August average values over 1988–2004, calculated from data in the IMPROVE database for the Yosemite NP site at Turtleback Dome, of 8 ± 5 µg m^{-3}. As can be seen in Figure 6.14, most of the difference in the fine aerosol mass concentrations between the two sites was due to higher concentrations of aerosol organic carbon at the Valley Floor site.

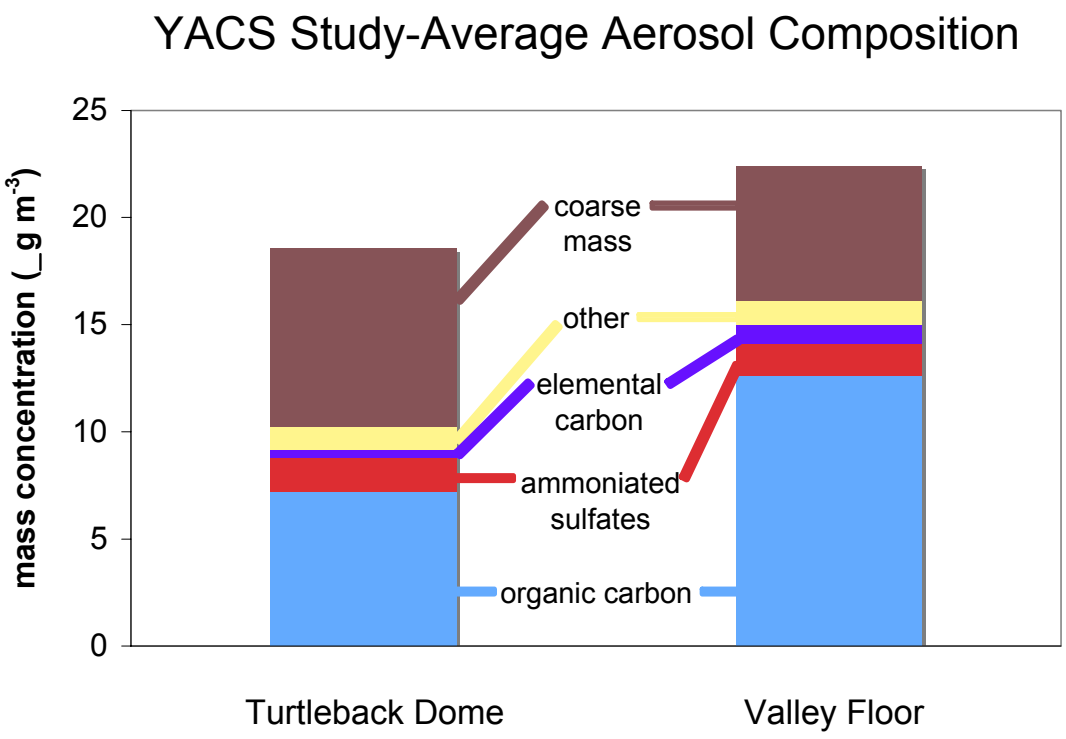

Figure 6.14. PM_{10} aerosol mass concentrations reconstructed from individual species concentration measurements, for the Turtleback Dome and Valley Floor sites.

- **Fine particles were the dominant contributor to visibility degradation at Turtleback Dome during summer 2002.**

- The average total (gas plus aerosol) extinction coefficient at Turtleback Dome was 57 ± 31 Mm^{-1}, representing the mean value ± one standard deviation. This corresponds to a visual range of approximately 69 km. The highest values of the extinction coefficient occurred in mid-August and were on the order of 191 Mm^{-1} (20-km visual range). This compares with the proposed annual average extinction coefficient for "natural background" conditions in the nonurban western United States of 15.8 Mm^{-1}.
- On average, 77% of the total light extinction coefficient was attributed to scattering by fine particles; absorption by fine particles and scattering by coarse mode particles contributed 8% and 15%, respectively (Figure 6.15).

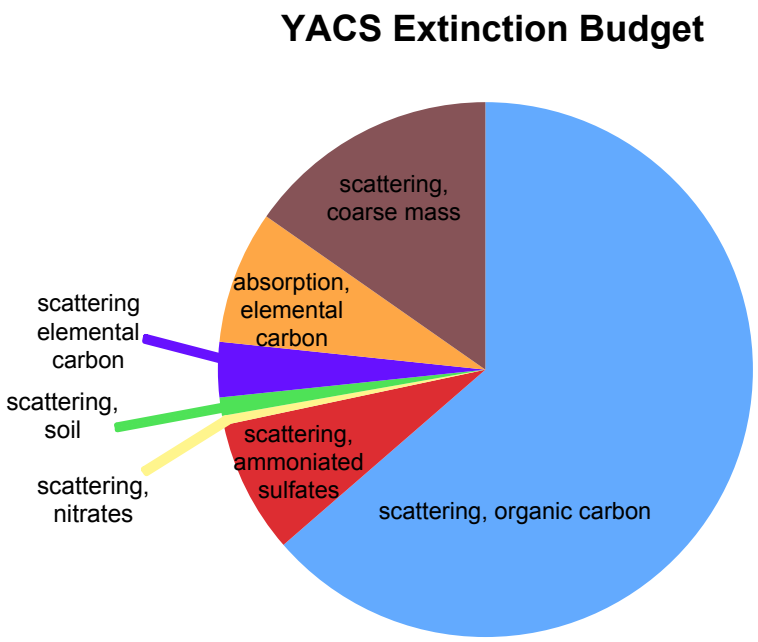

Figure 6.15. Reconstructed, study-averaged extinction budget at Turtleback Dome. All species except coarse mass are in the fine aerosol mode.

- **Natural (biogenic) sources dominated the total, and the variability in, particulate organic mass concentrations in summer 2002 at Turtleback Dome.**
  - Carbon isotope analyses of fine aerosol filter samples from Turtleback Dome determined a constant contribution from fossil fuel sources of 0.7 ± 0.1 µg m^{-3} to particulate organic matter. Contemporary (biogenically derived) carbon represented 2–9 µg m^{-3}. Sources of contemporary aerosol carbon include emissions from fires and vegetative emissions of reactive gases that subsequently form condensable species, both particulate primary emissions and volatile organic aerosol precursors that are later oxidized to secondary organic aerosols.
- **There is evidence that particulate matter sampled at Turtleback Dome was strongly influenced by the long-range transport of emissions from wildfires.**
  - During the summer of 2002, wildfires burned more than 7 million acres in the United States. Several of the largest and longest-lived fires were in southern Oregon and

California. Back and forward trajectories indicate that fire emissions were transported into California, and that a regional haze affected much of the state during August. Figure 6.16 shows an example satellite image from MODIS (http://modis.gsfc.nasa.gov/gallery/).

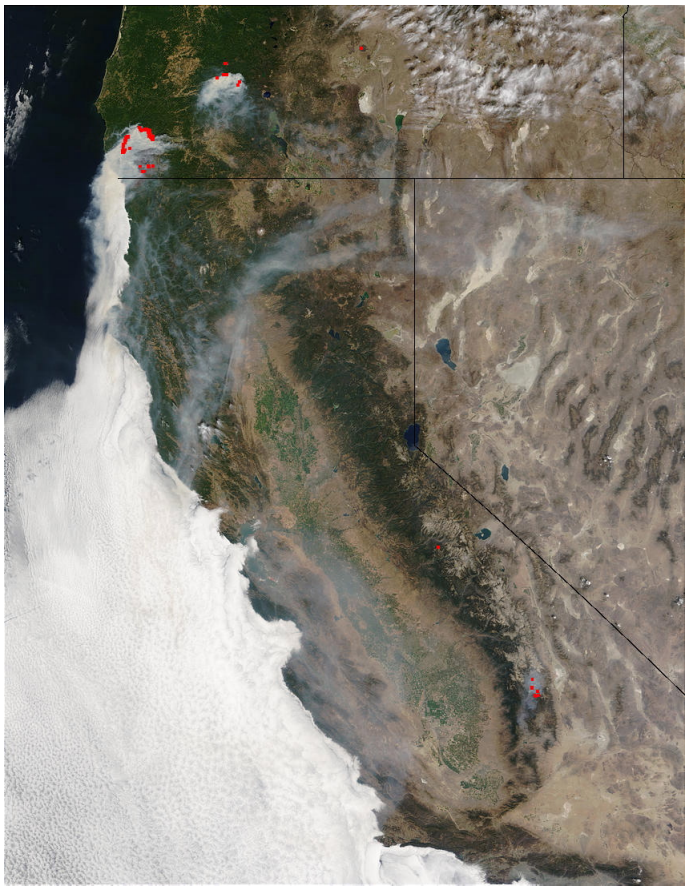

Figure 6.16. MODIS image (August 18) of smoke from fires (red areas) in Oregon and in Sequoia National Park transported into California's Central Valley.

- Back trajectory analyses and molecular marker techniques also confirmed the influence of smoke on aerosols sampled at the site. Figure 6.17 shows the study-average apportionment of $PM_{2.5}$ organic carbon measured at Turtleback Dome to various sources for which molecular markers and source signature profiles exist. The apportionment was highly variable in time, with primary wood smoke particles estimated to contribute <1% during the first week of the study to a high of 65% during the last week. Transportation sources contributed 4–19% on a weekly basis, and 10% on average, at this site. Most of the organic carbon mass could not be attributed to primary emissions from known sources and was thus assumed to be secondary in nature. Given the modern carbon signature observed in Turtleback Dome aerosol, most of the secondary material probably was derived from oxidation of biogenic volatile organic compound (VOC) emissions. VOCs associated with wildfire smoke appeared to be significant contributors to secondary organic aerosol.
- Although fewer measurements of organic aerosol speciation were available at the Valley

Floor site, data available from that location suggest a somewhat larger contribution of transportation sources to observed organic carbon.

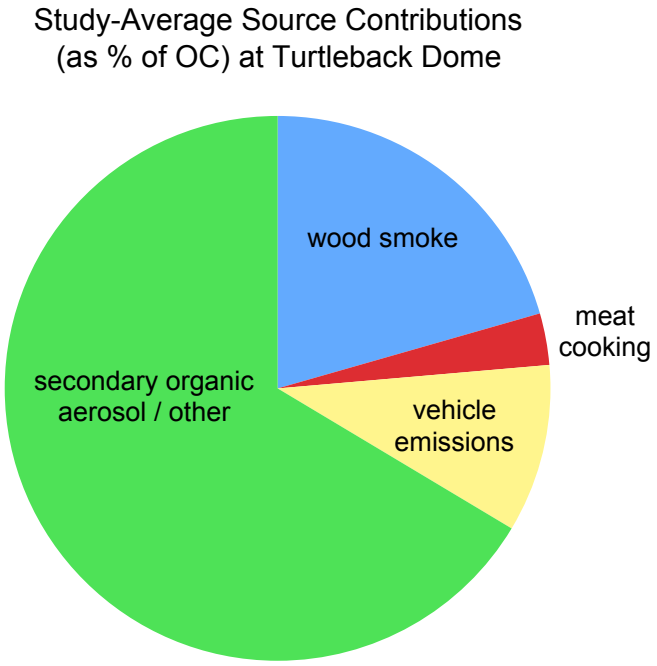

Figure 6.17. Study-averaged source contributions of fine aerosol organic carbon (expressed as % of OC) at Turtleback Dome.

6.3 EXECUTIVE SUMMARY: REVIEW OF THE IMPROVE EQUATION FOR ESTIMATING AMBIENT LIGHT EXTINCTION COEFFICIENTS

6.3.1 Introduction

Compliance under the Regional Haze Rule is based on Interagency Monitoring of Protected Visual Environments (IMPROVE) protocols for reconstructing aerosol $PM_{2.5}$ mass concentrations and light extinction coefficients (b_{ext}) from speciated mass concentrations. Dry $PM_{2.5}$ fine mass is computed using equations 1 and 2:

$$PM_{2.5} = (NH_4)_2SO_4+NH_4NO_3+POM+LAC+Soil \quad (1)$$

$$Soil = 2.2Al+2.49Si+1.94Ti+1.63Ca+2.42Fe \quad (2)$$

where sulfate is assumed to be fully neutralized ammonium sulfate ($(NH_4)_2SO_4$), nitrate is assumed to be in the form of ammonium nitrate (NH_4NO_3), and organic carbon is included as particulate organic material ($POM=R_{oc}\cdot OC$), computed by multiplying organic carbon (OC) concentrations by a molecular weight per carbon weight ratio (R_{oc}). Light-absorbing carbon is referred to as LAC. Fine soil concentrations include the contributions from assumed forms of elemental species (equation 2) (Malm et al., 1994). Mass concentrations are given in units of μg m^{-3}.

The current IMPROVE equation used to estimate total light extinction coefficients for visible wavelengths (λ) associated with measured aerosol species is

$$b_{ext}=(3.0)f(RH)[(NH_4)_2SO_4]+(3.0)f(RH)[NH_4NO_3]+(4.0)[POM]+(1.0)[Soil]+(0.6)[CM]+(10.0)[LAC] \quad (3)$$

where the nominal dry mass scattering and absorption efficiencies are in units of m^2 g^{-1} and b_{ext} is in units of inverse length. The forms of aerosol species are the same as in the reconstructed mass equations (equations 1 and 2). A value of R_{oc}=1.4 is used to compute POM. Coarse mass (CM) is computed as the difference between PM_{10} and $PM_{2.5}$ gravimetric mass ($CM=PM_{10}-PM_{2.5}$). The $f(RH)$ scattering enhancement curve accounts for the effects of relative humidity (RH) on particle growth and scattering for hygroscopic particles. Currently, it is computed assuming continuous particle growth starting at 40% relative humidity for fully neutralized pure ammonium sulfate. Only sulfates and nitrates are assumed to be hygroscopic.

Equation 3 reflects only the contribution of particulates to b_{ext}. Gaseous scattering and absorption can also be important under certain conditions. Scattering of light by air molecules is referred to as Rayleigh scattering (b_{ray}) and currently is assumed to be a constant 10 Mm^{-1} for all the IMPROVE sites, although it varies as a function of pressure and temperature. Absorption by NO_2 in visible wavelengths can also be important and is currently not included in the IMPROVE protocol.

The formulation of the equations used in the mass and IMPROVE b_{ext} reconstructions (equations 1–3) requires a number of assumptions. Each assumption has associated uncertainties with obvious consequences for reconstructed extinction, albeit to varying degrees. Uncertainty in estimated extinction is dependent on not only the assumed forms of each of the aerosol species and their respective mass scattering efficiencies and growth factors but also on measurement and

analytic accuracy and precision. We have recently reviewed the assumptions and some associated uncertainties inherent to this formulation (Hand and Malm, 2005). We suggest refinements when data exist to support modifications to the assumptions used to derive the IMPROVE equation. However, refinements of several of the assumptions are not possible at this time because existing data do not warrant them, or because further measurements are required. The suggested refinements of the IMPROVE equation include

- changing the R_{oc} factor used to compute particulate organic matter from 1.4 to 1.8
- modifying the *f(RH)* scattering enhancement curve to reflect some water associated with particles below a relative humidity of 40%
- including sea salt in reconstructed mass and extinction equations
- modifying values of dry mass scattering efficiencies to reflect current data and functional relationships between mass scattering efficiency and mass concentration
- site-specific Rayleigh scattering based on elevation and the annual average temperature of a monitoring site
- the addition of a NO_2 light absorption term used at sites with available data

The following discussion provides a brief description of the motivation behind these refinements.

6.3.2 Particulate Organic Matter and the R_{oc} Multiplier

Estimating the contributions of organic carbon aerosol to mass or scattering requires an estimate of the total mass associated with organic carbon. The organic carbon multiplier (R_{oc}) used to compute particulate organic material ($POM = R_{oc} \cdot OC$) is an estimate of the average molecular weight per carbon weight for organic carbon aerosol and takes into account contributions from other elements associated with the organic matter, such as N, O, and H. It is impossible to determine which and how many elements are associated with *POM* without knowing the chemical formula of the organic compound, and it is common for ~ 20–40% of organic aerosol mass to remain unidentified (Turpin and Lim, 2001).

Because the organic compounds that compose *POM* are largely unknown, the approach for taking into account other elements in *POM* mass has been to apply an average multiplier. The current value of 1.4 applied in the IMPROVE equation dates back to samples collected in Pasadena CA in the early 1970s and 1980s (Grosjean and Friedlander, 1975; White and Roberts, 1977; Van Vaeck and Van Cauwenberghe, 1978; Countess et al., 1980; Japar et al., 1984). More recently, Turpin and Lim (2001) reviewed estimates of R_{oc} in terms of the types of compounds known to compose *POM*. They recommend a factor of 1.6 ± 0.2 for urban organic aerosols, a factor of 2.1 ± 0.2 for nonurban organic aerosols, and values ranging from 2.2 to 2.6 for samples with impacts from biomass burning. El-Zanan et al. (2005) used solvent extractions from archived IMPROVE filters at five sites to directly measure *POM* mass and carbon content and derive an average R_{oc} of 1.92 (range of 1.58–2.58). Malm et al. (2005a) recently found that an R_{oc} factor of approximately 1.8 allowed for closure in fine mass and light scattering coefficients for periods that encompassed both pristine conditions as well as the impacts of biomass burning

and regional haze in Yosemite National Park. Poirot and Husar (2004) found better agreement between measured and reconstructed fine mass by applying an R_{oc} factor of 1.8 during a biomass burning event in the New England and mid-Atlantic state regions.

Malm and Hand (2006) estimated R_{oc} from IMPROVE data by applying an ordinary least square (OLS) multiple-linear regression (MLR) analysis using

$$PM_{2.5,i} = a_1[(NH_4)_2SO_4]_i + a_2[NH_4NO_3]_i + a_3[OC]_i + a_4[LAC]_i + a_5[soil]_i + a_6[sea\ salt]_i \quad (4)$$

where the aerosol species are the same chemical form as in equations 1 and 2, and *i* refers to a single sample (or time period). This type of analysis has inherent uncertainties, as discussed by Andrews et al. (2000) and El Zanan et al. (2005). If the mass for each species (other than *POM*) is accurately estimated and the regression is unbiased, then the regression coefficient (a_i) for a given species should equal 1. The regression coefficient for *POM* corresponds to the R_{oc} factor.

The annual mean value of R_{oc} derived from equation 4 is shown for all IMPROVE sites in Figure 6.18, with obvious spatial trends. The highest coefficients of 1.8–2.0 are just east of the Rocky Mountain range and may be reflective of wild and prescribed fire activity to the west of this region. Three of the four sites in Alaska (not shown) also have coefficients near 1.9, with the exception of Simeonof National Wildlife Refuge on the Alaskan peninsula. Other remote locations have R_{oc} values near 1.8. Coefficients ranging from 1.6 to 1.8 are found around most of the United States, with distinct regions having coefficients less than 1.6. Regions in the Northwest, interior Midwest, and Northeast are in this category.

The annual mean coefficient over all sites is R_{oc}=1.7±0.2, with 158 sites having significantly valid coefficients. On a seasonal basis the coefficients do not vary significantly. Based on estimates reported from other studies and the analysis performed here, we recommend a R_{oc} value of 1.8.

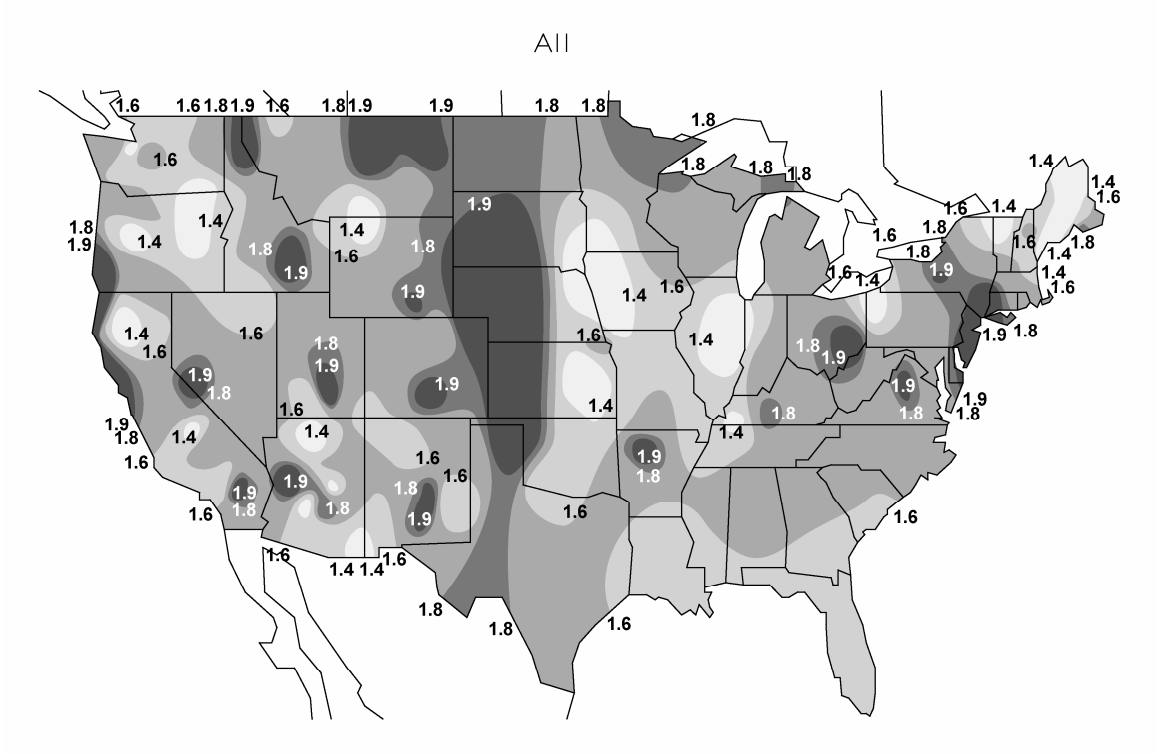

Figure 6.18. Annual mean value of R_{oc} multiplier derived from an ordinary least square multi-linear regression analysis.

6.3.3 Scattering Enhancement Curve (*f(RH)*)

The hygroscopicity of atmospheric aerosols is an important characteristic that determines how a particle will behave in a changing relative humidity (*RH*) environment. Soluble particles will uptake water, resulting in increased mass and particle size, both of which determine how efficiently particles scatter light, as well as their atmospheric lifetimes. A pure salt particle (e.g., ammonium sulfate) exposed to increasing *RH* will undergo an abrupt change from a solid particle to a droplet at a particular relative humidity (referred to as deliquescence) that is specific to its chemical composition. Above this point the particle continues to grow exponentially. As the *RH* decreases, the solution droplet will lose water by evaporation and remain in a metastable supersaturated state until it effloresces and returns to a solid particle at a lower RH than that at which it deliquesced. The metastable state can exist for indefinite periods of time. This behavior is also referred to as hysteresis because the particle follows a different path of growth and evaporation.

It is likely that a large fraction of hygroscopic particles exist in supersaturated equilibrium as aqueous droplets below their deliquescence *RH*, based on the numerous studies that report a smooth function of particle growth with relative humidity rather than step-wise growth behavior. This behavior has been observed for particle growth curves (D/D_o) in southeast Texas (Santarpia et al., 2004, 2005), Great Smoky Mountains National Park (Hand et al., 2000), and Yosemite National Park (Carrico et al., 2005). Smooth *f(RH)* curves have been observed in the Netherlands (ten Brink et al., 1996), Great Smoky Mountains, Grand Canyon, Big Bend, and Yosemite national parks (e.g., Malm and Day, 2001; Malm et al., 2003; 2005b), Portugal

(Carrico et al., 2000), China (Xu et al., 2002), North Carolina (Im et al., 2001), the Maldives (Eldering et al., 2002), and during the Aerosol Characterization Experiment in Asia (ACE-Asia) (Carrico et al., 2003). Although a variety of aerosol types likely exist at these locations, their smooth growth curves suggest these particles exist either in a equilibrium state, lacking growth characteristics like deliquescence points due to their nonsoluble/soluble mixture, or in a supersaturated equilibrium state with a very low efflorescence *RH* (i.e., acidic aerosols). In either case, water appears to be associated with these aerosols at low values of *RH*.

The current *f(RH)* growth curve used in the IMPROVE equation is based on an interpolated D/D_o curve between the ascending and descending branches of growth for ammonium sulfate and reaches a value 1 at 40% *RH* (no water is associated with the particles below 40% *RH*) (Sisler and Malm, 1994). We propose applying an *f(RH)* growth curve corresponding to equilibrium calculations for ammonium sulfate below the deliquescence point to 0% *RH* using the AIM (Aerosol Inorganics Model) model with the "no solids" option (Clegg et al., 1998). This smooth curve approximates the behavior observed for mixtures of aerosols as those observed in the studies cited above; it differs from the current curve in that it allows water to be associated with the aerosol for *RH* values below 40%. The *f(RH)* scattering enhancement curve is consistent with the value of dry mass scattering efficiency used to compute extinction coefficients; therefore modifications made to one parameter must also be made to the other. Organics are assumed to be nonhygroscopic because laboratory and field results suggest they are weakly to nonhygroscopic (Malm et al., 2003, Carrico et al., 2005; Malm et al. 2005b).

6.3.4 Sea Salt

Although contributions from sea salt to coarse mass (and indirectly to fine mass) currently are not included in the reconstructed mass equation, sea salt can be a significant fraction of the fine mass at many coastal locations, (e.g., the Virgin Islands), as well as contribute significantly to light scattering (e.g., Quinn et al., 2001, 2002, 2004). Because sea salt is hygroscopic, the added effects of water mass to light scattering in coastal higher *RH* environments could be important also. Difficulties in computing sea salt from data from the IMPROVE network arise because sodium ion data (the strongest indicator of sea salt) are not available. Elemental sodium data are available from X-ray fluorescence (XRF) analyses; however, sensitivity issues regarding poor detection of Na result in large uncertainties corresponding to Na from XRF (White et al., 2004). Issues also arise when using the chloride ion or chlorine to estimate sea salt because reaction of gaseous nitric acid with sea salt produces sodium nitrate particles and the release of gaseous HCl. The depletion of chloride during this reaction results in an underestimation of sea salt when using chloride to compute it. For noncoastal sites, the inclusion of sea salt is not expected to have a considerable impact on reconstructed light scattering, so underestimating the contribution at those sites is not significant.

The MLR analysis in equation 4 included sea salt as $1.6 \cdot Cl^-$ (NaCl). This analysis suggests that east and west coastal sites underestimate sea salt mass by about 10% on average, even with some chloride depletion. We recommend that sea salt be included in the reconstructed fine mass equation as $1.8 \cdot Cl^-$ (sea salt is 55% Cl by weight as defined by the composition of sea water by Seinfeld and Pandis, 1998) because of the uncertainties related to sodium measurements. A dry sea salt mass scattering efficiency of 1.7 $m^2 g^{-1}$ is recommended, corresponding to a dry lognormal size distribution with geometric mass mean diameter of 2.5

and geometric standard deviation of 2 (Quinn et al.,1996), a refractive index of 1.55, and a density of 1.9 g cm^{-3}. Hygroscopic effects of sea salt are taken into account by applying D/D_o particle growth curves for NaCl (Tang, 1997) and computing *f(RH)* curves with the above assumed size distribution.

6.3.5 Mass Scattering Efficiencies

Estimates of dry mass scattering efficiencies (α_{sp}) depend on the aerosol composition and size distribution, both of which vary temporally and spatially and typically are unknown without extensive measurements. A recent literature review (Hand and Malm, 2006) suggests the current values applied in the IMPROVE formulation are realistic; however, lowering mass scattering efficiencies for inorganic salts would be more consistent with available data. We also suggest that *POM* mass scattering efficiencies should also be decreased; however, at least under some circumstances, the *POM* scattering efficiency is most likely higher than what is currently assumed. We recommend no changes to mass scattering efficiencies for fine soil and coarse mass, nor do we recommend changes to the LAC mass absorption efficiency.

Investigations of estimates of mass scattering efficiency from IMPROVE mass and nephelometry data suggest a functional dependence of mass scattering efficiencies on mass concentrations in that, as mass concentrations increase, mass scattering efficiencies also tend to increase at most sites in an approximately linear fashion (Malm and Hand, 2006). This functional dependence is accounted for by assuming a bimodal size distribution. The smaller size mode corresponds to lower mass scattering efficiencies under low mass concentration conditions associated with younger particles. The large size mode corresponds to higher values of α_{sp} for higher mass concentration conditions assumed to be associated with aged or cloud-processed aerosols. The size modes are described by lognormal size distributions with geometric mass mean diameters and geometric standard deviations of 0.2 μm and 2.2 for the small mode and 0.5 μm and 1.5 for the large mode, respectively, and are assumed for ammonium sulfate, ammonium nitrate, and *POM*. The annual mean ammonium sulfate mass scattering efficiency is shown in Figure 6.19. Values tend to be lower in the Southwest compared to the eastern United States, ranging from 2.27 $m^2 g^{-1}$ in Jarbidge Wilderness NV (JARB) to 3.11 $m^2 g^{-1}$ in Mammoth Cave National Park KY (MACA), with a mean and standard deviation for all sites of 2.5±0.3 $m^2 g^{-1}$. The annual mean POM mass scattering efficiency for all sites is shown in Figure 6.20. The average (and one standard deviation) of all sites is 3.2±0.2 $m^2 g^{-1}$, ranging from 2.9 $m^2 g^{-1}$ in the Virgin Islands (VIIS) (not shown) to 3.71 $m^2 g^{-1}$ in Phoenix AZ (PHOE).

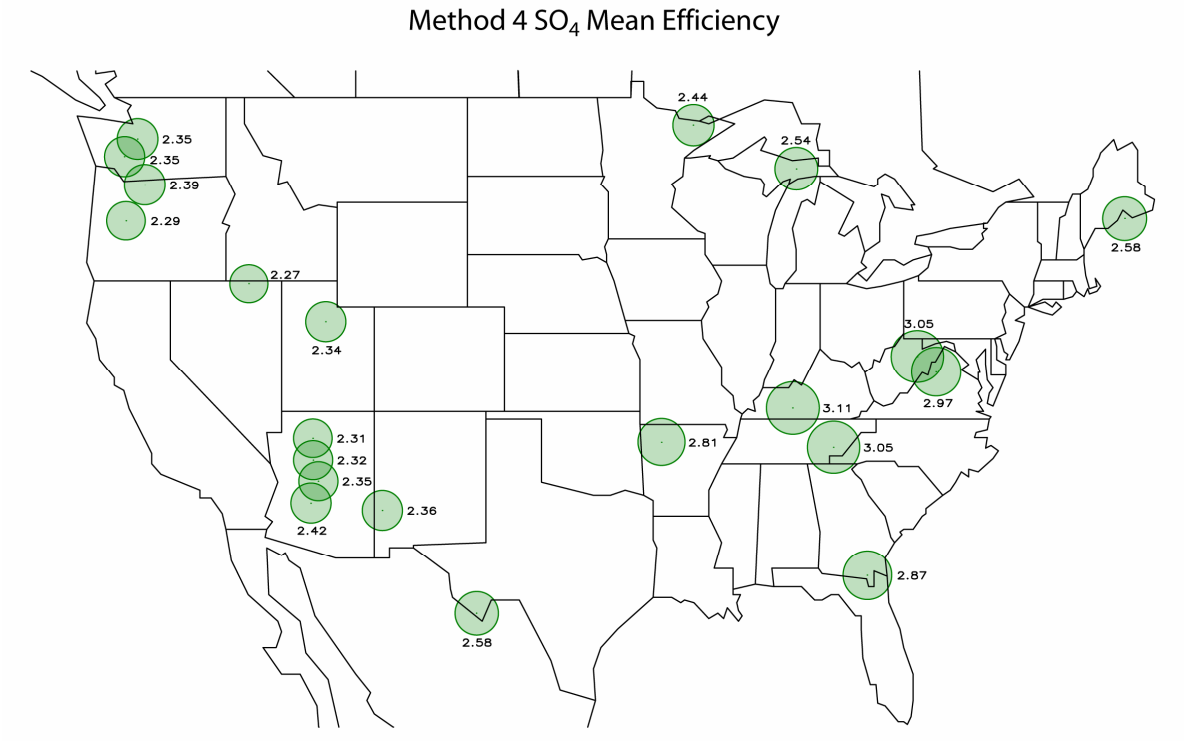

Figure 6.19. Map of the mean ammonium sulfate mass scattering efficiency (m^2 g^{-1}). The size of the circle reflects the magnitude of the efficiency, which is printed near the circle.

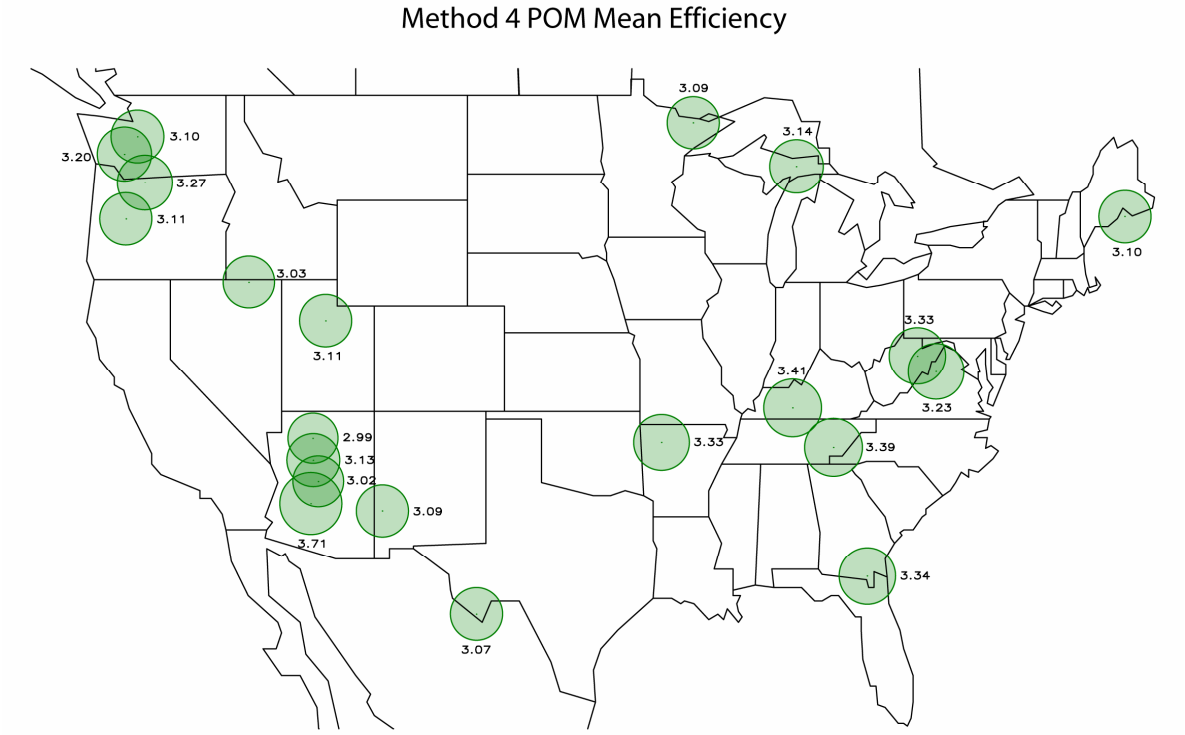

Figure 6.20. Map of the mean POM mass scattering efficiency (m^2 g^{-1}). The size of the circle reflects the magnitude of the efficiency, which is printed near the circle.

6.3.6 Site-Specific Rayleigh Scattering

The current IMPROVE equation assumes a constant value of 10 Mm^{-1} regardless of location. Rayleigh scattering depends on air density and varies with temperature and pressure. For each IMPROVE site b_{ray} was computed using the standard atmospheric pressure corresponding to the site elevation and the annual mean temperature. Values range from 8 Mm^{-1} for sites elevations around 12,000 feet to 12Mm^{-1} for sites near sea level.

6.3.7 Light Absorption by NO_2

The NO2 absorption efficiency is computed using equation 5:

$$PAE_{NO_2} = \frac{\sum_{350}^{750} PR(\lambda) \times AE(\lambda)}{\sum_{350}^{750} PR(\lambda)} \qquad (5)$$

where the NO_2 absorption efficiency ($AE(\lambda)$) is multiplied by the relative observer photopic response ($PR(\lambda)$) for viewing an image of 2º angular size (Dixon, 1940). This product is summed over the wavelengths from 350 to 750 nm and divided by the sum of the photopic response over the same wavelength range. The NO_2 absorption efficiency is 0.33 Mm^{-1}/ppb.

6.3.8 New IMPROVE Equation

The new IMPROVE equation is proposed as

$$\begin{aligned} b_{ext} = {} & 2.2 \cdot f_S(RH) \cdot [(NH_4)_2 SO_4]_S + 4.8 \cdot f_L(RH) \cdot [(NH_4)_2 SO_4]_L \\ & + 2.4 \cdot f_S(RH) \cdot [NH_4NO_3]_S + 5.1 \cdot f_L(RH) \cdot [NH_4NO_3]_L \\ & + 2.8 \cdot [POM]_S + 6.1 \cdot [POM]_L \\ & + 10 \cdot [LAC] \\ & + 1.0 \cdot [Soil] \\ & + 1.7 \cdot f_{SS}(RH) \cdot [Seasalt] \\ & + 0.6 \cdot [CM] \\ & + b_{ray} \\ & + 0.33 \cdot [NO_2(ppb)] \end{aligned}$$

where

$$[(NH_4)SO_4]_L = \frac{[total\ (NH_4)SO_4]}{20} \cdot [total\ (NH_4)SO_4],\ for\ [total\ (NH_4)SO_4] < 20\ \mu g\ m^{-3}$$

$$\left[(NH_4)SO_4\right]_L = \left[total\ (NH_4)SO_4\right],\ for\ \left[total\ (NH_4)SO_4\right] \geq 20\ \mu g\ m^{-3}$$

$$\left[(NH_4)SO_4\right]_S = \left[total\ (NH_4)SO_4\right] - \left[\ (NH_4)SO_4\right]_L$$

Similar equations hold for ammonium nitrate and POM.

For a more comprehensive review of the IMPROVE equation, download the final report at http://vista.cira.colostate.edu/improve/Publications/GrayLit/016_IMPROVEeqReview/IMPROVEeqReview.htm

References

Andrews, E., P. Saxena, S. Musarra, L. M. Hildemann, P. Koutrakis, P. H. McMurry, I. Olmez, W. H. White, Concentration and composition of atmospheric aerosols from the 1995 SEAVS experiment and a review of the closure between chemical and gravimetric measurements, *J. Air & Waste Manage. Assoc., 50,* 648-664, May 2000.

Carrico, C. M., M. J. Rood, J. A. Ogren, C. Neusüß, A. Wiedensohler, and J. Heintzenberg, Aerosol optical properties at Sagres, Portugal during ACE-2, *Tellus, 52B,* 694-715, 2000.

Carrico, C. M., M. H. Bergin, J. Xu, K. Baumann, and H. Maring, Urban aerosol radiative properties: Measurements during the 1999 Atlanta Supersite Experiment, *J. Geophys. Res., 108(D7)*, 8422, doi:10.1029/2001JD001222, 2003.

Carrico, C. M., S. M. Kreidenweis, W. C. Malm, D. E. Day, T. Lee, J. Carrillo, G. R. McMeeking, and J. L. Collett, Jr., Hygroscopic growth behavior of a carbon-dominated aerosol in Yosemite National Park, *Atmos. Environ., 39*, 1393-1404, 2005.

Clegg S.L., P. Brimblecombe, and A.S. Wexler, A thermodynamic model of the system H+-NH4+-Na+-SO42—NO3—Cl—H2O at 298.15 K, *J. of Phys. Chem.102A*, 2155-2171, 1998.

Countess, R. J., G. T. Wolff, and S. H. Cadle, The Denver winter aerosol: A comprehensive chemical characterization, *J. Air Pollution Control Assoc., 30,* 1194-1200, 1980.

Dixon, J. K., The absorption coefficient of nitrogen dioxide in the visible spectrum, *J. Chem. Phys., 8(2),* 157-160, 1940.

Eldering, A., J. A. Ogren, Z. Chowdhury, L. S. Hughes, and G. R. Cass, Aerosol optical properties during INDOEX based on measured aerosol particle size and composition, *J. Geophys. Res.,107(D22),* 8001, doi:10.1029/2001JD001572, 2002.

El-Zanan, H. S., D. H. Lowenthal, B. Zielinska, J. C. Chow, and N. Kumar, Determination of the organic aerosol mass to organic carbon ratio in IMPROVE samples, *Chemosphere, 60(4),* 485-496, 2005.

Grosjean, D., and S. K. Friedlander, Gas-particle distribution factors for organics and other pollutants in the Los Angeles atmosphere, *J. Air Pollution Control Assoc., 25,* 1038-1044, 1975.

Hand, J. L., R. B. Ames, S. M. Kreidenweis, D. E. Day and W. C. Malm, Estimates of particle hygroscopicity during the Southeastern Aerosol and Visibility Study, *J. Air & Waste Manage. Assoc., 50,* 677-685, May 2000.

Hand, J. L., and W. C. Malm, Review of the IMPROVE equation for estimating ambient light extinction coefficients (final report), http://vista.cira.colostate.edu/improve/Publications/GrayLit/016_IMPROVEeqReview/IMPROVEeqReview.htm, 2005.

Hand, J. L., and W. C. Malm, Review of aerosol mass scattering efficiencies from ground-based measurements since 1990, *In preparation for submission to J. Geophysical Res.,* 2006.

Im, J.-S., V. K. Saxena, and B. N. Wenny, An assessment of hygroscopic growth factors for aerosols in the surface boundary layer for computing direct radiative forcing, *J. Geophys. Res., 106(D17)*, 20213-20224, 2001.

Japar, S. M., A. C. Szkarlat, R. A. Gorse, Jr., E. K. Heyerdahl, R. L. Johnson, J. A. Rau, and J. J. Huntzicker, Comparison of solvent extraction and thermal optical carbon analysis methods: Application to diesel vehicle exhaust aerosol, *Environ. Sci. Techonol., 18,* 231-234, 1984.

Malm, W. C., J. F. Sisler, D. Huffman, R. A. Eldred, and T. A. Cahill, Spatial and seasonal trends in particle concentration and optical extinction in the United States, *J. Geophys. Res., 99(D1)*, 1347-1370, 1994.

Malm W.C. and D. E. Day, Estimates of aerosol species scattering characteristics as a function of relative humidity, *Atmos. Environ., 35,* 2845-2860, 2001.

Malm W.C., D. E. Day, S. M. Kreidenweis, J. L. Collett, Jr., T. Lee, T., Humidity dependent optical properties of fine particles during the Big Bend Regional Aerosol and Visibility Observational study (BRAVO), *J. Geophys. Res. 108(D9),* 4279, doi:10.1029/2002JD002998, 2003.

Malm W.C., D. E. Day, C. Carrico, S. M. Kreidenweis, J. L. Collett, Jr., G. McMeeking, T. Lee, J. Carrillo, Inter-comparison and closure calculations using measurements of aerosol species and optical properties during the Yosemite Aerosol Characterization Study, *J. Geophys. Res., 110,* D14302, doi:10.1029/2004JD005494*,* 2005a.

Malm, W. C., D. E. Day, S. M. Kreidenweis, J. L. Collett, Jr., C. Carrico, G. McMeeking, and T. Lee, Hygroscopic properties of organic-laden aerosol*, Atmos. Environ., 39,* 4969-4982, 2005b.

Malm, W. C. and Hand, J. L., An examination of aerosol physical and optical properties collected in the IMPROVE program, *Submitted to Atmos. Environ.,* 2006.

Poirot, R. L. and R. B.Husar, Chemical and physical characteristics of wood smoke in the northeastern U.S. during July 2002: Impacts from Quebec forest fires, Paper # 94, A&WMA Specialty conference: Regional and Global Perspectives on Haze: Causes, Consequences and Controversies, Asheville, NC, October 25-29, 2004.

Quinn, P. K., V. N. Kapustin, T. S. Bates and D. S. Covert, Chemical and optical properties of marine boundary layer aerosol particles of the mid-Pacific in relation to sources and meteorological transport, *J. Geophys. Res., 101(D3),* 6931-6951, 1996.

Quinn, P. K., D. J. Coffman, T. S. Bates, T. L. Miller, J. E. Johnson, K. Voss, E. J. Welton, and C. Neususs, Dominant aerosol chemical components and their contribution to extinction during the Aerosols99 cruise across the Atlantic, *J. Geophys. Res., 106(D18)*, 20783-20809, 2001.

Quinn, P. K., D. J. Coffman, T. S. Bates, T. L. Miller, J. E. Johnson, E. J. Welton, C. Neususs, M. Miller, and P. J. Sheridan, Aerosol optical properties during INDOEX 1999: Means, variability, and controlling factors, J. Geophys. Res., *107(D19), 8020,* doi:10.1029/2000JD000037, 2002.

Quinn, P. K., D. J. Coffman, T. S. Bates, E. J. Welton, D. S. Covert, T. L. Miller, J. E. Johnson, S. Maria, L. Russell, R. Arimoto, C. M. Carrico, M. J. Rood, and J. Anderson, Aerosol optical properties measured on board the *Ronald H. Brown* during ACE-Asia as a function of aerosol chemical composition and source region, *J. Geophys. Res., 109(D19S01)*, doi:10.1029/2003JD004010, 2004.

Santarpia, J. L., R. Li, and D. R. Collins, Direct measurement of the hydration state of ambient aerosol populations, *J. Geophys. Res.,109,* D18209*,* doi:10.1029/2004.

Santarpia, J. L., R. Gasparini, R. Li, and D. R. Collins, Diurnal variations in the hygroscopic growth cycles of ambient aerosol populations, *J. Geophys. Res.,110,* D03206, doi:10.1029/2004JD005279, 2005.

Seinfeld, J. H. and S. N. Pandis, *Atmospheric Chemistry and Physics: From Air Pollution to Climate Change,* John Wiley, New York, pp 444, 1998.

Sisler, J. F. and W. C. Malm, The relative importance of soluble aerosols to spatial and seasonal trends of impared visibility in the United States, *Atmos. Environ., 28(5),* 851-862, 1994.

Tang, I. N., Thermodynamic and optical properties of mixed-salt aerosols of atmospheric importance, *J. Geophys. Res.,102(D2),* 1883-1893, 1997.

ten Brink, H. M., J. P. Veefkind, A. Waijers-Ijpelaan, and J. C. Van der Hage, Aerosol light scattering in the Netherlands, *Atmos. Environ., 30(24),* 4251-4261, 1996.

Turpin, B. J., and H.-J. Lim, Species contributions to $PM_{2.5}$ mass concentrations: Revisiting common assumptions for estimating organic mass, *Aerosol Sci. Technol., 35,* 602-610, 2001.

Van Vaeck, L. and K. Van Cauwenberghe, Cascade impactor measurements of the size distribution of the major classes of organic pollutants in atmospheric particulate matter, *Atmos. Environ., 12,* 2239, 1978.

White, W. H. and P. T. Roberts, On the nature and origins of visibility-reducing aerosols in the Los Angels Air Basin, *Atmos. Environ., 11,* 803-812, 1977.

White, W. H., R. A. Eldred, P. J. Feeney, C. E. McDade, B. P. Perley, D. J. Shadoan, and P. H. Wakabayashi, Behavior of fine-particle elemental data near the detection limit, Paper # 24, A&WMA Specialty conference: Regional and Global Perspectives on Haze: Causes, Consequences and Controversies, Asheville, NC, October 25-29, 2004.

Xu, J., M. H. Bergin, X. Yu, G. Liu, J. Zhao, C. M. Carrico, and K. Baumann, Measurement of aerosol chemical, physical and radiative properties in the Yangtze delta region of China, *Atmos. Environ., 36,* 161-173, 2002.

6.4 COARSE PARTICLE SPECIATION AT SELECTED LOCATIONS IN THE RURAL CONTINENTAL UNITED STATES

Abstract

A few short-term special studies at national parks have shown that coarse mass (2.5–10 μm) may not be just crustal minerals but may consist of a substantial amount (≈ 40–50%) of carbonaceous material and inorganic salts such as calcium nitrate and sodium nitrate. To more fully investigate the composition of coarse particles, a program of coarse particle sampling and speciation analysis at nine of the IMPROVE sites was initiated 19 March 2003 and operated through the year 2004. Only the data for 2004 are reported here. Sites were selected to be representative of the continental United States and were operated according to IMPROVE protocol analytic procedures. Crustal minerals (soil) are the single largest contributor to coarse mass (CM) at all but one monitoring location. The average fractional contributions range from a high of 76% at Grand Canyon National Park to a low of 34% at Mount Rainier National Park. The second largest contributor to CM is organic mass, which on an average annual fractional basis is highest at Mount Rainier at 59%. At Great Smoky Mountains National Park, organic mass contributes 40% on average, while at four sites organic mass concentrations contribute between 20% and 30% of the CM. Nitrates are on average the third largest contributor to CM concentrations. The highest fractional contributions of nitrates to CM are at Brigantine National Wildlife Refuge, Great Smoky Mountains, and San Gorgonio wilderness area at 10–12%. Sulfates contribute less than about 5% at all sites.

6.4.1 Introduction

The Regional Haze Rule (U.S. Environmental Protection Agency, 1999) requires monitoring representative of 156 visibility-protected federal areas (VPFAs) beginning in January 2001. This entails particle sampling and analysis of the major aerosol components using methods patterned after those utilized since 1987 by the Interagency Monitoring of Protected Visual Environments (IMPROVE) network (Joseph, et al., 1987; Malm et al., 1994).

In 1999, the IMPROVE network consisted of 30 monitoring sites in VPFAs, 20 of which began operation in 1988, with the others starting in the early 1990s. About this time the EPA provided supplemental support to expand the network to about 110 monitoring sites. Additional information about the site selection process is available elsewhere (Malm et al., 2000a; Colorado State University, http://vista.cira.colostate.edu/improve/).

The aerosol data collected in the IMPROVE program have been widely analyzed to better understand the seasonal and spatial patterns of fine aerosol components and their contribution to light extinction (Eldred et al., 1993; Malm et al., 1994; Sisler and Malm, 2000; Malm et al., 2004). The spatial patterns of trace elements, e.g., selenium, vanadium, zinc, and bromine have also been examined (Eldred, 1997; Malm and Sisler, 2000). At sites where more than 10 years of data were collected, temporal trends in fine mass (FM) and its major aerosol components have been examined (Iyer et al., 2000; Patterson et al., 2000; Malm and Sisler, 2000; Malm et al., 2002).

However, fine particles (< 2.5 μm) are speciated, while coarse particles (2.5–10.0 μm) are not. A few short-term special studies at national parks have shown that coarse mass (CM) is not just crustal minerals but consists of a substantial amount (≈ 40–50%) of carbonaceous material and inorganic salts such as calcium nitrate and sodium nitrate (Malm and Day, 2000; Lee et al., 2004; Malm et al., 2005). To more fully investigate the composition of coarse particles, a program of coarse particle sampling and speciation analysis at nine of the IMPROVE sites was initiated between 19 March 2003 and 23 December 2003 and operated through the year 2004. Only data from the year 2004 are reported here. Sites were selected to be representative of the continental United States and are listed in Table 6.1, along with the fine particle monitoring start date, elevation, and location of each of the sites. This paper reports on monthly trends in speciated FM and CM concentrations derived from data collected during 2004 at these sites and compares them to historical trends.

Table 6.1. Site description.

Site	Elevation (M)	State	Latitude (Degrees)	Longitude (Degrees)	Start Date
Bondville	211	Illinois	40.0514	-88.3719	3/5/2001
Bridger wilderness area	2607	Wyoming	42.9749	-109.757	3/2/1988
Brigantine National Wildlife Refuge	5	New Jersey	39.465	-74.4492	9/18/1991
Grand Canyon National Park	2267	Arizona	35.9731	-111.984	3/12/1988
Great Smoky Mountains National Park	815	Tennessee	35.6334	-83.9417	3/2/1988
Mount Rainier National Park	427	Washington	46.7579	-122.123	3/2/1988
San Gorgonio wilderness area	1705	California	34.1924	-116.901	3/2/1988
Sequoia National Park	535	California	36.4894	-118.829	3/4/1992
Upper Buffalo wilderness area	723	Arkansas	35.8259	-93.2029	12/18/1991

6.4.2 Particulate Samplers

The basic IMPROVE sampler was designed for the IMPROVE network and has been operated extensively in the network and during field studies since the winter of 1987 (Malm et al., 1989; Malm et al., 1994). The IMPROVE sampler consists of four independent modules. Each module incorporates a separate inlet, filter pack, and pump assembly; however, all modules are controlled by the same timing mechanism. Twice-weekly 24-h duration samples are collected using the same schedule as the national particulate matter (PM) monitoring network operated by state and local governments.

The sampler has a four-filter manifold for each module. Modules A, B, and C are each equipped with a 2.5 μm cyclone. The module A Teflon filter is analyzed for gravimetric FM, nearly all elements with atomic mass number ≥ 11 (Na) and ≤ 82 (Pb) by x-ray florescence (XRF), elemental hydrogen by proton elastic scattering analysis, and for light absorption. For module B, the sampled air is drawn through a sodium carbonate denuder tube in the inlet to remove gaseous nitric acid; the material collected on the Nylasorb substrate is extracted ultrasonically in a de-ionized water bath and subsequently analyzed by ion chromatography for the anions sulfate, nitrate, nitrite, and chloride. Module C utilizes quartz fiber filters for the collection of fine particles that are subsequently analyzed for carbon. At some sites, tandem quartz filters are used so that the second filter is available for estimating the organic carbon artifact associated with hydrocarbon gases trapped in the filter substrate. Thermal optical

reflectance (TOR) is the analytical technique used for determination of organic and elemental/light-absorbing carbon (LAC) (Chow et al., 1993). Finally, module D, fitted with a PM_{10} inlet, utilizes a Teflon filter that is gravimetrically analyzed for mass (PM_{10}). In this study, a second set of modules B and C were operated with a PM_{10} inlet (and denoted modules E and F). These and the Teflon filter from the D module were analyzed, allowing for an estimate of species mass in the 2.5–10.0 μm range. It is this size range that will be referred to as the coarse mode.

6.4.3 Estimation of Aerosol Mass

The fine and coarse aerosol species concentrations at most continental sites can be classified into six major types: sulfates, nitrates, organics, LAC, crustal minerals (often referred to as soil), and sea salt. Details of standard methods for apportionment of measured mass to the various aerosol species concentrations are described in some detail in Malm et al. (1994), while Table 6.2 presents the standard equations currently used in the IMPROVE program for estimating the species concentrations.

Table 6.2. Assumed molecular forms of each particulate species and method of estimation used.

Species	Formula	Assumptions
Sulfate	4.125[S] or 1.37*[SO_4^{--}]	All elemental S is from sulfate. All sulfate is from ammonium sulfate.
Nitrate	1.29[NO_3^-]	Denuder efficiency is close to 100%. All nitrate is from ammonium nitrate.
LAC (light-absorbing carbon by channel C)	[EC1]+[EC2]+[EC3]-[OP]	All high temp carbon is elemental
OMC (Organic mass from carbon)	1.8{[O1]+[O2]+[O3]+[O4]+[OP]}	Average organic molecule is 56% carbon.
SOIL	2.2[Al]+2.19[Si] +1.63[Ca]+2.42[Fe] +1.94[Ti]	[Soil K]=0.6[Fe]. FeO and Fe_2O_3 are equally abundant. A factor of 1.16 is used for MgO, Na_2O, H_2O, CO_2
Sea salt	1.8*[Cl^-]	1.8 accounts for other salts than NaCl
RCFM (reconstructed fine mass)	[SULFATE]+[NITRATE] +[LAC]+[OMC]+[SOIL] +[SEA SALT]	Represents dry ambient fine aerosol mass for continental sites.
Coarse mass species	[PM_{10}] species - [$PM_{2.5}$] species	Difference between species found on the <10 μm and 2.5 μm substrates—coarse and fine species have same chemical form.

A number of measurement programs have shown that, during summer months in the eastern United States, the average sulfate ammoniation is nearer ammonium bisulfate, with ammonium-to-sulfate molar ratios that can approach sulfuric acid (Gebhart et al., 1994; Malm et al., 2000b; Lefer and Talbot, 2001). Measurements at Big Bend, Texas, showed ammonium-to-sulfate molar ratios of about 1.4 on average (Malm et al., 2003). However, because the ammonium ion is not routinely measured in the IMPROVE program, sulfates will be assumed to

be in the form of ammonium sulfate for the purpose of examining general spatial and temporal trends in sulfate mass concentrations.

Nitrates in the aerosol are assumed to be in the form of ammonium nitrate, but, again, special studies have shown that at some locations fine nitrates are the fine tail of the coarse particle nitrate size distribution, consisting of sodium nitrate or calcium nitrate, that has resulted from the reaction of nitric acid vapor with sea salt or crustal minerals (Malm et al., 2003). Assuming nitrates are in the molecular form of ammonium nitrate would underestimate nitrate mass concentrations by about 6% and by a factor of 2 if the true molecular compositions were sodium nitrate and calcium nitrate, respectively.

An average ambient particulate organic compound is assumed to have a constant fraction of carbon by weight. Particulate organic carbon mass concentration (POM) from module C is assumed to be [POM] = 1.8[OC], where OC is organic carbon as determined by TOR. The factor of 1.8 corrects the organic carbon mass for other elements associated with the assumed organic molecular composition (Turpin and Lim, 2001; Poirot and Husar, 2004; Malm et al., 2005; Malm and Hand, 2006).

Concentrations of crustal minerals, referred to as soil, are estimated by summing the elements predominantly associated with common crustal elements measured by XRF plus oxygen for the compounds (Al_2O_3, SiO_2, CaO, K_2O, FeO, Fe_2O_3, TiO_2) and applying an adjustment to account for other unmeasured compounds such as MgO, Na_2O, water, and carbonate.

Sea salt concentrations are typically computed from sea salt markers such as the sodium ion, chloride ion, or combination of ions (Quinn et al., 2001). Difficulties in computing sea salt from data from the IMPROVE network arise because positive ions are not analyzed; therefore sodium ion (the strongest indicator of sea salt) data are not available. Elemental sodium data are available from XRF analyses; however, sensitivity issues regarding poor detection of Na result in large uncertainties (White et al., 2004). Issues also arise when using the chloride ion or chlorine to estimate sea salt, because reaction of gaseous nitric acid with sea salt produces sodium nitrate particles and the release of gaseous HCl. The depletion of chloride during this reaction results in an underestimation of sea salt when using chloride to compute it. However, because the chloride ion is the only accurately measured marker for sea salt in the IMPROVE program, $1.8[Cl^-]$ will be used to estimate sea salt concentrations (sea salt is 55% Cl by weight as defined by the composition of sea water by Seinfeld and Pandis, 1998).

The self-consistency and overall quality of the measurements are assured by redundancy and intercomparisons between independently measured species. A description of validation and quality assurance procedures is available in Eldred et al. (1988), Sisler et al. (1993), and Malm et al. (1994). In the most general sense, validation is a matter of comparing chemically related species that have been measured in different modules. Fortunately, the design of the IMPROVE sampler allows for redundancy between certain module A measurements and module B and C measurements of the ions and carbons, enabling quality control checks. For example, elemental sulfur mass × 3 should agree with the sulfate ion measured in module B. Reconstructed fine mass (RCFM), defined and used in this paper as the sum of the individual species described above, should agree with measurements of gravimetric mass. However, when comparing gravimetric

FM to RCFM, a number of complicating factors must be dealt with. First, under some conditions, a large portion of the nitrates (≥ 50%) can volatilize from the module A Teflon filter. Second, because of water retention by soluble aerosol species, the amount of residual water on the filter is a function of the relative humidity (RH) at which the filter was weighed and the history of the RH to which the aerosol was exposed.

6.4.4 The Data Set

The combined FM and CM concentration data sets for the 2004 year of monitoring at the nine sites are summarized in Tables 6.3 and 6.4 as the mean, standard deviation, maximum, and minimum for each species measured. Also shown in the last column is the fraction of gravimetric mass for each species. There are a total of 1014 data points. Reconstructed mass is the sum of all species. Negative values occur for the FM species because filter blanks exceed measured values, while for the CM species, negative values are also associated with reported PM_{10} mass concentrations for a given species that are less than $PM_{2.5}$ mass concentrations. For FM, the mean reconstructed value is 7% greater than the mean measured mass, while for CM the mean reconstructed value is 3% less than the mean measured mass. Scatter plots of reconstructed versus measured FM and CM are presented in Figs. 6.21 and 6.22. For both data sets, the agreement is quite good. However, for the FM data set, reconstructed mass tends to be overestimated in the mid-range mass concentration values of 5–12 μg m^{-3}, and there is substantially more scatter around the 1:1 line for the CM than for the FM data set. With the intercept forced through 0, the ordinary least square (OLS) slopes for the data shown in Figs. 6.21 and 6.22 are 1.03 ± .004 and 0.95 ± .01, respectively. Corresponding R^2 values are 0.96 and 0.81.

Table 6.3. Statistical summary of all fine mass and fine mass species concentrations.

Variable (μg m^{-3})	Mean	Std. Dev.	Minimum	Maximum	% of FM
FM	6.64	5.44	0.09	39.75	
FM_{RECON}	7.12	5.49	0.19	36.00	107.2
$(NH_4)_2SO_4$	2.70	3.08	0.02	21.74	40.7
NH_4NO_3	1.19	2.07	0.00	27.97	17.9
POM	2.32	1.90	-0.03	14.17	34.9
LAC	0.27	0.20	0.01	2.07	4.1
SOIL	0.62	0.69	0.01	6.89	9.3
Sea salt	0.02	0.13	0.00	2.13	0.3

Table 6.4. Statistical summary of all coarse mass and coarse mass species concentrations.

Variable (μg m^{-3})	Mean	Std. Dev.	Minimum	Maximum	% of CM
CM	5.24	5.81	-1.75	49.93	
CM_{RECON}	5.07	5.97	-3.47	46.70	96.8
$(NH_4)_2SO_4$	0.03	0.50	-4.23	4.54	0.6
NH_4NO_3	0.41	0.50	-1.72	2.97	7.8
POM	1.28	1.41	-3.35	15.29	24.4
LAC	0.07	0.13	-0.54	1.52	1.3
SOIL	3.19	4.87	-0.02	39.73	60.9
Sea salt	0.10	0.51	-0.11	6.99	1.9

On the average, sulfate interpreted as ammonium sulfate and POM make up 41% and 35% of the FM, respectively, while ammonium nitrate contributes another 18%. Soil mass concentration is less than 10% of measured mass, LAC about 4%, and sea salt is negligible. For the CM fraction, the sulfate contribution is negligible and LAC and sea salt are only 1% and 2%, respectively. As expected, crustal minerals (soil) are the major component at 61%, but POM and ammonium nitrate contribute significantly at 24% and 8%, respectively.

6.4.5 Spatial Variability of Coarse and Fine Monthly Patterns in Species Mass Concentrations

Statistical summaries of FM and CM aerosol constituents in the form of averages, standard deviations, maximums, and minimums for data aggregations for the year 2004 are shown in Tables 6.5 and 6.6. Also presented in the tables are the percent contribution of each species to gravimetric mass and a comparison of gravimetric and reconstructed mass in the form of a percentage of reconstructed to gravimetric mass. These same summaries are available on a monthly basis at http://vista.cira.colostate.edu/IMPROVE/Data/Other/Data_CMSpeciation.htm. Figs. 6.23 and 6.24 present graphical summaries of these data in the form of average monthly concentrations as stacked bar plots, while Figs. 6.25 and 6.26 show the average fractional contribution of each species to gravimetric FM and CM. The sum of the fractional contributions of each species should sum to 1. Therefore, values greater or less than 1 show the over- or underestimation of reconstructed mass as compared to gravimetric mass. Also, for purposes of comparing the current data set to the historical record, selected average species concentrations are also presented in Figs. 6.23 and 6.24. In the case of FM (Fig. 6.23), historical averages of gravimetric mass and the main constituents of FM—ammonium sulfate, POM, and, in some cases, ammonium nitrate—mass concentrations are plotted. Because only values of coarse gravimetric mass have been routinely measured, only historic values of this variable are presented (Fig. 6.24).

Table 6.5. Statistical summary of annual fine mass and fine mass species concentrations by site.

Mount Rainier Fine Mass	N = 114				
Variable (μg m^{-3})	Mean	Std. Dev.	Minimum	Maximum	% of FM
FM	3.69	2.79	0.09	15.47	
FM_{RECON}	3.92	3.03	0.2	17.45	106.2
$(NH_4)_2SO_4$	0.91	0.71	0.02	2.9	24.7
NH_4NO_3	0.2	0.23	0	1.13	5.4
POM	2.27	2.06	-0.03	12.98	61.5
LAC	0.26	0.2	0.01	0.89	7.0
SOIL	0.25	0.3	0.01	1.45	6.8
Sea salt	0.04	0.11	0	0.67	1.1
San Gorgonio Fine Mass	N = 116				
Variable (μg m^{-3})	Mean	Std. Dev.	Minimum	Maximum	% of FM
FM	5.82	3.48	0.21	14.57	
FM_{RECON}	7.41	4.47	0.63	16.76	127.3
$(NH_4)_2SO_4$	1.6	1.13	0.09	5.83	27.5
NH_4NO_3	2.66	2.22	0.03	9.28	45.7
POM	2.03	1.38	0.15	8.21	34.9

LAC	0.29	0.16	0.05	0.82	5.0
SOIL	0.83	0.69	0.01	3.35	14.3
Sea salt	0	0	0	0.03	0.0
Sequoia Fine Mass	N = 112				
Variable ($\mu g\ m^{-3}$)	Mean	Std. Dev.	Minimum	Maximum	% of FM
FM	8.06	5.4	0.71	39.75	
FM_{RECON}	9.02	5.38	0.99	36	111.9
$(NH_4)_2SO_4$	1.99	1.39	0.13	6.69	24.7
NH_4NO_3	2.14	3.47	0.07	27.97	26.6
POM	3.49	1.94	0.55	8.85	43.3
LAC	0.33	0.16	0.04	0.83	4.1
SOIL	1.07	0.95	0.02	3.45	13.3
Sea salt	0	0	0	0.01	0.0
Grand Canyon Fine Mass	N = 116				
Variable ($\mu g\ m^{-3}$)	Mean	Std. Dev.	Minimum	Maximum	% of FM
FM	2.58	1.94	0.27	14.2	
FM_{RECON}	2.71	2.38	0.19	18.38	105.0
$(NH_4)_2SO_4$	0.8	0.43	0.09	2.57	31.0
NH_4NO_3	0.22	0.26	0.02	2.19	8.5
POM	1.02	1.74	-0.01	14.17	39.5
LAC	0.12	0.22	0.01	2.07	4.7
SOIL	0.55	0.5	0.01	2.37	21.3
Sea salt	0	0	0	0.02	0.0
Upper Buffalo Fine Mass	N = 106				
Variable ($\mu g\ m^{-3}$)	Mean	Std. Dev.	Minimum	Maximum	% of FM
FM	8.1	4.9	1.15	28.84	
FM_{RECON}	8.49	4.78	1.35	26.54	104.8
$(NH_4)_2SO_4$	3.42	2.37	0.38	11.01	42.2
NH_4NO_3	1.16	1.64	0.1	10.43	14.3
POM	2.88	2.25	0.56	13.83	35.6
LAC	0.27	0.16	0.07	1.05	3.3
SOIL	0.76	1.05	0.01	6.89	9.4
Sea salt	0	0	0	0.01	0.0
Bondville Fine Mass	N = 102				
Variable ($\mu g\ m^{-3}$)	Mean	Std. Dev.	Minimum	Maximum	% of FM
FM	10.25	5.72	3.33	33.56	
FM_{RECON}	10.53	5.48	3.24	34.38	102.7
$(NH_4)_2SO_4$	4.26	3.26	0.68	19.84	41.6
NH_4NO_3	2.74	3.11	0.19	24.5	26.7
POM	2.59	1.5	0.51	9.52	25.3
LAC	0.37	0.19	0.11	0.98	3.6
SOIL	0.56	0.34	0.06	1.78	5.5
Sea salt	0	0.02	0	0.12	0.0

Great Smoky Mountains Fine Mass	N = 112				
Variable (μg m^{-3})	Mean	Std. Dev.	Minimum	Maximum	% of FM
FM	10.42	6.06	0.97	28.36	
FM_{RECON}	10.47	5.37	1.55	24.96	100.5
$(NH_4)_2SO_4$	5.87	4.09	0.72	17.64	56.3
NH_4NO_3	0.62	0.77	0.09	4.95	6.0
POM	3.04	1.58	0.37	9.8	29.2
LAC	0.33	0.15	0.07	0.87	3.2
SOIL	0.61	0.58	0.03	4.3	5.9
Sea salt	0	0	0	0	0.0
Bridger Fine Mass	N = 122				
Variable (μg m^{-3})	Mean	Std. Dev.	Minimum	Maximum	% of FM
FM	2.11	1.68	0.28	9.97	
FM_{RECON}	2.28	1.68	0.24	9.56	108.1
$(NH_4)_2SO_4$	0.62	0.39	0.09	2.65	29.4
NH_4NO_3	0.16	0.14	0.01	0.8	7.6
POM	0.98	0.93	0.03	6.98	46.4
LAC	0.08	0.07	0.01	0.57	3.8
SOIL	0.45	0.67	0.01	5.02	21.3
Sea salt	0	0	0	0.01	0.0
Brigantine Fine Mass	N = 114				
Variable (μg m^{-3})	Mean	Std. Dev.	Minimum	Maximum	% of FM
FM	9.74	5.79	3.43	35.06	
FM_{RECON}	10.18	5.87	3.66	29.8	104.5
$(NH_4)_2SO_4$	5.26	4.14	1.11	21.74	54.0
NH_4NO_3	1.07	1	0.18	5.23	11.0
POM	2.83	1.75	0.7	11.26	29.1
LAC	0.38	0.2	0.02	1.03	3.9
SOIL	0.55	0.43	0.03	1.94	5.6
Sea salt	0.09	0.36	0	2.13	0.9

Table 6.6. Statistical summary of annual coarse mass and coarse mass species concentrations by site.

Mount Rainier Coarse Mass	N = 114				
Variable (μg m^{-3})	Mean	Std. Dev.	Minimum	Maximum	% of CM
CM	2.84	2.13	0.11	8.25	
CM_{RECON}	2.97	2.43	-3.47	10.09	104.6
$(NH_4)_2SO_4$	0.07	0.12	-0.31	0.59	2.5
NH_4NO_3	0.1	0.14	-0.06	0.67	3.5
POM	1.68	1.81	-3.33	8.38	59.2
LAC	0.08	0.15	-0.41	0.64	2.8
SOIL	0.95	1.42	-0.02	6.09	33.5
Sea salt	0.08	0.16	0	0.78	2.8

San Gorgonio Coarse Mass	N = 116				
Variable (μg m^{-3})	Mean	Std. Dev.	Minimum	Maximum	% of CM
CM	6.95	5.57	0.15	25.55	
CM_{RECON}	6.2	4.76	-0.31	18.53	89.2
$(NH_4)_2SO_4$	-0.07	0.19	-0.88	0.28	-1.0
NH_4NO_3	0.74	0.73	-0.34	2.97	10.6
POM	0.96	0.99	-2.81	5.7	13.8
LAC	0.05	0.11	-0.14	0.54	0.7
SOIL	4.51	3.67	0	16.13	64.9
Sea salt	0.01	0.02	0	0.08	0.1
Sequoia Coarse Mass	N = 112				
Variable (μg m^{-3})	Mean	Std. Dev.	Minimum	Maximum	% of CM
CM	10.33	8.6	-1.75	33	
CM_{RECON}	12.39	10.81	0.24	40.61	119.9
$(NH_4)_2SO_4$	0	0.28	-1.07	0.56	0.0
NH_4NO_3	0.69	0.65	-1.72	2.75	6.7
POM	2.52	1.44	0.38	6.78	24.4
LAC	0.06	0.08	-0.14	0.47	0.6
SOIL	9.28	9.46	0.04	32.72	89.8
Sea salt	0.02	0.04	0	0.3	0.2
Grand Canyon Coarse Mass	N = 116				
Variable (μg m^{-3})	Mean	Std. Dev.	Minimum	Maximum	% of CM
CM	2.55	2.22	0.08	10.31	
CM_{RECON}	2.41	2.26	-1.91	10.54	94.5
$(NH_4)_2SO_4$	0.09	0.12	-0.25	0.52	3.5
NH_4NO_3	0.14	0.11	0	0.43	5.5
POM	0.22	0.55	-3.35	2.64	8.6
LAC	0.01	0.06	-0.24	0.23	0.4
SOIL	1.94	1.81	0.04	8.86	76.1
Sea salt	0.01	0.04	-0.02	0.32	0.4
Upper Buffalo Coarse Mass	N = 106				
Variable (μg m^{-3})	Mean	Std. Dev.	Minimum	Maximum	% of CM
CM	8.03	6.48	0.28	40.24	
CM_{RECON}	6.49	5.12	0.48	27.85	80.8
$(NH_4)_2SO_4$	0.21	0.48	-1.03	1.81	2.6
NH_4NO_3	0.51	0.42	-0.15	2.04	6.4
POM	1.64	0.97	-0.22	5.86	20.4
LAC	0.09	0.12	-0.54	0.47	1.1
SOIL	4.03	4.25	0.06	23.47	50.2
Sea salt	0.02	0.04	0	0.24	0.2

Bondville Coarse Mass	N = 102				
Variable (μg m^{-3})	Mean	Std. Dev.	Minimum	Maximum	% of CM
CM	5.77	5.86	-0.81	31.88	
CM_{RECON}	6.03	6.35	0	46.7	104.5
$(NH_4)_2SO_4$	0.13	0.58	-1.08	3.71	2.3
NH_4NO_3	0.42	0.36	-0.65	1.59	7.3
POM	1.85	2.09	0.02	15.29	32.1
LAC	0.17	0.24	-0.15	1.52	2.9
SOIL	3.45	5.14	0.11	39.73	59.8
Sea salt	0	0.02	-0.11	0.07	0.0
Great Smoky Mountains Coarse Mass	N = 112				
Variable (μg m^{-3})	Mean	Std. Dev.	Minimum	Maximum	% of CM
CM	3.37	2.7	0.26	14.97	
CM_{RECON}	3.01	2.44	-0.28	12.91	89.3
$(NH_4)_2SO_4$	0	0.77	-4.23	1.51	0.0
NH_4NO_3	0.39	0.41	-0.07	2.24	11.6
POM	1.36	1.06	-0.17	4.29	40.4
LAC	0.08	0.11	-0.18	0.48	2.4
SOIL	1.43	1.4	-0.01	9.12	42.4
Sea salt	0.01	0.06	0	0.59	0.3
Bridger Coarse Mass	N = 122				
Variable (μg m^{-3})	Mean	Std. Dev.	Minimum	Maximum	% of CM
CM	1.81	2.07	-0.01	12.73	
CM_{RECON}	1.99	2.24	-1.34	14.31	109.9
$(NH_4)_2SO_4$	0.1	0.13	-0.1	0.81	5.5
NH_4NO_3	0.11	0.15	-0.14	1.06	6.1
POM	0.42	0.57	-1.51	4.63	23.2
LAC	0.03	0.06	-0.45	0.18	1.7
SOIL	1.33	1.72	0	11.23	73.5
Sea salt	0	0.01	0	0.1	0.0
Brigantine Coarse Mass	N = 114				
Variable (μg m^{-3})	Mean	Std. Dev.	Minimum	Maximum	% of CM
CM	6.11	6.37	1.02	49.93	
CM_{RECON}	4.67	3.88	-0.69	27.81	76.4
$(NH_4)_2SO_4$	0.14	0.86	-1.82	4.54	2.3
NH_4NO_3	0.6	0.49	-0.08	2.33	9.8
POM	1.08	0.93	-1.44	4.49	17.7
LAC	0.05	0.15	-0.5	0.67	0.8
SOIL	2.06	2.49	-0.02	18.69	33.7
Sea salt	0.74	1.35	0	6.98	12.1

In general, the temporal variability, as well as composition of FM species collected during the year 2004, was similar to the grand average over all years. However, some differences are apparent. In most cases, FM concentrations during the year 2004 were generally less than the historical averages, perhaps reflecting the general reduction in species concentrations over the past 15 years (Malm et al., 2002). Sulfate concentrations have decreased across most of the United States, as have POM in the Northwest and nitrates in the coastal areas of California and inland at San Gorgonio wilderness area. Historical comparison at the Bondville site is less meaningful because routine monitoring was only initiated in the year 2001. At all monitoring sites, sulfates tend to be highest during the spring/summer/fall months when more sunlight is available and photochemistry is enhanced, while nitrates tend be highest during the cooler winter months. This is especially true at Bondville and Sequoia National Park where nitrates are 40–50+% of the FM from November to April. It interesting to note that at both Bondville and Upper Buffalo wilderness area fine mass concentrations tend to peak in February, then decrease, and peak again in late summer/fall months. Also, note the fine soil mass fraction (Fig. 6.25) increases during the month of April throughout most of the monitoring sites in the West and at Upper Buffalo. This trend is also observed at most IMPROVE monitoring sites in the western United States (Malm et al., 2002). Fine POM concentrations show less seasonal variability at the eastern sites, but show large seasonal variability at those sites representing the interior West, the Colorado plateau, and the Northwest. At Mount Rainier National Park, the ratio of POM in July to that in January is almost a factor of 10 (8.6).

Fig. 6.25 shows that reconstructed and gravimetric FM compare quite well, as reflected in Fig. 6.21. There are, however, a variety of reasons why these two variables should not agree. First, average molecular structure is assumed for all species, and this may be most important in the R_{oc} factor, which scales organic carbon to mass of carbon plus other elements that make up the organic mass concentration. In this analysis, $R_{oc} = 1.8$ was used. In the East, sulfates tend to be acidic during summer months and therefore retain water at RH values found in laboratories where filters are weighed and gravimetric mass concentrations derived (about RH = 40%). Therefore gravimetric mass reflects retained water, as well as the mass of the sulfate aerosol. Another potentially important artifact is the loss of ammonium nitrate from the Teflon substrate that is used for gravimetric analysis. Notice that, at Great Smoky Mountains National Park and Bondville, reconstructed mass is less than gravimetric mass during summer months, possibly reflecting retained water, while at San Gorgonio and Sequoia, where nitrates are a substantial fraction of FM, reconstructed mass is always higher than gravimetric mass, possibly reflecting loss of nitrate from the Teflon substrates. This is also true at some monitoring sites during the winter months, although one would expect that the nitrate loss artifact from Teflon filters would be lower because of lower ambient temperatures. At Mount Rainier and possibly Bridger and Sequoia, where POM is a significant fraction of FM and reconstructed mass is larger than gravimetric mass, the R_{oc} factor of 1.8 may be too high. In fact, an OLS regression with FM as the dependent variable and the species as independent variables suggests that the R_{oc} multiplier should be about 1.4 rather than the 1.8 used in this analysis.

Referring to Fig. 6.26 and Table 6.6, one can see that, for the most part, reconstructed and gravimetric CM compare quite favorably. This is also evident from Fig. 6.22, a scatter plot of reconstructed and gravimetric CM. However, it is evident from Fig. 6.22 that, although the data points scatter around the 1:1 line, there are a number of sampling periods where the two variables disagree by as much as a factor of 2.

It is clear that soil is the single largest contributor to CM at all but one monitoring location. The average fractional contributions range from a high of 76% at Grand Canyon National Park to a low of 34% at Mount Rainier. With the exception of Mount Rainier, the western United States generally has the highest fractional contributions, while the East has an average annual fractional contribution of 40–60%. The highest average concentration is found at Sequoia at 9.28 μg m^{-3}. Sequoia also has the highest average monthly contribution at near 21.5 μg m^{-3} for the month of August. San Gorgonio and Bondville have the second highest soil dust contributions at 4.5 and 3.5 μg m^{-3}, respectively, while Mount Rainier has the lowest average concentration of 0.95 μg m^{-3}.

Fig. 6.24 shows the lowest coarse soil concentrations tend to occur in the winter, as do most other species, while the months with maximum coarse soil contributions tend to vary from location to location. One interesting feature is the elevated soil concentrations during the month of April at Bondville and Upper Buffalo that are consistent with the historically high CM that occurs during this month. After this increase of CM in April, there is a decrease, followed by another increase in CM at Bondville and Upper Buffalo during the fall months. Whereas fine soil concentrations tend to peak across the entire western United States during the month of April, coarse soil concentrations do not show this trend. In the western United States, coarse soil concentrations tend to peak more toward mid-summer, and at Sequoia the highest concentrations are found in the fall.

The second largest contributor to CM is organic mass, which on an average annual fractional basis is highest at Mount Rainier at 59%. During the months of September and October, the fractional contribution of POM to CM was more than 80%. Even though POM contributes 59% of the CM on average at Mount Rainier, its average concentration is less than at the Sequoia and Bondville sites. The highest POM concentration occurs at Sequoia at 2.52 μg m^{-3} and the second highest at Bondville at 1.85 μg m^{-3}. At Great Smoky Mountains, organic mass contributes 40% on average, while at four sites organic mass concentrations contribute between 20% and 30% of the CM. The lowest fractional contribution of organic mass occurs at Grand Canyon and San Gorgonio.

Nitrates are on average the third largest contributor to CM concentrations. The highest fractional contributions to CM by nitrates are at Brigantine, Great Smoky Mountains, and San Gorgonio at 10–12%. However, at coastal sites such as Brigantine, nitrates may well be in the form of sodium nitrate resulting from reactions of nitric acid with sea salt. San Gorgonio and Sequoia actually have the highest coarse nitrate contributions at 0.74 and 0.69 μg m^{-3}, respectively. Brigantine is nearly as high at 0.6 μg m^{-3}. Whereas nitrates at coastal sites may be in the form of sodium nitrate, in the interior West they are more likely to be associated with soil elements such as calcium. As with fine nitrates, coarse nitrate concentrations tend to be highest during the winter months.

At most sites sea salt concentrations are very low, the one exception being Brigantine where the average concentration is 0.74 μg m^{-3} and is 12% of the CM budget. At Mount Rainier, sea salt contributes about 3% to the CM, and at the rest of the monitoring sites average concentrations are near 0.

Sulfates' contribution to CM is negligible on average at most sites, with its fractional contribution less than a few percent. This is also true on average for LAC.

It is interesting to contrast species mass concentrations that make up the fine and coarse modes. In the East, FM is dominated by sulfates, with organics contributing significantly less but in second place, while for CM soil is the biggest contributor, with organic mass again being in second place. In most of the rest of the United States, FM is made up of about equal amounts of sulfates, organics, and soil, with organics being the more significant contributor in the northwestern United States. Nitrates contribute little to FM except in southern California and the Midwest. In the coarse mode, soil is almost always the most significant fraction of mass, with organics being a distant second at about 24%. Other species on average are less than 10%.

6.4.6 Summary

To more fully investigate the composition of coarse particles, a nine-station coarse particle speciation network was initiated on 19 March 2003 and was completely operational by 23 December 2003. Sites were selected to be representative of the continental United States and were operated according to IMPROVE protocols for the year 2004. Both $PM_{2.5}$ (FM) and PM_{10} ($CM = PM_{10}–PM_{2.5}$) mass concentrations were speciated for sulfates, nitrates, organic and light-absorbing carbon, crustal minerals (soil), and sea salt. For FM, the sum of species mass concentrations values was 7% greater than gravimetric on average, while for CM the sum was 3% less than gravimetric mass on average. Scatter plots of reconstructed FM and CM versus gravimetric FM and CM show OLS slopes with the intercept set equal to 0 to be $1.03 \pm .004$ and $0.95 \pm .01$, respectively.

On average for the nine monitoring sites, sulfate (interpreted as ammonium sulfate) and POM make up 41% and 35% of the FM, respectively, while ammonium nitrate contributes another 18%. Soil mass concentration is less than 10% of measured mass, LAC about 4%, and sea salt is negligible.

For the CM fraction, the sulfate contribution is negligible, and LAC and sea salt are only 1% and 2%, respectively. As expected, soil is the major component at 61%, but POM and ammonium nitrate contribute significantly at 24% and 8%, respectively. The average fractional contributions of soil to CM range from a high of 76% at Grand Canyon to a low of 34% at Mount Rainier. With the exception of Mount Rainier, the western United States generally has the highest fractional contributions, while the East has an average annual fractional contribution of 40–60%. The lowest soil concentrations tend to occur in the winter, as do most other species, while the months with maximum soil contributions tend to vary from location to location.

The second largest contributor to CM is organic carbon mass, which on an average annual fractional basis is highest at Mount Rainier at 59%. During the months of September and October, the fractional contribution of POM to CM was more than 80%. The lowest fractional contribution of organic mass occurs at Grand Canyon and San Gorgonio.

Nitrates are on average the third largest contributor to CM concentrations. The highest fractional contributions to CM by nitrates are at Brigantine, Great Smoky Mountains, and San Gorgonio at 10–12%. However, at coastal sites such as Brigantine, nitrates may well be in the

form of sodium nitrate, which results from reactions of nitric acid with sea salt. Whereas nitrates at coastal sites may be in the form of sodium nitrate, in the interior West they are more likely to be associated with soil elements such as calcium. As with fine nitrates, coarse nitrate concentrations tend to be highest during the winter months.

At most sites sea salt concentrations are very low, the one exception being Brigantine where the average contribution to CM is 12%. At Mount Rainier, sea salt contributes about 3% to the CM, and at the rest of the monitoring sites average concentrations are near 0. Sulfates' contribution to CM is negligible on average at most sites, with its fractional contribution less than a few percent. This is also true on average for LAC.

Disclaimer

The assumptions, findings, conclusions, judgments, and views presented herein are those of the authors and should not be interpreted as necessarily representing the National Park Service or the National Oceanic and Atmospheric Administration policies.

References

Chow J.C., Watson J.G., Pritchett L.C., Pierson W.R., Frazier C.A., Purcell R.G., 1993. The DRI thermal/optical reflectance carbon analysis system: Description, evaluation, & applications in U.S. air quality studies. Atmospheric Environment 27A, 1185-1201.

Eldred R.A., Cahill T.A., Pitchford M., Malm W.C., 1988. IMPROVE - A new remote area particulate monitoring system for visibility studies. Presented at the 81st Annual Meeting of the Air Pollution Control Association, Dallas.

Eldred R.A., Cahill T.A., Malm W.C., Pitchford M.L., 1993. Ten-year trends in sulfur concentrations at national parks throughout the United States. Presented at the 86th Annual Meeting of the Air & Waste Management Association, Denver.

Eldred R.A., 1997. Comparison of selenium and sulfur at remote sites throughout the United States. Journal of the Air & Waste Management Association 47, 204-211.

Gebhart K.A., Malm W.C., Day D., 1994. Examination of the effects of sulfate acidity & relative humidity on light scattering at Shenandoah National Park. Atmospheric Environment 28, 841-849.

Iyer H., Patterson P., Malm W.C., Delgado J., 2000. Trends in the extremes of sulfur concentration distributions. Journal of the Air & Waste Management Association 50, 802-808.

Joseph D., Metza B.J., Malm W.C., Pitchford M.L., 1987. A Federal Program to Monitor Visibility in Class I Areas; in: Bhardwaja P.J. (Ed.), Visibility Protection: Research and Policy Aspects, Air Pollution Control Association, Pittsburgh.

Lee T., Kreidenweis S.M., Collett J.L. Jr., 2004. Aerosol ion characteristics during the Big Bend Regional Aerosol and Visibility Observational Study. Journal of the Air & Waste Management Association 54, 585-592.

Lefer B.L., Talbot R.W., 2001. Summertime measurements of aerosol nitrate and ammonium at a northeastern U.S. site. Journal of Geophysical Research 106, 20365-20378.

Malm W.C., Gebhart K.A., Latimer D., Cahill T.A., Eldred R., Pielke R., Stocker R.A., Watson J.G., 1989. National Park Service Report on the Winter Haze Intensive Tracer Experiment, Final Report.

Malm W.C., Sisler J.F., Huffman D., Eldred R.A., Cahill T.A., 1994. Spatial and seasonal trends in particle concentration and optical extinction in the U.S. Journal of Geophysical Research 99, 1347-1370.

Malm W.C., Day D.E., 2000. Optical properties of aerosols at Grand Canyon National Park. Atmospheric Environment 34, 3373-3391.

Malm W.C., Sisler J.F., 2000. Spatial patterns of major aerosol species and selected heavy metals in the United States. Fuel Processing Technology 65, 473-501.

Malm W.C., Sisler J.F., Pitchford M.L., Scruggs M., Ames R., Copeland S., Gebhart K.A., Day D.E., 2000a. IMPROVE (Interagency Monitoring of Protected Visual Environments): Spatial and Seasonal Patterns and Temporal Variability of Haze and Its Constituents in the United States: Report III; CIRA Report ISSN: 0737-5352-47, Colorado State University, Fort Collins, CO.

Malm W.C., Day D.E., Kreidenweis S.M., 2000b. Light scattering characteristics of aerosols as a function of relative humidity: Part I: A comparison of measured scattering and aerosol concentrations using the theoretical models. Journal of the Air & Waste Management Association 50, 686-700.

Malm W.C., Schichtel B.A., Ames R.B., Gebhart K.A., 2002. A ten-year spatial and temporal trend of sulfate across the United States. Journal of Geophysical Research 107, doi:10.1029/2002JD002107.

Malm W.C., Day D.E., Kreidenweis S.M., Collett J.L., Lee T., 2003. Humidity-dependent optical properties of fine particles during the Big Bend Regional Aerosol and Visibility Observational Study. Journal of Geophysical Research 108, doi:10.1029/2002JD002998.

Malm W.C., Schichtel B.A., Pitchford M.L., Ashbaugh L.L., Eldred R.A., 2004. Spatial and monthly trends in speciated fine particle concentration in the United States. Journal of Geophysical Research 109, doi:10.1029/2003JD003739.

Malm W.C., Day D.E., Carrico C.A., Kreidenweis S.M., Collett J. Jr., McMeeking G., Lee T., Carrillo J., Schichtel, B.A., 2005. Intercomparison and closure calculations using measurements of aerosol species and optical properties during the Yosemite Aerosol Characterization Study. Journal of Geophysical Research 10, doi:10.1029/2004JD005494.

Malm W.C., Hand J.L., 2006. Mass scattering and extinction efficiencies derived from aerosol composition data using linear regression techniques. In preparation.

Patterson P., Iyer H.K., Sisler J.F., Malm W.C., 2000. An analysis of the yearly changes in sulfur concentrations at various national parks in the United States. Journal of the Air & Waste Management Association 50, 790-201.

Poirot R.L., R.B.Husar, 2004. Chemical and physical characteristics of wood smoke in the northeastern U.S. during July 2002: Impacts from Quebec forest fires. Paper # 94, Air and Waste Management Association Specialty Conference: Regional and Global Perspectives on Haze: Causes, Consequences and Controversies, Asheville, NC, October 25-29.

Quinn P.K., Coffman D.J., Bates T.S., Miller T.L., Johnson J.E., Voss K., Welton E.J., Neususs C., 2001. Dominant aerosol chemical components and their contribution to extinction during the Aerosols99 cruise across the Atlantic. Journal of Geophysical Research 106(D18), 20783-20809.

Seinfeld J.H., Pandis S.N., 1998. Atmospheric Chemistry and Physics: From Air Pollution to Climate Change, John Wiley, New York, p. 444.

Sisler J.F., Huffman D., Latimer D.A., 1993. Spatial and Temporal Patterns and the Chemical Composition of the Haze in the U.S.: An Analysis of Data from the IMPROVE Network, 1988-1991; CIRA Report ISSN 0737 5352 26, Colorado State University, Fort Collins, CO.

Sisler J.F., Malm W.C., 2000. Interpretation of trends of PM2.5 and reconstructed visibility from the IMPROVE network. Journal of the Air & Waste Management Association 50, 775-789.

Turpin B.J., Lim H.J., 2001. Species contributions to $PM_{2.5}$ mass concentrations: Revisiting common assumptions for estimating organic mass. Aerosol Science and Technology 35, 602-610.

U.S. Environmental Protection Agency, 1999. Regional Haze Regulations: Final Rule. 40 CFR Part 51, 64(126), Docket No. A-95-38, Federal Register.

White W.H., Eldred R.A., Feeney P.J., McDade C.E., Perley B.P., Shadoan D.J., Wakabayashi P.H., 2004. Behavior of fine-particle elemental data near the detection limit. Paper # 24, Air and Waste Management Association Specialty Conference: Regional and Global Perspectives on Haze: Causes, Consequences and Controversies, Asheville, NC, October 25-29.

Figure 6.21. Scatter plot of gravimetric and reconstructed fine mass. An ordinary least square slope with the intercept set equal to 0 is 1.03 ± 0.004 with an $R^2 = 96$.

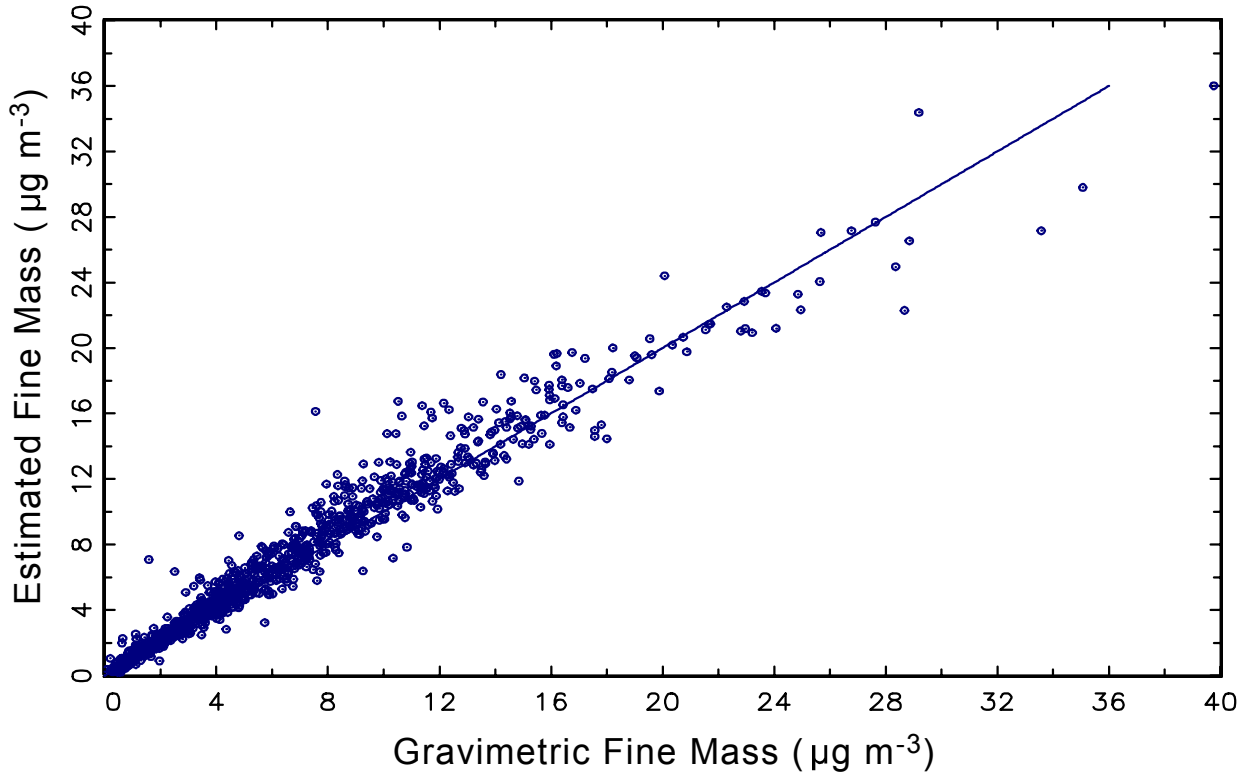

Figure 6.22. Scatter plot of gravimetric and reconstructed coarse mass. An ordinary least square slope with the intercept set equal to 0 is 0.95 ± 0.01 with an $R^2 = 81$.

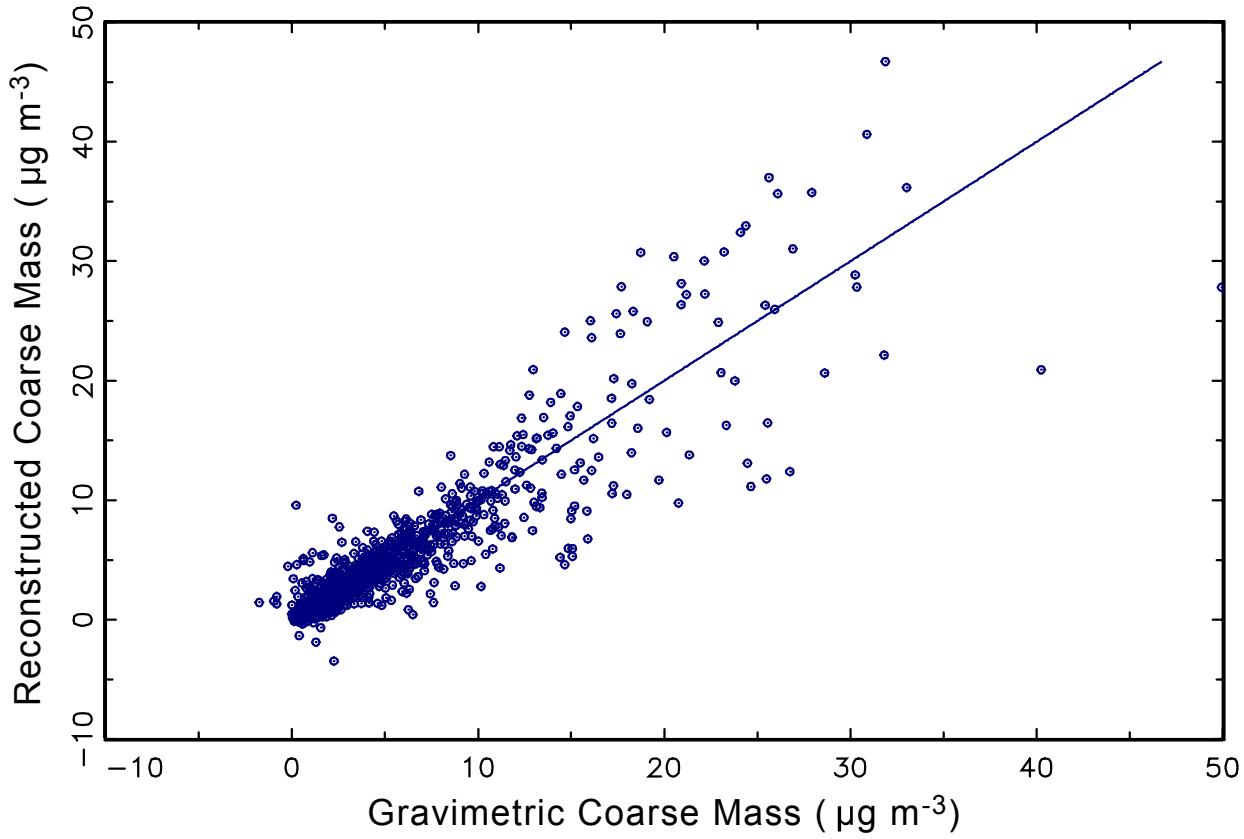

Figure 6.23. A map of stacked bar charts showing the fine mass concentration of each species at each of the nine locations at which measurements were made. The continuous lines are running averages of the data collected historically at each monitoring site.

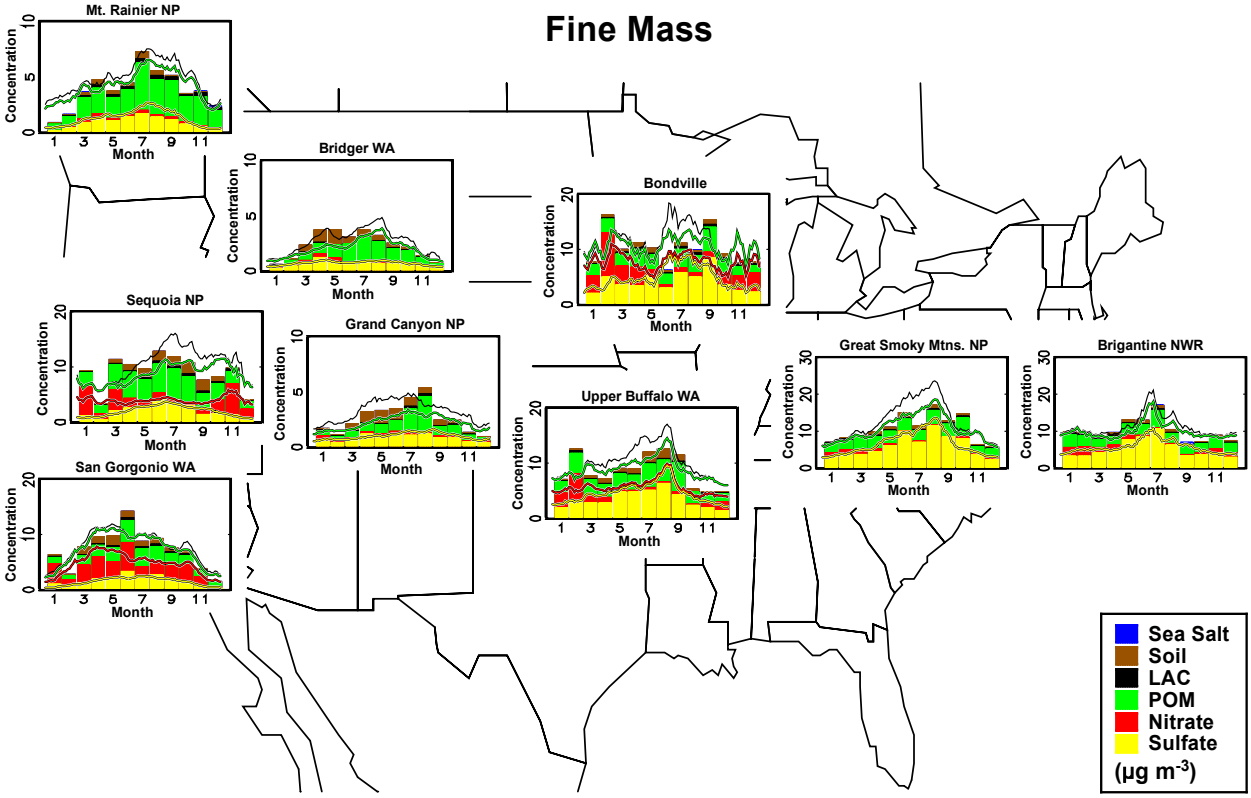

Figure 6.24. A map of stacked bar charts showing the coarse mass concentration of each species at each of the nine locations at which measurements were made. The continuous lines are running averages of the data collected historically at each monitoring site.

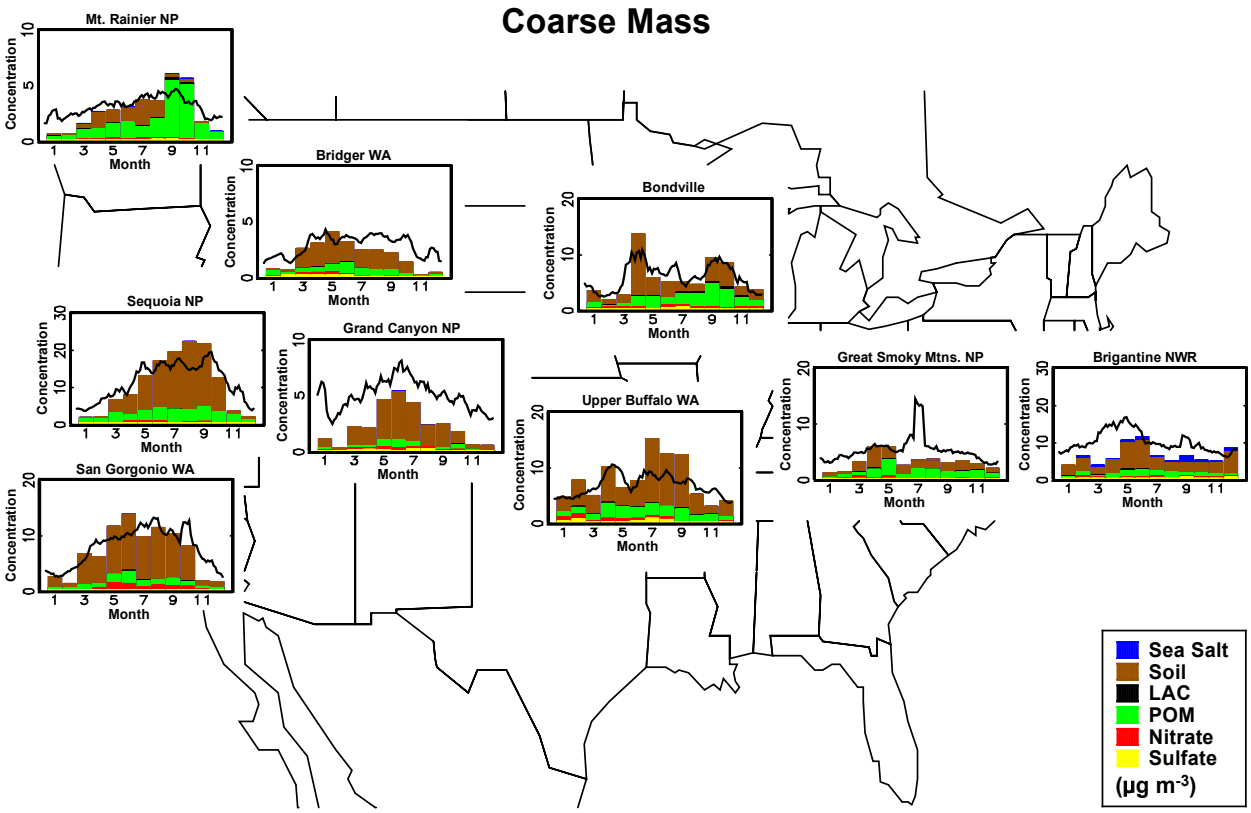

Figure 6.25. A map of stacked bar charts showing the fractional contribution of each fine mass species to gravimetric mass at each of the nine locations at which measurements were made.

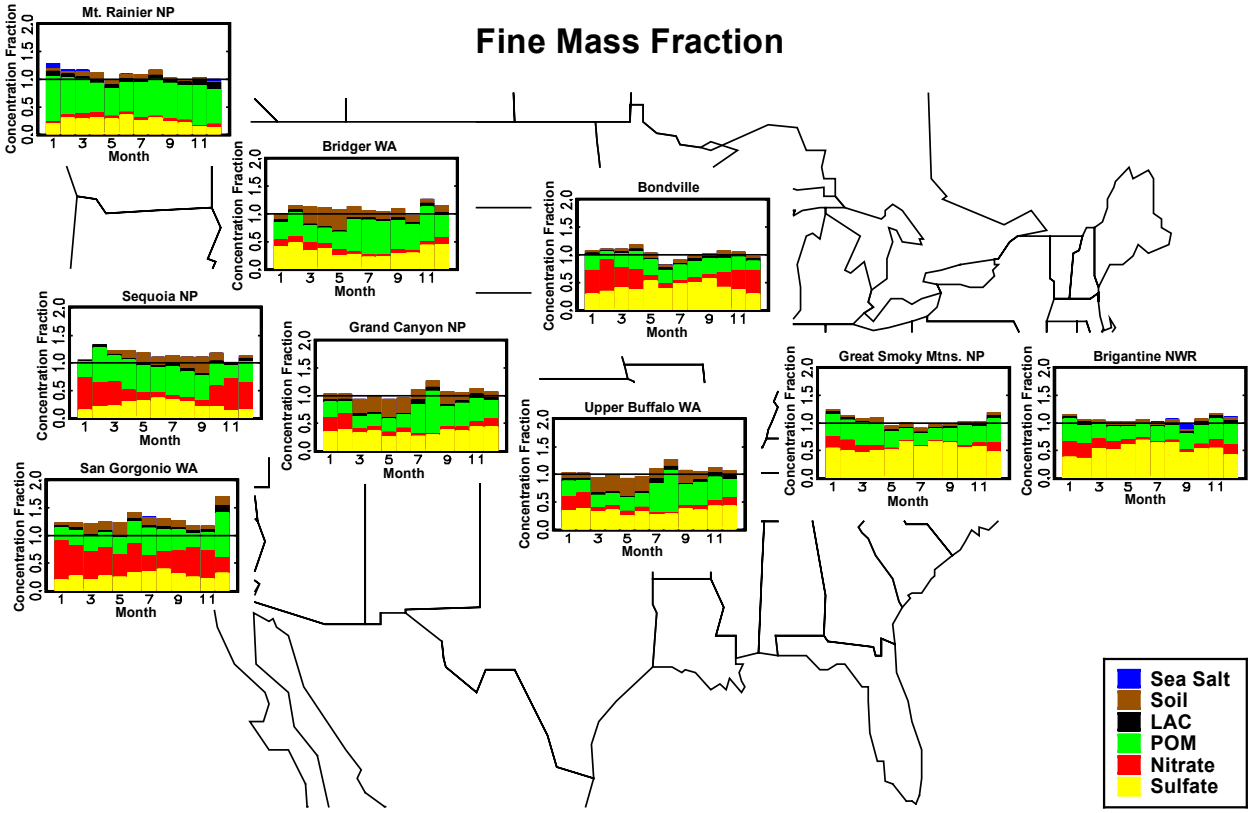

Figure 6.26. A map of stacked bar charts showing the fractional contribution of each coarse mass species to gravimetric mass at each of the nine locations at which measurements were made. The stacked bar chart for the month of January is not shown for Sequoia National Park because of a large uncertainty in PM_{10} gravimetric mass.

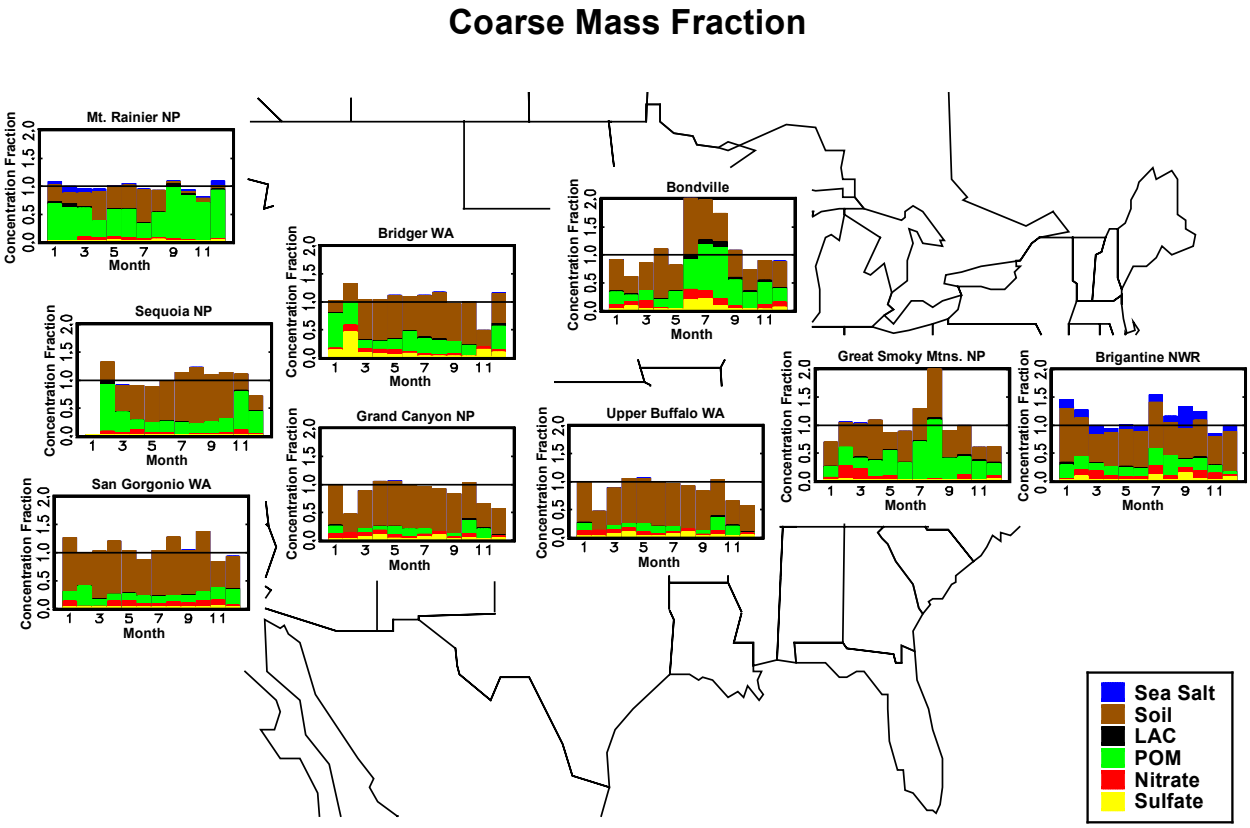

6.5 THE COMPARABILITY OF IMPROVE AND STN MEASUREMENTS—A SUMMARY OF THE RESULTS AND CONCLUSIONS FROM AN ANALYSIS OF COLLOCATED MEASUREMENTS DETAILED IN APPENDIX E

The $PM_{2.5}$ chemical Speciation Trends Network (STN) also monitors speciated fine aerosol mass concentrations at ~300 sites located primarily in urban and suburban areas, in contrast to IMPROVE, which has sites located primarily in remote rural locations. The STN was established in a manner such that it has similar measurements to those collected by IMPROVE—both networks collect 24-hour samples on appropriate filter media on a 1-in-3-day sampling schedule for quantifying $PM_{2.5}$ mass and its chemical constituents. The collocation of IMPROVE and STN sites in select urban and rural locations allows for analysis of the intercomparability between the two monitoring networks. Measurements from collocated IMPROVE and STN sites are expected to be the same within combined measurement uncertainty for most parameters. IMPROVE and STN utilize gravimetric analysis for quantification of $PM_{2.5}$ mass, IC for NO_3^- and $SO_4^=$, and XRF for elements including S, Al, Fe, Ca, Si, and Ti. However, the two networks use different samplers and different standard operating procedures for sample collection and analysis and maintain independent quality assurance programs.

Integrating data from the two networks provides more complete information on the spatial and temporal distributions of $PM_{2.5}$ aerosol mass and its major constituents throughout the United States. The in-network collocated data from IMPROVE and STN, as well as the cross-network collocated data, were explored to develop estimates on the comparability of multiyear mean concentrations between sites from the two networks. The purpose of this analysis was to provide an adequate framework for the spatial and temporal trends examined in Chapters 2 and 3 using data from both the IMPROVE and STN networks. The details of this study including data set descriptions, statistical methodology, and detailed results are given in Appendix E of this report.

The goal of these analyses was to answer the question, from a usability stand point, how comparable are the IMPROVE and STN data? The specific arena this study aimed to address is the comparability of collocated multiyear mean concentrations for each of the measurements utilized in the IMPROVE RCFM model, calculated utilizing all reported concentration values. Paired mean values were composed of between 4 months and 2+ years of data, depending on the length of the available data record; the IMPROVE-STN collocated samplers all had record lengths of at least 1 year and generally 2+ years.

The IMPROVE in-network collocated data were examined to 1) determine if the observed relative measurement errors were consistent with idealized random errors and 2) establish the typical uncertainty in mean concentrations calculated from the collocated IMPROVE measurements. The discussion of the in-network IMPROVE collocated data was included to provide context for analysis of the cross-network collocated data. The cross-network IMPROVE and STN collocated data were explored with the same objectives as the in-network IMPROVE collocated data, with appropriate statistical modifications to account for the expected differences in measurement errors between the two networks. Finally, the characteristic uncertainties observed in the in-network IMPROVE and in-network STN collocated data were used to calculate the expected characteristic uncertainties in the cross-network collocated data. The objective of this step was to evaluate the observed cross-network measurement uncertainty

in the context of what we would expect if the only information we had was the uncertainties observed in the individual networks.

The combined analysis of the in-network and cross-network collocated data populations led to a number of important conclusions regarding the observed measurement errors and the comparability of mean concentrations within and between IMPROVE and STN:

1. Biases between the IMPROVE and STN measurements of the soil elements and OC are readily apparent in the analysis of the cross-network collocated data. In the case of the soil elements, the biases are indicated by low R^2 values (<0.55) in the correlation analysis and median relative errors greater than 0. IMPROVE routinely reports higher values for the soil elements as compared to STN. The biases in OC were in the opposite direction; the median relative difference was less than 0, indicating that IMPROVE was consistently reporting lower OC values than STN. The bias observed in the OC measurements is consistent with only the IMPROVE measurements being blank corrected.

2. There are errors present in the IMPROVE and/or STN measurements that are identified in the IMPROVE-STN collocated data that are not apparent in the IMPROVE-IMPROVE or STN-STN collocated data. These additional errors are identified by larger than expected observed root mean square (rms) relative differences. The expectations were based upon simple propagation of error techniques, whereby the expected rms relative difference in the cross-network collocated data is the square root of the sum of the squared relative precision observed in each network's in-network collocated data. The observed rms relative differences observed in the IMPROVE-STN collocated data were 15–50 percentage points higher than expectations for all parameters besides S and SO_4. Analysis of cross-network collocated data identifies previously hidden errors, particularly measurement biases, which for most parameters are of considerable magnitude.

3. The analysis of the in-network IMPROVE collocated data revealed that there are nonrandom errors present in the IMPROVE measurements that are identified by larger than expected observed relative differences in the paired mean values. The expectations were based on the model of random errors, whereby independent random errors will "cancel each other out" as the sample size of the average value increases at the rate of $1/\sqrt{n}$. The parameters that had multiple aggregates with observed relative errors in the paired means more than 3 standard deviations away from expectations were SO_4, OC, Al, and Ca. These results suggest that, for these parameters, nonrandom errors (biases) are present such that the characteristic relative error for the parameter does not provide a meaningful estimate of the errors in the mean value under independent and identically distributed (i.i.d.) assumptions. This does not necessarily imply that the characteristic relative error for the parameter is too low; rather it could be that the assumption of completely independent measurement errors is incorrect. For example, a significant flow bias related to an annual calibration in one of the collocated samplers is not independent for each 24-hour sampling period during that year.

4. The IMPROVE measurement errors are inconsistent with idealized random errors—they are not i.i.d. nor are they Gaussian when the entire population is examined. Thus data analysts must be cautious in their use of any statistical techniques that require an assumption of i.i.d. or normal errors.

    a. There are significant nonrandom errors (biases) present in several of the IMPROVE measurements (see conclusion 4) that additionally are likely shared (dependent) among certain subsets of measurements. Sampling errors seem like the probable source for the biases between the collocated IMPROVE measurements, given that they were all analyzed batch-wise so that the analytical conditions should have been very similar.

    b. The IMPROVE measurement errors are heteroscedastic—they show significant relationships with both time and concentration in terms of central tendency and variability, indicating that the distribution of the errors is not the same for the entire sample population. Heteroscedastic measurement errors are expected when the measurement process spans concentrations from below minimum detection limits (mdl) to those that are well quantified. However, many statistical techniques are highly sensitive to heteroscedastic errors and require the data analyst to either pretreat the data by transforming the data to equalize the errors or to select robust techniques.

    c. The IMPROVE measurement errors do not follow a single normal distribution and for many parameters do not follow a single symmetrical distribution. This does not necessarily indicate that the error distribution at any fixed concentration is not Gaussian. For example, the high concentrations could all have errors drawn from a normal distribution with mean value $\mu = 0$ and standard deviation σ_1, $N(0, \sigma_1)$, and the lower concentrations have their errors drawn from a normal distribution with the same mean value and a larger standard deviation, $N(0, \sigma_2)$, where $\sigma_1 < \sigma_2$ and the result of grouping all these samples together would be a nonnormal error distribution.

5. The combined measurement errors observed in the cross-network collocated are additionally inconsistent with idealized i.i.d random errors in that they are heteroscedastic and as a whole nonnormal. As no analysis of the in-network STN collocated data was done, it is not possible to determine if this is just a result of IMPROVE having heteroscedastic measurement errors or if STN measurements exhibit the same inconsistencies. The same cautions, about applying statistics requiring i.i.d. or normal errors, apply to any joint analysis of the IMPROVE and STN data.

CHAPTER 7: BIBLIOGRAPHY OF JOURNAL ARTICLES USING IMPROVE DATA

Ames, R. B. and W. C. Malm (2001), Chemical species' contributions to the upper extremes of aerosol fine mass, *Atmospheric Environment*, *35*, 5193-5204.

Ames, R. B. and W. C. Malm (2001), Comparison of sulfate and nitrate particle mass concentrations measured by IMPROVE and the CDN, *Atmospheric Environment*, *35*, 905-916.

Andronache, C. (2004), Estimates of sulfate aerosol wet scavenging coefficient for locations in the Eastern United States, *Atmospheric Environment*, *38*, 795-804.

Ashbaugh, L. L. and R. A. Eldred (2004), Loss of particle nitrate from Teflon sampling filters: Effects on measured gravimetric mass in California and in the IMPROVE network, *Journal of the Air & Waste Management Association*, *54*, 93-104.

Begum, B. A., P. K. Hopke, and W. X. Zhao (2005), Source identification of fine particles in Washington, DC, by expanded factor analysis modeling, *Environmental Science & Technology*, *39*, 1129-1137.

Bennett, J. P. and S. Benson (2005), Elemental content of lichens of the Point Reyes Peninsula, northern California, *Science of the Total Environment*, *343*, 199-206.

Brewer, P. F. and J. P. Adlhoch (2005), Trends in speciated fine particulate matter and visibility across monitoring networks in the southeastern United States, *Journal of the Air & Waste Management Association*, *55*, 1663-1674.

Cao, J. J., S. C. Lee, K. F. Ho, S. C. Zou, K. Fung, Y. Li, J. G. Watson, and J. C. Chow (2004), Spatial and seasonal variations of atmospheric organic carbon and elemental carbon in Pearl River Delta Region, China, *Atmospheric Environment*, *38*, 4447-4456.

Cao, J. J., F. Wu, J. C. Chow, S. C. Lee, Y. Li, S. W. Chen, Z. S. An, K. K. Fung, J. G. Watson, C. S. Zhu, and S. X. Liu (2005), Characterization and source apportionment of atmospheric organic and elemental carbon during fall and winter of 2003 in Xi'an, China, *Atmospheric Chemistry and Physics*, *5*, 3127-3137.

Cao, J. J., S. C. Lee, J. C. Chow, Y. Cheng, K. F. Ho, K. Fung, S. X. Liu, and J. G. Watson (2005), Indoor/outdoor relationships for PM2.5 and associated carbonaceous pollutants at residential homes in Hong Kong - case study, *Indoor Air*, *15*, 197-204.

Castro, L. M., C. A. Pio, R. M. Harrison, and D. J. T. Smith (1999), Carbonaceous aerosol in urban and rural European atmospheres: estimation of secondary organic carbon concentrations, *Atmospheric Environment*, *33*, 2771-2781.

Chan, Y. C., G. H. McTainsh, R. W. Simpson, P. D. Vowles, D. D. Cohen, and G. M. Bailey (2002), Light degrading properties of size-fractionated PM10 aerosol samples collected from an industrial area in Brisbane, Australia, *Aerosol Science and Technology*, *36*, 890-898.

Chen, L. W. A., J. C. Chow, B. G. Doddridge, R. R. Dickerson, W. F. Ryan, and P. K. Mueller (2003), Analysis of a summertim PM2.5 and haze episode in the mid-Atlantic region, *Journal of the Air & Waste Management Association*, *53*, 946-956.

Cheung, H. C., T. Wang, K. Baumann, and H. Guo (2005), Influence of regional pollution outflow on the concentrations of fine particulate matter and visibility in the coastal area of southern China, *Atmospheric Environment*, *39*, 6463-6474.

Chow, J. C., J. G. Watson, D. Crow, D. H. Lowenthal, and T. Merrifield (2001), Comparison of IMPROVE and NIOSH carbon measurements, *Aerosol Science and Technology*, *34*, 23-34.

Chow, J. C. and J. G. Watson (2002), PM2.5 carbonate concentrations at regionally representative Interagency Monitoring of Protected Visual Environment sites, *Journal of Geophysical Research-Atmospheres*, *107*.

Chow, J. C., J. G. Watson, L. W. A. Chen, W. P. Arnott, and H. Moosmuller (2004), Equivalence of elemental carbon by thermal/optical reflectance and transmittance with different temperature protocols, *Environmental Science & Technology*, *38*, 4414-4422.

Chow, J. C., J. G. Watson, P. K. K. Louie, L. W. A. Chen, and D. Sin (2005), Comparison of PM2.5 carbon measurement methods in Hong Kong, China, *Environmental Pollution*, *137*, 334-344.

Copeland, S. A. (2005), A statistical analysis of visibility-impairing particles in federal class I areas, *Journal of the Air & Waste Management Association*, *55*, 1621-1635.

Corbin, K. C., S. M. Kreidenweis, and T. H. Vonder Haar (2002), Comparison of aerosol properties derived from Sun photometer data and ground-based chemical measurements, *Geophysical Research Letters*, *29*.

Day, D. E. and W. C. Malm (2001), Aerosol light scattering measurements as a function of relative humidity: a comparison between measurements made at three different sites, *Atmospheric Environment*, *35*, 5169-5176.

Debell, L. J., R. W. Talbot, J. E. Dibb, J. W. Munger, E. V. Fischer, and S. E. Frolking (2004), A major regional air pollution event in the northeastern United States caused by extensive forest fires in Quebec, Canada, *Journal of Geophysical Research-Atmospheres*, *109*.

Debell, L. J., M. Vozzella, R. W. Talbot, and J. E. Dibb (2004), Asian dust storm events of spring 2001 and associated pollutants observed in New England by the Atmospheric Investigation, Regional Modeling, Analysis and Prediction (AIRMAP) monitoring network, *Journal of Geophysical Research-Atmospheres*, *109*.

Eatough, D. J., D. A. Eatough, L. Lewis, and E. A. Lewis (1996), Fine particulate chemical composition and light extinction at Canyonlands National Park using organic particulate material concentrations obtained with a multisystem, multichannel diffusion denuder sampler, *Journal of Geophysical Research-Atmospheres*, *101*, 19515-19531.

Eatough, D. J., M. Green, W. Moran, and R. Farber (2001), Potential particulate impacts at the Grand Canyon from northwestern Mexico, *Science of the Total Environment*, *276*, 69-82.

Eatough, D. J., R. W. Long, W. K. Modey, and N. L. Eatough (2003), Semi-volatile secondary organic aerosol in urban atmospheres: meeting a measurement challenge, *Atmospheric Environment*, *37*, 1277-1292.

El-Zanan, H. S., D. H. Lowenthal, B. Zielinska, J. C. Chow, and N. Kumar (2005), Determination of the organic aerosol mass to organic carbon ratio in IMPROVE samples, *Chemosphere*, *60*, 485-496.

Eldred, R. A. and T. A. Cahill (1994), Trends in Elemental Concentrations of Fine Particles at Remote Sites in the United-States-Of-America, *Atmospheric Environment*, *28*, 1009-1019.

Eldred, R. A. and T. A. Cahill (1997), Sulfate sampling artifact from SO2 and alkaline soil, *Environmental Science & Technology*, *31*, 1320-1324.

Eldred, R. A., T. A. Cahill, and R. G. Flocchini (1997), Composition of PM(2.5) and PM(10) aerosols in the IMPROVE network, *Journal of the Air & Waste Management Association*, *47*, 194-203.

Eldred, R. A. (1997), Comparison of selenium and sulfur at remote sites throughout the United States, *Journal of the Air & Waste Management Association*, *47*, 204-211.

Frank, N. H. (2006), Retained nitrate, hydrated sulfates, and carbonaceous mass in Federal Reference Method fine particulate matter for six eastern US cities, *Journal of the Air & Waste Management Association*, *56*, 500-511.

Fung, K., J. C. Chow, and J. G. Watson (2002), Evaluation of OC/EC speciation by thermal manganese dioxide oxidation and the IMPROVE method, *Journal of the Air & Waste Management Association*, *52*, 1333-1341.

Gebhart, K. A., W. C. Malm, and M. Flores (2000), A preliminary look at source-receptor relationships in the Texas-Mexico border area, *Journal of the Air & Waste Management Association*, *50*, 858-868.

Gebhart, K. A., S. Copeland, and W. C. Malm (2001), Diurnal and seasonal patterns in light scattering, extinction, and relative humidity, *Atmospheric Environment*, *35*, 5177-5191.

Gebhart, K. A., S. M. Kreidenweis, and W. C. Malm (2001), Back-trajectory analyses of fine particulate matter measured at Big Bend National Park in the historical database and the 1996 scoping study, *Science of the Total Environment*, *276*, 185-204.

Gebhart, K. A., W. C. Malm, and L. L. Ashbaugh (2005), Spatial, temporal, and interspecies patterns in fine particulate matter in Texas, *Journal of the Air & Waste Management Association*, *55*, 1636-1648.

Gebhart, K. A., B. A. Schichtel, M. G. Barna, and W. C. Malm (2006), Quantitative back-trajectory apportionment of sources of particulate sulfate at Big Bend National Park, TX, *Atmospheric Environment*, *40*, 2823-2834.

Gego, E., P. S. Porter, C. Hogrefe, and J. S. Irwin (2006), An objective comparison of CMAQ and REMSAD performances, *Atmospheric Environment*, *40*, 4920-4934.

Gego, E. L., P. S. Porter, J. S. Irwin, C. Hogrefe, and S. T. Rao (2005), Assessing the comparability of ammonium, nitrate and sulfate concentrations measured by three air quality monitoring networks, *Pure and Applied Geophysics*, *162*, 1919-1939.

Green, M., R. Farber, N. Lien, K. Gebhart, J. Molenar, H. Iyer, and D. Eatough (2005), The effects of scrubber installation at the Navajo generating station on particulate sulfur and visibility levels in the Grand Canyon, *Journal of the Air & Waste Management Association*, *55*, 1675-1682.

Heald, C. L., D. J. Jacob, R. J. Park, B. Alexander, T. D. Fairlie, R. M. Yantosca, and D. A. Chu (2006), Transpacific transport of Asian anthropogenic aerosols and its impact on surface air quality in the United States, *Journal of Geophysical Research-Atmospheres*, *111*.

Hidy, G. M. and C. L. Blanchard (2005), The midlatitude North American background aerosol and global aerosol variation, *Journal of the Air & Waste Management Association*, *55*, 1585-1599.

Holmes, C. W. and R. Miller (2004), Atmospherically transported elements and deposition in the Southeastern United States: local or transoceanic?, *Applied Geochemistry*, *19*, 1189-1200.

Horvath, H. (1997), Comparision of the light absorption coefficient and carbon measures for remote aerosols: An independent analysis of data from the IMPROVE network I and II: Discussion, *Atmospheric Environment*, *31*, 2885-2887.

Huffman, H. D. (1996), Comparison of the light absorption coefficient and carbon measures for remote aerosols: An independent analysis of data from the IMPROVE network .1, *Atmospheric Environment*, *30*, 73-83.

Huffman, H. D. (1996), The reconstruction of aerosol light absorption by particle measurements at remote sites: An independent analysis of data from the IMPROVE network .2, *Atmospheric Environment*, *30*, 85-99.

Huffman, H. D. (1997), Comparison of the light absorption coefficient and carbon measures for remote aerosols: An independent analysis of data from the IMPROVE network I and II: Reply, *Atmospheric Environment*, *31*, 2889-2890.

Iyer, H., P. Patterson, and W. C. Malm (2000), Trends in the extremes of sulfur concentration distributions, *Journal of the Air & Waste Management Association*, *50*, 802-808.

Kim, E., P. K. Hopke, T. V. Larson, N. N. Maykut, and J. Lewtas (2004), Factor analysis of Seattle fine particles, *Aerosol Science and Technology*, *38*, 724-738.

Kim, E. and P. K. Hopke (2004), Source apportionment of fine particles in Washington, DC, utilizing temperature-resolved carbon fractions, *Journal of the Air & Waste Management Association*, *54*, 773-785.

Kim, E. and P. K. Hopke (2004), Improving source identification of fine particles in a rural northeastern US area utilizing temperature-resolved carbon fractions, *Journal of Geophysical Research-Atmospheres*, *109*.

Kim, E. and P. K. Hopke (2005), Improving source apportionment of fine particles in the eastern United States utilizing temperature-resolved carbon fractions, *Journal of the Air & Waste Management Association*, *55*, 1456-1463.

Kim, E., P. K. Hopke, D. M. Kenski, and M. Koerber (2005), Sources of fine particles in a rural Midwestern US area, *Environmental Science & Technology*, *39*, 4953-4960.

Kim, E. and P. K. Hopke (2006), Characterization of fine particle sources in the Great Smoky Mountains area, *Science of the Total Environment*, *368*, 781-794.

Kim, K. W., Y. J. Kim, and S. J. Oh (2001), Visibility impairment during Yellow Sand periods in the urban atmosphere of Kwangju, Korea, *Atmospheric Environment*, *35*, 5157-5167.

Kim, K. W., Z. S. He, and Y. J. Kim (2004), Physicochemical characteristics and radiative properties of Asian dust particles observed at Kwangju, Korea, during the 2001 ACE-Asia intensive observation period, *Journal of Geophysical Research-Atmospheres*, *109*.

Klouda, G. A., J. J. Filliben, H. J. Parish, J. J. Chow, J. G. Watson, and R. A. Cary (2005), Reference material 8785: Air particulate matter on filter media, *Aerosol Science and Technology*, *39*, 173-183.

Kreidenweis, S. M., L. A. Remer, R. Bruintjes, and O. Dubovik (2001), Smoke aerosol from biomass burning in Mexico: Hygroscopic smoke optical model, *Journal of Geophysical Research-Atmospheres*, *106*, 4831-4844.

Lansinger, J. M., C. F. Peistrup, W. G. Tank, and J. L. Isenogle (1977), Analysis of National-Park Service Visibility Data, *Bulletin of the American Meteorological Society*, *58*, 871.

Liu, W., P. K. Hopke, and R. A. VanCuren (2003), Origins of fine aerosol mass in the western United States using positive matrix factorization, *Journal of Geophysical Research-Atmospheres*, *108*.

Lowenthal, D. and N. Kumar (2006), Light scattering from sea-salt aerosols at Interagency Monitoring of Protected Visual Environments (IMPROVE) sites, *Journal of the Air & Waste Management Association*, *56*, 636-642.

Lowenthal, D. H., J. G. Watson, and P. Saxena (2000), Contributions to light extinction during project MOHAVE, *Atmospheric Environment*, *34*, 2351-2359.

Lowenthal, D. H. and N. Kumar (2003), PM2.5 mass and light extinction reconstruction in IMPROVE, *Journal of the Air & Waste Management Association*, *53*, 1109-1120.

Lowenthal, D. H. and N. Kumar (2004), Variation of mass scattering efficiencies in IMPROVE, *Journal of the Air & Waste Management Association*, *54*, 926-934.

Malm, W. C. and J. V. Molenar (1984), Visibility Measurements in National-Parks in the Western United-States, *Journal of the Air Pollution Control Association*, *34*, 899-904.

Malm, W. C. and G. Persha (1991), Considerations in the Accuracy of A Long-Path Transmissometer, *Aerosol Science and Technology*, *14*, 459-471.

Malm, W. C. (1992), Characteristics and Origins of Haze in the Continental United-States, *Earth-Science Reviews*, *33*, 1-36.

Malm, W. C., K. A. Gebhart, J. Molenar, T. Cahill, R. Eldred, and D. Huffman (1994), Examining the Relationship Between Atmospheric Aerosols and Light Extinction at Mount-Rainier-National-Park and North-Cascades-National-Park, *Atmospheric Environment*, *28*, 347-360.

Malm, W. C. and K. A. Gebhart (1997), Source apportionment of sulfur and light extinction using receptor modeling techniques, *Journal of the Air & Waste Management Association*, *47*, 250-268.

Malm, W. C. and M. L. Pitchford (1997), Comparison of calculated sulfate scattering efficiencies as estimated from size-resolved particle measurements at three national locations, *Atmospheric Environment*, *31*, 1315-1325.

Malm, W. C. and D. E. Day (2000), Optical properties of aerosols at Grand Canyon National Park, *Atmospheric Environment*, *34*, 3373-3391.

Malm, W. C. and J. F. Sisler (2000), Spatial patterns of major aerosol species and selected heavy metals in the United States, *Fuel Processing Technology*, *65*, 473-501.

Malm, W. C. and D. E. Day (2001), Estimates of aerosol species scattering characteristics as a function of relative humidity, *Atmospheric Environment*, *35*, 2845-2860.

Malm, W. C., B. A. Schichtel, R. B. Ames, and K. A. Gebhart (2002), A 10-year spatial and temporal trend of sulfate across the United States, *Journal of Geophysical Research-Atmospheres*, *107*.

Malm, W. C., B. A. Schichtel, M. L. Pitchford, L. L. Ashbaugh, and R. A. Eldred (2004), Spatial and monthly trends in speciated fine particle concentration in the United States, *Journal of Geophysical Research-Atmospheres*, *109*.

Malm, W. C., D. E. Day, C. Carrico, S. M. Kreidenweis, J. L. Collett, G. McMeeking, T. Lee, J. Carrillo, and B. Schichtel (2005), Intercomparison and closure calculations using measurements of aerosol species and optical properties during the Yosemite Aerosol Characterization Study, *Journal of Geophysical Research-Atmospheres*, *110*.

Matsui, T., S. M. Kreidenweis, R. A. Pielke, B. Schichtel, H. B. Yu, M. Chin, D. A. Chu, and D. Niyogi (2004), Regional comparison and assimilation of GOCART and MODIS aerosol optical depth across the eastern US, *Geophysical Research Letters*, *31*.

Maykut, N. N., J. Lewtas, E. Kim, and T. V. Larson (2003), Source apportionment of PM2.5 at an urban IMPROVE site in Seattle, Washington, *Environmental Science & Technology*, *37*, 5135-5142.

McDonald, K. and M. Shepherd (2004), Characterization of visibility impacts related to fine particulate matter in Canada, *Journal of the Air & Waste Management Association*, *54*, 1061-1068.

McMeeking, G. R., S. M. Kreidenweis, M. Lunden, J. Carrillo, C. M. Carrico, T. Lee, P. Herckes, G. Engling, D. E. Day, J. Hand, N. Brown, W. C. Malm, and J. L. Collett (2006), Smoke-impacted regional haze in California during the summer of 2002, *Agricultural and Forest Meteorology*, *137*, 25-42.

Mebust, M. R., B. K. Eder, F. S. Binkowski, and S. J. Roselle (2003), Models-3 community multiscale air quality (CMAQ) model aerosol component - 2. Model evaluation, *Journal of Geophysical Research-Atmospheres*, *108*.

Morris, R., B. Koo, and G. Yarwood (2005), Evaluation of multisectional and two-section particulate matter photochemical grid models in the western United States, *Journal of the Air & Waste Management Association*, *55*, 1683-1693.

Morris, R. E., B. Koo, A. Guenther, G. Yarwood, D. McNally, T. W. Tesche, G. Tonnesen, J. Boylan, and P. Brewer (2006), Model sensitivity evaluation for organic carbon using two multi-pollutant air quality models that simulate regional haze in the southeastern United States, *Atmospheric Environment*, *40*, 4960-4972.

Nejedly, Z., J. L. Campbell, J. Brook, R. Vet, and R. Eldred (2003), Evaluation of elemental and black carbon measurements from the GAViM and IMPROVE networks, *Aerosol Science and Technology*, *37*, 96-108.

O'Neill, S. M., B. K. Lamb, J. Chen, C. Claiborn, D. Finn, S. Otterson, C. Figueroa, C. Bowman, M. Boyer, R. Wilson, J. Arnold, S. Aalbers, J. Stocum, C. Swab, M. Stoll, M. Dubois, and M. Anderson (2006), Modeling ozone and aerosol formation and transport in the pacific northwest with the community multi-scale air quality (CMAQ) modeling system, *Environmental Science & Technology*, *40*, 1286-1299.

Odman, M. T., A. G. Russell, and J. W. Boylan (2004), Estimates of PM2.5 levels in the southeastern United States for the year 2010: What else can be done?, *Fuel Processing Technology*, *85*, 631-639.

Park, K., J. C. Chow, J. G. Watson, D. L. Trimble, P. Doraiswamy, K. Park, W. P. Arnott, K. R. Stroud, K. Bowers, R. Bode, A. Petzold, and A. D. A. Hansen (2006), Comparison of continuous and filter-based carbon measurements at the Fresno Supersite, *Journal of the Air & Waste Management Association*, *56*, 474-491.

Park, R. J., D. J. Jacob, M. Chin, and R. V. Martin (2003), Sources of carbonaceous aerosols over the United States and implications for natural visibility, *Journal of Geophysical Research-Atmospheres*, *108*.

Park, R. J., D. J. Jacob, B. D. Field, R. M. Yantosca, and M. Chin (2004), Natural and transboundary pollution influences on sulfate-nitrate-ammonium aerosols in the United States: Implications for policy, *Journal of Geophysical Research-Atmospheres*, *109*.

Park, S. S., M. S. Bae, J. J. Schauer, S. Y. Ryu, Y. J. Kim, S. Y. Cho, and S. J. Kim (2005), Evaluation of the TMO and TOT methods for OC and EC measurements and their characteristics in PM2.5 at an urban site of Korea during ACE-Asia, *Atmospheric Environment*, *39*, 5101-5112.

Patterson, P., H. Iyer, J. Sisler, and W. C. Malm (2000), An analysis of the yearly changes in sulfur concentrations at various national parks in the United States, 1980-1996, *Journal of the Air & Waste Management Association*, *50*, 790-801.

Pitchford, M. and M. Green (1997), Analyses of sulfur aerosol size distributions for a forty-day period in summer 1992 at Meadview, Arizona, *Journal of the Air & Waste Management Association*, *47*, 136-146.

Pitchford, M. L., B. A. Schichtel, K. A. Gebhart, M. G. Barna, W. C. Malm, I. H. Tombach, and E. M. Knipping (2005), Reconciliation and interpretation of the Big Bend National Park light extinction source apportionment: Results from the Big Bend Regional Aerosol and Visibility Observational study - Part II, *Journal of the Air & Waste Management Association*, *55*, 1726-1732.

Rosenfeld, D. and A. Givati (2006), Evidence of orographic precipitation suppression by air pollution-induced aerosols in the western United States, *Journal of Applied Meteorology and Climatology*, *45*, 893-911.

Ryan, P. A., D. Lowenthal, and N. Kumar (2005), Improved light extinction reconstruction in interagency monitoring of protected visual environments, *Journal of the Air & Waste Management Association*, *55*, 1751-1759.

Ryan, P. A. (2005), Precipitation in light extinction reconstruction, *Journal of the Air & Waste Management Association*, *55*, 1014-1018.

Schichtel, B. A., W. C. Malm, and M. L. Pitchford (2006), Critique of "Precipitation in light extinction reconstruction" by P.A. Ryan, *Journal of the Air & Waste Management Association*, *56*, 539-546.

Sciare, J., H. Cachier, K. Oikonomou, P. Ausset, R. Sarda-Esteve, and N. Mihalopoulos (2003), Characterization of carbonaceous aerosols during the MINOS campaign in Crete, July-August 2001: a multi-analytical approach, *Atmospheric Chemistry and Physics*, *3*, 1743-1757.

Sisler, J. F. and W. C. Malm (1990), Assessing the Visibility Impairment Associated with Various Sulfate Reduction Scenarios at Shenandoah-National-Park, *Abstracts of Papers of the American Chemical Society*, *200*, 108-ENVR.

Sisler, J. F. and W. C. Malm (1997), Characteristics of winter and summer aerosol mass and light extinction on the Colorado Plateau, *Journal of the Air & Waste Management Association*, *47*, 317-330.

Sister, J. F. and W. C. Malm (2000), Interpretation of trends of PM2.5 and reconstructed visibility from the IMPROVE network, *Journal of the Air & Waste Management Association*, *50*, 775-789.

Snow, J. A., J. B. Dennison, D. A. Jaffe, H. U. Price, J. K. Vaughan, and B. Lamb (2003), Aircraft and surface observations of air quality in Puget Sound and a comparison to a regional model, *Atmospheric Environment*, *37*, 4019-4032.

Todd, D. L., W. C. Keene, J. L. Moody, H. Maring, and J. N. Galloway (2003), Effects of wet deposition on optical properties of the atmosphere over Bermuda and Barbados, *Journal of Geophysical Research-Atmospheres*, *108*.

Veranth, J. M., T. A. Moss, J. C. Chow, R. Labban, W. K. Nichols, J. C. Walton, J. G. Watson, and G. S. Yost (2006), Correlation of in vitro cytokine responses with the chemical composition of soil-derived particulate matter, *Environmental Health Perspectives*, *114*, 341-349.

Vukovich, F. M. and J. Sherwell (2002), Comparison of fine particles and the relationship between particle variation and meteorology at an urban site and a remote site in the eastern United States, *Journal of the Air & Waste Management Association*, *52*, 573-584.

Walsh, K. and J. Sherwell (2002), Estimation of ambient PM2.5 concentrations in Maryland and verification by measured values, *Journal of the Air & Waste Management Association*, *52*, 1161-1175.

Walsh, K. J. and A. B. Gilliland (2001), Regional variations in sulfate and nitrate on annual, seasonal, and synoptic time scales, *Journal of the Air & Waste Management Association*, *51*, 1339-1345.

Wang, J., S. A. Christopher, U. S. Nair, J. S. Reid, E. M. Prins, J. Szykman, and J. L. Hand (2006), Mesoscale modeling of Central American smoke transport to the United States: 1. "Top-down" assessment of emission strength and diurnal variation impacts, *Journal of Geophysical Research-Atmospheres*, *111*.

Watson, J. G., J. C. Chow, D. H. Lowenthal, C. F. Cahill, D. L. Blumenthal, L. W. Richards, and H. G. Jorge (2001), Aerosol chemical and optical properties during the Mt. Zirkel Visibility Study, *Journal of Environmental Quality*, *30*, 1118-1125.

Watson, J. G. and J. C. Chow (2002), Comparison and evaluation of in situ and filter carbon measurements at the Fresno Supersite, *Journal of Geophysical Research-Atmospheres*, *107*.

Watson, J. G., J. C. Chow, D. H. Lowenthal, N. F. Robinson, C. F. Cahill, and D. L. Blumenthal (2002), Simulating changes in source profiles from coal-fired power stations: Use in chemical mass balance of PM2.5 in the Mount Zirkel Wilderness, *Energy & Fuels*, *16*, 311-324.

White, W. H. (1997), Deteriorating air or improving measurements? On interpreting concatenate time series, *Journal of Geophysical Research-Atmospheres*, *102*, 6813-6821.

White, W. H., L. L. Ashbaugh, N. P. Hyslop, and C. E. Mcdade (2005), Estimating measurement uncertainty in an ambient sulfate trend, *Atmospheric Environment*, *39*, 6857-6867.

Xu, J., D. DuBois, M. Pitchford, M. Green, and V. Etyemezian (2006), Attribution of sulfate aerosols in Federal Class I areas of the western United States based on trajectory regression analysis, *Atmospheric Environment*, *40*, 3433-3447.

Yu, S. C., R. L. Dennis, P. V. Bhave, and B. K. Eder (2004), Primary and secondary organic aerosols over the United States: estimates on the basis of observed organic carbon (OC) and elemental carbon (EC), and air quality modeled primary OC/EC ratios, *Atmospheric Environment*, *38*, 5257-5268.

Yu, X. Y., L. Taehyoung, B. Ayres, S. M. Kreidenweis, J. L. Collett, and W. Maim (2005), Particulate nitrate measurement using nylon filters, *Journal of the Air & Waste Management Association*, *55*, 1100-1110.

Yu, X. Y., T. Lee, B. Ayres, S. M. Kreidenweis, W. Malm, and J. L. Collett (2006), Loss of fine particle ammonium from denuded nylon filters, *Atmospheric Environment*, *40*, 4797-4807.

Zeller, K., D. Harrington, A. Riebau, and E. Donev (2000), Annual wet and dry deposition of sulfur and nitrogen in the snowy range, Wyoming, *Atmospheric Environment*, *34*, 1703-1711.

Zhang, R. J., Y. F. Xu, and Z. W. Han (2003), Inorganic chemical composition and source signature of PM2.5 in Beijing during ACE-Asia period, *Chinese Science Bulletin*, *48*, 1002-1005.

Zhang, Y., P. Liu, B. Pun, and C. Seigneur (2006), A comprehensive performance evaluation of MM5-CMAQ for the Summer 1999 Southern Oxidants Study episode - Part I: Evaluation protocols, databases, and meteorological predictions, *Atmospheric Environment*, *40*, 4825-4838.

Zhang, Y., P. Liu, A. Queen, C. Misenis, B. Pun, C. Seigneur, and S. Y. Wu (2006), A comprehensive performance evaluation of MM5-CMAQ for the Summer 1999 Southern Oxidants Study episode- Part II: Gas and aerosol predictions, *Atmospheric Environment*, *40*, 4839-4855.

Zhao, W. X. and P. K. Hopke (2004), Source apportionment for ambient particles in the San Gorgonio wilderness, *Atmospheric Environment*, *38*, 5901-5910.

Zhao, W. X. and P. K. Hopke (2006), Source investigation for ambient PM2.5 in Indianapolis, IN, *Aerosol Science and Technology*, *40*, 898-909.